ADVANCES IN MICROBIAL IRON CYCLING

EDITED BY: Lei Yan, Sujun Li, Orit Sivan and Sabine Kasten
PUBLISHED IN: Frontiers in Microbiology

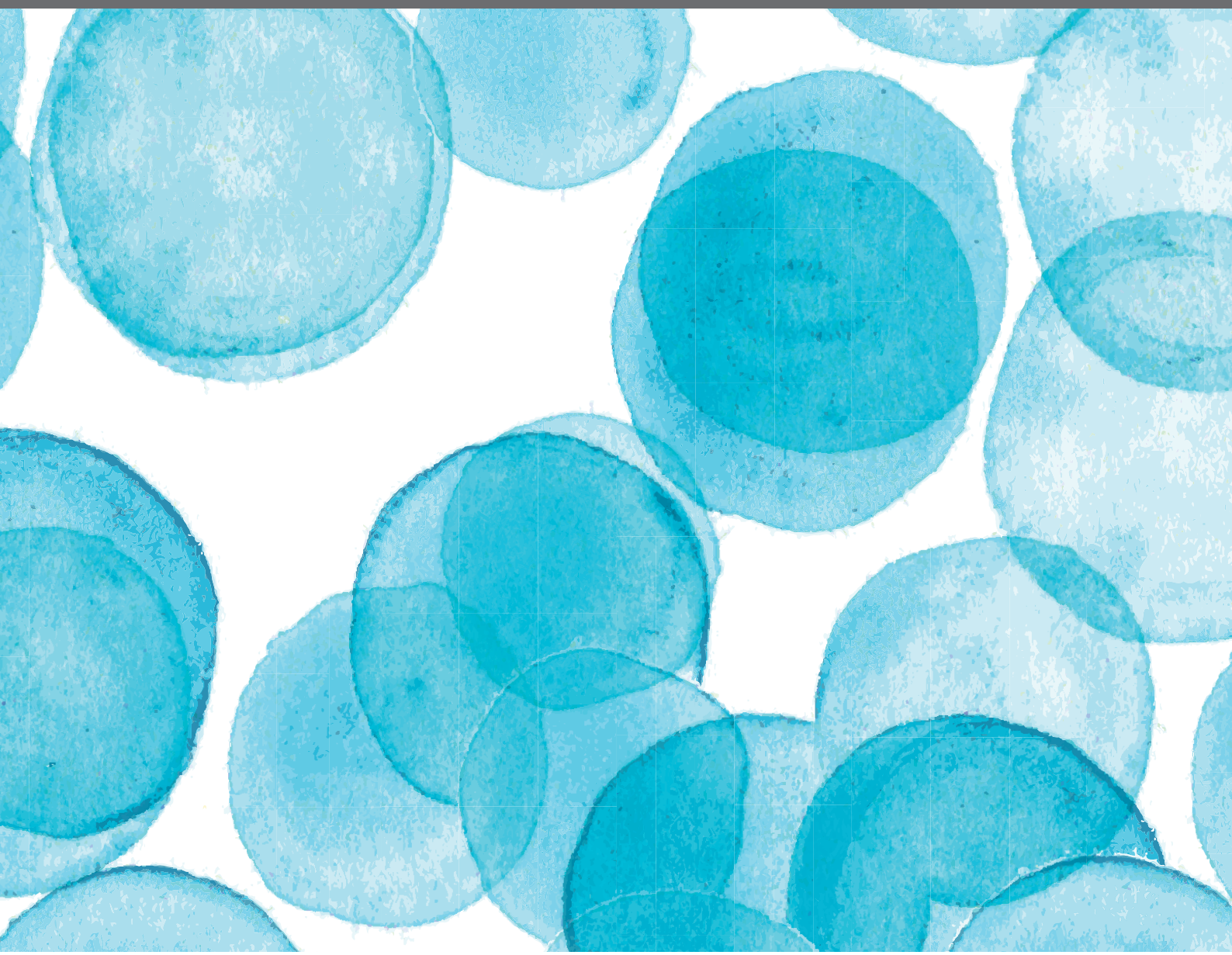

frontiers Research Topics

ISSN 1664-8714
ISBN 978-2-88976-563-8
DOI 10.3389/978-2-88976-563-8

About Frontiers

Frontiers is more than just an open-access publisher of scholarly articles: it is a pioneering approach to the world of academia, radically improving the way scholarly research is managed. The grand vision of Frontiers is a world where all people have an equal opportunity to seek, share and generate knowledge. Frontiers provides immediate and permanent online open access to all its publications, but this alone is not enough to realize our grand goals.

Frontiers Journal Series

The Frontiers Journal Series is a multi-tier and interdisciplinary set of open-access, online journals, promising a paradigm shift from the current review, selection and dissemination processes in academic publishing. All Frontiers journals are driven by researchers for researchers; therefore, they constitute a service to the scholarly community. At the same time, the Frontiers Journal Series operates on a revolutionary invention, the tiered publishing system, initially addressing specific communities of scholars, and gradually climbing up to broader public understanding, thus serving the interests of the lay society, too.

Dedication to Quality

Each Frontiers article is a landmark of the highest quality, thanks to genuinely collaborative interactions between authors and review editors, who include some of the world's best academicians. Research must be certified by peers before entering a stream of knowledge that may eventually reach the public - and shape society; therefore, Frontiers only applies the most rigorous and unbiased reviews.
Frontiers revolutionizes research publishing by freely delivering the most outstanding research, evaluated with no bias from both the academic and social point of view. By applying the most advanced information technologies, Frontiers is catapulting scholarly publishing into a new generation.

What are Frontiers Research Topics?

Frontiers Research Topics are very popular trademarks of the Frontiers Journals Series: they are collections of at least ten articles, all centered on a particular subject. With their unique mix of varied contributions from Original Research to Review Articles, Frontiers Research Topics unify the most influential researchers, the latest key findings and historical advances in a hot research area! Find out more on how to host your own Frontiers Research Topic or contribute to one as an author by contacting the Frontiers Editorial Office: frontiersin.org/about/contact

ADVANCES IN MICROBIAL IRON CYCLING

Topic Editors:
Lei Yan, Heilongjiang Bayi Agricultural University, China
Sujun Li, Indiana University, United States
Orit Sivan, Ben-Gurion University of the Negev, Israel
Sabine Kasten, Alfred Wegener Institute Helmholtz Centre for Polar and Marine Research (AWI), Germany

Citation: Yan, L., Li, S., Sivan, O., Kasten, S., eds. (2022). Advances in Microbial Iron Cycling. Lausanne: Frontiers Media SA. doi: 10.3389/978-2-88976-563-8

Table of Contents

frontiers | Frontiers in Microbiology

EDITORIAL
published: 21 June 2022
doi: 10.3389/fmicb.2022.931648

Editorial: Advances in Microbial Iron Cycling

Lei Yan[1]*, *Sujun Li*[2], *Orit Sivan*[3] and *Sabine Kasten*[4,5,6]

[1] Heilongjiang Provincial Key Laboratory of Environmental Microbiology and Recycling of Argo-Waste in Cold Region, College of Life Science and Biotechnology, Heilongjiang Bayi Agricultural University, Daqing, China, [2] Indiana University Bloomington, Bloomington, IN, United States, [3] Ben-Gurion University of the Negev Beersheba, Beersheba, Israel, [4] Alfred Wegener Institute Helmholtz Centre for Polar and Marine Research (AWI) Bremerhaven, Germany, [5] Faculty of Geosciences, University of Bremen, Bremen, Germany, [6] MARUM – Center for Marine Environmental Sciences, University of Bremen, Bremen, Germany

Keywords: iron cycling, iron redox cycling bacteria, mechanisms, metagenomics, biomineral

Editorial on the Research Topic

Advances in Microbial Iron Cycling

Iron is the fourth most abundant element in the Earth's crust and an essential nutrient for almost all living organisms (e.g., Frey and Reed, 2012). As a redox-sensitive transition element, iron is tightly associated with oxidation and reduction processes, and is linked to and also drives the cycling of other elements, including carbon, oxygen, nitrogen, phosphorus, sulfur, and manganese, through numerous processes (Sanyal et al., 2019). These processes are not only actuated by chemical reactions but also driven by microorganisms, which use iron compounds as both electron donors and acceptors and electron transfer in energy generating processes (e.g., Lovley, 1991; Weber et al., 2006; Riedinger et al., 2014; Sivan et al., 2014; Aromokeye et al., 2020).

A large number of microbiological research methods have been developed and shown the essential roles of iron-metabolizing microbes in global biogeochemical cycles (Konhauser et al., 2011). These iron redox cycling bacteria are distributed widely in nature, including marine, forest, and wetland ecosystems (e.g., Hori et al., 2010; Kanaparthi, 2013). Since discovering the first iron-metabolizing bacterium, we have significantly improved our understanding of the diversity, physiology, ecology, and environmental influence of the microorganisms that transform iron. Unraveling the contribution of certain biotic or abiotic processes during iron cycling is highly challenging, despite the availability of various microscopic, spectroscopic, molecular biological and other analytical methods to follow the abiotic and microbial transformation of dissolved, colloidal, and particulate iron redox species (e.g., Raiswell and Canfield, 2012; Kappler et al., 2021).

This Research Topic presents the leading edge of microbial iron cycling, focusing on the geochemical significance of microorganisms and microbial processes which can directly or indirectly contribute to iron cycling in nature. Ten submitted manuscripts had been accepted for publication. In a review article, Lucía et al. described the molecular mechanisms of regulating iron metabolism, focusing on *Saccharomyces cerevisiae*. The budding yeast *S. cerevisiae* has been used as a model organism to study the adaptation of eukaryotic cells to changes in iron availability. Upon iron deficiency, yeast utilizes two transcription factors, Aft1 and Aft2, to activate the expression of a set of genes known as the iron regulon, which are implicated in iron uptake, recycling, and mobilization. At high iron levels, the yeast Yap5, Msn2, and Msn4 transcription factors activate the expression of a vacuolar iron importer called Ccc1, which is the most important high-iron protecting factor devoted to detoxifying excess cytosolic iron that is stored in the vacuole for its mobilization upon scarcity.

OPEN ACCESS

Edited and reviewed by:
Bradley M. Tebo,
Oregon Health and Science University, United States

***Correspondence:**
Lei Yan
hekouyanlei@gmail.com
orcid.org/0000-0003-2596-6840

Specialty section:
This article was submitted to Microbiological Chemistry and Geomicrobiology, a section of the journal Frontiers in Microbiology

Received: *29 April 2022*
Accepted: *23 May 2022*
Published: *21 June 2022*

Citation:
Yan L, Li S, Sivan O and Kasten S (2022) Editorial: Advances in Microbial Iron Cycling. Front. Microbiol. 13:931648. doi: 10.3389/fmicb.2022.931648

Lambrecht et al. described an enrichment culture (BLA1) from meromictic ferruginous Brownie Lake, Minnesota, United States, which contains a Fe(II)-oxidizing Green sulfur bacteria (GSB) and a metabolically flexible putative Fe(III)-reducing anaerobe. "*Candidatus Chlorobium masyuteum*" is closely related to other phototrophic GSB, but distinct in genomic and physiological characteristics. It is able to grow photoautotrophically using Fe(II), and possibly acetate and H^2. The Fe(III)-reducing anaerobe "*Candidatus Pseudopelobacter ferreus*" grows in anoxic freshwater medium in defined coculture with "*Ca. C. masyuteum*". Investigation of BLA1 expands the genetic basis for phototrophic Fe(II) oxidation by GSB and highlights the role these organisms may play in Fe(II) oxidation and carbon cycling in ferruginous lakes.

Another article authored by Zhang et al. explored the impact of Fe(III) (Oxyhydr) oxides mineralogy on iron solubilization and associated microbial communities. The authors highlight the influence of Fe mineralogy on the abundance of *Geobacter* and *Shewanella* concerning Fe bio-reduction kinetics in a complex mixture of electron donors.

Garber et al. surveyed the microbial iron cycle in diverse subseafloor habitats using FeGenie (A database and bioinformatics tool that identifies microbial iron cycling genes and enables the development of testable hypotheses on the biogeochemical cycling of iron). They illuminated the diversity of microbial iron redox mechanisms that can occur across various geochemical regimes, suggesting that geochemical constraints likely play an important role in dictating the dominant mechanisms for iron cycling.

Also concerning microbial-mediated iron oxidation and reduction, Yang, Jiang et al. compared biogeographic patterns and composition of the iron redox cycling bacterial community between soil and water samples obtained from different types of peatlands across four regions in Northeast China using high-throughput DNA sequencing. The results suggest that the widespread bacteria involved in iron redox cycling exhibit distinct patterns of distribution and formation mechanisms of microbial community between soil and water in peatlands.

Calapa et al. reported the mass transport of iron and other solutes under flow conditions in subsurface groundwater and its effect on community structure dynamics and Fe(III)-reduction. The results demonstrate that removing inhibitory Fe(II) via mimicking the hydrologic flow of groundwater increases reduction rates and overall Fe-oxide dissolution, which in turn alters the hydrology of the Fe(III)-rich rocks. Reductive weathering of Fe(III)-rich rocks may be more substantial than previously understood.

Yücel et al. studied soluble, colloidal, and particulate iron across the hydrothermal vent mixing zones in Broken Spur and Rainbow, Mid-Atlantic Ridge. The persistence of a nanoparticulate/colloidal phase (retained within 20–200 nm filtrates) even in high-temperature samples, suggested this recalcitrant Fe pool- surviving immediate precipitation-contributes to maintaining high hydrothermal iron fluxes to the deep ocean.

Finally, three articles reported that the iron cycle is closely coupled with carbon, sulfur, nitrogen, phosphorus and manganese cycles. Yang, Li et al. investigated the activity of Anammox bacteria in the Feammox process using the ^{15}N isotopic tracing technique combined with 16S rRNA gene amplicon sequencing. A significantly positive relationship between rates of $^{15}N_2$ production and Fe(III) reduction indicated the occurrence of Feammox during incubation. They proposed that sole Anammox bacteria or cooperation between Anammox bacteria and Fe(III) reducers serve a potential role in the Feammox process.

Napieralski and Roden investigated the potential interactions among metabolically diverse microorganisms in the near-surface weathering of silicate rocks and confirmed the ability of ferrous iron [Fe(II)] oxidizing bacteria (FeOB) to grow via the oxidation of silicate-bound Fe(II). They suggested that chemolithotrophic and organotrophic microorganisms likely coexist and contribute synergistically to the overall weathering of the *in-situ* bedrock outcrop.

Nabeh et al. investigated and quantified the interactions between iron-sulfide minerals and biomass-derived organic carbon. The amounts of carbon and nitrogen associated with biogenic iron sulfide minerals increased with increasing cell biomass concentrations in the media, indicating that the microbial cells play an essential role in increasing organic carbon concentrations in iron sulfide minerals.

In summary, the collected articles show novel pathways for iron uptake and acquisition, intracellular and extracellular iron mineralization, microbially mediated iron cycling in natural and artificial environments, and advances in the analysis of the effect of the iron cycle on the cycling of other elements. This knowledge broadens our perspective on the iron cycle and will contribute to understanding the transformations of carbon, nitrogen and phosphorus.

AUTHOR CONTRIBUTIONS

LY initiated and wrote this Editorial and revised by SL, OS, and SK. All authors contributed to the article and approved the submitted version.

ACKNOWLEDGMENTS

The editors express their gratitude to all the researchers who contributed their valuable work to this topic, as well as the reviewers who provided their constructive criticisms to improve the articles and the topic work.

REFERENCES

Aromokeye, D. A., Kulkarni, A., Elvert, M., Wegener, G., Henkel, S., Coffinet, S., et al. (2020). Rates and microbial players of iron-driven anaerobic oxidation of methane in methanic marine sediments. *Front. Microbiol.* 10, 3041. doi: 10.3389/fmicb.2019.03041

Frey, P. A., and Reed, G. H. (2012). The ubiquity of iron. *ACS Chem. Biol.* 7, 1477–1481. doi: 10.1021/cb300323q

Hori, T., Müller, A., Igarashi, Y., Conrad, R., and Friedrich, M. W. (2010). Identification of iron-reducing microorganisms in anoxic rice paddy soil by ^{13}C-acetate probing. *ISME J.*, 4, 267–278. doi: 10.1038/ismej.2009.100

Kanaparthi, D. (2013). *Microbial redox cycling of iron in Lake Grosse Fuchskuhle*. Philipps-Universität Marburg.

Kappler, A., Bryce, C., Mansor, M., Lueder, U., Byrne, J. M., and Swanner, E. D. (2021). An evolving view on biogeochemical cycling of iron. *Nat. Rev. Microbiol.* 19, 360–374. doi: 10.1038/s41579-020-00502-7

Konhauser, K. O., Kappler, A., and Roden, E. E. (2011). Iron in microbial metabolisms. *Elements.* 7, 89–93. doi: 10.2113/gselements.7.2.89

Lovley, D. R. (1991). Dissimilatory Fe (III) and Mn (IV) reduction. *Microb. Physiol.* 55, 259–287. doi: 10.1128/mr.55.2.259-287.1991

Raiswell, R., and Canfield, D. E. (2012). The iron biogeochemical cycle past and present. *Geochem. Perspect.* 1, 1–220. doi: 10.7185/geochempersp.1.1

Riedinger, N., Formolo, M. J., Lyons, T. W., Henkel, S., Beck, A., and Kasten, S. (2014). An inorganic geochemical argument for coupled anaerobic oxidation of methane and iron reduction in marine sediments. *Geobiology.* 12, 172–81. doi: 10.1111/gbi.12077

Sanyal, S. K., Shuster, J., and Reith, F. (2019). Cycling of biogenic elements drives biogeochemical gold cycling. *Earth-Sci. Rev.* 190, 131–147. doi: 10.1016/j.earscirev.2018.12.010

Sivan, O., Antler, G., Turchyn, A. V., Marlow, J. J., and Orphan, V. J. (2014). Iron oxides stimulate sulfate-driven anaerobic methane oxidation in seeps. *Proc.Nat. Acad. Sci.* 111, E4139–E4147. doi: 10.1073/pnas.1412269111

Weber, K. A., Achenbach, L. A., and Coates, J. D. (2006). Microorganisms pumping iron: anaerobic microbial iron oxidation and reduction. *Nat. Rev. Microbiol.* 4, 752–764. doi: 10.1038/nrmicro1490

Conflict of Interest: The authors declare that the research was conducted in the absence of any commercial or financial relationships that could be construed as a potential conflict of interest.

frontiers in Microbiology

MINI REVIEW
published: 09 September 2020
doi: 10.3389/fmicb.2020.582830

Iron Regulatory Mechanisms in *Saccharomyces cerevisiae*

Lucía Ramos-Alonso[1†], Antonia María Romero[1†], María Teresa Martínez-Pastor[2] and Sergi Puig[1]*

[1] *Departamento de Biotecnología, Instituto de Agroquímica y Tecnología de Alimentos (IATA), Consejo Superior de Investigaciones Científicas (CSIC), Valencia, Spain,* [2] *Departamento de Bioquímica y Biología Molecular, Universitat de València, Valencia, Spain*

OPEN ACCESS

Edited by:
Lei Yan,
Heilongjiang Bayi Agricultural University, China

Reviewed by:
Nicoletta Guaragnella, University of Bari Aldo Moro, Italy
Claudina Rodrigues-Pousadaj, New University of Lisbon, Portugal
Upendarrao Golla, Pennsylvania State University, United States
Amparo Pascual-Ahuir, Universitat Politècnica de València, Spain
Vasanthi Nachiappan, Bharathidasan University, India

***Correspondence:**
Sergi Puig
spuig@iata.csic.es

†Present address:
Lucía Ramos-Alonso, Department of Microbiology, Oslo University Hospital, Oslo, Norway
Antonia María Romero, Department of Chemistry and Molecular Biology, University of Gothenburg, Gothenburg, Sweden

Specialty section:
This article was submitted to Microbiological Chemistry and Geomicrobiology, a section of the journal Frontiers in Microbiology

Received: *13 July 2020*
Accepted: *20 August 2020*
Published: *09 September 2020*

Citation:
Ramos-Alonso L, Romero AM, Martínez-Pastor MT and Puig S (2020) Iron Regulatory Mechanisms in Saccharomyces cerevisiae. Front. Microbiol. 11:582830. doi: 10.3389/fmicb.2020.582830

Iron is an essential micronutrient for all eukaryotic organisms because it participates as a redox cofactor in many cellular processes. However, excess iron can damage cells since it promotes the generation of reactive oxygen species. The budding yeast *Saccharomyces cerevisiae* has been used as a model organism to study the adaptation of eukaryotic cells to changes in iron availability. Upon iron deficiency, yeast utilizes two transcription factors, Aft1 and Aft2, to activate the expression of a set of genes known as the iron regulon, which are implicated in iron uptake, recycling and mobilization. Moreover, Aft1 and Aft2 activate the expression of Cth2, an mRNA-binding protein that limits the expression of genes encoding for iron-containing proteins or that participate in iron-using processes. Cth2 contributes to prioritize iron utilization in particular pathways over other highly iron-consuming and non-essential processes including mitochondrial respiration. Recent studies have revealed that iron deficiency also alters many other metabolic routes including amino acid and lipid synthesis, the mitochondrial retrograde response, transcription, translation and deoxyribonucleotide synthesis; and activates the DNA damage and general stress responses. At high iron levels, the yeast Yap5, Msn2, and Msn4 transcription factors activate the expression of a vacuolar iron importer called Ccc1, which is the most important high-iron protecting factor devoted to detoxify excess cytosolic iron that is stored into the vacuole for its mobilization upon scarcity. The complete sequencing and annotation of many yeast genomes is starting to unveil the diversity and evolution of the iron homeostasis network in this species.

Keywords: iron deficiency, iron excess, iron homeostasis, iron metabolism, yeast, *Saccharomyces cerevisiae*, transcriptional regulation, post-transcriptional regulation

INTRODUCTION

Iron is a vital micronutrient for all eukaryotic organisms. Its redox activity and its ability to bind to multiple ligands enables iron to participate as a cofactor in the form of heme, iron-sulfur clusters (ISC), mononuclear iron or oxo-diiron centers in numerous biological processes including respiration, DNA replication and repair, ribosome biogenesis, translation, photosynthesis, biosynthesis of lipids and oxygen transport. Iron is one of the most abundant elements in the Earth's crust, but the extremely low solubility of ferric iron (Fe^{3+}) at physiological pH has dramatically restricted its availability to living organisms. Consequently, iron deficiency anemia has become the most common nutritional disorder worldwide, affecting two billion people,

particularly women, children and older adults [reviewed in Chaparro and Suchdev (2019); Means (2020)]. The same redox properties that make iron indispensable for life also lead to cytotoxicity when present at high concentrations since it participates in Fenton reactions producing hydroxyl radicals that damage cells at the DNA, lipid and protein levels. Therefore, intracellular iron levels have to be tightly controlled. Defects in human iron homeostasis are directly related to disorders such as Friedreich's ataxia, myopathies and encephalomyopathies, hemochromatosis, multiple mitochondrial dysfunction syndromes, and to increased risk of infections and cancer [reviewed in Stehling et al. (2014); Muckenthaler et al. (2017)]. Iron deficiency is also a concern in agriculture because it induces chlorosis and reduces photosynthesis, affecting both the yield and the nutritional value of crops [reviewed in Puig et al. (2007); Zhang et al. (2019)]. For all these reasons, studying the molecular mechanisms that regulate iron metabolism is important to understand iron-related physiological alterations, to deal with its nutritional defect consequences, and to develop medical treatments and agricultural applications. The budding yeast *S. cerevisiae* has been used as a model organism to study many aspects of iron homeostasis and regulation in eukaryotes. In fact, recent systems biology approaches have proposed a comprehensive mechanistic model for iron metabolism that has also been integrated into a whole-yeast metabolic model (Dikicioglu and Oliver, 2019; Lindahl, 2019). Here, we briefly review the mechanisms that control the adaptation of *S. cerevisiae* to changes in iron bioavailability.

REGULATION IN RESPONSE TO IRON DEFICIENCY

Transcriptional Activation of the Iron Regulon by Aft1 and Aft2

In response to iron limitation, the yeast Aft1 and Aft2 (Aft1/Aft2) transcription factors accumulate in the nucleus, bind to iron-regulatory promoter elements (FeREs) with the consensus sequence PyPuCACCCPu (where Py is a pyrimidine and Pu is a purine), and activate the transcription of a group of genes collectively known as the iron regulon [reviewed by Philpott and Protchenko (2008); Kaplan and Kaplan (2009); Martins et al. (2018a)]. The following proteins belong to the yeast iron regulon: (1) the reductive iron uptake system, which is formed by four heme-containing cell surface metalloreductases (Fre1–Fre4), the copper-dependent high-affinity iron importer complex Fet3/Ftr1 and its copper-delivery proteins Atx1 and Ccc2, and the oxygen-independent low-affinity plasma membrane iron and copper transporter Fet4; (2) the non-reductive iron import machinery, which includes three cell wall mannoproteins (Fit1–Fit3) and four iron-xenosiderophore-specific transporters (Arn1–Arn4); (3) the vacuolar mobilization machinery constituted by the Fre6 metalloreductase, and the Fet5/Fth1 (paralogs of Fet3/Ftr1) and Smf3 iron exporters; (4) iron recycling proteins such as the Hmx1 heme oxygenase; (5) mitochondrial iron importers including Mrs4; (6) iron-independent alternatives to iron-using processes such as the biotin and 7-keto-8-aminopelargonic acid (KAPA) importers Vht1 and Bio5, respectively; and (7) the mRNA-binding proteins Cth1 and Cth2 implicated in iron metabolism remodeling (**Figure 1**). Recent studies have identified novel genes activated by Aft1 in response to iron depletion: (1) the trans-Golgi network K^+/H^+-exchanger gene *KHA1*, which product facilitates copper loading into apo-Fet3 multicopper-ferroxidase (Wu et al., 2016); (2) *MMT1* and *MMT2* mitochondrial iron exporter genes (Li et al., 2020); (3) *RNR1*, encoding for the catalytic subunit of the iron-dependent ribonucleotide reductase (RNR) enzyme; and (4) *RNR1* transcriptional activator *IXR1* (Ros-Carrero et al., 2020).

Genetic and biochemical studies have demonstrated that ISC assembly and export machineries are directly involved in the post-transcriptional regulation of iron metabolism in higher eukaryotes (through the iron regulatory proteins, IRPs) and transcriptional regulation and sensing of iron homeostasis in yeast cells via specific transcription factors including Aft1, Aft2, and Yap5 (see below) [reviewed in Muhlenhoff et al. (2015); Martinez-Pastor et al. (2017); Gupta and Outten (2020)]. Upon iron-sufficient or high-iron conditions, the activity of the Aft1/Aft2 transcription factors is limited to avoid the harmful consequences of excess iron acquisition. Curiously, yeast Aft1/Aft2 do not respond to cytoplasmic iron levels; instead they sense a mitochondrial signal from ISC biosynthesis that inhibits their function in iron-replete conditions (Chen et al., 2004; Rutherford et al., 2005; Hausmann et al., 2008). Thus, yeast cells with an impaired ISC system induce the extracellular iron uptake systems and accumulate iron in mitochondria (Kispal et al., 1999; Chen et al., 2004; Rutherford et al., 2005; Hausmann et al., 2008). Under iron-sufficient conditions, an uncharacterized sulfur-containing compound, denoted X-S, is exported to the cytoplasm by the yeast Atm1 (human ABCB7) mitochondrial transporter. After multiple steps, the X-S molecule is converted into a $[2Fe–2S]^{2+}$ cluster that is coordinated via cysteine residues to a homodimer of monothiol glutaredoxins (Grx3 or Grx4) and two glutathione molecules. Finally, the Bol2/Fra2 protein transfers the ISC to the Aft1/Aft2 transcription factors, which homodimerize, decreasing their affinity for DNA and being exported to the cytosol (Li and Outten, 2012, 2019; Poor et al., 2014). A recent study has shown that the mitogen-activated protein kinase (MAPK) Hog1 limits Aft1 function by directly phosphorylating specific serine residues and promoting its nuclear export (Martins et al., 2018b). Further data have demonstrated that when subcellular localization is impaired, Aft1/Aft2 transcriptional activity is still regulated via iron-dependent DNA-binding (Ueta et al., 2012; Poor et al., 2014). Nowadays, iron-sensing is an area of intense research in both yeast and mammals.

Post-transcriptional Remodeling of Iron Metabolism by the mRNA-Binding Protein Cth2

In response to iron limitation, yeast cells activate the expression of two tristetraprolin family members (Wells et al., 2017), called Cth1 and Cth2, characterized by the presence of a conserved

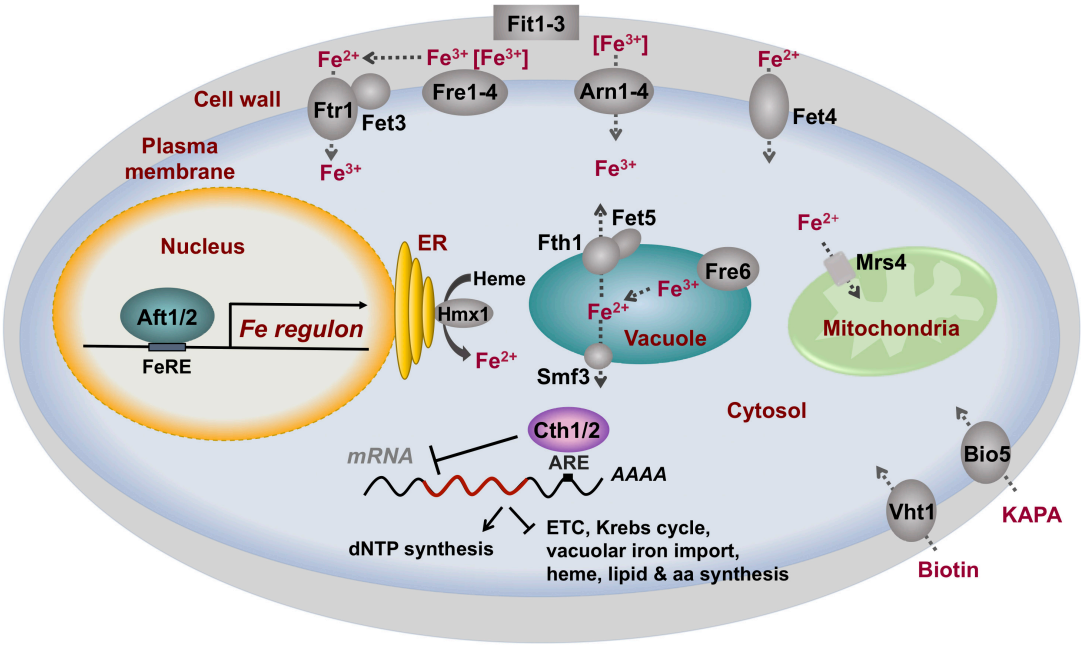

FIGURE 1 | The transcriptional factors Aft1 and Aft2 activate the iron regulon in response to iron deficiency in *S. cerevisiae*. Iron regulon members include genes that encode for proteins that enhance the acquisition of extracellular iron, the mobilization and recycling of intracellular iron, iron-independent alternatives to iron-using processes, and a metabolic remodeling response of iron-dependent processes mediated by the mRNA-binding proteins Cth1 and Cth2, among other processes. KAPA: 7-keto-8-aminopelargonic acid.

$Cx_8Cx_5Cx_3Hx_{18}Cx_8Cx_5Cx_3H$ tandem zinc finger (TZF) motif that directly interacts with adenosine and uridine-rich elements (AREs) in the 3′ untranslated region (3′UTR) of target mRNAs to post-transcriptionally limit their expression [(Puig et al., 2005, 2008; Pedro-Segura et al., 2008; Prouteau et al., 2008); reviewed in Martinez-Pastor et al. (2013a)]. *CTH1* expression remains low, whereas *CTH2* is highly induced upon iron deficiency (Puig et al., 2005, 2008). The higher relevance of Cth2 in the adaptation of yeast cells to iron depletion is highlighted by the growth defect that *cth2*Δ mutant cells display under these conditions, which is exacerbated in *cth1*Δ*cth2*Δ double mutants (Puig et al., 2005). Cth2 is a highly unstable nucleocytoplasmic shuttling protein (Vergara et al., 2011; Romero et al., 2018b). A nuclear localization signal (NLS) embedded in its TZF motif enables its import to the nucleus, where it co-transcriptionally associates to ARE-containing mRNAs (Prouteau et al., 2008; Vergara et al., 2011). Then, Cth2 either promotes the nuclear degradation of its bound transcripts or their export to the cytosol where it facilitates their 5′ to 3′ ARE-mediated decay (AMD) and translational inhibition (Pedro-Segura et al., 2008; Prouteau et al., 2008; Vergara et al., 2011; Ramos-Alonso et al., 2018a). Cth2 amino-terminal region is important for both AMD and translation repression, whereas its carboxy-terminal domain is only required to inhibit protein synthesis (Ramos-Alonso et al., 2018a, 2019). Cth2 does not contain any nuclear export signal; instead it relies on the mRNA export machinery to exit the nucleus (Vergara et al., 2011). Importantly, Cth2 nucleocytoplasmic shuttling is absolutely necessary for its mRNA regulatory function (Vergara et al., 2011). Very recent protein interaction data have demonstrated that Cth2 enters the nucleus in association to the Dhh1 RNA helicase and the Pop2/Caf1 deadenylase proteins, whereas the 5′ to 3′ Xrn1 exonuclease is only recruited after Cth2-binding to its target mRNAs (Perea-Garcia et al., 2020). Thus, when mRNA decay is impaired, Cth2 protein is trapped in microscopically visible foci where mRNA turnover takes place (cytosolic processing bodies), probably because the Cth2 TZF-embedded NLS is not available (Pedro-Segura et al., 2008). Yeast Cth2 is an excellent model to study how eukaryotic mRNA-binding proteins post-transcriptionally control mRNA expression.

In response to iron-deficient conditions, Cth2 post-transcriptionally inhibits the expression of ARE-containing mRNAs that encode proteins that directly bind iron or that are involved in iron-consuming pathways [reviewed in Sanvisens and Puig (2011); Philpott et al. (2012); Outten and Albetel (2013)]. The most numerous set of Cth2 mRNA targets encode for components of the mitochondrial electron transport chain, a highly iron-consuming process that is not essential for yeast cells, since they mostly ferment even in aerobic conditions. Consistent with this, Cth2 expression limits oxygen consumption (Ramos-Alonso et al., 2018b; Sato et al., 2018). Genome-wide studies have shown that, in addition to regulating respiration, Cth2 targeted mRNAs are implicated in other iron-dependent pathways including components of the tricarboxylic acid (TCA) cycle (such as aconitase and succinate dehydrogenase), the biosynthesis of unsaturated fatty acids, ergosterol and sphingolipids, and the synthesis of numerous amino acids (e.g., leucine, lysine, methionine, or glutamate) and cofactors such as biotin and lipoic acid (Puig et al., 2005, 2008). Cth2 also

limits the accumulation of iron into the vacuole when iron levels are low by promoting the degradation of the *CCC1* transcript encoding for the vacuolar iron importer (Puig et al., 2005). The overexpression of a functional *CTH1* or *CTH2* gene is highly cytotoxic (Thompson et al., 1996; Pedro-Segura et al., 2008; Romero et al., 2018b), so yeast cells have to tightly control their expression. Interestingly, both mRNAs contain AREs that allow a negative cross- and auto-regulation that limits their expression and that is important for the activation of respiration and for optimal adaptation to the transit from iron-deficient to iron-sufficient conditions (Martinez-Pastor et al., 2013b). Remarkably, Cth2 does not only down-regulate iron-consuming processes, but it also preferentially promotes iron-dependent activities that are essential or highly important for cells. An illustrating example is RNR, an oxo-diiron-containing enzyme that catalyzes the *de novo* synthesis of deoxyribonucleotides (dNTPs). Under normal conditions, the activity of RNR is limited by the different subcellular localization of its cytosolic large catalytic subunit R1 and its nuclear iron-containing small subunit R2. In response to iron deprivation, Cth2 promotes the degradation of the ARE-containing *WTM1* mRNA, which encodes for a nuclear R2 anchoring protein (Sanvisens et al., 2011). In this way, Cth2 facilitates the export of the small R2 subunit to the cytosol and the assembly of a functional RNR holoenzyme (Sanvisens et al., 2011). Therefore, Cth2 is a central coordinator of iron metabolism that prioritizes iron utilization in essential processes over dispensable iron-using ones.

Regulation of Metabolic and Cellular Processes in Response to Iron Depletion

In response to iron deficiency, the decrease in activity of some iron-dependent enzymes limits the levels of key metabolic intermediates that are used as coactivators of specific transcription factors (Ihrig et al., 2010). For instance, in response to low iron, there is a decrease in the expression of genes from the iron-dependent branched-chain amino acid biosynthesis pathway due to a drop in the levels of the metabolic intermediate α-isopropylmalate, which serves as a coactivator of the Leu3 transcription factor (Ihrig et al., 2010; **Figure 2**). Similarly, the decrease in heme levels that occurs under iron starvation conditions limits the activity of the Hap1 transcription factor, a regulatory process that contributes to the down-regulation of mitochondrial respiration (Ihrig et al., 2010; **Figure 2**). Furthermore, multiple molecular markers indicate that the nutrient-signaling pathway that depends on the target of rapamycin complex 1 (TORC1) is also inhibited during the advance of iron deficiency, although the triggering signal is currently unknown and would require further studies (Romero et al., 2019; **Figure 2**). As a consequence, there is a decrease in the transcriptional activity of all RNA polymerases that causes the down-regulation of genes encoding for ribosomal proteins (RPs) and ribosome biogenesis (RiBi) factors, as well as a significant drop of rRNAs and tRNAs levels that finally impair global translation (Romero et al., 2019, 2020; Ros-Carrero et al., 2020; **Figure 2**). Interestingly, iron deficiency also promotes the Gcn2-dependent phosphorylation of the translation initiation factor eIF2α, probably due to the presence of uncharged tRNAs, contributing to the repression of bulk translation (Romero et al., 2020; **Figure 2**). Consistent with a defect at the initiation step, the translation of the *GCN4* mRNA, which depends on short upstream open reading frames (uORFs), is enhanced (Romero et al., 2020). It is important to stress that translation is a highly energy consuming process that requires the conserved ISC-containing Rli1 (human ABCE1) protein for ribosome biogenesis and recycling (Kispal et al., 2005; Yarunin et al., 2005; Young et al., 2015).

Iron deficiency also triggers the activation of various signaling pathways beyond the Aft1/Aft2 iron regulon (Martins et al., 2018a). Upon iron scarcity, there is an increase in the transcription of genes belonging to the mitochondrial retrograde (RTG) response (*CIT1*, coding for the mitochondrial isoform of citrate synthase; *ACO1*, aconitase, and *IDH1* and *IDH2*, encoding NAD^+-dependent isocitrate dehydrogenases) via the Rtg1-Rtg3 transcription factor complex (**Figure 2**), probably due to TORC1 inhibition or to mitochondrial dysfunction (Romero et al., 2019). The activation of the RTG response during iron deficiency may provide sufficient α-ketoglutarate as a nitrogen donor for biosynthetic processes. Moreover, a decrease in the activity of the iron-dependent Δ9 fatty acid desaturase Ole1 in iron-deficient conditions causes a drop in the levels of unsaturated fatty acids (UFAs) that releases the endoplasmic reticulum (ER)-anchored Mga2 transcription factor and activates the transcription of *OLE1* (Romero et al., 2018a; **Figure 2**). UFA regulation of Mga2 is essential for growth in iron-depleted conditions (Romero et al., 2018a; Jorda et al., 2020). In fact, the levels of UFAs have been reported to be crucial for the Aft1-dependent activation of the iron regulon, although no mechanistic clues have been provided yet (Jorda et al., 2020). Moreover, both iron deficiency and defects in the mitochondrial ISC biogenesis activate the Mec1-Rad53-Dun1 DNA damage checkpoint kinase cascade that, in combination with Cth2 and Aft1 regulatory factors (see above), promote the activity of the iron-dependent RNR enzyme at multiple levels [(Sanvisens et al., 2011, 2014, 2016; Pijuan et al., 2015; Ros-Carrero et al., 2020); reviewed in Sanvisens et al. (2013); Puig et al. (2017)]. Upon iron limitation, Dun1 kinase enhances dNTP synthesis by promoting the degradation of the R1 inhibitor protein Sml1, and the R2 import protein Dif1 (Sanvisens et al., 2014, 2016). Future studies would determine whether the DNA damage checkpoint kinase cascade is activated when iron is scarce as a consequence of defects in the activity of the iron-dependent DNA polymerases and DNA repair enzymes (Puig et al., 2017).

Iron starvation also initiates the environmental stress response (ESR) program (Romero et al., 2019), that includes the transcriptional activation, via the general stress transcription factors Msn2 and Msn4, of ∼300 mRNAs mostly implicated in protecting cells against adverse stress conditions, and the repression of ∼600 transcripts encoding RPs, RiBis and other factors implicated in translation (Gasch et al., 2000). The substitution of iron-using processes by iron-independent alternatives is also a broad yeast response. In addition to the replacement of the iron-dependent biosynthesis of biotin by its uptake, yeast cells also decrease the expression of the

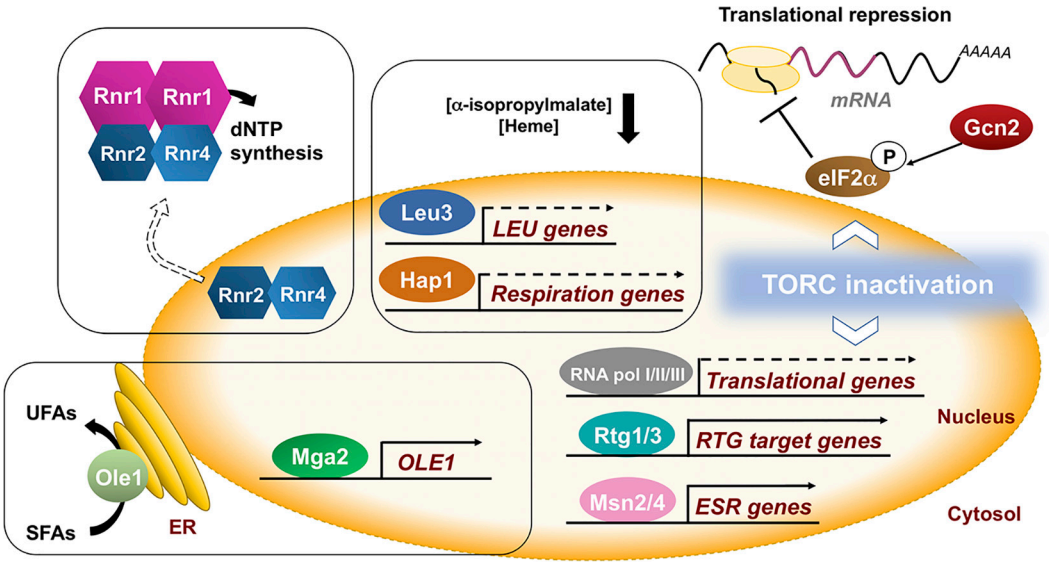

FIGURE 2 | Yeast adaptation to iron deficiency requires the remodeling of many cellular processes. In *S. cerevisiae*, multiple iron-related processes indirectly respond to iron deficiency. The lack of iron leads to a decrease in the availability of iron-dependent metabolites including amino acid intermediates, heme, unsaturated fatty acids (UFAs) and deoxyribonucleotides (dNTPs), leading to changes in the expression of genes implicated in their biosynthesis. Moreover, global nutrient signaling pathways (TORC1) and environmental stress responses (ESR) respond to iron limitation by causing a bulk decrease in transcription and translation, and the activation of specific metabolic pathways such as the mitochondrial retrograde (RTG) response. These observations highlight the huge amount of direct and indirect connections between iron and cellular metabolism. Further detailed studies are necessary to fully decipher how eukaryotic cells sense iron starvation and transduce this signal to a wide range of cellular processes.

ISC-dependent glutamate synthase enzyme Glt1 in favor of a glutamate dehydrogenase iron-independent route for nitrogen assimilation (Belli et al., 2004; Shakoury-Elizeh et al., 2004).

REGULATION IN RESPONSE TO IRON EXCESS

The yeast iron detoxification response is mostly triggered by the transcriptional activator protein of the Yap family, Yap5 [reviewed in Li and Ward (2018); Rodrigues-Pousada et al. (2019)]. Yap5 associates to Yap response elements (YREs) within the promoter of its target genes independently of iron levels, but only activates transcription when it associates to two [2Fe–2S] clusters through conserved cysteine-rich domains in a mitochondrial ISC-dependent but Grx3/4-independent manner (Li et al., 2008, 2012; Rietzschel et al., 2015). Thus, in response to high-iron, Yap5 activates the transcription of: (1) the *CCC1* vacuolar importer gene, which is the main iron storage yeast facilitator; (2) the *GRX4* monothiol glutaredoxin, which binds and transfers the iron-derived mitochondrial signal to Aft1 and Aft2 transcription factors limiting their activity; (3) *TYW1*, which encodes for a cytosolic [4Fe–4S] cluster-containing enzyme probably implicated in iron buffering; and (4) the copper metallothionein gene *CUP1* to protect cells from oxidative stress (Li et al., 2011; Pimentel et al., 2012).

Curiously, cells lacking *YAP5* are less sensitive to iron than *ccc1*Δ cells, suggesting that other transcriptional factors contribute to the expression of *CCC1* (Pimentel et al., 2012). In this sense, a recent study has discovered that yeast cells lacking the low-glucose sensor Snf1 or other components of this kinase complex display defects in *CCC1* expression under high-iron conditions that lead to iron sensitivity (Li et al., 2017). Remarkably, the Snf1 activation of *CCC1* does not depend on Yap5 or ISC biogenesis, but utilizes Msn2 and Msn4 transcription factors and other unidentified regulatory factors (Li et al., 2017). Consistent with this, the *msn2*Δ*msn4*Δ double mutant is sensitive to iron and the Msn4 protein translocates to the nucleus in response to excess iron (Du et al., 2012; Li et al., 2017). Further studies are necessary to decipher how iron modulates the activity of the Snf1 kinase complex since no changes in Snf1 phosphorylation have been reported upon exposure to high iron.

IRON HOMEOSTASIS DIVERSITY IN *S. cerevisiae* YEAST STRAINS

The utilization over the past decades of laboratory *S. cerevisiae* strains has allowed the characterization of the main features that govern eukaryotic iron homeostasis, including iron sensing, regulation, acquisition, distribution, storage, and utilization. However, the recent sequencing of the genome of numerous natural and human-domesticated yeast strains is opening novel horizons for studying iron homeostasis diversity and evolution that should be pursued in the future (Peter et al., 2018). In addition to the reductive strategy for iron uptake, some budding yeasts are also able to synthesize and acquire iron via siderophores. A recent

phylogenomic study has suggested that the genes implicated in the biosynthesis and utilization of the iron-binding molecule pulcherrimin were ancestral to *S. cerevisiae*, although lost in the majority but not all lineages (Krause et al., 2018). Another report has uncovered the acquisition by a group of budding yeasts of a whole bacterial operon implicated in siderophore iron transport through horizontal transfer (Kominek et al., 2019). A genetic study has unveiled the diversity of wild Malaysian *S. cerevisiae* strains, which have adapted their iron homeostasis network to their natural environment (Lee et al., 2013). These strains are particularly sensitive to iron due to defects in *YAP5* gene and especially in their *CCC1* vacuolar iron transporter allele, but display an *AFT1* allele that improves their adaptation to iron-deficient conditions (Lee et al., 2013). Whole-genome analyses of *S. cerevisiae* strains used for the production of sherry-like wine have also revealed an improved iron uptake system and an increased sensitivity to iron probably due to the presence of *AFT1*, *FRE* and *FIT* alleles also found in flor yeasts (Eldarov et al., 2018). In a broad phenotypic characterization of *S. cerevisiae* strains from different geographical and source origins, yeast strains were classified as iron-resistant and iron-sensitive (Martinez-Garay et al., 2016). Curiously, the most iron-resistant strains accumulate less iron than the sensitive ones, and grow poorly in iron-deficient conditions, whereas the iron-sensitive strains have better adapted to low iron environments (Martinez-Garay et al., 2016). A more detailed study of both the genotype and phenotype of these and other yeast strains will definitely contribute to a better understanding of iron homeostasis and evolution.

AUTHOR CONTRIBUTIONS

LR-A and SP wrote the original draft. MM-P and AR reviewed and edited the manuscript. All authors contributed to the article and approved the submitted version.

FUNDING

Work in our laboratory is supported by the Spanish Ministry of Science, Innovation and Universities (MICINN) grant BIO2017-87828-C2-1-P and FEDER (Fondo Europeo de Desarrollo Regional) funds. LR-A was recipient of predoctoral contract from MICINN. We acknowledge support of the publication fee by the CSIC Open Access Publication Support Initiative through its Unit of Information Resources for Research (URICI).

ACKNOWLEDGMENTS

We thank all the members of the Systems Biology in Yeast of Biotechnological Interest (SBYBI) group for their scientific contributions.

REFERENCES

Belli, G., Molina, M. M., Garcia-Martinez, J., Perez-Ortin, J. E., and Herrero, E. (2004). *Saccharomyces cerevisiae* glutaredoxin 5-deficient cells subjected to continuous oxidizing conditions are affected in the expression of specific sets of genes. *J. Biol. Chem.* 279, 12386–12395. doi: 10.1074/jbc.m311879200

Chaparro, C. M., and Suchdev, P. S. (2019). Anemia epidemiology, pathophysiology, and etiology in low- and middle-income countries. *Ann. N.Y. Acad. Sci.* 1450, 15–31.

Chen, O. S., Crisp, R. J., Valachovic, M., Bard, M., Winge, D. R., and Kaplan, J. (2004). Transcription of the yeast iron regulon does not respond directly to iron but rather to iron-sulfur cluster biosynthesis. *J. Biol. Chem.* 279, 29513–29518. doi: 10.1074/jbc.m403209200

Dikicioglu, D., and Oliver, S. G. (2019). Extension of the yeast metabolic model to include iron metabolism and its use to estimate global levels of iron-recruiting enzyme abundance from cofactor requirements. *Biotechnol. Bioeng.* 116, 610–621. doi: 10.1002/bit.26905

Du, Y., Cheng, W., and Li, W. F. (2012). Expression profiling reveals an unexpected growth-stimulating effect of surplus iron on the yeast *Saccharomyces cerevisiae*. *Mol. Cells* 34, 127–132. doi: 10.1007/s10059-012-2242-0

Eldarov, M. A., Beletsky, A. V., Tanashchuk, T. N., Kishkovskaya, S. A., Ravin, N. V., and Mardanov, A. V. (2018). Whole-genome analysis of three yeast strains used for production of sherry-like wines revealed genetic traits specific to flor yeasts. *Front. Microbiol.* 9:965. doi: 10.3389/fmicb.2018.00965

Gasch, A. P., Spellman, P. T., Kao, C. M., Carmel-Harel, O., Eisen, M. B., Storz, G., et al. (2000). Genomic expression programs in the response of yeast cells to environmental changes. *Mol. Biol. Cell* 11, 4241–4257. doi: 10.1091/mbc.11.12.4241

Gupta, M., and Outten, C. E. (2020). Iron-sulfur cluster signaling: the common thread in fungal iron regulation. *Curr. Opin. Chem. Biol.* 55, 189–201. doi: 10.1016/j.cbpa.2020.02.008

Hausmann, B., Lill, S. R., and Muhlenhoff, U. (2008). Cellular and mitochondrial remodeling upon defects in iron-sulfur protein biogenesis. *J. Biol. Chem.* 283, 8318–8330. doi: 10.1074/jbc.m705570200

Ihrig, J., Hausmann, A., Hain, A., Richter, N., Hamza, I., Lill, R., et al. (2010). Iron regulation through the back door: iron-dependent metabolite levels contribute to transcriptional adaptation to iron deprivation in *Saccharomyces cerevisiae*. *Eukaryot. Cell* 9, 460–471. doi: 10.1128/ec.00213-09

Jorda, T., Romero, A. M., Perea-Garcia, A., Rozes, N., and Puig, S. (2020). The lipid composition of yeast cells modulates the response to iron deficiency. *Biochim. Biophys. Acta Mol. Cell Biol. Lipids* 1865:158707. doi: 10.1016/j.bbalip.2020.158707

Kaplan, C. D., and Kaplan, J. (2009). Iron acquisition and transcriptional regulation. *Chem. Rev.* 109, 4536–4552. doi: 10.1021/cr9001676

Kispal, G., Csere, P., Prohl, C., and Lill, R. (1999). The mitochondrial proteins Atm1p and Nfs1p are essential for biogenesis of cytosolic Fe/S proteins. *EMBO J.* 18, 3981–3989. doi: 10.1093/emboj/18.14.3981

Kispal, G., Sipos, K., Lange, H., Fekete, Z., Bedekovics, T., Janaky, T., et al. (2005). Biogenesis of cytosolic ribosomes requires the essential iron-sulphur protein Rli1p and mitochondria. *EMBO J.* 24, 589–598. doi: 10.1038/sj.emboj.7600541

Kominek, J., Doering, D. T., Opulente, D. A., Shen, X. X., Zhou, X., DeVirgilio, J., et al. (2019). eukaryotic acquisition of a bacterial operon. *Cell* 176, 1356–1366. doi: 10.1016/j.cell.2019.01.034

Krause, D. J., Kominek, J., Opulente, D. A., Shen, X. X., Zhou, X., Langdon, Q. K., et al. (2018). Functional and evolutionary characterization of a secondary metabolite gene cluster in budding yeasts. *Proc. Natl. Acad. Sci. U.S.A.* 115, 11030–11035. doi: 10.1073/pnas.1806268115

Lee, H. N., Mostovoy, Y., Hsu, T. Y., Chang, A. H., and Brem, R. B. (2013). Divergence of iron metabolism in wild Malaysian yeast. *G3* 3, 2187–2194. doi: 10.1534/g3.113.008011

Li, H., and Outten, C. E. (2012). Monothiol CGFS glutaredoxins and BolA-like proteins: [2Fe-2S] binding partners in iron homeostasis. *Biochemistry* 51, 4377–4389. doi: 10.1021/bi300393z

Li, H., and Outten, C. E. (2019). The conserved CDC motif in the yeast iron regulator Aft2 mediates iron-sulfur cluster exchange and protein-protein interactions with Grx3 and Bol2. *J. Biol. Inorg. Chem.* 24, 809–815. doi: 10.1007/s00775-019-01705-x

Li, L., Bagley, D., Ward, D. M., and Kaplan, J. (2008). Yap5 is an iron-responsive transcriptional activator that regulates vacuolar iron storage in yeast. *Mol. Cell Biol.* 28, 1326–1337. doi: 10.1128/mcb.01219-07

Li, L., Bertram, S., Kaplan, J., Jia, X., and Ward, D. M. (2020). The mitochondrial iron exporter genes MMT1 and MMT2 in yeast are transcriptionally regulated by Aft1 and Yap1. *J. Biol. Chem.* 295, 1716–1726. doi: 10.1074/jbc.ra119.011154

Li, L., Jia, X., Ward, D. M., and Kaplan, J. (2011). Yap5 protein-regulated transcription of the TYW1 gene protects yeast from high iron toxicity. *J. Biol. Chem.* 286, 38488–38497. doi: 10.1074/jbc.m111.286666

Li, L., Kaplan, J., and Ward, D. M. (2017). The glucose sensor Snf1 and the transcription factors Msn2 and Msn4 regulate transcription of the vacuolar iron importer gene CCC1 and iron resistance in yeast. *J. Biol. Chem.* 292, 15577–15586. doi: 10.1074/jbc.m117.802504

Li, L., Miao, R., Bertram, S., Jia, X., Ward, D. M., and Kaplan, J. (2012). A role for iron-sulfur clusters in the regulation of transcription factor Yap5-dependent high iron transcriptional responses in yeast. *J. Biol. Chem.* 287, 35709–35721. doi: 10.1074/jbc.m112.395533

Li, L., and Ward, D. M. (2018). Iron toxicity in yeast: transcriptional regulation of the vacuolar iron importer Ccc1. *Curr. Genet.* 64, 413–416. doi: 10.1007/s00294-017-0767-7

Lindahl, P. A. (2019). A comprehensive mechanistic model of iron metabolism in *Saccharomyces cerevisiae*. *Metallomics* 11, 1779–1799. doi: 10.1039/c9mt00199a

Martinez-Garay, C. A., de Llanos, R., Romero, A. M., Martinez-Pastor, M. T., and Puig, S. (2016). Responses of *Saccharomyces cerevisiae* strains from different origins to elevated iron concentrations. *Appl. Environ. Microbiol.* 82, 1906–1916. doi: 10.1128/aem.03464-15

Martinez-Pastor, M. T., de Llanos, R., Romero, A. M., and Puig, S. (2013a). Post-transcriptional regulation of iron homeostasis in *Saccharomyces cerevisiae*. *Int. J. Mol. Sci.* 14, 15785–15809. doi: 10.3390/ijms140815785

Martinez-Pastor, M., Vergara, S. V., Puig, S., and Thiele, D. J. (2013b). Negative feedback regulation of the yeast Cth1 and Cth2 mRNA binding proteins is required for adaptation to iron deficiency and iron supplementation. *Mol. Cell Biol.* 33, 2178–2187. doi: 10.1128/mcb.01458-12

Martinez-Pastor, M. T., Perea-Garcia, A., and Puig, S. (2017). Mechanisms of iron sensing and regulation in the yeast *Saccharomyces cerevisiae*. *World J. Microbiol. Biotechnol.* 33:75.

Martins, T. S., Costa, V., and Pereira, C. (2018a). Signaling pathways governing iron homeostasis in budding yeast. *Mol. Microbiol.* 109, 422–432. doi: 10.1111/mmi.14009

Martins, T. S., Pereira, C., Canadell, D., Vilaca, R., Teixeira, V., Moradas-Ferreira, P., et al. (2018b). The Hog1p kinase regulates Aft1p transcription factor to control iron accumulation. *Biochim. Biophys. Acta Mol. Cell Biol. Lipids* 1863, 61–70. doi: 10.1016/j.bbalip.2017.10.001

Means, R. T. (2020). Iron deficiency and iron deficiency anemia: implications and impact in pregnancy, fetal development, and early childhood parameters. *Nutrients* 12:447. doi: 10.3390/nu12020447

Muckenthaler, M. U., Rivella, S., Hentze, M. W., Galy, B., and Red Carpet, A. (2017). A red carpet for iron metabolism. *Cell* 168, 344–361. doi: 10.1016/j.cell.2016.12.034

Muhlenhoff, U., Hoffmann, B., Richter, N., Rietzschel, N., Spantgar, F., Stehling, O., et al. (2015). Compartmentalization of iron between mitochondria and the cytosol and its regulation. *Eur. J. Cell Biol.* 94, 292–308. doi: 10.1016/j.ejcb.2015.05.003

Outten, C. E., and Albetel, A. N. (2013). Iron sensing and regulation in *Saccharomyces cerevisiae*: ironing out the mechanistic details. *Curr. Opin. Microbiol.* 16, 662–668. doi: 10.1016/j.mib.2013.07.020

Pedro-Segura, E., Vergara, S. V., Rodriguez-Navarro, S., Parker, R., Thiele, D. J., and Puig, S. (2008). The Cth2 ARE-binding protein recruits the Dhh1 helicase to promote the decay of succinate dehydrogenase SDH4 mRNA in response to iron deficiency. *J. Biol. Chem.* 283, 28527–28535. doi: 10.1074/jbc.m804910200

Perea-Garcia, P., Jimenez-Lorenzo, M. R., Martinez-Pastor, M. T., and Puig, S. (2020). Sequential recruitment of the mRNA decay machinery to the iron-regulated protein Cth2 in *Saccharomyces cerevisiae*. *Biochim. Biophys. Acta Gene Regul. Mech.* 1863:194595. doi: 10.1016/j.bbagrm.2020.194595

Peter, J., De Chiara, M., Friedrich, A., Yue, J. X., Pflieger, D., Bergstrom, A., et al. (2018). Genome evolution across 1,011 *Saccharomyces cerevisiae* isolates. *Nature* 556, 339–344. doi: 10.1038/s41586-018-0030-5

Philpott, C. C., Leidgens, S., and Frey, A. G. (2012). Metabolic remodeling in iron-deficient fungi. *Biochim. Biophys. Acta* 1823, 1509–1520. doi: 10.1016/j.bbamcr.2012.01.012

Philpott, C. C., and Protchenko, O. (2008). Response to iron deprivation in *Saccharomyces cerevisiae*. *Eukaryot Cell* 7, 20–27. doi: 10.1128/ec.00354-07

Pijuan, J., Maria, C., Herrero, E., and Belli, G. (2015). Impaired mitochondrial Fe-S cluster biogenesis activates the DNA damage response through different signaling mediators. *J. Cell Sci.* 128, 4653–4665. doi: 10.1242/jcs.178046

Pimentel, C., Vicente, C., Menezes, R. A., Caetano, S., Carreto, L., and Rodrigues-Pousada, C. (2012). The role of the Yap5 transcription factor in remodeling gene expression in response to Fe bioavailability. *PLoS One* 7:e37434. doi: 10.1371/journal.pgen.037434

Poor, C. B., Wegner, S. V., Li, H., Dlouhy, A. C., Schuermann, J. P., Sanishvili, R., et al. (2014). Molecular mechanism and structure of the *Saccharomyces cerevisiae* iron regulator Aft2. *Proc. Natl. Acad. Sci. U.S.A.* 111, 4043–4048. doi: 10.1073/pnas.1318869111

Prouteau, M., Daugeron, M. C., and Seraphin, B. (2008). Regulation of ARE transcript 3′ end processing by the yeast Cth2 mRNA decay factor. *EMBO J.* 27, 2966–2976. doi: 10.1038/emboj.2008.212

Puig, S., Andres-Colas, N., Garcia-Molina, A., and Penarrubia, L. (2007). Copper and iron homeostasis in *Arabidopsis*: responses to metal deficiencies, interactions and biotechnological applications. *Plant Cell Environ.* 30, 271–290. doi: 10.1111/j.1365-3040.2007.01642.x

Puig, S., Askeland, E., and Thiele, D. J. (2005). Coordinated remodeling of cellular metabolism during iron deficiency through targeted mRNA degradation. *Cell* 120, 99–110. doi: 10.1016/j.cell.2004.11.032

Puig, S., Ramos-Alonso, L., Romero, A. M., and Martinez-Pastor, M. T. (2017). The elemental role of iron in DNA synthesis and repair. *Metallomics* 9, 1483–1500. doi: 10.1039/c7mt00116a

Puig, S., Vergara, S. V., and Thiele, D. J. (2008). Cooperation of two mRNA-binding proteins drives metabolic adaptation to iron deficiency. *Cell Metab.* 7, 555–564. doi: 10.1016/j.cmet.2008.04.010

Ramos-Alonso, L., Romero, A. M., Polaina, J., Puig, S., and Martinez-Pastor, M. T. (2019). Dissecting mRNA decay and translation inhibition during iron deficiency. *Curr. Genet.* 65, 139–145. doi: 10.1007/s00294-018-0880-2

Ramos-Alonso, L., Romero, A. M., Soler, M. A., Perea-Garcia, A., Alepuz, P., Puig, S., et al. (2018a). Yeast Cth2 protein represses the translation of ARE-containing mRNAs in response to iron deficiency. *PLoS Genet.* 14:e1007476. doi: 10.1371/journal.pgen.1007476

Ramos-Alonso, L., Wittmaack, N., Mulet, I., Martinez-Garay, C. A., Fita-Torro, J., Lozano, M. J., et al. (2018b). Molecular strategies to increase yeast iron accumulation and resistance. *Metallomics* 10, 1245–1256. doi: 10.1039/c8mt00124c

Rietzschel, N., Pierik, A. J., Bill, E., Lill, R., and Muhlenhoff, U. (2015). The basic leucine zipper stress response regulator Yap5 senses high-iron conditions by coordination of [2Fe-2S] clusters. *Mol. Cell Biol.* 35, 370–378. doi: 10.1128/mcb.01033-14

Rodrigues-Pousada, C., Devaux, F., Caetano, S. M., Pimentel, C., da Silva, S., Cordeiro, A. C., et al. (2019). Yeast AP-1 like transcription factors (Yap) and stress response: a current overview. *Microb. Cell* 6, 267–285. doi: 10.15698/mic2019.06.679

Romero, A. M., Jorda, T., Rozes, N., Martinez-Pastor, M. T., and Puig, S. (2018a). Regulation of yeast fatty acid desaturase in response to iron deficiency. *Biochim. Biophys. Acta Mol. Cell Biol. Lipids* 1863, 657–668. doi: 10.1016/j.bbalip.2018.03.008

Romero, A. M., Martinez-Pastor, M., Du, G., Sole, C., Carlos, M., Vergara, S. V., et al. (2018b). Phosphorylation and proteasome recognition of the mRNA-binding protein Cth2 facilitates yeast adaptation to iron deficiency. *mBio* 9:e01694-18.

Romero, A. M., Ramos-Alonso, L., Alepuz, P., Puig, S., and Martinez-Pastor, M. T. (2020). Global translational repression induced by iron deficiency in yeast depends on the Gcn2/eIF2alpha pathway. *Sci. Rep.* 10:233.

Romero, A. M., Ramos-Alonso, L., Montella-Manuel, S., Garcia-Martinez, J., de la Torre-Ruiz, M. A., Perez-Ortin, J. E., et al. (2019). A genome-wide transcriptional study reveals that iron deficiency inhibits the yeast TORC1 pathway. *Biochim. Biophys. Acta Gene Regul. Mech.* 1862:194414. doi: 10.1016/j.bbagrm.2019.194414

Ros-Carrero, C., Ramos-Alonso, L., Romero, A. M., Bano, M. C., Martinez-Pastor, M. T., and Puig, S. (2020). The yeast Aft1 transcription factor activates ribonucleotide reductase catalytic subunit RNR1 in response to iron deficiency. *Biochim. Biophys. Acta Gene Regul. Mech.* 1863:194522. doi: 10.1016/j.bbagrm.2020.194522

Rutherford, J. C., Ojeda, L., Balk, J., Muhlenhoff, U., Lill, R., and Winge, D. R. (2005). Activation of the iron regulon by the yeast Aft1/Aft2 transcription factors depends on mitochondrial but not cytosolic iron-sulfur protein biogenesis. *J. Biol. Chem.* 280, 10135–10140. doi: 10.1074/jbc.m413731200

Sanvisens, N., Bano, M. C., Huang, M., and Puig, S. (2011). Regulation of ribonucleotide reductase in response to iron deficiency. *Mol. Cell* 44, 759–769. doi: 10.1016/j.molcel.2011.09.021

Sanvisens, N., de Llanos, R., and Puig, S. (2013). Function and regulation of yeast ribonucleotide reductase: cell cycle, genotoxic stress and iron availability. *Biomed. J.* 36, 51–58. doi: 10.4103/2319-4170.110398

Sanvisens, N., and Puig, S. (2011). "Causes and consequences of nutritional iron deficiency in living organisms," in *Biology of Starvation in Humans and Other Organisms*, ed. T. C. Merkin (Hauppauge, NY: Nova Science Publishers), 245–276.

Sanvisens, N., Romero, A. M., An, X., Zhang, C., de Llanos, R., Martinez-Pastor, M. T., et al. (2014). Yeast Dun1 kinase regulates ribonucleotide reductase inhibitor Sml1 in response to iron deficiency. *Mol. Cell Biol.* 34, 3259–3271. doi: 10.1128/mcb.00472-14

Sanvisens, N., Romero, A. M., Zhang, C., Wu, X., An, X., Huang, M., et al. (2016). Yeast Dun1 kinase regulates ribonucleotide reductase small subunit localization in response to iron deficiency. *J. Biol. Chem.* 291, 9807–9817. doi: 10.1074/jbc.m116.720862

Sato, T., Chang, H. C., Bayeva, M., Shapiro, J. S., Ramos-Alonso, L., Kouzu, H., et al. (2018). mRNA-binding protein tristetraprolin is essential for cardiac response to iron deficiency by regulating mitochondrial function. *Proc. Natl. Acad. Sci. U.S.A.* 115, E6291–E6300.

Shakoury-Elizeh, M., Tiedeman, J., Rashford, J., Ferea, T., Demeter, J., Garcia, E., et al. (2004). Transcriptional remodeling in response to iron deprivation in *Saccharomyces cerevisiae*. *Mol. Biol. Cell* 15, 1233–1243. doi: 10.1091/mbc.e03-09-0642

Stehling, O., Wilbrecht, C., and Lill, R. (2014). Mitochondrial iron-sulfur protein biogenesis and human disease. *Biochimie* 100, 61–77. doi: 10.1016/j.biochi.2014.01.010

Thompson, M. J., Lai, W. S., Taylor, G. A., and Blackshear, P. J. (1996). Cloning and characterization of two yeast genes encoding members of the CCCH class of zinc finger proteins: zinc finger-mediated impairment of cell growth. *Gene* 174, 225–233. doi: 10.1016/0378-1119(96)00084-4

Ueta, R., Fujiwara, N., Iwai, K., and Yamaguchi-Iwai, Y. (2012). Iron-induced dissociation of the Aft1p transcriptional regulator from target gene promoters is an initial event in iron-dependent gene suppression. *Mol. Cell Biol.* 32, 4998–5008. doi: 10.1128/mcb.00726-12

Vergara, S. V., Puig, S., and Thiele, D. J. (2011). Early recruitment of AU-rich element-containing mRNAs determines their cytosolic fate during iron deficiency. *Mol. Cell Biol.* 31, 417–429. doi: 10.1128/mcb.00754-10

Wells, M. L., Perera, L., and Blackshear, P. J. (2017). An ancient family of RNA-binding proteins: still important! *Trends Biochem. Sci.* 42, 285–296. doi: 10.1016/j.tibs.2016.12.003

Wu, X., Kim, H., Seravalli, J., Barycki, J. J., Hart, P. J., Gohara, D. W., et al. (2016). Potassium and the K+/H+ exchanger Kha1p promote binding of copper to ApoFet3p Multi-copper ferroxidase. *J. Biol. Chem.* 291, 9796–9806. doi: 10.1074/jbc.m115.700500

Yarunin, A., Panse, V. G., Petfalski, E., Dez, C., Tollervey, D., and Hurt, E. C. (2005). Functional link between ribosome formation and biogenesis of iron-sulfur proteins. *EMBO J.* 24, 580–588. doi: 10.1038/sj.emboj.7600540

Young, D. J., Guydosh, N. R., Zhang, F., Hinnebusch, A. G., and Green, R. (2015). Rli1/ABCE1 recycles terminating ribosomes and controls translation reinitiation in 3′UTRs in vivo. *Cell* 162, 872–884. doi: 10.1016/j.cell.2015.07.041

Zhang, X., Zhang, D., Sun, W., and Wang, T. (2019). The adaptive mechanism of plants to iron deficiency via iron uptake, transport, and homeostasis. *Int. J. Mol. Sci.* 20:2424. doi: 10.3390/ijms20102424

Conflict of Interest: The authors declare that the research was conducted in the absence of any commercial or financial relationships that could be construed as a potential conflict of interest.

frontiers in Microbiology

ORIGINAL RESEARCH
published: 20 November 2020
doi: 10.3389/fmicb.2020.571244

Impact of Fe(III) (Oxyhydr)oxides Mineralogy on Iron Solubilization and Associated Microbial Communities

Fengfeng Zhang[1,2], Fabienne Battaglia-Brunet[1,2], Jennifer Hellal[2], Catherine Joulian[2], Pascale Gautret[1] and Mikael Motelica-Heino[1]*

[1] Univ. Orléans, CNRS, BRGM, ISTO, UMR 7327, Orléans, France, [2] BRGM, Orléans, France

Iron-reducing bacteria (IRB) are strongly involved in Fe cycling in surface environments. Transformation of Fe and associated trace elements is strongly linked to the reactivity of various iron minerals. Mechanisms of Fe (oxyhydr)oxides bio-reduction have been mostly elucidated with pure bacterial strains belonging to *Geobacter* or *Shewanella* genera, whereas studies involving mixed IRB populations remain scarce. The present study aimed to evaluate the iron reducing rates of IRB enriched consortia originating from complex environmental samples, when grown in presence of Fe (oxyhydr)oxides of different mineralogy. The abundances of *Geobacter* and *Shewanella* were assessed in order to acquire knowledge about the abundance of these two genera in relation to the effects of mixed IRB populations on kinetic control of mineralogical Fe (oxyhydr)oxides reductive dissolution. Laboratory experiments were carried out with two freshly synthetized Fe (oxyhydr)oxides presenting contrasting specific surfaces, and two defined Fe-oxides, i.e., goethite and hematite. Three IRB consortia were enriched from environmental samples from a riverbank subjected to cyclic redox oscillations related to flooding periods (Decize, France): an unsaturated surface soil, a flooded surface soil and an aquatic sediment, with a mixture of organic compounds provided as electron donors. The consortia could all reduce iron-nitrilotriacetate acid (Fe(III)-NTA) in 1–2 days. When grown on Fe (oxyhydr)oxides, Fe solubilization rates decreased as follows: fresh Fe (oxyhydr)oxides > goethite > hematite. Based on a bacterial *rrs* gene fingerprinting approach (CE-SSCP), bacterial community structure in presence of Fe(III)-minerals was similar to those of the site sample communities from which they originated but differed from that of the Fe(III)-NTA enrichments. *Shewanella* was more abundant than *Geobacter* in all cultures. Its abundance was higher in presence of the most efficiently reduced Fe (oxyhydr)oxide than with other Fe(III)-minerals. *Geobacter* as a proportion of the total community was highest in the presence of the least easily solubilized Fe (oxyhydr)oxides. This study highlights the influence of Fe mineralogy on the abundance of *Geobacter* and *Shewanella* in relation to Fe bio-reduction kinetics in presence of a complex mixture of electron donors.

Keywords: iron-reducing bacteria, *Shewanella*, *Geobacter*, iron (oxyhydr)oxides, solubilization

OPEN ACCESS

Edited by:
Lei Yan,
Heilongjiang Bayi Agricultural University, China

Reviewed by:
Tongxu Liu,
Guangdong Institute of Eco-environmental and Soil Sciences (CAS), China
Emma Jayne Gagen,
The University of Queensland, Australia

***Correspondence:**
Fabienne Battaglia-Brunet
f.battaglia@brgm.fr

Specialty section:
This article was submitted to Microbiological Chemistry and Geomicrobiology, a section of the journal Frontiers in Microbiology

Received: *10 June 2020*
Accepted: *02 November 2020*
Published: *20 November 2020*

Citation:
Zhang F, Battaglia-Brunet F, Hellal J, Joulian C, Gautret P and Motelica-Heino M (2020) Impact of Fe(III) (Oxyhydr)oxides Mineralogy on Iron Solubilization and Associated Microbial Communities. Front. Microbiol. 11:571244. doi: 10.3389/fmicb.2020.571244

INTRODUCTION

Fe (oxyhydr)oxides are ubiquitous components in several compartments of the critical zone (e.g., soils, sediments, and aquifers) and are present in many different mineralogical forms. Understanding biogeochemical behavior and Fe cycling is fundamental for many scientific communities (Bonneville et al., 2004; Roden et al., 2004). Indeed, the mobility of associated trace elements (TE) is partly controlled by Fe speciation, mineralogy and reactivity (Cornell and Schwertmann, 2003). The natural solubility of crystalline Fe (oxyhydr)oxides is low. However, the interaction with microbes and organic substances can enhance the formation of soluble Fe(III) and increase the availability of Fe and associated TE (Colombo et al., 2014). Many biogeochemical aspects of Fe cycling, including the major microbially mediated and abiotic reactions, have been extensively covered (Melton et al., 2014), together with Fe redox transformations and availability of TE (Zhang et al., 2012), as well as Fe redox cycling in bacteriogenic Fe oxide-rich sediments (Gault et al., 2011). In aerobic environments at circumneutral pH conditions, Fe is generally relatively stable and highly insoluble in the form of (oxyhydr)oxides (e.g., $Fe(OH)_3$, FeOOH, Fe_2O_3). However, in anaerobic conditions these minerals can be reductively dissolved (Roden and Wetzel, 2002; Roden et al., 2004) by microbial and abiotic pathways (Bonneville et al., 2004; Hansel et al., 2004; Thompson et al., 2006; Shi et al., 2016). In particular, reductive dissolution of Fe (oxyhydr)oxides can be driven by dissimilatory iron-reducing bacteria (DIRB), significantly contributing to biogeochemical cycling of Fe and subsequent TE mobilization (Cooper et al., 2006; Ghorbanzadeh et al., 2017; Levar et al., 2017). Microbial dissimilatory iron reduction (DIR) is a ubiquitous biogeochemical process in suboxic environments (Lovley, 2000; Crosby et al., 2005; Wilkins et al., 2006; Schilling et al., 2019). DIRB use Fe (oxyhydr)oxides as electron acceptors instead of oxygen for oxidizing organic matter. Moreover, the rate of Fe(III) reduction will also influence mobility of TE initially immobilized on or in Fe (oxyhydr)oxides through adsorption or co-precipitation. Crystallinity, specific surface area and size among other factors may influence reactivity of Fe (oxyhydr)oxides in relation to the metabolic activity and diversity of DIRB (Cutting et al., 2009; Aino et al., 2018).

The role of iron-reducing bacteria (IRB) in Fe redox transformations has been evidenced for more than three decades (Lovley et al., 1987; Lovley, 1991; Stern et al., 2018; Meile and Scheibe, 2019; Su et al., 2020), during which more than 100 distinct IRB species have been found. However, *Geobacter* and *Shewanella* are the two most studied IRB genera up to now (Li et al., 2012; Han et al., 2018; Engel et al., 2019; Jiang et al., 2020). Some studies have focused on the observation of secondary mineral formation in presence of *Geobacter* or *Shewanella* strains during the bio-transformation of amorphous, poorly crystalline and highly crystalline iron (oxyhydr)oxides i.e., ferric (ferrihydrite, goethite, hematite, lepidocrocite), ferrous (siderite, vivianite), and mixed valence (magnetite, green rust) (Fredrickson et al., 1998; Zachara et al., 2002; Han et al., 2018). Moreover, molecular mechanisms that occur during Fe reduction have been characterized by electro microbiology for *Geobacter* and *Shewanella* (Nealson, 2017; Shi et al., 2019). Additionally, IRB communities may be influenced by initial Fe mineralogy and the nature of available electron donors. Lentini et al. (2012) compared IRB cultures obtained with different organic substrates, i.e., glucose, lactate and acetate, and different Fe(III)-minerals, i.e., ferrihydrite, goethite and hematite. Type of electron donor was the most important factor influencing community structure, that also varied with the nature of the Fe(III)-mineral. The availability of carbon sources, other than acetate, induced the development of sulfate-reducing bacteria, that could indirectly dissolve Fe(III)-minerals through the production of H_2S, whereas acetate alone induced the dissolution of ferrihydrite and the development of *Geobacter*. Hori et al. (2015) obtained IRB enrichments from diverse environments with only acetate that favored the selection and isolation of organisms belonging to the *Geobacter* genus. Acetate is a common small organic acid that cannot support fermentation, thus its consumption is generally linked to respiratory mechanisms. However, mixtures of organic substrates can be found in soils and sediments. In order to obtain complementary information on complex IRB communities that could be helpful to make the link with previous experiments involving pure strains only, the present study was performed with a mixture of simple (acetate, formate, lactate, glucose) and complex (peptone) electron donors and focused on the abundance of the two model genera, *Geobacter* and *Shewanella*, in bacterial communities originating from natural environments. Bio-reduction of four different Fe (oxyhydr)oxides presenting contrasting specific surfaces, crystallinity and solubility features, i.e., two freshly synthetized Fe (oxyhydr)oxides, and the two defined Fe-oxides goethite and hematite, was investigated with the obtained IRB enrichments. The objective of this experiment was to assess (1) the dissolution rate of these minerals in presence of mixed IRB communities while inhibiting sulfate reduction, and (2) the influence of the type of Fe(III)-mineral on the relative abundances of *Shewanella* and *Geobacter*, when a complex mixture of organic substrates is provided.

MATERIALS AND METHODS

Soil and Sediment Sampling and Enrichment of Iron-Reducing Bacteria (IRB)

Soils and riverbanks periodically subjected to flooding and thus to cyclic redox oscillations represent one of the surface environments where IRB should actively contribute to Fe bio-reduction. This study was based on IRB enrichments from soil and sediment samples from a riverbank, in a site already studied in terms of Fe and TE total concentration profiles in sediment cores (Dhivert et al., 2015). The sampling site is located in a Loire river channel, in Decize, France (Dhivert et al., 2015). Three samples were collected using an auger and stored under a N_2 atmosphere: soil from the riverbank (10–15 cm depth), soil from flooded ground (0–7 cm depth) and under-water sediment (7–17 cm depth), which were named D1,

D2, and D3, respectively. In order to obtain cultures enriched in Fe(III)-reducing bacteria, enrichment medium containing Fe(III) as electron acceptor and Na-molybdate to inhibit the development of sulfate-reducing bacteria was used. 10 g of each soil sample were inoculated into 200 mL basic medium (composition detailed in the **Supplementary Figure S1**, Lovley, 2006; Huguet, 2009) autoclaved (121°C, 20 min) then flushed with sterile N_2 just after autoclaving. The headspace of vials (small volume because 200 mL bottles were used) was N_2. The following components were added to this medium: 10 mM of Fe(III) Nitrilotriacetic Acid as electron acceptor, 1.5 g L^{-1} peptone, 10 mM of acetate, lactate, and formate, 2 mM glucose as electron donors (Lovley et al., 1989; Coates et al., 1996; Shelobolina et al., 2007; Kwon et al., 2016) in anaerobic conditions, and 0.4 mM of sodium molybdate. Fe(III)-NTA (100 mM stock solution) was prepared by dissolving 1.64 g of $NaHCO_3$ in 80 ml water, adding 2.56 g $C_6H_6NO_6Na_3$ and 2.7 g $FeCl_3{\cdot}6H_2O$, bringing the solution up to 100 ml, flushing with N_2 and filter sterilizing (0.2 μm, Millex-GP Syringe Filter, 33 mm diameter) into a sterile, anaerobic serum bottle. Sterilization of the electron donors was performed by autoclaving for acetate, lactate and formate, and filtration at 0.2 μm for peptone and glucose. Sodium molybdate was autoclaved. All stock solutions were kept anaerobic under N_2 after sterilization. Cultures were incubated at 20°C under agitation (100 rpm) for 10 days. Samples (1.5–2 mL) were collected in an anaerobic glove box, filtered at 0.45 μm (Millex -GP Syringe Filter, 33 mm diameter) and analyzed for Fe(II) content in order to evaluate Fe(III) reduction. After 3–5 steps of sub-culturing (inoculation at 10% in fresh medium, every 2 weeks), the three Fe-reducing cultures were able to reduce 10 mM Fe(III) into 1–2 days, and were used as inocula for the following IRB incubation experiments (see section "IRB Incubation Experiments").

Fe(III) (Oxyhydr)oxides

Two fresh Fe (oxyhydr)oxides were synthesized in the laboratory under the modified protocol of Schwertmann and Cornell (2008). The Fe (oxyhydr)oxide named FoF was prepared according to the protocol for ferrihydrite, by dissolving 40 g $Fe(NO_3)_3$ $9H_2O$ in 500 mL distilled water and adding 330 mL of 1 M KOH to adjust the pH to 7–8. The mixture was centrifuged at 5,000 rpm for 10 min and the supernatant was subsequently removed. The solid fraction was then washed five times with Milli-Q water. The Fe (oxyhydr)oxide named FoL was prepared according to the protocol for lepidocrocite with 11.93 g of unoxidized $FeCl_2{\cdot}4H_2O$ salts dissolved into 300 mL distilled water by stirring. The solution was adjusted to pH 6.7–6.9 with NaOH using a pH-stat under aeration (100 mL/min air). Washing was performed as described for FoF. Both synthesized minerals were freeze-dried. Goethite from Sigma-Aldrich (CAS No. 20344-49-4) and hematite from VWR Chemicals (CAS No. 1309-37-1) were also used. Mineralogical morphologies of all Fe (oxyhydr)oxides were characterized using a scanning electron microscope (SEM) and Brunauer, Emmett and Teller (BET) surface area measurement (determined by multipoint BET N_2 adsorption) (Brunauer et al., 1938). Specific surface areas were determined from N_2 adsorption isotherms in the best linear range (with a minimum of 15 points) between the relative pressure P/Po 0.03 and 0.33 (Cavelan et al., 2019).

Specific surface areas of Fe (oxyhydr)oxides varied from 11.7 to 337 m^2 g^{-1} (**Table 1**), and compared well to some other synthetic (oxyhydr)oxides (Larsen and Postma, 2001; Bonneville et al., 2004; Pedersen et al., 2005; Das et al., 2013). SEM was performed on a TM 3000 coupled to a SwiftED3000 X-Stream module (Hitachi), and operated at 15 kV accelerating voltage (Thouin et al., 2016). The corresponding observed morphologies (**Supplementary Figure S2**) are given in **Table 1**.

IRB Incubation Experiments

Incubation experiments were performed in 50 mL glass bottles containing 50 mL medium, equipped with chlorobutyl rubber stoppers, using 10% (v/v) of inocula from D1, D2, and D3 [see section "Soil and Sediment Sampling and Enrichment of Iron-Reducing Bacteria (IRB)"] enriched from the site samples of Decize and the four Fe (oxyhydr)oxides presenting contrasting specific surfaces (FoF, FoL, goethite, and hematite), under anaerobic conditions. The compositions of the different solutions used to prepare the culture medium were the same as for the enrichment cultures and are also listed in **Supplementary Figure S1**. The total Fe(III) concentration added as Fe (oxyhydr)oxides was adjusted to be close to 20 mM, as Fe(III)-NTA or solid iron oxides, based on the theoretical formula of each (**Supplementary Table S1**). The inoculation of Fe-reducing cultures was performed in an anaerobic glove box. The gas phase of the bottles was N_2 and the bottles were flushed with N_2 before and after sampling. The flasks were incubated at 20°C, under agitation (100 rpm). Not inoculated controls were prepared in the same conditions. Samples (1.5–2 mL) were collected as described in section "Soil and Sediment Sampling and Enrichment of Iron-Reducing Bacteria (IRB)" and analyzed for total dissolved iron ($[FeT]_D$). The Fe solubilization rates were calculated using the data of $[FeT]_D$ collected during the first phase of the incubation, when this parameter increased linearly. After 27 days incubation, the remaining cultures were centrifuged at 5,000 rpm for 10 min. Supernatants were removed and solids freeze-dried for observation under SEM-XEDS.

Fe Analyses and pH/Eh

For Fe analyses, 1.5 mL aliquot was sampled with a syringe and filtered through a 0.2 μm filter into 5 mL tubes and immediately acidified with concentrated HCl in the glove box.

TABLE 1 | Characteristics of Fe(III) oxides submitted to Fe-reducing bacteria.

Iron oxide	Assumed morphology[a]	Surface area[b] (m^2g^{-1})
goethite	Acicular	11.7
hematite	cylinder/rod	31.4
FoF	Blocky	232
FoL	Blocky	337

[a]For use in estimating mean particle size from morphology by SEM-EDS [TM3000 accompanied by a SwiftED3000 X-Stream module (Hitachi)]. [b]Determined by multipoint BET N_2 adsorption.

$[FeII]_D$ (dissolved Fe(II) concentration) was determined using the ortho-phenanthroline colorimetry method (Murti et al., 1966; Mamindy-Pajany et al., 2013). $[FeT]_D$ was determined using the same method but with the addition of hydroquinone to reduce dissolved total ferric iron ($[FeIII]_D$) into total ferrous iron ($[FeII]_D$). pH and redox potential (Eh, ref. Ag/AgCl) were measured in samples taken from the incubation flasks using standard hand-held portable meters (WTW Multi340i set) in glove box before and after the incubation.

DNA Extraction and qPCR of 16S rRNA Genes

DNA extractions were performed on all samples at the end of the experiments. Biomass was harvested by centrifugation at 10,000 rpm for 10 min of 2 mL of culture. Microbial DNA was extracted using the Fast DNA™ SPIN Kit for Soil (MP Biomedicals, United States) according to the manufacturer's instructions. The integrity of the DNA products was checked with agarose gel electrophoresis. The DNA concentrations were determined with a Quantus™ Fluorometer (Promega, United States).

Quantification of *Shewanella* and *Geobacter* were performed by quantitative PCR (qPCR) of a fragment of the gene encoding 16S rRNA (*rrs* gene) (abbreviated *Shewanella* 16S and *Geobacter* 16S), using a CFX96 Touch™ Real-Time PCR Detection System (Bio-Rad, United States). Primers Sw 640-F (5′-RAC TAG AGT CTT GTA GAG G-3′) and Sw 815-R (5′-AAG DYA CCA AAY TCC GAG TA-3′) specific to *Shewanella rrs* gene (Snoeyenbos-West et al., 2000; Li et al., 2018), and primers Geo 564-F (5′-AAG CGT TGT TCG GAW TTA T-3′) and Geo 840-R (5′-GGC ACT GCA GGG GTC AAT A-3′) specific to *Geobacter rrs* gene (Kim et al., 2012) were used. qPCR reactions were performed in a total volume of 20 μL containing: 7.68 μL of sterile nuclease- and nucleic acids-free water, 10 μL of SSO Advanced Universal SYBR Green Supermix (Bio-Rad), 0.16 μL of each primer at 50 μM, and 2 μL of DNA (1–5 ng·μL^{-1}). qPCR reaction programs were as follows: for *Shewanella*, 1 min at 95°C, followed by 40 cycles: 5 s at 95°C/30 s at 55°C/30 s at 72°C/30 s at 80°C; for *Geobacter*, 2 min at 95°C, followed by 45 cycles: 10 s at 95°C/20 s at 60°C/20 s at 72°C/30 s at 80°C. Plasmid DNA containing the target genes were constructed from *Shewanella putrefaciens* and *Geobacter metallireducens rrs* gene, PCR amplified with primers 640F/815R and 564F/840R, respectively, and cloned using the TOPO™ TA Cloning™ Kit for Sequencing (Invitrogen, United States) according to the instructions. A calibration curve was obtained from serial dilutions of a known quantity of linearized plasmids containing known copy numbers of *S. putrefaciens* or *G. metallireducens rrs* genes. All samples, controls and standards were analyzed in duplicates. Results were reported as gene copies per gram or microliter of culture. Generation of a specific PCR product was confirmed by DNA melting curve analysis and agarose gel electrophoresis.

Quantification of the bacterial *rrs* gene coding 16S rRNA (abbreviated bacterial 16S), was performed with primers 341-F (5′-CCT ACG GGA GGC AGC AG-3′) and 515-R (5′-TGC CAG CAG CCG CGG TAA T-3′), as described for *Shewanella* and *Geobacter* except 0.2 μL T4GP32 at 500 ng·μL^{-1} was added into the reaction mixture. qPCR reaction program was as follows: 3 min at 95°C, followed by 35 cycles: 30 s at 95°C/30 s at 60°C/30 s at 72°C/30 s at 80°C. Plasmid DNA containing the bacterial *rrs* gene of *Pseudomonas putida* KT 2440 was 10-fold serially diluted to obtain a calibration curve of known copy numbers of *P. putida* KT 2440 *rrs* gene.

CE-SSCP Fingerprints

Capillary Electrophoresis-Single Strand Conformational Polymorphism (CE-SSCP) (Delbès et al., 2000) profiles were performed in order to characterize the bacterial community structure in cultures. About 200 bp of the V3 region of the bacterial *rrs* gene was amplified from DNA extracts with the forward primer w49 (5′-ACGGTCCAGACTCCTACGGG-3′; *Escherichia coli* position, 331) and the reverse primer w34 (5′-TTACCGCGGCTGCTGGCAC-3′; *E. coli* position, 533), 5′end labeled with the fluorescent dye FAM, using 25 cycles, hybridization at 61°C, and 30 s elongation at 72°C. 1 μL of diluted (20 or 50 fold in nuclease-free water) PCR product was added to a mixture of 18.6 μL of deionized formamide and 0.4 μL of Genescan-600 LIZ internal standard (Applied Biosystems). To obtain single-strand DNA, samples were heat-denaturized for 5 min at 95°C, and immediately cooled on ice. CE-SSCP analyses were performed on an ABI Prism 310 genetic analyzer using a 47-cm length capillary, a non-denaturing 5.6% CAP polymer (Applied Biosystems) and the following electrophoresis conditions: run temperature 32°C, sample injection for 5 s at 15 kV, data collection for 35 min at 12 kV. CE-SSCP data analyzes and lining CE-SSCP profiles up to the internal standard and to a common baseline were performed using BioNumerics V7.5 (Applied Maths).

Determination of Iron Oxides Solubilisation Parameters

The total dissolved Fe (Fe solubilization) was calculated from the $[FeT]_D$ curves during all the incubation period for the batch experiments. The initial Fe reduction rate (mg L^{-1}·h^{-1}) was calculated for the period of rapid increase of $[FeT]_D$ during the first stage (3–8 days) of the batch experiments. The total dissolved Fe and initial Fe (oxyhydr)oxide dissolution rates are indicated as "Fe solubilization" and "solubilization rate" in the following statistics.

Statistics

DNA quantification and qPCR data were analyzed using a Kruskal–Wallis test with XLSTAT software (version 2019 21.1.3) to determine the significant differences between each culture or between iron oxides. Variations in bacterial community structure were further analyzed by Non-Metric multiDimensional Scaling (nMDS) and ANOSIM analysis applied to a Bray-Curtis dissimilarity matrix of CE-SSCP data (generated in BioNumerics V7.5), using R-Studio software (Vegan Package) (R Studio Team, 2015).

Principal component analysis (PCA) was used to summarize the relationships between chemical (Fe-reducing speed for the first few days and Fe reduction proportion) and microbial (molecular biomass, i.e., DNA concentration, and *Geobacter* and *Shewanella* gene abundances) data with XLSTAT software (version 2019 21.1.3).

RESULTS

Dissolution of Fe (Oxyhydr)oxides

Fe (oxyhydr)oxide solubilization in the incubations was mainly influenced by the type of Fe (oxyhydr)oxide. For all cultures, D1 (**Figure 1A**), D2 (**Figure 1B**), and D3 (**Figure 1C**), the highest iron solubilization rates were observed in presence of FoL. The iron solubilization rates during the first week of the experiment, regardless of mineral structure, roughly matched the order of specific surface area except for goethite/hematite with D1 and D2 (**Supplementary Table S2**). In abiotic control flasks, iron dissolution remained lower than 0.4% (**Supplementary Figure S3**).

Initial pH of the medium was close to 7.5. This parameter did not significantly change during the incubation in presence of FoL and goethite. The final pH increased slightly to 7.6 in presence of FoF and decreased to 7.4 in presence of hematite. The initial Eh was −30 mV (ref. Ag/AgCl). This parameter decreased to -230 ± 10 mV after incubation in presence of bacteria. In abiotic control flasks, the Eh value decreased down to −130 mV.

According to the $[FeT]_D$ during the incubation period, total dissolved Fe from Fe (oxyhydr)oxides was calculated (**Figure 2**). Considering that total Fe provided as Fe minerals was close to 20 mM, the percentage of Fe solubilization was in the range from 1 to 15%. The highest quantities of dissolved Fe were obtained for FoL, with 0.074 mg iron per mL with D3 inoculum. The extent of FoL solubilization was more than three times higher than that of hematite with the same inoculum. For goethite, low solubilization, around 0.022 mg iron per mL, were obtained, with no significant differences between the three inocula. Moreover, when Fe (oxyhydr)oxides are grouped without distinguishing the origin of the inocula, the solubilization of FoL was significantly different to that of goethite and hematite (**Figure 2**), and that of FoF was significantly different to that of hematite. For the same data set, the significant differences shown between the different inocula (**Supplementary Figure S4**) shows that for both D1 and D2, FoL solubilization was significantly different to that of hematite. However, there was no significant difference in iron solubilization between iron oxides with D3. This suggests that D3 could be less influenced by Fe mineralogy than the other two inocula.

Biological Parameters

Soil Samples

Globally, *Geobacter* was clearly present in higher proportions than *Shewanella* in the bacterial communities present in the environmental samples used to enrich D1, D2, and D3.

Effect of Fe (Oxyhydr)oxides on Bacterial Community Structure

The bacterial community structure profiles of the initial soil and sediment samples, the Fe-NTA enrichments and the cultures in presence of the four different (oxyhydr)oxides were compared using an nMDS ordination approach (**Figure 4**). Full CE-SSCP profiles are available in **Supplementary Figure S5**. These profiles show a high diversity with many peaks.

The structures of the initial communities were modified after inoculation on solid Fe (oxyhydr)oxides (**Figure 4**): enrichments on Fe(III)-NTA are grouped on the right side of the representation, whereas communities obtained by cultures with iron oxides are gathered on the left side. The three initial communities from environmental samples are located between these two poles. No clear separation is observed between the communities obtained with the four pure iron oxides. Although, according to ANOSIM analysis, no significant difference in community composition was found between initial inocula (significance > 0.05), a significant dissimilarity was found between community origins (i.e., initial soils and form of Fe(III) provided to the consortia) ($R = 0.345$ and significance = 0.0249).

Bacterial Abundance and Abundances of *Shewanella* and *Geobacter*

The *rrs* gene abundances and *Geobacter* 16S, *Shewanella* 16S/bacterial 16S ratios did not highlight any significant differences between the three initial soils D1, D2, and D3 (**Figure 3B**). As shown in **Figure 3A**, globally, the *rrs* gene abundance in goethite samples was significantly different to FOF samples. Conversely, the abundance of the two quantified IRB, i.e., *Geobacter* and *Shewanella*, differ between the types of Fe oxides provided as Fe(III) source (**Figures 3C,E**). Globally, compared with *Geobacter*, *Shewanella* was present in a larger proportion in all bacterial communities with the four iron oxides. Moreover, the number of gene copies of *Shewanella* for FoL is significantly different in D1 from that in presence of other iron oxides but there are no significant differences between the cultures for FoF, goethite and hematite samples (**Figure 3F**). When the type of inocula is not taken into account, the proportion of *Shewanella* 16S genes for FoL samples is significantly different for goethite and hematite samples (**Figure 3E**).

Considering specifically each quantified genus, the cultures in presence of goethite inoculated with D3 bacteria contained a significantly different proportion of *Geobacter* 16S genes than the same culture (D3) with FoL (**Figure 3F**). In the other conditions (D1, D2 with all oxides), no significant differences between the proportion of *Geobacter* 16S genes in the global bacterial population was observed.

DISCUSSION

Influence of the Type of Iron Oxide on Bacterial Iron Solubilisation

FoL and FoF were synthetized in the laboratory and were more amorphous, thus more reactive, than goethite and hematite (Usman et al., 2012). According to the literature, abiotic rates

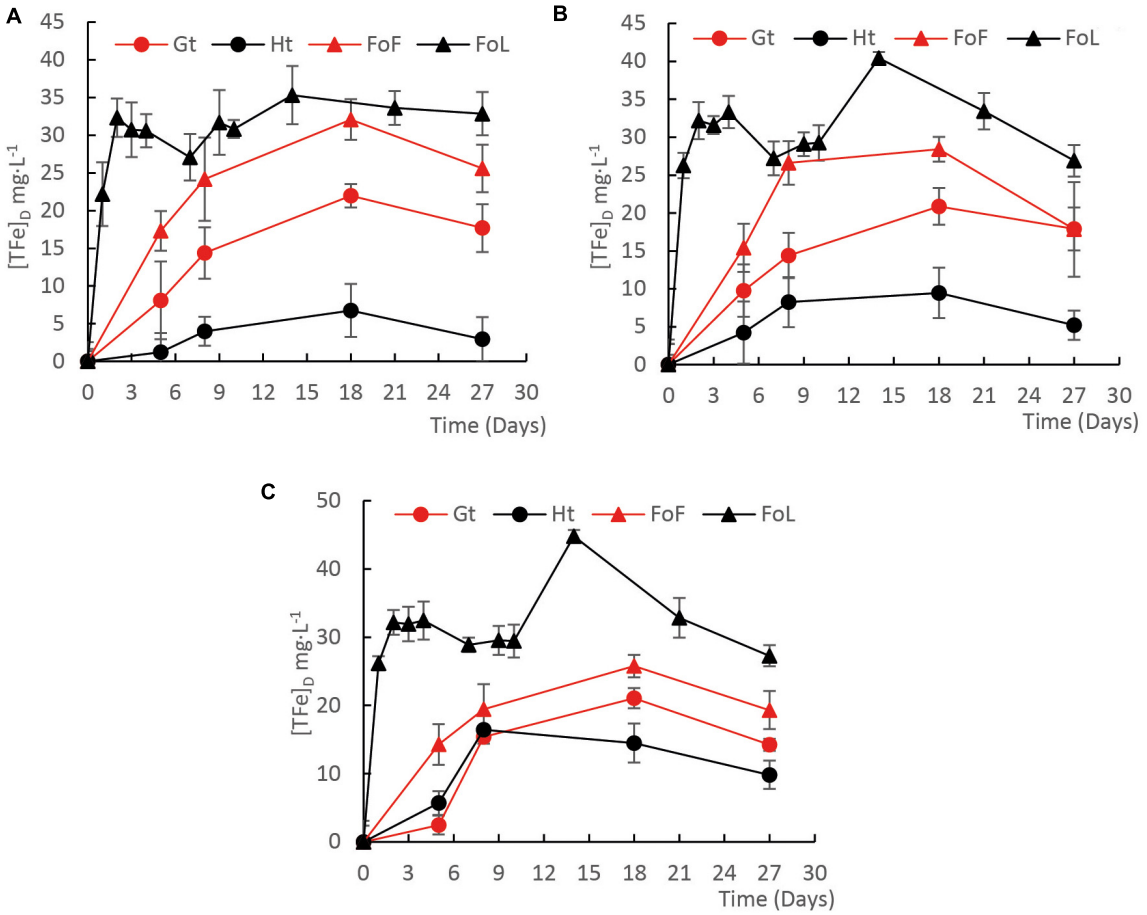

FIGURE 1 | Evolution of the concentration of total Fe during incubation experiments with four Fe(III) (oxyhydr)oxides in presence of D1 **(A)**, D2 **(B)**, and D3 **(C)** iron-reducing cultures with a mixture of C sources, *Fe(III)-NTA* is given in **Supplementary Figure S3**. Error bars represent the standard deviation of triplicate measurements.

of reductive iron dissolution are correlated with the solubility of Fe (oxyhydr)oxides (Larsen and Postma, 2001). The rates of this abiotic reductive bulk dissolution decrease according to ferrihydrite > lepidocrocite > goethite > hematite, emphasizing the importance of the crystal structure on the dissolution rate (Larsen and Postma, 2001). However, Roden (2006) found that in presence of IRB, oxides' mineralogical and thermodynamical properties exert a minor influence on reduction rates compared with the abundance of available oxide surface sites controlled by oxide surface areas and the accumulation of surface-bound biogenic Fe(II). This last process, of the precipitation of new Fe(II) minerals (Urrutia et al., 1998; Zachara et al., 2002), could explain the late decrease of soluble Fe (**Figure 1**). Present results are partially in accordance with this last hypothesis, as Fe solubilization effectiveness increased with the specific surface, in particular for the two freshly synthesized oxides. Here, the fresh mineral prepared with the protocol of lepidocrocite (FoL) synthesis presented a higher specific surface than the mineral produced using the protocol for ferrihydrite (FoF). Synthetic lepidocrocites can present a very large range of specific surface areas, depending on their level of crystallinity (Schwertmann, 1973). In the present case, the specific area of synthetic FoL (337 $m^2.g^{-1}$) is much higher than for other Fe (oxyhydr)oxides, possibly due to a rapid oxidation of Fe(II) during synthesis that produced poor crystallization and formation of lepidocrocite impurities (Schwertmann and Taylor, 1979). Schwertmann (1973) showed that the specific surface of lepidocrocite increases with its solubility in presence of oxalate, and this specific surface area is anti-correlated with the crystallinity. In the present experiment, at the end of the incubation, we detected 8 $mg.L^{-1}$ total Fe in the FoL abiotic control, but almost no Fe in FoF abiotic control. This supports the idea that FoL was more soluble than FoF. The high specific surface area and probable poor crystallinity of FoL could have favored solubilization by IRB.

Fe solubilization rates were limited after a few days, probably due to evolution of the composition of the liquid medium, or the accumulation of surface-bound biogenic Fe(II) (Roden, 2006), as Fe(III) was not the limiting factor. Parameters such as humic substances, quinones, and organic carbon can strongly influence microbial Fe(III) reduction rates for *Shewanella* (Adhikari et al., 2017) or *Geobacter* (Wolf et al., 2009) in natural environments.

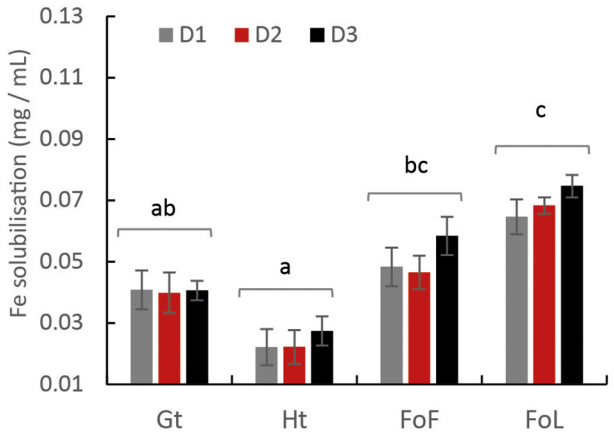

FIGURE 2 | Final total amount of solubilized Fe from Fe (oxyhydr)oxides: goethite, hematite, FoF and FoL in presence of D1, D2, and D3 inocula with a mixture of C sources. The letters "a" and "b" represent the significance of differences (Kruskal–Wallis test at $p < 0.05$) between cultures. Values in the same Fe (oxyhydr)oxides group are not significantly different from one another. Error bars represent the standard deviation of triplicate measurements.

Generally, in these studies, the highest reducing rates were observed during the first few days of microbial Fe(III) reduction. In our study, the influence of the type of Fe (oxyhydr)oxides on initial iron oxide-reducing rates were consistent with those of previous studies performed with pure strains.

Bacterial Communities

The structures of the initial bacterial communities present in the environmental samples were modified by the enrichment in Fe(III)-NTA medium, and again showed an evolution when the enrichments were grown in presence of solid Fe (oxyhydr)oxides (**Figure 3**). This last result could be due to the difference of bio-availability of Fe with minerals compared to Fe(III)-NTA. Cai et al. (2019) also showed an influence of bio-available Fe(III) on microbial community structure. Here, the accessibility of Fe(III) in the Fe(III)-NTA incubations favored the iron reducing community that may have rapidly consumed available organic substrates and probably lowered the development of other bacteria. With minerals, however, Fe(III) is less accessible and competition for Fe(III) may induce changes in community structure. For example, Zhuang et al. (2011) indicated that *Rhodoferax* and *Geobacter* species were acetate-oxidizing Fe(III)-reducers that compete in anoxic subsurface environments and this competition could influence the *in situ* bioremediation of uranium-contaminated groundwater by changing diversity structure. On the other hand, no clear effect of the type of Fe mineral on the global community profile was observed. This may be linked to the culture medium composition. Indeed, the addition of diverse C sources could enable fermentative bacteria to develop without using Fe(III) for their growth. In contrast, Lentini et al. (2012) observed an effect of the type of Fe (oxyhydr)oxide, i.e., FoF, goethite or hematite, on the structure of bacterial communities in enrichment cultures using T-RFLP fingerprints. However, these authors did not use an initial Fe(III)-NTA enrichment step and did not use a sulfate-reduction inhibitor, as in our study.

Geobacter and *Shewanella* 16S Genes Abundances

The relative abundance of *Geobacter* and *Shewanella* in the initial soils and sediment used as sources of IRB in our experiment could be linked to the redox conditions of the environment. Indeed, *Geobacter* and *Shewanella* were present in higher proportions in the river sediment D3, than in the flooded soil D2, itself richer than the non-saturated soil D1. This suggests that the reducing conditions in the aquatic sediment was more favorable for anaerobic bacteria, such as IRB.

Shewanella and *Geobacter* represented in our incubation experiments a small proportion of the total community, however we made a focus on these two genera because they are the most studied iron reducing bacteria. However, the other members of the community could contribute either directly or indirectly to the iron solubilization process. Considering the evolution of the two targeted IRB genera, namely *Geobacter* and *Shewanella*, after the enrichment with Fe(III)-NTA, the *Shewanella*/*Geobacter* abundance ratio increased significantly compared to the site samples (**Supplementary Figure S6** compared with **Figure 3B**), suggesting that the presence of a large amount of bio-available Fe(III) in the enrichment culture medium was in favor of *Shewanella*. Another explanation for the sharp increase of *Shewanella* compared to *Geobacter* could be the composition of the culture medium in terms of organic substrates. *Geobacter* can use acetate as electron donors while performing the dissimilatory Fe reduction (Caccavo et al., 1994; Coates et al., 1996), but does not use lactate nor glucose. Conversely, some *Shewanella* species were shown to be able to use glucose and can present either respiratory or fermentative types of metabolisms (Nogi et al., 1998; Ziemke et al., 1998; Ivanova et al., 2004). Lentini et al. (2012) showed that the presence of *Geobacter* was favored by acetate whereas the growth of *Shewanella* was rather stimulated by lactate. Moreover, these authors suggested that production of acetate through incomplete degradation of lactate by *Shewanella* could benefit *Geobacter* (Hori et al., 2015). Our medium contained both acetate, formate, lactate and glucose, thus it should potentially support growth of both *Shewanella* and *Geobacter*. However, a fermentative metabolism could explain the selection of *Shewanella* over *Geobacter* in our enrichments and in all incubation conditions, because this genus can grow either using fermentation or Fe(III) reduction (Bowman, 2015). Moreover, Leyva-Díaz et al. (2017) showed that peptone was a better substrate for the growth of *Shewanella baltica* than glucose or acetate. As our medium contained 1.5 g L^{-1} peptone, this substrate could also favor the growth of bacteria belonging to the *Shewanella* genus.

When these communities were grown in presence of solid iron oxides, the abundance of *Shewanella* (average of D1, D2, and D3) was 112, 30, 52, and 3058 times higher than the abundance of *Geobacter*, for FoF, goethite, hematite and

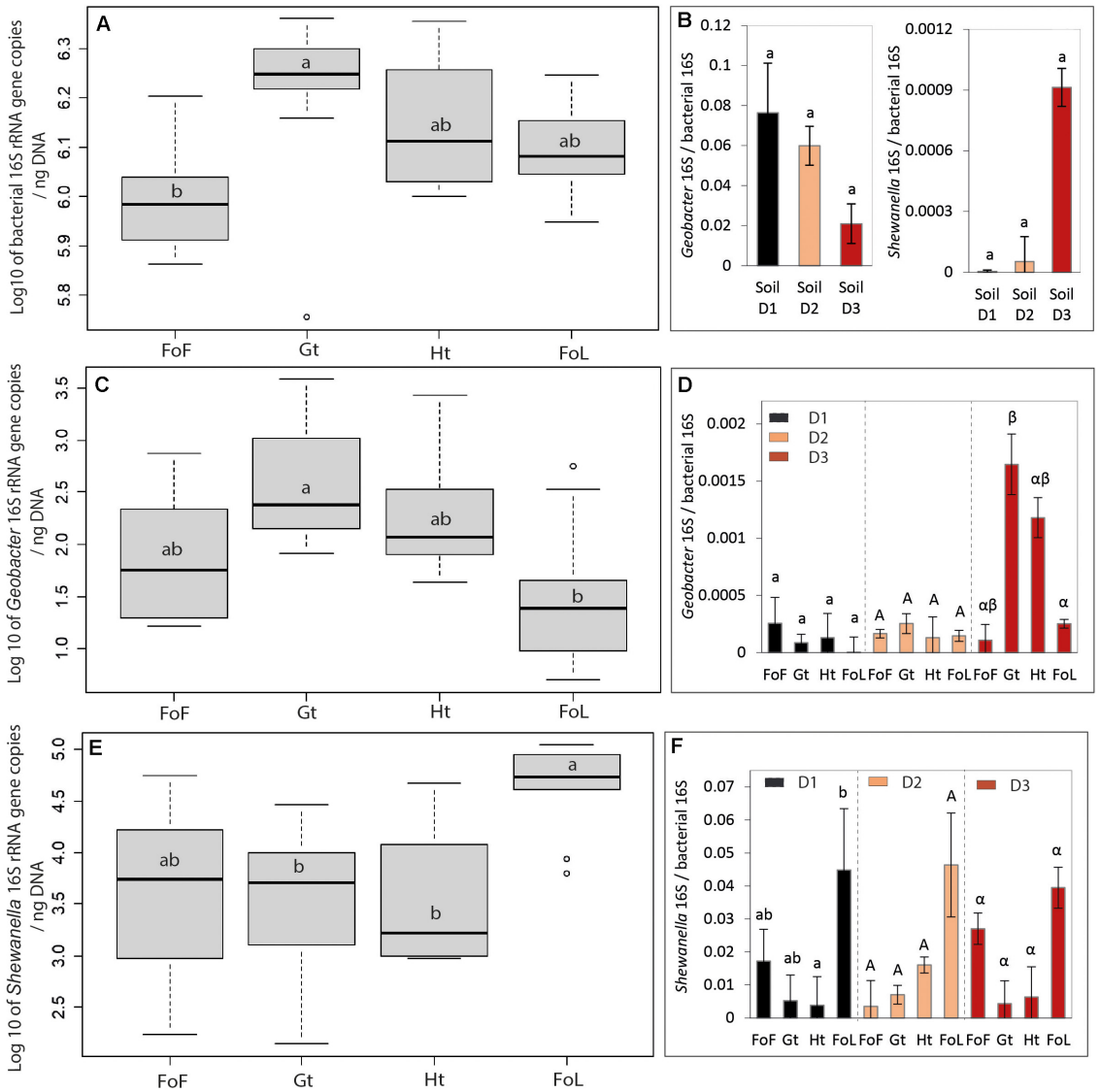

FIGURE 3 | Parameters linked to bacterial abundance: **(A)** Log10 of bacterial 16S rRNA (*rrs* gene) copies, **(B)** Ratio of *Shewanella* and *Geobacter* over bacterial 16S rRNA (*rrs* gene) copies for all three site samples D1, D2, and D3, **(C)** Log 10 of *Geobacter* 16S gene copies, **(D)** Ratio *Geobacter* 16S over bacterial 16S rRNA (*rrs* gene) copies, **(E)** Log 10 of *Shewanella* 16S gene copies, and **(F)** Ratio *Shewanella* 16S over bacterial 16S rRNA (*rrs* gene) copies. Details of bacterial, *Shewanella* and *Geobacter* 16S rRNA (*rrs* gene) copies for all three site samples D1, D2, and D3 are given in **Supplementary Figure S6**. The letters "a" and "b" differed significantly (Kruskal–Wallis test at $p < 0.05$) between group of iron oxide for graph "(a), (b), (c), and (e)"; the small letter, capital letter and Greek letter were used for differing significantly by group of inocula D1, D2, and D3 for graphs "(d) and (f)." Data represent average values of three experimental replicates and their standard deviation (σ) for graph "(b), (d), and (f)," 3 inocula × 3 replicates for graphs "(a), (c), and (e)." Ht: hematite; Fh: FoF; Lp: FoL; Gt: goethite. Error bars represent the standard deviation of triplicate measurements.

FoL, respectively. Moreover, we found that the cultures in presence of goethite inoculated with D3 bacteria contained higher proportions of *Geobacter* than the same culture (D3) with FoL. These results might suggest that *Geobacter* could be more favored, in the competition with other IRB such as *Shewanella*, for growth in presence of goethite and hematite than for growth in presence of the more easily dissolved oxides, i.e., FoF and FoL. The type of Fe mineral can exert a selection pressure on the communities of IRB, as previously shown by Lentini et al. (2012). This result could be linked to a higher affinity of *Geobacter* for Fe(III), that would favor this organism at low Fe(III) availability levels. Reported Ks values for Fe(III) are 1.0 mM with *Geobacter sulfurreducens* (Esteve-Núñez et al., 2005) compared to 29 mM with *S. putrefaciens* (Liu et al., 2001).

Yet, the solubility of ferrihydrite and lepidocrocite are higher than that of goethite and hematite (Cornell and Schwertmann, 2003; Liu et al., 2007), thus the availability of Fe(III) could be higher with the first two oxides. *Shewanella* might be favored by high bio-available Fe(III), but could be less efficient

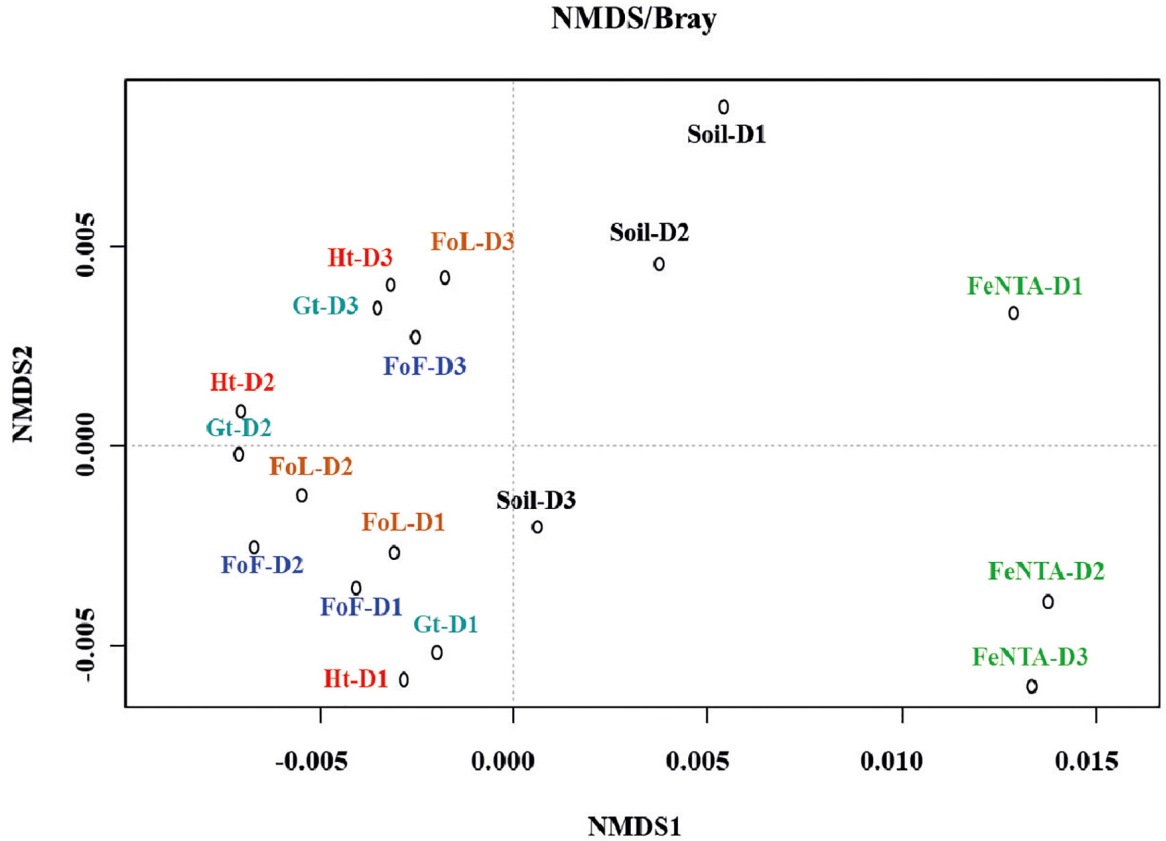

FIGURE 4 | nMDS ordination of D1, D2, and D3 community fingerprints applied to a Bray-Curtis dissimilarity matrix. Plot stress = 0.15. Ht: hematite; Fh: FoF; Lp: FoL; Gt: goethite.

for growth in presence of less soluble Fe-oxides such as goethite and hematite. The anaerobic respiration of *Shewanella* was highly dependent on electron shuttles. Nevin and Lovley (2002) suggested that *Shewanella alga* strain BrY released compounds that could solubilize Fe(III) from Fe(III) oxides, however, *G. metallireducens* did not produce electron shuttles or Fe(III) chelators to solubilize Fe(III) oxides (Nevin and Lovley, 2002). Kotloski and Gralnick (2013) determined the contribution of flavin electron shuttles in extracellular electron transfer by *Shewanella oneidensis* and Wu et al. (2020) showed that exogenous electron mediators (EMs) favored high density current production and increased the synthesis of extracellular polymeric substances which promoted biofilm formation during electron shuttling process (Wu et al., 2020). The conduction of electrons along pili or other filamentous structures is one of the mechanisms proposed for electron transfer to solid iron oxides. Leang et al. (2010) showed that OmcS, a cytochrome that is required for Fe(III) reduction by *G. sulfurreducens*, was localized along the pili (Leang et al., 2010). The electrically conductive pili play a major role in the adaptation of *Geobacter* to perform DIR in natural environments (Liu et al., 2019). These differences in the Fe(III)-reducing mechanisms between the two species might explain their difference of affinity for Fe(III) (Liu et al., 2001; Esteve-Núñez et al., 2005) and the relative increase of *Geobacter* abundance, observed here in presence of goethite and hematite, with the enrichment culture that was the most efficient for Fe-oxide solubilization, i.e., culture D3.

Relation Between Iron Solubilisation Effectiveness and *Geobacter* and *Shewanella* Abundances

In batch experiments, the three inocula D1, D2, and D3, enriched from soil from the river bank, flooded soil and an aquatic sediment of the Decize site gave similar results in terms of Fe solubilization effectiveness of iron (oxyhydr)oxides. However, there were differences between different Fe (oxyhydr)oxides: the type of Fe (oxyhydr)oxides had more influence on Fe solubilization effectiveness than the origin of the inocula. Fe solubilization rates were slower with goethite and hematite compared to FoF and FoL. The same tendency was observed by Bonneville et al. (2004), who found that, with the pure strain *S. putrefaciens* in presence of 20 mM Fe(III), reduction of 6-line ferrihydrite was faster than that obtained with lepidocrocite, and faster than that obtained with low surface area hematite. Li et al. (2012) reported similar results for the microbial reduction

of Fe(III) oxides by *Shewanella decolorationis* strain S12, the reducing speed decreasing according to the following order: lepidocrocite > goethite > hematite.

Principal component analysis integrating chemical (**Supplementary Table S2**) and molecular data was performed to identify the relationships and contributions between iron solubilization effectiveness and *Geobacter*/*Shewanella* abundances in batch experiment samples (Mercier et al., 2014; Zhu et al., 2014; Hong et al., 2015). In this study, a biplot (**Supplementary Figure S7**) summarizes PCA results. The first principal component is strongly influenced by the iron solubilization effectiveness (higher on the right than on the left side of the representation), with higher values associated with FoL, and the lowest associated with goethite and hematite (not separated), FoF being in an intermediary position. Meanwhile proportion of *Shewanella* in the bacterial community, but not to the proportion of *Geobacter*, seems to be correlated to FoL. The second principal component reflects high values of the proportion of *Geobacter* in the bacterial communities. Thus, the proportion of *Shewanella* seems to be more correlated to iron solubilization parameters than *Geobacter*. PCA allows clear discrimination with different groups of iron oxides, however not for the different types of inoculum (D1, D2, and D3).

According to Bonneville et al. (2004), the dissolution and solubility of goethite and hematite are lower than that of ferrihydrite and lepidocrocite in the presence of *Shewanella*. Cutting et al. (2009) indicated that hematite and goethite are susceptible to limited Fe(III) reduction in presence of *G. sulfurreducens*. Moreover, Poggenburg et al. (2016) mentioned that Fe(III)-organic compounds (coprecipitates from solutions of $FeCl_3$ and natural organic matter) reduction by *S. putrefaciens* was influenced by the amount of available electron shuttling molecules induced by sorbed natural organic matter. Fe(III)-organic compounds' reduction by *G. metallireducens* was more influenced by particle size, physicochemical properties and iron (oxyhydr)oxides (composition of sorbed natural organic matter and aggregation state) (Poggenburg et al., 2016). In our study, FoL samples with a higher proportion of *Shewanella* in their bacterial communities were correlated with high initial iron solubilization rates and electron shuttling molecules might have a role in this phenomenon. In contrast, *Geobacter* was not specifically associated to FoL but was found in higher proportions with goethite in one condition. This tendency is in accordance with findings of previous research performed with the less soluble iron oxides (Crosby et al., 2007), showing that *G. sulfurreducens* reduced 0.7% hematite and 4.0% goethite while *S. putrefaciens* reduced only 0.5% of hematite 3.1% goethite after 280 days of incubation. Thus, our results suggest that *Geobacter* might suffer less from the competition with *Shewanella* in low bio-available Fe(III) conditions, whereas the contribution of this genus, present in lower quantities than *Shewanella*, to the iron solubilization effectiveness is not demonstrated. Moreover, other members in the community of IRB might have potential contribution to Fe solubilization. Our culture medium contained substrates such as glucose and peptone that could support the growth of fermentative organisms. Lentini et al. (2012) and Gagen et al. (2019) indicated that fermentation likely plays a key role in reduction of crystalline iron oxides by diverse species, such as *Telmatospirillum*, both through direct reduction and by the production of H_2, potentially used by dissimilatory iron reducers, during fermentation.

CONCLUSION

Microbial enrichments containing IRB, obtained with a mixture of simple and complex electron donors, were able to grow and reduce Fe(III) in a short time. Experiments performed with fresh Fe (oxyhydr)oxides, goethite and hematite confirmed that the type of Fe mineral could influence Fe solubilization rates and the abundances of two IRB commonly involved as pure strains in Fe-reducing experiments, i.e., *Geobacter* and *Shewanella*.

The present study's results showed that: (1) the sub-culturing of IRB enrichments from Fe(III)-NTA to pure iron oxides significantly modified the bacterial communities; (2) in our experimental conditions, bacterial diversity was not significantly different from one type of pure (oxyhydr)oxide to another; (3) the type of Fe oxide can influence the proportion of *Geobacter* and *Shewanella*. Meanwhile, the nature of Fe (oxyhydr)oxides seems to have exerted a selection on the ratio of *Geobacter* and *Shewanella*, whereas it did not impact the bacterial community fingerprints. The concentration of bio-available Fe(III) and the mixture of electron donors in the enrichment medium favored the development of *Shewanella* compared with *Geobacter* genus. However, the culture medium included a large amount of electron donors that is not representative of most natural systems. Therefore, complementary studies, performed with lower concentrations of electron donors provided in continuous feeding conditions would help to make the link with real environments. In presence of iron oxides, the highest proportions of *Shewanella* in bacterial communities were obtained with FoL and corresponded to the highest levels of iron solubilization, possibly linked to the fact that FoL was the most soluble (oxyhydr)oxide in our experiments. This result is consistent with the hypothesis that *Shewanella* development could be favored by a high bioavailability of Fe(III). In contrast, *Geobacter* was detected in higher proportions with goethite that is less easily dissolved, when D3 culture was used.

Globally, all results suggested that both initial community composition of the sample used to prepare the enrichments, as well as the type of Fe(III) oxide used as electron acceptor influenced the final proportions and abundances of *Geobacter* and *Shewanella*. A better knowledge of complementary biological parameters associated with these two organisms, such as their activity during Fe(III) solubilization and reduction in complex communities and distribution between planktonic and Fe(III)-mineral-attached cells, could help to elucidate their role in natural environments. As biofilms in soils and sediments contain a large part of the bacterial biomass, future research could be focused on

the distribution and activity of *Geobacter* and *Shewanella* attached on iron oxides surfaces.

DATA AVAILABILITY STATEMENT

The original contributions presented in the study are included in the article/**Supplementary Material**, further inquiries can be directed to the corresponding author.

AUTHOR CONTRIBUTIONS

FB-B, JH, and MM-H conceived and designed the experiments and arranged funds. FZ performed major experiments. FZ and FB-B were responsible for manuscript preparation. MM-H, FB-B, JH, and FZ arranged sampling from Decize, France. PG and FZ performed SEM. CJ, JH, and FZ performed the qPCR of *Shewanella*/*Geobacter* and bacterial 16S rRNA (*rrs* gene) quantification. All authors contributed to the article and approved the submitted version.

FUNDING

This research work was performed in the frame of a Ph.D. project, a scholarship co-funded by the BRGM – Région Centre-Val de Loire 2017–2020, contract N° SIRET 582 056 149 00120. Additionally, the INSU-EC2CO project "Dycyfer" also contributed to this work. This work was supported by a grant overseen by the French National Research Agency (ANR) as part of the "Investments d'Avenir" Program LabEx VOLTAIRE, 10-LABX-0100.

SUPPLEMENTARY MATERIAL

The Supplementary Material for this article can be found online at: https://www.frontiersin.org/articles/10.3389/fmicb.2020.571244/full#supplementary-material

Supplementary Figure 1 | Design and initial compositions of the batch experiments.

Supplementary Figure 2 | SEM observations of iron oxides: Morphology of initial FoF **(A)**, FoL **(B)**, hematite **(C)**, and goethite **(D)**.

Supplementary Figure 3 | Concentration of Fe(II) and total Fe (FeT) of D1, D2, and D3 incubated on Fe(III)-NTA medium **(A)**, and evolution of the concentration of total Fe during incubation experiments with four abiotic Fe(III) (oxyhydr)oxides **(B)**. Error bars represent the standard deviation of triplicate measurements.

Supplementary Figure 4 | Dissolution of Fe(III) oxides: goethite, hematite, FoF and FoL in presence of D1, D2, and D3 inocula. The small letters, capital letters and Greek letters were used for differing statistical significance (Kruskal–Wallis test at $p < 0.05$) per group of inocula D1, D2, and D3 for the different iron oxides. Error bars represent the standard deviation of triplicate measurements.

Supplementary Figure 5 | CE-SSCP diversity profiles of the site samples (Soil), the Fe(III)-NTA enrichments (Fe-NTA) and cultures in presence of the four iron oxides: FoF, FoL, goethite (Gt) and hematite (Ht). D1: soil from river bank; D2: sediment interface, flooded soil; D3: sediment under water.

Supplementary Figure 6 | Parameters linked to bacterial abundance: **(A)** Log10 of bacterial 16S rRNA (*rrs* gene) copies, **(B)** Log 10 of *Geobacter* 16S gene copies, **(C)** Log 10 of *Shewanella* 16S gene copies, for the three site samples D1, D2, and D3; Ratios of *Shewanella* 16S **(D)** and *Geobacter* 16S **(E)** over bacterial 16S rRNA genes copies in Fe(III)-NTA enrichments. Error bars represent the standard deviation of triplicate measurements.

Supplementary Figure 7 | Principal component analysis (F1 × F2) biplot map generated from iron solubilization (percentage and rate of iron solubilization) and ratios of *Shewanella* (*Shewanella* 16S/bacterial 16S) and *Geobacter* (*Geobacter* 16S/bacterial 16S) in the bacterial community, obtained for the FoF, goethite hematite and FoL incubations with D1, D2, and D3.

REFERENCES

Adhikari, D., Zhao, Q., Das, K., Mejia, J., Huang, R., Wang, X., et al. (2017). Dynamics of ferrihydrite-bound organic carbon during microbial Fe reduction. *Geochim. Cosmochim. Acta* 212, 221–233. doi: 10.1016/j.gca.2017.06.017

Aino, K., Hirota, K., Okamoto, T., Tu, Z., Matsuyama, H., and Yumoto, I. (2018). Microbial communities associated with indigo fermentation that thrive in anaerobic alkaline environments. *Front. Microbiol.* 9:2196. doi: 10.3389/fmicb.2018.02196

Bonneville, S., Van Cappellen, P., and Behrends, T. (2004). Microbial reduction of iron (III) oxyhydroxides: effects of mineral solubility and availability. *Chem. Geol.* 212, 255–268. doi: 10.1016/j.chemgeo.2004.08.015

Bowman, J. P. (2015). Shewanella. Bergey's Manual of Systematics of Archaea and Bacteria. New Jersey: John Wiley & Sons, Inc., 1–22.

Brunauer, S., Emmett, P. H., and Teller, E. (1938). Adsorption of gases in multimolecular layers. *J. Am. Chem. Soc.* 60, 309–319. doi: 10.1021/ja01269a023

Caccavo, F., Lonergan, D. J., Lovley, D. R., Davis, M., Stolz, J. F., and McInerney, M. J. (1994). *Geobacter sulfurreducens* sp. nov., a hydrogen-and acetate-oxidizing dissimilatory metal-reducing microorganism. *Appl. Environ. Microbiol.* 60, 3752–3759. doi: 10.1128/aem.60.10.3752-3759.1994

Cai, Y., Hu, K., Zheng, Z., Zhang, Y., Guo, S., Zhao, X., et al. (2019). Effects of adding EDTA and Fe2+ on the performance of reactor and microbial community structure in two simulated phases of anaerobic digestion. *Bioresour. Technol.* 275, 183–191. doi: 10.1016/j.biortech.2018.12.050

Cavelan, A., Boussafir, M., Le Milbeau, C., Rozenbaum, O., and Laggoun-Défarge, F. (2019). Effect of organic matter composition on source rock porosity during confined anhydrous thermal maturation: example of Kimmeridge-clay mudstones. *Int. J. Coal Geol.* 212:103236. doi: 10.1016/j.coal.2019.103236

Coates, J. D., Phillips, E. J., Lonergan, D. J., Jenter, H., and Lovley, D. R. (1996). Isolation of *Geobacter* species from diverse sedimentary environments. *Appl. Environ. Microbiol.* 62, 1531–1536. doi: 10.1128/aem.62.5.1531-1536.1996

Colombo, C., Palumbo, G., He, J.-Z., Pinton, R., and Cesco, S. (2014). Review on iron availability in soil: interaction of Fe minerals, plants, and microbes. *J. Soils Sediments* 14, 538–548. doi: 10.1007/s11368-013-0814-z

Cooper, D. C., Picardal, F. F., and Coby, A. J. (2006). Interactions between microbial iron reduction and metal geochemistry: effect of redox cycling on transition metal speciation in iron bearing sediments. *Environ. Sci. Technol.* 40, 1884–1891. doi: 10.1021/es051778t

Cornell, R. M., and Schwertmann, U. (2003). *The Iron Oxides: Structure, Properties, Reactions, Occurrences and Uses*. Hoboken, NJ: John Wiley & Sons.

Crosby, H. A., Johnson, C. M., Roden, E. E., and Beard, B. L. (2005). Coupled Fe (II)-Fe (III) electron and atom exchange as a mechanism for Fe isotope fractionation during dissimilatory iron oxide reduction. *Environ. Sci. Technol.* 39, 6698–6704. doi: 10.1021/es0505346

Crosby, H. A., Roden, E. E., Johnson, C. M., and Beard, B. L. (2007). The mechanisms of iron isotope fractionation produced during dissimilatory Fe (III) reduction by *Shewanella putrefaciens* and *Geobacter sulfurreducens*. *Geobiology* 5, 169–189. doi: 10.1111/j.1472-4669.2007.00103.x

Cutting, R., Coker, V., Fellowes, J., Lloyd, J., and Vaughan, D. (2009). Mineralogical and morphological constraints on the reduction of Fe (III) minerals by *Geobacter sulfurreducens*. *Geochim. Cosmochim. Acta* 73, 4004–4022. doi: 10.1016/j.gca.2009.04.009

Das, S., Hendry, M. J., and Essilfie-Dughan, J. (2013). Adsorption of selenate onto ferrihydrite, goethite, and lepidocrocite under neutral pH conditions. *Appl. Geochem.* 28, 185–193. doi: 10.1016/j.apgeochem.2012.10.026

Delbès, C., Moletta, R., and Godon, J. J. (2000). Monitoring of activity dynamics of an anaerobic digester bacterial community using 16S rRNA polymerase chain reaction–single−strand conformation polymorphism analysis. *Environ. Microbiol.* 2, 506–515. doi: 10.1046/j.1462-2920.2000.00132.x

Dhivert, E., Grosbois, C., Rodrigues, S., and Desmet, M. (2015). Influence of fluvial environments on sediment archiving processes and temporal pollutant dynamics (Upper Loire River, France). *Sci. Total Environ.* 505, 121–136. doi: 10.1016/j.scitotenv.2014.09.082

Engel, C. E. A., Schattenberg, F., Dohnt, K., Schröder, U., Müller, S., and Krull, R. (2019). Long-term behavior of defined mixed cultures of *Geobacter sulfurreducens* and *Shewanella oneidensis* in bioelectrochemical systems. *Front. Bioeng. Biotechnol.* 7:60. doi: 10.3389/fbioe.2019.00060

Esteve-Núñez, A., Rothermich, M., Sharma, M., and Lovley, D. (2005). Growth of *Geobacter sulfurreducens* under nutrient−limiting conditions in continuous culture. *Environ. Microbiol.* 7, 641–648. doi: 10.1111/j.1462-2920.2005.00731.x

Fredrickson, J. K., Zachara, J. M., Kennedy, D. W., Dong, H., Onstott, T. C., Hinman, N. W., et al. (1998). Biogenic iron mineralization accompanying the dissimilatory reduction of hydrous ferric oxide by a groundwater bacterium. *Geochim. Cosmochim. Acta* 62, 3239–3257. doi: 10.1016/s0016-7037(98)00243-9

Gagen, E. J., Zaugg, J., Tyson, G. W., and Southam, G. (2019). Goethite reduction by a neutrophilic member of the alphaproteobacterial genus *Telmatospirillum*. *Front. Microbiol.* 10:2938. doi: 10.3389/fmicb.2019.02938

Gault, A. G., Ibrahim, A., Langley, S., Renaud, R., Takahashi, Y., Boothman, C., et al. (2011). Microbial and geochemical features suggest iron redox cycling within bacteriogenic iron oxide-rich sediments. *Chem. Geol.* 281, 41–51. doi: 10.1016/j.chemgeo.2010.11.027

Ghorbanzadeh, N., Lakzian, A., Halajnia, A., Choi, U. K., Kim, K. H., Kim, J. O., et al. (2017). Impact of bioreduction on remobilization of adsorbed cadmium on iron minerals in anoxic condition. *Water Environ. Res.* 89, 519–526. doi: 10.2175/106143017x14902968254449

Han, R., Liu, T., Li, F., Li, X., Chen, D., and Wu, Y. (2018). Dependence of secondary mineral formation on Fe (II) production from ferrihydrite reduction by *Shewanella oneidensis* MR-1. *ACS Earth Space Chem.* 2, 399–409. doi: 10.1021/acsearthspacechem.7b00132

Hansel, C. M., Benner, S. G., Nico, P., and Fendorf, S. (2004). Structural constraints of ferric (hydr) oxides on dissimilatory iron reduction and the fate of Fe (II). *Geochim. Cosmochim. Acta* 68, 3217–3229. doi: 10.1016/j.gca.2003.10.041

Hong, C., Si, Y., Xing, Y., and Li, Y. (2015). Illumina MiSeq sequencing investigation on the contrasting soil bacterial community structures in different iron mining areas. *Environ. Sci. Pollut. Res.* 22, 10788–10799. doi: 10.1007/s11356-015-4186-3

Hori, T., Aoyagi, T., Itoh, H., Narihiro, T., Oikawa, A., Suzuki, K., et al. (2015). Isolation of microorganisms involved in reduction of crystalline iron (III) oxides in natural environments. *Front. Microbiol.* 6:386. doi: 10.3389/fmicb.2015.00386

Huguet, L. (2009). *Caractérisation Biogéochimique et Potentiel de Méthylation du Mercure de Biofilms en Milieu Tropical (Retenue de Petit Saut et estuaire du Sinnamary, Guyane Française)*. Doctoral dissertation, Nancy 1, Nancy.

Ivanova, E. P., Gorshkova, N. M., Bowman, J. P., Lysenko, A. M., Zhukova, N. V., Sergeev, A. F., et al. (2004). *Shewanella pacifica* sp. nov., a polyunsaturated fatty acid-producing bacterium isolated from sea water. *Int. J. Syst. Evol. Microbiol.* 54(Pt 4), 1083–1087. doi: 10.1099/ijs.0.02993-0

Jiang, Z., Shi, M., and Shi, L. (2020). Degradation of organic contaminants and steel corrosion by the dissimilatory metal-reducing microorganisms *Shewanella* and *Geobacter* spp. *Int. Biodeterior. Biodegradation* 147:104842. doi: 10.1016/j.ibiod.2019.104842

Kim, S.-J., Koh, D.-C., Park, S.-J., Cha, I.-T., Park, J.-W., Na, J.-H., et al. (2012). Molecular analysis of spatial variation of iron-reducing bacteria in riverine alluvial aquifers of the Mankyeong River. *J. Microbiol.* 50, 207–217. doi: 10.1007/s12275-012-1342-z

Kotloski, N. J., and Gralnick, J. A. (2013). Flavin electron shuttles dominate extracellular electron transfer by *Shewanella oneidensis*. *MBio* 4:e00553-12. doi: 10.1128/mBio.00553-12

Kwon, M. J., O'Loughlin, E. J., Boyanov, M. I., Brulc, J. M., Johnston, E. R., Kemner, K. M., et al. (2016). Impact of organic carbon electron donors on microbial community development under iron-and sulfate-reducing conditions. *PLoS One* 11:e0146689. doi: 10.1371/journal.pone.0146689

Larsen, O., and Postma, D. (2001). Kinetics of reductive bulk dissolution of lepidocrocite, ferrihydrite, and goethite. *Geochim. Cosmochim. Acta* 65, 1367–1379. doi: 10.1016/s0016-7037(00)00623-2

Leang, C., Qian, X., Mester, T., and Lovley, D. R. (2010). Alignment of the c-type cytochrome OmcS along pili of *Geobacter sulfurreducens*. *Appl. Environ. Microbiol.* 76, 4080–4084. doi: 10.1128/aem.00023-10

Lentini, C. J., Wankel, S. D., and Hansel, C. M. (2012). Enriched iron (III)-reducing bacterial communities are shaped by carbon substrate and iron oxide mineralogy. *Front. Microbiol.* 3:404. doi: 10.3389/fmicb.2012.00404

Levar, C. E., Hoffman, C. L., Dunshee, A. J., Toner, B. M., and Bond, D. R. (2017). Redox potential as a master variable controlling pathways of metal reduction by *Geobacter sulfurreducens*. *ISME J.* 11, 741–752. doi: 10.1038/ismej.2016.146

Leyva-Díaz, J. C., Poyatos, J. M., Barghini, P., Gorrasi, S., and Fenice, M. (2017). Kinetic modeling of *Shewanella baltica* KB30 growth on different substrates through respirometry. *Microb. Cell Fact.* 16:189.

Li, B.-B., Cheng, Y.-Y., Fan, Y.-Y., Liu, D.-F., Fang, C.-Y., Wu, C., et al. (2018). Estimates of abundance and diversity of *Shewanella* genus in natural and engineered aqueous environments with newly designed primers. *Sci. Total Environ.* 637-638, 926–933. doi: 10.1016/j.scitotenv.2018.05.051

Li, X., Liu, T., Li, F., Zhang, W., Zhou, S., and Li, Y. (2012). Reduction of structural Fe (III) in oxyhydroxides by *Shewanella* decolorationis S12 and characterization of the surface properties of iron minerals. *J. Soils Sediments* 12, 217–227. doi: 10.1007/s11368-011-0433-5

Liu, C., Kota, S., Zachara, J. M., Fredrickson, J. K., and Brinkman, C. K. (2001). Kinetic analysis of the bacterial reduction of goethite. *Environ. Sci. Technol.* 35, 2482–2490. doi: 10.1021/es001956c

Liu, H., Li, P., Zhu, M., Wei, Y., and Sun, Y. (2007). Fe (II)-induced transformation from ferrihydrite to lepidocrocite and goethite. *J. Solid State Chem.* 180, 2121–2128. doi: 10.1016/j.jssc.2007.03.022

Liu, X., Ye, Y., Xiao, K., Rensing, C., and Zhou, S. (2019). Molecular evidence for the adaptive evolution of *Geobacter sulfurreducens* to perform dissimilatory iron reduction in natural environments. *Mol. Microbiol.* 113, 783–793. doi: 10.1111/mmi.14443

Lovley, D. (2006). Dissimilatory Fe (III)-and Mn (IV)-reducing prokaryotes. *Prokaryotes* 2, 635–658. doi: 10.1007/0-387-30742-7_21

Lovley, D. R. (1991). Dissimilatory Fe (III) and Mn (IV) reduction. *Microbiol. Mol. Biol. Rev.* 55, 259–287. doi: 10.1128/mmbr.55.2.259-287.1991

Lovley, D. R. (2000). "Fe (III) and Mn (IV) reduction," in *Environmental Microbe-Metal Interactions*, ed. D. R. Lovley (Washington, DC: American Society of Microbiology), 3–30.

Lovley, D. R., Phillips, E. J., and Lonergan, D. J. (1989). Hydrogen and formate oxidation coupled to dissimilatory reduction of iron or manganese by *Alteromonas putrefaciens*. *Appl. Environ. Microbiol.* 55, 700–706. doi: 10.1128/aem.55.3.700-706.1989

Lovley, D. R., Stolz, J. F., Nord, G. L., and Phillips, E. J. (1987). Anaerobic production of magnetite by a dissimilatory iron-reducing microorganism. *Nature* 330, 252–254. doi: 10.1038/330252a0

Mamindy-Pajany, Y., Bataillard, P., Séby, F., Crouzet, C., Moulin, A., Guezennec, A.-G., et al. (2013). Arsenic in marina sediments from the Mediterranean coast: speciation in the solid phase and occurrence of thioarsenates. *Soil Sediment Contam.* 22, 984–1002. doi: 10.1080/15320383.2013.770441

Meile, C., and Scheibe, T. D. (2019). Reactive transport modeling of microbial dynamics. *Elements* 15, 111–116. doi: 10.2138/gselements.15.2.111

Melton, E. D., Swanner, E. D., Behrens, S., Schmidt, C., and Kappler, A. (2014). The interplay of microbially mediated and abiotic reactions in the biogeochemical Fe cycle. *Nat. Rev. Microbiol.* 12, 797–808. doi: 10.1038/nrmicro3347

Mercier, A., Joulian, C., Michel, C., Auger, P., Coulon, S., Amalric, L., et al. (2014). Evaluation of three activated carbons for combined adsorption and biodegradation of PCBs in aquatic sediment. *Water Res.* 59, 304–315. doi: 10.1016/j.watres.2014.04.021

Murti, G. K., Volk, V., and Jackson, M. (1966). Colorimetric determination of iron of mixed valency by orthophenanthroline. *Soil Sci. Soc. Am. J.* 30, 663–664. doi: 10.2136/sssaj1966.03615995003000050037x

Nealson, K. H. (2017). Bioelectricity (electromicrobiology) and sustainability. *Microb. Biotechnol.* 10, 1114–1119. doi: 10.1111/1751-7915.12834

Nevin, K. P., and Lovley, D. R. (2002). Mechanisms for Fe (III) oxide reduction in sedimentary environments. *Geomicrobiol. J.* 19, 141–159. doi: 10.1080/01490450252864253

Nogi, Y., Kato, C., and Horikoshi, K. (1998). Taxonomic studies of deep-sea barophilic *Shewanella* strains and description of *Shewanella violacea* sp. nov. *Arch. Microbiol.* 170, 331–338. doi: 10.1007/s002030050650

Pedersen, H. D., Postma, D., Jakobsen, R., and Larsen, O. (2005). Fast transformation of iron oxyhydroxides by the catalytic action of aqueous Fe (II). *Geochim. Cosmochim. Acta* 69, 3967–3977. doi: 10.1016/j.gca.2005.03.016

Poggenburg, C., Mikutta, R., Sander, M., Schippers, A., Marchanka, A., Dohrmann, R., et al. (2016). Microbial reduction of ferrihydrite-organic matter coprecipitates by *Shewanella putrefaciens* and *Geobacter metallireducens* in comparison to mediated electrochemical reduction. *Chem. Geol.* 447, 133–147. doi: 10.1016/j.chemgeo.2016.09.031

Roden, E. E. (2006). Geochemical and microbiological controls on dissimilatory iron reduction. *C. R. Geosci.* 338, 456–467. doi: 10.1016/j.crte.2006.04.009

Roden, E. E., Sobolev, D., Glazer, B., and Luther, G. W. (2004). Potential for microscale bacterial Fe redox cycling at the aerobic-anaerobic interface. *Geomicrobiol. J.* 21, 379–391. doi: 10.1080/01490450490485872

Roden, E. E., and Wetzel, R. G. (2002). Kinetics of microbial Fe (III) oxide reduction in freshwater wetland sediments. *Limnol. Oceanogr.* 47, 198–211. doi: 10.4319/lo.2002.47.1.0198

Schilling, K., Borch, T., Rhoades, C. C., and Pallud, C. E. (2019). Temperature sensitivity of microbial Fe (III) reduction kinetics in subalpine wetland soils. *Biogeochemistry* 142, 19–35. doi: 10.1007/s10533-018-0520-4

Schwertmann, U. (1973). Use of oxalate for Fe extraction from soils. *Can. J. Soil Sci.* 53, 244–246. doi: 10.4141/cjss73-037

Schwertmann, U., and Cornell, R. M. (2008). *Iron Oxides in the Laboratory: Preparation and Characterization*. Hoboken, NJ: John Wiley & Sons.

Schwertmann, U., and Taylor, R. M. (1979). Natural and synthetic poorly crystallized lepidocrocite. *Clay Miner.* 14, 285–293. doi: 10.1180/claymin.1979.014.4.05

Shelobolina, E. S., Nevin, K. P., Blakeney-Hayward, J. D., Johnsen, C. V., Plaia, T. W., and Krader, P. (2007). *Geobacter pickeringii* sp. nov., *Geobacter argillaceus* sp. nov. and *Pelosinus fermentans* gen. nov., sp. nov., isolated from subsurface kaolin lenses. *Int. J. Syst. Evol. Microbiol.* 57(Pt 1), 126–135. doi: 10.1099/ijs.0.64221-0

Shi, L., Dong, H., Reguera, G., Beyenal, H., Lu, A., Liu, J., et al. (2016). Extracellular electron transfer mechanisms between microorganisms and minerals. *Nat. Rev. Microbiol.* 14, 651–662. doi: 10.1038/nrmicro.2016.93

Shi, M., Jiang, Y., and Shi, L. (2019). Electromicrobiology and biotechnological applications of the exoelectrogens *Geobacter* and *Shewanella* spp. *Sci. China Technol. Sci.* 62, 1670–1678. doi: 10.1007/s11431-019-9509-8

Snoeyenbos-West, O., Nevin, K., Anderson, R., and Lovley, D. (2000). Enrichment of *Geobacter* species in response to stimulation of Fe (III) reduction in sandy aquifer sediments. *Microb. Ecol.* 39, 153–167. doi: 10.1007/s002480000018

Stern, N., Mejia, J., He, S., Yang, Y., Ginder-Vogel, M., and Roden, E. E. (2018). Dual role of humic substances as electron donor and shuttle for dissimilatory iron reduction. *Environ. Sci. Technol.* 52, 5691–5699. doi: 10.1021/acs.est.7b06574

Su, C., Zhang, M., Lin, L., Yu, G., Zhong, H., and Chong, Y. (2020). Reduction of iron oxides and microbial community composition in iron-rich soils with different organic carbon as electron donors. *Int. Biodeterior. Biodegradation* 148:104881. doi: 10.1016/j.ibiod.2019.104881

RStudio Team (2015). *RStudio: Integrated Development for R*. Boston, MA: RStudio Inc., 700.

Thompson, A., Chadwick, O. A., Rancourt, D. G., and Chorover, J. (2006). Iron-oxide crystallinity increases during soil redox oscillations. *Geochim. Cosmochim. Acta* 70, 1710–1727. doi: 10.1016/j.gca.2005.12.005

Thouin, H., Le Forestier, L., Gautret, P., Hube, D., Laperche, V., Dupraz, S., et al. (2016). Characterization and mobility of arsenic and heavy metals in soils polluted by the destruction of arsenic-containing shells from the Great War. *Sci. Total Environ.* 550, 658–669. doi: 10.1016/j.scitotenv.2016.01.111

Urrutia, M., Roden, E., Fredrickson, J., and Zachara, J. (1998). Microbial and surface chemistry controls on reduction of synthetic Fe (III) oxide minerals by the dissimilatory iron−reducing bacterium *Shewanella alga*. *Geomicrobiol. J.* 15, 269–291. doi: 10.1080/01490459809378083

Usman, M., Hanna, K., Abdelmoula, M., Zegeye, A., Faure, P., and Ruby, C. (2012). Formation of green rust via mineralogical transformation of ferric oxides (ferrihydrite, goethite and hematite). *Appl. Clay Sci.* 64, 38–43. doi: 10.1016/j.clay.2011.10.008

Wilkins, M. J., Livens, F. R., Vaughan, D. J., and Lloyd, J. R. (2006). The impact of Fe (III)-reducing bacteria on uranium mobility. *Biogeochemistry* 78, 125–150. doi: 10.1007/s10533-005-3655-z

Wolf, M., Kappler, A., Jiang, J., and Meckenstock, R. U. (2009). Effects of humic substances and quinones at low concentrations on ferrihydrite reduction by *Geobacter metallireducens*. *Environ. Sci. Technol.* 43, 5679–5685. doi: 10.1021/es803647r

Wu, Y., Luo, X., Qin, B., Li, F., Haggblom, M. M., and Liu, T. (2020). Enhanced current production by exogenous electron mediators via synergy of promoting biofilm formation and the electron shuttling process. *Environ. Sci. Technol.* 54, 7217–7225. doi: 10.1021/acs.est.0c00141

Zachara, J. M., Kukkadapu, R. K., Fredrickson, J. K., Gorby, Y. A., and Smith, S. C. (2002). Biomineralization of poorly crystalline Fe (III) oxides by dissimilatory metal reducing bacteria (DMRB). *Geomicrobiol. J.* 19, 179–207. doi: 10.1080/01490450252864271

Zhang, C., Ge, Y., Yao, H., Chen, X., and Hu, M. (2012). Iron oxidation-reduction and its impacts on cadmium bioavailability in paddy soils: a review. *Front. Environ. Sci. Eng.* 6, 509–517. doi: 10.1007/s11783-012-0394-y

Zhu, Y., Wang, H., Li, X., Hu, C., Yang, M., and Qu, J. (2014). Characterization of biofilm and corrosion of cast iron pipes in drinking water distribution system with UV/Cl2 disinfection. *Water Res.* 60, 174–181. doi: 10.1016/j.watres.2014.04.035

Zhuang, K., Izallalen, M., Mouser, P., Richter, H., Risso, C., Mahadevan, R., et al. (2011). Genome-scale dynamic modeling of the competition between *Rhodoferax* and *Geobacter* in anoxic subsurface environments. *ISME J.* 5, 305–316. doi: 10.1038/ismej.2010.117

Ziemke, F., Höfle, M. G., Lalucat, J., and Rossellö-Mora, R. (1998). Reclassification of *Shewanella putrefaciens* Owen's genomic group II as *Shewanella baltica* sp. nov. *Int. J. Syst. Evol. Microbiol.* 48, 179–186. doi: 10.1099/00207713-48-1-179

Conflict of Interest: The authors declare that the research was conducted in the absence of any commercial or financial relationships that could be construed as a potential conflict of interest.

frontiers in Microbiology

ORIGINAL RESEARCH
published: 14 December 2020
doi: 10.3389/fmicb.2020.601907

The Weathering Microbiome of an Outcropping Granodiorite

Stephanie A. Napieralski and Eric E. Roden**

Department of Geoscience, University of Wisconsin-Madison, Madison, WI, United States

Microorganisms have long been recognized for their capacity to catalyze the weathering of silicate minerals. While the vast majority of studies on microbially mediated silicate weathering focus on organotrophic metabolism linked to nutrient acquisition, it has been recently demonstrated that chemolithotrophic ferrous iron [Fe(II)] oxidizing bacteria (FeOB) are capable of coupling the oxidation of silicate mineral Fe(II) to metabolic energy generation and cellular growth. In natural systems, complex microbial consortia with diverse metabolic capabilities can exist and interact to influence the biogeochemical cycling of essential elements, including iron. Here we combine microbiological and metagenomic analyses to investigate the potential interactions among metabolically diverse microorganisms in the near surface weathering of an outcrop of the Rio Blanco Quartz Diorite (DIO) in the Luquillo Mountains of Puerto Rico. Laboratory based incubations utilizing ground DIO as metabolic energy source for chemolithotrophic FeOB confirmed the ability of FeOB to grow via the oxidation of silicate-bound Fe(II). Dramatically accelerated rates of Fe(II)-oxidation were associated with an enrichment in microorganisms with the genetic capacity for iron oxidizing extracellular electron transfer (EET) pathways. Microbially oxidized DIO displayed an enhanced susceptibility to the weathering activity of organotrophic microorganisms compared to unoxidized mineral suspensions. Our results suggest that chemolithotrophic and organotrophic microorganisms are likely to coexist and contribute synergistically to the overall weathering of the *in situ* bedrock outcrop.

Keywords: iron oxidation, weathering, chemolithotrophy, metagenomics, extracellular electron transfer (EET)

OPEN ACCESS

Edited by:
Bradley M. Tebo,
Oregon Health & Science University, United States

Reviewed by:
Eva Pakostova,
Coventry University, United Kingdom
Axel Schippers,
Federal Institute for Geosciences and Natural Resources, Germany

****Correspondence:***
Stephanie A. Napieralski
snapieralski@wisc.edu
Eric E. Roden
eroden@geology.wisc.edu

Specialty section:
This article was submitted to Microbiological Chemistry and Geomicrobiology, a section of the journal Frontiers in Microbiology

Received: *01 September 2020*
Accepted: *26 November 2020*
Published: *14 December 2020*

Citation:
Napieralski SA and Roden EE (2020) The Weathering Microbiome of an Outcropping Granodiorite. Front. Microbiol. 11:601907. doi: 10.3389/fmicb.2020.601907

INTRODUCTION

The weathering of Earth's continental crust involves a complex set of physical, geochemical, and biological reactions. As microorganisms are ubiquitous in soils and sedimentary environments, often preferentially associated with mineral surfaces (Hazen et al., 1991) they have vast potential to enhance mineral weathering thus impacting the cycling of bioessential elements between the lithosphere and the biosphere. Microbiological impacts on weathering processes, from the aid in physical disaggregation by mechanical forcing to enhancement of chemical dissolution have long been recognized and are extensively described (Banfield et al., 1999; Uroz et al., 2009). Well established mechanisms of microbially enhanced mineral dissolution revolve around organotrophic metabolisms, where microorganisms solubilize mineral components to meet their nutritional needs for conveyance of a growth benefit (Bennett et al., 2001) and provide valuable ecosystem services for higher biota (Calvaruso et al., 2006; Lambers et al., 2009). Acidolysis and chelation by organic

acids (Drever and Stillings, 1997; Uroz et al., 2009) as well as siderophores (Kalinowski et al., 2000; Liermann et al., 2000; Buss et al., 2007) have been extensively invoked when relating microbial activity to mineral weathering.

Redox active elements, such as Fe, are often present in igneous rocks. If Fe constitutes a considerable component of the mineral structure, redox reactions can occur prior to bulk dissolution if the kinetics of electron transfer are faster than structural disintegration (White, 1990). Oxidation of structural Fe(II) is in fact often rate limiting in terms of Fe(II) mineral weathering (Hering and Stumm, 1990). Fe(II) silicate minerals in fresh rock, in disequilibrium with Earth's oxidizing surficial environment, represent a vast supply of electrons to potentially fuel microbial metabolism and growth, including by chemolithotrophic Fe(II)-oxidizing bacteria (FeOB). FeOB are known to occupy distinct environmental niches where opposing gradients of ferrous iron [Fe(II)] and oxidants (e.g., O_2) intersect, such as aquatic sediments, freshwater iron seeps, and hydrothermal vents (Sobolev and Roden, 2002; Roden et al., 2004; Emerson et al., 2010). By analogy, the interface between reduced igneous rock and the oxidizing atmosphere represents such a gradient, albeit a very sharp, solid phase one, that theoretically can provide energy to fuel biomass production (Jakosky and Shock, 1998; Buss et al., 2005; Shock, 2009). While studies have suggested that FeOB are capable of direct utilization of the structural Fe(II) in silicate minerals (Popa et al., 2012; Roden, 2012; Shelobolina et al., 2012b) and glasses (Bailey et al., 2009; Henri et al., 2015), only recently has the ability of FeOB to utilize crystalline silicate-bound Fe(II) in rocks for metabolic energy generation and subsequent growth been demonstrated (Napieralski et al., 2019). By combining microbiological and metagenomic based approaches, Napieralski et al. (2019) demonstrated that FeOB can dramatically accelerate the oxidation of silicate mineral bound Fe(II) via extracellular electron transfer (EET) coupled to cellular growth, and that the subsequent oxidative weathering of the minerals biotite and hornblende within granitic rocks resulted in subtle changes to the surface structure that rendered the mineral more susceptible to proton promoted dissolution via dilute acid. While not explicitly demonstrated, the redox driven mineralogical transformations associated with FeOB activity should then also affect the efficiency at which organotrophic microorganisms are able to solubilize cations for nutritional purposes.

It is important to consider the entire suite of biogeochemical reactions that may be mediated by complex microbial communities in natural systems. Our previous work specifically investigated the role of chemolithotrophic FeOB in the subsurface (ca. 8 m) weathering of the Rio Blanco Quartz Diorite (Napieralski et al., 2019), well below the rooting zone where organic carbon content is minimal. In contrast, the near surface, where inputs from plant derived organic matter are of substantial concern (Banfield et al., 1999), a more complex interplay between organotrophically and lithotrophically mediated processes may be involved in the weathering of Fe(II)-silicates. In order to address this potential interplay, samples were collected for enrichment culturing and metagenomic analysis from near-surface outcrop of the rapidly weathering Rio Blanco Quartz Diorite of the Luquillo Mountains, Puerto Rico (Buss et al., 2008; **Figure 1**). After establishment, Fe(II)-silicate oxidizing enrichment cultures were amended with additional carbon to assess the degree to which prior lithotrophic activity might enhance the cation solubilizing ability of organotrophic microorganisms. Our results indicate that chemolithotrophic and organotrophic microorganisms can coexist and work synergistically to enhance the weathering of near surface silicate rock.

MATERIALS AND METHODS

Field Sampling

In June of 2017, samples were collected from a road cut exposure of the Rio Blanco Quartz Diorite (abbreviated hereafter as "DIO") previously described by Buss et al. (2008) (See **Figure 1**). Rindlets nearest the weathering corestone were carefully excavated using a rock hammer and spatula previously sterilized by ethanol soaking and flame and placed into sterile Whirlpack bags. Samples were then placed in coolers and shipped overnight to The University of Wisconsin-Madison where portions were promptly placed at −80°C and 4°C for DNA extraction and enrichment culturing, respectively.

Chemolithotrophic Enrichment Culturing

Chemolithotrophic Fe(II)-oxidizing cultures were established as previously described with DIO and Fe(II)-free quartz sand (QTZ) (Napieralski et al., 2019). Briefly, 5.0 g of ground and sieved (<45 μM) DIO or quartz sand (Acros Chemicals 140–381 μm) were added to 50 mL of Luquillo artificial ground water (L-AGW), autoclaved anoxically, and aerated with sterile air. 5 v/v% CO_2 was added to the headspace and the appropriate bottles were inoculated with ca. 1.0 g of material from the DIO outcrop that had been aseptically fragmented. No mineral amendment controls were also prepared by adding ca. 1.0 g of inocula to 50 mL of L-AGW without additional minerals (NoMin). Samples were taken immediately following inoculation and at 41, 82, 105, 130, 182, 252, 334, and 615 days for analyses as described below.

Organotrophic Incubations

After 615 days of initial chemolithotrophic incubation, 5.0 mL of DIO from one replicate (to ensure consistency of substrate) of both live/inoculated and abiotic control reactors was removed and the solids separated via centrifugation. The aqueous phase was discarded, and the solids were resuspended in 40 mL of fresh L-AGW. The resultant slurries (temporarily denoted as DIO-Ox and DIO-Cont) were each transferred in equal amounts (20 mL) to two sterile bottles. The bottles were reseeded with ca. 0.1 g of DIO outcrop material and 1.0 mM of filter sterilized glucose was added; these reactors are referred to as DIO-Ox + Glu-Inoc and DIO-Cont + Glu-Inoc. For abiotic controls, 5.0 mL of the second replicate of the abiotic control from the chemolithotrophic incubations was similarly prepared in fresh L-AGW with glucose but was left uninoculated; these reactors are referred to as DIO-Cont + Gluc-Sterile (see **Figure 2**). Samples were taken at T_0,

FIGURE 1 | Outcrop scale photo of a weathering corestone of Rio Blanco Quartz Diorite exposed by road cutting **(A)**. The corestone exhibits spheroidal weathering, with partially altered "rindlets" surrounding the unaltered rock **(B)**. Material for this study was collected near the rindlet-corestone interface **(C)**. Pocket knife for scale (ca. 9 cm).

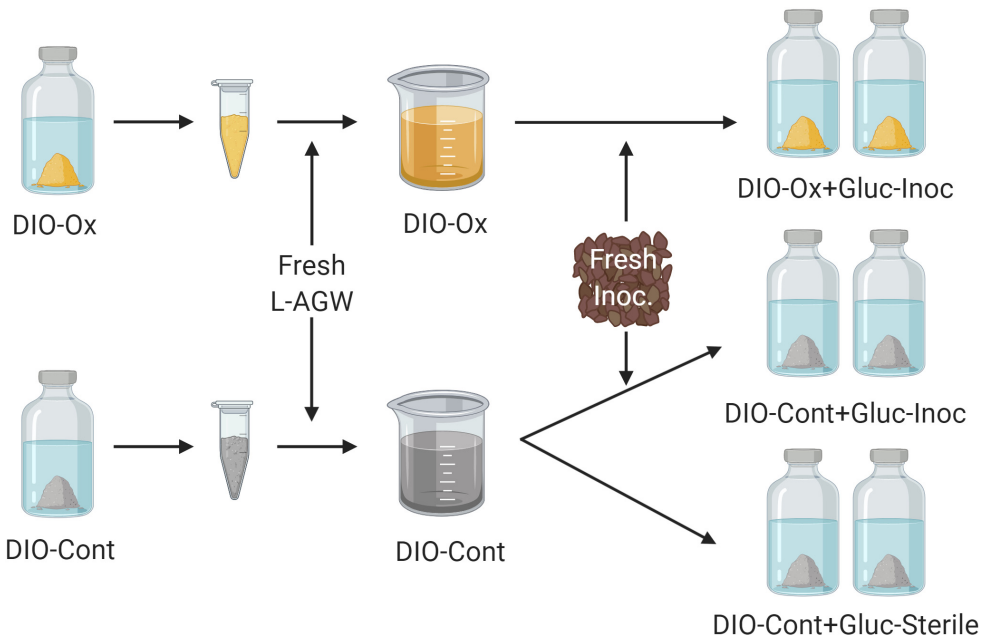

FIGURE 2 | Conceptual cartoon of the generation of organotrophic incubations. The solids were isolated from the initial lithotrophic incubations for both live inoculated (DIO-Ox) and uninoculated control experiments (DIO-Cont) and resuspended in fresh Luquillo artificial river water (L-AGW). The resultant slurries were divided into duplicate reactors, and either reinoculated (Inoc) or left as a sterile control and stoppered. 1.0 mM filter sterilized glucose (Gluc) was added to each reactor via needle and syringe.

and after 1, 3, 14, 28, and 60 days of incubation for the analyses described below.

Analytical Methods

ATP

ATP content of enrichment cultures was determined via luminescence using BacTiter-Glo^{TM} (Promega, Madison, WI, United States) as previously described (Napieralski et al., 2019).

Solid-Phase Fe(II)

The ratio of Fe(II) to total Fe released by 0.5 M HCl extraction was determined on the solid phase of 1.0 mL of total enrichment culture subsamples. The solids were separated via centrifugation and extracted for 24 h in 5 mL of 0.5 M HCl on an orbital shaker. Fe(II) of each extract was determined by the standard Ferrozine assay (Stookey, 1970) and the measurement was repeated after the addition of hydroxylamine-HCl for determination of Fe(total).

Cations

The aqueous phase from duplicate reactors was pooled, diluted 1:5 in 5 mM HNO_3 and filtered through a 0.22 μm filter. Major cation concentrations (Ca, K, Mg, and Na) were determined using inductively coupled plasma optical emission spectroscopy (ICP-OES).

Particulate Organic Matter

The POC content of triplicate samples of the weathered material at the rindlet-corestone interface (see **Figure 1C**) used to establish initial enrichment cultures was determined via high temperature combustion utilizing a Flash EA 1112 Flash Combustion Analyzer.

DNA Extraction, Metagenomic Sequencing, and Assembly

DNA was extracted from duplicate outcrop (Gb-OC) and 182 days enrichment culture material (DIO-Inoc, QTZ-Inoc, and NoMin-Inoc) utilizing previously described (Napieralski et al., 2019) adaptations to the SDS-based DNA extraction method of Zhou et al. (1996). DNA was submitted to the University of Wisconsin-Madison Biotechnology Sequencing Center for shotgun metagenomic library preparation and 2 × 250 sequencing on the Illumina HiSeq 2500 rapid platform. Raw reads were quality filtered using the default parameters Trim-Galore. Concatenated reads from all samples were assembled using IDBA-UD (Peng et al., 2012) utilizing the high-performance computing cluster at the Center for High Throughput Computing at University of Wisconsin-Madison.

Metagenomic Analysis

Metagenome assembled genomes (MAGs) were obtained from the metagenomic co-assembly using the Bin Refinement module of metaWRAP (Uritskiy et al., 2018) with initial bin sets generated using MetaBat2 (Kang et al., 2019) and Concoct (Alneberg et al., 2014). Quality, completion and initial taxonomy of refined MAGs were assessed using CheckM (Parks et al., 2015). Final consensus taxonomy of MAGs was determined using the Classify Bins module of metaWRAP and extraction of essential single-copy genes as described by He et al. (2016) for each MAG. The relative abundance of each MAG (genomes per million reads) across all samples in the co-assembly was determined using the Bin Quantification module of metaWRAP. Open reading frames (ORFs) were predicted and annotated using Prokka (Seemann, 2014). Subcellular location of putative proteins was predicted using Cello (Yu et al., 2006). Putative extracellular electron transfer (EET) pathways for iron oxidation were identified as previously described (He et al., 2017) using BLASTP and HMMsearch for homologs to the Cyc2-type system of *Acidithiobacillus ferrooxidans* (Castelle et al., 2008) and MtoAB of *Sideroxydans lithotrophicus* ES-1 (Liu et al., 2012). Putative siderophore biosynthesis pathways were identified using HMMsearch for the PFAMs associated with non-ribosomal peptide synthesis (NRPS) condensation and adenylation domains as well as the conserved IucAC domains of NPRS-independent synthesis (NIS) (Hopkinson and Barbeau, 2012). Selected MAGs were investigated for the presence of carbohydrate active enzymes using the dbCAN webserver (Yin et al., 2012).

RESULTS

Initial Chemolithotrophic Enrichment

Over the course of the 615-days chemolithotrophic incubation, Fe(II)/Fe(total) declined from an average of 0.857 to 0.664 in the live DIO reactors; no systematic change in Fe(II)/Fe(total) was observed in sterile, abiotic controls (**Figure 3A**). The ATP content of all inoculated reactors decline precipitously from initial values of ca. 1.3 nM over the first 130 days of incubation (**Figure 3B**). In DIO cultures, ATP content stabilized at an average of ca. 0.6 nM for the duration of the experiment, whereas ATP continued to decline to ca. 0.13 and 0.15 nM in QTZ and NoMin (inoculum only) cultures, respectively. No net change in background ATP (abiotic control) was observed.

The release of major rock forming cations (Ca, Mg, K, and Na) was detected in all DIO amended reactors (**Figure 4**). Both Ca and Na concentrations showed a modest increase in net release in inoculated reactors relative to sterile abiotic controls (**Figures 4A,B**). Final Ca concentrations reached 0.124 and 0.160 mM in control and live inoculated reactors, respectively, corresponding to increases in concentration of 50 and 91 μM Ca over the course of the experiment. Final Na concentrations increased to 0.288 and 0.326 mM in the control and live reactors, respectively. Thus, 41 and 37 μM more Ca and Na, respectively, was released in the presence of a live inoculum relative to sterile controls. Ca and Na release was also detected in the

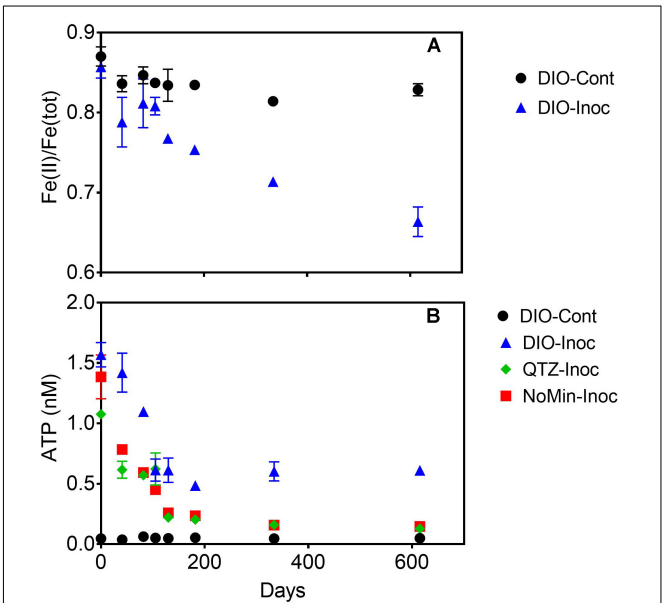

FIGURE 3 | Fe(II)/Fe(tot) of dilute HCl extractable Fe in abiotic uninoculated (DIO-Cont) and live inoculated (DIO-Inoc) diorite enrichment cultures **(A)**. ATP content (nM) of control DIO and inoculated DIO, quartz (QTZ), and inocula only (NoMin) cultures **(B)**. Data point and error bars denote the mean and range of duplicate reactors.

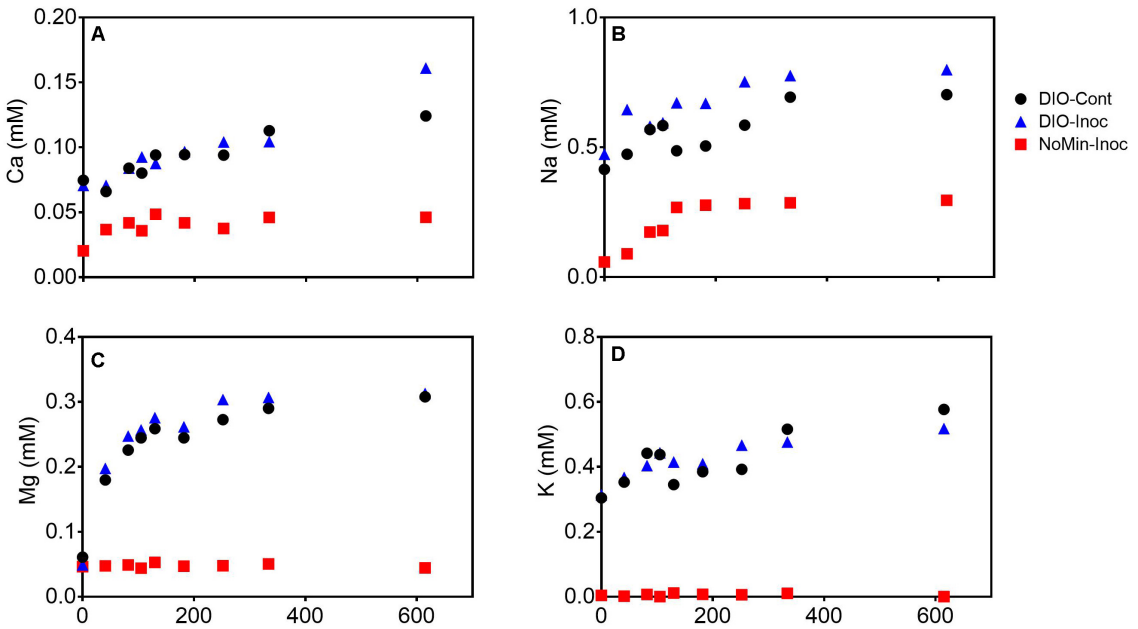

FIGURE 4 | Ca **(A)**, Na **(B)**, Mg **(C)**, and K **(D)** concentrations (mM) in pooled duplicate control (DIO-Cont), live inoculated (DIO-Inoc), and inocula only (NoMin-Inoc) reactors.

inoculum only NoMin reactors, indicating release from DIO in the inoculum. No difference in Mg concentration between control and live reactors was observed, nor was there any release of Mg in NoMin reactors (**Figure 4C**). K release was also not detected in NoMin reactors, and in contrast to Ca and Na, overall release of K was higher in abiotic reactors relative to live inoculated (**Figure 4D**), with 0.06 mM more K released in abiotic reactors over the course of the experiment.

Organotrophic Incubation

Addition of glucose to stimulate organotrophic metabolism after imposed chemolithotrophic conditions resulted in immediate cell growth, with ATP increasing to 6–7 nM in live reactors after 1 day (**Figure 5B**). After initial growth, ATP content of the reactors declined over the remaining 60 days to an average final concentration of ca. 1.1 nM. Small changes were observed in Fe(II)/Fe(tot) for both glucose amended reactor sets, declining from an average of 0.664 to 0.633 in live cultures containing microbially oxidized DIO from the previous chemolithotrophic enrichment culture (DIO-Ox + Gluc-Inoc), and from an average of 0.829 to 0.794 in live cultures containing unoxidized DIO from previous abiotic controls (DIO-Cont + Gluc-Inoc) (**Figure 5A**). No oxidation was observed in the glucose-amended abiotic control (DIO-Cont + Gluc-Sterile) containing DIO from previous abiotic controls.

The release of all cations was stimulated in live cultures containing both previously oxidized and unoxidized DIO relative to unoxidized abiotic controls (**Figure 6**). Average final concentrations and total release of Ca and Mg were slightly higher (ca. 0.04 mM) in live cultures containing previously oxidized DIO compared to unoxidized (**Figures 6A,C**). The opposite trend was observed in K release, with final K concentrations being an average of 0.040 mM higher in DIO-Cont + Gluc-Inoc reactors (**Figure 6D**). Final average Na concentrations overlapped within the error of the replicates, though an average of 0.022 mM more Na was released in DIO-Cont + Gluc-Inoc vs. DIO-Ox + Gluc-Inoc reactors (**Figure 6B**).

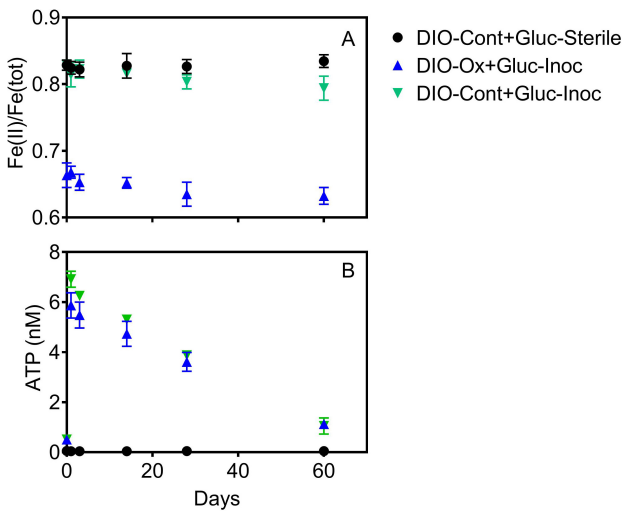

FIGURE 5 | Fe(II)/Fe(tot) **(A)** and ATP content **(B)** after supplementation with 1.0 mM glucose in live cultures containing microbially oxidized DIO from the previous chemolithotrophic enrichment culture (DIO-Ox-Gluc-Inoc), live cultures containing unoxidized DIO from previous abiotic controls (DIO-Cont-Gluc-Inoc), or sterile controls containing unoxidized DIO from previous abiotic controls (DIO-Cont + Gluc-Sterile).

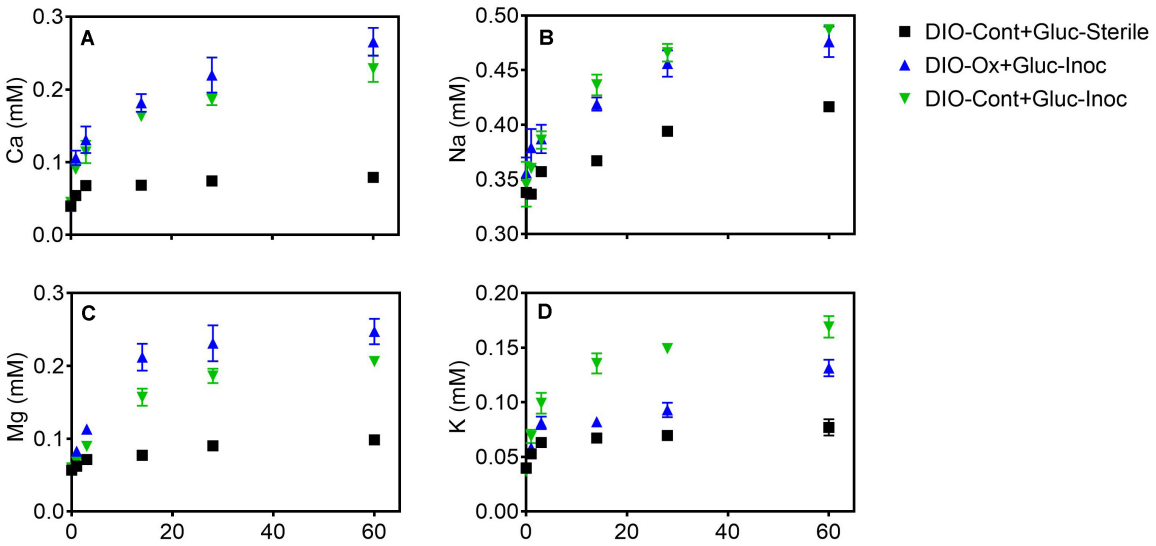

FIGURE 6 | Ca **(A)**, Na **(B)**, Mg **(C)**, and K **(D)** concentrations after supplementation with 1.0 mM glucose in live cultures containing microbially oxidized DIO from the previous chemolithotrophic enrichment culture (DIO-Ox-Gluc-Inoc), live cultures containing unoxidized DIO from previous abiotic controls (DIO-Cont-Gluc-Inoc), or sterile controls containing unoxidized DIO from previous abiotic controls (DIO-Cont + Gluc-Sterile).

Metagenomic Analysis

A total of 84 MAGs (>70% complete, <10% redundant) were obtained from the metagenomic co-assembly. Of these MAGs, 12 contained homologs to EET pathways putatively involved in Fe(II) oxidation, with nine MAGs containing Cyc2 homologs, three containing MtoAB, and one containing both. Of these putative FeOB MAGs, five also contained RuBisCO (**Figure 7**). In reactors amended with DIO, putative chemolithotrophic FeOB were enriched relative to the *in situ* samples and diorite free (NoMin and QTZ) reactors (**Figure 7**). The most abundant MAG in each replicate of the diorite oxidizing cultures was a putative chemolithoautotrophic γ-proteobacteria, most closely affiliated with the family *Acidiferrobacteraceae*. However, each replicate was dominated by a different *Acidiferrobacteraceae* MAG. While the most abundant MAG in DIO-OC-A contained homologs to both Cyc2 and MtoAB, the dominant MAG in DIO-OC-B contained only Cyc2. Putative siderophore biosynthesis pathways were identified in 9 MAGs (**Figure 7**). Compared to the diorite oxidizing enrichment cultures, MAGs containing putative siderophore biosynthesis pathways are overall more abundant *in situ*.

The two most abundant MAGs in both *in situ* libraries is a Sphingobacteriaceae, putatively of the genus *Mucilaginibacter* (**Figure 7**). In addition to containing a putative NRPS-type siderophore biosynthesis pathway, the *Mucilaginibacter* MAGs are enriched in carbohydrate active enzymes, particularly glycosyltransferases and glycoside hydrolases. Also abundant are β-proteobacteria, with four of the top 10 most abundant MAGs in both *in situ* metagenomes belonging to this class, three of which to the order *Burkholderiales*. In addition, two of the top 10 MAGs contain putative EET pathways but did not contain RuBisCO or other carbon fixation pathway, an MtoAB in a β-proteobacteria and Cyc2 in a *Nitrospiraceae*.

DISCUSSION

Initial Chemolithotrophic Enrichments

The results of this study confirm the previously reported (Napieralski et al., 2019) ability of chemolithotrophic microorganisms from the Rio Blanco quartz diorite weathering environment to catalyze oxidation of Fe(II)-silicate phases in fresh rock (**Figures 3A**, **5A**). In contrast to our previous findings, biologically enhanced release of Ca and Na was observed during initial chemolithotrophic incubation under all experimental conditions, including during incubation of endogenous DIO in the inoculum. Our 2019 study on the potential role of FeOB in DIO weathering utilized inocula from the subsurface rindlet-saprolite interface, well below the rooting zone where organic carbon content is very low (Buss et al., 2005). As such, transfer of labile organics and actively metabolizing organotrophic cells upon inoculation of enrichment cultures was likely to have been limited. The present study is thus fundamentally different in that the initial inoculum was obtained from a surficially exposed outcrop with visible roots and vegetation (see **Figure 1**), and organic matter was transferred into the enrichment cultures upon inoculation. The addition of 1.0 g of natural inoculum with an average POC content of 0.269 ± 0.012 wt% to the 50 mL reactors would result in an initial average organic carbon content of 4.48 ± 0.18 mM, representing a maximum possible amount of carbon, though the bioavailable fraction may be less. While it is well established that microorganisms can enhance the release of major rock forming cations from granitic material in the presence of glucose amendments (Wu et al., 2008; Frey et al., 2010), similar results have also been noted in a study of granitic gneisses and diorites incubated with only natural sediment and glacial waters without carbon or other nutrient amendment (Montross et al., 2013). These results indicate that even small

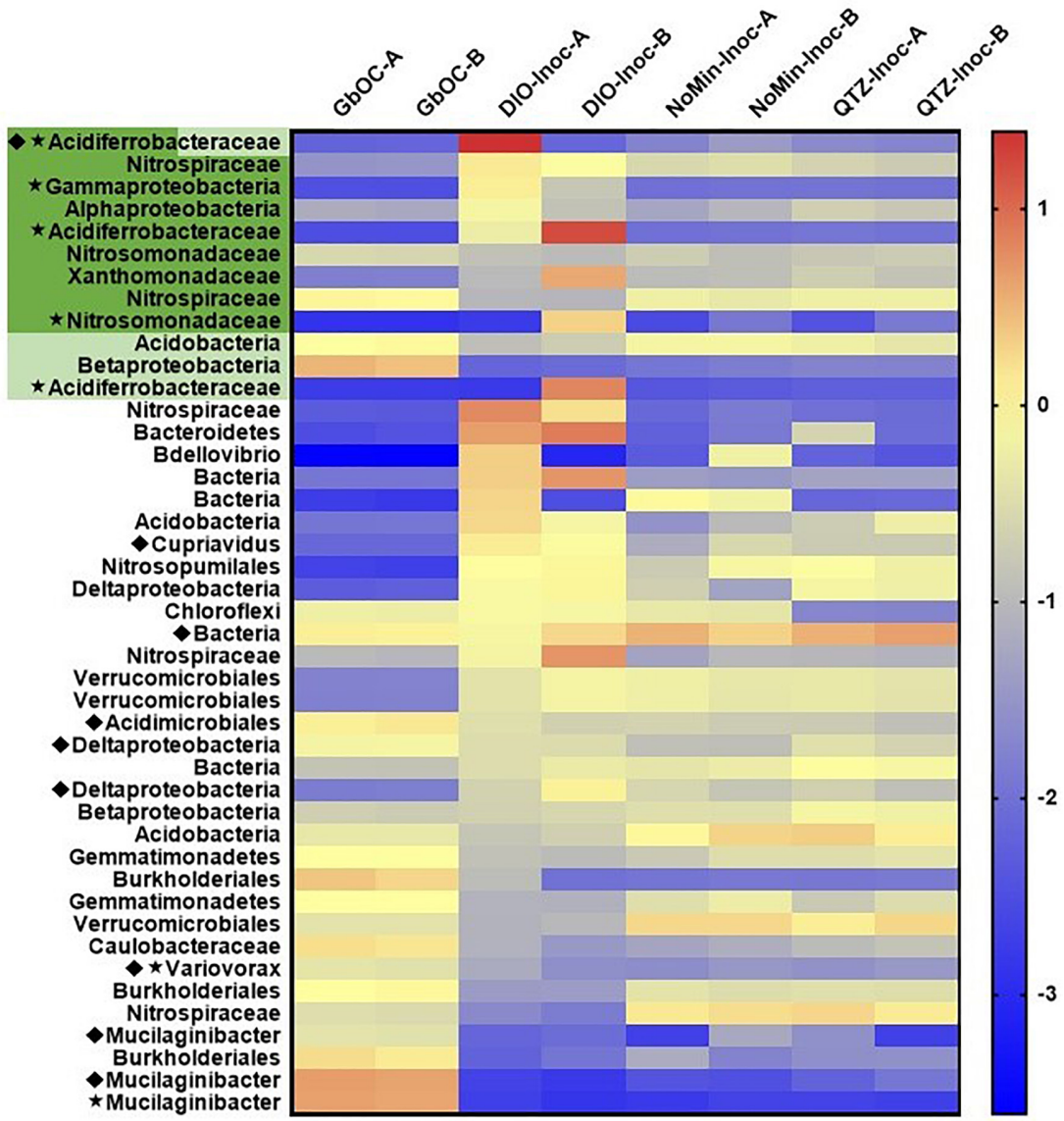

FIGURE 7 | Heat map of the abundance (log genomes per million reads) of selected MAGs (the 10 most abundant MAGs in each sample and all MAGs with EET and siderophore biosynthesis pathways) across all samples in the metagenomic co-assembly including duplicate *in situ* outcrop (GbOC) and duplicate inocula only (NoMin-Inoc), quartz (QTZ-Inoc) and diorite (DIO-Inoc) enrichment cultures. Putative FeOB are highlighted, with the presence of Cyc2 homologs in dark green and MtoAB in light green. The presence of RuBisCO is indicated by a star and siderophore biosynthesis by a diamond.

amounts of naturally derived, potentially more complex forms of organic carbon are capable of supporting microbially enhanced mineral dissolution.

Due to the input of carbon and active organotrophic biomass in the inoculum, we are presently unable to directly link oxidation of the DIO to FeOB growth. ATP concentrations declined over time in all inoculated reactors (**Figure 3**), which suggests that microbial growth coupled to Fe(II) oxidation was insufficient to compensate for the decline in organotrophic biomass initially present in the inoculum. These results are consistent with a recent study utilizing microbially colonized shale for the establishment of chemolithotrophic pyrite-oxidizing enrichment cultures (Napieralski, 2020). Nevertheless, the rate and extent of the decline in ATP concentration was lower in reactors amended with DIO compared to those without added DIO (QTZ and NoMin; see **Figure 3**), suggestive of ATP generation linked to chemolithotrophic metabolism. The final "steady-state" ATP concentration of ca. 0.6 nM observed here is comparable to that reported by Napieralski et al. (2019) in the previous study on the chemolithotrophic oxidation of the DIO, where growth yield calculations were consistent with previously reported for yields for FeOB in opposing gradient media (Sobolev and Roden, 2004). Thus, the accelerated oxidation of mineral-associated Fe(II) (**Figure 2**) and presence and enrichment of multiple MAGs

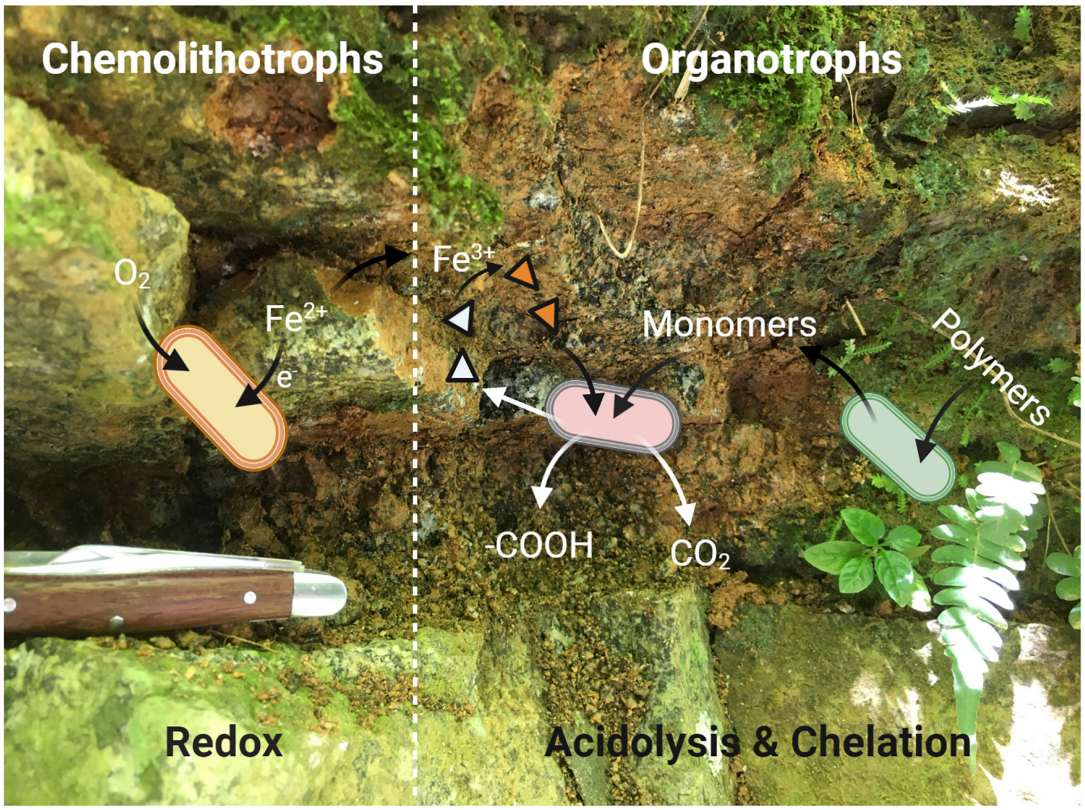

FIGURE 8 | A simplified conceptual cartoon of the potential interactions between members of the "weathering microbiome" of a surficial exposure of the Rio Blanco Quartz Diorite, based on the mechanisms of microbial weathering described by Uroz et al. (2009). Redox based weathering is performed via chemolithotrophic FeOB (yellow cells) which oxidize mineral-bound Fe(II) via EET. The resultant mineralogical transformations render the minerals more susceptible to weathering by organotrophic bacteria (pink and green cells). The organotrophic degradation of complex, plant derived organics provides monomers which can be readily utilized by soil microorganisms, leading to acidolysis by organic and carbonic acids. The Fe(III) generated by FeOB provides a suitable substrate for chelation by siderophores (triangles, empty when unbound) which may be produced by either organotrophic or chemolithotrophic (not shown in diagram for simplicity) taxa.

containing Fe(II)-oxidizing EET systems (**Figure 7**) is consistent with the growth of chemolithotrophic FeOB in the present study.

Putative Chemolithotrophic Pathways

In both replicates of the diorite oxidizing enrichment cultures, the most abundant MAG belonged to the family *Acidiferrobacteraceae* (**Figure 7**) and contained a Cyc2 homolog as ribulose 1,5-bisphosphate carboxylase/oxygenase (RuBisCO), indicating their ability to grow chemolithoautotrophically. The family *Acidiferrobacteraceae* is currently described as harboring acidiphilic Fe and S oxidizers (Issotta et al., 2018), as well as neutrophilic S oxidizers (Kojima et al., 2015, 2016). Members of the genus *Acidiferrobacter* encompassing the acidophilic FeOB have been shown to contain homologs to Cyc2 as well as rusticyanin (Issotta et al., 2018), an acid-stable copper protein utilized by *Acidithiobacillus ferrooxidans* for electron transfer during Cyc2 dependent Fe(II) oxidation (Castelle et al., 2008), but not present in neutrophilic FeOB genomes (Barco et al., 2015; He et al., 2017; McAllister et al., 2020). Rusticyanin homologs were not identified in any of the *Acidiferrobacteraceae* MAGs obtained in this study. While there are currently no described neutrophilic FeOB within the *Acidiferrobacteraceae,* Meier et al. (2019) identified 16S rRNA gene sequences related to *Acidiferrobacteraceae* as being potentially involved in soil formation at a site selected to be free of influence of sulfides and where the pH was circumneutral. As our knowledge of the diversity of metabolic capacity of FeOB is rapidly expanding with the increase of environmental metagenomic data, the possibility remains that there are previously unrecognized neutrophilic FeOB within the family *Acidiferrobacteraceae.*

The taxonomy of the putative FeOB MAGs obtained in this study largely varied from the MAGs obtained from the subsurface weathering cultures, which included β-proteobacteria of the genus *Cupriavidus* and order Burkholderiales (Napieralski et al., 2019). A notable exception is the presence of a highly abundant *Xanthomonadaceae* MAG closely related to the non-autotrophic soil bacterium *Dyella japonica* A8 (Chen and Chan, 2012) which we previously identified as containing a homolog to Cyc2. Interestingly, Uroz et al. (2009) noted the ability of a *Dyella* sp. to solubilize biotite and other *Dyella* sp. have been isolated or identified from weathering environments (Uroz et al., 2011; Zhao et al., 2013), though no genomes are available to assess whether they contained Cyc2 homologs. In addition to the *Xanthomonadaceae* MAG, four additional MAGs identified in

this study contained putative EET pathways but lacked RuBisCO. While alternative carbon fixation pathways exist, they tend to be phylogenetically restricted, with the vast majority of α, β and γ-proteobacteria utilizing the Calvin Cycle (Hugler and Sievert, 2011). Two of the MAGs containing EET but not RuBisCO belong to organisms of the phylum *Nitrospirae*, which are known to use the reductive tricarboxylic acid cycle (rTCA) for carbon assimilation. Although the rTCA cycle shares many of the same genes as the TCA cycle, the unique enzyme 2-oxoglutarate synthase can be used to distinguish the two pathways (Hugler and Sievert, 2011). As this gene was not present in either *Nitrospirae* MAG, it seems likely that they cannot grow autotrophically. The differences in the taxonomy of the putative chemolithotrophic FeOB identified in this study compared to the study on subsurface weathering of the DIO suggests that the ability to utilize mineral-bound Fe(II) for metabolic energy generation may not be a unique feature of any given FeOB. Rather, it may be a trait shared among FeOB, an idea supported by previous studies where phylogenetically diverse bacteria, putatively FeOB, were isolated on Fe(II)-phyllosilicate minerals (Shelobolina et al., 2012a; Benzine et al., 2013).

Effect of Prior Oxidation on Mineral Weatherability

In line with previous observations on organotrophically driven mineral weathering (Bennett et al., 2001; Wu et al., 2008), the addition of organic carbon stimulated the release of major cations relative to sterile controls (**Figure 6**). Cellular uptake has been shown to be a potential sink for cations during the microbial weathering of basaltic rock (Stranghoener et al., 2018). However, the stimulated cation release observed here was probably not influenced significantly by cellular uptake, as a maximum of a few μM of Ca, K, Mg, and Na would be required for nutritional purposes given the relatively low cell densities in our cultures, [ca. 10^6–10^7 cells mL^{-1} for the chemolithotrophic and organotrophic enrichments, respectively, based on measured ATP concentrations of the cultures and typical cellular ATP contents (Balkwill et al., 1988)] and the typical elemental composition of bacterial cells (Heldal et al., 1985). Likewise, although bacterial cells sorb major cations and silica, the affinity of cells for these ions is much lower than for transitions metals and metalloids (Urrutia, 1997), and this process is not expected to have significantly altered aqueous speciation in our experiments. In any case, due to the possibility of cellular uptake and sorption to cell surfaces, the enhanced release of cations observed in our experiments represents a conservative estimate of the amount of cations released to solution as a result of microbial activity.

With the exception of Na (**Figure 6B**), prior microbial DIO oxidation had a small but detectable influence on subsequent organotrophically mediated cation release. In the DIO, Na resides primarily in the mineral plagioclase (Na-Ca feldspar), which is unresponsive to Fe(II) oxidation due to the lack of Fe in the crystal structure. Thus, plagioclase would not be expected to be subjected to crystallographic defects associated with charge imbalance generated by the oxidation of structural Fe (Shelobolina et al., 2012b; Napieralski et al., 2019). A modest increase in the amount of Ca released was observed in DIO-Ox + Gluc-Inoc vs. DIO-Cont + Gluc-Inoc reactors (**Figure 5A**), although this difference was not outside of the error (range) of duplicate reactors. Plagioclase constitutes ca. 56.4 wt% of the DIO compared to the ca 6.3% of hornblende (White et al., 1998), the two mineral phases in which Ca is concentrated. Thus, the input of Ca from the redox-responsive hornblende is likely to be low compared to that from plagioclase. An enhanced release of Mg was also observed from previously oxidized diorites (**Figure 6C**). Mg is primarily sourced from the redox active minerals hornblende and biotite, which can account for enhanced release from the oxidized DIO. Biotite is also the major source of K in the DIO. Similar to our previous observations (Napieralski et al., 2019), we observed that K release was repressed when biotite was oxidized (**Figure 6D**). This surprising effect is best attributed to the assertation by Gilkes et al. (1973a; 1973b) that oxidation of Fe(II) in biotite changes the orientation of biotite hydroxyl groups, creating a more stable environment for the interlayer cation. However, this is not to say that K cannot become depleted from biotite via microbial activity, as K concentrations are clearly higher in DIO-Ox + Gluc-Inoc and DIO-Cont + Gluc-Inoc than in the abiotic, unoxidized control (DIO-Cont + Gluc-Sterile) (**Figure 6D**). As biotite found in soils is often already at least partially oxidized/altered (Wilson, 2004), this observation is not at odds with the dogma that microbial activity in the rhizosphere plays an important role in soil fertility by increasing K availability. Put more plainly, the biologically enhanced release of K from partially oxidized biotite is greater than the abiotic release of K in fresh, unoxidized biotite, despite the fact that the prior oxidation of biotite repressed the release of K overall in chemolithotrophic experiments. All together this work is consistent with our previous observation that ferromagnesian minerals which have undergone modest surface oxidation are more susceptible acidolysis by mineral acids, and the supposition that FeOB activity may enhance the weatherability of ferromagnesian minerals (Napieralski et al., 2019).

Potential Metabolic Interactions *in situ*

We have used microbiological and metagenomic analyses to inform the potential metabolic interactions between community members involved in the surficial weathering of the DIO, and a conceptual model is provided in **Figure 8**. It is clear from the *in situ* metagenomes (GbOC-A and GbOC-B) that degradation of complex organics is an important metabolic pathway. Multiple MAGs, including putative *Mucilaginibacter,* are enriched in carbohydrate active enzymes. *Mucilaginibacter* sp. have been reported to degrade complex organics such as cellulose and hemicellulose and play an important role in degradation of plant biomass in forest soils (López-Mondéjar et al., 2016). While not directly related to weathering, the enzymatic degradation of complex organic carbon to oligosaccharides facilitates the release of plant-derived carbon to the soil solution (Guggenberger et al., 1994). Once depolymerized, plant derived organic carbon would then be available to other regolith organotrophs, including multiple β-proteobacteria also abundant in the *in situ* libraries. β-proteobacteria, particularly the

Burkholderiales, have been shown to be abundant in weathering systems, and while genomic markers of their ability to enhance mineral weathering are lacking, they have been previously reported to correlate with mineral dissolution *in vitro* (Lepleux et al., 2012; Stranghoener et al., 2018). With the exception of a single *Cupriavidus* MAG, no siderophore biosynthesis pathways were associated with *Burkholderiales* MAGs. This suggests that their ability to enhance mineral dissolution may rely on mechanisms other than chelation by siderophores, such as organic acid production.

Although it might be tempting to think that the availability of carbon would limit chemolithoautotrophic metabolisms, the data presented herein do not necessarily support that assumption. In the early stages of chemolithotrophic incubation, ATP declined across all experimental conditions (**Figure 3A**), suggesting an overall decline in microbial biomass. However, ATP in DIO free reactors (NoMin and QTZ) remains elevated above the abiotic control for the duration of the experiment, indicating actively metabolizing cells, likely oxidizing residual carbon. Assuming a relatively equal input of carbon occurred during inoculation of each reactor, sufficient carbon would similarly be available in diorite amended reactors. As Fe(II)/Fe(tot) declines over the entire course of the experiment (**Figure 3A**), and the most abundant MAG obtained from each DIO reactor has the genetic capacity for chemolithoautotrophic growth, it does not seem likely that chemolithoautotrophs were inhibited by the presence of residual carbon and organotrophic activity. This is further supported by slight decline in Fe(II)/Fe(tot) in glucose amended DIO reactors (**Figure 5A**). It thus seems possible that the putative chemolithoautotrophs, detected in the metagenomic co-assembly can co-exist and metabolize Fe(II) *in situ,* with the oxidative weathering activity of FeOB contributing to the ability of organotrophic microorganisms to further weather ferromagnesian minerals via other mechanisms, including acidolysis and chelation by siderophores. As siderophores are highly specific to Fe(III), with a low affinity for Fe(II), (Neilands, 1995), the implication is that their mechanism of action in enhanced Fe(II) mineral dissolution must almost certainly require prior oxidation, either chemically or biologically, to obtain a suitable substrate. Thus, the oxidation of mineral bound Fe(II) by FeOB may act to increase Fe(III) availability for cellular uptake via siderophores.

FUTURE PERSPECTIVES

We have identified the potential involvement FeOB in silicate mineral weathering in both a subsurface (Napieralski et al., 2019) and surficial quartz diorite weathering environment and have also identified a potential marker for microbial oxidative weathering in Cyc2. In both the present study and our previous work on subsurface weathering, MAGs containing Cyc2 homologs are abundant in Fe(II)-oxidizing enrichment cultures, and the functionality of Cyc2 as an Fe(II) oxidase in neutrophilic FeOB has recently been validated (McAllister et al., 2020). While most studies on *in situ* weathering rely on 16S rRNA gene-based surveys (Liermann et al., 2014; Wild et al., 2019), taxonomic information alone is often not enough to make metabolic inferences, and the role of non-canonical FeOB in terrestrial weathering is likely to be under recognized. Although metagenomic investigations are helping to unravel microbial pathways and biogeochemical implications in a variety of geological habitats (Anantharaman et al., 2016a,b; Fortney et al., 2018; Colman et al., 2019), the terrestrial "weathering microbiome" remains largely unexplored, with the genetic mechanism for biogeochemical weathering only beginning to be revealed (Uroz et al., 2013). This work thus provides a framework and additional genomic target for future investigations into the role of microorganisms in biogeochemical weathering.

DATA AVAILABILITY STATEMENT

Sequencing data generated in the study, including raw reads for individual metagenomes (BioSamples SAMN15518762-69) have been deposited in the National Center for Biotechnology Information database under the BioProject ID PRJNA645909.

AUTHOR CONTRIBUTIONS

SN and ER designed the research. SN conducted the field and laboratory work, performed the data analysis, and wrote the manuscript with input from ER. Both authors contributed to the article and approved the submitted version.

FUNDING

This research was supported by NASA project no. NNA13AA94A, administered by the NASA Astrobiology Institute, and University of Wisconsin-Madison Microbiome Initiative award.

ACKNOWLEDGMENTS

We thank the NSF Luquillo Critical Zone Observatory for access to facilities and assistance with fieldwork in addition to field work assistance provided by Dr. Nathaniel Fortney. **Figures 2**, **8** were created with BioRender.com.

REFERENCES

Alneberg, J., Bjarnason, B. S., de Bruijn, I., Schirmer, M., Quick, J., Ijaz, U. Z., et al. (2014). Binning metagenomic contigs by coverage and composition. *Nat. Methods* 11, 1144–1146. doi: 10.1038/nmeth.3103

Anantharaman, K., Breier, J. A., and Dick, G. J. (2016a). Metagenomic resolution of microbial functions in deep-sea hydrothermal plumes across the Eastern Lau Spreading Center. *ISME J.* 10, 225–239. doi: 10.1038/ismej.2015.81

Anantharaman, K., Brown, C. T., Hug, L. A., Sharon, I., Castelle, C. J., Probst, A. J., et al. (2016b). Thousands of microbial genomes shed light on interconnected

biogeochemical processes in an aquifer system. *Nat. Commun.* 7:13219. doi: 10.1038/ncomms13219

Bailey, B., Templeton, A., Staudigel, H., and Tebo, B. M. (2009). Utilization of substrate components during basaltic glass colonization by *Pseudomonas* and shewanella isolates. *Geomicrobiol. J.* 26, 648–656. doi: 10.1080/01490450903263376

Balkwill, D. L., Leach, F. R., Wilson, J. T., McNabb, J. F., and White, D. C. (1988). Equivalence of microbial biomass measures based on membrane lipid and cell wall components, adenosine triphosphate, and direct counts in subsurface aquifer sediments. *Microb. Ecol.* 16, 73–84. doi: 10.1007/BF02097406

Banfield, J. F., Barker, W. W., Welch, S. A., and Taunton, A. (1999). Biological impact on mineral dissolution: application of the lichen model to understanding mineral weathering in the rhizosphere. *Proc. Natl. Acad. Sci. U.S.A.* 96, 3404–3411. doi: 10.1073/pnas.96.7.3404

Barco, R. A., Emerson, D., Sylvan, J. B., Orcutt, B. N., Jacobson Meyers, M. E., Ramirez, G. A., et al. (2015). New insight into microbial iron oxidation as revealed by the proteomic profile of an obligate iron-oxidizing chemolithoautotroph. *Appl. Environ. Microbiol.* 81, 5927–5937. doi: 10.1128/AEM.01374-15

Bennett, P. C., Rogers, J. R., Choi, W. J., and Hiebert, F. K. (2001). Silicates, silicate weathering, and microbial ecology. *Geomicrobiol. J.* 18, 3–19. doi: 10.1080/01490450151079734

Benzine, J., Shelobolina, E., Xiong, M. Y., Kennedy, D. W., McKinley, J. P., Lin, X., et al. (2013). Fe-phyllosilicate redox cycling organisms from a redox transition zone in Hanford 300 Area sediments. *Front. Microbiol.* 4:388. doi: 10.3389/fmicb.2013.00388

Buss, H. L., Bruns, M. A., Schultz, M. J., Moore, J., Mathur, C. F., and Brantley, S. L. (2005). The coupling of biological iron cycling and mineral weathering during saprolite formation, Luquillo mountains, Puerto Rico. *Geobiology* 3, 247–260. doi: 10.1111/j.1472-4669.2006.00058.x

Buss, H. L., Lüttge, A., and Brantley, S. L. (2007). Etch pit formation on iron silicate surfaces during siderophore-promoted dissolution. *Chem. Geol.* 240, 326–342. doi: 10.1016/j.chemgeo.2007.03.003

Buss, H. L., Sak, P. B., Webb, S. M., and Brantley, S. L. (2008). Weathering of the Rio Blanco quartz diorite, Luquillo Mountains, Puerto Rico: coupling oxidation, dissolution, and fracturing. *Geochim. Cosmochim. Acta* 72, 4488–4507. doi: 10.1016/j.gca.2008.06.020

Calvaruso, C., Turpault, M. P., and Frey-Klett, P. (2006). Root-associated bacteria contribute to mineral weathering and to mineral nutrition in trees: a budgeting analysis. *Appl. Environ. Microbiol.* 72, 1258–1266. doi: 10.1128/AEM.72.2.1258-1266.2006

Castelle, C., Guiral, M., Malarte, G., Ledgham, F., Leroy, G., Brugna, M., et al. (2008). A new iron-oxidizing/O2-reducing supercomplex spanning both inner and outer membranes, isolated from the extreme acidophile *Acidithiobacillus ferrooxidans*. *J. Biol. Chem.* 283, 25803–25811. doi: 10.1074/jbc.M802496200

Chen, J. W., and Chan, K. G. (2012). Genome sequence of Dyella japonica strain A8, a quorum-quenching bacterium that degrades N-acylhomoserine lactones, isolated from Malaysian tropical soil. *J. Bacteriol.* 194:6331. doi: 10.1128/JB.01637-12

Colman, D. R., Lindsay, M. R., and Boyd, E. S. (2019). Mixing of meteoric and geothermal fluids supports hyperdiverse chemosynthetic hydrothermal communities. *Nat. Commun.* 10:681. doi: 10.1038/s41467-019-08499-1

Drever, J. I., and Stillings, L. L. (1997). The role of organic acids in mineral weathering. *Coll. Surf. A Physicochem. Eng. Aspects* 120, 167–181. doi: 10.1016/S0927-7757(96)03720-X

Emerson, D., Fleming, E. J., and McBeth, J. M. (2010). Iron-oxidizing bacteria: an environmental and genomic perspective. *Annu. Rev. Microbiol.* 64, 561–583. doi: 10.1146/annurev.micro.112408.134208

Fortney, N. W., He, S., Converse, B. J., Boyd, E. S., and Roden, E. E. (2018). Investigating the composition and metabolic potential of microbial communities in chocolate pots hot springs. *Front. Microbiol.* 9:2075. doi: 10.3389/fmicb.2018.02075

Frey, B., Rieder, S. R., Brunner, I., Plotze, M., Koetzsch, S., Lapanje, A., et al. (2010). Weathering-associated bacteria from the *Damma glacier* forefield: physiological capabilities and impact on granite dissolution. *Appl. Environ. Microbiol.* 76, 4788–4796. doi: 10.1128/AEM.00657-10

Gilkes, R. J., Young, R. C., and Quirk, J. P. (1973a). Artificial weathering of oxidized biotite: I. potassium removal by sodium chloride and sodium tetraphenylboron solutions. *Soil Sci. Soc. Am. J.* 37, 25–28. doi: 10.2136/sssaj1973.03615995003700010013x

Gilkes, R. J., Young, R. C., and Quirk, J. P. (1973b). Artificial weathering of oxidized biotite: II. rates of dissolution in 0.1, 0.01, 0.001M HCl. *Soil Sci. Soc. Am. J.* 37, 29–33. doi: 10.2136/sssaj1973.03615995003700010014x

Guggenberger, G., Zech, W., and Schulten, H. R. (1994). Formation and mobilization pathways of dissolved organic matter: evidence from chemical structural studies of organic matter fractions in acid forest floor solutions. *Organ. Geochem.* 21, 51–66. doi: 10.1016/0146-6380(94)90087-6

Hazen, T. C., Jiménez, L., López de Victoria, G., and Fliermans, C. B. (1991). Comparison of bacteria from deep subsurface sediment and adjacent groundwater. *Microb. Ecol.* 22, 293–304. doi: 10.1007/BF02540231

He, S., Barco, R. A., Emerson, D., and Roden, E. E. (2017). Comparative genomic analysis of neutrophilic iron(II) oxidizer genomes for candidate genes in extracellular electron transfer. *Front. Microbiol.* 8:1584. doi: 10.3389/fmicb.2017.01584

He, S., Tominski, C., Kappler, A., Behrens, S., and Roden, E. E. (2016). Metagenomic analyses of the autotrophic Fe(II)-oxidizing, nitrate-reducing enrichment culture KS. *Appl. Environ. Microbiol.* 82, 2656–2668. doi: 10.1128/AEM.03493-15

Heldal, M., Norland, S., and Tumyr, O. (1985). X-ray microanalytic method for measurement of dry matter and elemental content of individual bacteria. *Appl. Environ. Microbiol.* 50, 1251–1257. doi: 10.1128/aem.50.5.1251-1257.1985

Henri, P. A., Rommevaux-Jestin, C., Lesongeur, F., Mumford, A., Emerson, D., Godfroy, A., et al. (2015). Structural iron (II) of basaltic glass as an energy source for zetaproteobacteria in an abyssal plain environment, off the mid atlantic ridge. *Front. Microbiol.* 6:1518. doi: 10.3389/fmicb.2015.01518

Hering, J. G., and Stumm, W. (1990). Oxidative and reductive dissolution of minerals. *Rev. Mineral. Geochem.* 23, 427–465. doi: 10.1515/9781501509131-015

Hopkinson, B. M., and Barbeau, K. A. (2012). Iron transporters in marine prokaryotic genomes and metagenomes. *Environ. Microbiol.* 14, 114–128. doi: 10.1111/j.1462-2920.2011.02539.x

Hugler, M., and Sievert, S. M. (2011). Beyond the Calvin cycle: autotrophic carbon fixation in the ocean. *Ann. Rev. Mar. Sci.* 3, 261–289. doi: 10.1146/annurev-marine-120709-142712

Issotta, F., Moya-Beltran, A., Mena, C., Covarrubias, P. C., Thyssen, C., Bellenberg, S., et al. (2018). Insights into the biology of acidophilic members of the Acidiferrobacteraceae family derived from comparative genomic analyses. *Res. Microbiol.* 169, 608–617. doi: 10.1016/j.resmic.2018.08.001

Jakosky, B. M., and Shock, E. L. (1998). The biological potential of Mars, the early Earth, and Europa. *J. Geophys. Res.: Planets* 103, 19359–19364. doi: 10.1029/98je01892

Kalinowski, B. E., Liermann, L. J., Brantley, S. L., Barnes, A., and Pantano, C. G. (2000). X-ray photoelectron evidence for bacteria-enhanced dissolution of hornblende. *Geochim. Cosmochim. Acta* 64, 1331–1343. doi: 10.1016/S0016-7037(99)00371-3

Kang, D. D., Li, F., Kirton, E., Thomas, A., Egan, R., An, H., et al. (2019). MetaBAT 2: an adaptive binning algorithm for robust and efficient genome reconstruction from metagenome assemblies. *PeerJ* 7:e7359. doi: 10.7717/peerj.7359

Kojima, H., Shinohara, A., and Fukui, M. (2015). *Sulfurifustis variabilis* gen. nov., sp. nov., a sulfur oxidizer isolated from a lake, and proposal of Acidiferrobacteraceae fam. nov. and Acidiferrobacterales ord. nov. *Int. J. Syst. Evol. Microbiol.* 65, 3709–3713. doi: 10.1099/ijsem.0.000479

Kojima, H., Watanabe, T., and Fukui, M. (2016). *Sulfuricaulis limicola* gen. Nov., sp. nov., a sulphur oxidizer isolated from a lake. *Int. J. Syst. Evol. Microbiol.* 66, 266–270. doi: 10.1099/ijsem.0.000709

Lambers, H., Mougel, C., Jaillard, B., and Hinsinger, P. (2009). Plant-microbe-soil interactions in the rhizosphere: an evolutionary perspective. *Plant Soil* 321, 83–115. doi: 10.1007/s11104-009-0042-x

Lepleux, C., Turpault, M. P., Oger, P., Frey-Klett, P., and Uroz, S. (2012). Correlation of the abundance of betaproteobacteria on mineral surfaces with mineral weathering in forest soils. *Appl. Environ. Microbiol.* 78, 7114–7119. doi: 10.1128/AEM.00996-12

Liermann, L. J., Albert, I., Buss, H. L., Minyard, M., and Brantley, S. L. (2014). Relating microbial community structure and geochemistry in deep regolith developed on Volcaniclastic Rock in the Luquillo Mountains, Puerto Rico. *Geomicrobiol. J.* 32, 494–510. doi: 10.1080/01490451.2014.964885

Liermann, L. J., Kalinowski, B. E., Brantley, S. L., and Ferry, J. G. (2000). Role of bacterial siderophores in dissolution of hornblende. *Geochim. Cosmochim. Acta* 64, 587–602. doi: 10.1016/S0016-7037(99)00288-4

Liu, J., Wang, Z., Belchik, S. M., Edwards, M. J., Liu, C., Kennedy, D. W., et al. (2012). Identification and characterization of MtoA: a decaheme c-type cytochrome of the neutrophilic Fe(II)-oxidizing bacterium *Sideroxydans lithotrophicus* ES-1. *Front. Microbiol.* 3:37. doi: 10.3389/fmicb.2012.00037

López-Mondéjar, R., Zühlke, D., Becher, D., Riedel, K., and Baldrian, P. (2016). Cellulose and hemicellulose decomposition by forest soil bacteria proceeds by the action of structurally variable enzymatic systems. *Sci. Rep.* 6:25279. doi: 10.1038/srep25279

McAllister, S. M., Polson, S. W., Butterfield, D. A., Glazer, B. T., Sylvan, J. B., and Chan, C. S. (2020). Validating the Cyc2 neutrophilic iron oxidation pathway using meta-omics of zetaproteobacteria iron mats at marine hydrothermal vents. *mSystems* 5:e00553-19. doi: 10.1128/mSystems.00553-19

Meier, L. A., Krauze, P., Prater, I., Horn, F., Schaefer, C. E. G. R., Scholten, T., et al. (2019). Pedogenic and microbial interrelation in initial soils under semiarid climate on James Ross Island, Antarctic Peninsula region. *Biogeosciences* 16, 2481–2499. doi: 10.5194/bg-16-2481-2019

Montross, S. N., Skidmore, M., Tranter, M., Kivimäki, A.-L., and Parkes, R. J. (2013). A microbial driver of chemical weathering in glaciated systems. *Geology* 41, 215–218. doi: 10.1130/g33572.1

Napieralski, S. A. (2020). *Microbiological and Metagenomic Insights into The Biogeochemical Weathering of Fe(II)-Silicates and Pyrite by Chemolithotrophic Bacteria*. Ph.D. Dissertation, University of Wisconsin-Madison, Madison, WI.

Napieralski, S. A., Buss, H. L., Brantley, S. L., Lee, S., Xu, H., and Roden, E. (2019). Microbial chemolithotrophy mediates oxidative weathering of granitic bedrock. *PNAS* 116, 26394–26401. doi: 10.1073/pnas.1909970117

Neilands, J. B. (1995). Siderophores: structure and function of microbial iron transport compounds. *J. Biol. Chem.* 270, 26723–26726. doi: 10.1074/jbc.270.45.26723

Parks, D. H., Imelfort, M., Skennerton, C. T., Hugenholtz, P., and Tyson, G. W. (2015). CheckM: assessing the quality of microbial genomes recovered from isolates, single cells, and metagenomes. *Genome Res.* 25, 1043–1055. doi: 10.1101/gr.186072.114

Peng, Y., Leung, H. C., Yiu, S. M., and Chin, F. Y. (2012). IDBA-UD: a de novo assembler for single-cell and metagenomic sequencing data with highly uneven depth. *Bioinformatics* 28, 1420–1428. doi: 10.1093/bioinformatics/bts174

Popa, R., Smith, A. R., Popa, R., Boone, J., and Fisk, M. (2012). Olivine-respiring bacteria isolated from the rock-ice interface in a lava-tube cave, a Mars analog environment. *Astrobiology* 12, 9–18. doi: 10.1089/ast.2011.0639

Roden, E. E. (2012). Microbial iron-redox cycling in subsurface environments. *Biochem. Soc. Trans.* 40, 1249–1256. doi: 10.1042/BST20120202

Roden, E. E., Sobolev, D., Glazer, B., and Luther, G. W. (2004). Potential for microscale bacterial fe redox cycling at the aerobic-anaerobic interface. *Geomicrobiol. J.* 21, 379–391. doi: 10.1080/01490450490485872

Seemann, T. (2014). Prokka: rapid prokaryotic genome annotation. *Bioinformatics* 30, 2068–2069. doi: 10.1093/bioinformatics/btu153

Shelobolina, E., Konishi, H., Xu, H., Benzine, J., Xiong, M. Y., Wu, T., et al. (2012a). Isolation of phyllosilicate-iron redox cycling microorganisms from an illite-smectite rich hydromorphic soil. *Front. Microbiol.* 3:134. doi: 10.3389/fmicb.2012.00134

Shelobolina, E., Xu, H., Konishi, H., Kukkadapu, R., Wu, T., Blothe, M., et al. (2012b). Microbial lithotrophic oxidation of structural Fe(II) in biotite. *Appl. Environ. Microbiol.* 78, 5746–5752. doi: 10.1128/AEM.01034-12

Shock, E. L. (2009). Minerals as energy sources for microorganisms. *Econ. Geol.* 104, 1235–1248. doi: 10.2113/gsecongeo.104.8.1235

Sobolev, D., and Roden, E. (2004). Characterization of a neutrophilic, chemolithoautotrophic Fe(II)-oxidizing β-Proteobacterium from freshwater wetland sediments. *Geomicrobiol. J.* 21, 1–10. doi: 10.1080/01490450490253310

Sobolev, D., and Roden, E. E. (2002). Evidence for rapid microscale bacterial redox cycling of iron in circumneutral environments. *Antonie Van Leeuwenhoek Int. J. Gen. Mol. Microbiol.* 81, 587–597.

Stookey, L. L. (1970). Ferrozine-A new spectrophotometric reagent for iron. *Anal. Chem.* 42, 778–781. doi: 10.1021/ac60289a016

Stranghoener, M., Schippers, A., Dultz, S., and Behrens, H. (2018). Experimental microbial alteration and Fe mobilization from basaltic rocks of the ICDP HSDP2 drill core, Hilo, Hawaii. *Front. Microbiol.* 9:1252. doi: 10.3389/fmicb.2018.01252

Uritskiy, G. V., DiRuggiero, J., and Taylor, J. (2018). MetaWRAP-a flexible pipeline for genome-resolved metagenomic data analysis. *Microbiome* 6:158. doi: 10.1186/s40168-018-0541-1

Uroz, S., Calvaruso, C., Turpault, M. P., and Frey-Klett, P. (2009). Mineral weathering by bacteria: ecology, actors and mechanisms. *Trends Microbiol.* 17, 378–387. doi: 10.1016/j.tim.2009.05.004

Uroz, S., Ioannidis, P., Lengelle, J., Cebron, A., Morin, E., Buee, M., et al. (2013). Functional assays and metagenomic analyses reveals differences between the microbial communities inhabiting the soil horizons of a Norway spruce plantation. *PLoS One* 8:e55929. doi: 10.1371/journal.pone.0055929

Uroz, S., Turpault, M. P., Van Scholl, L., Palin, B., and Frey-Klett, P. (2011). Long term impact of mineral amendment on the distribution of the mineral weathering associated bacterial communities from the beech *Scleroderma citrinum* ectomycorrhizosphere. *Soil Biol. Biochem.* 43, 2275–2282. doi: 10.1016/j.soilbio.2011.07.010

Urrutia, M. M. (1997). "General bacterial sorption processes," in *Biosorbents for Metal Ions*, eds J. D. A. Wase and C. Forster (Philadelphia: Taylor and Frances), 39–66.

White, A. F. (1990). Heterogeneous electrochemical reactions associated with oxidation of ferrous oxide and silicate surfaces. *Rev. Mineral. Geochem.* 23, 467–509. doi: 10.1515/9781501509131-016

White, A. F., Blum, A. E., Schulz, M. S., Vivit, D. V., Stonestrom, D. A., Larsen, M., et al. (1998). Chemical weathering in a tropical watershed, Luquillo Mountains, Puerto Rico: I. Long-term versus short-term weathering fluxes. *Geochim. Cosmochim. Acta* 62, 209–226. doi: 10.1016/S0016-7037(97)00335-9

Wild, B., Daval, D., Beaulieu, E., Pierret, M.-C., Viville, D., and Imfeld, G. (2019). In-situ dissolution rates of silicate minerals and associated bacterial communities in the critical zone (Strengbach catchment, France). *Geochim. Cosmochim. Acta* 249, 95–120. doi: 10.1016/j.gca.2019.01.003

Wilson, M. J. (2004). Weathering of the primary rock-forming minerals: processes, products and rates. *Clay Miner.* 39, 233–266. doi: 10.1180/0009855043930133

Wu, L., Jacobson, A. D., and Hausner, M. (2008). Characterization of elemental release during microbe–granite interactions at T=28°C. *Geochim. Cosmochim. Acta* 72, 1076–1095. doi: 10.1016/j.gca.2007.11.025

Yin, Y., Mao, X., Yang, J., Chen, X., Mao, F., and Xu, Y. (2012). DbCAN: a web resource for automated carbohydrate-active enzyme annotation. *Nucleic Acids Res.* 40, W445–W451. doi: 10.1093/nar/gks479

Yu, C. S., Chen, Y. C., Lu, C. H., and Hwang, J. K. (2006). Prediction of protein subcellular localization. *Proteins* 64, 643–651. doi: 10.1002/prot.21018

Zhao, F., Guo, X. Q., Wang, P., He, L. Y., Huang, Z., and Sheng, X. F. (2013). *Dyella jiangningensis* sp. nov., a gamma-proteobacterium isolated from the surface of potassium-bearing rock. *Int. J. Syst. Evol. Microbiol.* 63(Pt 9), 3154–3157. doi: 10.1099/ijs.0.048470-0

Zhou, J., Bruns, M. A., and Tiedje, J. M. (1996). DNA recovery from soils of diverse composition. *Appl. Environ. Microbiol.* 62, 316–322. doi: 10.1128/aem.62.2.316-322.1996

Conflict of Interest: The authors declare that the research was conducted in the absence of any commercial or financial relationships that could be construed as a potential conflict of interest.

frontiers in Microbiology

ORIGINAL RESEARCH
published: 25 May 2021
doi: 10.3389/fmicb.2021.674411

Geographical Distribution of Iron Redox Cycling Bacterial Community in Peatlands: Distinct Assemble Mechanism Across Environmental Gradient

Liang Yang[1,2,3], *Ming Jiang*[1,3]*, *Yuanchun Zou*[1,3], *Lei Qin*[1,3] and *Yingyi Chen*[1,2,3]

[1] Northeast Institute of Geography and Agroecology, Chinese Academy of Sciences, Changchun, China, [2] University of Chinese Academy of Sciences, Beijing, China, [3] Jilin Provincial Joint Key Laboratory of Changbai Mountain Wetland and Ecology, Changchun, China

Microbial-mediated iron (Fe) oxidation and reduction greatly contribute to the biogeochemistry and mineralogy of ecosystems. However, knowledge regarding the composition and distribution patterns of iron redox cycling bacteria in peatlands remains limited. Here, using high-throughput sequencing, we compared biogeographic patterns and assemblies of the iron redox cycling bacterial community between soil and water samples obtained from different types of peatland across four regions in Northeast China. A total of 48 phylotypes were identified as potential iron redox bacteria, which had greater than 97% similarity with Fe(II)-oxidizing bacteria (FeOB) and Fe(III)-reducing bacteria (FeRB). Among them, *Rhodoferax*, *Clostridium*, *Geothrix*, *Sideroxydans*, *Geobacter*, *Desulfovibrio*, and *Leptothrix* could be used as bioindicators in peatlands for characterizing different hydrological conditions and nutrient demands. Across all samples, bacterial communities associated with iron redox cycling were mainly affected by pH, dissolved organic carbon (DOC), and Fe^{2+}. Distance–decay relationship (DDR) analysis indicated that iron redox cycling bacterial communities in soil, but not in water, were highly correlated with geographic distance. Additionally, null model analysis revealed that stochastic processes substituted deterministic processes from minerotrophic fens to ombrotrophic bogs in soils, whereas deterministic processes were dominant in water. Overall, these observations suggest that bacteria involved in iron redox cycling are widespread in diverse habitats and exhibit distinct patterns of distribution and community assembly mechanisms between soil and water in peatlands.

Keywords: iron redox cycling bacteria, biogeographic distribution, community assembly, peatlands, Northeast China

OPEN ACCESS

Edited by:
Lei Yan,
Heilongjiang Bayi Agricultural University, China

Reviewed by:
Meng Wang,
Northeast Normal University, China
Baogang Zhang,
China University of Geosciences, China

***Correspondence:**
Ming Jiang
jiangm@iga.ac.cn

Specialty section:
This article was submitted to Microbiological Chemistry and Geomicrobiology, a section of the journal Frontiers in Microbiology

Received: *01 March 2021*
Accepted: *12 April 2021*
Published: *25 May 2021*

Citation:
Yang L, Jiang M, Zou Y, Qin L and Chen Y (2021) Geographical Distribution of Iron Redox Cycling Bacterial Community in Peatlands: Distinct Assemble Mechanism Across Environmental Gradient. Front. Microbiol. 12:674411. doi: 10.3389/fmicb.2021.674411

INTRODUCTION

The redox reactions involving iron are vital for the biogeochemical cycling of iron in terrestrial and aquatic ecosystems and are interconnected with the cycling of other elements, including carbon, nitrogen, phosphorus, sulfur, and manganese, through numerous processes in the biogeochemical iron cycle (Jickells et al., 2005; Raiswell and Canfield, 2012; Riedel et al., 2013). Owing to the redox

sensitivity of iron, iron cycling occurs largely through reduction and oxidation processes. In the early 20th century, iron redox cycling was assumed to be purely abiotic. However, the contribution of abiotic processes alone could not explain the observed spatiotemporal distribution of Fe redox cycling species in some environments, such as in the soil, plant rhizospheres, or even rust-colored flocculent mats (Melton et al., 2014). A better understanding of the biogeochemistry of ecosystems and the development of the microbiological research methods has led to the recognition that iron-metabolizing microorganisms are extremely important for biogeochemical processes globally (Emerson and Floyd, 2005; Weber et al., 2006).

Peatlands store approximately 30% of soil organic carbon and 10% of all freshwater, despite covering only 3% of the Earth's landmass (Gorham, 1991; Yu et al., 2010). Meanwhile, different types of peatlands exhibit different redox conditions and nutrition statuses, suggesting that they are replete in carbon, nitrogen, and/or sulfur sources that are readily available for microbial metabolic and redox processes (Kügler et al., 2019). Studies have shown that Fe(II)/Fe(III) as electron donors/acceptors are widely present in peatlands (Todorova and Costello, 2006; Reiche et al., 2008). Owing to the recurrent fluctuations of the redox potential in the upper layer of peatlands, iron redox cycling microorganisms can utilize a variety of terminal electron donors (such as ammonium, humus, and hydrogen) and electron acceptors (such as nitrate and metal cations) in peatland biogeochemical cycling (Küsel et al., 2008; Lüdecke et al., 2010). Therefore, we hypothesized that microorganisms involved in iron redox cycling would be widely distributed in peatlands and that the biogeographic patterns and assembly processes would differ between peatland soil and water samples.

Fe(II)-oxidizing bacteria (FeOB) and Fe(III)-reducing bacteria (FeRB) play important roles in microbial groups capable of iron redox functions. Numerous studies have documented that these iron redox cycling bacteria are widespread in the environment, including in marine, forest, and wetland ecosystems (Haaijer et al., 2008; Dubinsky et al., 2010; Emerson et al., 2010). Simultaneously, they have important environmental implications; for example, FeOB/FeRB can be harnessed for bioremediation purposes. For instance, Fe(III)-reducing bacteria (e.g., *Geobacter*, *Shewanella*, and *Anaeromyxobacter*) or Fe(II)-oxidizing bacteria (e.g., *Gallionella*, *Leptothrix*, and *Sideroxydans*) remove contaminants by altering the valence state of iron coupled with the oxidation or reduction of organic and inorganic material, such as hydrocarbons, pesticides, explosives, and heavy metals (Herath et al., 2010; Glodowska et al., 2020; Lu et al., 2020). Also, Fe(II)-oxidizing bacteria oxidize Fe(II) to Fe(III) (oxyhydr)oxides, which detoxify the environment by absorbing or co-precipitating heavy metals (Huang et al., 2012; Smith et al., 2017; Xu et al., 2017). In addition, Kappler et al. (2021) recently reported that microbial Fe(III) reduction coupled to methane and ammonium oxidation exists in various ecosystems, and provided new insights for the comprehensive assessment of greenhouse gas (GHG). Although there is evidence to support their potential roles in biogeochemical processes (Weber et al., 2006; Melton et al., 2014), how the biogeographical distribution of FeOB/FeRB is shaped by ecological factors at regional scales remains unknown.

To date, the lack of specific primers that could encompass all iron redox cycling microorganisms has limited investigation into their biogeographical distribution (Konstantinidis and Tiedje, 2007; Parro et al., 2007). Küsel et al. (2008) and Lüdecke et al. (2010) addressed the composition of FeOB and FeRB in peatlands using a combination of molecular technology and enrichment culture. However, these studies did not elucidate the biogeographical distribution of FeOB/FeRB in peatlands, because changes in substrate type and concentration fundamentally modify the niche of these microorganisms (Yi et al., 2013; Pierra et al., 2015). Owing to its high resolution and cost-effectiveness, high-throughput sequencing (HTS) has become the method of choice for identifying microbial phylotypes (Rousk et al., 2010; Yuan et al., 2016). To open new insights into the biogeographic distribution of iron-cycling bacteria, HTS data were compared against the National Center for Biotechnology Information (NCBI) 16S rRNA database using the BLAST algorithm. Here we studied what was the geographical distribution of the iron redox cycling bacterial community and how environmental gradients affected their assemble mechanism across environmental gradients in three different types of peatland across Northeast China. Our objectives were to (i) investigate the biogeographic distribution of bacteria involved in iron redox cycling in soil and water across peatlands and (ii) identify the assembly mechanism and the driving factors of abundance and community composition of iron redox cycling bacteria in peatlands.

MATERIALS AND METHODS

Study Sites and Sample Collection

The study sites were located in Helongjiang and Jilin provinces in Northeast China. These study sites have four regions, Sanjiang Plain (SJ), Lesser Khingan Mountain (LK), Greater Khingan Mountain (GK), and Changbai Mountain (CB), comprising three peatland types: minerotrophic fens (fen), ombrotrophic bogs (bog), and mixed peatlands (fen–bog complex). Sanjiang Plain is a temperate continental monsoon climate with seasonally frozen soil; the mean annual temperature is 2.5°C. Changbai Mountain is a temperate continental monsoon climate with seasonally frozen soil; the mean annual temperature is 3.3°C. Lesser Khingan Mountain is a temperate continental monsoon climate with island-shaped permafrost; the mean annual temperature is −1.0°C. Greater Khingan Mountain is a cold temperate continental monsoon climate with continuous permafrost; the mean annual temperature is −4.0°C (Man et al., 2010; Zhu et al., 2015; Han et al., 2018; Jiang et al., 2018). The peatlands of all sites are natural due to local protection or less anthropogenic disturbances. The soils in all sites are classified as peat soil with high content of organic matter. Detailed site characteristics are shown in **Supplementary Table 1**. Sampling was carried out in July 2019. Surface soil samples (30 cm) were obtained using a peat sampler (BJ7R-0409, Netherlands), and visible plant residues were removed. Water samples were extracted with a

syringe and then filtered. For each site, three replicate plots were established and randomly arranged. At each plot, both the soil and water samples were collected at five sampling points and mixed to obtain one composite sample. All samples were sealed on ice and transported to the laboratory, where they were divided into three subsamples: one subsample was used for physicochemical analyses, one was transferred into 0.5 M HCl for Fe(II) determination, and one was stored at −80°C for subsequent molecular analysis.

Measurements of Soil Physicochemical Properties

The pH was measured with a pH meter (PHS-3C, Shanghai, China) from a soil: distilled water (1:5, *w/v*) solution. Organic matter (OM) was determined by potassium dichromate oxidation-outer heating (Lu, 1999). Dissolved organic carbon (DOC) concentrations were measured in filtrates (0.4-μm filters) with a TOC-V CPN (Shimadzu, Tokyo, Japan) analyzer using high-temperature (680°C) combustion. Total nitrogen (TN) was measured with an elemental analyzer (VarioEL III, Germany). Ammonia (NH_4^+) and nitrate (NO_3^-) were extracted with 2 M KCl. Total phosphorus (TP) was assayed by HF-$HClO_4$ digestion, and phosphate (PO_4^{3-}) was extracted by sodium bicarbonate extraction. NH_4^+, NO_3^-, TP, and PO_4^{3-} were measured using a continuous-flow analyzer (Skalar Analytical BV, Breda, Netherlands). Total sulfur (TS), total manganese (TMn), and total iron (TFe) were assayed by HF-$HClO_4$ digestion and 10% HNO_3 extraction. Soil sulfate (SO_4^{2-}) was assayed from a soil: distilled water (1:5, *w/v*) solution. TS, SO_4^{2-}, TMn, and TFe concentrations were measured using the ICPS-7500 sequential plasma spectrometer (Shimadzu, Tokyo, Japan). Ferrous ion (Fe^{2+}) and ferric ion (Fe^{3+}) contents were analyzed using the ferrozine–ultraviolet absorbance method (Stookey, 1970). The oxidation–reduction potential (ORP) of water samples was assessed in the field using an ORP meter (PHS-JPB-607A, Shanghai, China).

DNA Extraction, PCR Amplification, and Illumina Sequencing

Bacterial DNA was isolated from samples using the Power Soil DNA Isolation Kit (MoBio Laboratories, Inc., Carlsbad, CA, United States) according to the manufacturer's protocol. DNA quality and quantity were assessed by the optical density at wavelength 260/230-nm and 260/280-nm ratios, respectively. The 16S rRNA V3–V4 region was amplified for each sample using the 338F (5′-ACTCCTACGGGAGGCAGCA-3′) and 806R (5′-GGACTACHVGGGTWTCTAAT-3′) primer pair. The primers were modified to contain a unique 8-nucleotide barcode at the 5′ end (Mori et al., 2014). PCR amplification and quantification details have been previously described (Yang et al., 2019a). Briefly, thermal cycling conditions of the first PCR step were as follows: an initial denaturation at 95°C for 5 min, followed by 15 cycles at 95°C for 1 min, 50°C for 1 min, and 72°C for 1 min, with a final extension at 72°C for 7 min. The thermal cycling conditions of second PCR step were as follows: an initial denaturation at 98°C for 30 s, followed by 10 cycles at 98°C for 10 s, 65°C for 30 s min, and 72°C for 30 s, with a final extension at 72°C for 5 min. Then, the amplified products were purified and recovered using the 1.0% agarose gel electrophoresis method. HTS analysis of bacterial rRNA genes was performed on purified samples using the Illumina HiSeq 2500 platform (2 × 250 paired ends). All raw sequences have been deposited into the NCBI Sequence Read Archive with the accession number SRP270023.

Processing of the Sequencing Data

Raw Illumina fastq files were demultiplexed, quality filtered, and analyzed using QIIME 2. Sequencing reads were merged using FLASH (version 1.2.7[1]) based on overlapping regions within paired-end reads (Magoc and Salzberg, 2011). The trimmed sequences were compared to the primers, and the tags with more than six mismatches were discarded using the FASTX-Toolkit. Tags with an average quality score of <20 in a 50-bp sliding window were truncated using Trimmomatic (version 0.33), and tags shorter than 350 bp were removed. Chimeras were detected and removed using UCHIME (version 4.2). High-quality sequences were clustered using USEARCH (version 10.0), and the tags were clustered into operational taxonomic units (OTUs) at a 97% similarity threshold. Taxonomy was assigned to all OTUs by searching against the SILVA databases (release 128[2]).

Iron redox cycling bacteria were initially identified at the genus level *via* the Functional Annotation of Prokaryotic Taxa database (Louca et al., 2016). Wang et al. (2009) used the BLAST 16S rRNA database to identify novel 16S rRNA primers targeting Gallionella-related bacteria, and thus all OTU sequences of iron redox cycling bacteria at the genus level in our research were compared with existing sequences using the online BLAST 16S rRNA database[3]. Sequences showing >97% similarity with FeOB and FeRB were retained and defined as potential iron redox cycling bacteria (Weber et al., 2006; Emerson et al., 2010; Melton et al., 2014). Additionally, these bacteria of FeOB and FeRB were selected for phylogenetic tree reconstruction to clarify their taxonomic status in MEGA-X using the neighbor-joining algorithm (Kumar et al., 2018).

Statistical and Bioinformatic Analysis

Alpha diversity indices relating to community diversity (Shannon and Simpson) and sequencing depth (Good's coverage) were calculated by Mothur (version 1.30[4]). Alpha diversity indices were tested for differences among three peatland types and four regions by one-way analysis of variance (ANOVA) using SPSS 17.0 for Windows (IBM SPSS Inc., United States). For beta diversity, non-metric multidimensional scaling (NMDS), coupled with analysis of similarity (ANOSIM), was used to visualize the differences in composition among peatland types (fen, bog, and fen–bog complex) and regions (SJ, CB, LK, and GK), and significance tests of differences were performed using the Bray–Curtis dissimilarity. The independent influences of regions, soil physicochemical properties, and iron redox cycling

[1]https://ccb.jhu.edu/software/FLASH/

[2]http://www.arb-silva.de

[3]http://www.ncbi.nlm.nih.gov

[4]http://www.mothur.org

bacterial community composition were assessed by Mantel's test. To identify the main physicochemical properties that were significantly correlated with bacterial communities involved in iron redox cycling, redundancy analysis (RDA) combined with forward selection was applied using the forward.sel function in the R package. The proportion of variation in the iron redox cycling bacterial communities that could be explained by spatial variables (geographical distances) and environmental variables was calculated by variation partitioning analysis (VPA). The NMDS, ANOSIM, Mantel's test, RDA, and VPA were conducted in the R platform with the vegan package (R Development Core Team, 2006).

Distance–decay describes how the similarity in species composition between two communities varies with the geographic distance that separates them (Morlon et al., 2008). To visualize distance–decay relationships (DDRs) of iron redox cycling bacterial community similarity and environmental dissimilarity, iron redox cycling bacterial community similarity was calculated *via* the Bray–Curtis dissimilarity and the environmental heterogeneity of each sample was calculated based on the Euclidean distance. Regarding environmental heterogeneity, except for soil pH, all other environmental variables were first standardized at the same scale and checked using the Shapiro–Wilk test and then log $(x + 1)$-transformed to improve homoscedasticity and normality (Mo et al., 2018). The microbial community similarity, environmental dissimilarity, and geographic distance matrixes were linearized using the vegan package and the DDRs were linearized in the R platform.

To investigate the community assembly mechanism (deterministic process vs. stochastic process), a null model analysis was conducted using abundance-based similarity metrics. A null model is a pattern-generating model that is based on randomization of ecological data or random sampling from a known or imagined distribution (Gotelli and Graves, 1996). Permutational multivariate analysis of variance (PERMANOVA), a non-parametric permutation test, was used to test the significance of the differences between the observed similarity matrices and the null model expectation of the iron redox cycling bacterial communities. If community assembly is primarily driven by deterministic processes, the actual bacterial communities will be significantly different from the corresponding null expectations. In contrast, if community assembly is primarily driven by stochastic processes, the actual similarity observed will be statistically indistinguishable from that of the random null expectation (Zhang et al., 2019). In addition, the standardized effect size (SES) was calculated as the differences in beta diversity between the real communities and the mean value of null communities divided by the standardized deviation of the beta diversity in the null communities. The relative importance of stochastic processes increases when SES is closer to zero (Ren et al., 2017). Null model analysis and PERMANOVA were performed using Vegan and Parallel packages in the R platform.

To identify indicative taxa, the linear discriminant analysis (LDA) effect size (LEfSe) method was used based on a normalized relative abundance matrix. The LEfSe method uses the Kruskal–Wallis test to identify the features that differed significantly among peatland types. An LDA threshold score of 4.0 and a significant P of 0.05 were used to detect indicator species among treatments. Significant taxa were used to generate taxonomic cladograms illustrating differences between sample genera using the website http://huttenhower.sph.harvard.edu/galaxy (Segata et al., 2011).

RESULTS

Physicochemical Properties of Surface Soil and Water

The physicochemical properties of soil and water samples differed from each other (**Tables 1**, **2**). The pH showed wide variation, ranging from 4.11 to 5.59 in soil and from 5.01 to 7.12 in water. Fe^{2+} was significantly and negatively correlated with pH ($r = -0.451$, $p < 0.01$) and NH_4^+ ($r = -0.302$, $p < 0.05$) and significantly and positively correlated with DOC ($r = 0.741$, $p < 0.01$) in water. In contrast, Fe^{3+} showed a significant positive correlation with pH ($r = 0.302$, $p < 0.05$) and NH_4^+ ($r = 0.352$, $p < 0.05$) and a significant negative correlation with DOC ($r = -0.390$, $p < 0.01$) in soil.

Composition of Bacteria Involved in Iron Redox Cycling

We identified 48 phylotypes showing >97% sequence similarity with verified FeOB and FeRB across the NCBI database. These OTUs belonged to four genera of FeOB and nine genera of FeRB (**Figure 1**). *Sideroxydans* and *Pedomicrobium* were the most enriched genera among the FeOB, while *Geobacter*, *Geothrix*, *Clostridium*, *Rhodoferax*, and *Pseudomonas* were the most enriched genera among the FeRB. The relative abundance of FeRB was approximately one to two orders of magnitude higher than that of FeOB at all sites. On average, FeOB accounted for 0.15% and 0.56% of the total bacteria in soil and water, respectively, and FeRB for 3.15% and 11.05%, respectively (**Figure 2**).

Cladogram analysis revealed that several groups of iron redox cycling bacteria in soil and water were associated with peatland type (**Figure 3**). In soil samples, the relative abundance of *Clostridium* was greatly enriched in fens. The relative abundances of *Geothrix*, *Desulfovibrio*, and *Sideroxydans* were markedly enriched in bogs (**Figure 3A**). In water samples, the relative abundances of *Rhodoferax*, *Geobacter*, and *Leptothrix* were highest in fen peatland, while that of *Desulfovibrio* was highest in bog (**Figure 3B**).

Assembly of Iron Redox Cycling Bacteria

Overall, we observed that community diversity was higher in FeRB than in FeOB in both water and soil samples (**Figure 4**). In soil samples, FeRB diversity was greatest in SJ. In water samples, FeRB diversity was significantly greater in SJ than in GK ($p < 0.05$). Meanwhile, the Shannon indices of fen FeRB were significantly greater than those of bog FeRB ($p < 0.05$). In addition, FeRB diversity in soil samples was greatest in fen. The above results indicated that the community diversity

TABLE 1 | Physicochemical properties of soil samples in peatlands (n = 3).

Site	Latitude and longitude	pH	TN (g kg^{-1})	NH_4^+ (mg kg^{-1})	NO_3^- (mg kg^{-1})	TP (g kg^{-1})	PO_4^{3-} (mg kg^{-1})	OM (%)	DOC (g kg^{-1})	TS (g kg^{-1})	SO_4^{2-} (mg kg^{-1})	Fe^{2+} (g kg^{-1})	Fe^{3+} (g kg^{-1})	TFe (g kg^{-1})	TMn (mg kg^{-1})
QL	47°46′N, 132°54′E	5.56	15.38	27.83	29.15	1.95	23.13	34.27	2.58	1.40	234.67	10.65	0.32	21.48	229.19
HH2	47°47′N, 133°38′E	5.29	28.79	28.35	4.06	1.07	4.79	72.32	2.41	1.41	71.23	3.43	0.14	5.96	331.72
BL	47°32′N, 133°54′E	5.59	21.27	37.27	34.53	1.03	15.08	43.29	2.75	1.44	91.37	5.46	0.33	13.12	231.59
JC1	42°21′N, 126.22′E	5.59	21.08	46.48	6.45	0.74	2.61	65.68	2.05	1.48	72.73	5.70	0.31	9.37	185.76
JC2	42°21′N, 126.22′E	5.15	19.98	55.14	4.63	0.70	2.72	65.77	3.00	1.67	70.68	4.12	0.50	8.46	219.02
JC3	42°21′N, 126.22′E	5.23	18.71	60.58	4.10	0.75	2.67	60.83	3.10	1.42	123.43	3.92	0.27	9.17	166.78
JC4	42°21′N, 126.22′E	5.20	19.89	40.95	5.33	0.80	2.35	67.55	2.13	1.47	87.42	4.73	0.48	7.60	126.36
WY1	48°34′N, 129°27′E	4.95	13.84	26.14	4.63	1.39	14.94	45.53	2.68	1.46	96.37	9.76	0.51	18.56	309.35
WY2	48°34′N, 129°27′E	4.83	14.63	21.90	5.31	1.25	9.78	60.04	3.34	1.63	117.55	6.95	0.38	11.13	261.21
WY3	48°33′N, 129°28′E	4.80	9.48	39.72	6.23	0.87	5.26	64.86	4.00	1.70	99.10	5.81	1.52	9.88	319.82
TB1	48°25′N, 129°08′E	4.48	13.08	21.29	3.74	1.23	5.47	57.37	4.22	1.73	76.76	3.27	7.31	18.39	228.58
TB2	48°25′N, 129°08′E	4.84	13.53	16.32	5.04	1.23	5.29	48.82	2.44	1.45	68.87	7.96	0.10	17.21	162.62
JS	51°08′N, 124°10′E	5.21	26.83	20.48	5.60	1.94	10.90	64.32	4.62	3.33	97.76	3.43	5.11	12.90	181.27
TQ2	52°57′N, 122°52′E	5.57	22.26	18.96	4.68	1.71	15.92	68.72	3.34	1.77	79.15	6.96	6.91	17.72	965.42
HT	51°37′N, 123°59′E	4.11	12.91	27.38	5.19	0.96	7.90	73.70	3.70	1.19	50.63	2.13	1.44	4.40	61.70

TN, total nitrogen; NH_4^+, ammonium; NO_3^-, nitrate; TP, total phosphorus; PO_4^{3-}, phosphate; OM, organic matter; DOC, dissolved organic carbon; TS, total sulfur; SO_4^{2-}, sulfate; Fe^{2+}, ferrous ion; Fe^{3+}, ferric ion; TFe, total iron; TMn, total manganese.

TABLE 2 | Physicochemical properties of water samples in peatlands (n = 3).

Site	Latitude and longitude	pH	TN (mg L^{-1})	NH_4^+ (mg L^{-1})	NO_3^- (mg L^{-1})	TP (mg L^{-1})	PO_4^{3-} (mg L^{-1})	OM (mg L^{-1})	DOC (mg L^{-1})	SO_4^{2-} (mg L^{-1})	Fe^{2+} (mg L^{-1})	Fe^{3+} (mg L^{-1})	TFe (mg L^{-1})	TMn (10^{-3} mg kg^{-1})	ORP (mV)
QL	47°46′N, 132°54′E	7.12	2.77	1.70	0.11	0.08	0.03	126.40	13.66	10.41	0.51	0.85	1.36	3.84	120.33
HH1	47°43′N, 133°35′E	6.20	2.04	0.04	1.04	0.05	0.01	243.73	41.71	0.95	1.01	2.71	3.72	3.58	111.00
HH2	47°47′N, 133°38′E	6.20	2.98	0.02	1.02	0.15	0.05	392.33	63.08	1.30	1.18	0.46	1.63	5.48	118.00
BL	47°32′N, 133°54′E	7.08	2.44	0.05	0.97	0.13	0.06	244.37	19.14	0.93	1.02	1.16	2.51	2.27	145.67
SJZ	47°32′N, 133°54′E	6.34	2.62	0.04	1.03	0.08	0.03	279.00	59.03	0.79	1.03	1.33	2.36	4.80	124.67
JC1	42°21′N, 126°22′E	6.19	2.22	0.07	0.66	0.08	0.03	386.87	96.39	2.00	1.84	11.52	13.36	6.42	81.67
JC2	42°21′N, 126°22′E	6.17	2.37	0.07	0.86	0.07	0.02	405.30	78.87	2.03	1.91	8.58	10.49	8.71	83.00
JC3	42°21′N, 126°22′E	6.29	1.83	0.06	0.45	0.07	0.02	365.00	105.35	2.56	1.72	3.96	5.68	4.22	111.00
JC4	42°21′N, 126°22′E	6.05	2.21	0.06	0.33	0.10	0.02	400.93	34.92	2.30	2.10	7.73	9.83	12.14	93.33
WY1	48°34′N, 129°27′E	5.63	1.39	0.01	0.07	0.24	0.13	627.00	133.13	2.78	3.76	7.64	11.39	3.80	98.00
WY2	48°34′N, 129°27′E	5.17	2.18	0.03	0.18	0.26	0.12	938.13	163.20	0.98	3.84	5.29	9.13	15.63	156.33
WY3	48°33′N, 129°28′E	5.06	1.86	0.04	0.22	0.17	0.04	704.67	159.47	1.75	3.34	1.89	5.23	12.96	204.67
WY4	48°33′N, 129°28′E	5.29	1.28	0.01	0.07	0.08	0.01	510.20	61.42	1.24	1.49	1.21	2.71	16.84	106.00
TB2	48°25′N, 129°08′E	6.07	0.96	0.01	0.08	0.12	0.05	321.50	58.34	1.22	2.27	1.59	3.86	19.91	120.33
JS	51°08′N, 124°10′E	6.14	1.12	0.04	0.16	0.07	0.01	222.67	74.82	3.51	2.74	3.04	5.78	4.03	75.33
TQ1	52°57′N, 122°52′E	5.97	1.52	0.01	0.11	0.08	0.01	532.90	65.39	0.76	1.27	0.54	1.81	16.78	120.67
TQ2	52°57′N, 122°52′E	6.02	1.17	0.02	0.07	0.33	0.01	453.87	66.00	0.96	1.34	1.42	2.76	6.13	176.33
HT	51°37′N, 123°59′E	5.01	1.41	0.04	0.31	0.12	0.03	437.03	93.94	1.16	1.39	0.44	1.83	4.03	229.33

TN, total nitrogen; NH_4^+, ammonium; NO_3^-, nitrate; TP, total phosphorus; PO_4^{3-}, phosphate; OM, organic matter; DOC, dissolved organic carbon; SO_4^{2-}, sulfate; Fe^{2+}, ferrous ion; Fe^{3+}, ferric ion; TFe, total iron; TMn, total manganese; T, temperature; DO, dissolved oxygen; ORP, oxidation-reduction potential.

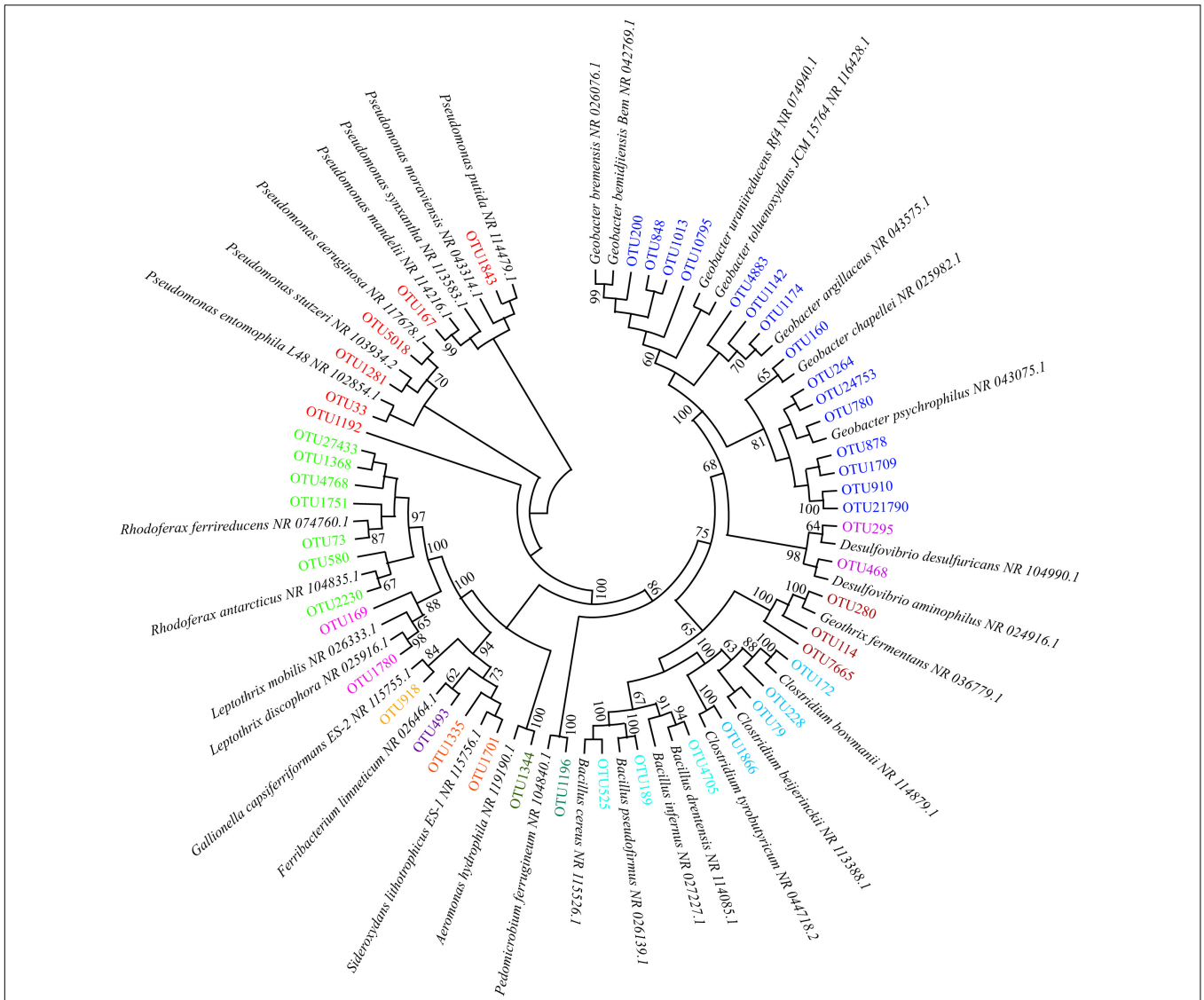

FIGURE 1 | Neighbor-joining phylogenetic tree of sequences obtained from peatland soil and water. Bootstrap values are shown near the nodes (based on 1,000 replicate trees). The phylotypes (operational taxonomic units [OTUs]) with sequence similarity with known Fe(II)-oxidizing and Fe(III)-reducing bacteria greater than 97% are labeled in different colors. The phylotypes labeled in the same color represent the same genus. For example, the phylotypes labeled in red represent *Pseudomonas*.

of iron redox cycling bacteria was correlated with distribution and peatland type.

Water-derived iron redox cycling bacterial communities showed no differences between region and peatland type (**Figure 5B**). Interestingly, regional distribution (r = 0.42, p = 0.001) had a greater effect on soil-derived iron redox cycling bacterial communities than peatland type (r = 0.28, p = 0.001) (**Figure 5A**).

We found that the similarity among observed communities was largely distinguishable from that of the null expectation for water, such as the water samples obtained from LK (p = 0.002) and Greater Khingan Mountain (p = 0.003). However, no notable differences (p > 0.05) were detected between the similarity among observed communities and that of the null expectation for soil. In addition, the similarity among observed communities was distinguishable from that of the null expectation for all peatland types (p < 0.05), except for soil samples from fen–bog complex and bog. The SES value was greater than zero in the samples from both soil and water, indicating deterministic and stochastic processes involved in the assembly of iron redox cycling bacteria, although their relative importance differed (**Table 3**).

Distribution Pattern of Iron Redox Cycling Bacteria

The pairwise similarity among iron redox cycling bacterial communities in soil samples decreased significantly with increasing geographic distance and environmental heterogeneity,

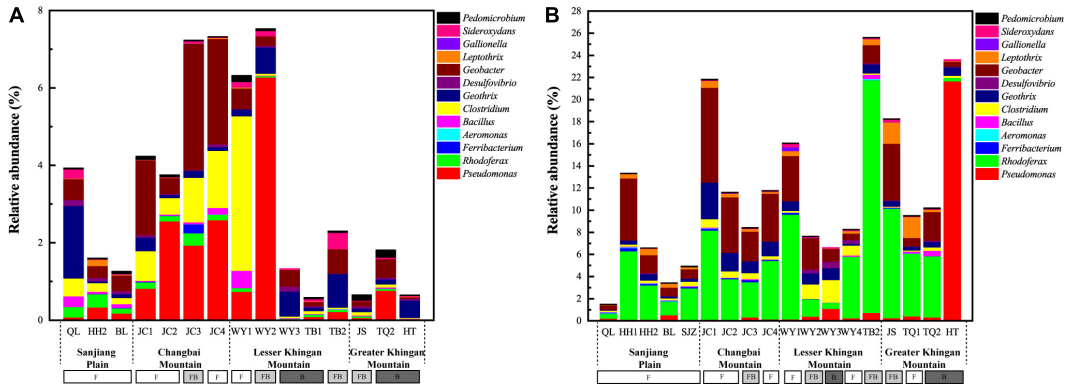

FIGURE 2 | The relative abundance of iron redox cycling bacteria in soil **(A)** and water **(B)**. F, fen; FB, fen–bog complex; B, bog.

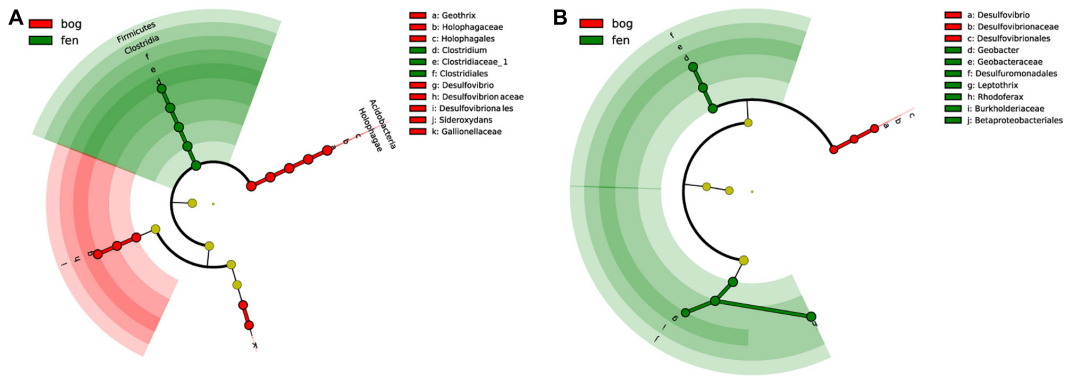

FIGURE 3 | Cladograms indicating the phylogenetic distribution of iron redox cycling bacterial lineages associated with regions in soil **(A)** and water **(B)**. Lineages were identified by linear discriminant analysis effect size (LEfSe) using a LDA score threshold of over 4.0. Circles represent phylogenetic levels from domain to species inside out. Labels are shown for the phylum and genus levels.

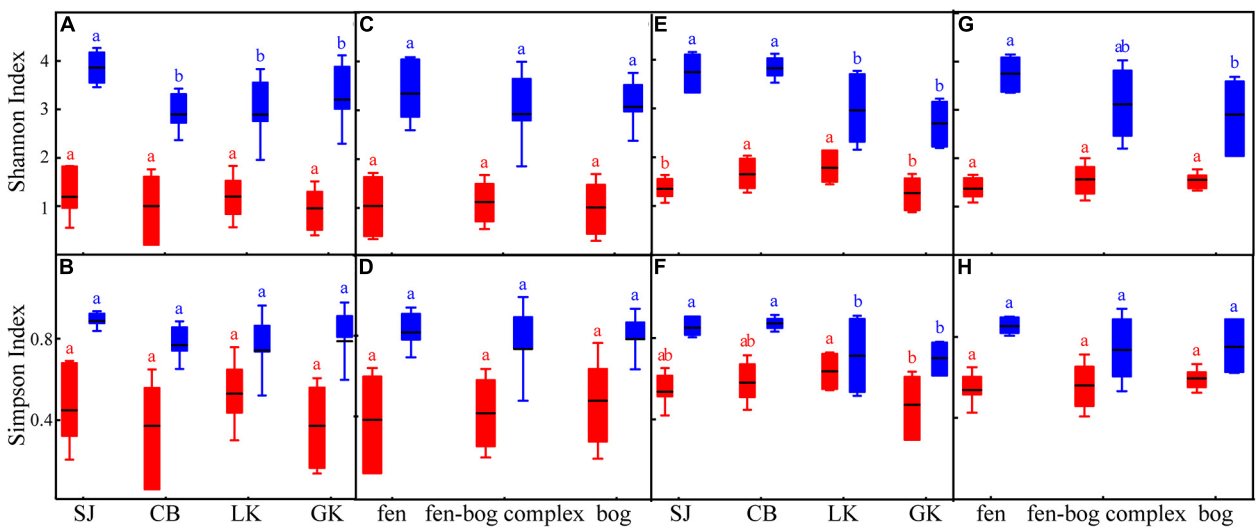

FIGURE 4 | The alpha diversity of iron redox cycling bacteria in soil **(A–D)** and water **(E–H)** of the different regions (Sanjiang Plain [SJ], Changbai Mountain [CB], Lesser Khingan Mountain [LK], and Greater Khingan Mountain [GK]) and peatland types (fen, fen–bog complex, bog). The red box represents iron-oxidizing bacteria; the blue box represents iron-reducing bacteria. Different letters indicate statistical significance among the different levels.

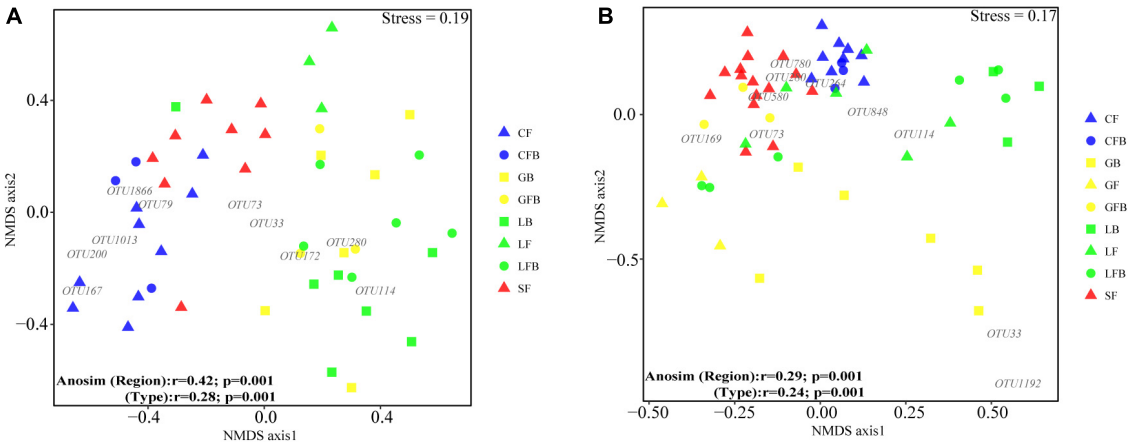

FIGURE 5 | Non-metric multidimensional scaling (NMDS) and two-way analysis of similarity (ANOSIM) of bacterial communities involved in iron redox cycling in soil **(A)** and water **(B)** based on Bray–Curtis dissimilarity. Red, blue, green, and yellow represent Sanjiang Plain, Changbai Mountain, Lesser Khingan Mountain, and Great Khingan Mountain, respectively. Triangles, circles, and squares represent fen, fen–bog complex, and bog, respectively. For example, blue triangles represent the fen in Changbai Mountain.

TABLE 3 | Significance test of the similarity between the observed bacterial communities and null model simulations and the standardized effect size (SES) across different sampling regions and peatland types based on weighted Bray–Curtis distances for iron redox cycling bacterial communities.

	Region and type	Mean of observed similarity	Mean of null expected similarity	*F*	*p*	SES	Ecological processes
Soil	Sanjiang Plain	0.430	0.545	2.862	0.117	1.724	Stochasticity
	Changbai Mountain	0.400	0.458	0.889	0.341	0.694	Stochasticity
	Lesser Khingan Mountain	0.277	0.351	1.220	0.256	1.865	Stochasticity
	Great Khingan Mountain	0.362	0.363	0.004	0.943	0.087	Stochasticity
	Fen	0.297	0.448	12.310	**0.001**	2.533	Determinism
	Fen–bog complex	0.217	0.302	3.075	0.086	2.036	Stochasticity
	Bog	0.333	0.398	1.096	0.301	0.725	Stochasticity
Water	Sanjiang Plain	0.449	0.523	1.942	0.189	2.277	Stochasticity
	Changbai Mountain	0.628	0.651	0.132	0.705	0.273	Stochasticity
	Lesser Khingan Mountain	0.410	0.587	14.249	**0.002**	2.513	Determinism
	Great Khingan Mountain	0.370	0.594	10.443	**0.003**	2.318	Determinism
	Fen	0.426	0.531	5.785	**0.029**	2.027	Determinism
	Fen–bog complex	0.461	0.613	9.395	**0.004**	2.288	Determinism
	Bog	0.299	0.533	14.983	**0.001**	2.909	Determinism

Permutational multivariate analysis of variance (PERMANOVA) was conducted. p-values <0.05 were in bold.

demonstrating that their variations were attributable to the joint effects of dispersal limitation and environmental selection. However, iron redox cycling bacterial community similarity in water samples was not correlated with geographic distance (p = 0.249) (**Figure 6**). In addition, Mantel path analysis showed that, in soil, the correlation coefficients of regions and peatland types with FeOB/FeRB community composition were greater than those between environmental factors and FeOB/FeRB community composition (**Supplementary Figure 1A**). However, the opposite trend was observed in water samples (**Supplementary Figure 1B**), indicating that the FeOB/FeRB community composition in water was more directly influenced by environmental factors.

Variance partitioning analysis (VPA) was used to quantify the relative contributions of environmental factors and spatial limitation to the community structure of iron redox cycling bacteria (**Figure 7**). Physicochemical properties and geographic distance explained 25.18% and 33.37% of the observed variation in soil and water, respectively. The contribution of geographic distance to the iron redox cycling bacterial community was significantly higher in soil (4.96%) than in water (0.30%). Regardless of whether samples were collected in soil or water, the relative contributions of physicochemical properties were significantly higher than those of geographic distance. RDA showed that pH appeared to be an important factor regulating the composition of iron redox cycling bacterial communities in both soil and water (**Figure 8**). For nutrients, NH_4^+, DOC, Fe^{2+}, and NO_3^- contributed more to mediate iron redox cycling bacterial communities in soil, while water-related bacterial communities involved in

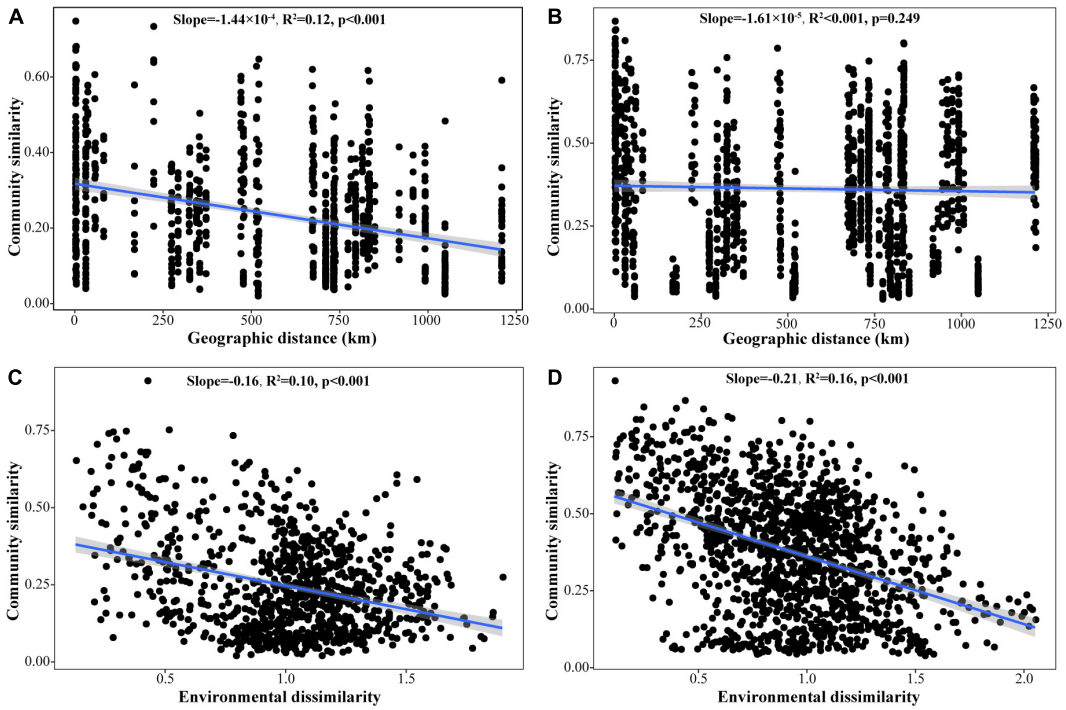

FIGURE 6 | Distance–decay relationships among iron redox cycling bacterial community similarity, geographic distance, and environmental dissimilarity for all sites in soil **(A,C)** and water **(B,D)**. Community similarity was calculated by 1-Bray–Curtis dissimilarity. Environmental dissimilarity was calculated by Euclidean distance.

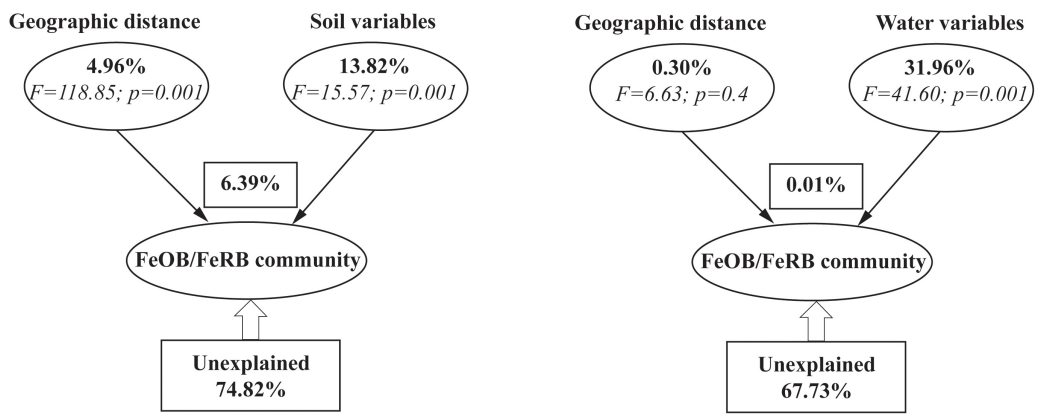

FIGURE 7 | Variation partitioning analysis of the effects of geographic distance and environmental variables on the phylogenetic structure of iron redox cycling bacterial communities.

iron redox cycling were mainly affected by N: P, DOC, TFe, and Fe^{2+}.

DISCUSSION

The Response of Iron Redox Cycling Bacteria to Physicochemical Properties

Several studies have reported that microbes are the primary oxidizers in anaerobic environments or environments with an oxygen content of less than 50 μM (Rentz et al., 2007; Chan et al., 2016). Additionally, we previously found that the relative abundance of iron redox cycling bacteria increased with increased soil moisture content during wetland restoration (Yang et al., 2019a). In the current study, we observed that the relative abundances of FeOB and FeRB were higher in flooded environments than in water-saturated environments. Intriguingly, minerotrophic fens were mostly flooded and ombrotrophic bogs were mostly water-saturated in our sampling sites. We speculated that the distribution of iron redox cycling bacteria may have been related to the type of peatland, which was consistent with the changing patterns of relative abundance

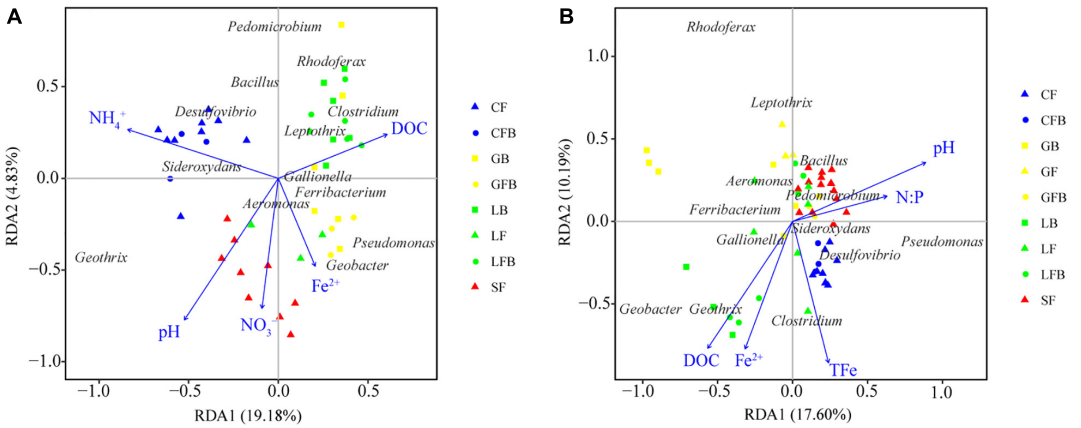

FIGURE 8 | Redundancy analysis of bacterial communities involved in iron redox cycling and environmental variables in soil **(A)** and water **(B)**. Red, blue, green, and yellow represent Sanjiang Plain, Changbai Mountain, Lesser Khingan Mountain, and Great Khingan Mountain, respectively. Triangles, circles, and squares represent fen, fen–bog complex, and bog, respectively. For example, the blue triangle represents the fen in Changbai Mountain.

and diversity of the iron redox cycling bacteria (**Figures 4**, **5**). For instance, the relative abundances of FeOB and FeRB in the peatlands of LK were both ranked in the order fen > fen–bog complex > bog (**Figure 2**). These findings demonstrated that iron redox cycling bacteria were more abundant in reducing conditions and may reflect the alternation of dry and wet conditions and hydrological fluctuation in peatlands (Küsel et al., 2008). The Fe cycle can be accompanied by migration and transformation of C, N, and P, indicating that iron redox cycling bacteria are relevant to ecological stoichiometry (Melton et al., 2014; Downie et al., 2018). Phosphorus has a strong affinity for iron oxyhydroxides, especially those associated with the sheaths of FeOB (Rentz et al., 2009). In addition, most nitrate-reducing FeOB require an organic co-substrate, such as acetate, to continually oxidize Fe(II) to Fe(III) (Muehe et al., 2009). In this study, the NMDS analysis revealed that the C:N and N:P ratios were significantly correlated with iron redox cycling bacteria (**Supplementary Table 2**). Du et al. (2020) evaluated the spatial characteristics of global N and P limitation based on the ratio of site-averaged leaf N and P resorption efficiencies of the dominant species and revealed that the natural terrestrial land area in Northeast China could be co-limited by N and P or weakly limited by either nutrient alone. This suggested that the interaction and balance of nutrient restricted individuals and communities of iron redox cycling bacteria. Furthermore, the results of the RDA revealed that NH_4^+ was also an important factor for the iron redox cycling bacterial community. Ammonium concentration is closely associated with iron redox cycling bacteria, both as an electron donor for iron oxidation and as a product of metabolism for use in iron reduction. For instance, *Geothrix* has been suggested to couple FeS_2 oxidation to NO_3^- reduction (Haaijer et al., 2007). Moreover, Zhou et al. (2016) recently reported that FeRB such as *Geobacter* play key roles in the Feammox (anaerobic ammonium oxidation coupled to iron(III) reduction) process.

We also observed that DOC and Fe^{2+} concentrations were common factors shaping the structure of iron redox cycling bacterial communities in both soil and water samples (**Figure 8**). DOC can not only constitute a carbon source for the growth of microorganisms but also improve the accessibility of other elements for microorganisms (Marschner and Kalbitz, 2003; Stenson, 2009). Daugherty et al. (2017) showed that complexation by organic ligands can increase the bioavailability of Fe(III). Besides, DOC can also be used as an electron donor and acceptor for repeated iron redox cycling (Klüpfel et al., 2014; Kügler et al., 2019). Intriguingly, the effect of pH on the regulation of community structure observed in our study was not in line with previously reported results. Numerous studies have documented that pH range is the primary factor regulating bacterial community composition. However, we observed that, although pH was indeed one of the influencing factors, it was not the most important limiting factor in shifting redox-cycling bacterial communities, even with variations in pH ranges of 1.48 and 2.11 units in soil and water samples, respectively. These results indicated that the selective pressure of environmental factors on whole bacterial communities or functional microorganisms such as iron redox cycling bacterial communities might be variable (Liu et al., 2016; Shi et al., 2020).

Indicative Taxa Across the Peatlands of Northeast China

Based on recently reported definitions of rare taxa (Xue et al., 2018), we found that 72.9%–87.5% of OTUs associated with iron redox cycling bacterial belonged to rare taxa (**Supplementary Table 3**). Zhou et al. (2020) demonstrated that rare bacterial species are more sensitive than abundant taxa to environmental changes. Therefore, iron redox cycling bacteria might play indicative roles in peatlands. In this study, we identified four genera of indicator bacteria in soil and four in water among the different peatland types (**Figure 3**).

Hydrological conditions restrict the distribution of some microbial groups (Yang et al., 2019b). Although the soil samples were collected on the surface layer in this study, fen soil samples

presented relatively reducing conditions due to the flooded conditions. In contrast, soil samples from bog exposed to the air exhibited relatively oxidizing conditions. As obligate anaerobic microorganisms, *Clostridium* and *Geobacter* are better suited to anoxic environments such as those found in wetlands, freshwater sediments, and oceans (Mohr et al., 2013; Zhou et al., 2014), likely explaining why the relative abundances of *Clostridium* in soil and *Geobacter* in water were higher in fens than in bogs. Finneran et al. (2003) found that *Rhodoferax* are facultative anaerobic bacteria that can oxidize acetate *via* the reduction of Fe(III), which might explain why *Rhodoferax* was enriched in fen water samples.

Except for *Desulfovibrio*, we found that the other indicator species in the water and soil showed inconsistencies. Based on the database of Functional Annotation of Prokaryotic Taxa (FAPROTAX) created by Louca et al. (2016), these indicator species are connected to the C cycle (ligninolysis, aromatic compound degradation, and fumarate respiration), N cycle (nitrification, denitrification, and nitrite ammonification), and S cycle (sulfate respiration, dissimilatory reduction of elemental sulfur, sulfite oxidation, and respiration). Our study showed that C concentration was significantly correlated with *Geothrix* and *Sideroxydans*, while N and S concentrations were significantly correlated with *Rhodoferax*, *Desulfovibrio*, *Geothrix*, and *Sideroxydans*. Intriguingly, we found that the genera *Geobacter*, *Desulfovibrio*, *Geothrix*, and *Sideroxydans* were significantly related to Fe^{2+} or total Fe (**Supplementary Table 4**). These results imply that metabolism may vary according to the microbial group, and further study is needed to identify potential interactions between those indicative taxa and link them to community composition and ecological functions.

Deterministic and Stochastic Processes in the Structuring of Iron Redox Cycling Bacterial Communities

The ecological mechanisms (determinism vs. stochasticity) associated with community assembly play important roles in shaping microbial community composition and structure. In general, a deterministic process is a non-random and niche-based ecological process, including environmental filtering and various biological interactions (e.g., competition, facilitation, mutualisms, and predation). However, a stochastic process is a random ecological process, including probabilistic dispersal, random speciation and extinction, and ecological drift (Stegen et al., 2012; Zhou and Ning, 2017). In our study, SES statistics confirmed that both deterministic and stochastic processes were involved in the assembly of bacterial communities involved in iron redox cycling. However, the DDR analysis indicated that deterministic processes played a more important role in regulating iron redox cycling-related bacterial communities in water compared with that in soil. Intriguingly, null model tests revealed that deterministic processes were dominant in water samples across the different peatland types, whereas stochastic processes substituted deterministic processes from minerotrophic fens to ombrotrophic bogs in soils. This indicated that iron redox cycling bacteria in soil were more likely to be governed by dispersal limitation. The differences in assembly mechanisms between iron redox cycling bacteria in water and soil across peatlands were mainly due to the different microbial types present as a result of environmental conditions (Wang et al., 2017; Mo et al., 2018). Zhou et al., 2002) proved that water disrupted the spatial isolation of soil bacteria and increased the interaction of bacterial communities; thus, we speculate that the dispersal limitation of iron redox cycling bacteria in soil could be alleviated by water.

Notably, iron redox cycling bacteria in soil and water were affected by environmental factors and spatial patterns, with the former having a greater impact than the latter (**Figure 7**). This was consistent with previous results reported in the black soils of northeast China (Liu et al., 2014, 2016). Nevertheless, the contribution of environmental variables was greater in water (31.96%) than in soil (13.82%), and the contribution of region was substantially greater in soil (4.96%) than in water (0.30%). One explanation may be that the soil environment is more complicated due to larger variations in temperature, hydrology, and nutrition, among other factors (Nie et al., 2009; Peralta et al., 2014; Wu et al., 2015). In contrast, the fluidity and solubility of water may, to some extent, homogenize environmental conditions (Jäger et al., 2016). Mantel path analysis also indicated that water-derived bacterial communities associated with iron redox cycling were more affected by environmental factors than by region or type of peatland, while the soil samples showed the opposite trend (**Supplementary Figure 1**). Consistent with this, DDR analysis indicated that iron redox cycling bacterial communities were mainly affected by environmental factors and that environmental factors exerted a more direct effect on iron redox cycling bacterial communities in water. These results indicated that environmental factors were more important than geographic location in determining the distribution of iron redox cycling bacterial communities in peatlands.

CONCLUSION

This study was the first to investigate the biogeographic distribution and mechanism of assembly of bacterial communities associated with iron redox cycling in surface soil and water samples collected from peatlands. Iron redox cycling bacteria were detected in all the samples; however, iron-reducing bacteria showed higher relative abundance and diversity than FeOB. To some extent, *Rhodoferax*, *Clostridium*, *Geothrix*, *Sideroxydans*, *Geobacter*, *Desulfovibrio*, and *Leptothrix* could be used as bioindicators in peatlands for characterizing different hydrological conditions and nutrient demands. Overall, DOC, Fe^{2+}, and pH were the key factors affecting the abundance and community composition of iron redox cycling bacteria. Distance–decay analysis indicated that bacterial communities associated with iron redox cycling in water displayed greater environmental heterogeneity, while those in soil displayed greater spatial limitation. Null model analysis based on species distribution further revealed that stochastic and deterministic

processes played important roles in mediating the assembly of bacterial communities involved in iron redox cycling in soil and water, respectively.

DATA AVAILABILITY STATEMENT

The data analyzed in this study is subject to the following licenses/restrictions: Further inquiries can be directed to the corresponding author. Requests to access these datasets should be directed to LY, yangliang@iga.ac.cn.

AUTHOR CONTRIBUTIONS

LY contributed to the investigation, methodology, and writing—original draft. MJ contributed to the supervision, funding acquisition, conceptualization, and writing—review and editing. YZ contributed to the funding acquisition and validation. LQ and YC contributed to the sampling and formal analysis. All authors contributed to the article and approved the submitted version.

FUNDING

This work was supported by the Joint Funds of the National Natural Science Foundation of China (U19A2042) and the National Natural Science Foundation of China (41771120 and 41971136).

ACKNOWLEDGMENTS

We thank the editor and the reviewers who helped improve the manuscript.

SUPPLEMENTARY MATERIAL

The Supplementary Material for this article can be found online at: https://www.frontiersin.org/articles/10.3389/fmicb.2021.674411/full#supplementary-material

Supplementary Figure 1 | Mantel path analysis linking the taxonomic composition of bacterial communities involved in iron redox cycling to different regions, peatland types, and physicochemical properties. **(A)** Soil; **(B)** water. Solid lines represent Mantel correlation coefficients; *p*-values are in parentheses.

REFERENCES

Chan, C. S., McAllister, S. M., Leavitt, A. H., Glazer, B. T., Krepski, S. T., and Emerson, D. (2016). The architecture of iron microbial mats reflects the adaptation of chemolithotrophic iron oxidation in freshwater and marine environments. *Front*. Microbiol. 7:796. doi: 10.3389/fmicb.2016.00796

Daugherty, E. E., Gilbert, B., Nico, P. S., and Borch, T. (2017). Complexation and redox buffering of iron(II) by dissolved organic matter. *Environ. Sci. Technol.* 51, 11096–11104. doi: 10.1021/acs.est.7b03152

Downie, H. F., Standerwick, J. P., Burgess, L., Natrajan, L. S., and Lloyd, J. R. (2018). Imaging redox activity and Fe(II) at the microbe-mineral interface during Fe(III) reduction. *Res. Microbiol.* 169, 582–589. doi: 10.1016/j.resmic.2018.05.012

Du, E., Terrer, C., Pellegrini, A., Ahlström, A., van Lissa, C. J., Zhao, X., et al. (2020). Global patterns of terrestrial nitrogen and phosphorus limitation. *Nat. Geosci.* 13, 221–226. doi: 10.1038/s41561-019-0530-4

Dubinsky, E. A., Silver, W. L., and Firestone, M. K. (2010). Tropical forest soil microbial communities couple iron and carbon biogeochemistry. *Ecology* 91, 2604–2612. doi: 10.1890/09-1365.1

Emerson, D., Fleming, E. J., and McBeth, J. M. (2010). Iron-oxidizing bacteria: an environmental and genomic perspective. *Annu. Rev. Microbiol.* 64, 561–583. doi: 10.1146/annurev.micro.112408.134208

Emerson, D., and Floyd, M. M. (2005). Enrichment and isolation of iron-oxidizing bacteria at neutral pH. *Method. Enzymol.* 397, 112–123. doi: 10.1016/S0076-6879(05)97006-7

Finneran, K. T., Johnsen, C. V., and Lovley, D. R. (2003). Rhodoferax ferrireducens sp. nov., a psychrotolerant, facultatively anaerobic bacterium that oxidizes acetate with the reduction of Fe(III). *Int. J. Syst. Evol. Micr.* 53, 669–673. doi: 10.1099/ijs.0.02298-0

Glodowska, M., Stopelli, E., Schneider, M., Rathi, B., Straub, D., Lightfoot, A., et al. (2020). Arsenic mobilization by anaerobic iron-dependent methane oxidation. *Commu. Earth. Environ.* 1:67. doi: 10.1038/s43247-020-00037-y

Gorham, E. (1991). Northern peatlands: role in the carbon cycle and probable responses to climatic warming. *Ecol. Appl.* 1, 182–195. doi: 10.2307/1941811

Gotelli, N. J., and Graves, G. R. (1996). *Null Models in Ecology*. Washington, D.C: Smithsonian Institution Press, 1–20.

Haaijer, S. C. M., Harhangi, H. R., Meijerink, B. B., Arjan Pol, M. S., Smolders, A. J. P., Verwegen, K., et al. (2008). Bacteria associated with iron seeps in a sulfur-rich, neutral pH, freshwater ecosystem. *ISME. J.* 2, 1231–1242. doi: 10.1038/ismej.2008.75

Haaijer, S. C. M., Lamers, L. P. M., Smolders, A. J. P., and Jetten, M. S. M. (2007). Iron sulphide and pyrite as potential electron donors for microbial nitrate reduction in freshwater wetlands. *Geomicrobiol. J.* 24, 391–401.

Han, Y. Y., Wang, M., Wang, S. Z., et al. (2018). Characteristics of soil enzyme activity of peat bog in jinchuan, changbai mountain. *Wetland Sci.* 16, 671–678. doi: 10.13248/j.cnki.wetlandsci.2018.05.014

Herath, I., Zhao, F. J., Bundschuh, J., Wang, P., Wang, J., Ok, Y. S., et al. (2010). Microbe mediated immobilization of arsenic in the rice rhizosphere afterincorporation of silica impregnated biochar composites. *J. Hazard. Mater.* 398:123096. doi: 10.1016/j.jhazmat.2020.123096

Huang, H., Zhu, Y. G., Chen, Z., Yin, X., and Sun, G. (2012). Arsenic mobilization and speciation during iron plaque decomposition in a paddy soil. *J. Soils. Sediments.* 12, 402–410. doi: 10.1007/s11368-011-0461-1

Jäger, A., Bertmer, M., and Schaumann, G. E. (2016). The relation of structural mobility and water sorption of soil organic matter studied by 1H and 13C solid-state NMR. *Geoderma* 284, 144–151. doi: 10.1016/j.geoderma.2016.08.024

Jiang, L., Song, C. C., and Song, Y. Y. (2018). Indoor simulation study on carbon and nitrogen contents and enzyme activities of soils in permafrost region in greater khingan mountains. *Wetland Sci.* 16, 295–302. doi: 10.13248/j.cnki.wetlandsci.2018.03.003

Jickells, T. D., An, Z. S., Andersen, K. K., Baker, A. R., Bergametti, G., Brooks, N., et al. (2005). Global iron connections between desert dust, ocean biogeochemistry, and climate. *Science* 308, 67–71. doi: 10.1126/science.1105959

Kappler, A., Bryce, C., Mansor, M., Lueder, U., Byrne, J. M., Swanner, E. D., et al. (2021). An evolving view on biogeochemical cycling of iron. *Nat. Rev. Microbiol.* doi: 10.1038/s41579-020-00502-7

Klüpfel, L., Piepenbrock, A., Kappler, A., and Sander, M. (2014). Humic substances as fully regenerable electron acceptors in recurrently anoxic environments. *Nat. Geosci.* 7, 195–200. doi: 10.1038/ngeo2084

Konstantinidis, K. T., and Tiedje, J. M. (2007). Prokaryotic taxonomy and phylogeny in the genomic era: advancements and challenges ahead. *Curr. Opin. Microbiol.* 10, 504–509. doi: 10.1016/j.mib.2007.08.006

Kügler, S., Cooper, R. E., Wegner, C. E., Mohr, J. F., Wichard, T., and Küsel, K. (2019). Iron-organic matter complexes accelerate microbial iron cycling in an

iron-rich fen. *Sci. Total. Environ.* 646, 972–988. doi: 10.1016/j.scitotenv.2018.07.258

Kumar, S., Stecher, G., Li, M., Knyaz, C., and Tamura, K. (2018). MEGA X: molecular evolutionary genetics analysis across computing platforms. *Mol. Biol. Evol.* 35, 1547–1549. doi: 10.1093/molbev/msy096

Küsel, K., Blothe, M., Schulz, D., Reiche, M., and Drake, H. L. (2008). Microbial reduction of iron and porewater biogeochemistry in acidic peatlands. *Biogeo. Sci.* 5, 1537–1549. doi: 10.5194/bg-5-1537-2008

Liu, J., Sui, Y., Yu, Z., Shi, Y., Chu, H., Jin, J., et al. (2014). High throughput sequencing analysis of biogeographical distribution of bacterial communities in the black soils of northeast china. *Soil. Biol. Biochem.* 70, 113–122. doi: 10.1016/j.soilbio.2013.12.014

Liu, J., Sui, Y., Yu, Z., Yao, Q., Shi, Y., Chu, H., et al. (2016). Diversity and distribution patterns of acidobacterial communities in the black soil zone of northeast china. *Soil. Biol. Biochem.* 95, 212–222. doi: 10.1016/j.soilbio.2015.12.021

Louca, S., Parfrey, L. W., and Doebeli, M. (2016). Decoupling function and taxonomy in the global ocean microbiome. *Science* 353, 1272–1277. doi: 10.1126/science.aaf4507

Lu, J., Zhang, B., He, C., and Borthwick, A. G. L. (2020). The role of natural Fe(II)-bearing minerals in chemoautotrophic chromium (VI) bio-reduction in groundwater. *J. Hazard. Mater.* 389:121911. doi: 10.1016/j.jhazmat.2019.121911

Lu, R. K. (1999). *Soil Argrochemistry Analysis Protocoes*. Beijing: China Agriculture Science Press, 107.

Lüdecke, C., Reiche, M., Eusterhues, K., Nietzsche, S., and Küsel, K. (2010). Acid-tolerant *Microaerophilic* Fe(II)-oxidizing bacteria promote Fe(III)-accumulation in a fen. *Environ. Microbiol.* 12, 2814–2825. doi: 10.1111/j.1462-2920.2010.02251.x

Magoc, T., and Salzberg, S. L. (2011). Flash: fast length adjustment of short reads to improve genome assemblies. *Bioinformatics* 27, 2957–2963. doi: 10.1093/bioinformatics/btr507

Man, X. L., Liu, B., and Li, Y. (2010). Distribution characteristics of organic carbon, nitrogen and phosphorus in the soils of herbaceous peat swamps in the Xiaoxing'an mountains. *J. Beijing Forest. Univ.* 32, 48–53.

Marschner, B., and Kalbitz, K. (2003). Controls of bioavailability and biodegradability of dissolved organic matter in soils. *Geoderma.* 113, 211–235. doi: 10.1016/S0016-7061(02)00362-2

Melton, E. D., Swanner, E. D., Behrens, S., Schmidt, C., and Kappler, A. (2014). The interplay of microbially mediated and abiotic reactions in the biogeochemical Fe cycle. *Nat. Rev. Microbiol.* 12, 797–808. doi: 10.1038/nrmicro3347

Mo, Y., Zhang, W., Yang, J., Lin, Y., Yu, Z., and Lin, S. (2018). Biogeographic patterns of abundant and rare bacterioplankton in three subtropical bays resulting from selective and neutral processes. *ISME. J.* 12, 2198–2210. doi: 10.1038/s41396-018-0153-6

Mohr, G., Hong, W., Zhang, J., Cui, G. Z., Yang, Y., Cui, Q., et al. (2013). A targetron system for gene targeting in thermophiles and its application in clostridium thermocellum. *PLos One* 8:e69032. doi: 10.1371/journal.pone.0069032

Mori, H., Maruyama, F., Kato, H., Toyoda, A., Dozono, A., Ohtsubo, Y., et al. (2014). Design and experimental application of a novel non-degenerate universal primer set that amplifies prokaryotic 16S rRNA genes with a low possibility to amplify eukaryotic rRNA genes. *DNA. Res.* 21, 217–227. doi: 10.1093/dnares/dst052

Morlon, H., Chuyong, G., Condit, R., Hubbell, S., Kenfack, D., Thomas, D., et al. (2008). A general framework for the distance–decay of similarity in ecological communities. *Ecol. Lett.* 11, 904–917. doi: 10.1111/j.1461-0248.2008.01202.x

Muehe, E. M., Gerhardt, S., Schink, B., and Kappler, A. (2009). Ecophysiology and the energetic benefit of mixotrophic Fe(II) oxidation by various strains of nitrate-reducing bacteria. *FEMS Microbiol. Ecol.* 70, 335–343. doi: 10.1111/j.1574-6941.2009.00755.x

Nie, M., Zhang, X., Wang, J., Jiang, L., Yang, J., Quan, Z., et al. (2009). Rhizosphere effects on soil bacterial abundance and diversity in the yellow river deltaic ecosystem as influenced by petroleum contamination and soil salinization. *Soil. Biol. Biochem.* 41, 2535–2542. doi: 10.1016/j.soilbio.2009.09.012

Parro, V., Moreno-Paz, M., and Gonzalez-Toril, E. (2007). Analysis of environmental transcriptomes by DNA microarrays. *Environ. Microbiol.* 9, 453–464. doi: 10.1111/j.1462-2920.2006.01162.x

Peralta, A. L., Ludmer, S., Matthews, J. W., and Kent, A. D. (2014). Bacterial community response to changes in soil redox potential along a moisture gradient in restored wetlands. *Ecol. Eng.* 73, 246–253. doi: 10.1016/j.ecoleng.2014.09.047

Pierra, M., Carmona-Martínez, A. A., Trably, E., Godon, J. J., and Bernet, N. (2015). Microbial characterization of anode-respiring bacteria within biofilms developed from cultures previously enriched in dissimilatory metal-reducing bacteria. *Bioresource. Technol.* 195, 283–287. doi: 10.1016/j.biortech.2015.07.010

R Development Core Team. (2006). *R, a Language and Environment for Statistical Computing*. Vienna, Austria: R 21. Foundation for Statistical Computing.

Raiswell, R., and Canfield, D. E. (2012). The iron biogeochemical cycle past and present. *Geochem. Perspect.* 1, 1–2. doi: 10.7185/geochempersp.1.1

Reiche, M., Torburg, G., and Küsel, K. (2008). Competition of Fe(III) reduction and methanogenesis in an acidic fen. *FEMS. Microbiol. Ecol.* 65, 88–101. doi: 10.1111/j.1574-6941.2008.00523.x

Ren, L., He, D., Chen, Z., Jeppesen, E., Lauridsen, T. L., Søndergaard, M., et al. (2017). Warming and nutrient enrichment in combination increase stochasticity and beta diversity of bacterioplankton assemblages across freshwater mesocosms. *ISME. J.* 11, 613–625. doi: 10.1038/ismej.2016.159

Rentz, J., Turner, I. P., and Ullman, J. L. (2009). Removal of phosphorus from solution using biogenic iron oxides. *Water. Res.* 43, 2029–2035. doi: 10.1016/j.watres.2009.02.021

Rentz, J. A., Kraiya, C., Luther, G. W. I. I. I., and Emerson, D. (2007). Control of ferrous iron oxidation within circumneutral microbial iron mats by cellular activity and autocatalysis. *Environ. Sci. Technol.* 41, 6084–6089. doi: 10.1021/es062203e

Riedel, T., Zak, D., Biester, H., and Dittmar, T. (2013). Iron traps terrestrially derived dissolved organic matter at redox interfaces. *Proc. Natl. Acad. Sci. U. S. A.* 110, 10101–10105. doi: 10.1073/pnas.1221487110

Rousk, J., Bååth, E., Brookes, P. C., Lauber, C. L., Lozupone, C., Caporaso, J. G., et al. (2010). Soil bacterial and fungal communities across a pH gradient in an arable soil. *ISME. J.* 4, 1340–1351. doi: 10.1038/ismej.2010.58

Segata, N., Izard, J., Waldron, L., Gevers, D., Miropolsky, L., Garrett, W. S., et al. (2011). Metagenomic biomarker discovery and explanation. *Genome. Biol.* 12:R60. doi: 10.1186/gb-2011-12-6-r60

Shi, Y., Jiang, Y., Wang, S., Wang, X., and Zhu, G. (2020). Biogeographic distribution of comammox bacteria in diverse terrestrial habitats. *Sci. Total. Environ.* 717:137257. doi: 10.1016/j.scitotenv.2020.137257

Smith, R. L., Kent, D. B., Repert, D. A., and Böhlke, J. K. (2017). Anoxic nitrate reduction coupled with iron oxidation and attenuation of dissolved arsenic and phosphate in a sand and gravel aquifer. *Geochim. Cosmochim. Acta.* 196, 102–120. doi: 10.1016/j.gca.2016.09.025

Stegen, J., Lin, X., Konopka, A. E., and Fredrickson, J. K. (2012). Stochastic and deterministic assembly processes in subsurface microbial communities. *ISME. J.* 6, 1653–1664. doi: 10.1038/ismej.2012.22

Stenson, A. C. (2009). Fourier transform ion cyclotron resonancemass spectral characterization of metal-humic binding. *Rapid Commun. Mass Spectrom.* 23, 465–476. doi: 10.1002/rcm.3889

Stookey, L. L. (1970). Ferrozine - a new spectrophotometric reagent for iron. *Anal. Chem.* 42, 779–781. doi: 10.1021/ac60289a016

Todorova, S. G., and Costello, A. M. (2006). Design of Shewanella-specific 16S rRNA primers and application to analysis of Shewanella in a minerotrophic wetland. *Environ. Microbiol.* 8, 426–432. doi: 10.1111/j.1462-2920.2005.00908.x

Wang, J., Muyzer, G., Bodelier, P. L. E., and Laanbroek, H. J. (2009). Diversity of iron oxidizers in wetland soils revealed by novel 16S rRNA primers targeting gallionella-related bacteria. *ISME. J.* 3, 715–725. doi: 10.1038/ismej.2009.7

Wang, J., Zhang, T., Li, L., Li, J., Feng, Y., and Lu, Q. (2017). The patterns and drivers of bacterial and fungal β-diversity in a typical dryland ecosystem of northwest china. *Front. Microbiol.* 8:2126. doi: 10.3389/fmicb.2017.02126

Weber, K. A., Achenbach, L. A., and Coates, J. D. (2006). Microorganisms pumping iron: anaerobic microbial iron oxidation and reduction. *Nature* 4, 752–764. doi: 10.1038/nrmicro1490

Wu, J., Xiong, J., Hu, C., Shi, Y., Wang, K., and Zhang, D. (2015). Temperature sensitivity of soil bacterial community along contrasting warming gradient. *Appl. Soil. Ecol.* 94, 40–48. doi: 10.1016/j.apsoil.2015.04.018

Xu, X. W., Chen, C., Wang, P., Kretzschmar, R., and Zhao, F. J. (2017). Control of arsenic mobilization in paddy soils by manganese and iron oxides. *Environ. Pollut.* 231, 37–47. doi: 10.1016/j.envpol.2017.07.084

Xue, Y., Chen, H., Yang, J., Liu, M., Huang, B., and Yang, J. (2018). Distinct patterns and processes of abundant and rare eukaryotic plankton communities following a reservoir cyanobacterial bloom. *ISME. J.* 12, 2263–2277. doi: 10.1038/s41396-018-0159-0

Yang, L., Jiang, M., Zhu, W. H., Han, L. S., and Qin, L. (2019a). Soil bacterial communities with an indicative function response to nutrients in wetlands of northeastern china that have undergone natural restoration. *Ecol. Indic.* 101, 562–571. doi: 10.1016/j.ecolind.2019.01.037

Yang, F., Zhang, D., Wu, J., Chen, Q., Long, C., Li, Y., et al. (2019b). Anti-seasonal submergence dominates the structure and composition of prokaryotic communities in the riparian zone of the three gorges reservoir, china. *Sci. Total Environ.* 663, 662–672. doi: 10.1016/j.scitotenv.2019.01.357

Yi, W., You, J., Zhu, C., Wang, B., and Qu, D. (2013). Diversity, dynamic and abundance of geobacteraceae species in paddy soil following slurry incubation. *Eur. J. Soil. Biol.* 56, 11–18. doi: 10.1016/j.ejsobi.2013.01.004

Yu, Z., Loisel, J., Brosseau, D. P., Beilman, D. W., and Hunt, S. J. (2010). Global peatland dynamics since the last glacial maximum. *Geophys. Res. Lett.* 37:L13402. doi: 10.1029/2010gl043584

Yuan, H. Y., Ding, L. J., Wang, N., Chen, S. C., Deng, Y., Li, X. M., et al. (2016). Geographic distance and amorphous iron affect the abundance and distribution of *Geobacteraceae* in paddy soils in China. *J. Soil. Sediment.* 16, 2657–2665. doi: 10.1007/s11368-016-1462-x

Zhang, Z., Deng, Y., Feng, K., Cai, W., Li, S., Yin, H., et al. (2019). Deterministic assembly and diversity gradient altered the biofilm community performances of bioreactors. *Environ. Sci. Technol.* 53, 1315–1324. doi: 10.1021/acs.est.8b06044

Zhou, G., Yang, X., Li, H., Marshall, C. W., Zheng, B., Yan, Y., et al. (2016). Electron shuttles enhance anaerobic ammonium oxidation coupled to iron(III) reduction. *Environ. Sci. Technol.* 50, 9298–9307. doi: 10.1021/acs.est.6b02077

Zhou, J., and Ning, D. (2017). Stochastic community assembly: does it matter in microbial ecology? *Microbiol. Mol. Biol. Rev.* 81, e00002–e17. doi: 10.1128/MMBR.00002-17

Zhou, J., Xia, B., Treves, D. S., Wu, L. Y., Marsh, T. L., O'Neill, R. V., et al. (2002). Spatial and resource factors influencing high microbial diversity in soil. *Appl. Environ. Microbiol.* 68, 326–334. doi: 10.1128/AEM.68.1.326-334.2002

Zhou, L., Zhou, Y., Yao, X., Cai, J., Liu, X., Tang, X., et al. (2020). Decreasing diversity of rare bacterial subcommunities relates to dissolved organic matter along permafrost thawing gradients. *Environ. Int.* 134:105330. doi: 10.1016/j.envint.2019.105330

Zhou, S., Yang, G., Lu, Q., and Wu, M. (2014). Geobacter soli sp. nov., a dissimilatory Fe(III)-reducing bacterium isolated from forest soil. *Int. J. Sys. Evol. Micr.* 64, 3786–3791. doi: 10.1099/ijs.0.066662-0

Zhu, X. Y., Song, C. C., Guo, Y. D., Shi, F., Zhang, J., Qiao, T., et al. (2015). The porewater methane concentration and controlling factors from the peatlands in the sanjiang plain. *Acta Sci. Circumst.* 35, 2233–2239.

Conflict of Interest: The authors declare that the research was conducted in the absence of any commercial or financial relationships that could be construed as a potential conflict of interest.

frontiers in Microbiology

ORIGINAL RESEARCH
published: 09 July 2021
doi: 10.3389/fmicb.2021.695260

"*Candidatus* Chlorobium masyuteum," a Novel Photoferrotrophic Green Sulfur Bacterium Enriched From a Ferruginous Meromictic Lake

*Nicholas Lambrecht[1], Zackry Stevenson[1], Cody S. Sheik[2,3], Matthew A. Pronschinske[1], Hui Tong[1,4] and Elizabeth D. Swanner[1]**

[1] Department of Geological and Atmospheric Sciences, Iowa State University, Ames, IA, United States, [2] Department of Biology, University of Minnesota Duluth, Duluth, MN, United States, [3] Large Lakes Observatory, University of Minnesota Duluth, Duluth, MN, United States, [4] Guangdong Key Laboratory of Integrated Agro-environmental Pollution Control and Management, National-Regional Joint Engineering Research Center for Soil Pollution Control and Remediation in South China, Guangdong Institute of Eco-environmental Science and Technology, Guangdong Academy of Sciences, Guangzhou, China

OPEN ACCESS

Edited by:
Lei Yan, Heilongjiang Bayi Agricultural University, China

Reviewed by:
Katharine J. Thompson, University of British Columbia, Canada
Petra Pjevac, University of Vienna, Austria

***Correspondence:**
Elizabeth D. Swanner
eswanner@iastate.edu

Specialty section:
This article was submitted to Microbiological Chemistry and Geomicrobiology, a section of the journal Frontiers in Microbiology

Received: *14 April 2021*
Accepted: *07 June 2021*
Published: *09 July 2021*

Citation:
Lambrecht N, Stevenson Z, Sheik CS, Pronschinske MA, Tong H and Swanner ED (2021) "Candidatus Chlorobium masyuteum," a Novel Photoferrotrophic Green Sulfur Bacterium Enriched From a Ferruginous Meromictic Lake. Front. Microbiol. 12:695260. doi: 10.3389/fmicb.2021.695260

Anoxygenic phototrophic bacteria can be important primary producers in some meromictic lakes. Green sulfur bacteria (GSB) have been detected in ferruginous lakes, with some evidence that they are photosynthesizing using Fe(II) as an electron donor (i.e., photoferrotrophy). However, some photoferrotrophic GSB can also utilize reduced sulfur compounds, complicating the interpretation of Fe-dependent photosynthetic primary productivity. An enrichment (BLA1) from meromictic ferruginous Brownie Lake, Minnesota, United States, contains an Fe(II)-oxidizing GSB and a metabolically flexible putative Fe(III)-reducing anaerobe. "*Candidatus* Chlorobium masyuteum" grows photoautotrophically with Fe(II) and possesses the putative Fe(II) oxidase-encoding *cyc2* gene also known from oxygen-dependent Fe(II)-oxidizing bacteria. It lacks genes for oxidation of reduced sulfur compounds. Its genome encodes for hydrogenases and a reverse TCA cycle that may allow it to utilize H_2 and acetate as electron donors, an inference supported by the abundance of this organism when the enrichment was supplied by these substrates and light. The anaerobe "*Candidatus* Pseudopelobacter ferreus" is in low abundance (~1%) in BLA1 and is a putative Fe(III)-reducing bacterium from the *Geobacterales* ord. nov. While "*Ca.* C. masyuteum" is closely related to the photoferrotrophs *C. ferrooxidans* strain KoFox and *C. phaeoferrooxidans* strain KB01, it is unique at the genomic level. The main light-harvesting molecule was identified as bacteriochlorophyll *c* with accessory carotenoids of the chlorobactene series. BLA1 optimally oxidizes Fe(II) at a pH of 6.8, and the rate of Fe(II) oxidation was 0.63 ± 0.069 mmol day^{-1}, comparable to other photoferrotrophic GSB cultures or enrichments. Investigation of BLA1 expands the genetic basis for phototrophic Fe(II) oxidation by GSB and highlights the role these organisms may play in Fe(II) oxidation and carbon cycling in ferruginous lakes.

Keywords: photoferrotrophy, Brownie Lake, meromictic, green sulfur bacterium, phototrophic Fe(II) oxidation, early Earth biogeochemistry, iron cycling, geomicrobiology

INTRODUCTION

Iron is a major redox-active element on Earth (Raiswell and Canfield, 2012). The biogeochemical cycling between the two main redox states, Fe(II) and Fe(III), is accomplished by both aerobic and anaerobic microbes, as well as abiotic chemical reactions (Melton et al., 2014). Active redox cycling mediated by microbes at the interface of oxic and anoxic settings couples the Fe biogeochemical cycles at Earth's surface to that of several other major elemental cycles (e.g., C, O, S, N; Kappler et al., 2021), underscoring the necessity to elucidate microbiological pathways that transform Fe and the controls on their activity in the environment.

Investigation of modern Fe cycling organisms may also help to constrain microbial processes in Precambrian (i.e., >540 million years ago; Ma) oceans, which were characterized by widespread and persistent ferruginous (anoxic and Fe-rich) conditions (Poulton and Canfield, 2011). Prior to the development of oxygenated surface waters after the Great Oxidation Event (GOE) at ∼2.4 billion years ago (Ga), anoxygenic photosynthetic bacteria (APB) that could utilize Fe(II) in the photic zone may have been the major marine primary producers fueling the biosphere in the Archean (4.0–2.5 Ga), sustaining up to 10% of modern-day primary productivity prior to the evolution of oxygenic photosynthesis by Cyanobacteria (Canfield et al., 2006; Jones et al., 2015). These organisms, collectively known as photoferrotrophs, are bacteria that use light energy, Fe(II) as an electron donor, and inorganic carbon to perform anoxygenic photosynthesis (Ehrenreich and Widdel, 1994; Kappler et al., 2005):

$$\text{light } (h\nu) + 4Fe^{2+} + CO_2 + 11H_2O \rightarrow 4Fe(OH)_3 + (CH_2O) + 8H^+ \quad (1)$$

Photoferrotrophs have been implicated as major contributors to primary productivity in ferruginous Kabuno Bay of Lake Kivu (Llirós et al., 2015; Morana et al., 2016). They fix carbon in ferruginous Lake Svetloe (Savvichev et al., 2017). In ferruginous Lake La Cruz, photoferrotrophic activity was detected despite these organisms being only a small fraction of the APB community (Walter et al., 2014). However, the presence of sunlight and ferruginous conditions are not strong indicators that photoferrotrophy is occurring or is biogeochemically significant; increasing genomic evidence suggests photoferrotrophic APB are potentially widespread and active in many lakes (Tsuji et al., 2020; Garcia et al., 2021).

Photoferrotrophs are phylogenetically diverse and include the classes Alphaproteobacteria (purple non-sulfur bacteria, PNSB), Gammaproteobacteria (purple sulfur bacteria, PSB), and the family *Chlorobiaceae* within the class Chlorobia (green sulfur bacteria, GSB). Isolates or defined co-cultures of photoferrotrophs include the freshwater PNSB *Rhodobacter ferrooxidans* strain SW2 (Ehrenreich and Widdel, 1994) and *Rhodopseudomonas palustris* strain TIE-1 (Jiao et al., 2005); the PSB include the freshwater *Thiodictyon* sp. (Ehrenreich and Widdel, 1994; Croal et al., 2004) and the marine *Rhodovulum robiginosom* and *Rhodovulum iodosum* (Straub et al., 1999); and the GSB include the marine *Chlorobium* sp. strain N1 enrichment (Laufer et al., 2017; Bryce et al., 2019), the freshwater *Chlorobium ferrooxidans* strain KoFox, which grows in coculture with *Geospirillum* sp. strain KoFum (Heising et al., 1999), the freshwater coculture of a strain closely related to *Chlorobium ferrooxidans* that grows in coculture with a strain closely related to *Rhodopseudomonas palustris* (Schmidt et al., 2021), and the isolate *Chlorobium phaeoferrooxidans* strain KB01 (Crowe et al., 2017). *C. phaeoferrooxidans* strain KB01 is the first photoferrotroph to be isolated from a ferruginous water column (Llirós et al., 2015).

In addition to Fe(II) oxidation, some APB can exploit sulfide as a photosynthetic electron donor (Straub et al., 1999; Laufer et al., 2017). APB utilize bacteriochlorophyll (Bchl) molecules and accessory pigments such as carotenoids to harvest light energy. Previous studies have documented the presence of Bchl *e* and increased methylation of hopanoids under ferruginous conditions and attributed their presence to photoferrotrophic activity (Eickhoff et al., 2013; Crowe et al., 2014). The detection of degradation products of such biomolecules (e.g., biomarkers) in ancient rocks has been used as evidence for euxinic conditions, i.e., free sulfide present, in the Phanerozoic (e.g., Summons and Powell, 1986; Grice et al., 2005; Mallorquí et al., 2005; Hays et al., 2007) and Paleoproterozoic oceans (e.g., Brocks et al., 2005; Brocks and Schaeffer, 2008). However, specific pigments do not always indicate the electron donor being used [i.e., Fe(II) or sulfide] and, by implication, ferruginous or euxinic environmental conditions. Rather, the presence of these biomarkers establishes paleoenvironments in which light reached anoxic portions of ancient water columns, inferring the presence of obligate anoxygenic phototrophs. To fully understand and interpret the biomarker record, identification of potential biomarkers produced by diverse modern photoferrotrophs, especially those active under ferruginous conditions, is required.

Here, we describe the enrichment and characterization of a novel pelagic Fe(II)-oxidizing photoferrotroph from a meromictic and ferruginous lake that is closely related to other phototrophic GSB, but distinct in genomic and physiological characteristics. Similar to other photoferrotrophic GSB (Heising et al., 1999; Bryce et al., 2019; Schmidt et al., 2021), this organism could not be isolated, but is the most abundant organism in the enrichment. The characterization of novel photoferrotrophs informs the framework for understanding how APB, specifically GSB, influence carbon and iron cycling within ferruginous systems. The organism described here is only the second photoferrotroph to be brought into enrichment from a ferruginous water column, which highlights the difficulties, but also value, in bringing these organisms into culture.

MATERIALS AND METHODS

Enrichment and Cultivation

Freshwater from Brownie Lake in Minneapolis, Minnesota, United States, was taken from the chemocline (5.5 m) in

May 2016. The field site and geochemical conditions have been described previously (Lambrecht et al., 2018). Site water (1 ml) was added to Hungate tubes containing 9 ml of freshwater (FW) medium amended with anoxic ferrous chloride ($FeCl_2$).

The FW medium for enrichment and cultivation had a salinity of 1.6. Per liter, the medium contained the following salts: 0.14 g KH_2PO_4, 0.3 g NH_4Cl, 0.5 g $MgSO_4 \times 7H_2O$, and 0.1 g $CaCl_2 \times 2H_2O$. The medium was degassed under N_2/CO_2 (90:10 v/v) and buffered with 22 mM $NaHCO_3$ (1.85 g l^{-1}). Lastly, the following supplements were added in 1-ml volumes per liter: vitamin solution (1 mg biotin, 10 mg nicotinate, 5 mg aminobenzoic acid, 2.5 mg Ca-D(+) pantothenate, 25 mg pyridoxamine dihydrochloride, 5 mg thiamine dihydrochloride, and 100 mg vitamin B_{12} in 100 ml Millipore water), selenium-tungstate solution (0.4 g NaOH, 6 mg $Na_2SeO_3 \times 5H_2O$, and 8 mg $Na_2WO_4 \times 2H_2O$ in 1 l Millipore water), and a trace element solution (10 ml of 25% HCl, 2.86 g H_3BO_3, 0.5 g $MnCl_2 \times 4H_2O$, 180 mg $ZnCl_2$, 36 mg $Na_2MoO_4 \times 2H_2O$, 2 mg $CuCl_2 \times 2H_2O$, 24 mg $NiCl_2 \times 6H_2O$, 190 mg $CoCl_2 \times 6H_2O$, and 1.5 g $FeCl_2 \times 4H_2O$ in 1 l Millipore water). The pH was adjusted using sterile anoxic 1 M HCl or 0.5 M Na_2CO_3 after autoclaving. Anoxic $FeCl_2$, prepared according to Hegler et al. (2008), was subsequently added (∼3 mM final conc.), and precipitation with phosphate and carbonate was allowed to occur at 4°C for 48 h. Following precipitation, the media was filtered (0.2 polyethersulfone filter) in an anoxic chamber (100% N_2), dispensed in serum bottles, and the headspace promptly exchanged for N_2/CO_2 (90:10 v/v).

Enrichment was done at 20°C with illumination from two fluorescent bulbs, one warm (2,700 K) and one cool (5,000 K), to provide the full spectrum of photosynthetically active radiation (PAR). Delivery of the full PAR spectrum from the two fluorescent bulbs was verified with a MSC15 spectral light meter (Gigahertz-Optik). A long-pass light filter (Edmund Optics) was initially used to allow only wavelengths longer than 700 nm to the tubes to exclude growth by oxygenic photosynthesis. After several months and four transfers, a series of two serial dilutions to extinctions were performed in an effort to isolate a single organism from the enrichment. A serial 10-fold dilution series prepared up to a dilution of 10^{-9}. The last dilution showing evidence of Fe(II) oxidation was transferred. Following dilution to extinction, and for all experiments subsequently described, the enrichment was incubated with the full PAR spectrum. For standard cultivation, a 4% inoculum was used.

DNA Sequencing and Bioinformatic Processing

To identify which organisms were present in the enrichment before dilution to extinction, DNA was extracted using the DNeasy PowerSoil Kit (Qiagen) according to the instructions of the manufacturer. Near full-length 16S rRNA gene sequences were obtained using the universal bacterial primers 27F (5′-AGAGTTTGATCCTGGCTCAG-3′) and 1492R (5′-TACGGYTACCTTGTTACGACTT-3′) (Lane, 1991). The PCR products were cloned into a plasmid vector with an ampicillin-resistant marker using the TOPO TA Cloning Kit (Thermo Fisher). Vectors were transformed into One Shot Top10 competent cells ThermoFisher (Waltham, MA, United States) that were afterward plated onto the LB medium containing ampicillin. Colonies were picked and tested for their correct size using the M13F (5′-CAGGAAACAGCTATGAC-3′) and M13R (5′-GTAAAACGACGGCCAG-3′) primer pair. The PCR product with the correct insert was purified with the PureLink PCR purification kit (Invitrogen). Sanger sequencing was performed on an Applied Biosystems 3730xl DNA Analyzer at the ISU DNA Facility. All clones sequenced were aligned with ClustalW (Thompson et al., 2003).

For genome sequencing after dilution to extinction, DNA was extracted using the DNeasy PowerSoil Kit (Qiagen, Germantown, MD, United States) and sent to the University of Minnesota Genomics Core for sequencing. Sequencing libraries were created using the Nextera-XT kit (Illumina) and sequenced on the MiSeq platform with 2 × 300 bp paired-end sequencing. Prior to assembly, raw reads were trimmed of adapters and screened for quality with FastP (Chen et al., 2018). The cleaned reads were assembled with SPAdes v. 3.14.0 (Nurk et al., 2013). Genome quality was assessed using Quast (Gurevich et al., 2013). Searches of 16S rRNA genes in the assembly with Barrnap (Seemann, 2018) revealed that the culture was not axenic and required genome binning. The assembly was binned with MetaBat1, Metabat2, and Maxbin2 (Kang et al., 2015; Wu et al., 2016; Kang et al., 2019). DASTool was used to select the highest-quality bins from the assemblies (Sieber et al., 2018). Genomes were assessed for completeness with CheckM (Parks et al., 2015) and taxonomy using GTDB-Tk (Chaumeil et al., 2019). The recovered genomes were genes called and annotated with MetaErg (Dong and Strous, 2019) and DRAM (Shaffer et al., 2020). FeGenie, a bioinformatics tool used to identify genes associated with Fe cycling, was used to screen the recovered genomes in the BLA1 enrichment for genes implicated in Fe cycling, specifically Fe(II) oxidation and Fe(III) reduction (Garber et al., 2020). The distance allowed between genes to be identified as a cluster was set to 5. A phylogenomic tree of the dominant recovered genomes with other closely related genomes was generated using GToTree (Lee, 2019). Genomes were downloaded from GTDB, and single-copy genes were identified with Hmmer[1]. Sixteen single-copy genes were used to assess the phylogenomic association (see Hug et al., 2016), as they have been shown to be robust for phylogenetic relationships. Prior to concatenation, the single-copy genes were individually aligned with Muscle (Edgar, 2004) and trimmed with trimAL (Capella-Gutiérrez et al., 2009). A maximum likelihood phylogenetic tree was created with IQ-TREE using default parameters (Nguyen et al., 2015). Genome relatedness of the *Chlorobia* genomes was assessed using Average Nucleotide Identity (ANI; Jain et al., 2018) and Digital DNA–DNA hybridization (DDH) with Genome-to-Genome Distance Tool (GGDC) (Meier-Kolthoff et al., 2013). The

[1]http://hmmer.org/

two genomes from this study were deposited to the National Center for Biotechnology Information (NCBI, Bioproject PRJNA611822) and the sequences to the sequence read archive (SRA; SRR11292469).

Characterization of Growth Substrates

Screening of Electron Donors

The enrichment was tested on the following electron donors for anoxygenic phototrophic growth: acetate, hydrogen (H_2) gas, hydrogen sulfide, thiosulfate, and sulfite. Acetate was added at a final concentration of 5 mM. Hydrogen gas was supplied to the culture by flushing the headspace every second day with H_2/CO_2 gas (90:10 v/v). The final concentrations of inorganic electron donors were as follows: sodium sulfide (2 mM), sodium thiosulfate (2 mM), and sodium sulfite (2 mM). Spectrophotometry at 600 nm was used to assess growth of the enrichment on alternative substrates.

Growth Experiments With Fe(II)

Fe(II) oxidation was tracked in two different types of experiments on the enrichment. The first was using triplicate bottles at different pH to determine the pH optimum. For this, three 50-ml serum bottles were filled with 25 ml of Fe(II) medium at each of the five initial pH conditions(6.7, 6.8, 6.9, 7.0, and 7.1) set with the bicarbonate-N_2/CO_2 buffer system and capped with rubber butyl stoppers. PAR intensity was measured with a LI-190R quantum sensor coupled to a LI-250A light meter (LiCOR). Cultures were kept in a 20°C incubator at an intensity of ∼4 μM photons m^{-2} s^{-1}. Fe(II) was assessed on unfiltered samples acidified directly into 1 N HCl and measured promptly with a ferrozine assay following a protocol adapted from Stookey (1970) and Viollier et al. (2000) using an Epoch 2 Microplate Reader (Biotek). The starting concentration of Fe(II) was ∼2.5 mM.

To determine cell-specific Fe(II) oxidation rates, triplicate 100-ml bottles were filled with 50 ml Fe(II) medium adjusted to pH 6.8. Controls included dark conditions with cells and light without cells (control for photo-oxidation). Fe(II) concentrations were tracked as above. For growth quantification, samples were extracted and immediately fixed with paraformaldehyde (final conc. 3.8%) and stored at 4°C. Fe-oxide digestion and filtration onto black filters were conducted following Wu et al. (2014). Cells were stained with Sytox (1:50 dilution). Fluorescent images were collected using a Leica DFC7000T microscope. Twenty fields of view or 1,000 cells were enumerated for each replicate at each time point. Cell counting was aided by the 3D Objects Counter from ImageJ (Abràmoff et al., 2004). The maximum rate of Fe(II) oxidation was calculated for each replicate by linear regression of the steepest part of their respective Fe(II) vs. time plots (minimum three points).

Photosynthetic Pigment Identification

Pigment Extraction

Pigment extraction was performed following an in-house protocol created by the Metabolomics Lab at ISU based on published protocols (Costas et al., 2012; Bóna-Lovász et al., 2013). The enrichment was grown with ferrous iron, in stationary phase, and was centrifuged at 1,000 rpm for 15 min followed by removal of the supernatant. An acetone/methanol solution (7:2 v/v) was added to the spun-down cells and sonicated in a water bath for 10 min, then vortexed for 10 min at maximum speed. After centrifugation at 1,000 rpm for 10 min, the supernatant containing the pigments was transferred to a clean tube and dried under a constant stream of N_2 gas. Once dried, concentrated pigments were resuspended in ∼0.4 ml of the acetone/methanol solution.

UHPLC and MS(n) Analysis

Concentrated Bchl compounds were detected and quantified using the Agilent 6540 UHD Q-TOF LC/MS system. Chromatographic separation was performed using an Agilent 1290 Infinity series UHPLC, equipped with a diode array detector. A Zorbex Eclipse Plus C18 RRHD column (2.1 × 100 mm, 1.8 μm) was used to separate the isolated sample. Temperature during separation was held at 45°C. Analysis was performed using a 10-μl injection of sample and a flow rate of 0.5 ml min^{-1}. The mobile phase consisted of Solvent A, a 7:2:1 (water:methanol:acetonitrile) mixture, and Solvent B, a 3:1:1 (acetonitrile:MTBE:methanol) mixture. A gradient starting from 60% A and 40% B was followed by 25% A and 75% B for 5 min, and then 100% B for 15 min. After, the sample was held for 20 min. This was followed by a return to initial conditions (60% A, 40% B) held for a 6-min post-analysis equilibration. All spectra were captured at a range of absorbance from 300 to 950 nm, by a step of 4 nm, and a 0.62-Hz scan rate.

MS/MS analysis was performed using the Agilent 6540 UHD Q-Tof Mass Spectrometer, operating in positive ion mode. Mass spectra were obtained using the Agilent QTOF 6540 mass spectrometer equipped with the JetStream ESI ion source. The mass spectrometer was scanned from m/z 100 to 1,700 and operated in the 4-GHz HRes mode. Accurate mass measurement was achieved by constantly infusing a reference calibrant (ions at m/z 121.0508 and 922.0098). An Agilent Technologies 1100 Series HPLC system coupled to an Agilent Technologies Mass Selective Trap SL detector equipped with an atmospheric pressure chemical ionization source was used for MS^5 analysis of selected Bchl molecules using directed infusion. All pigments were identified by comparison with published reference absorption spectra (Jensen, 1965; Airs and Keely, 2002).

Microscopy

A 2-μl aliquot from the enrichment grown with Fe(II) was placed onto a carbon film grid (Electron Microscopy Sciences) and allowed to settle for 1 min. After additional liquid was wicked from the grid, 2 μl of aqueous 2% uranyl acetate was immediately added and allowed 30 s to fully immerse the grid. Following a final wick of the grid, it was allowed to dry leaving a thin film of cells. Transmission electron microscopy (TEM) images were obtained using JEOL 2100 STEM in the Roy J. Carver High Resolution Microscopy facility at ISU. The images were captured under normal high vacuum conditions at 200 kV with a Gatan OneView 4K camera. Fluorescence images were obtained as described in section "Growth Experiments With Fe(II)."

RESULTS AND DISCUSSION

Enrichment of BLA1

Initial enrichment of lake water from the chemocline on FW medium containing Fe(II) with a long-pass light filter resulted in growth as assessed by visible Fe(II) oxidation and precipitation. After dilution-to-extinction and propagation for several generations, DNA was extracted, and the 16S rRNA gene was amplified and cloned to identify dominant taxa in the enrichment. All clones sequenced (17 of 17) were identical and had close matches to photoferrotrophic GSB.

Metagenomics was then performed on the enrichment after dilution to extinction. The number of assembled contigs and total size of the assembly suggested more than one genome may be present. Searches of assembled 16S rRNA genes with Barrnap[2] revealed two unique 16S rRNA sequences. The enrichment was subsequently named "BLA1," as the first enrichment (A1) from Browne Lake (BL), and this epithet is applied to the dominant strain within the enrichment. The dominant genome (∼300 × coverage) was predicted to be 99% complete with 0% contamination. Taxonomic identification of the genome bin with GTDB-TK identified it as a novel species belonging to the *Chlorobium* genus based on average nucleotide differences. The 16S rRNA gene from the *Chlorobium* sp. BLA1 genome matched 100% by BLAST (Altschul et al., 1990) to the 16S rRNA clones which initially recovered "BLA1" enrichment. The recovered *Chlorobium* sp. BLA1 genome was closely related to other known photoferrotrophic GSB, particularly *C. ferrooxidans* and *C. phaeoferrooxidans* KB01 (**Figure 1**). The second and less abundant genome (4 × coverage) was 97% complete with 2% contamination. *Pseudopelobacter* sp. SKOL is taxonomically associated with the novel order Geobacterales and novel family *Pelobacteraceae* (**Figure 2**; Waite et al., 2020). GTDB-TK identified the genome as a novel species within the *Pseudopelobacter* genus and is similar to a preexisting genome, *Pseudopelobacter* sp001802125 (GTDB taxonomy, NCBI name GWC2_55_20).

Morphology and Growth of BLA1

TEM revealed that the dominant cell type in BLA1 was rod-shaped, ca. 0.8–0.9 μm long and 0.4–0.6 μm wide (**Figure 3**). Cells did not contain flagella and are immotile, consistent with all other photoferrotrophs assessed for motility (Ehrenreich and Widdel, 1994; Heising et al., 1999; Straub et al., 1999). Cell morphology appeared similar to *C. ferrooxidans* strain KoFox (Heising et al., 1999).

The pH optimum for BLA1 growth on Fe(II) was pH 6.8 as determined by the Fe(II) oxidation rate (**Figure 4**). This is similar to the optimum for other photoferrotrophs (Straub et al., 1999), although a freshwater photoferrotrophic *Chlorobium* sp. isolated from Lake Constance had an optimum of pH 7.4–7.6 (Schmidt et al., 2021). Protons are a product of Eq. 1, which likely explains the preference of many photoferrotrophs for circumneutral pH. The pH of water decreases with depth through the chemocline of Brownie Lake and is seasonally variable, but is generally from 8 near the epilimnion down to 6.5 near the monimolimnion. Fe(II) oxidation rates were slowest at pH 7.0 (**Figure 4**), indicating that ideal conditions for this organism and Fe(II) oxidation may occur near the bottom of the chemocline.

The rate of Fe(II) oxidation in other photoferrotrophic organisms has also been shown to increase with higher Fe(II) concentrations and increasing light intensity (e.g., Michaelis–Menten kinetics; Hegler et al., 2008; Wu et al., 2014; Laufer et al., 2017). The effect of these additional factors on Fe(II) oxidation rate was not explored here. However, PAR in the chemocline of Brownie Lake varied from a maximum of 1–2 μmol photons m^{-2} s^{-1} at the top of the chemocline down to 0.1 μmol photons m^{-2} s^{-1}. Such conditions are consistent with GSB being able to inhabit some of the lowest light environments of all photosynthetic bacteria (Overmann and Garcia-Pichel, 2013).

Iron oxidation was followed in triplicate incubations at pH 6.8 with an initial density of ∼2.2 × 10^7 cells ml^{-1} and at a light intensity of 4.2 μmol photons m^{-2} s^{-1}. Serum bottles of FW medium containing Fe(II) showed evidence of Fe(II) oxidation after 8–10 days. No oxidation of Fe(II) was observed in cultures incubated in the dark or in uninoculated samples incubated in the light (**Figure 4**). The average rate of Fe(II) oxidation at 20°C and 4.2 μM photons m^{-2} s^{-1} was 0.63 ± 0.069 mmol day^{-1}. After 16 days, 95% of the Fe(II) was oxidized. The Fe(II) oxidation rate of BLA1 is commensurate with other photoferrotrophic enrichments containing *Chlorobium* sp., such as the marine *Chlorobium* sp. strain N1, 0.77 ± 0.02 mmol day^{-1} (Laufer et al., 2017). It is also similar to the freshwater purple non-sulfur *R. ferrooxidans* strain SW2, 0.40 mM day^{-1} (Kappler et al., 2005). Cell numbers increased under Fe(II) growth conditions to 3.8 × 10^8 cells ml^{-1} at day 16 (**Figure 4**). The doubling time during Fe(II) oxidation was 0.6 days (14.3 h). This doubling time is comparable to *Chlorobium* sp. strain N1 (0.4 days or 9.6 h; Laufer et al., 2017) but is faster than *C. ferrooxidans* strain KoFox (5.3 days; Heising et al., 1999). At 3.8 × 10^8 cells ml^{-1}, the average cell-specific Fe(II) oxidation rate for *Chlorobium* sp. BLA1 was 1.68 ± 0.26 fmol $cell^{-1}$ day^{-1}. This is comparable to *Chlorobium* sp. strain N1 (1.15 fmol $cell^{-1}$ day^{-1}; Laufer et al., 2017), but ∼1,000 × lower than for photoferrotrophs inhabiting the chemocline of Kabuno Bay (1.25 pmol $cell^{-1}$ day^{-1}; Llirós et al., 2015).

Similar to many other enriched or isolated photoferrotrophic *Chlorobium* sp., the BLA1 enrichment did not show evidence for growth with reduced sulfur compounds (**Table 1**). The exception is *Chlorobium* sp. N1, which was enriched from marine sediments (Laufer et al., 2017) where sulfur compounds are generally more abundant than lake water. *Chlorobium* sp. from ferruginous lakes have sometimes also been determined to have the capacity for photosynthetic oxidation of both Fe(II) and reduced sulfur compounds (Crowe et al., 2014; Tsuji et al., 2020), perhaps indicating that selection for and utilization of photoferrotrophy in the environment is dependent on the specific environmental conditions, such as low sulfur. Brownie Lake, from which BLA1 was enriched, does have 50–100 μM sulfate and hydrogen sulfide is periodically detected in anoxic water (Lambrecht et al., 2018).

The BLA1 enrichment was able to grow with both H_2 and acetate (**Table 1**). This finding is very similar to a freshwater

[2]https://github.com/tseemann/barrnap

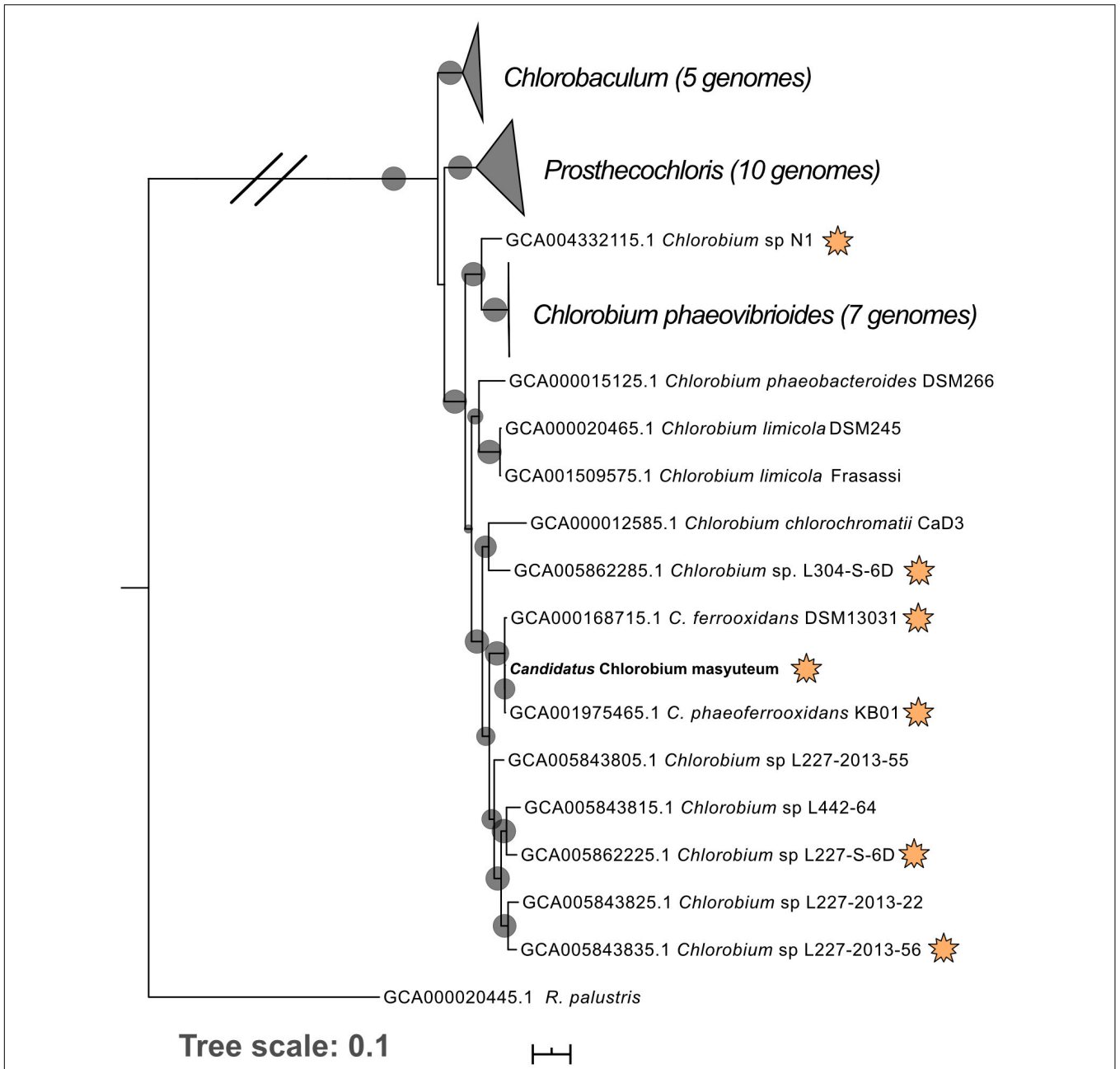

FIGURE 1 | Phylogenomic tree of "*Ca*. C. masyuteum" with other Chlorobia isolates and metagenome assembled genomes. Genomes highlighted with orange stars are either experimentally verified or inferred from the genome to photo-oxidize Fe(II). Bootstrap values (>75%) are represented by black circles. Orange stars represent organisms with either tested or inferred photoferrotrophy capability.

enrichment of a photoferrotrophic *Chlorobium* sp. with a photosynthetic *Rhodopseudomonas* sp. (Schmidt et al., 2021). In that study, detailed experiments and subsequent isolation of the *Rhodopseudomonas* sp. revealed that while only the *Chlorobium* sp. was capable of photosynthetic Fe(II) oxidation, both strains were capable of H_2 oxidation, and only the *Rhodopseudomonas* sp. was capable of growth using acetate (**Table 1**). For BLA1, observable growth on H_2 was seen approximately 10–14 days following inoculation, and growth on acetate often required a lag time of 8–14 days. Direct Sanger sequencing of the 16S rRNA gene amplified from DNA extracted when BLA1 was grown with H_2 or acetate resulted in a clean sequence matching of the 16S rRNA recovered from the *Chlorobium* sp. BLA1 genome, suggesting robust growth by that organism on these substrates.

Nevertheless, there is the possibility for a close relationship with the *Pseudopelobacter* sp., much like what was observed by Schmidt et al. (2021) in their enrichment. It seems unlikely to involve simultaneous Fe(III) reduction by *Pseudopleobacter* sp.

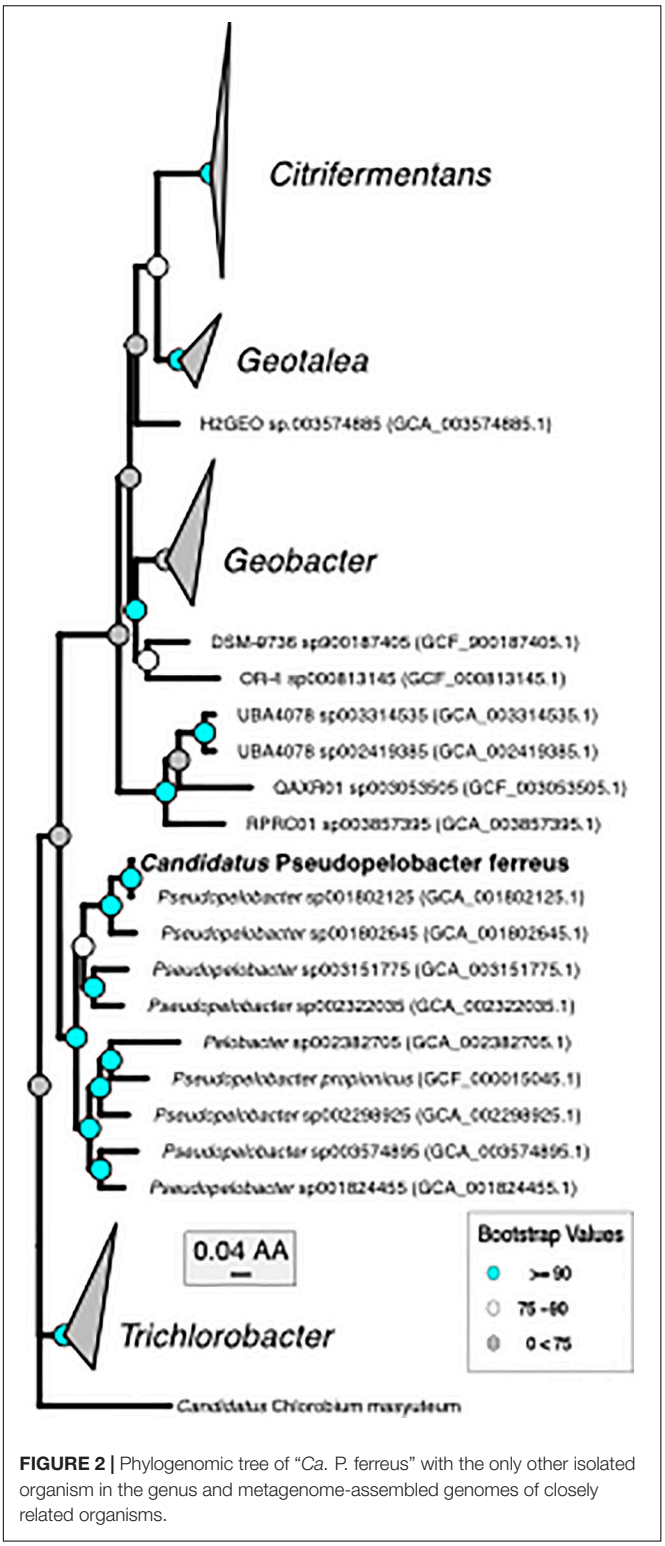

FIGURE 2 | Phylogenomic tree of "*Ca.* P. ferreus" with the only other isolated organism in the genus and metagenome-assembled genomes of closely related organisms.

SKOL during Fe(II) oxidation in the absence of acetate (see below for a discussion of functional capabilities encoded in both genomes) as no Fe(III) reduction was observed after all Fe(II) had been oxidized (**Supplementary Figure 1**). However, acetate and formate are detectable in the chemocline of Brownie Lake, suggesting redox cycling of Fe between these two organisms could be possible. No H_2 measurements have been made in Brownie Lake.

Phylogenomics of BLA1 Enrichment Genomes

Chlorobium sp. BLA1 is > 99% similar by the 16S rRNA gene to *C. ferrooxidans* and *C. phaeoferrooxidans*, and the three genomes are similar in size, %GC, and gene number (**Table 2**). This result is congruent with the phylogeny of sequenced genomes (**Figure 1**). All three of these strains are genetically distinct from other anoxygenic phototrophic Chlorobia that lack the ability to oxidize Fe(II). For instance, the *Chlorobium* sp. BLA1 16S rRNA sequence is only 97% similar to that of *Chlorobium clathratiforme*. Therefore, to distinguish whether *Chlorobium* sp. BLA1 is a new species or a subspecies of either *C. ferrooxidans* or *C. phaeoferrooxidans*, we used two independent measures of genome relatedness, digital DNA–DNA hybridization (DDH) and average nucleotide identity (ANI). Both DDH and ANI values indicate that *Chlorobium* sp. BLA1 is a novel species (**Table 2**). DDH values for all the closest related genomes were well below the accepted cutoff of 70% (Meier-Kolthoff et al., 2013). Additionally, ANI values for these genomes were also below the 95% cutoff for species level (Jain et al., 2018). These results indicate that at the genome level, *Chlorobium* sp. BLA1 is sufficiently divergent from *C. ferrooxidans* and *C. phaeoferrooxidans* to be considered a distinct species. Thus, we assign the name "*Candidatus* Chlorobium masyuteum."

The second organism, *Pseudopelobacter* sp. SKOL, is taxonomically associated with the Order *Geobacterales* and was far less abundant in the assembly (4 × coverage). The genome is most closely related to *Pseudopelobacter sp001802645* (95.5% similar by ANI), a metagenome-assembled genome (MAG) from groundwater in Rifle, CO (Anantharaman et al., 2016). Currently, there is one isolated species, *Pseudopelobacter propionicus*, from this proposed genus. We propose the name "*Candidatus* Pseudopelobacter ferreus."

Predicted Functional Capability of BLA1 Genomes

"*Candidatus* Chlorobium masyuteum"

The "*Ca.* C. masyuteum" genome consists of 17 contigs, with 2,312 predicted genes, and two rRNA operons. Gene and protein families predicted to function in key physiological activities of "*Ca.* C. masyuteum" are presented in **Figure 5A**. As with other members of the class Chlorobia, "*Ca.* C. masyuteum" has a type 1 photosynthetic reaction center (RC). Chlorosomes are unique membrane-bound photosynthetic antenna complexes found exclusively in GSB that contain large numbers of Bchl molecules (Imhoff, 2014). Chlorosome genes (*csmE*, *csmAC*, *csmB*, and *csmIJ*) appeared on four separate contigs. The *fmoA* gene encoding for the Fenna–Matthews–Olson protein are also present. The Fenna–Matthews–Olson protein participates in energy transfer from chlorosomes to the RC in the *Chlorobiaceae* (Fenna et al., 1974). *Chlorobiales* synthesize Bchl *a* and Chl *a*, as

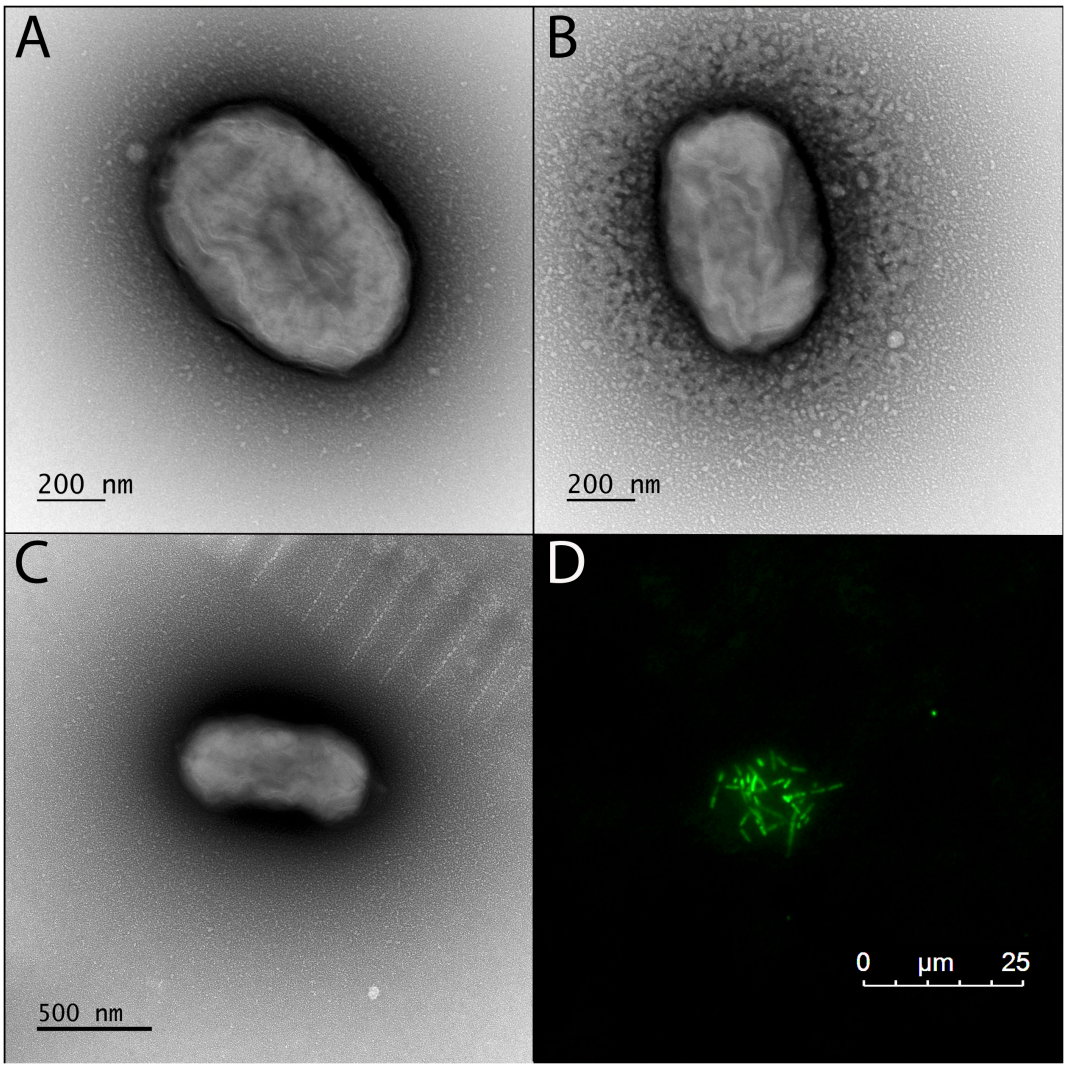

FIGURE 3 | Transmission electron microscopy (TEM) and fluorescence microscope images of the BLA1 enrichment grown in FW medium with Fe(II). **(A–C)** TEM; cell surfaces appear wrinkled, while still maintaining the structure of the cell, due to dehydration during TEM preparation. **(D)** Fluorescence image of live cells clustered on an Fe(III) mineral.

well as major Bchl (*c*, *d*, or *e*) to harvest light (Bryant and Liu, 2013). The genome of "*Ca.* C. masyuteum" contained at least six protein families corresponding to the synthesis of Bchl *a* and two corresponding to Chl *a* synthesis (**Figure 5A** and **Supplementary Table 1**). Additionally, two protein families specific to the Bchl *c* synthesis pathway, BchU and BchV, were present (Maresca et al., 2004; Chew, 2007).

The functional hallmark of the BLA1 enrichment is the ability to grow photoautotrophically using Fe(II). In photoferrotrophic purple bacteria, the *pioABC* operonis a three-gene operon coding for a periplasmic decaheme c-type cytochrome that transfers electrons (*pioA*), an outer membrane β-barrel protein (*pioB*), and a periplasmic high potential iron-sulfur cluster protein that participates in anaerobic electron transport (*pioC*; Jiao and Newman, 2007). This operon is found in *R. vannielii* strain ATCC 17100 (He et al., 2017) and *R. palustris* (Jiao and Newman, 2007). The *foxEYZ* operonis another three-gene operon that encodes for a c-type cytochrome (*foxE*), a putative protein containing the cofactor pyrroloquinoline (*foxY*), and a putative protein with transport function (*foxZ*) and is found in *R. ferrooxidans* (Croal et al., 2007). Annotation of the "*Ca.* C. masyuteum" genome indicates that the *pio* and *fox* operons are absent. This finding is similar to other GSB photoferrotrophs (Bryce et al., 2018; Tsuji et al., 2020), leading us to screen for other genes with potential Fe(II) oxidase activity.

Recently, homologs to an outer-membrane c-type cytochrome that functions in Fe(II) oxidation, encoded by the gene *cyc2*, have been detected in both acidophilic and neutrophilic oxygen-dependent Fe(II) oxidizing bacteria. *Acidothiobacillus ferrooxidans, Mariprofundus* sp., *Acidothiobacillus ferrooxidans, Mariprofundus* sp., *Gallionellaceae*, and *Zetaproteobacteria* are

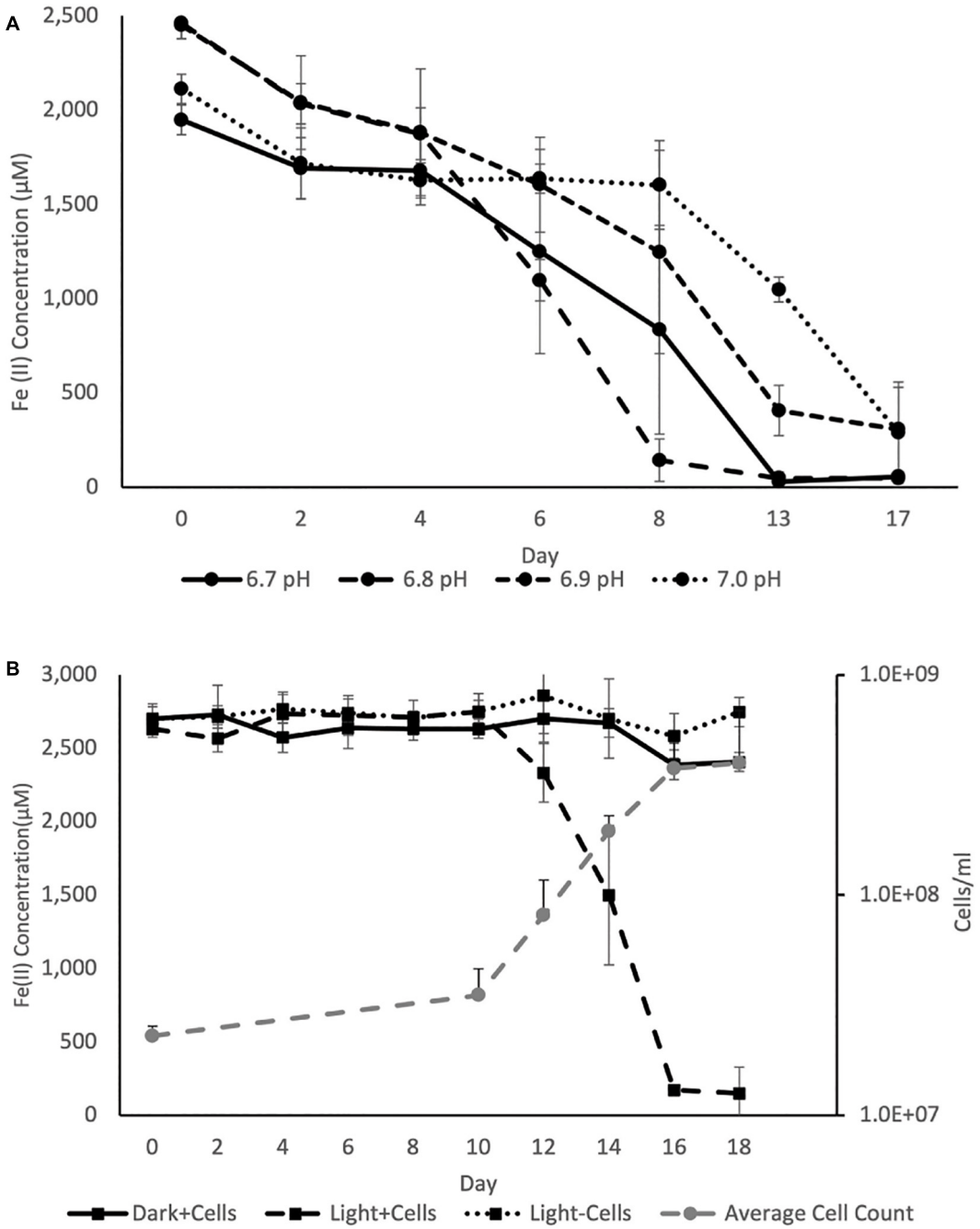

FIGURE 4 | (A) Average Fe(II) oxidation curves for triplicate BLA1 incubations under illumination at different pH, showing optimal activity at pH 6.8. **(B)** Representative growth and Fe(II) oxidation of BLA1 from one triplicate. Error bars represent the standard deviation of analytical triplicates for Fe(II) (in all cases smaller than symbol size) and the standard deviation of all fields of view counted for cell counts.

such examples (Castelle et al., 2008; Barco et al., 2015; Chan et al., 2018; McAllister et al., 2020). Subsequently, the *cyc2* gene was found in the genomes of *C. ferrooxidans* and *C. phaoferrooxidans* (He et al., 2017; Chan et al., 2018) and have been detected in *Chlorobium* metagenomes in enrichments from ferruginous lakes (Tsuji et al., 2020). We identified *cyc2* in the genome of "*Ca.* C. masyuteum." In addition, we identified two genes, *afuBC*, which are integral and cytoplasmic membrane proteins of the ferric iron ABC transport system in "*Ca.* C. masyuteum" (**Figure 5A**).

The BLA1 enrichment was not able to oxidize sulfide, sulfite, or thiosulfate (**Table 1**). The "*Ca.* C. masyuteum" genome was in agreement with growth experiments, as genes implicated in sulfide (*dsr*) or thiosulfate (*sox*) oxidation were absent (**Figure 5A**). This differs from the GSB *Chlorobium* sp. strain N1

TABLE 1 | Commonly used sole organic and inorganic electron donors to assess additional photoautotrophic growth of true photoferrotrophic isolates or enrichments.

Photoferrotroph	Iron(II)	Acetate	Hydrogen	Sulfide	Thiosulfate	Source
"*Ca.* C. masyuteum"	+	(+)	(+)	-	-	This study
C. ferrooxidans strain KoFox	+	-	+	-	-	Heising et al., 1999
						Hegler et al., 2008
C. phaeoferrooxidans strain KB01	+	n. d.	n. d.	n. d.	n. d.	Crowe et al., 2017
Chlorobium sp.	+	(+)	+	-	-	Schmidt et al., 2021
Chlorobium sp. strain N1	+	+	+	+	+	Laufer et al., 2017
Thiodycton sp. strains Thd2 and F4	+	+	+	-	-	Ehrenreich and Widdel, 1994
						Hegler et al., 2008
*R. palustris*strain TIE-1	+	+	+	-	+	Jiao et al., 2005
*R. ferrooxidans*strain SW2	+	+	+	-	n. d.	Ehrenreich and Widdel, 1994
R. iodosum	+	+	+	+	+	Straub et al., 1999
R. rubiginosum	+	+	+	+	+	Straub et al., 1999

(+) indicates growth on this substrate may not be attributed solely to this strain. Thiodycton strain L7 in Ehrenreich and Widdel (1994) was given accession number X78718, and this accession number in GenBank recognizes this isolate as strain Thd2. n.d. = no data.

TABLE 2 | Isolate genome characteristics and comparisons to other *Chlorobia* genomes.

Reference genome	Strain name	DDH	Model C.I. (%)	ANI	%GC	Genome size (Mb)	No. genes
"*Ca.* Chlorobium masyuteum"	BLA1	–	–	–	50.6	2.56	2,312
Chlorobium ferrooxidans	DSM 13031	54.8	52.1–57.5	94.1	50.1	2.54	2,308
Chlorobium phaeoferrooxidans	KB01	51.5	48.9–54.2	93.4	49.7	2.57	2,486
Chlorobium sp.	L227-2013-55	19.9	17.7–22.3	78.9	48.5	2.38	2,338
Chlorobium sp.	L227-2013-22	19.9	17.7–22.3	78.7	45.9	2.55	2,459
Chlorobium sp.	L227-S-6D	18.9	16.8–21.3	78	46.8	2.49	2,383
Chlorobium sp.	L227-2013-56	18.5	16.3–20.9	77.6	43.9	2.89	1,991
Chlorobium sp.	L442-64	19.7	17.5–22.1	78.1	48.3	1.9	1,851
Chlorobium phaeobacteroides	DSM 266	19.2	17–21.6	77.6	48.4	3.13	2,819
Chlorobium sp.	N1	17.9	15.8–20.3	77.6	61.5	2.37	2,284

*Reference genome identifiers correspond to isolates in **Figure 1**.*

(Laufer et al., 2017) and the PSB *R. iodosum* and *R. rubiginosum* (Straub et al., 1999). *R. palustris* strain TIE-1 is able to oxidize thiosulfate, but no reports indicate the oxidation of sulfide by TIE-1 or closely related strains (Jiao et al., 2005; Schmidt et al., 2021). The ability to oxidize these sulfur compounds is also absent from the well-studied *C. ferrooxidans* strain KoFox (Heising et al., 1999). Genes implicated in sulfite oxidation, *aprAB* and *sat*, were present in the "*Ca.* C. masyuteum" genome but are likely also used for the assimilation of sulfur as no sulfite oxidation was observed. The *sat* genes are absent in other photoferrotrophic *Chlorobium* sp. (Thompson et al., 2017). No other sulfur oxidation genes were present.

In addition, the genome of "*Ca.* C. masyuteum" contains *cys*, *sat*, and *sir* genes which participate in assimilatory sulfate reduction (ASR). Other photoferrotrophic *Chlorobium* sp. (e.g., *C. phaeoferrooxidans*, *C. ferrooxidans*, "*Ca.* C. canadense" L304-6D, and L227 enrichment S-6D) have been shown to contain ASR genes, particularly *cys* (Thompson et al., 2017; Tsuji et al., 2020), and sulfate assimilation has been biochemically verified in the first two strains. During isolation of *Chlorobium* sp. strain N1, the authors suggested sulfate could be utilized as a sulfur source; however, ASR activity was not directly tested (Laufer et al., 2017).

Nitrogen fixation has been recognized in *Chlorobium* sp. for quite some time (Heda and Madigan, 1986; Bryant et al., 2012), and GSB may be important sources of fixed nitrogen in stratified water columns (Halm et al., 2009; Swanner et al., 2020). Although fixed nitrogen was always provided in the FW medium, the "*Ca.* C. masyuteum" genome does contain *nifDKH* genes encoding a Mo-requiring nitrogenase (**Figure 5A**). These genes have also been detected and growth without fixed nitrogen verified in the closely related photoferrotrophs *C. ferrooxidans* and *C. phaeoferrooxidans* (Thompson et al., 2017).

Genes necessary to fix carbon using the reverse tricarboxylic acid cycle typical for *Chlorobium* sp. are present in "*Ca.* C. masyuteum" (Tang and Blankenship, 2010). The BLA1 enrichment was also able to grow with acetate. As acetate utilization is an unusual capability for organisms within the *Chlorobiaceae* family (Imhoff, 2014), it is possible that this mode of growth may have required some type of syntrophy with "*Ca.* P. ferreus," although acetate cultures were dominated by "*Ca.* C. masyuteum" based on Sanger sequencing. Other photoferrotrophic *Chlorobium* that are able to use acetate but only in coculture are *Chlorobium ferrooxidans* (strain KoFox) with *Geospirillum sp.* strain Kofum (Heising et al., 1999) and the closely related *Chlorobium* sp. obligately in coculture with

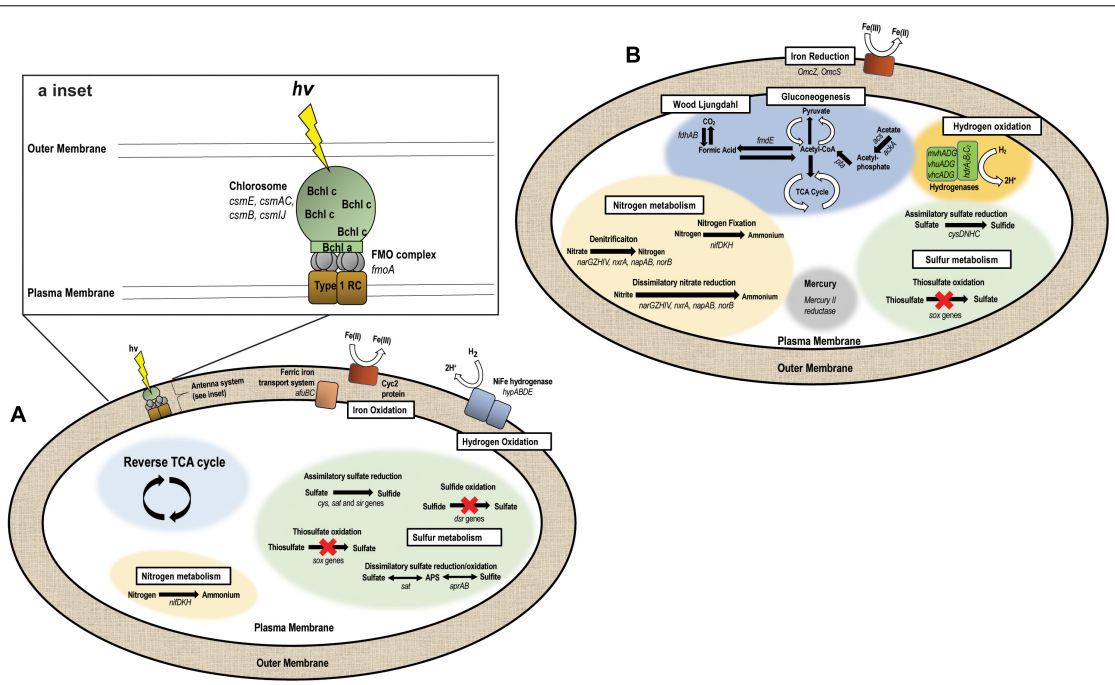

FIGURE 5 | Metabolic pathways encoded by the two genomes recovered from the BLA1 enrichment. **(A)** "*Ca.* C. masyuteum" (APS—adenylyl sulfate). Inset shows the antenna system (RC—reaction center, FMO—Fenna–Matthews–Olson, Bchl—Bacteriochlorophyll). **(B)** "*Ca.* P. ferreus."

acetate utilizing *Rhodopseudomonas* sp. (Schmidt et al., 2021). Considering we did observe robust growth dominated by "*Ca.* C. masyuteum" on acetate, we suggest it could also be possible for "*Ca.* C. masyuteum" to use its reverse TCA cycle or run the reverse TCA in the forward direction to assimilate acetate, such as has been observed for *C. tepidum* (Tang and Blankenship, 2010).

Oxidation of H_2 for photoautotrophic growth requires membrane-bound NiFe hydrogenases (Schwartz et al., 2006). The "*Ca.* C. masyuteum" genome contains *hypABDE* genes encoding for a Group 1d Ni-Fe hydrogenase (**Figure 5A**), similar to the genomes of *C. ferrooxidans* and *C. phaoferrooxidans*. This, along with growth experiments, suggests that "*Ca.* C. masyuteum" is able to grow photoautotrophically utilizing H_2. However, growth on H_2 was not observed by *C. phaoferrooxidans* despite the presence of *hyp* genes (Thompson, 2020). Further work to establish whether *hypABDE* genes encode photosynthetic hydrogen oxidation may help to determine which genes can be used as genetic markers for photosynthetic hydrogen oxidation by GSB in environmental contexts (Thompson, 2020; Tsuji et al., 2020; Garcia et al., 2021).

"*Candidatus* Pseudopelobacter ferreus"

The "*Ca.* P. ferreus" genome is 4.5 Mb, consists of 139 contigs, with 4,019 predicted genes, and one 16S rRNA gene, and has a GC content of 54.6%. Although it is not photosynthetic, this organism is metabolically flexible, with gene and protein families predicted to function in transformation of C, Fe, N, S, H, and Hg (**Figure 5B**). The "*Ca.* P. ferreus" genome encodes for the reductive acetyl-CoA or Wood–Ljungdahl pathway for carbon fixation common among the Delta Proteobacteria (Hügler and Sievert, 2011).

"*Ca.* P. ferreus" seems likely to function as an FeRB when grown in the BLA1 enrichment, considering that the genome contains gene homologs for dissimilatory Fe(III) reduction and the detection of Fe(III) reduction activity in BLA1 after complete Fe(II) oxidation and acetate addition (**Supplementary Figure 1**). These homologs include *omcS* and *omcZ*, putatively thought to be involved in long-distance extracellular electron transfer (Santos et al., 2015; Wang et al., 2019), and additional hypothetical proteins involved in electron transfer including porins, periplasmic cytochromes, and outer-membrane cytochromes (Garber et al., 2020). The low abundance of the "*Ca.* P. ferreus" genome in the BLA1 enrichment in combination with no subsequent Fe(III) reduction before acetate was added suggests that Fe(III) reduction is likely not occurring during photoferrotrophic growth in the absence of added electron donors.

Fe(III) reduction by "*Ca.* P. ferreus" can likely be coupled to oxidation of H_2. The genome encodes for the cytoplasmic heterodisulfide reductase (HdrABC) as well as a NiFe hydrogenase (MvhAGD). This complex seems to function in H_2 oxidation and possibly electron bifurcation in a number of anaerobes, including methanogenic Archaea and *Geobacter sulfurreducens* (Wischgoll et al., 2005; Wagner et al., 2017). Fe(III) reduction activity with H_2 was not assessed for BLA1.

Although it is capable of autotrophy, "*Ca.* P. ferreus" encodes multiple pathways for the incorporation of organics. Since BLA1 grew when amended with acetate, we have focused on possible pathways to explain this phenomenon (**Figure 5B**). Acetate could

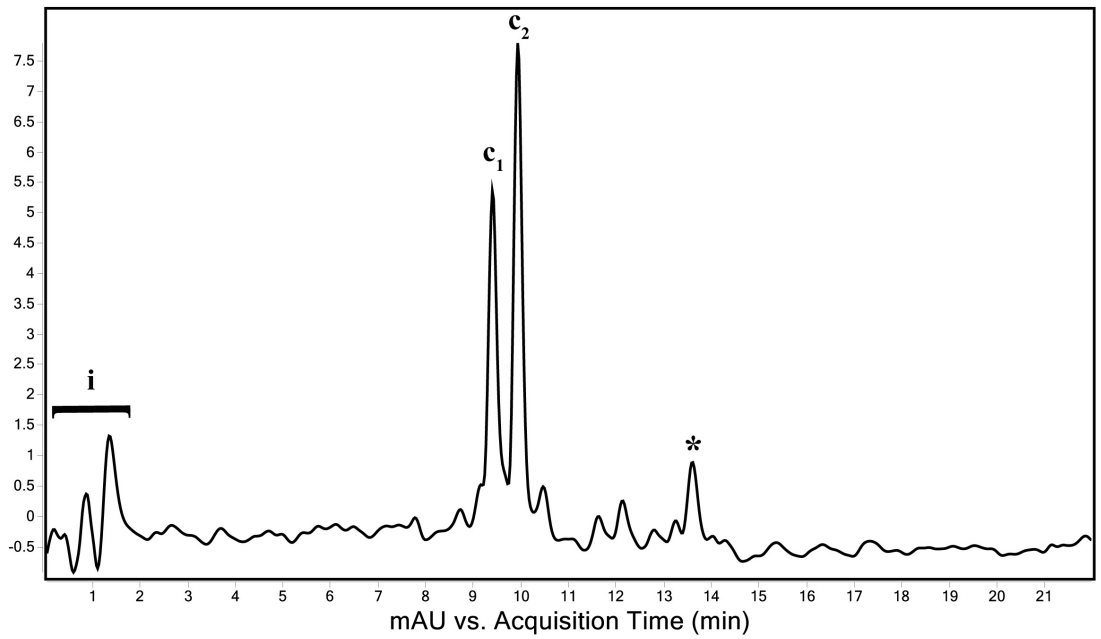

FIGURE 6 | Total wavelength chromatogram depicting the major pigments of "*Ca.* C. masyuteum." i—sample injection peaks; c_1 and c_2—bacteriopheophytins corresponding to bacteriochlorophyll *c*; *chlorobactene.

be incorporated as acetyl phosphate (*via acs* and *ackA*) and converted to acetyl-CoA (*pta*). Acetyl-CoA could then feed into the TCA cycle or gluconeogenesis after conversion to pyruvate. Another possibility is that acetate is incorporated as acetyl-CoA by reversing the Wood–Ljungdahl pathway, such as occurs in some methanogens and anaerobes (Zhuang et al., 2014).

In addition to its potential role in Fe(III) reduction, the genome of "*Ca.* P. ferreus" also encodes a mercury(II) reductase. Similar functionality has been detected in other Geobacterales (Lu et al., 2016). The genome also encodes for Mo-requiring nitrogenase *via nifDKH* and contained genes for ASR (i.e., *cysDNHC*).

Pigments Produced by "*Ca.* C. masyuteum"

The genome of "*Ca.* C. masyuteum" consisted of protein families for important minor pigments Chl *a* and Bchl *a*, as well as the major light-harvesting pigment Bchl *c*. To confirm that Bchl *c*, as opposed to Bchl *d* or *e*, is the major light-harvesting pigment, an extract from the BLA1 enrichment grown on Fe(II) was examined using a Q-TOF LC/MS system. The resulting chromatogram (**Figure 6**) displayed three major peaks corresponding to light-harvesting molecules. The first peak, denoted as c_1, eluted between 9.3 and 9.7 min and gave rise to a major ion at *m/z* 785 (**Figure 7A**). The second peak, denoted as c_2, eluted later between 9.9 and 10.2 min and displayed an increasing mass difference of 14 Da (*m/z* 799; **Figure 7B**). Peaks of low relative abundance were detected in the mass spectra indicating the presence of numerous background ions. As "*Ca.* C. masyuteum" was the dominant organism under these growth conditions, and "*Ca.* P. ferreus" is non-photosynthetic, we interpret the detected pigments as sourcing from "*Ca.* C. masyuteum."

Peaks c_1 and c_2 were identified as bacteriopheophytins (Bphes), suggestive of two structural isomers of Bchl *c* based on previous identification with similar mass spectra (Airs and Keely, 2002). The detection of Bphes in place of Bchl *c* is likely due to post-column demetallation of the center Mg^{2+} (**Table 2**; Airs and Keely, 2002). The verification of the Bphes peaks as derivatives of Bchl *c* was assessed by performing a MS^5 analysis, which creates fragmentation patterns unique to Bchl *c*, *d*, or *e*. The fragmentation pattern was as compared to work performed by Airs and Keely (2002) and indicative of Bchl *c* (**Supplementary Figure 2A**). The corresponding UV/vis spectrum agreed with the MS^5 analysis, which depicted major absorption peaks characteristic of Bchl *c* at 412 and 668 nm (**Supplementary Figure 2B**). This is similar to what has been observed by Airs and Keely (2002). However, the peak at 412 nm is shifted to the left (412 nm instead of 435 nm) of what was observed by Airs and Keely (2002), likely due to the loss of the Mg^{2+} ion. The utilization of Bchl *c* as the main light-harvesting pigment is yet another feature that distinguishes "*Ca.* C. masyuteum" and its close relatives. *C. ferrooxidans* synthesizes Bchl *c* as well (Heising et al., 1999). However, *C. phaoferrooxidans* synthesizes Bchl *e* (Thompson, 2020).

The last of the major peaks eluted between 13.6 and 13.8 min (**Figure 7**). LC/MS analysis detected two molecules with overlapping retention times at this peak. Both molecules, γ-carotene and chlorobactene, likely contributed to the absorbance peak at ∼13.7 min. However, MS/MS fragmentation revealed major ions for chlorobactene [*m/z* 532.4 (radical) and *m/z* 533*z* 533.4 ($M+H^+$)] and minor ions for γ-carotene

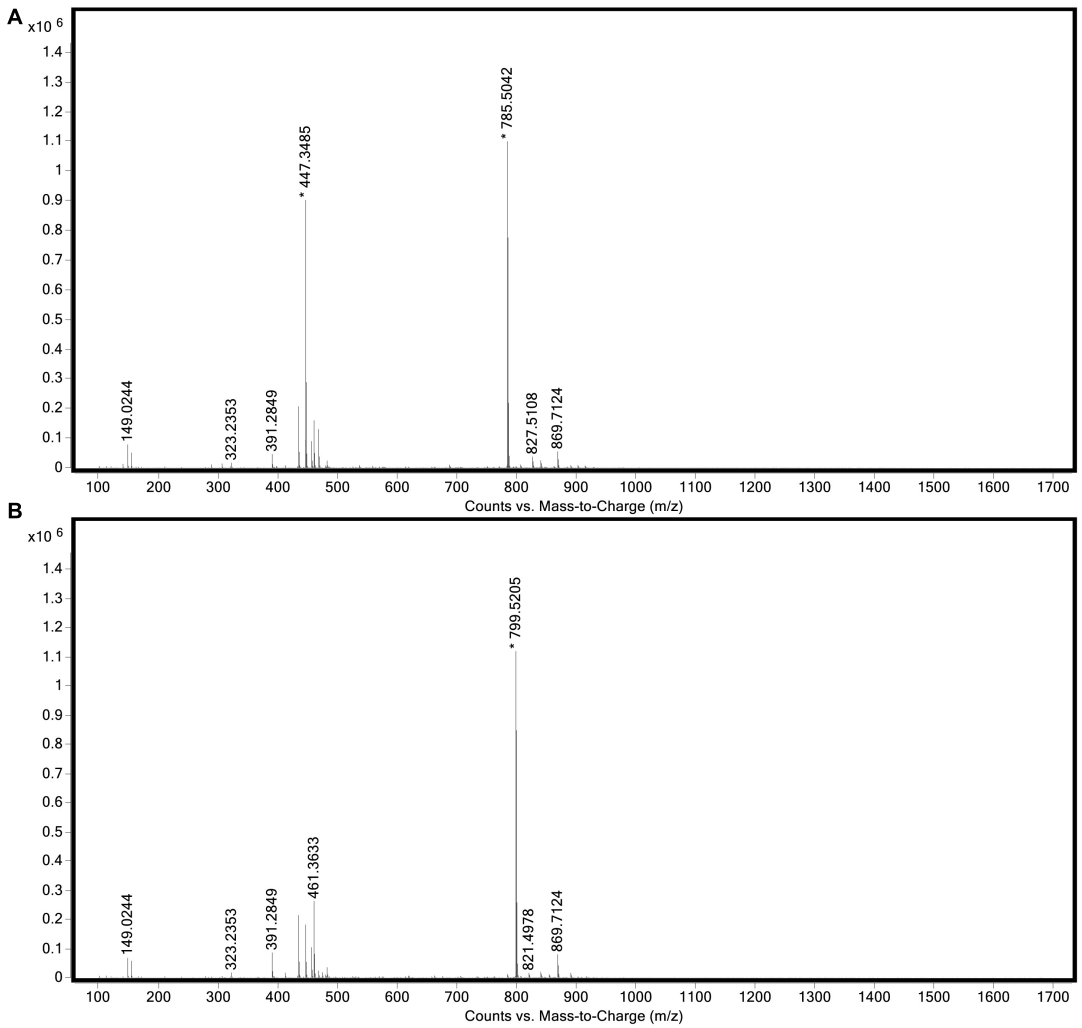

FIGURE 7 | Full mass spectra of **(A)** peak c_1 and **(B)** peak c_2 obtained during LC/MS analysis of the extract from "*Ca.* C. masyuteum."

[*m/z* 536.4 (radical) and *m/z 537.4* ($M+H^+$); **Supplementary Figure 3A**]. The UV/vis spectrum of the major MS/MS fragmentation peak had three absorption maxima at 437, 460, and 488 nm (**Supplementary Figure 3B**). This sequence, when compared to reference absorption spectra (Jensen, 1965), corresponded to the aromatic carotenoid chlorobactene. The presence of both Bchl *c* and the accessory pigment chlorobactene in the extract agrees with previous work on GSB (Maresca et al., 2008). A similar absorption spectrum for chlorobactene was observed in extracts from the photoferrotroph *C. ferrooxidans* strain KoFox (Hegler et al., 2008).

The activity of photoferrotrophs in ferruginous oceans prior to the GOE has been implicated in the formation of massive Fe-Si deposits known as banded iron formations (BIF; Konhauser et al., 2002; Kappler et al., 2005; Hegler et al., 2008; Bekker et al., 2010; Mloszewska et al., 2012; Posth et al., 2013). However, ambiguity in assigning specific stable isotopic signatures exclusively to photoferrotrophy (e.g., Fe, see Swanner et al., 2015; Wu et al., 2017) indicates a need for other indicators of these organisms and their activity. Biomarkers are organic molecules that resist degradation and alteration and can be indicative of certain taxonomic groups (e.g., Bchl, aromatic carotenoids). Recent work has suggested that certain isoprenoids can act as biomarkers, linking APB to phototrophic Fe(II) oxidation in a Mesoproterozoic iron formation (Xiamaling Formation; 1.4 Ga) that shares similarities to Archean-aged BIFs (Canfield et al., 2018).

Chlorobactene exists as a monoaromatic carotenoid associated with green-pigmented GSB (i.e., *Chlorobiaceae*) and has been utilized as a proxy for GSB in the rock record as far back as 1.64 Ga (e.g., Barney Creek Formation; Summons and Powell, 1986). The presence of chlorobactene in the Barney Creek Formation, as well as other Precambrian deposits mentioned previously, has typically signified euxinic conditions. However, GSB phototrophs such as "*Ca.* C. masyutem" are capable of oxidizing iron but not reduced sulfur compounds (**Table 1**), and thus chlorobactene (or its derivatives) may not be a definitive indicator of euxinia. However, if found in

combination with paleoredox proxies that indicate ferruginous conditions, detection of chlorobactene might serve as a line of evidence in support of photoferrotrophy. Continued effort is needed to better describe the environmental conditions under which sulfur vs. Fe(II)-oxidizing phototrophs are active, as cryptic phototrophic sulfur cycling has been detected in ferruginous environments (Crowe et al., 2014), and cryptic phototrophic iron cycling is noted from euxinic environments (Berg et al., 2016).

CONCLUSION

In summary, two novel organisms were co-enriched from ferruginous meromictic Brownie Lake, Minnesota, United States. The most abundant organism in the BLA1 enrichment is "*Ca.* C. masyuteum," a photoferrotrophic GSB that is genetically and physiologically unique when compared to close relatives. It is able to grow photoautotrophically using Fe(II), and possibly acetate and H_2. It produces bacteriochlorophyll c as well as chlorobactene. The presence of the *cyc2* gene in "*Ca.* C. masyuteum" adds compounding evidence that this gene can be used as a marker for Fe(II) oxidation in GSB in ferruginous environments. The lack of sulfur oxidation pathways in this organism or observed reduced sulfur oxidation in the enrichment suggests that it likely performs photoferrotrophy in the environment but may also be able to use fermentation by-products like H_2 or organic acids as electron donors for photosynthesis. The genome also encodes for a Mo-utilizing nitrogenase, suggesting a role for alleviation of nitrogen fixation in the redoxcline of Brownie Lake (Swanner et al., 2020).

"*Ca.* C. masyuteum" could not be isolated, and metagenomic sequencing revealed that a novel and metabolically flexible organism comprised about 1% of the BLA1 enrichment. "*Ca.* P. ferreus" is a putative FeRB that likely oxidizes acetate and/or H_2. Two other photoferrotrophic GSB also live in defined coculture (Heising et al., 1999; Bryce et al., 2019), suggesting that close associations with other organisms may be a common strategy among photoferrotrophic GSB.

Description of "*Candidatus* Chlorobium masyuteum" (ma.syu.te for the phrase *mas'yúte*, meaning "eats iron" in the Dakota language spoken by the first caretakers of Brownie Lake). Short rod-like bacterium (0.8 μm by 0.4–0.6 μm in size). Selective enrichment from freshwater at 20°C with a long-pass light filter (i.e., > 700 nm). Grows autotrophically in freshwater medium with Fe(II) or molecular hydrogen as electron donors, in defined coculture with a *Pseudopelobacter* sp. Basis of assignment: digital DDH and ANI relatedness measures indicate a significant divergence at the genome to level from its closest *Chlorobium* relatives. Belongs to class Chlorobia, order *Chlorobiales*, and family *Chlorobiaceae*. Identified from a water sample of Brownie Lake, Minneapolis, Minnesota, United States.

Description of "*Candidatus* Pseudopelobacter ferreus" (fer're.us. L. masc. adj. ferreus pertaining to iron). Selective enrichment from freshwater at 20°C. Grows in anoxic freshwater medium in defined coculture with "*Ca.* C. masyuteum." Basis of assignment: digital DDH and ANI relatedness measures indicate a significant divergence at the genome to level from its closest *Pseudopelobacter* relatives. Belongs to proposed phylum Desulfurbacterota, Desulfuromonadia class nov., *Geobacterales* order nov., and *Pseudopelobacteraceae* fam. nov. (Waite et al., 2020). Identified from a water sample of Brownie Lake, Minneapolis, Minnesota, United States.

DATA AVAILABILITY STATEMENT

The datasets presented in this study can be found in online repositories. The names of the repository/repositories and accession number(s) can be found in the article/ **Supplementary Material**.

AUTHOR CONTRIBUTIONS

NL, ZS, and ES wrote the manuscript with input from all authors. NL and ES collected the field samples. MP, NL, ZS, and HT conducted the laboratory experiments with the isolate. CS, ZS, and NL analyzed and annotated the genomes, and created the figures and tables for the manuscript.

FUNDING

This work was sponsored by the National Science Foundation (NSF) collaborative research grant (EAR—1660691 to ES and EAR—1660761 to CS). This work was also supported by the National Aeronautics and Space Administration (NASA) Interdisciplinary Consortium for Astrobiology Research grant 80NSSC21K0592, Metal Utilization and Selection across Eons (MUSE).

ACKNOWLEDGMENTS

Chad Wittkop and Sergei Katsev helped to collect water samples. We acknowledge the W. M. Keck Metabolomics Research Laboratory (Office of Biotechnology, Iowa State University) for providing analytical instrumentation and we thank Lucas Showman for his assistance and support. Tracey Stewart at the Roy J. Carver High Resolution Microscopy Facility at Iowa State University facilitated TEM sample preparation and imaging. Šišóka Dúta and Alexander Hall assisted with developing the species epithets. The Minneapolis Parks and Recreation Board supplied permits to work at Brownie Lake. This manuscript was originally part of a dissertation accepted by Iowa State University and edited for publication.

SUPPLEMENTARY MATERIAL

The Supplementary Material for this article can be found online at: https://www.frontiersin.org/articles/10.3389/fmicb.2021.695260/full#supplementary-material

REFERENCES

Abràmoff, M. D., Magalhães, P. J., and Ram, S. J. (2004). Image processing with ImageJ. *Biophotonics Int.* 11, 36–42.

Airs, R. L., and Keely, B. J. (2002). Atmospheric pressure chemical ionisation liquid chromatography/mass spectrometry of bacteriochlorophylls from Chlorobiaceae: characteristic fragmentations. *Rapid Commun. Mass Spectrom.* 16, 453–461. doi: 10.1002/rcm.598

Altschul, S. F., Gish, W., Miller, W., Myers, E. W., and Lipman, D. J. (1990). Basic local alignment search tool. *J. Mol. Biol.* 215, 403–410.

Anantharaman, K., Brown, C. T., Hug, L. A., Sharon, I., Castelle, C. J., Probst, A. J., et al. (2016). Thousands of microbial genomes shed light on interconnected biogeochemical processes in an aquifer system. *Nat. Comm.* 7:13219. doi: 10.1038/ncomms13219

Barco, R. A., Emerson, D., Sylvan, J. B., Orcutt, B. N., Jacobson Meyers, M. E., Ramírez, G. A., et al. (2015). New insight into microbial iron oxidation as revealed by the proteomic profile of an obligate iron-oxidizing chemolithoautotroph. *Appl. Environ. Microbiol.* 81, 5927–5937. doi: 10.1128/AEM.01374-15

Bekker, A., Slack, J. F., Planavsky, N., Krapez, B., Hofmann, A., Konhauser, K. O., et al. (2010). Iron formation: the sedimentary product of a complex interplay among mantle, tectonic, oceanic, and biospheric processes. *Econ. Geol.* 105, 467–508. doi: 10.2113/gsecongeo.105.3.467

Berg, J. S., Michellod, D., Pjevac, P., Martinez-Perez, C., Buckner, C. R. T., Hach, P. F., et al. (2016). Intensive cryptic microbial iron cycling in the low iron water column of the meromictic Lake Cadagno. *Environ. Microbiol.* 18, 5288–5302. doi: 10.1111/1462-2920.13587

Bóna-Lovász, J., Bóna, A., Ederer, M., Sawodny, O., and Ghosh, R. (2013). A rapid method for the extraction and analysis of carotenoids and other hydrophobic substances suitable for systems biology studies with photosynthetic bacteria. *Metabolites* 3, 912–930. doi: 10.3390/metabo3040912

Brocks, J. J., and Schaeffer, P. (2008). Okenane, a biomarker for purple sulfur bacteria (Chromatiaceae), and other new carotenoid derivatives from the 1640 Ma Barney Creek Formation. *Geochim. Cosmochim. Acta* 72, 1396–1414. doi: 10.1016/j.gca.2007.12.006

Brocks, J. J., Love, G. D., Summons, R. E., Knoll, A. H., Logan, G. A., and Bowden, S. A. (2005). Biomarker evidence for green and purple sulphur bacteria in a stratified Palaeoproterozoic sea. *Nature* 437:866. doi: 10.1038/nature04068

Bryant, D. A., and Liu, Z. (2013). Green bacteria: insights into green bacterial evolution through genomic analyses. *Adv. Bot. Res.* 66, 99–150.

Bryant, D. A., Liu, Z., Li, T., Zhao, F., Costas, A. M. G., Klatt, C. G., et al. (2012). "Comparative and functional genomics of anoxygenic green bacteria from the taxa chlorobi, chloroflexi, and acidobacteria," in *Functional Genomics and Evolution of Photosynthetic Systems*, eds R. Burnap and W. Vermaas (Dordrecht: Springer), 47–102. doi: 10.1007/978-94-007-1533-2_3

Bryce, C., Blackwell, N., Schmidt, C., Otte, J., Huang, Y. M., Kleindienst, S., et al. (2018). Microbial anaerobic Fe (II) oxidation–ecology, mechanisms and environmental implications. *Environ. Microbiol.* 20, 3462–3483. doi: 10.1111/1462-2920.14328

Bryce, C., Blackwell, N., Straub, D., Kleindienst, S., and Kappler, A. (2019). Draft genome sequence of chlorobium sp. strain N1, a marine Fe(II)-oxidizing green sulfur bacterium. *Microbiol. Resour. Announc.* 8, 1–2. doi: 10.1128/mra.00080-19

Canfield, D. E., Rosing, M. T., and Bjerrum, C. (2006). Early anaerobic metabolisms. *Philos. Trans. R. Soc. B Biol. Sci.* 361, 1819–1836. doi: 10.1098/rstb.2006.1906

Canfield, D. E., Zhang, S., Wang, H., Wang, X., Zhao, W., Su, J., et al. (2018). A mesoproterozoic iron formation. *Proc. Natl. Acad. Sci. U.S.A.* 115, E3895–E3904.

Capella-Gutiérrez, S., Silla-Martínez, J. M., and Gabaldón, T. (2009). trimAl: a tool for automated alignment trimming in large-scale phylogenetic analyses. *Bioinformatics* 25, 1972–1973. doi: 10.1093/bioinformatics/btp348

Castelle, C., Guiral, M., Malarte, G., Ledgham, F., Leroy, G., Brugna, M., et al. (2008). A new iron-oxidizing/O2-reducing supercomplex spanning both inner and outer membranes, isolated from the extreme acidophile *Acidithiobacillus ferrooxidans*. *J. Biol. Chem.* 283, 25803–25811. doi: 10.1074/jbc.M802496200

Chan, C., McAllister, S. M., Garber, A., Hallahan, B. J., and Rozovsky, S. (2018). Fe oxidation by a fused cytochrome-porin common to diverse Fe-oxidizing bacteria. *bioRxiv* [Preprint]. doi: 10.1101/228056

Chaumeil, P.-A., Mussig, A. J., Hugenholtz, P., and Parks, D. H. (2019). GTDB-Tk: a toolkit to classify genomes with the genome taxonomy database. *Bioinformatics* 36, 1925–1927.

Chen, S., Zhou, Y., Chen, Y., and Gu, J. (2018). fastp: an ultra-fast all-in-one FASTQ preprocessor. *Bioinformatics* 34, i884–i890.

Chew, A. G. M. (2007). *Elucidation of the Bacteriochlorophyll c Biosynthesis Pathway in Green Sulfur Bacterium Chlorobium Tepidum*. State College, PA: The Pennsylvania State University.

Costas, A. M. G., Tsukatani, Y., Rijpstra, W. I. C., Schouten, S., Welander, P. V., Summons, R. E., et al. (2012). Identification of the bacteriochlorophylls, carotenoids, quinones, lipids, and hopanoids of "*Candidatus* chloracidobacterium thermophilum". *J. Bacteriol.* 194, 1158–1168. doi: 10.1128/JB.06421-11

Croal, L. R., Jiao, Y., and Newman, D. K. (2007). The fox operon from *Rhodobacter* strain SW2 promotes phototrophic Fe (II) oxidation in *Rhodobacter capsulatus* SB1003. *J. Bacteriol.* 189, 1774–1782. doi: 10.1128/jb.01395-06

Croal, L. R., Johnson, C. M., Beard, B. L., and Newman, D. K. (2004). Iron isotope fractionation by Fe (II)-oxidizing photoautotrophic bacteria. *Geochim. Cosmochim. Acta* 68, 1227–1242. doi: 10.1016/j.gca.2003.09.011

Crowe, S. A., Hahn, A. S., Morgan-Lang, C., Thompson, K. J., Simister, R. L., Llirós, M., et al. (2017). Draft genome sequence of the pelagic photoferrotroph *Chlorobium phaeoferrooxidans*. *Genome Announc.* 5:e01584-16.

Crowe, S. A., Maresca, J. A., Jones, C., Sturm, A., Henny, C., Fowle, D. A., et al. (2014). Deep-water anoxygenic photosynthesis in a ferruginous chemocline. *Geobiology* 12, 322–339. doi: 10.1111/gbi.12089

Dong, X., and Strous, M. (2019). An integrated pipeline for annotation and visualization of metagenomic contigs. *Front. Genet.* 10:999. doi: 10.3389/fgene.2019.00999

Edgar, R. C. (2004). MUSCLE: multiple sequence alignment with high accuracy and high throughput. *Nucleic Acids Res.* 32, 1792–1797. doi: 10.1093/nar/gkh340

Ehrenreich, A., and Widdel, F. (1994). Anaerobic oxidation of ferrous iron by purple bacteria, a new type of phototrophic metabolism. *Appl. Environ. Microbiol.* 60, 4517–4526. doi: 10.1128/aem.60.12.4517-4526.1994

Eickhoff, M., Birgel, D., Talbot, H. M., Peckmann, J., and Kappler, A. (2013). Oxidation of F e (II) leads to increased C-2 methylation of pentacyclic triterpenoids in the anoxygenic phototrophic bacterium *Rhodopseudomonas palustris* strain TIE-1. *Geobiology* 11, 268–278. doi: 10.1111/gbi.12033

Fenna, R. E., Matthews, B. W., Olson, J. M., and Shaw, E. K. (1974). Structure of a bacteriochlorophyll-protein from the green photosynthetic bacterium *Chlorobium limicola*: crystallographic evidence for a trimer. *J. Mol. Biol.* 84, 231–240. doi: 10.1016/0022-2836(74)90581-6

Garber, A. I., Nealson, K. H., Okamoto, A., McAllister, S. M., Chan, C. S., Barco, R. A., et al. (2020). FeGenie: a comprehensive tool for the identification of iron genes and iron gene neighborhoods in genome and metagenome assemblies. *Front. Microbiol.* 11:37. doi: 10.3389/fmicb.2020.00037

Garcia, S. L., Mehrshad, M., Buck, M., Tsuji, J. M., Neufeld, J. D., McMahon, K. D., et al. (2021). Freshwater Chlorobia exhibit metabolic specialization among cosmopolitan and endemic populations. *mSystems* 6:e001196-20. doi: 10.1128/mSystems.01196-20

Grice, K., Cao, C., Love, G. D., Böttcher, M. E., Twitchett, R. J., Grosjean, E., et al. (2005). Photic zone euxinia during the Permian-Triassic superanoxic event. *Science* 307, 706–709. doi: 10.1126/science.1104323

Gurevich, A., Saveliev, V., Vyahhi, N., and Tesler, G. (2013). QUAST: quality assessment tool for genome assemblies. *Bioinformatics* 29, 1072–1075. doi: 10.1093/bioinformatics/btt086

Halm, H., Musat, N., Lam, P., Langlois, R., Musat, F., Peduzzi, S., et al. (2009). Co-occurrence of denitrification and nitrogen fixation in a meromictic lake, Lake Cadagno (Switzerland). *Environ. Microbiol.* 11, 1945–1958. doi: 10.1111/j.1462-2920.2009.01917.x

Hays, L. E., Beatty, T., Henderson, C. M., Love, G. D., and Summons, R. E. (2007). Evidence for photic zone euxinia through the end-Permian mass extinction in the Panthalassic Ocean (Peace River Basin, Western Canada). *Palaeoworld* 16, 39–50. doi: 10.1016/j.palwor.2007.05.008

He, S., Barco, R. A., Emerson, D., and Roden, E. E. (2017). Comparative genomic analysis of neutrophilic iron (II) oxidizer genomes for candidate genes in extracellular electron transfer. *Front. Microbiol.* 8:1584. doi: 10.3389/fmicb.2017.01584

Heda, G. D., and Madigan, M. T. (1986). Aspects of nitrogen fixation in *Chlorobium*. *Arch. Microbiol.* 143, 330–336. doi: 10.1007/BF00412798

Hegler, F., Posth, N. R., Jiang, J., and Kappler, A. (2008). Physiology of phototrophic iron (II)-oxidizing bacteria: implications for modern and ancient environments. *FEMS Microbiol. Ecol.* 66, 250–260. doi: 10.1111/j.1574-6941.2008.00592.x

Heising, S., Richter, L., Ludwig, W., and Schink, B. (1999). *Chlorobium ferrooxidans* sp. nov., a phototrophic green sulfur bacterium that oxidizes ferrous iron in coculture with a "Geospirillum" sp. strain. *Arch. Microbiol.* 172, 116–124. doi: 10.1007/s002030050748

Hug, L. A., Baker, B. J., Anantharaman, K., Brown, C. T., Probst, A. J., Castelle, C. J., et al. (2016). A new view of the tree of life. *Nat. Microbiol.* 1, 1–6. doi: 10.1038/nmicrobiol.2016.48

Hügler, M., and Sievert, S. M. (2011). Beyond the Calvin cycle: autotrophic carbon fixation in the ocean. *Ann. Rev. Mar. Sci.* 3, 261–289. doi: 10.1146/annurev-marine-120709-142712

Imhoff, J. F. (2014). "The family Chlorobiaceae," in *The Prokaryotes: Other Major Lineages of Bacteria and The Archaea*, eds E. Rosenberg, E. F. DeLong, S. Lory, E. Stackebrandt, and F. Thompson (Berlin: Springer), 501–514. doi: 10.1007/978-3-642-38954-2_142

Jain, C., Rodriguez-R, L. M., Phillippy, A. M., Konstantinidis, K. T., and Aluru, S. (2018). High throughput ANI analysis of 90K prokaryotic genomes reveals clear species boundaries. *Nat. Commun.* 9:5114. doi: 10.1038/s41467-018-07641-9

Jensen, S. L. (1965). Bacterial carotenoids. *Acta Chem. Scand.* 19, 1025–1030.

Jiao, Y., and Newman, D. K. (2007). The pio operon is essential for phototrophic Fe (II) oxidation in *Rhodopseudomonas palustris* TIE-1. *J. Bacteriol.* 189, 1765–1773. doi: 10.1128/jb.00776-06

Jiao, Y., Kappler, A., Croal, L. R., and Newman, D. K. (2005). Isolation and characterization of a genetically tractable photoautotrophic Fe (II)-oxidizing bacterium, *Rhodopseudomonas palustris* strain TIE-1. *Appl. Environ. Microbiol.* 71, 4487–4496. doi: 10.1128/aem.71.8.4487-4496.2005

Jones, C., Nomosatryo, S., Crowe, S. A., Bjerrum, C. J., and Canfield, D. E. (2015). Iron oxides, divalent cations, silica, and the early earth phosphorus crisis. *Geology* 43, 135–138. doi: 10.1130/g36044.1

Kang, D. D., Froula, J., Egan, R., and Wang, Z. (2015). MetaBAT, an efficient tool for accurately reconstructing single genomes from complex microbial communities. *PeerJ* 3:e1165. doi: 10.7717/peerj.1165

Kang, D. D., Li, F., Kirton, E., Thomas, A., Egan, R., An, H., et al. (2019). MetaBAT 2: an adaptive binning algorithm for robust and efficient genome reconstruction from metagenome assemblies. *PeerJ* 7:e7359. doi: 10.7717/peerj.7359

Kappler, A., Bryce, C., Mansor, M., Lueder, U., Byrne, J. J. M., Swanner, E. E. D., et al. (2021). An evolving view on the biogeochemical iron cycle. *Nat. Rev. Microbiol.* 19, 360–374. doi: 10.1038/s41579-020-00502-7

Kappler, A., Pasquero, C., Konhauser, K. O., and Newman, D. K. (2005). Deposition of banded iron formations by anoxygenic phototrophic Fe(II)-oxidizing bacteria. *Geology* 33, 865–868. doi: 10.1130/G21658.1

Konhauser, K. O., Hamade, T., Raiswell, R., Morris, R. C., Ferris, F. G., Southam, G., et al. (2002). Could bacteria have formed the Precambrian banded iron formations? *Geology* 30, 1079–1082. doi: 10.1130/0091-7613(2002)030<1079:cbhftp>2.0.co;2

Lambrecht, N., Wittkop, C., Katsev, S., Fakhraee, M., and Swanner, E. D. (2018). Geochemical characterization of two ferruginous meromictic lakes in the Upper Midwest, USA. *J. Geophys. Res. Biogeosci.* 123, 3403–3422. doi: 10.1029/2018jg004587

Lane, D. J. (1991). "16S/23S rRNA sequencing," in *Nucleic Acid Techniques in Bacterial Systematics*, eds E. Stackebrandt and M. Goodfellow (Chichester: John Wiley & Sons), 115–174.

Laufer, K., Niemeyer, A., Nikeleit, V., Halama, M., Byrne, J. M., and Kappler, A. (2017). Physiological characterization of a halotolerant anoxygenic phototrophic Fe (II)-oxidizing green-sulfur bacterium isolated from a marine sediment. *FEMS Microbiol. Ecol.* 93:fix054.

Lee, M. D. (2019). GToTree: a user-friendly workflow for phylogenomics. *Bioinformatics* 35, 4162–4164. doi: 10.1093/bioinformatics/btz188

Llirós, M., García–Armisen, T., Darchambeau, F., Morana, C., Triadó–Margarit, X., Inceoğlu, Ö, et al. (2015). Pelagic photoferrotrophy and iron cycling in a modern ferruginous basin. *Sci. Rep.* 5:13803.

Lu, X., Liu, Y., Johs, A., Zhao, L., Wang, T., Yang, Z., et al. (2016). Anaerobic mercury methylation and demethylation by *Geobacter bemidjiensis* Bem. *Environ. Sci. Technol.* 50, 4366–4373. doi: 10.1021/acs.est.6b00401

Mallorquí, N., Arellano, J. B., Borrego, C. M., and García-Gil, L. J. (2005). Signature pigments of green sulfur bacteria in lower Pleistocene deposits from the Banyoles lacustrine area (Spain). *J. Paleolimnol.* 34, 271–280. doi: 10.1007/s10933-005-3731-3

Maresca, J. A., Chew, A. G. M., Ponsatí, M. R., Frigaard, N. U., Ormerod, J. G., and Bryant, D. A. (2004). The bchU gene of *Chlorobium tepidum* encodes the C-20 methyltransferase in bacteriochlorophyll c biosynthesis. *J. Bacteriol.* 186, 2558–2566. doi: 10.1128/jb.186.9.2558-2566.2004

Maresca, J. A., Romberger, S. P., and Bryant, D. A. (2008). Isorenieratene biosynthesis in green sulfur bacteria requires the cooperative actions of two carotenoid cyclases. *J. Bacteriol.* 190, 6384–6391. doi: 10.1128/jb.00758-08

McAllister, S. M., Polson, S. W., Butterfield, D. A., Glazer, B. T., Sylvan, J. B., and Chan, C. S. (2020). Validating the Cyc2 neutrophilic iron oxidation pathway using meta-omics of zetaproteobacteria iron mats at marine hydrothermal vents. *mSystems* 5:e00553-19.

Meier-Kolthoff, J. P., Auch, A. F., Klenk, H.-P., and Göker, M. (2013). Genome sequence-based species delimitation with confidence intervals and improved distance functions. *BMC Bioinformatics* 14:60. doi: 10.1186/1471-2105-14-60

Melton, E. D., Swanner, E. D., Behrens, S., Schmidt, C., and Kappler, A. (2014). The interplay of microbially mediated and abiotic reactions in the biogeochemical Fe cycle. *Nat. Rev. Microbiol.* 12:797. doi: 10.1038/nrmicro3347

Mloszewska, A. M., Pecoits, E., Cates, N. L., Mojzsis, S. J., O'Neil, J., Robbins, L. J., et al. (2012). The composition of Earth's oldest iron formations: the Nuvvuagittuq Supracrustal Belt (Québec, Canada). *Earth Planet. Sci. Lett.* 317, 331–342. doi: 10.1016/j.epsl.2011.11.020

Morana, C., Roland, F. A. E., Crowe, S. A., Llirós, M., Borges, A. V., Darchambeau, F., et al. (2016). Chemoautotrophy and anoxygenic photosynthesis within the water column of a large meromictic tropical lake (Lake Kivu, East Africa). *Limnol. Oceanogr.* 61, 1424–1437. doi: 10.1002/lno.10304

Nguyen, L. T., Schmidt, H. A., Von Haeseler, A., and Minh, B. Q. (2015). IQ-TREE: a fast and effective stochastic algorithm for estimating maximum-likelihood phylogenies. *Mol. Biol. Evol.* 32, 268–274. doi: 10.1093/molbev/msu300

Nurk, S., Bankevich, A., Antipov, D., Gurevich, A., Korobeynikov, A., Lapidus, A., et al. (2013). "Assembling genomes and mini-metagenomes from highly chimeric reads," in *Proceedings of the Annual International Conference on Research in Computational Molecular Biology*, eds M. Deng, R. Jiang, F. Sun, and X. Zhang (Berlin: Springer), 158–170. doi: 10.1007/978-3-642-37195-0_13

Overmann, J., and Garcia-Pichel, F. (2013). "The phototrophic way of life BT – the prokaryotes: prokaryotic communities and ecophysiology," in *The Prokaryotes*, eds E. Rosenberg, E. F. DeLong, S. Lory, E. Stackebrandt, and F. Thompson (Berlin: Springer), 203–257. doi: 10.1007/978-3-642-30123-0_51

Parks, D. H., Imelfort, M., Skennerton, C. T., Hugenholtz, P., and Tyson, G. W. (2015). CheckM: assessing the quality of microbial genomes recovered from isolates, single cells, and metagenomes. *Genome Res.* 25, 1043–1055. doi: 10.1101/gr.186072.114

Posth, N. R., Konhauser, K. O., and Kappler, A. (2013). Microbiological processes in banded iron formation deposition. *Sedimentology* 60, 1733–1754. doi: 10.1111/sed.12051

Poulton, S. W., and Canfield, D. E. (2011). Ferruginous conditions: a dominant feature of the ocean through Earth's history. *Elements* 7, 107–112. doi: 10.2113/gselements.7.2.107

Raiswell, R., and Canfield, D. E. (2012). The iron biogeochemical cycle past and present. *Geochem. Perspect.* 1, 1–2. doi: 10.7185/geochempersp.1.1

Santos, T. C., Silva, M. A., Morgado, L., Dantas, J. M., and Salgueiro, C. A. (2015). Diving into the redox properties of *Geobacter sulfurreducens* cytochromes: a model for extracellular electron transfer. *Dalt. Trans.* 44, 9335–9344. doi: 10.1039/c5dt00556f

Savvichev, A. S., Kokryatskaya, N. M., Zabelina, S. A., Rusanov, I. I., Zakharova, E. E., Veslopolova, E. F., et al. (2017). Microbial processes of the carbon and sulfur cycles in an ice-covered, iron-rich meromictic Lake Svetloe (Arkhangelsk region, Russia). *Environ. Microbiol.* 19, 659–672. doi: 10.1111/1462-2920.13591

Schmidt, C., Nikeleit, V., Schaedler, F., Leider, A., Lueder, U., Bryce, C., et al. (2021). Metabolic responses of a phototrophic co-culture enriched from a freshwater sediment on changing substrate availability and its relevance for biogeochemical iron cycling. *Geomicrobiol. J.* 38, 267–281. doi: 10.1080/01490451.2020.1837303

Schwartz, E., Fritsch, J., and Friedrich, B. (2006). "The H2-metabolizing prokaryotes," in *The Prokaryotes*, eds M. Dworkin, S. Falkow, E. Rosenberg, K. H. Schleifer, and E. Stackebrandt (New York, NY: Springer), 496–563. doi: 10.1007/0-387-30742-7_17

Seemann, T. (2018). *Barrnap 0.9: Rapid Ribosomal RNA Prediction*. Available online at: https://github.com/tseemann/barrnap. (accessed January 2019).

Shaffer, M., Borton, M. A., McGivern, B. B., Zayed, A. A., La Rosa, S. L., Solden, L. M., et al. (2020). DRAM for distilling microbial metabolism to automate the curation of microbiome function. *Nucleic Acids Res.* 48, 8883–8900. doi: 10.1093/nar/gkaa621

Sieber, C. M. K., Probst, A. J., Sharrar, A., Thomas, B. C., Hess, M., Tringe, S. G., et al. (2018). Recovery of genomes from metagenomes via a dereplication, aggregation and scoring strategy. *Nat. Microbiol.* 3, 836–843. doi: 10.1038/s41564-018-0171-1

Stookey, L. L. (1970). Ferrozine - a new spectrophotometric reagent for iron. *Anal. Chem.* 42, 779–781.

Straub, K. L., Rainey, F. A., and Widdel, F. (1999). *Rhodovulum iodosum* sp. nov. and *Rhodovulum robiginosum* sp. nov., two new marine phototrophic ferrous-iron-oxidizing purple bacteria. *Int. J. Syst. Evol. Microbiol.* 49, 729–735. doi: 10.1099/00207713-49-2-729

Summons, R. E., and Powell, T. G. (1986). Chlorobiaceae in Palaeozoic seas revealed by biological markers, isotopes and geology. *Nature* 319:763. doi: 10.1038/319763a0

Swanner, E. D., Lambrecht, N., Wittkop, C., Harding, C., Katsev, S., Torgeson, J., et al. (2020). The biogeochemistry of ferruginous lakes and past ferruginous oceans. *Earth-Science Rev.* 211, 103430. doi: 10.1016/j.earscirev.2020.103430

Swanner, E. D., Wu, W., Hao, L., Wüstner, M. L., Obst, M., Moran, D. M., et al. (2015). Physiology, Fe(II) oxidation, and Fe mineral formation by a marine planktonic *Cyanobacterium* grown under ferruginous conditions. *Front. Earth Sci.* 3:60. doi: 10.3389/feart.2015.00060

Tang, K. H., and Blankenship, R. E. (2010). Both forward and reverse TCA cycles operate in green sulfur bacteria. *J. Biol. Chem.* 285, 35848–35854. doi: 10.1074/jbc.M110.157834

Thompson, J. D., Gibson, T. J., and Higgins, D. G. (2003). Multiple sequence alignment using ClustalW and ClustalX. *Curr. Protoc. Bioinformatics* Chapter 2:Unit 2.3.

Thompson, K. J. (2020). *Phototrophic Iron Oxidation and Implications for Biogeochemical Cycling in the Archean Eon*. Vancouver, BC: University of British Columbia. doi: 10.14288/1.0392002

Thompson, K. J., Simister, R. L., Hahn, A. S., Hallam, S. J., and Crowe, S. A. (2017). Nutrient acquisition and the metabolic potential of photoferrotrophic Chlorobi. *Front. Microbiol.* 8:1212. doi: 10.3389/fmicb.2017.01212

Tsuji, J. M., Tran, N., Schiff, S. L., Venkiteswaran, J. J., Molot, L. A., Tank, M., et al. (2020). Anoxygenic photosynthesis and iron–sulfur metabolic potential of Chlorobia populations from seasonally anoxic Boreal Shield lakes. *ISME J.* 14, 2732–2747. doi: 10.1038/s41396-020-0725-0

Viollier, E., Inglett, P. W., Hunter, K., Roychoudhury, A. N., and Van Cappellen, P. (2000). The ferrozine method revisited: Fe(II)/Fe(III) determination in natural waters. *Appl. Geochemistry* 15, 785–790. doi: 10.1016/S0883-2927(99)00097-9

Wagner, T., Koch, J., Ermler, U., and Shima, S. (2017). Methanogenic heterodisulfide reductase (HdrABC-MvhAGD) uses two noncubane [4Fe-4S] clusters for reduction. *Science* 357, 699–703. doi: 10.1126/science.aan0425

Waite, D. W., Chuvochina, M., Pelikan, C., Parks, D. H., Yilmaz, P., Wagner, M., et al. (2020). Proposal to reclassify the proteobacterial classes deltaproteobacteria and oligoflexia, and the phylum thermodesulfobacteria into four phyla reflecting major functional capabilities. *Int. J. Syst. Evol. Microbiol.* 70, 5972–6016. doi: 10.1099/ijsem.0.004213

Walter, X. A., Picazo, A., Miracle, M. R., Vicente, E., Camacho, A., Aragno, M., et al. (2014). Phototrophic Fe (II)-oxidation in the chemocline of a ferruginous meromictic lake. *Front. Microbiol.* 5:713. doi: 10.3389/fmicb.2014.00713

Wang, F., Gu, Y., O'Brien, J. P., Yi, S. M., Yalcin, S. E., Srikanth, V., et al. (2019). Structure of microbial nanowires reveals stacked hemes that transport electrons over micrometers. *Cell* 177, 361–369. doi: 10.1016/j.cell.2019.03.029

Wischgoll, S., Heintz, D., Peters, F., Erxleben, A., Sarnighausen, E., Reski, R., et al. (2005). Gene clusters involved in anaerobic benzoate degradation of *Geobacter metallireducens*. *Mol. Microbiol.* 58, 1238–1252. doi: 10.1111/j.1365-2958.2005.04909.x

Wu, W., Swanner, E. D., Hao, L., Zeitvogel, F., Obst, M., Pan, Y., et al. (2014). Characterization of the physiology and cell–mineral interactions of the marine anoxygenic phototrophic Fe (II) oxidizer *Rhodovulum iodosum*–implications for Precambrian Fe (II) oxidation. *FEMS Microbiol. Ecol.* 88, 503–515. doi: 10.1111/1574-6941.12315

Wu, W., Swanner, E. D., Kleinhanns, I. C., Schoenberg, R., Pan, Y., and Kappler, A. (2017). Fe isotope fractionation during Fe (II) oxidation by the marine photoferrotroph *Rhodovulum iodosum* in the presence of Si–implications for Precambrian iron formation deposition. *Geochim. Cosmochim. Acta* 211, 307–321. doi: 10.1016/j.gca.2017.05.033

Wu, Y. W., Simmons, B. A., and Singer, S. W. (2016). MaxBin 2.0: an automated binning algorithm to recover genomes from multiple metagenomic datasets. *Bioinformatics* 32, 605–607. doi: 10.1093/bioinformatics/btv638

Zhuang, W.-Q., Yi, S., Bill, M., Brisson, V. L., Feng, X., Men, Y., et al. (2014). Incomplete Wood–Ljungdahl pathway facilitates one-carbon metabolism in organohalide-respiring *Dehalococcoides mccartyi*. *Proc. Natl. Acad. Sci. U.S.A.* 111, 6419–6424. doi: 10.1073/pnas.1321542111

Conflict of Interest: The authors declare that the research was conducted in the absence of any commercial or financial relationships that could be construed as a potential conflict of interest.

frontiers in Microbiology

ORIGINAL RESEARCH
published: 14 July 2021
doi: 10.3389/fmicb.2021.696534

Hydrologic Alteration and Enhanced Microbial Reductive Dissolution of Fe(III) (hydr)oxides Under Flow Conditions in Fe(III)-Rich Rocks: Contribution to Cave-Forming Processes

*Kayla A. Calapa[1], Melissa K. Mulford[2], Tyler D. Rieman[3], John M. Senko[1,2,3], Augusto S. Auler[4], Ceth W. Parker[5] and Hazel A. Barton[1,2,3]**

[1] Department of Biology, University of Akron, Akron, OH, United States, [2] Integrated Bioscience, University of Akron, Akron, OH, United States, [3] Department of Geosciences, University of Akron, Akron, OH, United States, [4] Instituto do Carste, Belo Horizonte, Brazil, [5] Planetary Protection Center of Excellence, NASA Jet Propulsion Laboratory, Pasadena, CA, United States

OPEN ACCESS

Edited by:
Sujun Li,
Indiana University, United States

Reviewed by:
James F. Holden,
University of Massachusetts Amherst, United States
Xiaolong Liang,
Washington University in St. Louis, United States

***Correspondence:**
Hazel A. Barton
bartonh@uakron.edu

Specialty section:
This article was submitted to Microbiological Chemistry and Geomicrobiology, a section of the journal Frontiers in Microbiology

Received: *16 April 2021*
Accepted: *21 June 2021*
Published: *14 July 2021*

Citation:
Calapa KA, Mulford MK, Rieman TD, Senko JM, Auler AS, Parker CW and Barton HA (2021) Hydrologic Alteration and Enhanced Microbial Reductive Dissolution of Fe(III) (hydr)oxides Under Flow Conditions in Fe(III)-Rich Rocks: Contribution to Cave-Forming Processes. Front. Microbiol. 12:696534. doi: 10.3389/fmicb.2021.696534

Previous work demonstrated that microbial Fe(III)-reduction contributes to void formation, and potentially cave formation within Fe(III)-rich rocks, such as banded iron formation (BIF), iron ore and canga (a surficial duricrust), based on field observations and static batch cultures. Microbiological Fe(III) reduction is often limited when biogenic Fe(II) passivates further Fe(III) reduction, although subsurface groundwater flow and the export of biogenic Fe(II) could alleviate this passivation process, and thus accelerate cave formation. Given that static batch cultures are unlikely to reflect the dynamics of groundwater flow conditions *in situ*, we carried out comparative batch and column experiments to extend our understanding of the mass transport of iron and other solutes under flow conditions, and its effect on community structure dynamics and Fe(III)-reduction. A solution with chemistry approximating cave-associated porewater was amended with 5.0 mM lactate as a carbon source and added to columns packed with canga and inoculated with an assemblage of microorganisms associated with the interior of cave walls. Under anaerobic conditions, microbial Fe(III) reduction was enhanced in flow-through column incubations, compared to static batch incubations. During incubation, the microbial community profile in both batch culture and columns shifted from a Proteobacterial dominance to the Firmicutes, including Clostridiaceae, Peptococcaceae, and Veillonellaceae, the latter of which has not previously been shown to reduce Fe(III). The bacterial Fe(III) reduction altered the advective properties of canga-packed columns and enhanced permeability. Our results demonstrate that removing inhibitory Fe(II) via mimicking hydrologic flow of groundwater increases reduction rates and overall Fe-oxide dissolution, which in turn alters the hydrology of the Fe(III)-rich rocks. Our results also suggest that reductive weathering of Fe(III)-rich rocks such as canga, BIF, and iron ores may be more substantial than previously understood.

Keywords: cave (speleogenic) and alluvial deposits (formations), iron reduction bacteria, hydrology and water, *Desulfosporosinus*, *Veillonella*

INTRODUCTION

The Southern Espinhaço Mountain Range (SE) of southeastern Brazil contains commercially important, high-grade iron ore hosted by the Serra da Serpentina Group, a stratigraphic unit which includes the iron-rich Serra do Sapo Formation (Auler et al., 2019). These sedimentary units were formed by the precipitation of Fe(III) and Si phases from solution during the Proterozoic Eon (Weber et al., 2006; Rosière et al., 2019; Silveira Braga et al., 2021). Iron ores can include magnetite (Fe_3O_4), hematite (α-Fe_2O_3), or a ferric oxyhydroxide like goethite (α-FeOOH) or limonite ($FeO(OH)\cdot n(H_2O)$, and high-grade ore averages between 60 and 67% Fe (Dorr, 1964; Beukes et al., 2003; Rolim et al., 2016). The SE and Quadrilátero Ferrífero (Iron Quadrangle; QF) located ∼150 km south of SE, contain abundant Fe(III)-rich minerals, which can be found in intact banded iron formation (BIF), Si-depleted ore, and canga rock (Beukes et al., 2003; Souza et al., 2015; Auler et al., 2019). BIF contains alternating bands of quartz (SiO_2) and either magnetite or hematite that range from a few millimeters to a few centimeters in thickness, and averages between 15 and 38% iron (Smith, 2015; Rolim et al., 2016). Canga is a brecciated duricrust containing clasts of iron oxide (usually BIF) with an iron-oxide cement matrix that averages between 57 and 62% iron (Dorr, 1964; Spier et al., 2007; Gagen et al., 2019). Canga contains the most poorly crystalline Fe(III) of the three major phases (i.e. canga, BIF, and ore), with goethite the most prominent mineral phase (Parker et al., 2013).

Canga and BIF are generally considered highly resistant to both mechanical and chemical weathering at pH $\geq$ 3 (Dorr, 1964; Johnson et al., 2012; Auler et al., 2014; Spier et al., 2018; Gagen et al., 2019), and canga covers the slopes and valleys of the SE region. Yet this area is also associated with hundreds of caves (iron formation caves; IFCs) that form mostly at the BIF/canga boundary (Auler et al., 2019). The identification of these caves suggests that processes leading to Fe(III) weathering and removal increase porosity at the canga/BIF interface, despite the resistance of both types of rocks to dissolution. At circumneutral pH, Fe solubility can be enhanced by microbially mediated reductive dissolution of Fe(III) phases to relatively soluble Fe(II). This activity may facilitate the mass transport necessary for the increased porosity and the formation of the observed IFCs (Parker et al., 2013, 2018). In support of this hypothesis, while the walls of the IFCs are lined with a hard, oxidized layer of canga, the interior (approximately 3 cm behind) of the wall surface contains a soft, gooey, water-saturated material that contains abundant microbial cells (Parker et al., 2018). Given the inhibition of Fe-reduction by oxygen, we wondered whether this material was involved in promoting Fe-reduction and increased porosity, leading to formation of the IFCs. Canga is a rather porous media, and active vertical percolation of water occurs during rainfall, the patterns of which can be irregular, depending on season (Mesquita et al., 2017; Parker et al., 2018). As such, intermittent periods of extensive water circulation around and within caves and their hosting rocks can occur, followed by water stagnation or dry periods.

Prior enrichment of canga-associated microorganisms from IFCs demonstrated that the microbial communities present were capable of Fe(III) reduction to extents that could contribute to IFC formation (Parker et al., 2018), but Fe(II) that accumulates during Fe(III) (hydr)oxide reduction can adsorb to Fe(III) phase surfaces and induce mineral (trans)formations (Roden et al., 2000; Benner et al., 2002; Hansel et al., 2003, 2005; Gonzalez-Gil et al., 2005). These consequences of Fe(III) reduction could self-limit further Fe(III) (hydr)oxide reduction, although subsurface water flow could help overcome these limitations by advective transport of Fe(II) (Gonzalez-Gil et al., 2005; Minyard and Burgos, 2007; Wefer-Roehl and Kübeck, 2014). Additionally, it remained unclear if the extents of microbiological Fe(III) (hydr)oxide dissolution observed were sufficient to induce hydrologic alterations that would culminate in cave formation. To understand whether this hydrologic flow could influence Fe-reduction rates and enhance IFC formation we compared batch cultures [where Fe(II) will accumulate] to columns [where Fe(II) is removed via flow] to evaluate how water flow influenced microbiologically mediated Fe(III) reduction, and whether such activity could influence the hydraulic properties of canga.

MATERIALS AND METHODS

Sample Collection and Preparation for Batch Incubations and Column Experiments

Five IFCs were sampled in the SE region of Brazil in December 2018. The cave designations are: CSS-0009, CSS-0080, CSS-0010, CSS-0107, and CSS-0074. Authorization for sampling during the destruction of these caves through mining had been approved by the Brazilian environmental agency, and the sampling was part of a final recovery effort prior to mining. Canga was collected from the interior of a cave that was forming at a BIF-canga interface. Large (0.5–5.5 kg) chunks of canga were removed from cave walls using an electric demolition hammer during the final sampling effort prior to cave destruction and placed in plastic bags. The soft, microbial-rich material behind the walls (*sub muros*) was collected by first removing the rigid oxide layer and then using a sterile garden shovel to place this material in sterile glass jars and sealed with plastic tape to maintain anaerobic/microaerobic conditions. Samples were placed in a refrigerator upon return from the field. Collected canga was pulverized for column experiments by cutting large chunks into smaller pieces with a water-cooled trim saw with a 25 cm blade, which were then processed through a ball mill (SPEX Industries, Inc., Metuchen, NJ, United States) until all the material passed through a 1.44 mm sieve. This pulverized canga was sterilized by autoclaving at 121°C for 15 min, allowing a 1 h recovery, and then autoclaved again to assure deactivation of spore-forming bacteria. This sterilized canga was then dried at 65°C for 14–16 h in an oven.

Batch Incubations

Preparation of batch incubations was carried out in a Coy anaerobic glove bag (Coy Laboratory Products, Inc., Grass Lake, MI, United States) filled with 3-5% H_2, balance N_2. Synthetic porewater (SPW) composition was based on characterization of IFC porewaters, and contained 5 mM $CaCl_2$, 0.1 mM Na_2SO_4, and 0.1 mM KH_2PO_4. Sodium lactate (5.0 mM) was included as an electron donor and carbon source, and the pH of the SPW was adjusted to either pH 4.75 or pH 6.8 with HCl or NaOH, respectively, which were chosen to approximate the pH of porewaters we have observed in IFCs (Parker et al., 2018). O_2 was removed from the SPW by bringing the liquid to nearly boiling, then cooling under a stream of N_2 gas for 45 min. Once cooled, SPW-containing bottles were sealed, transferred to the anaerobic glove bag, and filter-sterilized with a 0.2 μm PES filter (VWR, Radnor, PA, United States) until use in incubation bottles or column experiments. Batch sediment incubations contained 20 g of pulverized canga (equivalent to approximately 120 mmol Fe(III)) and 60 mL of SPW in 160 mL serum bottles that were sealed with butyl rubber stoppers held in place with aluminum crimp seals. Where appropriate, 5 g of *sub muros* material and associated microbial community was used as inoculum for non-sterile incubations. Incubations were carried out in triplicate.

Column Assembly and Operation

All materials used for packing columns were acid-washed and sterilized prior to use, and all columns (10 cm × 1 cm Econo-Columns; Bio-Rad Laboratories, Hercules, CA, United States) were packed and operated in a Coy anaerobic glove bag as described. Approximately 2 g of 3 and 2 mm diameter glass beads were placed at the bottom of the column, respectively, to prevent sediment clogging. The uninoculated columns were packed with pulverized sterile canga using a "lift" technique: a 2 g lift of canga was added, followed by the injection of 200–500 μL SPW (described above) through bottom of the column. After the addition of each lift, the columns were tapped to remove air bubbles, and sediments were allowed to settle for 1–2 min. A suspension of *sub muros* was prepared with 8 g pulverized canga and 8 g *sub muros* in 6 mL SPW, which was added 250 μL at a time after each lift of canga/SPW during column packing. The final amount of *sub muros* added was ∼2 mL, which resulted in $\sim 9.2 \times 10^7$ cells/g column material (as determined by direct cell counting; see below). All columns received 4 g of 2 mm beads followed by 2 g of 3 mm beads added to on top of the sediments to prevent clogging. After packing, columns contained a total of 16 g of solids and 7 mL liquid (either SPW only in uninoculated columns or SPW and microbial suspension in inoculated columns). All column incubations were carried out in triplicate in the anaerobic glove bag for 14 days prior to the first sampling.

Synthetic porewater was delivered to columns in an upward flow during sampling using a Masterflex L/S Precision Variable-Speed Console peristaltic pump with Masterflex L/S 8-Channel Pump Head (Cole-Parmer, Vernon Hills, IL, United States), and 1.6 mm inner diameter Tygon tubing (Fischer Scientific, Pittsburgh, PA, United States). The columns were subsequently incubated statically for 7 days at room temperature between sampling events, whereupon 3–5 column void volumes of SPW were passed through at a flow rate of 0.2 mL/min, and during this period samples were collected from each column volume for measurement of pH, sulfate concentration, and dissolved Fe(II) concentration (described below). At the completion of the experiments, breakthrough curves were determined with 1 mM NaBr-amended (Acros Organics, Morris, NJ, United States) SPW at a flow rate of 0.2 mL/min, and samples were periodically collected for bromide quantification (described below). At the conclusion of the experiments, columns were deconstructed and sediments were removed for analysis of the microbial communities and quantification of total Fe(II) and microbial cells.

Sample Processing and Analytical Techniques

Column effluent samples for dissolved Fe(II) quantification were preserved in 0.5 M HCl, while those intended for measurement of pH, sulfate, and bromide were untreated. Solids were removed from the samples by centrifugation at 12,100 × *g* for 5 min. To measure solid-associated Fe(II) in column sediments, approximately 0.5 g of material was placed in microcentrifuge tubes with 1 mL 0.5 M HCl (Lovley and Phillips, 1987) and solids were then separated from the solution by centrifugation before measurement of Fe(II) in the supernatant. Fe(II) was quantified by ferrozine assay (Stookey, 1970). pH was measured using a SevenGo Pro pH/Ion meter (Mettler Toledo, Columbus, OH, United States). Sulfate, bromide, phosphate, nitrate, and chloride were measured by ion chromatography with a Dionex DX-120 System with an IonPac AS22 Column and conductivity detection (Thermo Fisher Scientific, Waltham, MA, United States). To analyze the mineralogy of the column at the end of the experiment, approximately 1 mL of column contents were dried in a closed container with $CaCl_2$ (Acros Organics, Morris, NJ, United States) as a drying agent under anaerobic conditions. Mineral characterization of the homogenized rock was determined by X-Ray Diffraction (XRD) with a Rigaku Ultima IV (Rigaku, Woodlands, TX, United States). Samples were analyzed with a 2θ between 5° and 70° and diffraction patterns were compared to those standards available on the American Mineralogist Crystal Structure Database (Downs and Hall-Wallace, 2003).

Microbial Community Analysis

Microbial cells in the *sub muros* inoculum, batch incubations, and in the columns at the conclusion of the experiments were enumerated by direct cell counting. Briefly, ∼1 g samples were collected while the columns remained in the anaerobic glove bag and mixed with 1 mL of filter-sterilized Dulbecco pH 7.4 phosphate buffered saline (PBS) (Thermo Fisher Scientific, Waltham, MA, United States) and vigorously shaken by hand to mix the contents. One hundred microliter of this mixture was then added to 9.9 mL sterile PBS and 1X thiazole green DNA stain (Biotium, Fremont, CA, United States). This mixture was incubated in the dark for 30 min at room temperature and then

filtered onto a 0.2 μm GTBP Isopore polycarbonate membrane filter via a Millipore stainless steel filtration unit (Millipore Sigma, Darmstadt, Germany). The filter was removed and placed on a glass slide with 25 μL SlowFade Gold Antifade Mountant with DAPI (Thermo Fisher Scientific, Waltham, MA, United States) and cells were counted using a BX53 fluorescent microscope (Olympus America Inc., Center Valley, PA, United States). The total cell number was calculated based on 100 fields-of-view (FOV) at 1,000× magnification, with the average number of cells per FOV multiplied by the total dilution factor, area of the filter membrane, and standardized against the absolute weight of the material/g (Hershey et al., 2018).

For DNA analyses, genomic DNA was extracted from samples using either then DNeasy PowerLyzer PowerSoil or PowerBiofilm Kit (Qiagen, Germantown, MD, United States). Subsamples from the triplicate batch incubations were pooled before DNA extraction. PCR amplification of the 16S rRNA V3 and V4 regions using the primers 806R (5′-GGA CTA CHV GGG TWT CTA AT-3′) and 515F (5′-GTG CCA GCM GCC GCG GTA A-3′), with samples identified using unique barcodes along with Illumina adapter sequences (Integrated DNA Technologies, Coralville, IA, United States). Amplification was using a Mastercycler Nexus Gradient (Eppendorf, Enfield, CT, United States), including a 3 min 94°C hot start, followed by 30 cycles of: denaturing at 94°C for 45 s, annealing at 50°C for 60 s, and then a 72°C extension for 90 s, followed by a final extension step at 72°C for 10 min. The PCR products were gel purified, and quantified using a Qubit dsDNA HS Assay Kit (Life Technologies, Waltham, MA, United States). Samples were then sequenced on an Illumina MiSeq and de-multiplexed in QIIME2 (version 2020.2; Bolyen et al., 2019) using *cutadapt demux*-paired and a quality check was carried out using *q2-deblur-denoise-16S* and *quality-filter-q-score*. OTU picking and taxonomic assignments were completed using the *feature-classifier-classify-sklearn* (Bolyen et al., 2019).

RESULTS AND DISCUSSION

Fe(III) Reduction in Static Incubations

To evaluate the canga-Fe(III) reducing activities of the microbial communities in the *sub muric* material, static batch incubations were conducted. Canga was provided as the Fe(III) source with SPW at a pH of 4.75 or 6.8, which matched the measured pH values *in situ* (Parker et al., 2018). Minimal Fe(II) was generated in uninoculated incubations, but accumulated in the *sub muros*-inoculated incubations at both pH 4.75 and 6.8 (**Figure 1A**). The concentration of dissolved Fe(II) that accumulated in the *sub muros*-inoculated batch incubations (approximately 5 mM) exceeded previous batch incubation work in which *Shewanella oneidensis* MR-1 was used to catalyze canga-Fe(III) reduction (less than 0.6 mM; Parker et al., 2013). Indeed, mean total Fe(II) concentration of *sub muros*-inoculated incubations exceeded 80 mmol/L (**Figure 1B**). In previous work, a maximum of 3% of canga-Fe(III) could be reduced by *S. oneidensis* MR-1 (Parker et al., 2013); however, greater extents of Fe(III) reduction have been observed by fermentative enrichments and isolates from canga by ourselves and other researchers (Parker et al., 2018; Gagen et al., 2019). The drivers of this enchanced reduction remain unclear at this time and represent a good target for future research.

In previous cultures using various Fe(III) mineral phases (including canga; Parker et al., 2018) we used a PIPES-buffered (also at pH 4.75 and 6.8) mineral salts medium for growth. In these cultures we saw a shift in microbial community structure from the Proteobacteria-dominated *sub muros* to one dominated by the Firmicutes, representing >97% of sequences (**Figure 2**). In these previous experiments, we had assumed that the shift in community structure had been driven in part by the high amount of organic carbon, while the closed nature of the experiment allowed H_2 to accumulate and drive fermentative Fe-reduction by members of the Clostridia (Shah et al., 2014; Parker et al., 2018). We tested this hypothesis in this study, using a basal medium (SPW) and 5 mM lactate as a carbon source. Analysis of partial 16S rRNA gene sequences in the batch incubations after 85 days revealed a similar dominance by fermentative Firmicutes (**Figure 2**). Nonetheless, using SPW/lactate, the Proteobacteria remained abundant, comprising 23 and 15% of the sequences recovered from pH 4.75 and 6.8 incubations, respectively. We also saw a small, but significant population of Actinobacteria (6% at pH 4.75 and 3% at pH 6.8) and Bacteriodetes (2.5% only at pH 6.8) that had not been observed previously (**Figure 2**). The pH of the uninoculated controls averaged 5.44, regardless of whether the pH 4.75 or 6.8 SPW was used to initiate the experiment, suggesting that canga buffered the pH; however, in the inoculated batch cultures, the SPW/lactate pH 4.75 culture increased to pH 6.10, while the SPW pH 6.8 culture remained reasonably constant at pH 6.67. There was no dramatic change in pH of the cultures following the addition of *sub muros* at day 0. This suggests Fe(III) reduction through microbial activity likely raises the pH (Eq 1):

$$Fe(OH)_3 + 3H^+ + e^- \rightarrow Fe^{2+} + 3H_2O \quad (1)$$

The similarity in pH of the final culture conditions may explain the similarity of the final observed community profiles (**Figure 2**).

At the genus level within the dominant Firmicutes (**Figure 3**), the SPW/lactate batch cultures displayed a different structural diversity to our previous work. Previously, at pH 4.75 the batch cultures were dominated by members of the genus *Clostridium* (Family Clostridiales; 71%), with a small but significant representation by the *Desulfosporosinus* (Family Peptococcaceae; 6%), while at pH 6.8, the PIPES batch cultures were dominated by both the *Desulfosporosinus* (38%) and *Clostridium* (36%) (Parker et al., 2018). Both cultures also contained minor populations of the *Paenibacilli* (Family Bacillales; 3% at both pH 4.75 and 6.8). In the batch cultures presented here, we saw a similar dominance by members of the Clostridia (31% at pH 4.75 and 47% at pH 6.8), and *Desulfosporosinus* (20 and 24% at pH 4.75 and 6.8, respectively). The *Desulfosporosinus* sp. are normally associated with sulfate reduction, but have also been shown to reduce Fe(III) enzymatically (Senko et al., 2009; Sato et al., 2019). If not enzymatic, the production of a minor amount of sulfide could be sufficient to enable Fe(III) reduction via S as an electron shuttle (Hansel et al., 2015). Members of the *Paenibacilli*, which have recently been demonstrated to play an

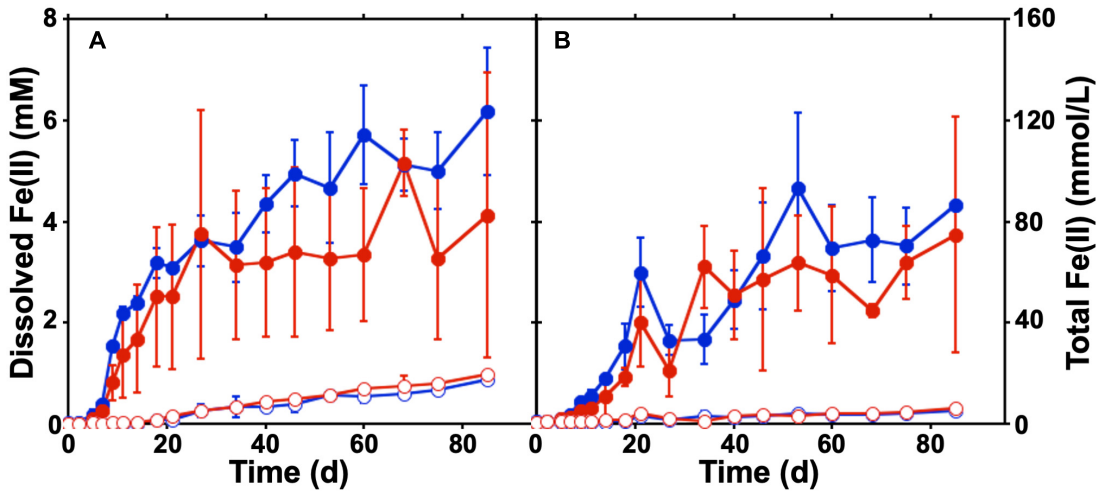

FIGURE 1 | Batch cultures of Fe(III) reduction in SPW canga. The concentration of dissolved Fe(II) **(A)** and total Fe(II) **(B)** were measured under static conditions over 3 months. Comparisons were made between sterile canga (open circles) or canga inoculated with *sub muros* material (closed circles), with a basal SPW medium pH of 4.75 (red) or pH 6.8 (blue). Error bars represent the standard deviation of triplicate incubations.

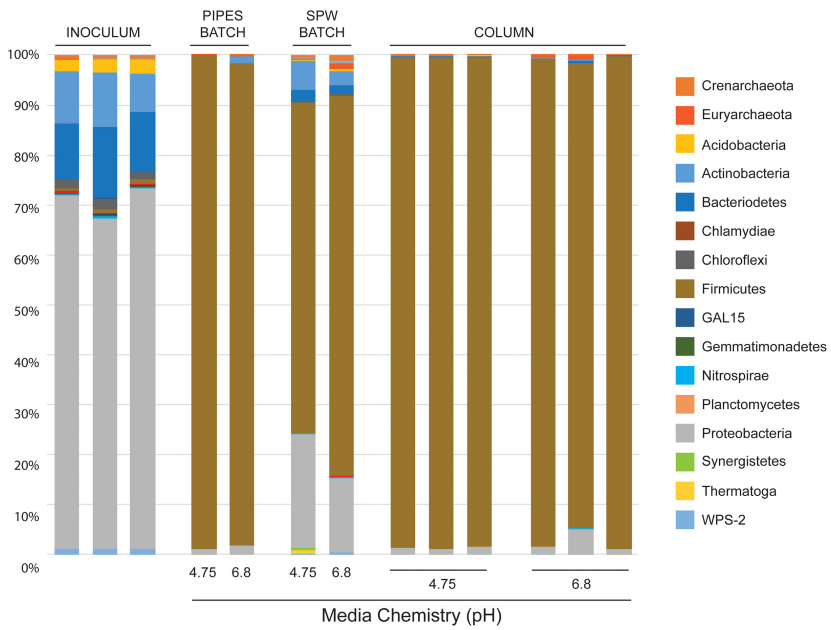

FIGURE 2 | Illumina sequencing results of phylum-level community diversity in batch and column cultures. Illumina sequencing of *sub muros* inoculated samples at day 0 are shown (inoculum). The diversity in our previous batch culture experiments, where the basal media was buffered with PIPES is shown (indicated as PIPES BATCH; Parker et al., 2018), followed by the cultures presented here using SPW with lactate (SPW BATCH). Illumina data is also provided for each of the individual columns in the flow-through experiments (COLUMN). The basal pH of each media formulation at day 0 is shown (Media Chemistry pH).

important role in iron oxide weathering in soils (including in Brazil; Loyaux-Lawniczak et al., 2019) were also represented at both pH 4.75 and 6.8 (4% of total diversity; **Figure 3**). Interestingly, we saw a higher percentage of members of the *Coprococcus* (Family Lachnospiraceae; 2%) at both pH 4.75 and 6.8. The genus *Coprococcus* includes strict anaerobes that play an important role in carbohydrate fermentation in the mammalian rumen, including lactate (Rainey, 2009). It is unclear as to why members of this genus would be enriched under the batch culture conditions; however, their growth is stimulated by fermentable carbohydrates, suggesting that the use of lactate may have enhanced their growth (Cotta and Forster, 2006; Rainey, 2009). Members of this genus have not been associated with Fe-reduction, or isolated from iron-rich environments, although the production of H_2 during fermentation may contribute to the overall culture Fe-reduction conditions (Cotta and Forster, 2006;

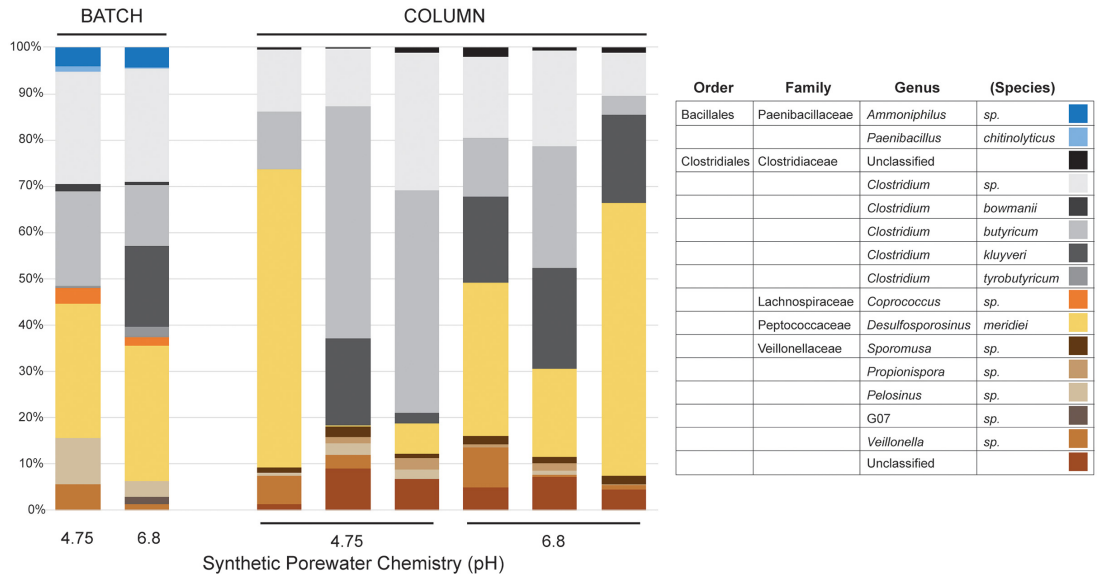

FIGURE 3 | Illumina sequencing results of genus-level community diversity within the Firmicutes from the batch and column cultures. Only the SPW/lactate results are shown. The distribution of genera in the batch cultures (BATCH) and individual columns (COLUMN) are shown, along with the basal pH of the SPW at day 0 is shown. Given the myriad of Family- and Genera-level distributions within the Firmicutes, the Order/Family/Genus classification is provided for each identified species.

Parker et al., 2018). We also observed a significant representation by members of the Family Veillonellaceae, with 11% at pH 4.75 and 5% at pH 6.8 (**Figure 3**). Recently, genera within the Veillonellaceae, such as *Sporomusa* spp. and *Propionispora* spp., have been shown to carry out Fe(III) reduction (Sass et al., 2004; Kato et al., 2015); however, rather using respiratory Fe(III) reduction, the *Sporomusa* appear to use Fe(III) as an electron sink in acetogenesis (Igarashi and Kato, 2021).

Fe(III) Reduction in Column Incubations

The underlying hypothesis of our work is that microbiological Fe(III) reducing activities are sufficient to induce porosity generation within the host rocks (i.e., canga, BIF, and iron ore); however, we have not observed hydrologic alterations of cave hosting rocks. Biogenic Fe(II) can limit the extent of Fe(III) (hydr)oxide reduction (Roden and Zachara, 1996; Urrutia et al., 1999; Roden and Urrutia, 2002; Roden, 2004, 2006), and induce mineralogical changes that would otherwise limit further Fe(III) reduction or limit the export of soluble Fe(II) (i.e., the formation of secondary minerals; Benner et al., 2002; Hansel et al., 2003, 2005). Nonetheless, the advective removal of biogenic Fe(II) as water flows through Fe(III) (hydr)oxide-rich rocks could enhance their reduction (Roden and Urrutia, 1999; Roden et al., 2000; Royer et al., 2004; Minyard and Burgos, 2007). For example, 95% of Fe(III) coating on sand was reduced over six months by *Shewanella putrefaciens* CN32 in flow-through columns, compared to 13% of the Fe(III) in batch incubations (Roden et al., 2000).

The climate regime in the SE area is highly seasonal, with over 80% of the ∼1,400 mm/year rainfall concentrated in November-March. Canga is a highly porous rock, with values between 24 and 29% (Costa and Sá, 2018), while the friable ore underneath the canga is highly impermeable with values as low as 10^{-8} m/s (Mesquita et al., 2017). Thus, rainfall infiltrates quickly through the canga towards the caves and then drains rapidly toward the surface, with very little retention of water, except in a few shallow internal ponds. Despite the robust Fe(III) reducing activity observed in the batch incubations (**Figure 1**; Parker et al., 2018), they do not mimic the hydrologic flow associated with the rocks of the SE or QF in which cave formation occurs with Fe(II) accumulating in the cultures. To mimic flow conditions in a laboratory setting, we packed canga into columns under conditions analogous to the batch incubations, and introduced flow into the system. This approach allowed us to answer the two major questions of this work: (1) does advective removal of biogenic Fe(II) enhance further canga-Fe(III) reduction and (2) are the Fe(III) reducing microbial activities associated with the *sub muric* material sufficient to induce hydrologic alterations to the host rock.

The columns were packed with crushed canga alone, or with crushed canga mixed with *sub muric* material. The columns were incubated statically for 14 days, allowing Fe(III) reduction to initiate, before four column volumes of SPW were then passed through the column and collected separately for analysis of effluent chemistry (**Figure 4**). This process of static incubation followed by introduced flow was then repeated at 7 day intervals. Minimal dissolved Fe(II) was detected in the effluent of uninoculated control columns throughout the incubation (**Figure 4**), and effluent pH was ∼4.5–5.0, regardless of influent SPW pH. This is slightly lower than the values obtained in the batch experiments shown in **Figure 1**. In the inoculated columns, progressively higher concentrations of dissolved Fe(II) accumulated over the course of the incubation, with maximum Fe(II) concentrations of approximately 3 mM Fe(II) detected

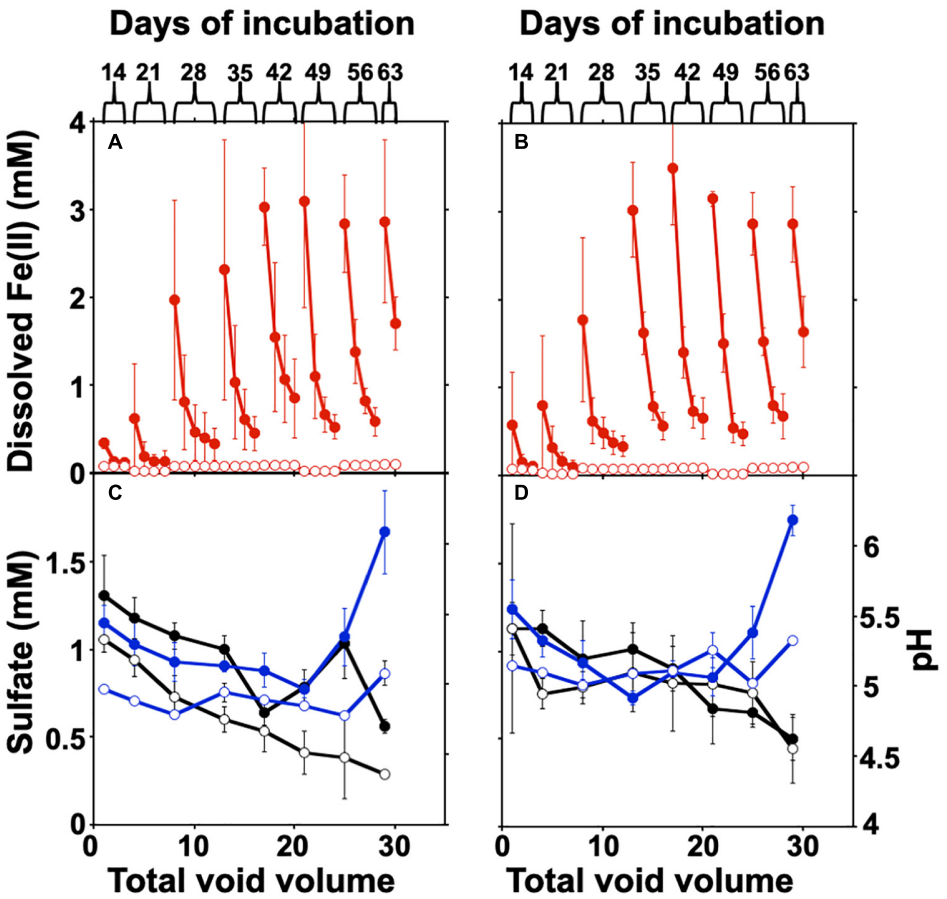

FIGURE 4 | Fe(III) reduction and changes in sulfate and pH in the column experiments. **(A,B)** Columns were operated semi-continuously, and sulfate and pH were measured in each pore volume (four volumes) recovered after each static incubation. The column was disassembled after two column volumes at day 63 for post mortem analysis. Error bars represent one standard deviation of triplicate columns. The concentration of dissolved Fe(II) is shown at pH 4.75 **(A)** and 6.8 **(B)**. Sulfate concentrations (black) and pH (blue) in column effluents are shown in panels **(C)** (pH 4.75) and **(D)** (pH 6.8). The values for uninoculated columns are shown with open circles, with the *sub muros*-inoculated columns represented by closed circles.

after the fifth round of static incubation at both pH 4.75 and 6.8 (**Figures 4A,B**).

The concentration of total Fe(II) (dissolved and solid-associated) produced in the columns incubated at either pH 4.75 or 6.8 SPW are shown in **Table 1**. A two-sample *t*-test assuming unequal variances suggested that there was no significant difference ($P = 0.97$) in total dissolved Fe(II) accumulation in the columns receiving SPW with pH 4.75 and 6.8 (**Figure 4**). The pH of the column effluent suggests that there was an increase in pH above 6.0 (**Figure 4C**), similar to the batch cultures. The increase in Fe(III) reduction in the pH 4.75 column as the experiment progressed may reflect a change in column community structure as the cultures move toward similar pH conditions. The increase in pH conditions is correlated with the increasing observation of *Clostridium kluyveri* (**Figure 3**) and may suggest either the selection of this species und these pH conditions, or a role in driving Fe(III)-reduction.

While canga is composed mostly of goethite and poorly crystalline Fe(III) (hydr)oxides (Parker et al., 2013), if we assume dissolved Fe(II) is derived from $Fe(OH)_3$, approximately 40 mg of $Fe(OH)_3$ were reductively dissolved and exported as Fe(II) from the packing material of inoculated columns, with minimal export of Fe from uninoculated columns (**Table 1**). In the batch

TABLE 1 | Post mortem analysis of column contents.

	pH 4.75 with *sub muros*	pH 4.75 uninoculated	pH 6.8 with *sub muros*	pH 6.8 uninoculated
Total Fe(II) (μmol/g)	60 ± 15	4.4 ± 0.2	89 ± 19	4.3 ± 0.1
Cell abundances t = 0 (cell/g wet)	$9.3 \times 10^7 \pm 2.3 \times 10^5$	N/D	$9.1 \times 10^7 \pm 1.8 \times 10^5$	N/D
Cell abundances t = 63 (cell/g wet)	$4.0 \times 10^8 \pm 8.1 \times 10^7$	N/D	$4.2 \times 10^8 \pm 4.7 \times 10^7$	N/D
$Fe(OH)_3$ removed as Fe^{2+} (mg)	38 ± 18	2.3 ± 0.2	40 ± 3.5	2.3 ± 0.01

incubations, only ~30 mg of $Fe(OH)_3$ were reductively dissolved (**Figure 1**). After two porewater replacement events (21 days), the dissolved Fe(II) concentration in effluent from *sub muros*-inoculated columns exceeded 6 mM in total in pH 6.8 columns and over 5 mM total in pH 4.75 columns; iron reduction levels which only accumulated after 60 days continuous culture in batch incubations (**Figures 1A**, **4A,B**). These results indicate that water flow enhances the reductive solubilization of Fe from canga and separation of the Fe(II) products from solid phases.

Microbial Communities in Column Incubations

The microbial community composition in the batch incubations suggested that non-respiratory Fe(III) reduction could play a role in the observed iron reduction (**Figure 3**). To determine the extent of growth during column operation, we counted cells associated with the *sub muros* inoculum and at the conclusion of the column experiments. All the columns seeded with *sub muros* were initially inoculated at ~9.2×10^7 cells/g. At 63 days, the population had increased in the columns at pH 4.75 by 4.3×, with the cell number in the pH 6.8 column increasing 4.6×. These data suggested an increase in microbial growth, and indeed the higher cell number is the pH 6.8 columns matches a higher-level of Fe(III) reduction. No microbial cells were detected in the uninoculated controls (**Table 1**).

DNA extraction from the inoculated columns produced sufficient DNA for Illumina sequencing, but repeated attempts to extract DNA from the uninoculated columns failed, matching the observations by direct cell counting. Illumina sequencing of the microbial communities in the columns matched our observations in batch culture (**Figures 2**, **3**); there had been a shift from dominance by the Proteobacteria, to dominance by members of the Firmicutes. At the genus level, the columns were similarly dominated by members of *Clostridium, Desulfosporosinus,* and *Veillonella,* which represented ≥90% of the identified partial 16S rRNA gene sequences (**Figure 3**); however, members of the *Paenibacilli* were not observed. There was some inter-column variability under each of the pH conditions, particularly in regard to the dominance of *Clostridium* relative to *Desulfosporosinus* (**Figure 3**). In the *Desulfosporosinus*-dominated columns, we saw a darkening of the column material, which could indicate sulfidogenesis, but there was no decrease in the effluent sulfate concentration over the course of the incubations (**Figures 4C,D**). This suggests that while members of the *Desulfosporosinus* are accumulating in these columns, they may be functioning as Fe(III) reducers. Indeed, members of this genus have been shown to be the primary Fe(III) reducers under oligotrophic conditions (Nixon et al., 2017; Bomberg et al., 2019). Fe(III) reduction is widespread among the Clostridia, including a strain of *Clostridium beijerinckii* (Dobbin et al., 1999; Lehours et al., 2010; Shah et al., 2014; List et al., 2019). Indeed, in our previous batch cultures were capable of extensive (in some cases, complete) Fe(III) reduction (Parker et al., 2018), and Lentini et al. (2012) have demonstrated that *Clostridium*-enriched cultures are capable of extensive reduction of goethite- and hematite-Fe(III).

Microbially Induced Hydrologic Alterations of Canga Columns

Based on dissolved Fe(II) in column effluents, approximately 40 mg of $Fe(OH)_3$ were removed from the columns due to microbiological Fe(III) reduction (**Table 1**). To determine if this export of mass impacted the hydraulic properties of the columns, we pumped bromide-amended SPW through the columns. Bromide breakthrough in the *sub muros*-inoculated columns preceded that of the uninoculated columns, and breakthrough was spread out in comparison to that of the uninoculated columns, which had a sharper curve (**Figure 5**). These observations indicate that flow through the uninoculated

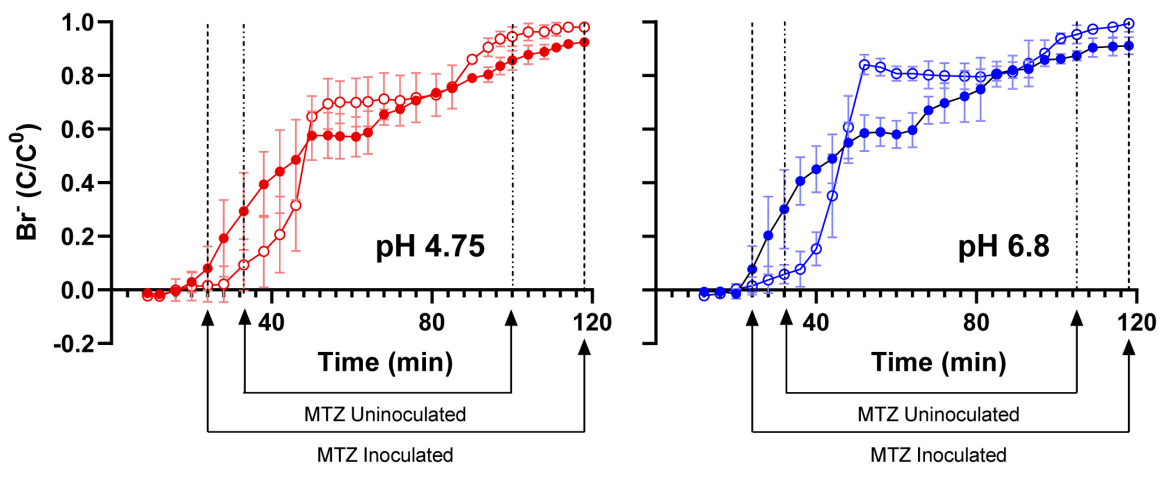

FIGURE 5 | Bromide breakthrough curves of *sub muros*-inoculated (closed shapes) and uninoculated (open shapes) columns after 63 days of operation. The columns that received the basal SPW pH 4.75 media are in red, with the SPW pH 6.8 in blue. Mass transfer zone (MTZ) lines represent initial breakthrough point where bromide-amended SPW is mixing with bromide-free SPW and adsorption exhaustion point where column is saturated with bromide-amended SPW. SPW was fed to columns at a rate of 0.2 mL/min. Error bars represent one standard deviation of triplicate columns.

columns did not experience the same mass transfer resistance seen in the columns in which microbiological Fe(III) reduction occurred (Lassabatere et al., 2004; Koestel et al., 2011; Safadoust et al., 2016). The porosity that allowed earlier bromide breakthrough is due to reductive dissolution of Fe(III) phases and export of dissolved Fe(II). In similar column experiments, Liang et al. (2019) found that bioreduction of sediment-associated Fe(III) led to the structural breakdown of particles in the columns and led to the earlier breakthrough of poorly-diffusible 2,6-difluorobenzoate. No change in more diffusible bromide breakthrough was observed after Fe(III) bioreduction (Liang et al., 2019). In the work presented here, Fe(III) bioreduction was more extensive, with maximal effluent Fe(II) concentrations of approximately 3 mM, in comparison to the maximal Fe(II) concentration of 0.3 mM observed by Liang et al. (2019). Taken together, the extensive Fe(III) bioreduction observed in these column experiments induced changes to the water flow paths in the packed canga.

Biogeochemical Implications

The results of our experiments indicate that the Fe(III) reducing activities of microorganisms associated with IFCs can induce reductive dissolution of Fe(III) phases, resulting in the transport of dissolved Fe(II) and hydrologic changes that are consistent with cave formation. While the Fe(III)-rich rocks of this region were generally considered to be resistant to weathering (Schuster et al., 2012; Monteiro et al., 2014), it is becoming increasingly clear that microbiological activities may induce extensive transformations to these rocks, especially canga (Parker et al., 2013, 2018; Levett et al., 2016, 2020; Gagen et al., 2018, 2019; Paz et al., 2020). Previous work has focused on the transformations of canga-Fe as a mechanism of canga permanence, whereby the weathering resistance of canga is owed to the alternating reductive dissolution of Fe(III) (hydr)oxides and abiotic or microbiological reoxidation of Fe(II) back to Fe(III) (Levett et al., 2016, 2020; Gagen et al., 2018, 2019, 2020; Paz et al., 2020). In this way, canga appears to be continuously weathering and reforming. The work here indicates that the Fe(III) rich phases could be more extensively weathered and removed from the systems, driven by the increased rates of Fe-reduction induced by water flow. Thus, Fe may be extensively mobilized from rocks in the SE and QF by microbiological weathering via microbial Fe(III) reduction (either through respiratory activity or as an electron sink) and separation, which can be enhanced by groundwater flow. These results should be applicable to other iron formation areas in Brazil and help explain why caves are larger in the iron deposits of Carajás, in the wetter Amazon Basin (Auler et al., 2019). A positive feedback mechanism, in which fast infiltration water would lead to increased porosity and thus even faster water percolation could operate, enhancing the mass transfer mechanisms required to mobilize Fe(II). Our observations indicate that microorganisms associated with these systems are capable of robust Fe(III) reducing activity, which could induce sufficient reductive dissolution of Fe(III) phases to form a cave. The numerous caves of the SE and QF (>3,000; Auler et al., 2019) indicate that the activity is extensive and continuously occurring. Indeed, we have observed remarkably high dissolved Fe concentrations in water circulating around caves in the QF (Parker et al., 2018). This extensive weathering of SE and QF Fe(III) phases may represent a previously underappreciated component of regional, and perhaps global Fe budgets.

DATA AVAILABILITY STATEMENT

The datasets presented in this study can be found in online repositories. The names of the repository/repositories and accession number(s) can be found in the article/supplementary material.

AUTHOR CONTRIBUTIONS

KC, MM, and TR carried out the lab work. JS, AA, CP, and HB carried out the fieldwork. All authors were involved in the design of the experiments and contributed to the manuscript.

FUNDING

This research was funded by the NSF grant #1645180 from NSF Geobiology and Low-temperature Geochemistry program to HB and JS.

REFERENCES

Auler, A. S., Parker, C. W., Barton, H. A., and Soares, G. A. (2019). "Iron formation caves: genesis and ecology," in *Encyclopedia of Caves*, eds W. B. White, D. C. Culver, and T. Pipan (London: Academic Press), 559–566.

Auler, A. S., Piló, L. B., Parker, C. W., Senko, J. M., Sasowsky, I. D., and Barton, H. A. (2014). "Hypogene cave patterns in iron ore caves: convergence of forms or processes," in *Hypogene Cave Morphologies*, eds K. Klimchou, I. D. Sasowsky, J. Mylroie, and A. S. Engel (Lewisburg, PA: Karst Waters Institute), 15–19.

Benner, S. G., Hansel, C. M., Wielinga, B. W., Barber, T. M., and Fendorf, S. (2002). Reductive dissolution and biomineralization of iron hydroxide under dynamic flow conditions. *Environ. Sci. Technol.* 36, 1705–1711. doi: 10.1021/es0156441

Beukes, N. J., Gutzmer, J., and Mukhopadhyay, J. (2003). The geology and genesis of high-grade hematite iron ore deposits. *Appl. Earth Sci.* 112, 18–25. doi: 10.1179/037174503225011243

Bolyen, E., Rideout, J. R., Dillon, M. R., Bokulich, N. A., Abnet, C. C., Al-Ghalith, G. A., et al. (2019). Reproducible, interactive, scalable and extensible microbiome data science using QIIME 2. *Nat. Biotech.* 37, 852–857. doi: 10.1038/s41587-019-0209-9

Bomberg, M., Claesson, L. L., Lamminmäki, T., and Kontula, A. (2019). Highly diverse aquatic microbial communities separated by permafrost in Greenland show distinct features according to environmental niches. *Front. Microbiol.* 10:1583. doi: 10.3389/fmicb.2019.01583

Costa, T., and Sá, G. (2018). "Soft iron ores: geotechnical characteristics," in *Guidelines for Open Pit Slope Design in Weak Rocks*, eds D. Martin, and P. Stacey (Clayton South, VIC: CSIRO Publishing), 273–285.

Cotta, M., and Forster, R. (2006). "The family *Lachnospiraceae*, including the genera *Butyrivibrio*, *Lachnospira* and *Roseburia*," in *The Prokaryotes*, Vol. 4, eds M. Dworkin, S. Falkow, E. Rosenberg, K. H. Schleifer, and E. Stackebrandt (New York, NY: Springer), 1002–1021.

Dobbin, P. S., Carter, J. P., San Juan, C. G.-S., von Hobe, M., Powell, A. K., and Richardson, D. J. (1999). Dissimilatory Fe(III) reduction by *Clostridium beijerinckii* isolated from freshwater sediment using Fe(III) maltol enrichment. *FEMS Microbiol. Lett.* 176, 131–138. doi: 10.1111/j.1574-6968.1999.tb13653.x

Dorr, J. V. N. (1964). Supergene iron ores of minas Gerais, Brazil. *Econ. Geol.* 59, 1203–1240. doi: 10.2113/gsecongeo.59.7.1203

Downs, R. T., and Hall-Wallace, M. (2003). The American Mineralogist crystal structure database. *Am. Mineral.* 88, 247–250.

Gagen, E. J., Levett, A., Paz, A., Bostlemann, H., da Silva Valadares, R. B., Bitencourt, J. A. P., et al. (2020). Accelerating microbial iron cycling promotes re-cementation of surface crusts in iron ore regions. *Microb. Biotechnol.* 13, 1960–1971. doi: 10.1111/1751-7915.13646

Gagen, E. J., Levett, A., Paz, A., Gustauer, M., Caldeira, C. F., da Silva Valadares, R. B., et al. (2019). Biogeochemical processe in canga ecosystems: armoring of iron ore against erosion and importance in iron duricrust restoration in Brazil. *Ore Geol. Rev.* 107, 573–586. doi: 10.1016/j.oregeorev.2019.03.013

Gagen, E. J., Levett, A., Shuster, J., Fortin, D., Vasconcelos, P. M., and Southam, G. (2018). Microbial diversity in actively forming iron oxides from weathered banded iron formation systems. *Microbes Environ.* 33, 385–393. doi: 10.1264/jsme2.ME18019

Gonzalez-Gil, G., Amonette, J. E., Romine, M. F., Gorby, Y. A., and Geesey, G. G. (2005). Bioreduction of natural specular hematite under flow conditions. *Geochem. Cosmochim. Acta* 69, 1145–1155. doi: 10.1016/j.gca.2004.08.014

Hansel, C. M., Benner, S. G., and Fendorf, S. (2005). Competing Fe(II)-induced mineralization pathways of ferrihydrite. *Environ. Sci. Technol.* 29, 7147–7153. doi: 10.1021/es050666z

Hansel, C. M., Benner, S. G., Neiss, J., Dohnalkova, A., Kukkadapu, R. K., and Fendrof, S. (2003). Secondary mineralization pathways induced by dissimilatory iron reduction of ferrihydrite under advective flow. *Geochem. Cosmochim. Acta* 67, 2977–2992. doi: 10.1016/S0016-7037(03)00276-X

Hansel, C. M., Lentini, C. J., Tang, Y., Johnston, D. T., Wankel, S. D., and Jardine, P. M. (2015). Dominance of sulfur-fueled iron oxide reduction in low-sulfate freshwater sediments. *ISME J.* 9, 2400–2412. doi: 10.1038/ismej.2015.50

Hershey, O. S., Kallmeyer, J., Wallace, A., Barton, M. D., and Barton, H. A. (2018). High microbial diversity despite extremely low biomass in a deep karst aquifer. *Front. Microbiol.* 9:2823. doi: 10.3389/fmicb.2018.02823

Igarashi, K., and Kato, S. (2021). Reductive transformation of Fe(III) (oxyhydr)oxides by mesophilic momoacetogens in the genus *Sporomusa*. *Front. Microbiol.* 12:600808. doi: 10.3389/fmicb.2021.600808

Johnson, D. B., Kanao, T., and Hedrich, S. (2012). Redox transformations of iron at extremely low pH: fundamental and applied aspects. *Front. Microbiol.* 3:96. doi: 10.3389/fmicb.2012.00096

Kato, S., Yumoto, I., and Kamagata, Y. (2015). Isolation of acetogenic bacteria that induce biocorrosion by utilizing metallic iron as the sole electron donor. *Appl. Environ. Microbiol.* 81, 67–73. doi: 10.1128/AEM.02767-14

Koestel, J. K., Moeys, J., and Jarvis, N. J. (2011). Meta-analysis of the effects of soil properties, site factors and experimental conditions on preferential solute transport. *Hydrol. Earth Syst. Sci. Discuss.* 8, 10007–10052. doi: 10.5194/hessd-8-10007-2011

Lassabatere, L., Winiarski, T., and Galvez-Cloutier, R. (2004). Retention of three heavy metals (Zn, Pb, and Cd) in a calcareous soil controlled by the modification of flow with geotextiles. *Environ. Sci. Technol.* 38, 4215–4221. doi: 10.1021/es035029s

Lehours, A.-C., Rabiet, M., Morel-Desrosiers, N., Morel, J.-P., Jouve, L., Arbeille, B., et al. (2010). Ferric iron reduction by fermentative strain BS2 isolated from an iron-rich anoxic environment (Lake Pavin, France). *Geomicrobiol. J.* 27, 714–722. doi: 10.1080/01490451003597663

Lentini, C. J., Wankel, S. D., and Hansel, C. M. (2012). Enriched iron(III)-reducing bacterial communities are shaped by carbon substrate and iron oxide mineralogy. *Front. Microbiol.* 3:404. doi: 10.3389/fmicb.2012.00404

Levett, A., Gagen, E., Shuster, J., Rintoul, L., Tobin, M., Vongsvivut, J., et al. (2016). Evidence of biogeochemical processes in iron duricrust formation. *J. S. Am. Earth Sci.* 71, 131–142. doi: 10.1016/j.jsames.2016.06.016

Levett, A., Vasconcelos, P. M., Gagen, E. J., Rintoul, L., Spier, C., Guagliardo, P., et al. (2020). Microbial weathering signatures in lateritic ferrginous duricrusts. *Earth Planet. Sci. Lett.* 538:116209. doi: 10.1016/j.epsl.2020.116209

Liang, X., Radosevich, M., Löffler, F., Schaeffer, S. M., and Zhuang, J. (2019). Impact of microbial iron oxide reduction on the transport of diffusible tracers and non-diffusible nanoparticles in soils. *Chemosphere* 220, 391–402. doi: 10.1016/j.chemosphere.2018.12.165

List, C., Hosseini, Z., Meibom, K. L., Hatzimanikatis, V., and Bernier-Latmani, R. (2019). Impact of iron reduction on the metabolism of *Clostridium acetobutylicum*. *Environ. Microbiol.* 21, 3548–3563. doi: 10.1111/1462-2920.14640

Lovley, D. R., and Phillips, E. J. P. (1987). Rapid assay for microbially reducible ferric iron in aquatic sediments. *Appl. Envir. Microbiol.* 53, 1536–1540. doi: 10.1128/aem.53.7.1536-1540.1987

Loyaux-Lawniczak, S., Vuilleumier, S., and Geoffroy, V. A. (2019). Efficient reduction of iron oxides by *Paenibacillus* spp. strains isolated from tropical soils. *Geomicrobiol. J.* 36, 423–432. doi: 10.1080/01490451.2019.1566415

Mesquita, D. C., Dantas, J. C. M., Paula, R. S., and Guerra, K. J. (2017). Estudo dos parâmetros hidrodinâmicos obtidos em ensaios de campo em itabiritos brandos da porção sudoeste do Quadrilátero Ferrífero, MG. *Geonomos* 25, 12–19.

Minyard, M. L., and Burgos, W. D. (2007). Hydrologic flow controls on biologic iron(III) reduction in natural sediments. *Environ. Sci. Technol.* 41, 1218–1224. doi: 10.1021/es0619657

Monteiro, H. S., Vasconcelos, P. M., Farley, K. A., Spier, C. A., and Mello, C. L. (2014). (U-Th)/He geochronology of goethite and the origin and evolution of cangas. *Geochim. Cosmochim. Acta* 131, 267–289. doi: 10.1016/j.gca.2014.01.036

Nixon, S. L., Telling, J. P., Wadham, J. L., and Cockell, C. S. (2017). Viable cold-tolerant iron-reducing microorganisms in geographically diverse subglacial environments. *Biogeosciences* 14, 1445–1455. doi: 10.5194/bg-14-1445-2017

Parker, C. W., Auler, A. S., Barton, M. D., Sasowsky, I. D., Senko, J. M., and Barton, H. A. (2018). Fe (III) reducing microorganisms from iron ore caves demonstrate fermentative Fe (III) reduction and promote cave formation. *Geomicrobiol. J.* 35, 311–322. doi: 10.1080/01490451.2017.1368741

Parker, C. W., Wolf, J. A., Auler, A. S., Barton, H. A., and Senko, J. M. (2013). Microbial reducibility of Fe (III) phases associated with the genesis of iron ore caves in the Iron Quadrangle, Minas Gerais, Brazil. *Minerals* 3, 395–411. doi: 10.3390/min3040395

Paz, A., Gagen, E. J., Levett, A., Zhao, Y., Kopittke, P. M., and Southam, G. (2020). Biogeochemical cycling of iron oxides in the rhizosphere of plants grown on ferruginous duricrust (canga). *Sci. Total Environ.* 713:136637. doi: 10.1016/j.scitotenv.2020.136637

Rainey, F. A. (2009). "Family V. *Lachnospiraceae* fam. nov," in *Bergey's Manual of Systematic Bacteriology*, Vol. 3, eds P. De Vos, G. M. Garrity, D. Jones, N. R. Krieg, W. Ludwig, F. A. Rainey, et al. (Dordrecht: Springer), 921–968.

Roden, E. E. (2004). Analysis of long-term bacterial vs. chemical Fe(III) oxide reduction kinetics. *Geochem. Cosmochim. Acta* 68, 3205–3216. doi: 10.1016/j.gca.2004.03.028

Roden, E. E. (2006). Geochemical and microbiological controls on dissimilatory iron reduction. *C. R. Geosci.* 338, 456–467. doi: 10.1016/j.crte.2006.04.009

Roden, E. E., and Urrutia, M. M. (1999). Ferrous iron removal promotes microbial reduction of crystalline iron(III) oxides. *Environ. Sci. Technol.* 33, 1847–1853. doi: 10.1021/es9809859

Roden, E. E., and Urrutia, M. M. (2002). Influence of biogenic Fe(II) on bacterial crystalline Fe(III) oxide reduction. *Geomicrobiol. J.* 19, 209–251. doi: 10.1080/01490450252864280

Roden, E. E., Urrutia, M. M., and Mann, C. J. (2000). Bacterial reductive dissolution of crystalline Fe(III) oxide in continuous-flow column reactors. *Appl. Environ. Microbiol.* 66, 1062–1065. doi: 10.1128/AEM.66.3.1062-1065.2000

Roden, E. E., and Zachara, J. M. (1996). Microbial reduction of crystalline iron(III) oxides: influence of oxide surface area and potential for cell growth. *Environ. Sci. Technol.* 30, 1618–1628. doi: 10.1021/es9506216

Rolim, V. K., Rosière, C. A., Santos, J. O. S., and McNaughton, N. J. (2016). The Orosirian-Statherian banded iron formation-bearing sequences of the southern border of the Espinhaço Range, Southeast Brazil. *J. S. Am. Earth Sci.* 65, 43–66. doi: 10.1016/j.jsames.2015.11.003

Rosière, C., Bekker, A., Rolim, V., and Santos, J. (2019). Post-Great Oxidation Event Orosirian–Statherian iron formations on the São Francisco craton: geotectonic implications. *I. Arc* 28:e12300. doi: 10.1111/iar.12300

Royer, R. A., Dempsey, B. A., Jeon, B.-H., and Burgos, W. D. (2004). Inhibition of biological reductive dissolution of hematite by ferrous iron. *Environ. Sci. Technol.* 38, 187–193. doi: 10.1021/es026466u

Safadoust, A., Khaboushan, E. A., Mahboubi, A. A., Gharabaghi, B., Mosaddeghi, M. H., Ahrens, B., et al. (2016). Comparison of three models describing bromide transport affected by different soil structure types. *Arch. Agron. Soil Sci.* 62, 674–687. doi: 10.1080/03650340.2015.1074184

Sass, H., Overmann, J., Rütters, H., Babenzien, H.-D., and Cypionka, H. (2004). *Desulfosporomusa polytropa* gen. nov., sp. nov., a novel sulfate-reducing bacterium from sediments of an oligotrophic lake. *Arch. Microbiol.* 182, 204–211. doi: 10.1007/s00203-004-0703-3

Sato, Y., Hamai, T., Hori, T., Aoyagi, T., Inaba, T., Kobayashi, M., et al. (2019). *Desulfosporosinus* spp. were the most predominant sulfate-reducing bacteria in pilot- and laboratory-scale passive bioreactors for acid mine drainage treatment. *Appl. Microbiol. Biotechnol.* 103, 7783–7793. doi: 10.1007/s00253-019-10063-2

Schuster, D. L., Farley, K. A., Vasconcelos, P. M., Balco, G., Monteiro, H. S., Waltenberg, K., et al. (2012). Cosmogenic ^{3}He in hematite and goetite from Brazilian canga duricrust demonstrates the extreme stability of these surfaces. *Earth Planet. Sci. Lett.* 329–330, 41–50. doi: 10.1016/j.epsl.2012.02.017

Senko, J. M., Zhang, G., McDonough, J. T., Bruns, M. A., and Burgos, W. D. (2009). Metal reduction at low pH by a *Desulfosporosinus* species: implications for the biological treatment of acidic mine drainage. *Geomicrobiol. J.* 26, 71–82. doi: 10.1080/01490450802660193

Shah, M., Lin, C.-C., Kukkadapu, R., Engelhard, M. H., Zhao, X., Wang, Y., et al. (2014). Syntrophic effects in a subsurface Clostridial consortium on Fe(III)-(oxyhydr)oxide reduction and secondary mineralization. *Geomicrobiol. J.* 31, 101–115. doi: 10.1080/01490451.213.806601

Silveira Braga, F. C., Rosière, C. A., Schneider Santos, J. O., Hagemann, S. G., Danyushevsky, L., and Valle Salles, P. (2021). Geochemical and tectonic constraints on the genesis of iron formation-hosted magnetite-hematite deposits at the Guanhães Block (Brazil) by contact metasomatism with pegmatite intrusions. *Ore Geol. Rev.* 129:103931. doi: 10.1016/j.oregeorev.2020.103931

Smith, A. J. B. (2015). The life and times of banded iron formations. *Geology* 43, 1111–1112. doi: 10.1130/focus122015.1

Souza, A., Figueiredo e Silva, R., Rosière, C., Dias, G., and Morais, F. (2015). Estudos geoquímicos de iabiritos da Serra do Sapo, espinhaço meridional, Minas Gerais. *Rev. Geonomos* 22, 1–17. doi: 10.18285/geonomos.v22i2.313

Spier, C. A., de Oliveira, S. M. B., Sial, A. N., and Rios, F. J. (2007). Geochemistry and genesis of the banded iron formations of the Cauê Formation, Quadrilátero Ferrífero, Minas Gerais, Brazil. *Precambrian Res.* 152, 170–206. doi: 10.1016/j.precamres.2006.10.003

Spier, C. A., Levett, A., and Rosière, C. A. (2018). Geochemistry of canga (ferricrete) and evolution of the weathering profile developed on itabirite and iron ore in the Quadrilátero Ferrífero, Minas Gerais, Brazil. *Miner. Depos.* 54, 983–1010. doi: 10.1007/s00126-018-0856-7

Stookey, L. L. (1970). Ferrozine—a new spectrophotometric reagent for iron. *Anal. Chem.* 42, 779–781.

Urrutia, M. M., Roden, E. E., and Zachara, J. M. (1999). Influence of aqueous and solid-phase Fe(II) complexants on microbial reduction of crystalline iron(III) oxides. *Environ. Sci. Technol.* 33, 4022–4028. doi: 10.1021/es990447b

Weber, K. A., Achenbach, L. A., and Coates, J. D. (2006). Microorganisms pumping iron: anaerobic microbial iron oxidation and reduction. *Nat. Rev. Microbiol.* 4, 752–764. doi: 10.1038/nrmicro1490

Wefer-Roehl, A., and Kübeck, C. (2014). *Guidelining Protocol for Soil-Column Experiments Assessing Fate and Transport of Trace Organics. 308339*. Available online at: http://demeau-fp7.eu/sites/files/D123a Guidelines Column experiments.pdf (accessed June 14, 2018).

Conflict of Interest: The authors declare that the research was conducted in the absence of any commercial or financial relationships that could be construed as a potential conflict of interest.

frontiers in Microbiology

ORIGINAL RESEARCH
published: 03 September 2021
doi: 10.3389/fmicb.2021.667944

Metagenomic Insights Into the Microbial Iron Cycle of Subseafloor Habitats

Arkadiy I. Garber[1], Ashley B. Cohen[2], Kenneth H. Nealson[3], Gustavo A. Ramírez[4,5], Roman A. Barco[3], Tristan C. Enzingmüller-Bleyl[6], Michelle M. Gehringer[6] and Nancy Merino[7]**

[1] School of Life Sciences, Arizona State University, Tempe, AZ, United States, [2] School of Marine and Atmospheric Sciences, Stony Brook University, Stony Brook, NY, United States, [3] Department of Earth Sciences, University of Southern California, Los Angeles, CA, United States, [4] Department of Marine Biology, Leon H. Charney School of Marine Sciences, University of Haifa, Haifa, Israel, [5] College of Veterinary Medicine, Western University of Health Sciences, Pomona, CA, United States, [6] Department of Microbiology, Technical University of Kaiserslautern, Kaiserslautern, Germany, [7] Biosciences & Biotechnology Division, Lawrence Livermore National Laboratory, Livermore, CA, United States

OPEN ACCESS

Edited by:
Sabine Kasten,
Alfred Wegener Institute Helmholtz Centre for Polar and Marine Research (AWI), Germany

Reviewed by:
Mark Alexander Lever,
ETH Zürich, Switzerland
Karrie A. Weber,
University of Nebraska–Lincoln, United States
Orit Sivan,
Ben-Gurion University of the Negev, Israel

***Correspondence:**
Arkadiy I. Garber
agarber4@asu.edu
Nancy Merino
merino4@llnl.gov

Specialty section:
This article was submitted to Microbiological Chemistry and Geomicrobiology, a section of the journal Frontiers in Microbiology

Received: 15 February 2021
Accepted: 30 July 2021
Published: 03 September 2021

Citation:
Garber AI, Cohen AB, Nealson KH, Ramírez GA, Barco RA, Enzingmüller-Bleyl TC, Gehringer MM and Merino N (2021) Metagenomic Insights Into the Microbial Iron Cycle of Subseafloor Habitats. Front. Microbiol. 12:667944. doi: 10.3389/fmicb.2021.667944

Microbial iron cycling influences the flux of major nutrients in the environment (e.g., through the adsorptive capacity of iron oxides) and includes biotically induced iron oxidation and reduction processes. The ecological extent of microbial iron cycling is not well understood, even with increased sequencing efforts, in part due to limitations in gene annotation pipelines and limitations in experimental studies linking phenotype to genotype. This is particularly true for the marine subseafloor, which remains undersampled, but represents the largest contiguous habitat on Earth. To address this limitation, we used FeGenie, a database and bioinformatics tool that identifies microbial iron cycling genes and enables the development of testable hypotheses on the biogeochemical cycling of iron. Herein, we survey the microbial iron cycle in diverse subseafloor habitats, including sediment-buried crustal aquifers, as well as surficial and deep sediments. We inferred the genetic potential for iron redox cycling in 32 of the 46 metagenomes included in our analysis, demonstrating the prevalence of these activities across underexplored subseafloor ecosystems. We show that while some processes (e.g., iron uptake and storage, siderophore transport potential, and iron gene regulation) are near-universal, others (e.g., iron reduction/oxidation, siderophore synthesis, and magnetosome formation) are dependent on local redox and nutrient status. Additionally, we detected niche-specific differences in strategies used for dissimilatory iron reduction, suggesting that geochemical constraints likely play an important role in dictating the dominant mechanisms for iron cycling. Overall, our survey advances the known distribution, magnitude, and potential ecological impact of microbe-mediated iron cycling and utilization in sub-benthic ecosystems.

Keywords: metagenomics, marine sediment, marine aquifer, FeGenie, iron cycling, iron acquisition, iron oxidation, iron reduction

INTRODUCTION

Iron is the dominant redox-active element in the Earth's crust and an important nutrient for almost all known life. In many environments, iron cycling is intimately linked to biogeochemical cycling of other elements, including carbon (e.g., CO_2, CH_4, and organic carbon), nitrogen (Laufer et al., 2016b; McAllister et al., 2020b), and heavy metals (Cooper et al., 2006). Thus, even though biologically available iron is comparatively rare/transient in many ecosystems, its speciation and flux considerably impacts the overall activities and productivity of diverse ecosystems. Research on the genetic basis for microbial iron cycling is in its infancy, and annotation pipelines annotate genes related to iron oxidation or reduction as "hypothetical" or simply "cytochrome c." Accordingly, the extent of information that can be gained from metagenomes or metagenome-assembled genomes (MAGs), derived from shotgun sequencing, in relation to the potential for microbial iron redox cycling in the environment remains poorly constrained. This is particularly true of the marine subsurface, an extremely remote and difficult to access/sample environment, that is nevertheless significantly influenced by microbe-mineral interactions, particularly those related to iron oxidation and reduction (Edwards et al., 2003a; Roden, 2012).

While there have been studies, largely in ecosystems where iron-oxidizing and –reducing bacteria are conspicuously present (Riedinger et al., 2014; Laufer et al., 2016a,b; Beam et al., 2018; Bryce et al., 2018; Aromokeye et al., 2020; McAllister et al., 2020b), the extent of microbial iron cycling in other environments, including marine sediment and sediment-buried crustal aquifers, remains comparatively underexplored. Even though microbes capable of iron redox can form only a small proportion of the community in the latter habitats (e.g., rare biosphere), their influence on iron-cycling has potential to significantly impact the surrounding geochemistry. We previously developed FeGenie (Garber et al., 2020), a database and bioinformatics tool, to aid in annotating the iron redox genes and other genes involved in many aspects of the microbial iron cycle, including iron transport, storage, and regulation; we are also continuously updating the library of iron genes to include more genes and processes, such as siderophore transport and biosynthesis (Neilands, 1995), and fermentative iron reduction (Jones et al., 1984), which will be included in the next release. Herein, we used FeGenie, with an updated set of hidden Markov models (HMMs) for iron redox cycling and iron transport (**Supplementary Table 1**), to systematically profile the microbial iron cycle in recently published metagenomes representing six marine sediment sites and two sediment-buried crustal aquifer sites (**Table 1**). These metagenomes, published over the last decade, have recently illuminated the microbial lifestyle under the often harsh conditions imposed by subsurface geochemical regimes. Some of the original analyses of these metagenomes provided evidence for microbial iron oxidation and reduction occurring in the subseafloor, but these conclusions were inferred by using a limited iron redox gene database (Meyer et al., 2016; Tully and Heidelberg, 2016; Tully et al., 2018; Smith et al., 2019). Using FeGenie, we re-analyzed these metagenomes with a focus on iron cycling, using a standardized approach that includes all known genetic markers for dissimilatory iron reduction and oxidation. We note that these metagenomes were generated using a variety of wet-lab and *in silico* methods, limiting the cross-comparisons that can be carried out. Nonetheless, we highlight the potential for microbial iron cycling in the marine subsurface and demonstrate FeGenie's capability to provide added valuable insights into iron cycling and acquisition/storage mechanisms in subseafloor habitats.

MATERIALS AND METHODS

Data Acquisition and Assembly

Metagenome assemblies representing North Pond fluids, which were made available by Tully et al. (2018), were downloaded from figshare (see original publication for figshare link). For the Guaymas Basin metagenome, in lieu of an assembly, we downloaded the 551 MAGs published by Dombrowski et al. (2018), and concatenated the contigs. Thus, due to the great amount of data available from these MAGs, no unbinned fraction from that dataset was evaluated. For all other metagenomic datasets, listed in **Table 1**, raw metagenome reads were obtained using the SRA Toolkit (release 2.10.0, SRA Toolkit Development Team). Reads were quality trimmed using Trimmomatic v0.36 (minimum length = 36 bp, sliding window = 4 bp, minimum quality score = 15, adaptors used = ILLUMINACLIP:TruSeq3-PE:2:30:10) (Bolger et al., 2014), and assembled using Spades v3.13.0 (default k-mers, Bankevich et al., 2012). Metagenome assemblies were then subjected to FeGenie analysis (Garber et al., 2020). For those metagenomes where metagenome-assembled genomes (MAGs) were publically available (Guaymas Basin, Loki's Castle, Eastern Gulf of Mexico, Juan de Fuca ridge aquifer fluids, Juan de Fuca ridge olivine biofilms, and North Pond aquifer fluids), those were downloaded and also analyzed with FeGenie.

FeGenie Analysis

We used FeGenie to identify iron genes in metagenome assemblies and MAGs. FeGenie was run with the –meta flag, directing the gene-calling software Prodigal, part of the FeGenie pipeline, to use its metagenomic procedure. Iron redox genes from the FeGenie output files were extracted using a custom python script (**Supplementary File 1**) and organized into pathways. To identify the closest sequenced relatives of identified iron genes, the protein sequences were extracted from FeGenie and queried (e-value cutoff: 1E-6) against the non-redundant protein database (release 240) from the National Center for Biotechnology Information (NCBI) using DIAMOND v2.0.4.142 (Buchfink et al., 2015). The closest phylogenetic relatives were then inferred from the top 50 DIAMOND matches and summarized in **Supplementary File 2.**

Siderophore biosynthesis clusters that were identified with FeGenie were confirmed using AntiSMASH v.5 (Blin et al., 2019). Contigs containing putative siderophore cluster genes were extracted using the grep command and subsequently subjected to AntiSMASH analysis (–cb-general, –cb-subclusters, –cb-knownclusters, –clusterhmmer, –asf, all other parameters were

TABLE 1 | Metadata for metagenome samples in which iron redox genes were detected with FeGenie.

Location	Longitude	Latitude	Depth below seafloor (bsf)	Depth below sealevel	NCBI BioProject ID	Metagenome references	Iron content	Iron references
Juan de Fuca U1362A (R/V Atlantis cruise ATL18-07)	47.761	−127.761	428–527 m (193–292 m below basement)	2,650 m	PRJNA269163	Jungbluth et al., 2017	0–1.1 μM aqueous Fe	Jungbluth et al., 2016
Juan de Fuca U1362B (R/V Atlantis cruise ATL18-07)	47.758	−127.762	264–352 m (29–117 m below basement)	2,650 m	PRJNA269163	Jungbluth et al., 2017	0–1.1 μM aqueous Fe	Jungbluth et al., 2016
Juan de Fuca 1301A (olivine biofilm)	47.754	−127.764	275–287 m	2,650 m	PRJNA264811	Smith et al., 2019	NA	NA
North Pond U1382A	22.750	−46.083	191.4–311.4 m (90–210 m below basement)	∼4,500 m	PRJNA391950	Tully et al., 2018	<1 μM Fe(II)	Bach, 2016; Meyer et al., 2016
North Pond U1383C	22.750	−46.083	123.6–285.6 m (70–232 m below basement)	∼4,500 m	PRJNA391950	Tully et al., 2018	<1 μM Fe(II)	Bach, 2016; Meyer et al., 2016
South Pacific Gyre (Expedition Knox-02RR)	−39.310	−139.801	0–5 cm	5,283 m	PRJNA297058	Tully and Heidelberg, 2016	5.6–7.3% Fe_2O_3	D'Hondt et al., 2011; Dunlea, 2016
Arctic mid-ocean ridge (Loki's Castle)	73.763	8.464	3-11 m	∼3,250 m	PRJNA504765	Dharamshi et al., 2020	0–220 μM Fe(II) in pore water	Jørgensen et al., 2012, 2013
Costa Rica (IODP Expedition 334: U1378)	8.592	−84.077	2–93 m	∼1,000 m	PRJEB11766	Martino et al., 2019; Farag et al., 2020	Non-iron bearing clays	Expedition. 344 Scientists, 2011
Guaymas Basin	27.006	−111.409	0–60 cm	∼2,000 m	PRJNA362212	Dombrowski et al., 2018	NA	NA
Adriatic Sea (MET2 sample)	45.062	13.652	30 cm	NA	PRJEB13497	Gacesa et al., 2018	NA	NA
The solent	50.714	−1.464	0–8 cm	23.9–31.7 m	PRJEB6766	Smith et al., 2015	NA	NA
Eastern Gulf of Mexico (Site E26)	26.590	87.510	0–20 cm	2,800 m	PRJNA485648	Dong et al., 2019; Li et al., 2020	NA	NA
Western Gulf of Mexico (Chapopote, Oily sediment in the vicinity of the asphalt volcano)	21.964	93.226	0–10 cm	2,925 m	PRJEB32776	Laso-Pérez et al., 2019; Li et al., 2020	NA	NA
Santa Monica Basin (Eastern Pacific Ocean)	33.789	118.668	0–12 cm	860 m	PRJNA431796	Scheller et al., 2016; Yu et al., 2018; Li et al., 2020	NA	NA
Håkon Mosby Mud Volcano	72.004	14.730	0–10 cm	1,250 m	PRJNA248084	Ruff et al., 2019; Li et al., 2020	NA	NA

NA, not available.

default). Results were then visually inspected for confirmation of potential for siderophore synthesis.

The R packages ggplot2 (Wickham et al., 2020), ggdendro (de Vries and Ripley, 2020), and Pvclust (Suzuki and Shimodaira, 2006), were used to generate plots presented in this article.

Site Descriptions

North Pond

The ∼8 Mya North Pond aquifer lies beneath a Mid-Atlantic ridge sediment basin and is composed of basaltic rocks, an important source of iron in this habitat, which are subject to chemical weathering by seawater due to advective fluid flow (Langseth et al., 1992; Meyer et al., 2016). Major solid weathering products include iron and manganese oxides, as well as carbonate minerals. Although classified as an oxic environment, the periodic presence of anaerobes and marker genes for low-O_2 metabolisms suggests the occurrence of anaerobic microenvironments and redox oscillations (Tully et al., 2018). The frequency of redox oscillations is likely related to the seawater residence time in fractures, as well as the redox-buffering capacity of the rocks, in which anaerobic zones may occur due to fluid stagnation and consumption of oxygen through reaction with reduced minerals (MacQuarrie and Mayer, 2005; Trinchero et al., 2019). In contrast, intersecting fractures may result in fluid mixing of deep and shallow seawater, leading to microbial hot spots supported by fluctuating O_2 concentrations that are ideal for iron-reducing and -oxidizing bacteria, something that has been previously observed in a terrestrial fractured rock aquifer (Bochet et al., 2020).

Juan de Fuca

The ∼3.5 Mya Juan de Fuca (JdF) ridge crustal aquifer is a basalt-hosted habitat located along a mid-ocean ridge flank with hydrothermal fluid circulation (Jungbluth et al., 2016). In comparison to North Pond, the geochemical signature of JdF fluids is more representative of extensive water-rock interactions due to longer fluid residence times and elevated fluid temperatures (Edwards et al., 2012). Seawater recharge occurs slowly due to the impermeability of the surrounding sediment and spreads laterally along fractures. Along the flowpath, fluid is heated and reduced, interacting with the basaltic rock, and is subsequently further altered by diffusive exchange with the overlying sediment pore water. The latter is most intense along the strong redox gradient at the sediment-rock boundary, where fluids are enriched in Fe, Mn, ammonium, Si, and Ca, and depleted in nitrate and oxygen (Wheat et al., 2013). Iron enrichment is particularly substantial and can be approximately 3000-fold higher in concentration relative to seawater and other JdF fluids in the flow path (Wheat et al., 2013).

Marine sediments

The metabolic potential for iron oxidation and reduction in marine sediments, hosting an estimated 0.18–3.6% of Earth's total living biomass (Kallmeyer et al., 2012), remains understudied. Potential for oxidized iron to serve as an important electron sink and contribute significantly to the breakdown of organic carbon in sediment was recognized as early as 1963 (Kamura et al., 1963; Takai et al., 1963a,b). More recently, it was determined that *Zetaproteobacteria* are rare within marine sediments (estimated global abundance of 0.11%) but can contribute $\sim 8 \times 10^{15}$ g of Fe in sedimentary iron oxides annually (Beam et al., 2018). Here, to survey the genetic capacity for iron cycling across diverse sedimentary regimes, we examine 27 marine sediment metagenomes (from 10 geographical sites, **Table 1**), including a low productivity oligotrophic site in the South Pacific Gyre, and high productivity sites like the Arctic Mid-Ocean Ridge (Dharamshi et al., 2020), Costa Rica Margin (Martino et al., 2019), and Guaymas Basin (Dombrowski et al., 2018).

RESULTS AND DISCUSSION

The Impact of Shifting Redox Conditions on Iron Cycling in the North Pond Aquifer

Recent work, including metagenomic, metatranscriptomic, and colonization/poised-electrode experiments, provide evidence for iron oxidation within the North Pond aquifer. Metagenomic (Tully et al., 2018) and metatranscriptomic (Seyler et al., 2020) studies revealed the presence of genes associated with iron oxidation, specifically, *cyc2* [encoding an outer membrane porin-cytochrome fusion; (Appia-Ayme et al., 1998; Castelle et al., 2008; Barco et al., 2015; He et al., 2017, Keffer et al., 2021)] and *foxE* (encoding a periplasmic cytochrome; Croal et al., 2007; Pereira et al., 2017). Tully et al. (2018) also reconstructed metagenome-assembled genomes (MAGs) affiliated with the iron-oxidizing Zetaproteobacteria, which are known to adapt to fluctuating O_2 concentrations and advective flow regimes (Chiu et al., 2017; Blackwell et al., 2020), further solidifying the presence and significant contribution that iron-oxidizing bacteria make to the aquifer community. Recent mineral colonization and current generation on poised electrodes also demonstrated the presence of iron oxidizing bacteria and provided evidence for their ability to utilize insoluble electron acceptors (Jones et al., 2020).

Our survey of 18 metagenome assemblies from the North Pond crustal aquifer (Tully et al., 2018) using the FeGenie library confirmed the presence of previously reported iron oxidases (**Figure 1**) (Tully et al., 2018; Seyler et al., 2020), which we phylogenetically linked to Zetaproteobacteria (*cyc2*) and Rhodospirillaceae (*foxE*) (**Supplementary File 2**). Linking *cyc2* to Zetaproteobacteria is important because this gene is highly diverse and is often encoded by taxa not known to be capable of iron oxidation; thus, only a handful of *cyc2* genes have been experimentally shown to be iron oxidases (Castelle et al., 2008; Jeans et al., 2008; Barco et al., 2015; McAllister et al., 2020a; Keffer et al., 2021). Further, we also documented the presence of genes associated with iron reduction [*mtrCAB* (Pitts et al., 2003; Hartshorne et al., 2007; Edwards et al., 2020) within seven of the timepoints, which span 2 years (**Figure 1**)]. The *mtrCAB* genes are most closely related to the dissimilatory iron reducer *Shewanella benthica* (**Supplementary File 2**), which was also enriched in mineral colonizations from the North Pond aquifer (Jones et al., 2020). We also identified nine MAGs (Tully et al., 2018), encoding copies of genes linked to respiratory iron oxidation or reduction (**Supplementary Table 2**). Notably, two MAGs that encode *cyc2* belong to the family Mariprofundaceae,

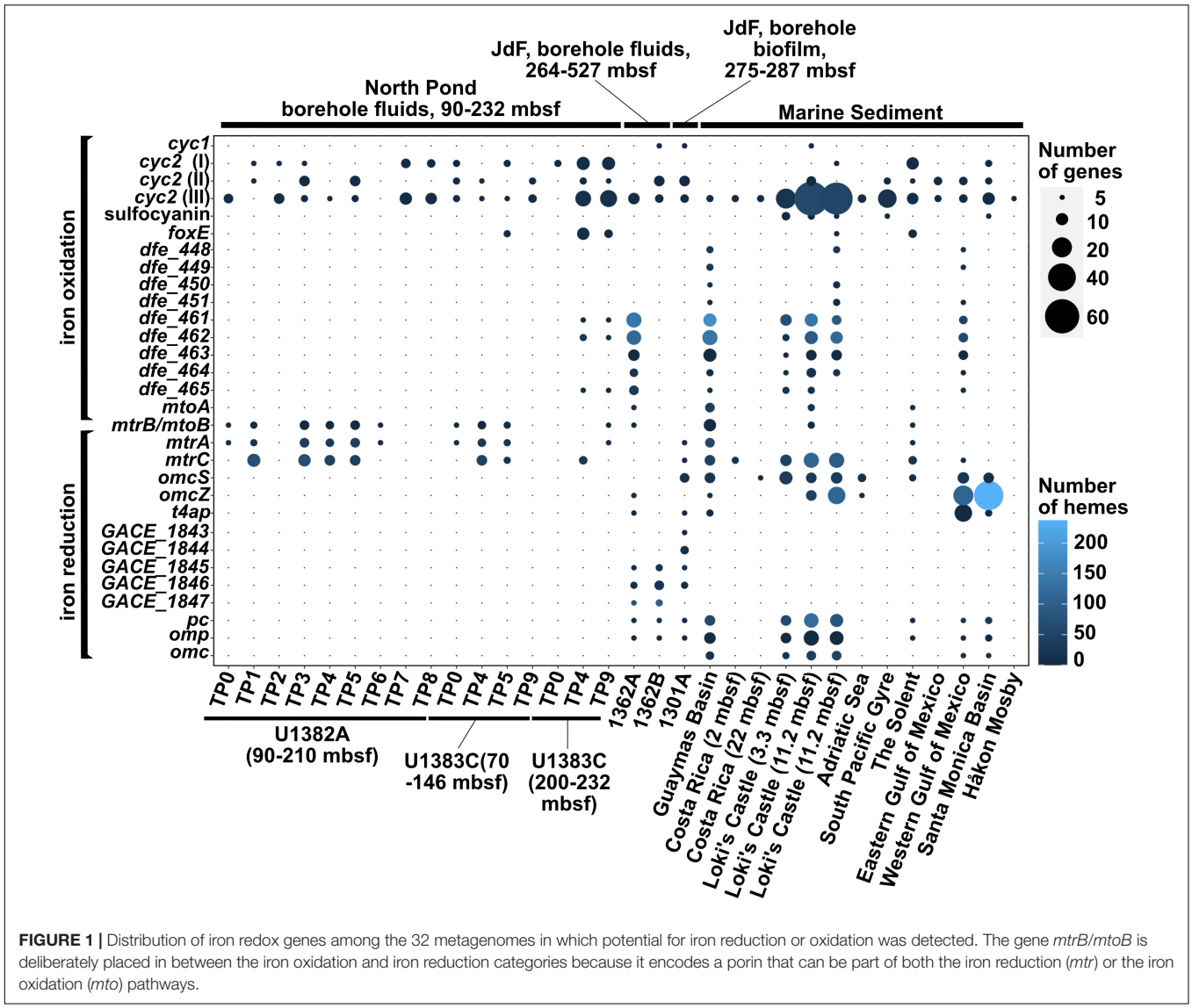

FIGURE 1 | Distribution of iron redox genes among the 32 metagenomes in which potential for iron reduction or oxidation was detected. The gene *mtrB*/*mtoB* is deliberately placed in between the iron oxidation and iron reduction categories because it encodes a porin that can be part of both the iron reduction (*mtr*) or the iron oxidation (*mto*) pathways.

known to encompass at least eight isolated strains of iron oxidizers (Emerson and Moyer, 2002; McBeth et al., 2011; Mumford et al., 2016; Barco et al., 2017; Chiu et al., 2017; McAllister et al., 2019). Another MAG, which belongs to the genus *Shewanella*, encodes two copies of the *mtrCAB* operon for iron reduction. Other putative iron oxidizers and reducers are shown in **Supplementary Table 2**. 16S rRNA gene amplicon sequencing presented by Jones et al. (2020), showed that *Geobacter*-related spp. were also enriched on minerals; however, we did not detect any *Geobacter*-related gene markers for iron reduction (*omcS*, *omcZ*, and type IV aromatic/electroactive pili [*t4ap*]), suggesting that this lineage may be part of the rare biosphere and undetectable with metagenomic approaches, at least in the aquifer fluids. Additionally, two metagenomes, derived from bottom water sampled near the North Pond aquifer, showed potential for iron oxidation via *cyc2*, *foxE*, and sulfocyanin, a blue-copper protein used as a genetic marker for iron oxidation in Archaea (Castelle et al., 2015). However, these sequences were not related to known iron-oxidizing bacteria (e.g., Mariprofundaceae), and no iron reduction genes were detected.

The co-occurrence of iron oxidizers and reducers in the North Pond aquifer supports potential for coupling of iron redox processes. Mutualistic interactions between iron oxidizers and reducers have been reported in various habitats (Weber et al., 2006; Blöthe and Roden, 2009; Emerson, 2009; Roden et al., 2012; Elliott et al., 2014; Byrne et al., 2015). While the coupling of iron reduction with oxidation may be less apparent in an iron-rich habitat like the Loihi Seamount (Emerson and Moyer, 2002), iron reducers and iron oxidizers may be more dependent on each other's metabolic by-products in the North Pond aquifer, where dissolved iron and carbon concentrations are much lower. As noted above, the presence of anaerobes within the North Pond aquifer hints at the possibility of sub-oxic microenvironments and varying redox conditions (Tully et al., 2018). This variability may be reflected in the observed fluctuation of iron oxidases and reductases over the 2-year sampling period (**Figure 1**).

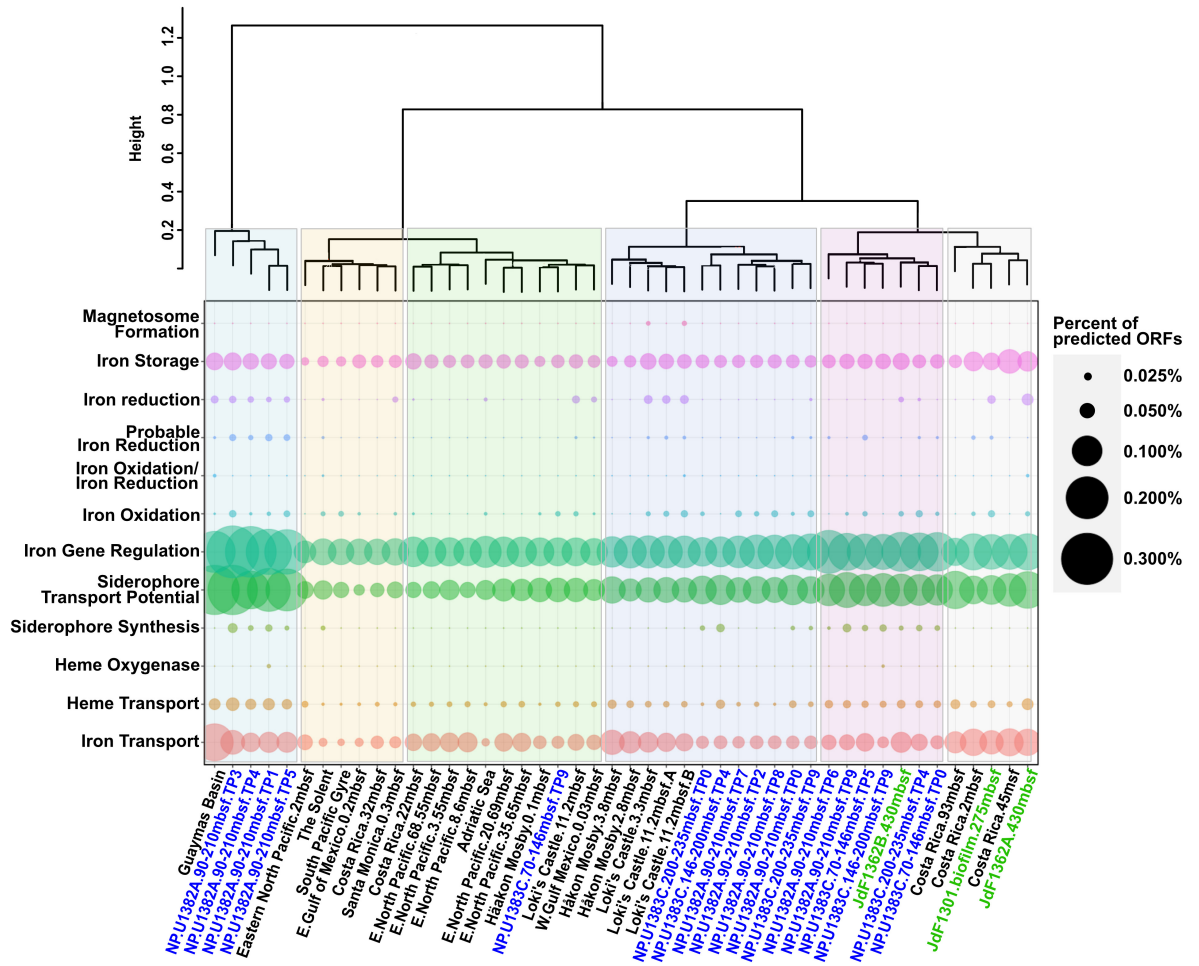

FIGURE 2 | Dotplot summary of iron genes in marine subcrustal aquifers and sediment identified by FeGenie, showing the variation among iron genes from different time points from North Pond. North Pond metagenomes are colored blue, while metagenomes from the Juan de Fuca ridge are colored green. Metagenomes derived from sediment samples are colored black. While certain pathways appear to be universal (iron acquisition and storage), other processes appear to vary in abundance (iron redox cycling and siderophore synthesis), while others still (magnetosome formation and heme oxygenases) appear to be quite rare. "Percent of predicted ORFs" was calculated by dividing the total number of genes identified from each iron gene category by the total number of predicted ORFs from each respective metagenome.

Consistent with this, hierarchical clustering of the metagenomes based on the overall iron gene composition (including iron acquisition and storage) demonstrated the dissimilarity between different North Pond timepoints (**Figure 2**), consistent with the observed temporal separation between iron reducers and oxidizers. Iron-oxidizers and reducers can take advantage of redox oscillations (Coby et al., 2011; Jewell et al., 2016), and in the North Pond aquifer, dominance of either iron reducers and oxidizers may be cyclical.

Different Iron Redox Strategies Between Planktonic and Biofilm Communities of the Juan de Fuca Ridge

Evidence for iron oxidation at the JdF first came in the form of a chemolithoautotrophic iron-oxidizing isolate (Edwards et al., 2003b), and then with the identification of biogenic iron oxides resembling those formed by iron-oxidizing bacteria, like *Mariprofundus* and *Leptothrix* (Kennedy et al., 2003; Toner et al., 2008). However, this evidence is from seafloor samples collected in the vicinity of the JdF aquifer. For example, the biogenic iron oxides were either (i) found in iron oxide mounds (Kennedy et al., 2003) or (ii) enriched from mineral incubations deployed at the seafloor (Toner et al., 2008). No sequence-based analysis has been performed on these iron oxide-rich samples, and the exact identity and mechanisms for iron-cycling in microbial communities associated with those iron oxides remains unknown. Three metagenomes representing the planktonic (2 samples) and crust-associated (1 sample) microbial communities from the sediment buried crustal aquifer at the JdF have since been published, allowing molecular interrogation of genetic potential for iron-related metabolisms. Two crustal aquifer planktonic metagenomes (Jungbluth et al., 2017) were collected at subseafloor observatories retrofitted with

Circulation Obviation Retrofit Kits [CORKs; Edwards et al. (2012)]; one biofilm metagenome is derived from an olivine chip biofilm incubated *in situ* for 4 years within a Flow-through Osmotic Colonization System [FLOCS; Orcutt et al. (2010)] (Smith et al., 2019).

FeGenie analysis revealed the genetic potential for iron oxidation, via *cyc2*, in all three JdF metagenomes, while *mtoAB*, a larger multi-protein porin-cytochrome complex (Jiao and Newman, 2007; Liu J. et al., 2012), was detected in only one of the crustal fluid metagenomes (**Figure 1**). The JdF crustal biofilm was previously reported to not support iron oxidation through the analysis of MAGs alone (Smith et al., 2019). Analysis of the whole metagenome assembly, including the unbinned fraction (contigs that were not included in the MAGs), identified at least eight *cyc2* gene copies. Seven of these *cyc2* copies were in the unbinned fraction of the assembly, and one was detected in JdFRolivine-5, a MAG (within the class Clostridia) constructed and published by Smith et al. (2019). Despite its significant homology, the *cyc2* copy in JdFRolivine-5 has unclear function, as it is considerably shorter than most other *cyc2* genes.

Smith et al. (2019) also reported that the MAG JdFRolivine-10 is related to the known iron reducer *Geoglobus* (Slobodkina et al., 2009; Mardanov et al., 2015) and encodes some of the cytochromes implicated in iron reduction in *Geoglobus acetivorans* (Mardanov et al., 2015). Three multiheme cytochromes encoded by JdFRolivine-10 match those in FeGenie's HMM library (**Supplementary Table 2**), which were previously linked to extracellular electron transfer: DFE_0449 (14-heme iron oxidase; Deng et al., 2018), GACE_1846 (4-heme iron reductase), and GACE_1847 (22-heme iron reductase) (Mardanov et al., 2015). The outer membrane cytochrome with locus tag GACE_1847 was predicted to encode an outer membrane anchor domain, as well as two hematite-binding sites (Mardanov et al., 2015). These cytochromes are all located on different contigs in JdFRolivine-10's genome and were identified using the new FeGenie flag –all_results, allowing us to bypass FeGenie's built-in operon-evaluating algorithm. FeGenie also confirmed the presence of a hematite-binding motif (a new feature in FeGenie's pipeline, see **Supplementary Methods** for details). The presence of heme-binding and transmembrane domains encoded on the GACE_1847 homolog provides a clue to one of the possible mechanisms for iron reduction within the JdF aquifer biofilm. Other genes related to iron reduction were also detected in the unbinned fraction of the metagenome from JdF olivine biofilms: *omcS* (Mehta et al., 2005; Qian, 2011; Wang et al., 2019), *mtrC* (Hartshorne et al., 2007), *mtrA* (Pitts et al., 2003), and *t4ap* (Bray et al., 2020), further supporting the potential for iron reduction within crustal biofilms. However, since olivine contains only reduced iron (Fe^{2+}), it likely has been oxidized first by iron-oxidizing bacteria, supporting a potential cryptic iron cycle on the surface of the olivine mineral (**Supplementary Figure 1**); and since JdF is an anoxic system, this implicates anaerobic iron oxidation, possibly nitrate-dependent.

In the crustal fluid metagenomes, we detected potential for iron reduction via *t4ap* (Bray et al., 2020), *omcZ* (Inoue et al., 2010), and the flavin-based extracellular electron transfer mechanism recently reported in *Listeria monocytogenes* (Light et al., 2018). Potential for iron oxidation was detected via the *dfeEFGHI* operon (Deng et al., 2018). Unlike the olivine biofilms, *omcS* was not detected in the fluid metagenomes. This gene is associated with *Geobacter* species (Qian, 2011; Wang et al., 2019), which prefer anaerobic environments and less likely to dominate fluids subject to redox gradients (Lin et al., 2004; Lovley et al., 2011; Engel et al., 2020). Indeed, four *omcS* copies detected in the biofilm were phylogenetically linked to *Geoalkalibacter subterraneus* and *Malonomonas rubra* (**Supplementary File 2** and **Supplementary Table 4**), both obligate anaerobes that taxonomically fall within the *Desulfuromonadales* order, which also contains *Geobacter* spp. Because the planktonic community in the anoxic crustal fluids is sourced from oxic bottom waters, we hypothesize that these iron reducers, rare in seawater, remain rare in the chemically evolved anoxic fluids. Eventually, these lineages may transition from planktonic to biofilm lifestyles where the activities of previous microbial communities (e.g., iron-oxidizing and sulfur-reducing bacteria) provide them with oxidized iron substrates (Toner et al., 2008; Ramírez et al., 2016). For example, as mentioned above, we did not detect any *Geobacter*-related gene markers from the North Pond aquifer metagenomes; however, recent mineral incubations enriched an electroactive consortia that includes *Geobacter* (Jones et al., 2020), supporting the latent presence of this lineage in redox-fluctuating fluids.

A Survey of Iron Redox Potential in Globally Dispered Marine Sediment

Potential for benthic iron reduction is prevalent among the locations under relatively high water-column productivity (e.g., Loki's Castle, Guaymas Basin, and Western Gulf of Mexico), but is absent in the oligotrophic South Pacific Gyre (SPG) (**Figure 1**). The lack of iron reduction in SPG is consistent with previous analysis of these sediments (Tully and Heidelberg, 2016). High water column productivity results in benthic conditions ideal for iron reduction (low oxygen and high organic carbon deposition rates). The South Pacific Gyre sediments are far from this ideal, as they are low in carbon and oxic throughout the entire sediment column (D'Hondt et al., 2009). Two of the four cold-seep sediment metagenomes (Håkon Mosby Mud Volcano and Eastern Gulf of Mexico) also lacked any detectable genes for iron reduction. The surveyed metagenome sample from the Håkon Mosby Mud Volcano represents the top cm of young, freshly-erupted mud with ongoing aerobic activities, and, thus, is also not primed for iron reduction (Ruff et al., 2019). It is unclear why we did not detect genes for iron reduction in the Eastern Gulf of Mexico sediment (Dong et al., 2019); this site represent a petroleum seep where benthic communities may be dominated by hydrocarbon-degrading microbes that are not capable of iron reduction. It is important to note that technical (e.g., number of contigs, contig lengths, etc.) and environmental (community richness) differences can significantly influence inferences from broad metagenomic surveys; often, several factors (e.g., quality and concentration of DNA, strain-level diversity, prevalence of repetitive DNA sequences) can play a major role in determining the quality of the metagenome assemblies, as evidenced from the

substantial variation in the distribution of contig lengths obtained from different metagenome assemblies (**Supplementary File 3**). This can affect the capacity of annotation pipelines, like FeGenie or AntiSMASH, to detect certain pathways.

Higher productivity sites demonstrated a diverse array of genes for iron reduction, including *omcS*, *omcZ*, and *mtrCAB*, etc. *Geobacter*-related iron reductases [e.g., *omcS*, *omcZ*, and other porin-cytochrome complexes (Shi et al., 2014)] were more common in the marine sediment sites compared with the surveyed aquifer metagenomes, with only the Guaymas Basin encoding the *mtrCAB* operon. Numerous copies of the aromatically dense type IV pili (Bray et al., 2020) gene were detected. These are particularly prevalent in marine sediment from the Western Gulf of Mexico (Laso-Pérez et al., 2019).

Potential for iron oxidation was detected in nearly all surveyed marine sediment sites (**Figure 1**). Specifically, *cyc2* [more specifically, *cyc2*-cluster 3 (McAllister et al., 2020a)] appears to be the most common gene putatively linked to iron oxidation. In the North Pond aquifer, many *cyc2* homologs were found to be closely related to those encoded by the iron-oxidizing *Mariprofundus*. However, in marine sediments, *cyc2* homologs appear to have a different phylogenetic distribution, with associated taxa that have not previously been linked to iron oxidation (e.g., Acidobacteria, Desulfobacterales, *Ralstonia solanacearum*, etc.). In these taxa with no experimental evidence for iron oxidation, the function of *cyc2* is less clear. While *cyc2* appears to be most widely distributed porin-cytochrome putative iron oxidase, *mtoAB* is also present in three sediment sites: Guaymas Basin, Loki's Castle, and The Solent. Other genetic markers for iron oxidation were also detected: sulfocyanin was detected in three of the marine sediment sites (Loki's Castle, South Pacific Gyre, and Santa Monica Basin); the periplasmic cytochrome-encoding *foxE* was found in two sites (Loki's Castle and The Solent). The Solent, which represents the only sediment metagenome from the photic zone, was found to have a variety of different markers for iron oxidation and reduction. Thus, unlike other sites that are well below the photic zone (**Table 1**), where iron oxidation has potential to fuel chemolithoautotrophy, in The Solent, iron oxidation may fuel photoferrotrophy. While the oxic South Pacific Gyre sediment may support aerobic iron oxidation, the other surficial sediment sites, with higher productivity and lower oxygen content, may support continuous iron oxidation at the surface or during periods of oxygenation [e.g., via bioturbation (Beam et al., 2018)].

Magnetosome Formation at Loki's Castle, but Absent From Other Sediment and Aquifer Metagenomes

Magnetosomes are organelles of magnetotactic bacteria that contain biomineralized magnetite (Frankel et al., 1979; Uebe and Schüler, 2016). This allows bacteria to sense the Earth's magnetic field, facilitating orientation along geochemical gradients. We detected nine separate loci encoding genes for magnetosome formation at Loki's Castle sediment (**Figure 2**). The genetic loci for magnetosome formation identified at Loki's Castle presented a mixed phylogenetic distribution, with amino acid identities near 50%, likely indicating a lack of closely related sequenced organisms. However, some of the most closely related sequences in NCBI's non-redundant protein database appear to be from the Magnetococcales order, which includes *Magnetococcus marinus*, a marine magnetotactic bacterium isolated from the oxic-anoxic sediment-boundary off the coast of Rhode Island (Bazylinski et al., 2013). Magnetosomes are conceivably advantageous in environments with geochemical gradients, and are considered to be ubiquitous in aquatic habitats (Lefèvre and Bazylinski, 2013). Thus, the apparent lack of magnetosome formation operons in most marine sediment and all aquifer metagenomes is somewhat surprising. It is possible that magenetosome formation is heavily dependent on the availability and speciation of iron, which varies as a function of the spatial distribution of the redox cascade. Alternatively, the dearth of magnetosome formation operons (*mam*) can be a result of FeGenie's strict rules for its detection (requiring the presence of at least 5 of the 10 diagnostic genes); while the assembly qualities for most of the metagenomes used in our survey are high (**Supplementary File 3**), detection of magnetosome formation operons requires contigs greater than 5,000 bases in length, and these make up a relatively small proportion (∼0.1–20%) of contigs in each assembly. In support of the latter hypothesis, we identified a MAG with genetic potential for iron oxidation (via *foxE*) – this MAG, with a ∼75% complete genome, is closely related to the *mam*-encoding *Magnetovibrio blakemorei*, but only has 2/10 of the *mam* genes, which are found on two different contigs; this is below FeGenie's detection threshold.

Iron Acquisition and Storage Is Common, but Siderophore Synthesis Is Limited to Subsurface Aquifers and One Sediment Site

In addition to genes for iron redox cycling and magnetosome formation, we also report the distribution of genes for iron acquisition and storage, which are not directly linked to respiration, but are essential functions for the majority of living organisms (**Figure 2**). As expected, metagenomes examined in this study have the genes necessary for ferrous and ferric iron transport [*efeUOB, fbpAB(C), feoAB(C)*, *futABC*], iron storage within ferritin (PF00210), as well as iron gene regulation (*dtxR, fecR, feoC*, and *fur*) (**Supplementary Table 3**). Potential for transport of iron-chelating molecules like siderophores (Butler, 2005) and heme via the TonB-ExbB-ExbD system was also detected (Krewulak and Vogel, 2011). We note that TonB-dependent transport is not specific to iron-chelating compounds (Noinaj et al., 2010). Even though heme can also be transported by this pathway (Noinaj et al., 2010; Krewulak and Vogel, 2011), the marine sediment metagenomes were largely devoid of heme oxygenase and storage homologs, except for one copy of *pigA* (heme oxygenase; Friedman et al., 2003, 2004) and a few copies of *hutZ* (heme storage; Liu X. et al., 2012) in the North Pond metagenomes.

The North Pond metagenomes harbored several siderophore synthesis gene clusters that share similarity to the known clusters encoding desferrioxamine E, crochelin A, amonabactin

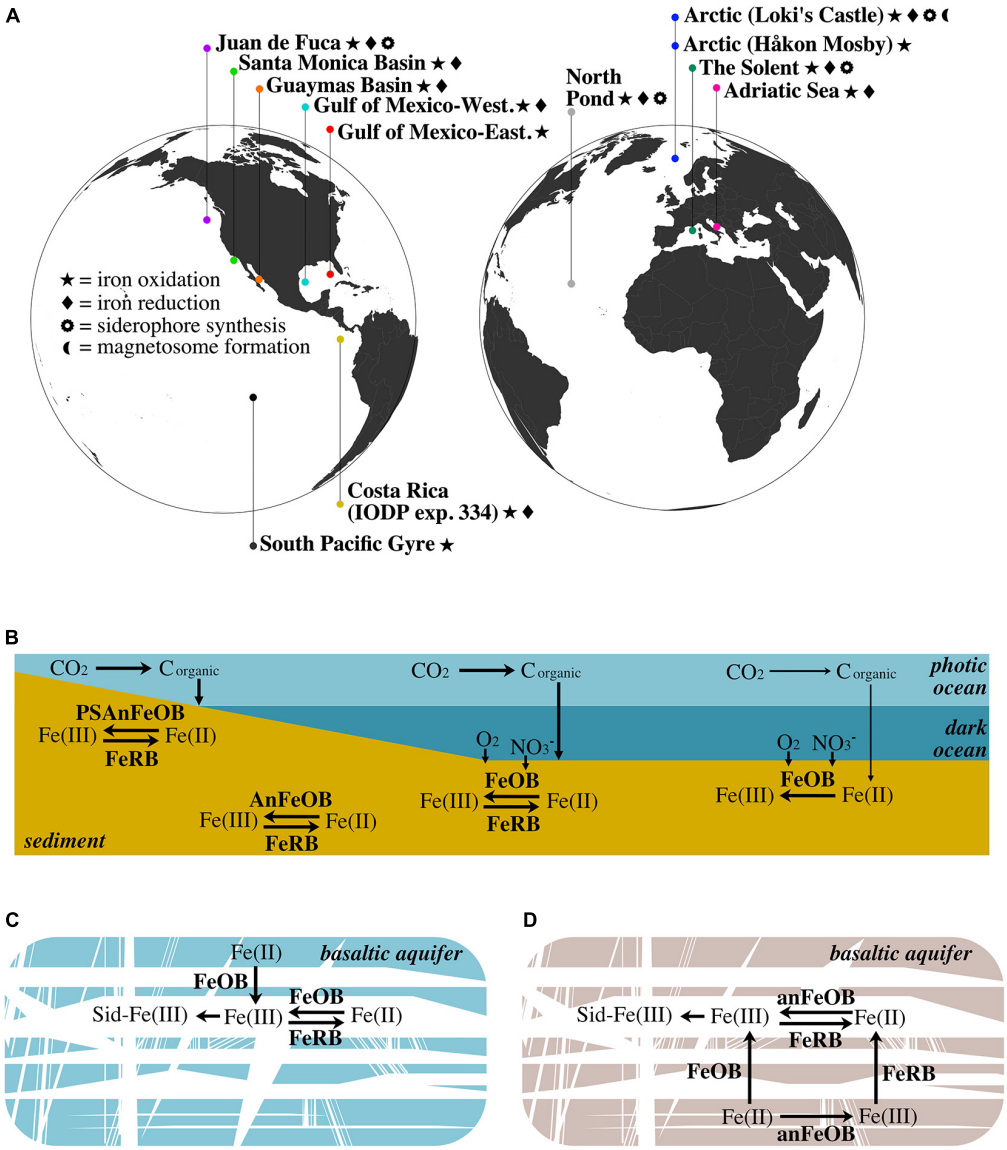

FIGURE 3 | (A) Geographic distribution of marine aquifer and sediment sites from which metagenome samples are derived. **(B)** Schematic of the iron redox cycle in various types of marine sediment. In shallow sediment within the photic zone (e.g., The Solent), photoferrotrophy can drive iron oxidation. Below the photic zone, aerobic iron oxidation in surficial sediment (e.g., Guaymas Basin, Santa Monica Basin, and Western Gulf of Mexico) is contrasted with anaerobic iron oxidation (e.g., nitrate-dependent) in deep anoxic sediment (e.g., Costa Rica and Loki's Castle). In these aforementioned sediments, iron reduction is present and represents the other half of the iron cycle. Conversely, in oxic sediments, such as those underlying areas of low productivity (e.g., South Pacific Gyre), aerobic iron oxidation is the dominant process, with no detectable iron reduction. The lower productivity is denoted by thinner arrows that signify carbon fixation and sedimentation. **(C)** Iron cycling within the cold and oxic North Pond aquifer: iron is released from the young, largely ferrous (Bach and Edwards, 2003), basaltic crust via iron oxidation, where it is free to cycle between the ferric and ferrous forms, and subject to the chelating activity of siderophores. **(D)** Iron cycling within the warm, anoxic JdF aquifer: since the waters circulating in this aquifer are anoxic, iron oxidation is likely dependent on anaerobic metabolisms. Similar to North Pond, JdF basaltic crust is young and the iron content is largely ferrous (Bach and Edwards, 2003); thus, iron is first released via oxidation. Detection of iron reduction on the surface of an olivine chip suggests that iron oxides may be deposited on the olivine mineral after oxidation by iron-oxidizing microbes. FeOB, aerobic iron-oxidizing bacteria; AnFeOB, anaerobic iron-oxidizing bacteria; PSAnFeOB, photosynthetic anaerobic iron-oxidizing bacteria; FeRB, iron-reducing bacteria; Sid, siderophores.

P, vicibactin, and vibrioferrin (**Supplementary Table 5**). The percent of genes in these identified clusters with significant BLAST hits to genes within known siderophore clusters ranged from 33–80%, as determined by AntiSMASH (Blin et al., 2019). Putative siderophore synthesis was also confirmed in several North Pond MAGs (**Supplementary Table 2**). MAGs taxonomically identified as *Pseudomonas tetraodonis*, *Halomonas alkaliantarctica*, and *Paracoccus* sp. may produce siderophores related to desferrioxamine E (75% gene similarity), crochelin A (46%), and amonabactin P (42%), respectively. Other North Pond MAGs encode siderophore gene clusters similar to aerobactin (33%; *Moritella* sp000170855), bisucaberin

B (100%; Flavobacteriaceae sp.), and unknown siderophores. The presence of siderophore synthesis clusters in the North Pond metagenomes and MAGs with low similarity to known siderophore biosynthesis genes suggests potential for synthesizing structurally related or novel siderophores. Siderophore clusters are genetically diverse and modular systems that are impacted by several evolutionary processes, including gene loss and gene acquisition (e.g., through horizontal gene transfer) (Cruz-Morales et al., 2017; Thode et al., 2018). This leads to variation in siderophore structures (e.g., Seyedsayamdost et al., 2012), which is likely required to prevent uptake by non-siderophore-producing microorganisms, in what is known as siderophore piracy (Hibbing et al., 2010; Butaitë et al., 2017).

We also detected a siderophore synthesis locus in one of the JdF aquifer fluid metagenomes (**Supplementary Table 5**). Using AntiSMASH, this cluster was confirmed to be related to the acinetoferrin biosynthesis cluster.

Out of the 24 surveyed metagenomes from marine sediment, only one, The Solent, appears to encode a siderophore biosynthesis cluster, confirmed using AntiSMASH, to be most closely related to xanthoferrin. The overall lack of siderophore production in marine sediments may be due to the greater bioavailability of iron in those habitatis, or the potential presence of siderophores derived from the water column. The metagenomes may also harbor siderophore synthesis loci that share no or undetectable similarity to known siderophore synthesis clusters/models. Siderophores are necessary to obtain insoluble Fe(III) from the environment, and ferrisiderophore complexes become an important source of iron when soluble Fe(II) is limited. At Loki's Castle and Guaymas Basin sediments, pore water Fe(II) concentrations can reach ∼200 μM (**Table 1**), which may obviate the need to synthesize siderophores. In the South Pacific Gyre sediment, with extremely low productivity and metabolic activities, the synthesis of siderophores may be too energetically costly. In contrast, siderophore synthesis in North Pond and JdF fluids concur with the minimal amounts of bioavailable iron present (**Table 1**), although JdF fluids have been shown to have highly variable iron concentrations between boreholes (Wheat et al., 2013). Within North Pond, oxic conditions (∼213–216 μM O_2) result in the biotic and abiotic removal of soluble iron, leading to extremely low iron concentrations. This is consistent with the relatively high numbers of different siderophore synthesis loci identified there. The apparent lack of siderophore production in iron-limited sediment, like Costa Rica sediments, mainly composed of non-iron bearing clays (Vannucchi et al., 2013), and South Pacific Gyre sediments, which are oxygenated and contain only 5.6–7.3% Fe_2O_3 (D'Hondt et al., 2011; Dunlea, 2016) suggests dependence on exogenous siderophores, or other iron-chelating molecules (D'Onofrio et al., 2010). For example, in higher-productivity areas, sedimentation of biomass may deliver sufficient amounts of iron and iron-bearing molecules to benthic communities (Boyd and Ellwood, 2010; Gledhill and Buck, 2012; Boiteau et al., 2016). Additionally, release of reduced iron from sediment, which can also be catalyzed by iron-reducing bacteria, can potentially contribute to the iron budget of resident microbes. Alternatively, as mentioned above with regard to the apparent lack of magnetosome formation operons, the lack of siderophore biosynthesis operons may also be due to the fact that, similar to the magnetosome formation operon, siderophore biosynthesis operons are often >10,000 bases in length and involve multiple genes; thus, reliable detection of siderophore biosynthesis requires contigs that are relatively rare in metagenome assemblies.

CONCLUDING REMARKS

Our reanalysis of globally distributed marine subsurface metagenomes using FeGenie's comprehensive iron gene library illuminates the diversity of microbial iron redox mechanisms that can occur across a range of geochemical regimes (**Figure 3A**). Further, we demonstrate FeGenie's utility in providing a standardized pipeline for the comparison of iron genes among many large genomic datasets. We note that the data used in our survey were generated from multiple studies; inherent differences in sampling collection and processing, sequencing, and *in silico* methods, thus, make it difficult to generate overarching conclusions. Despite these potential limitations, our results support a hypothesis that geochemical constraints may influence the distribution of iron redox genes, potentially playing an important role in determining the dominant strategy for iron cycling (**Figures 3B–D**). At high-productivity sites (e.g., Guaymas Basin, Santa Monica Basin, Western Gulf of Mexico, Costa Rica), iron cycling is likely based on the penetration of oxygen and/or nitrate into surficial sediment, or deeper due to bioturbation, enabling microbial iron oxidation processes until these electron acceptors are diminished and iron reduction dominates. In oxic sediment, such as that underlying areas of low productivity (e.g., South Pacific Gyre), iron cycling is likely dominated by iron oxidation – with no or limited biological iron reduction. In cold and oxic subseafloor aquifers like North Pond, the flux of oxygen and organic carbon are possibly key factors influencing the abundances of iron-oxidizers and iron-reducers (**Figure 3C**), while in the warm and anoxic waters circulating within the JdF aquifer, iron cycling is dependent on anaerobic metabolisms (e.g., iron reduction and nitrate-dependent iron oxidation) (**Figure 3D**).

In nearly every site where iron redox cycling was detected, porin-cytochrome combinations were present and may constitute an important vector for dissimilatory electron transfer to and from soluble and insoluble iron (although porin-cytochrome genes are also the most common genetic markers currently available). For example, the porin-cytochrome fusion encoded by *cyc2* appears nearly ubiquitous in our surveyed data; *cyc2*, whose phylogenetic distribution implies rampant lateral transfer among prokaryotes (McAllister et al., 2020a), may thus represent a widespread mechanism for respiratory iron oxidation. Alternatively, it is possible that Cyc2 acts as an iron detoxification mechanism (Bradley et al., 2020). In addition to porin-cytochromes, other mechanisms for iron redox were detected in diverse habitats. For example, the *Geobacter*-type *omcS*, *omcZ*, and electroactive pili genes demonstrate another strategy that may be largely relegated to sediment and biofilm

niches. Although, detection of *omcZ* and *t4ap* genes in one of the JdF aquifer plankton metagenomes supports the possibility that this strategy may be utilized in planktonic niches, at least those where anoxic conditions prevail.

Geochemical constraints also seem to impact other aspects of the microbial iron cycle. Unlike the near-ubiquitous occurrence of genes associated with iron transport, iron storage, iron gene regulation, heme transport, and siderophore transport amongst the surveyed metagenomes, siderophore biosynthesis gene clusters were restricted to subseafloor aquifers, with only one sediment site encoding a siderophore biosynthesis cluster. Similarly, magnetosome formation genes were detected in only one of the sediment metagenomes (and none in the subsurface aquifers). It is possible that these biosynthesis operons are in short supply due to geochemical factors influencing the supply of iron or energy needed to synthesize them. However, we also cannot rule out the possibility that siderophore biosynthesis and magnetosome formation are more prevalent but undetected, either due to high level of sequence divergence from pre-existing HMMs used by FeGenie, or due to low abundances in the sequenced samples. For example, FeGenie retains the ability to detect potentially novel types of siderophore biosynthesis clusters, but detection of magnetosome formation depends on gene markers from a single known operon. In summary, our survey provides a comprehensive overview using the currently available genetic markers, generating testable hypotheses and providing insights into the distribution of iron genes in subsurface biomes across the world.

DATA AVAILABILITY STATEMENT

The original contributions generated for this study are included in the article/**Supplementary Material**, further inquiries can be directed to the corresponding authors.

ETHICS STATEMENT

Ethical review and approval was not required for the study on human participants in accordance with the local legislation and institutional requirements. Written informed consent for participation was not required for this study in accordance with the national legislation and the institutional requirements.

AUTHOR CONTRIBUTIONS

AG and NM conceived the study. AG and NM carried out the bioinformatics analysis. AG, NM, AC, GR, RB, TE-B, MG, and KN interpreted the results and wrote the manuscript. All authors contributed to the article and approved the submitted version.

FUNDING

MG and TE-B were funded by the German Research Foundation under the SPP1833 programme. Lawrence Livermore National Laboratory is operated by Lawrence Livermore National Security, LLS, for the United States Department of Energy, National Nuclear Security Administration under Contract DE-AC52-07NA27344 (IM #: LLNL-JRNL-819591).

ACKNOWLEDGMENTS

We sincerely thank Clara Chan for insights and comments on this manuscript. Thanks to Sean McAllister and Siavash Atashgahi for insightful discussions and input regarding iron cycling. Thanks to Martin Van-Den-Berghe for providing insights regarding siderophore utilization in the deep biosphere. We are grateful to Mike Russell for feedback on this manuscript. Finally, we thank Michał Sitko for making a FeGenie Dockerfile and Natasha Pavlovikj for creating a Conda recipe for FeGenie.

SUPPLEMENTARY MATERIAL

The Supplementary Material for this article can be found online at: https://www.frontiersin.org/articles/10.3389/fmicb.2021.667944/full#supplementary-material

Supplementary Figure 1 | Cryptic iron cycling on the surface of an olivine mineral incubated within the Juan de Fuca aquifer (borehole 1301A). The green trapezoid represents the olivine mineral with the chemical formula $(Mg^{2+}, Fe^{2+})_2SiO_4$. Oxidation of reduced iron within the olivine mineral by iron-oxidizing bacteria (FeOB) results in the formation of iron(III) oxyhydroxides, and chemical formula $Fe(OH)_3$, a by-product of microbial iron oxidation. The iron oxyhydroxides can then be used as terminal electron acceptors by iron-reducing bacteria (FeRB), releasing reduced iron from the mineral. Cyc2 and GACE_1847 are shown as putative iron oxidases and iron reductases, respectively, in this schematic.

REFERENCES

Appia-Ayme, C., Bengrine, A., Cavazza, C., Giudici-Orticoni, M.-T., Bruschi, M., Chippaux, M., et al. (1998). Characterization and expression of the co-transcribed cyc1 and cyc2 genes encoding the cytochrome cR (cSSP) and a high-molecular-mass cytochrome c from *Thiobacillus ferrooxidans* ATCC 33020. *FEMS Microbiol. Lett.* 167, 171–177.

Aromokeye, D. A., Kulkarni, A. C., Elvert, M., Wegener, G., Henkel, S., Coffinet, S., et al. (2020). Rates and microbial players of iron-driven anaerobic oxidation of methane in methanic marine sediments. *Front. Microbiol.* 10:3041. doi: 10.3389/fmicb.2019.03041

Bach, W. (2016). Some compositional and kinetic controls on the bioenergetic landscapes in oceanic basement. *Front. Microbiol.* 7:107. doi: 10.3389/fmicb.2016.00107

Bach, W., and Edwards, K. J. (2003). Iron and sulfide oxidation within the basaltic ocean crust: implications for chemolithoautotrophic microbial biomass production. *Geochim. Cosmochim. Acta* 67, 3871–3887. doi: 10.1016/s0016-7037(03)00304-1

Bankevich, A., Nurk, S., Antipov, D., Gurevich, A. A., Dvorkin, M., Kulikov, A. S., et al. (2012). SPAdes: a new genome assembly algorithm and its applications to single-cell sequencing. *J. Comput. Biol.* 19, 455–477. doi: 10.1089/cmb.2012.0021

Barco, R. A., Emerson, D., Sylvan, J. B., Orcutt, B. N., Meyers, M. E. J., Ramírez, G. A., et al. (2015). New insight into microbial iron oxidation as revealed by the proteomic profile of an obligate iron-oxidizing chemolithoautotroph. *Appl. Environ. Microbiol.* 81, 5927–5937. doi: 10.1128/AEM.01374-15

Barco, R. A., Hoffman, C. L., Ramírez, G. A., Toner, B. M., Edwards, K. J., and Sylvan, J. B. (2017). In-situ incubation of iron-sulfur mineral reveals a

diverse chemolithoautotrophic community and a new biogeochemical role for *Thiomicrospira*. *Environ. Microbiol.* 19, 1322–1337. doi: 10.1111/1462-2920.13666

Bazylinski, D. A., Williams, T. J., Lefèvre, C. T., Berg, R. J., Zhang, C. L., Bowser, S. S., et al. (2013). *Magnetococcus marinus* gen. nov., sp. nov., a marine, magnetotactic bacterium that represents a novel lineage (Magnetococcaceae fam. nov., Magnetococcales ord. nov.) at the base of the Alphaproteobacteria. *Int. J. Syst. Evol. Microbiol.* 63, 801–808. doi: 10.1099/ijs.0.038927-0

Beam, J. P., Scott, J. J., McAllister, S. M., Chan, C. S., McManus, J., Meysman, F. J. R., et al. (2018). Biological rejuvenation of iron oxides in bioturbated marine sediments. *ISME J.* 12, 1389–1394. doi: 10.1038/s41396-017-0032-6

Blackwell, N., Bryce, C., Straub, D., Kappler, A., and Kleindienst, S. (2020). Genomic Insights into Two Novel Fe(II)-Oxidizing Zetaproteobacteria isolates reveal lifestyle adaption to coastal marine sediments. *Appl. Environ. Microbiol.* 86:e01160-20. doi: 10.1128/AEM.01160-20

Blin, K., Shaw, S., Steinke, K., Villebro, R., Ziemert, N., Lee, S. Y., et al. (2019). antiSMASH 5.0: updates to the secondary metabolite genome mining pipeline. *Nucleic Acids Res.* 47, W81–W87. doi: 10.1093/nar/gkz310

Blöthe, M., and Roden, E. E. (2009). Microbial iron redox cycling in a circumneutral-pH groundwater seep. *Appl. Environ. Microbiol.* 75, 468–473. doi: 10.1128/AEM.01817-08

Bochet, O., Bethencourt, L., Dufresne, A., Farasin, J., Pédrot, M., Labasque, T., et al. (2020). Iron-oxidizer hotspots formed by intermittent oxic–anoxic fluid mixing in fractured rocks. *Nat. Geosci.* 13, 149–155. doi: 10.1038/s41561-019-0509-1

Boiteau, R. M., Mende, D. R., Hawco, N. J., McIlvin, M. R., Fitzsimmons, J. N., Saito, M. A., et al. (2016). Siderophore-based microbial adaptations to iron scarcity across the eastern Pacific Ocean. *Proc. Natl. Acad. Sci. U.S.A.* 113, 14237–14242. doi: 10.1073/pnas.1608594113

Bolger, A. M., Lohse, M., and Usadel, B. (2014). Trimmomatic: a flexible trimmer for Illumina sequence data. *Bioinform. Oxf. Engl.* 30, 2114–2120. doi: 10.1093/bioinformatics/btu170

Boyd, P. W., and Ellwood, M. J. (2010). The biogeochemical cycle of iron in the ocean. *Nat. Geosci.* 3, 675–682. doi: 10.1038/ngeo964

Bradley, J. M., Svistunenko, D. A., Wilson, M. T., Hemmings, A. M., Moore, G. R., and Le Brun, N. E. (2020). Bacterial iron detoxification at the molecular level. *J. Biol. Chem.* 295, 17602–17623. doi: 10.1074/jbc.rev120.007746

Bray, M. S., Wu, J., Padilla, C. C., Stewart, F. J., Fowle, D. A., Henny, C., et al. (2020). Phylogenetic and structural diversity of aromatically dense pili from environmental metagenomes. *Environ. Microbiol. Rep.* 12, 49–57. doi: 10.1111/1758-2229.12809

Bryce, C., Blackwell, N., Schmidt, C., Otte, J., Huang, Y.-M., Kleindienst, S., et al. (2018). Microbial anaerobic Fe(II) oxidation – Ecology, mechanisms and environmental implications. *Environ. Microbiol.* 20, 3462–3483. doi: 10.1111/1462-2920.14328

Buchfink, B., Xie, C., and Huson, D. H. (2015). Fast and sensitive protein alignment using DIAMOND. *Nat. Methods* 12, 59–60. doi: 10.1038/nmeth.3176

Butaitë, E., Baumgartner, M., Wyder, S., and Kümmerli, R. (2017). Siderophore cheating and cheating resistance shape competition for iron in soil and freshwater *Pseudomonas* communities. *Nat. Commun.* 8:414. doi: 10.1038/s41467-017-00509-4

Butler, A. (2005). Marine siderophores and microbial iron mobilization. *Biometals* 18, 369–374. doi: 10.1007/s10534-005-3711-0

Byrne, J. M., Klueglein, N., Pearce, C., Rosso, K. M., Appel, E., and Kappler, A. (2015). Redox cycling of Fe(II) and Fe(III) in magnetite by Fe-metabolizing bacteria. *Science* 347, 1473–1476. doi: 10.1126/science.aaa4834

Castelle, C., Guiral, M., Malarte, G., Ledgham, F., Leroy, G., Brugna, M., et al. (2008). A new iron-oxidizing/O2-reducing supercomplex spanning both inner and outer membranes, isolated from the extreme acidophile *Acidithiobacillus ferrooxidans*. *J. Biol. Chem.* 283, 25803–25811. doi: 10.1074/jbc.M802496200

Castelle, C. J., Roger, M., Bauzan, M., Brugna, M., Lignon, S., Nimtz, M., et al. (2015). The aerobic respiratory chain of the acidophilic archaeon *Ferroplasma acidiphilum*: a membrane-bound complex oxidizing ferrous iron. *Biochim. Biophys. Acta* 1847, 717–728. doi: 10.1016/j.bbabio.2015.04.006

Chiu, B. K., Kato, S., McAllister, S. M., Field, E. K., and Chan, C. S. (2017). Novel pelagic iron-oxidizing Zetaproteobacteria from the chesapeake bay oxic–anoxic transition zone. *Front. Microbiol.* 8:1280. doi: 10.3389/fmicb.2017.01280

Coby, A. J., Picardal, F., Shelobolina, E., Xu, H., and Roden, E. E. (2011). Repeated anaerobic microbial redox cycling of iron. *Appl. Environ. Microbiol.* 77, 6036–6042. doi: 10.1128/AEM.00276-11

Cooper, D. C., Picardal, F. F., and Coby, A. J. (2006). Interactions between microbial iron reduction and metal geochemistry: effect of redox cycling on transition metal speciation in iron bearing sediments. *Env. Sci Technol.* 40, 1884–1891. doi: 10.1021/es051778t

Croal, L. R., Jiao, Y., and Newman, D. K. (2007). The fox operon from rhodobacter strain SW2 promotes phototrophic Fe(II) oxidation in *Rhodobacter capsulatus* SB1003. *J. Bacteriol.* 189, 1774–1782. doi: 10.1128/JB.01395-06

Cruz-Morales, P., Ramos-Aboites, H. E., Licona-Cassani, C., Selem-Mójica, N., Mejía-Ponce, P. M., Souza-Saldívar, V., et al. (2017). Actinobacteria phylogenomics, selective isolation from an iron oligotrophic environment and siderophore functional characterization, unveil new desferrioxamine traits. *FEMS Microbiol. Ecol.* 93:fix086. doi: 10.1093/femsec/fix086

de Vries, A., and Ripley, B. D. (2020). *ggdendro: Create Dendrograms and Tree Diagrams Using "ggplot2."*. Available online at: https://CRAN.R-project.org/package=ggdendro (accessed February 13, 2021).

Deng, X., Dohmae, N., Nealson, K. H., Hashimoto, K., and Okamoto, A. (2018). Multi-heme cytochromes provide a pathway for survival in energy-limited environments. *Sci. Adv.* 4:eaao5682. doi: 10.1126/sciadv.aao5682

Dharamshi, J. E., Tamarit, D., Eme, L., Stairs, C. W., Martijn, J., Homa, F., et al. (2020). Marine sediments illuminate chlamydiae diversity and evolution. *Curr. Biol.* 30, 1032.e7–1048.e7. doi: 10.1016/j.cub.2020.02.016

D'Hondt, S., Inagaki, F., Alvarez Zarikian, C. A., and Expedition 329 Scientists (2011). *Expedition 329 Reports*. Tokyo: Integrated Ocean Drilling Program Management International, Inc.

D'Hondt, S., Spivack, A. J., Pockalny, R., Ferdelman, T. G., Fischer, J. P., Kallmeyer, J., et al. (2009). Subseafloor sedimentary life in the South Pacific Gyre. *Proc. Natl. Acad. Sci. U.S.A.* 106, 11651–11656. doi: 10.1073/pnas.0811793106

Dombrowski, N., Teske, A. P., and Baker, B. J. (2018). Expansive microbial metabolic versatility and biodiversity in dynamic Guaymas Basin hydrothermal sediments. *Nat. Commun.* 9:4999. doi: 10.1038/s41467-018-07418-0

Dong, X., Greening, C., Rattray, J. E., Chakraborty, A., Chuvochina, M., Mayumi, D., et al. (2019). Metabolic potential of uncultured bacteria and archaea associated with petroleum seepage in deep-sea sediments. *Nat. Commun.* 10:1816. doi: 10.1038/s41467-019-09747-0

D'Onofrio, A., Crawford, J. M., Stewart, E. J., Witt, K., Gavrish, E., Epstein, S., et al. (2010). Siderophores from neighboring organisms promote the growth of uncultured bacteria. *Chem. Biol.* 17, 254–264. doi: 10.1016/j.chembiol.2010.02.010

Dunlea, A. G. (2016). *Biogeochemistry and Geochemical Paleoceanography of the South Pacific Gyre*. Available online at: https://open.bu.edu/handle/2144/19711 (accessed February 12, 2021).

Edwards, K. J., Bach, W., and Rogers, D. R. (2003a). Geomicrobiology of the ocean crust: a role for chemoautotrophic Fe-bacteria. *Biol. Bull.* 204, 180–185. doi: 10.2307/1543555

Edwards, K. J., Rogers, D. R., Wirsen, C. O., and McCollom, T. M. (2003b). Isolation and characterization of novel psychrophilic, neutrophilic, Fe-oxidizing, chemolithoautotrophic α- and γ-*Proteobacteria* from the Deep Sea. *Appl. Environ. Microbiol.* 69, 2906–2913. doi: 10.1128/AEM.69.5.2906-2913.2003

Edwards, K. J., Wheat, C. J., Orcutt, B. N., Hulme, S., Becker, K., Bach, W., et al. (2012). *Design and Deployment of Borehole Observatories and Experiments During IODP Expedition 336, Mid-Atlantic Ridge flank at North Pond*. Tokyo: Integrated Ocean Drilling Program Management International, Inc.

Edwards, M. J., White, G. F., Butt, J. N., Richardson, D. J., and Clarke, T. A. (2020). The crystal structure of a biological insulated transmembrane molecular wire. *Cell* 181, 665.e10–673.e10. doi: 10.1016/j.cell.2020.03.032

Elliott, A. V. C., Plach, J. M., Droppo, I. G., and Warren, L. A. (2014). Collaborative microbial Fe-redox cycling by pelagic floc bacteria across wide ranging oxygenated aquatic systems. *Chem. Geol.* 366, 90–102. doi: 10.1016/j.chemgeo.2013.11.017

Emerson, D. (2009). Potential for iron-reduction and iron-cycling in iron oxyhydroxide-rich microbial mats at loihi seamount. *Geomicrobiol. J.* 26, 639–647. doi: 10.1080/01490450903269985

Emerson, D., and Moyer, C. L. (2002). Neutrophilic Fe-oxidizing bacteria are abundant at the loihi seamount hydrothermal vents and play a major role in Fe

oxide deposition. *Appl. Environ. Microbiol.* 68, 3085–3093. doi: 10.1128/AEM.68.6.3085-3093.2002

Engel, C. E. A., Vorländer, D., Biedendieck, R., Krull, R., and Dohnt, K. (2020). Quantification of microaerobic growth of *Geobacter sulfurreducens*. *PLoS One* 15:e0215341. doi: 10.1371/journal.pone.0215341

Expedition. 344 Scientists (2011). Costa Rica Seismogenesis Project (CRISP): sampling and quantifying input to the seismogenic zone and fluid output. *Int. Ocean Discov. Program* 334:13. doi: 10.2204/iodp.proc.344.2013

Farag, I. F., Biddle, J. F., Zhao, R., Martino, A. J., House, C. H., and León-Zayas, R. I. (2020). Metabolic potentials of archaeal lineages resolved from metagenomes of deep Costa Rica sediments. *ISME J.* 14, 1345–1358. doi: 10.1038/s41396-020-0615-5

Frankel, R. B., Blakemore, R. P., and Wolfe, R. S. (1979). Magnetite in freshwater magnetotactic bacteria. *Science* 203, 1355–1356. doi: 10.1126/science.203.4387.1355

Friedman, J., Lad, L., Deshmukh, R., Li, H., Wilks, A., and Poulos, T. L. (2003). Crystal structures of the NO- and CO-bound heme oxygenase from *Neisseriae meningitidis*. Implications for O2 activation. *J. Biol. Chem.* 278, 34654–34659. doi: 10.1074/jbc.M302985200

Friedman, J., Lad, L., Li, H., Wilks, A., and Poulos, T. L. (2004). Structural basis for novel delta-regioselective heme oxygenation in the opportunistic pathogen *Pseudomonas aeruginosa*. *Biochemistry* 43, 5239–5245. doi: 10.1021/bi049687g

Gacesa, R., Baranasic, D., Starcevic, A., Diminic, J., Korlević, M., Najdek, M., et al. (2018). Bioprospecting for genes encoding hydrocarbon-degrading enzymes from metagenomic samples isolated from northern adriatic sea sediments. *Food Technol. Biotechnol.* 56, 270–277. doi: 10.17113/ftb.56.02.18.5393

Garber, A. I., Nealson, K. H., Okamoto, A., McAllister, S. M., Chan, C. S., Barco, R. A., et al. (2020). FeGenie: a comprehensive tool for the identification of iron genes and iron gene neighborhoods in genome and metagenome assemblies. *Front. Microbiol.* 11:37. doi: 10.3389/fmicb.2020.00037

Gledhill, M., and Buck, K. N. (2012). The organic complexation of iron in the marine environment: a review. *Front. Microbiol.* 3:69. doi: 10.3389/fmicb.2012.00069

Hartshorne, R. S., Jepson, B. N., Clarke, T. A., Field, S. J., Fredrickson, J., Zachara, J., et al. (2007). Characterization of *Shewanella oneidensis* MtrC: a cell-surface decaheme cytochrome involved in respiratory electron transport to extracellular electron acceptors. *JBIC J. Biol. Inorg. Chem.* 12, 1083–1094. doi: 10.1007/s00775-007-0278-y

He, S., Barco, R. A., Emerson, D., and Roden, E. E. (2017). Comparative genomic analysis of neutrophilic iron(II) oxidizer genomes for candidate genes in extracellular electron transfer. *Front. Microbiol.* 8:1584. doi: 10.3389/fmicb.2017.01584

Hibbing, M. E., Fuqua, C., Parsek, M. R., and Peterson, S. B. (2010). Bacterial competition: surviving and thriving in the microbial jungle. *Nat. Rev. Microbiol.* 8, 15–25. doi: 10.1038/nrmicro2259

Inoue, K., Qian, X., Morgado, L., Kim, B.-C., Mester, T., Izallalen, M., et al. (2010). Purification and Characterization of OmcZ, an outer-surface, octaheme c-type cytochrome essential for optimal current production by geobacter sulfurreducens. *Appl. Environ. Microbiol.* 76, 3999–4007. doi: 10.1128/AEM.00027-10

Jeans, C., Singer, S. W., Chan, C. S., VerBerkmoes, N. C., Shah, M., Hettich, R. L., et al. (2008). Cytochrome 572 is a conspicuous membrane protein with iron oxidation activity purified directly from a natural acidophilic microbial community. *ISME J.* 2, 542–550. doi: 10.1038/ismej.2008.17

Jewell, T. N. M., Karaoz, U., Brodie, E. L., Williams, K. H., and Beller, H. R. (2016). Metatranscriptomic evidence of pervasive and diverse chemolithoautotrophy relevant to C, S, N and Fe cycling in a shallow alluvial aquifer. *ISME J.* 10, 2106–2117. doi: 10.1038/ismej.2016.25

Jiao, Y., and Newman, D. K. (2007). The pio operon is essential for phototrophic Fe(II) oxidation in rhodopseudomonas palustris TIE-1. *J. Bacteriol.* 189, 1765–1773. doi: 10.1128/JB.00776-06

Jones, J. G., Gardener, S., and Simon, B. M. (1984). Reduction of ferric iron by heterotrophic bacteria in lake sediments. *Microbiology* 130, 45–51. doi: 10.1099/00221287-130-1-45

Jones, R. M., D'Angelo, T., and Orcutt, B. N. (2020). Using cathodic poised potential experiments to investigate extracellular electron transport in the crustal deep biosphere of North Pond, mid-atlantic ridge. *Front. Environ. Sci.* 8:11. doi: 10.3389/fenvs.2020.00011

Jørgensen, S. L., Hannisdal, B., Lanzen, A., Baumberger, T., Flesland, K., Fonseca, R., et al. (2012). Correlating microbial community profiles with geochemical data in highly stratified sediments from the Arctic Mid-Ocean Ridge. *Proc. Natl. Acad. Sci. U.S.A.* 109, E2846–E2855. doi: 10.1073/pnas.1207574109

Jørgensen, S. L., Thorseth, I. H., Pedersen, R. B., Baumberger, T., and Schleper, C. (2013). Quantitative and phylogenetic study of the Deep Sea Archaeal Group in sediments of the Arctic mid-ocean spreading ridge. *Front. Microbiol.* 4:299. doi: 10.3389/fmicb.2013.00299

Jungbluth, S. P., Amend, J. P., and Rappé, M. S. (2017). Metagenome sequencing and 98 microbial genomes from Juan de Fuca Ridge flank subsurface fluids. *Sci. Data* 4:170037. doi: 10.1038/sdata.2017.37

Jungbluth, S. P., Bowers, R. M., Lin, H.-T., Cowen, J. P., and Rappé, M. S. (2016). Novel microbial assemblages inhabiting crustal fluids within mid-ocean ridge flank subsurface basalt. *ISME J.* 10, 2033–2047. doi: 10.1038/ismej.2015.248

Kallmeyer, J., Pockalny, R., Adhikari, R. R., Smith, D. C., and D'Hondt, S. (2012). Global distribution of microbial abundance and biomass in subseafloor sediment. *Proc. Natl. Acad. Sci. U.S.A.* 109, 16213–16216. doi: 10.1073/pnas.1203849109

Kamura, T., Takai, Y., and Ishikawa, K. (1963). Microbial reduction mechanism of ferric iron in paddy soils (Part I). *Soil Sci. Plant Nutr.* 9, 5–9. doi: 10.1080/00380768.1963.10431048

Keffer, J. L., McAllister, S. M., Garber, A. I., Hallahan, B. J., Sutherland, M. C., Rozovsky, S., et al. (2021). Iron oxidation by a fused cytochrome-porin common to diverse iron-oxidizing bacteria. *mBio*. doi: 10.1128/mBio.01074-21 [Epub ahead of print].

Kennedy, C. B., Scott, S. D., and Ferris, F. G. (2003). Characterization of bacteriogenic iron oxide deposits from axial volcano, Juan de Fuca Ridge, Northeast Pacific Ocean. *Geomicrobiol. J.* 20, 199–214. doi: 10.1080/01490450303873

Krewulak, K. D., and Vogel, H. J. (2011). TonB or not TonB: is that the question? *Biochem. Cell Biol.* 89, 87–97. doi: 10.1139/O10-141

Langseth, M. G., Becker, K., Herzen, R. P. V., and Schultheiss, P. (1992). Heat and fluid flux through sediment on the western flank of the Mid-Atlantic Ridge: a hydrogeological study of North Pond. *Geophys. Res. Lett.* 19, 517–520. doi: 10.1029/92GL00079

Laso-Pérez, R., Hahn, C., van Vliet, D. M., Tegetmeyer, H. E., Schubotz, F., Smit, N. T., et al. (2019). Anaerobic degradation of non-methane alkanes by " candidatus methanoliparia" in hydrocarbon seeps of the Gulf of Mexico. *mBio* 10:e01814-19. doi: 10.1128/mBio.01814-19

Laufer, K., Byrne, J. M., Glombitza, C., Schmidt, C., Jørgensen, B. B., and Kappler, A. (2016a). Anaerobic microbial Fe(II) oxidation and Fe(III) reduction in coastal marine sediments controlled by organic carbon content. *Environ. Microbiol.* 18, 3159–3174. doi: 10.1111/1462-2920.13387

Laufer, K., Nordhoff, M., Røy, H., Schmidt, C., Behrens, S., Jørgensen, B. B., et al. (2016b). Coexistence of microaerophilic, nitrate-reducing, and phototrophic Fe(II) oxidizers and Fe(III) reducers in coastal marine sediment. *Appl. Environ. Microbiol.* 82, 1433–1447. doi: 10.1128/AEM.03527-15

Lefèvre, C. T., and Bazylinski, D. A. (2013). Ecology, diversity, and evolution of magnetotactic bacteria. *Microbiol. Mol. Biol. Rev.* 77, 497–526. doi: 10.1128/MMBR.00021-13

Li, Z., Pan, D., Wei, G., Pi, W., Wang, J.-H., Peng, Y., et al. (2020). Deep sea sediments associated with cold seeps are a subsurface reservoir of viral diversity. *bioRxiv* [Preprint]. doi: 10.1101/2020.09.08.284018

Light, S. H., Su, L., Rivera-Lugo, R., Cornejo, J. A., Louie, A., Iavarone, A. T., et al. (2018). A flavin-based extracellular electron transfer mechanism in diverse Gram-positive bacteria. *Nature* 562, 140–144. doi: 10.1038/s41586-018-0498-z

Lin, W. C., Coppi, M. V., and Lovley, D. R. (2004). Geobacter sulfurreducens can grow with oxygen as a terminal electron acceptor. *Appl. Environ. Microbiol.* 70, 2525–2528. doi: 10.1128/aem.70.4.2525-2528.2004

Liu, J., Wang, Z., Belchik, S. M., Edwards, M. J., Liu, C., Kennedy, D. W., et al. (2012). Identification and characterization of MtoA: a decaheme c-type cytochrome of the neutrophilic Fe(II)-oxidizing bacterium *Sideroxydans lithotrophicus* ES-1. *Front. Microbiol.* 3:37. doi: 10.3389/fmicb.2012.00037

Liu, X., Gong, J., Wei, T., Wang, Z., Du, Q., Zhu, D., et al. (2012). Crystal structure of HutZ, a heme storage protein from *Vibrio cholerae*: a structural mismatch

observed in the region of high sequence conservation. *BMC Struct. Biol.* 12:23. doi: 10.1186/1472-6807-12-23

Lovley, D. R., Ueki, T., Zhang, T., Malvankar, N. S., Shrestha, P. M., Flanagan, K. A., et al. (2011). Geobacter: the microbe electric's physiology, ecology, and practical applications. *Adv. Microb. Physiol.* 59, 1–100.

MacQuarrie, K. T. B., and Mayer, K. U. (2005). Reactive transport modeling in fractured rock: a state-of-the-science review. *Earth Sci. Rev.* 72, 189–227. doi: 10.1016/j.earscirev.2005.07.003

Mardanov, A. V., Slododkina, G. B., Slobodkin, A. I., Beletsky, A. V., Gavrilov, S. N., Kublanov, I. V., et al. (2015). The *Geoglobus acetivorans* genome: Fe(III) reduction, acetate utilization, autotrophic growth, and degradation of aromatic compounds in a hyperthermophilic archaeon. *Appl. Environ. Microbiol.* 81, 1003–1012. doi: 10.1128/AEM.02705-14

Martino, A., Rhodes, M. E., León-Zayas, R., Valente, I. E., Biddle, J. F., and House, C. H. (2019). Microbial diversity in sub-seafloor sediments from the costa rica margin. *Geosciences* 9:218. doi: 10.3390/geosciences9050218

McAllister, S. M., Moore, R. M., Gartman, A., Luther, G. W. III, Emerson, D., and Chan, C. S. (2019). The Fe(II)-oxidizing Zetaproteobacteria: historical, ecological and genomic perspectives. *FEMS Microbiol. Ecol.* 95:fiz015. doi: 10.1093/femsec/fiz015

McAllister, S. M., Polson, S. W., Butterfield, D. A., Glazer, B. T., Sylvan, J. B., and Chan, C. S. (2020a). Validating the Cyc2 neutrophilic iron oxidation pathway using meta-omics of Zetaproteobacteria iron mats at marine hydrothermal vents. *mSystems* 5:e00553-19. doi: 10.1128/mSystems.00553-19

McAllister, S. M., Vandzura, R., Keffer, J. L., Polson, S. W., and Chan, C. S. (2020b). Aerobic and anaerobic iron oxidizers together drive denitrification and carbon cycling at marine iron-rich hydrothermal vents. *ISME J.* 15, 1271–1286. doi: 10.1038/s41396-020-00849-y

McBeth, J. M., Little, B. J., Ray, R. I., Farrar, K. M., and Emerson, D. (2011). Neutrophilic iron-oxidizing "Zetaproteobacteria" and mild steel corrosion in nearshore marine environments. *Appl. Environ. Microbiol.* 77, 1405–1412. doi: 10.1128/AEM.02095-10

Mehta, T., Coppi, M. V., Childers, S. E., and Lovley, D. R. (2005). Outer membrane c-type cytochromes required for Fe(III) and Mn(IV) oxide reduction in *Geobacter sulfurreducens*. *Appl. Environ. Microbiol.* 71, 8634–8641. doi: 10.1128/AEM.71.12.8634-8641.2005

Meyer, J. L., Jaekel, U., Tully, B. J., Glazer, B. T., Wheat, C. G., Lin, H.-T., et al. (2016). A distinct and active bacterial community in cold oxygenated fluids circulating beneath the western flank of the Mid-Atlantic ridge. *Sci. Rep.* 6:22541. doi: 10.1038/srep22541

Mumford, A. C., Adaktylou, I. J., and Emerson, D. (2016). Peeking under the iron curtain: development of a microcosm for imaging the colonization of steel surfaces by *Mariprofundus* sp. strain DIS-1, an oxygen-tolerant Fe-oxidizing bacterium. *Appl. Environ. Microbiol.* 82, 6799–6807. doi: 10.1128/AEM.01990-16

Neilands, J. B. (1995). Siderophores: structure and function of microbial iron transport compounds. *J. Biol. Chem.* 270, 26723–26726. doi: 10.1074/jbc.270.45.26723

Noinaj, N., Guillier, M., Barnard, T. J., and Buchanan, S. K. (2010). TonB-dependent transporters: regulation, structure, and function. *Annu. Rev. Microbiol.* 64, 43–60. doi: 10.1146/annurev.micro.112408.134247

Orcutt, B., Wheat, C. G., and Edwards, K. J. (2010). Subseafloor ocean crust microbial observatories: development of FLOCS (FLow-through osmo colonization system) and evaluation of borehole construction materials. *Geomicrobiol. J.* 27, 143–157. doi: 10.1080/01490450903456772

Pereira, L., Saraiva, I. H., Oliveira, A. S. F., Soares, C. M., Louro, R. O., and Frazão, C. (2017). Molecular structure of FoxE, the putative iron oxidase of *Rhodobacter ferrooxidans* SW2. *Biochim. Biophys. Acta BBA Bioenerg.* 1858, 847–853. doi: 10.1016/j.bbabio.2017.07.002

Pitts, K. E., Dobbin, P. S., Reyes-Ramirez, F., Thomson, A. J., Richardson, D. J., and Seward, H. E. (2003). Characterization of the *Shewanella oneidensis* MR-1 decaheme cytochrome MtrA. *J. Biol. Chem.* 278, 27758–27765. doi: 10.1074/jbc.M302582200

Qian, X. (2011). Biochemical characterization of purified OmcS, a c-type cytochrome required for insoluble Fe(III) reduction in *Geobacter sulfurreducens*. *Biochim. Biophys. Acta* 1807, 404–412. doi: 10.1016/j.bbabio.2011.01.003

Ramírez, G. A., Hoffman, C. L., Lee, M. D., Lesniewski, R. A., Barco, R. A., Garber, A., et al. (2016). Assessing marine microbial induced corrosion at santa catalina Island, California. *Front. Microbiol.* 7:1679. doi: 10.3389/fmicb.2016.01679

Riedinger, N., Formolo, M. J., Lyons, T. W., Henkel, S., Beck, A., and Kasten, S. (2014). An inorganic geochemical argument for coupled anaerobic oxidation of methane and iron reduction in marine sediments. *Geobiology* 12, 172–181. doi: 10.1111/gbi.12077

Roden, E. E. (2012). Microbial iron-redox cycling in subsurface environments. *Biochem. Soc. Trans.* 40, 1249–1256. doi: 10.1042/BST20120202

Roden, E. E., McBeth, J. M., Blöthe, M., Percak-Dennett, E. M., Fleming, E. J., Holyoke, R. R., et al. (2012). The microbial ferrous wheel in a neutral pH groundwater seep. *Front. Microbiol.* 3:172. doi: 10.3389/fmicb.2012.00172

Ruff, S. E., Felden, J., Gruber-Vodicka, H. R., Marcon, Y., Knittel, K., Ramette, A., et al. (2019). In situ development of a methanotrophic microbiome in deep-sea sediments. *ISME J.* 13, 197–213. doi: 10.1038/s41396-018-0263-1

Scheller, S., Yu, H., Chadwick, G. L., McGlynn, S. E., and Orphan, V. J. (2016). Artificial electron acceptors decouple archaeal methane oxidation from sulfate reduction. *Science* 351, 703–707. doi: 10.1126/science.aad7154

Seyedsayamdost, M. R., Cleto, S., Carr, G., Vlamakis, H., João Vieira, M., Kolter, R., et al. (2012). Mixing and matching siderophore clusters: structure and biosynthesis of serratiochelins from *Serratia* sp. V4. *J. Am. Chem. Soc.* 134, 13550–13553. doi: 10.1021/ja304941d

Seyler, L. M., Trembath-Reichert, E., Tully, B. J., and Huber, J. A. (2020). Time-series transcriptomics from cold, oxic subseafloor crustal fluids reveals a motile, mixotrophic microbial community. *ISME J.* 15, 1192–1206. doi: 10.1038/s41396-020-00843-4

Shi, L., Fredrickson, J. K., and Zachara, J. M. (2014). Genomic analyses of bacterial porin-cytochrome gene clusters. *Front. Microbiol.* 5:657. doi: 10.3389/fmicb.2014.00657

Slobodkina, G. B., Kolganova, T. V., Querellou, J., Bonch-Osmolovskaya, E. A., and Slobodkin, A. I. (2009). *Geoglobus acetivorans* sp. nov., an iron(III)-reducing archaeon from a deep-sea hydrothermal vent. *Int. J. Syst. Evol. Microbiol.* 59, 2880–2883. doi: 10.1099/ijs.0.011080-0

Smith, A. R., Kieft, B., Mueller, R., Fisk, M. R., Mason, O. U., Popa, R., et al. (2019). Carbon fixation and energy metabolisms of a subseafloor olivine biofilm. *ISME J.* 13, 1737–1749. doi: 10.1038/s41396-019-0385-0

Smith, O., Momber, G., Bates, R., Garwood, P., Fitch, S., Pallen, M., et al. (2015). Sedimentary DNA from a submerged site reveals wheat in the British Isles 8000 years ago. *Science* 347, 998–1001. doi: 10.1126/science.1261278

Suzuki, R., and Shimodaira, H. (2006). Pvclust: an R package for assessing the uncertainty in hierarchical clustering. *Bioinformatics* 22, 1540–1542. doi: 10.1093/bioinformatics/btl117

Takai, Y., Koyama, T., and Kamura, T. (1963a). Microbial metabolism in reduction process of paddy soils (Part 2). *Soil Sci. Plant Nutr.* 9, 10–14. doi: 10.1080/00380768.1963.10431049

Takai, Y., Koyama, T., and Kamura, T. (1963b). Microbial metabolism in reduction process of paddy soils (Part 3). *Soil Sci. Plant Nutr.* 9, 1–5. doi: 10.1080/00380768.1963.10431054

Thode, S. K., Rojek, E., Kozlowski, M., Ahmad, R., and Haugen, P. (2018). Distribution of siderophore gene systems on a Vibrionaceae phylogeny: database searches, phylogenetic analyses and evolutionary perspectives. *PLoS One* 13:e0191860. doi: 10.1371/journal.pone.0191860

Toner, B. M., Santelli, C. M., Marcus, M. A., Wirth, R., Chan, C. S., McCollom, T., et al. (2008). Biogenic iron oxyhydroxide formation at mid-ocean ridge hydrothermal vents: juan de Fuca Ridge. *Geochim. Cosmochim. Acta* 73, 388–403. doi: 10.1016/j.gca.2008.09.035

Trinchero, P., Sidborn, M., Puigdomenech, I., Svensson, U., Ebrahimi, H., Molinero, J., et al. (2019). Transport of oxygen into granitic rocks: role of physical and mineralogical heterogeneity. *J. Contam. Hydrol.* 220, 108–118. doi: 10.1016/j.jconhyd.2018.12.001

Tully, B. J., and Heidelberg, J. F. (2016). Potential mechanisms for microbial energy acquisition in oxic deep-sea sediments. *Appl. Environ. Microbiol.* 82, 4232–4243. doi: 10.1128/AEM.01023-16

Tully, B. J., Wheat, C. G., Glazer, B. T., and Huber, J. A. (2018). A dynamic microbial community with high functional redundancy inhabits the cold, oxic subseafloor aquifer. *ISME J.* 12, 1–16. doi: 10.1038/ismej.2017.187

Uebe, R., and Schüler, D. (2016). Magnetosome biogenesis in magnetotactic bacteria. *Nat. Rev. Microbiol.* 14, 621–637. doi: 10.1038/nrmicro.2016.99

Vannucchi, P., Ujiie, K., Stroncik, N., and the IODP Exp. 334 Scientific Party (2013). IODP expedition 334: an investigation of the sedimentary record, fluid flow and state of stress on top of the seismogenic zone of an erosive subduction margin. *Sci. Drill.* 15, 23–30. doi: 10.5194/sd-15-23-2013

Wang, F., Gu, Y., O'Brien, J. P., Yi, S. M., Yalcin, S. E., Srikanth, V., et al. (2019). Structure of microbial nanowires reveals stacked hemes that transport electrons over micrometers. *Cell* 177, 361.e10–369.e10. doi: 10.1016/j.cell.2019.03.029

Weber, K. A., Achenbach, L. A., and Coates, J. D. (2006). Microorganisms pumping iron: anaerobic microbial iron oxidation and reduction. *Nat. Rev. Microbiol.* 4, 752–764. doi: 10.1038/nrmicro1490

Wheat, C. G., Hulme, S. M., Fisher, A. T., Orcutt, B. N., and Becker, K. (2013). Seawater recharge into oceanic crust: IODP Exp 327 Site U1363 grizzly bare outcrop. *Geochem. Geophys. Geosyst.* 14, 1957–1972. doi: 10.1002/ggge.20131

Wickham, H., Chang, W., Henry, L., Pedersen, T. L., Takahashi, K., Wilke, C., et al. (2020). *ggplot2: Create Elegant Data Visualisations Using the Grammar of Graphics*. Available online at: https://CRAN.R-project.org/package=ggplot2 (accessed February 13, 2021).

Yu, H., Susanti, D., McGlynn, S. E., Skennerton, C. T., Chourey, K., Iyer, R., et al. (2018). Comparative genomics and proteomic analysis of assimilatory sulfate reduction pathways in anaerobic methanotrophic archaea. *Front. Microbiol.* 9:2917. doi: 10.3389/fmicb.2018.02917

Conflict of Interest: The authors declare that the research was conducted in the absence of any commercial or financial relationships that could be construed as a potential conflict of interest.

Publisher's Note: All claims expressed in this article are solely those of the authors and do not necessarily represent those of their affiliated organizations, or those of the publisher, the editors and the reviewers. Any product that may be evaluated in this article, or claim that may be made by its manufacturer, is not guaranteed or endorsed by the publisher.

frontiers in Microbiology

ORIGINAL RESEARCH
published: 10 September 2021
doi: 10.3389/fmicb.2021.717249

Anammox Bacteria Are Potentially Involved in Anaerobic Ammonium Oxidation Coupled to Iron(III) Reduction in the Wastewater Treatment System

*Xiao-Ru Yang[1,2], Hu Li[1,2], Jian-Qiang Su[1,2] and Guo-Wei Zhou[1,2,3]**

[1] Key Lab of Urban Environment and Health, Institute of Urban Environment, Chinese Academy of Sciences (CAS), Xiamen, China, [2] Center for Excellence in Regional Atmospheric Environment, Institute of Urban Environment, Chinese Academy of Sciences (CAS), Xiamen, China, [3] School of Resources and Environmental Engineering, Anhui University, Hefei, China

Anaerobic ammonium oxidation coupled to nitrite reduction (termed as Anammox) was demonstrated as an efficient pathway to remove nitrogen from a wastewater treatment system. Recently, anaerobic ammonium oxidation was also identified to be linked to iron(III) reduction (termed Feammox) with dinitrogen, nitrite, or nitrate as end-product, reporting to enhance nitrogen removal from the wastewater treatment system. However, little is known about the role of Anammox bacteria in the Feammox process. Here, slurry from wastewater reactor amended with ferrihydrite was employed to investigate activity of Anammox bacteria in the Feammox process using the ^{15}N isotopic tracing technique combined with 16S rRNA gene amplicon sequencing. A significantly positive relationship between rates of $^{15}N_2$ production and iron(III) reduction indicated the occurrence of Feammox during incubation. Relative abundances of Anammox bacteria including *Brocadia*, *Kuenenia*, *Jettenia*, and unclassified Brocadiaceae were detected with low relative abundances, whereas Geobacteraceae dominated in the treatment throughout the incubation. $^{15}N_2$ production rates significantly positively correlated with relative abundances of *Geobacter*, unclassified Geobacteraceae, and Anammox bacteria, revealing their contribution to nitrogen generation *via* Feammox. Overall, these findings suggested Anammox bacteria or cooperation between Anammox bacteria and iron(III) reducers serves a potential role in Feammox process.

Keywords: Feammox, Anammox bacteria, ammonium oxidation, iron(III) reduction, $^{15}N_2$ production

OPEN ACCESS

Edited by:
Lei Yan,
Heilongjiang Bayi Agricultural University, China

Reviewed by:
Nan Li,
Tianjin University, China
Kevin Thomas Finneran,
Clemson University, United States

****Correspondence:***
Guo-Wei Zhou
gwzhou@ahu.edu.cn

Specialty section:
This article was submitted to Microbiological Chemistry and Geomicrobiology, a section of the journal Frontiers in Microbiology

Received: *30 May 2021*
Accepted: *04 August 2021*
Published: *10 September 2021*

Citation:
Yang X-R, Li H, Su J-Q and Zhou G-W (2021) Anammox Bacteria Are Potentially Involved in Anaerobic Ammonium Oxidation Coupled to Iron(III) Reduction in the Wastewater Treatment System. Front. Microbiol. 12:717249. doi: 10.3389/fmicb.2021.717249

INTRODUCTION

Feammox [anaerobic ammonium oxidation coupled to iron(III) reduction] is a pathway of nitrogen cycling identified recently and makes a contribution to nitrogen loss in various environments, such as terrestrial (e.g., wetland, tropical rainforest, and paddy soils) and aquatic ecosystem (e.g., freshwater and marine) in addition to denitrification, co-denitrification, and anaerobic ammonium oxidation (Clement et al., 2005; Yang et al., 2012; Ding et al., 2014, 2017, 2019; Huang and Jaffé, 2014; Zhou et al., 2016). Previous studies showed that iron(III)-reducing bacteria such as *Anaeromyxobacter*, *Pseudomonas*, *Geobacter*, *Desulfosporosinus*, *Dechloromonas*,

and *Geothrix* always dominated in the Feammox "pool" (Zhou et al., 2016; Li et al., 2019); however, these iron(III) reducers prefer to utilize organic carbon for iron(III) reduction. Only a minor part of iron(III) reduction (0.4–6.1%) by these bacteria is estimated to be associated with Feammox in the natural or artificial environments (Yang et al., 2012; Ding et al., 2014, 2017, 2019; Li et al., 2015; Zhou et al., 2016). As a replacement, $^{15}NH_4^+$ is generally employed to trace the occurrence of Feammox; however, it is hard to directly identify the Feammox microbes through DNA or RNA stable isotope probing because the Feammox process results in conversion of $^{15}NH_4^+$ to $^{15}N_2/^{15}NO_3^-/^{15}NO_2^-$ but not assimilation of $^{15}NH_4^+$ into DNA and RNA. As a result, "Feammox microbes" are difficult to be directly captured from the incubation.

Sawayama (2006) has reported that the possibility of Feammox happened in a wastewater treatment system, which is recently expected to become another important way to remove nitrogen from the sludge of wastewater in addition to Anammox. Anammox is another anaerobic ammonium oxidation pathway that used nitrite as an electron acceptor with forming dinitrogen (Rikmann et al., 2014). Furthermore, the addition of iron(III) oxides is indicated to increase the efficiency of nitrogen removal in the system (Chen et al., 2014; Wang et al., 2016; Li H. et al., 2018; Yin et al., 2019). These discoveries further suggest the occurrence of Feammox in the Anammox-based nitrogen removal system of a wastewater treatment reactor. However, the Feammox-involving microorganisms in the wastewater treatment system is still under-characterized. Anammox bacteria, including members of the Planctomycetales such as *Brocadia*, *Kuenenia*, *Anammoxoglobus*, *Jettenia*, *Anammoximicrobium moscowii*, and *Scalindua* (Rikmann et al., 2014), possesses a versatile metabolism involved in the utilization of diverse electron donors (e.g., NH_4^+ and propionate) and acceptors (e.g., NO_2^-, NO_3^-, and SO_4^{2-}) (Strous et al., 2002; Cervantes et al., 2009; Rikmann et al., 2014; Rios-Del Toro and Cervantes, 2016; Rios-Del Toro et al., 2018). Inspired by these recent findings, we hypothesized that Fe(III) can play as terminal electron acceptors in anaerobic ammonium oxidation mediated by Anammox bacteria in the sludge from a wastewater treatment reactor.

In order to verify our hypothesis, sludge from a wastewater treatment reactor, which has been demonstrated to employ the Anammox process to remove nitrogen (Zhang et al., 2012), was used in this study. Through the $^{15}NH_4^+$-based isotopic tracing technique with 16S rRNA gene Illumina sequencing, we amended the sludge with ferrihydrite to investigate whether (1) Feammox occurred in the Anammox enrichment and (2) the Anammox organisms were involved in Feammox process.

MATERIALS AND METHODS

Experimental Procedures

The sludge was obtained from a wastewater treatment reactor (Zhang et al., 2012). The dominant electron donor and acceptor were NH_4^+ and NO_2^- in the wastewater treatment reactor, respectively, which has been established as a stable, completely autotrophic nitrogen removal process over nitrite (Canon). Theoretically, the Canon is a process combining partial nitrification with Anammox within a single reactor, which has been shown to be a cost-efficient autotrophic process for nitrogen removal, as it has no need for a carbon source and has low requirement for oxygen (Zhang et al., 2012). The characteristic of the sludge is detailed in **Supplementary Table 1**. The Feammox experiment was initiated by inoculating 10% (v/v) sludge into 20 ml basal medium and incubated at 30°C in the dark. The basal medium (pH 6.8–7.2) consists of $MgCl_2{\cdot}6H_2O$ (0.4 g L^{-1}), $CaCl_2{\cdot}H_2O$ (0.1 g L^{-1}), $^{14}NH_4Cl$ (0.027 g L^{-1}), KH_2PO_4 (0.6 g L^{-1}), 1 ml L^{-1} vitamin solution (Lovley and Phillips, 1988), 1 ml L^{-1} trace element solution (Lovley and Phillips, 1988), 30 mmol L^{-1} bicarbonate buffer, and 4 mmol L^{-1} Fe(III). The headspace of the serum vials was flushed with ultrapure helium. Ferrihydrite was synthesized as previously described (Kappler et al., 2014) and used as the Fe(III) source. The basal medium and ferrihydrite were autoclaved (120°C for 20 min) before use, and the vitamin solution and trace element solution were filtrated with a 0.22-μm filter from the stock solutions. In order to enrich the Feammox-associated microbial population, the cultures were anaerobically transferred (10%, v/v) to fresh medium for three generations once the Fe(III) was used up.

For the labeled experiment, $^{14}NH_4Cl$ was replaced by $^{15}NH_4Cl$ (^{15}N, 99.14%; Cambridge Isotope Laboratories, Andover, MA, United States) to prepare the fresh medium. In brief, aliquots (2 ml) of the Feammox enrichment were centrifuged and washed three times with sterile deionized water before inoculating into the 20 ml of fresh $^{15}NH_4Cl$-labeled medium. Three treatments were set up: (1) NH_4^+: Feammox enrichment was inoculated in the 20 ml of $^{15}NH_4Cl$-added basal medium amended without ferrihydrite; (2) Fe(III): Feammox enrichment was inoculated in the 20 ml of ferrihydrite-containing basal medium amended without $^{15}NH_4Cl$; and (3) Fe(III) + NH_4^+: Feammox enrichment was inoculated in the 20 ml of basal medium amended with both ferrihydrite and $^{15}NH_4Cl$. The final concentrations of $^{15}NH_4Cl$ and ferrihydrite were 0.5 and 4 mmol L^{-1} in the treatments, respectively. The number of serum vials for each treatment was 4, 4, and 24, respectively. All the treatments were incubated at 30°C in a dark under anaerobic condition.

Chemical Analysis

Ferrous iron and total iron were determined as described previously (Kappler et al., 2005). Briefly, Fe(II) was determined by anaerobically transferring 100 μl of culture suspension with a syringe into 900 μl of 40 mmol L^{-1} sulfamic acid and incubating for 1 h at room temperature. Total Fe was extracted using a mixture of 20 mmol L^{-1} hydroxylamine hydrochloride and 20 mmol L^{-1} sulfamic acid (v:v = 1:1) (Klueglein et al., 2015). A 100-μl extract was then added with 1 ml ferrozine solution (1 g ferrozine in 50 mmol L^{-1} HEPES buffer, pH 7) to generate the ferrous complex, which was quantified at 562 nm UV/Vis spectrometer. Change in Fe(II) concentrations between two given time points (23 days) were used to calculate iron(III) reduction rates.

For the ^{15}N-N_2 analysis, vials were shaken vigorously to equilibrate the dissolved phase with gaseous phase, and 1 ml of gas samples was collected from the headspace using gas-tight syringes and then injected into 12-ml glass vials (Exetainer; Labco, Lampeter, United Kingdom). The gas samples were taken on days 1, 4, 8, 10, 12, 14, 18, and 22, respectively. $^{30}N_2$ and $^{29}N_2$ concentrations were calculated by multiplying the moles of total N_2 in the headspace by the $^{30}N_2$ and $^{29}N_2$ mole fractions (Zhou et al., 2016). The total N_2 and N_2O concentration in the headspace was measured using a robotized system coupled to a gas chromatograph (Agilent Technologies, Santa Clara, CA, United States) as previously described (Zhou et al., 2016). The mole fractions of $^{30}N_2$ and $^{29}N_2$ were determined by isotope ratio mass spectrometry (IRMS; Thermo Finnigan Delta V Advantage, Bremen, Germany) coupled with Gasbench II, respectively (Zhou et al., 2016). After gas collection, the remaining cultures were immediately centrifuged at 14,000 × *g* for 15 min and the pellets were used for DNA extraction. The resulting supernatant was filtered through 0.22-μm filters and then subjected to measurement of NH_4^+, NO_2^-, and NO_3^- concentrations by ion chromatography (Dionex ICS-3000 system; Diones, Sunnyvale, CA, United States). All the liquid was sampled in the anaerobic glovebox (Shel Lab Bactron IV; Shel Lab, Cornelius, OR, United States) to avoid chemical oxidation. pH was analyzed using a dual-channel pH-ion-conductivity-dissolved oxygenmeter (X60; Thermo Fisher Scientific, Carlsbad, CA, United States) in the anaerobic glovebox.

DNA Extraction and Illumina Sequencing

DNA was extracted using FastDNA Spin Kit (MP Biomedical, Illkirch-Graffenstaden, France) according to the manufacturer's protocol and stored at −20°C for the molecular analyses. Since the biomass in the treatments amended with only Fe(III) or NH_4^+ was extremely low, there was enough DNA extracted from these treatments.

To investigate the bacterial community structures and compositions, the V4–V5 region of bacterial was amplified using the DNA extracted from the samples in the treatment of Fe(III) + NH_4^+ as template. The amplicons were purified, quantified, pooled, and then sequenced on an Illumina Miseq PE 250 platform (Novogene, Beijing, China) (Zhou et al., 2016). The forward primer was 515F (5′-GTGCCAGCMGCCGCGG-3′), and the reverse primer consisted of a 6-bp barcode and 907R (5′-CCGTCAATTCMTTTRAGTTT-3′) (Ren et al., 2014). Quantitative Insights into Microbial Ecology toolkit-version 1.9.0 (QIIME) was used to process and analyze sequences as previously described (Su et al., 2015). After removal of low-quality or ambiguous reads, operational taxonomic units (OTU) were determined at 97% similarity level using UCLUST clustering in accordance with the online instruction of QIIME for open-reference OTU pick, definition, and determination (Wang et al., 2007). The representative sequences of each OTU were assigned to taxonomy using an RDP classifier (Version 11).[1]

[1]http://rdp.cme.msu.edu

Quantitative PCR

The abundance of relevant genes and microbial organisms, including bacterial 16S rRNA gene, *Geobacteraceae* spp., *Acidimicrobiaceae* spp. (the reported potential microbe responsible for Feammox) (Huang and Jaffé, 2014), *hzsB* (hydrazine synthase), *nirS* (nitrite reductase), and *nosZ* (nitrous oxide reductase) was analyzed with a real-time PCR Detection System (Roche 480; Roche, Indianapolis, IN, United States). The primer sets and thermal cycles were detailed in **Supplementary Table 2**. The 20-μl qPCR reaction contained 10 μl 2 × TransStart® Top Green qPCR SuperMix (AQ131; Transgen Biotech, Beijing, China), 0.25 μM each primer, 0.8 μl bovine serum albumin (BSA, 20 mg ml^{-1}), and 2 μl of fivefold diluted DNA as a template. The standard curve was obtained using 10-fold serial dilutions of plasmid DNA with target-genes. Three non-template controls were carried out for each quantitative assay. A melting curve for each reaction showed that only one special peak was detected. Only the reactions with efficiencies between 90 and 110%, and standard curves with correlation coefficient above 0.99 were employed in this study.

Statistical Analyses

Analysis of variance (ANOVA) and Pearson correlation analysis were conducted by SPSS 18.0 (SPSS Inc., Chicago, IL, United States) and Origin 9.0 (OriginLab, Northampton, MA, United States). Statistical significance was performed using Duncan's multiple range test and denoted at $p < 0.05$. The differences of the bacterial communities were analyzed by non-metric multidimensional scaling (NMDS) based on weighted UniFrac dissimilarity among samples, which was represented by the ordination axes (Tunney et al., 2013).

Data Accessibility

The 16S rRNA gene sequences have been deposited in GenBank with accession number SRP116169.

RESULTS

Iron(III) Reduction and Changes of N Species in the Enrichment

In the Fe(III) + NH_4^+ treatment, Fe(II) increased up to 1.83 ± 0.010 mmol L^{-1} after 22-day anaerobic incubation (**Figure 1A**). In comparison, iron(III) reduction was not detected in the treatments only amended with Fe(III) or NH_4^+ after the 22-day incubation (**Figure 1A**).

Significant ($p < 0.05$) accumulation of $^{30}N_2$ was detected in the Fe(III) + NH_4^+ treatment (0.36 μmol L^{-1}) compared to that in the treatment of Fe(III) (0.064 μmol L^{-1}) or NH_4^+ (0.080 μmol L^{-1}) during the incubation (**Figure 1B** and **Supplementary Figure 1**). The $^{29}N_2$ production rates showed similar trends to that of $^{30}N_2$ (**Figure 1B** and **Supplementary Figure 1**). Headspace N_2O exhibited a higher concentration in the treatment of Fe(III) + NH_4^+ (2.89×10^{-3} μmol L^{-1}) than that in the treatment of Fe(III) (8.00×10^{-4} μmol L^{-1}) or NH_4^+

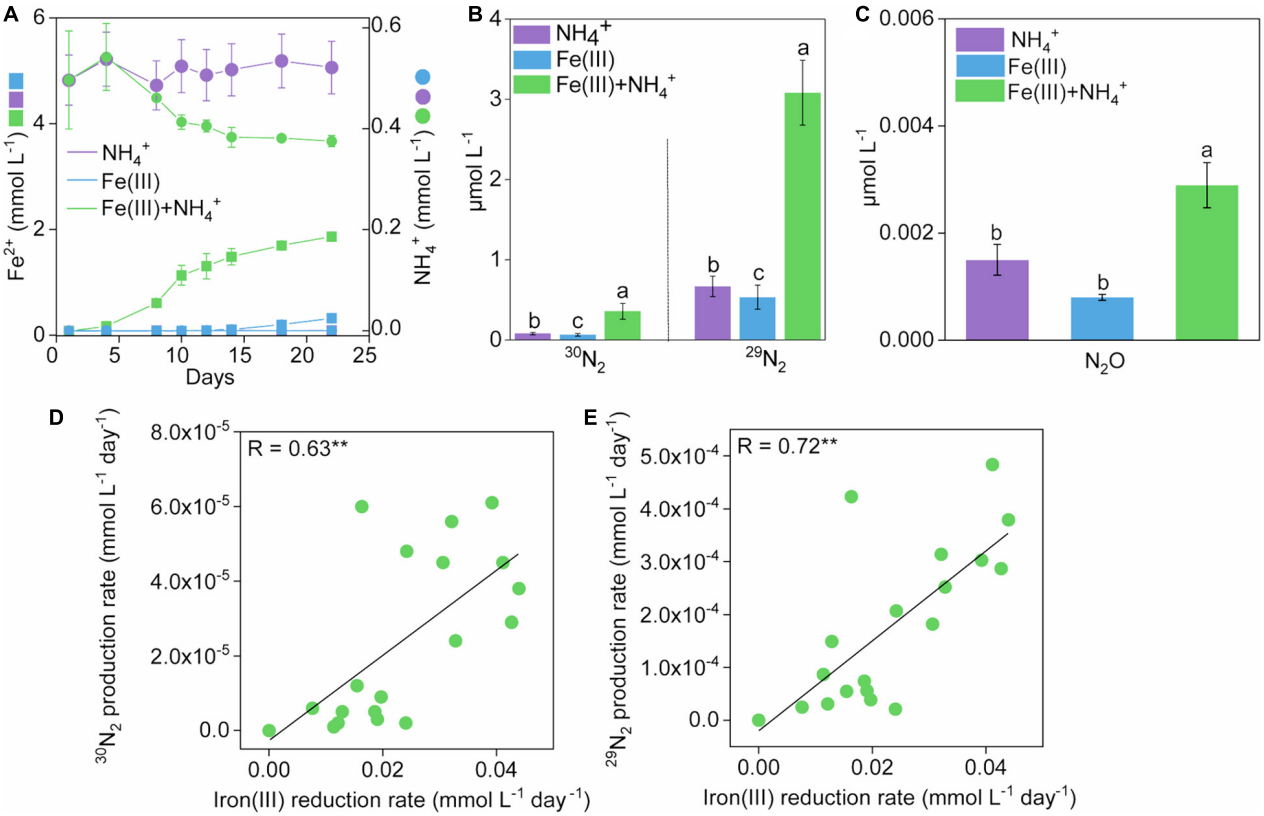

FIGURE 1 | Development of Fe(II), NH_4^+ and N_2 production in treatments during 22-day incubation. Kinetics of Fe(II) **(A)**, NH_4^+ **(B)**, and N_2 **(C)** production in treatments of NH_4^+, Fe(III), and Fe(III) + NH_4^+ during 22-day incubation. Error bars represent standard deviations of three replications. The different lowercase letters above the error bar denote statistically significant ($p < 0.05$) differences among different treatments. **(D,E)** The correlation between rates of iron(III) reduction and $^{15}N_2$ production in treatments of Fe(III) + NH_4^+ during 22-day incubation. "*" and "**" represent a statistically significant relationship between rates of iron(III) reduction and $^{15}N_2$ production, which is denoted at $p < 0.05$ and $p < 0.01$, respectively.

(9.01×10^{-4} μmol L^{-1}) during the incubation (**Figure 1C**). An amount of 0.12 mmol L^{-1} NH_4^+ was consumed in the treatment of Fe(III) + NH_4^+ (**Figure 1A**). Almost no utilization of NH_4^+ was observed in the NH_4^+ treatment (**Figure 1A**).

The rates of $^{30}N_2$ and $^{29}N_2$ production were significantly ($p < 0.001$) correlated with iron(III) reduction rates in the Fe(III) + NH_4^+ treatment (**Figures 1D,E**).

Changes in Abundances of Bacteria and the N Cycling-Relevant Genes

16S rRNA gene copy number increased up to 2.36×10^{10} copies L^{-1} medium after incubation in the Fe(III) + NH_4^+ treatment (**Figure 2A**). Also, the abundances of *hzsB*, *nirS*, and *nosZ* rapidly elevated in the treatment of Fe(III) + NH_4^+ after 12 days (**Figure 2** and **Supplementary Figure 2**). Especially, the gene copy numbers were higher for the genes *nirS* (1.26×10^7) and *nosZ* (2.62×10^7) than that for the gene *hzsB* (7.36×10^6 copies L^{-1} medium) in the treatment of Fe(III) + NH_4^+ (**Figure 2A**).

The abundance of *Geobacteraceae* spp. was about 2.03×10^6 copies L^{-1} medium after 22-day incubation in the treatment of Fe(III) + NH_4^+ (**Figure 2B**). By contrast, *Acidimicrobiaceae* spp. kept constantly low abundance throughout the incubation (**Figure 2B**).

Shift of Bacterial Community Composition

In the initial inoculant, 42.94% of the total bacterial community were affiliated to the family of Ignavibacteriaceae, followed by unclassified Anaerolineae (23.68%) and unclassified Chlorobi (8.02%) (**Figure 3**). While in the treatment of Fe(III) + NH_4^+, Geobacteraceae was the family with the highest relative abundance, followed by Comamonadaceae, Pelobacteraceae, and Pseudomonadaceae (**Figure 3**). These four families occupied up to 96.13% of the total microbial community (**Figure 3**).

Shift in the Relative Abundances of Iron(III)-Reducers and Anammox Bacteria

The detected iron(III) reducers included *Geobacter*, *Pseudomonas*, *Clostridium*, *Bacillus*, *Thiobacillus*, unclassified *Geobacteraceae*, *Desulfotomaculum*, *Desulfovibrio*, *Desulfobulbus*, and *Pelobacter* in the treatment of Fe(III) + NH_4^+ (**Figure 4A**). In comparison with the initial inoculant, the genera of *Geobacter*,

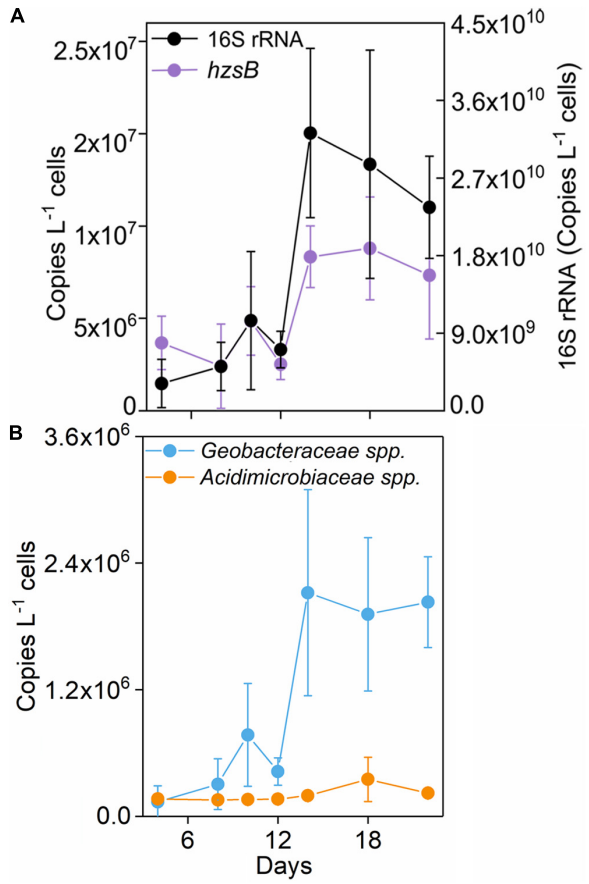

FIGURE 2 | Copy numbers of 16S *rRNA* gene, and *nosZ* **(A)**, *Geobacteraceae* spp., and *Acidimicrobiaceae* spp. **(B)** in the treatment of Fe(III) + NH_4^+ during 22-day incubation. Error bars represent standard deviations of three replication.

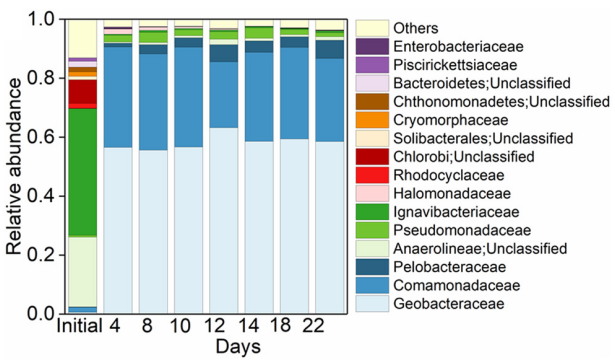

FIGURE 3 | Pattern of microbial community in treatments. Top 15 taxa at family level in the initial Anammox inoculant and the Anammox inoculant-based treatment of Fe(III) + NH_4^+ during the 22-day incubation.

Pseudomonas, *Clostridium*, *Desulfovibrio*, Desulfotomaculum, and *Pelobacter* were significantly enriched, while the relative abundance of *Bacillus* and *Thiobacillus* decreased in the treatment of Fe(III) + NH_4^+ during the incubation (**Figure 4A**). Of all the iron(III) reducers, the change in relative abundances of *Geobacter* and unclassified Geobacteraceae were significantly ($p < 0.05$) correlated with the $^{30}N_2$ and $^{29}N_2$ production rates in the treatment of Fe(III) + NH_4^+ (**Figure 4B**).

The Anammox-relevant Planctomycetes remained with low relative abundances in the treatment of Fe(III) + NH_4^+ after 22-day incubation. Dynamics of relative abundances of Anammox-relevant taxa, including unclassified Brocadiaceae, *Brocadia*, *Kuenenia*, and *Jettenia*, displayed a similar pattern in the treatment of Fe(III) + NH_4^+. These relative abundances of Anammox bacteria reached a peak on days 10–12 and then decreased during the incubation (**Figure 4C**). The relative abundances of these Anammox bacteria significantly ($p < 0.05$) correlated with the rates of $^{30}N_2$ and $^{29}N_2$ production (**Figure 4D**).

DISCUSSION

Feammox is a recently identified pathway of dinitrogen generation, expecting to be applied to remove nitrogen from a wastewater treatment system. In this study, we aimed to verify the occurrence of Feammox and investigate the Feammox-associated microbes in the sludge of a wastewater treatment system. Detection of $^{15}N_2$ production from sludge amended with iron(III) indicated the existence of Feammox in the incubation. Anammox bacteria such as Brocadiaceae, *Kuenenia*, and *Jettenia* and iron(III) reducers including *Geobacter* and unclassified Geobacteraceae were found potentially involved in the Feammox process.

The Feammox incubation was established using the sludge as inoculant, which was subjected to three generations with freshly prepared medium under anaerobic condition. As a result, the major electron acceptor for anaerobic oxidation of ^{15}N-NH_4^+ was ferrihydrite during the incubation. Previous reports suggested that Anammox can be linked to the microbial reduction of natural organic matters (Rios-Del Toro et al., 2018), likely originating from the breakdown of dead biomass, for example, carbohydrate residues including cellulose and lignin (Siemann et al., 2012). The transformation between oxidized and reduced state enables the quinone group-abundant organic matters serving as electron shuttles to mediate anaerobic oxidation of ammonium to N_2 (Westereng et al., 2015; Rios-Del Toro et al., 2018). However, the standard Gibbs free energy released from this process ($NH_4^+ + 1.5$ quinone-$NOM_{ox} \rightarrow 0.5N_2 + 1.5$ quinoneH_2-$NOM_{red} + 4H^+$) ranged from 5.8 kJ mol^{-1} to −124.6 kJ mol^{-1} (Rios-Del Toro et al., 2018), greatly lower than that produced from the Feammox process [$3Fe(OH)_3 + 5H^+ + NH_4^+ \rightarrow 3Fe^{2+} + 9H_2O + 0.5N_2$, $\Delta_rG_m = -245$ kJ mol^{-1}; $6Fe(OH)_3 + 10H^+ + NH_4^+ \rightarrow 6Fe^{2+} + 16H_2O + NO_2^-$, $\Delta_rG_m = -164$ kJ mol^{-1}; $8Fe(OH)_3 + 14H^+ + NH_4^+ \rightarrow 8Fe^{2+} + 21H_2O + NO_3^-$, $\Delta_rG_m = -207$ kJ mol^{-1}] (Yang et al., 2012). Therefore, Anammox was probably coupled to ferrihydrite reduction during the incubation. The significant accumulation of $^{30}N_2$ provided a solid evidence for the occurrence of Feammox in the treatment

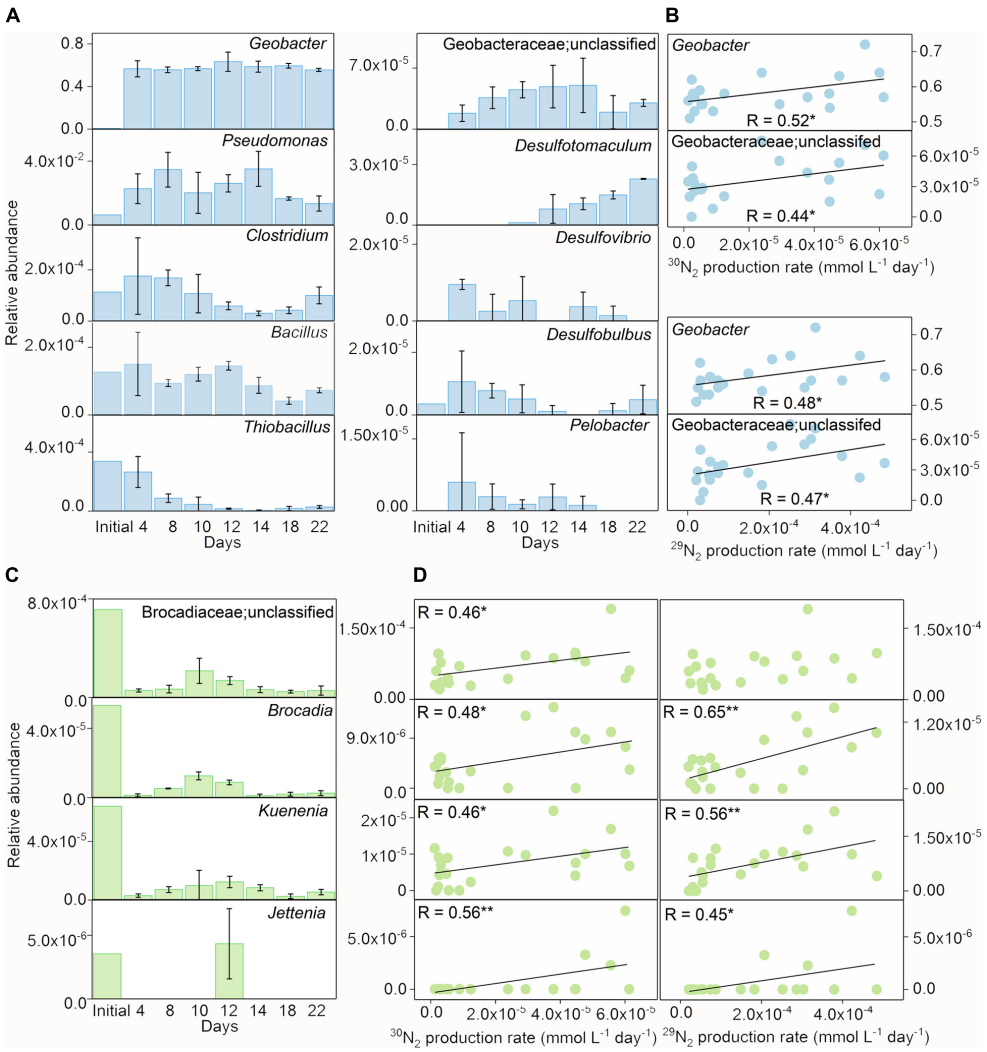

FIGURE 4 | The relative abundances of iron(III) reducers and Anammox bacteria during incubation. The relative abundances of iron(III) reducers **(A)** and the correlation between the relative abundances of *Geobacter*/unclassified Geobacteraceae and $^{15}N_2$ production rates **(B)** in the inoculant-based treatment of Fe(III) + NH_4^+ during 22-day incubation. Error bars represent standard deviations of three replications. The relative abundances of Brocadiaceae (unclassified), *Brocadia*, *Kuenenia*, and *Jettenia* **(C)**, and the correlation between the relative abundance of *Geobacter* and $^{15}N_2$ production rates **(D)** in the inoculant-based treatment of Fe(III) + NH_4^+. Error bars represent standard deviations of three replication. "*" and "**" represent a statistically significant relationship between relative abundances of iron(III) reducers, Anammox bacteria, and $^{15}N_2$ production, which is denoted at $p < 0.05$ and $p < 0.01$, respectively.

of Fe(III) + NH_4^+. Codenitrification is another potential source of $^{30}N_2$ (Laughlin and Stevens, 2002). However, it can be ruled out in this study because other ^{15}N-labeled nitrogen compounds (e.g., hydrazine and amino compounds) that could reduce $^{15}NO_2^-$ and $^{15}NO_3^-$ to N_2 were not available in the culture. Under these conditions, direct N_2 production from Feammox, or Feammox-produced NO_2^- or NO_3^- followed by denitrification or Anammox are the possible pathways for $^{30}N_2$ generation, supporting the occurrence of Feammox in the treatment of Fe(III) + NH_4^+. The positive correlation ($p < 0.0001$; **Figures 1D,E**) between Fe(III) reduction and $^{30}N_2/^{29}N_2$ production rates further verified the existence of Feammox in the treatment of Fe(III) + NH_4^+ during the anoxic incubation.

The amount of $^{15}N_2$, N_2O, and $^{15}NO_x^-$ (3.63 μmol L^{-1}; **Supplementary Table 3**) produced from the treatment of Fe(III) + NH_4^+ was far less than that of NH_4^+ depleted during the incubation, indicating that the majority of NH_4^+ was assimilated into microbial biomass (Tupas and Koike, 1990). The abundant genera such as *Pseudomonas* and *Bacillus* detected in this study, which are able to assimilate ammonia during their growth (Kim and Hollocher, 1982; Kanamori et al., 1989), may be the major NH_4^+ consumers in the treatment of Fe(III) + NH_4^+.

The molar ratio of reduced Fe (III) to the total NH_4^+ oxidation was about 15.41 in the Fe(III) + NH_4^+ treatment (**Figure 1**), which did not match the stoichiometry (ranging from 3 to 8) in the three Feammox equations (Yang et al., 2012; Ding et al., 2014; Zhou et al., 2016). This suggested that only

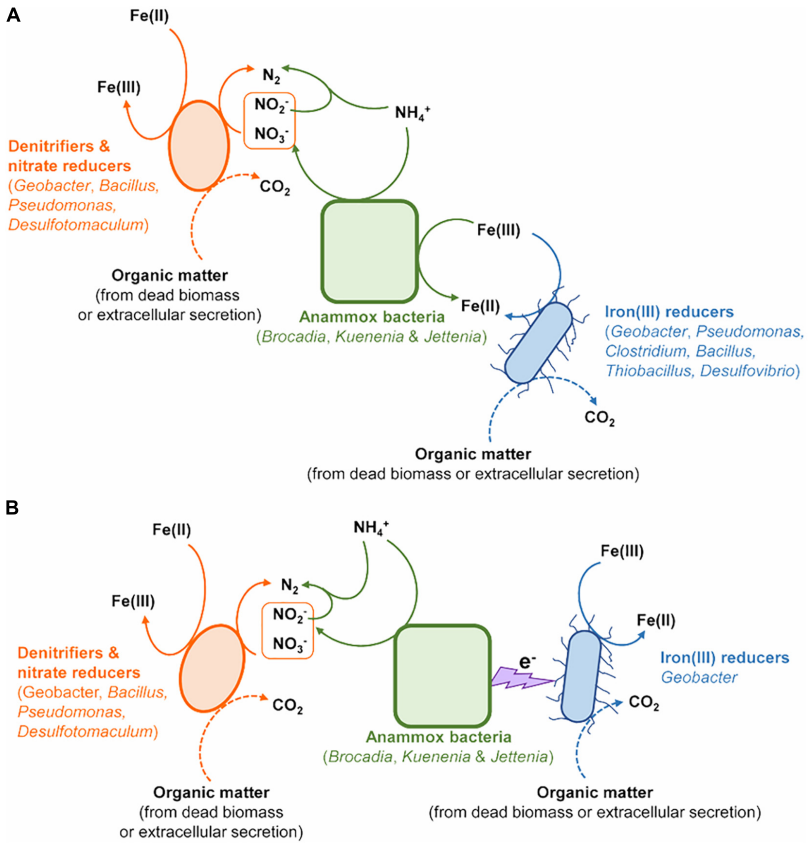

FIGURE 5 | The potential models of microorganisms contributing to N removal *via* Feammox. **(A)** Anammox bacteria directly involved in the Feammox-associated N removal. **(B)** Interaction between Anammox bacteria and *Geobacter* linked to Feammox-associated N removal.

a minor fraction of reduced Fe(III) was linked to the NH_4^+ oxidation in the Fe(III) + NH_4^+ treatment. According to the thermodynamic calculations, the amount of iron reduction associated with Feammox was 0.36–0.96 mmol L^{-1}, accounting for 19.67–52.46% of total Fe(III) reduction in the treatment of Fe(III) + NH_4^+. Thus, a majority of the reduced Fe(III) was linked to the oxidation of other substrates mediated by microorganisms. Because exogenous organic matter was not added in the treatment of Fe(III) + NH_4^+, the substrates might be organic compounds sourced from the dead biomass or extracellular secretion from the microbes. Among all the iron(III)-reducing bacteria, the family of Geobacteraceae was abundant in the treatment of Fe(III) + NH_4^+ (**Figure 3**). The genus of *Geobacter* is able to reduce Fe(III) associated with organic substrate oxidation to support its growth (Lovley, 1991). The relative abundance of Geobacteraceae showed an increase on days 10 and 12, which was in agreement with the rapidly increasing copy number of *Geobacter* after 12-day incubation in the treatment of Fe(III) + NH_4^+ (**Figures 2B**, **3**, **4A**), indicating *Geobacter* was the dominant genus in Geobacteraceae. The positive correlation between the abundance of *Geobacter* and accumulation of $^{15}N_2$ in the treatment of Fe(III) + NH_4^+ (**Figure 4B**) suggested that *Geobacter* may exert a potential role in Feammox.

The abundance of Anammox bacteria, including Brocadiaceae, *Kuenenia*, and *Jettenia*, showed significant correlation with $^{15}N_2$ production in the treatment of Fe(III) + NH_4^+ (**Figure 4D**), suggesting Anammox bacteria were linked with Feammox during the incubation. Although the mechanism about the role of Anammox bacteria as Feammox players was still unknown, a variety of reports have shown their versatile metabolism. Firstly, Anammox bacteria are capable of anaerobically oxidizing ammonium *via* anammoxosome coupled with other electron acceptors such as sulfate in addition to nitrite (Liu et al., 2008; Rikmann et al., 2014). The ΔG_o of sulfate-reducing anaerobic ammonium oxidation proceeded by Anammox species *Anammoxoglobus sulfate* ($2NH_4^+ + SO_4^{2-} \rightarrow S_o + N_2 + 4H_2O$ $\Delta G_o = -46$ kJ mol^{-1}; $8NH_4^+ + 3SO_4^{2-} \rightarrow HS^- + 4N_2 + 12H_2O + 5H^+$ $\Delta G_o = -22$ kJ mol^{-1}) is obviously lower than that of Feammox (Liu et al., 2008; Rikmann et al., 2014), suggesting that Anammox bacteria in the enrichment should favor Feammox. Secondly, genera of *Brocadia* and *Kuenenia* have iron(III)-reducing ability using organic matter (e.g., formate, acetate, and propionate) as electron donor (Graaf et al., 1996; Zhao et al., 2014); 80% of the ferric iron reductase in these Anammox bacteria locates in the membrane fraction and part of them termed as dissimilatory ferric iron reductases are the essential terminal reductase of the Fe(III) respiratory

pathway in iron(III)-reducing bacteria (Schröder et al., 2003; Zhao et al., 2014). It provided a cue that the Anammox bacteria detected in our study, including Brocadiaceae, *Kuenenia*, and *Jettenia*, were capable of reducing iron(III) linked to oxidizing ammonium anaerobically at same time. Moreover, several publications demonstrated the potential role of Anammox bacteria in Feammox based on the increase in the N_2 production after amendment with iron(III) oxides in the Anammox sludge (Chen et al., 2014; Wang et al., 2016; Li H. et al., 2018; Li X. et al., 2018; Yin et al., 2019). The Feammox bacteria *Acidimicrobiaceae* sp. were previously identified in acid soil with pH between 3.5 and 4.5 (Huang and Jaffé, 2014); however, the gene copy of the *Acidimicrobiaceae* spp. was extremely low (**Figure 2B**), and members of this family were not detected *via* Illumina sequencing in this study, which might indicate that this reported family made very little contribution to Feammox-linked N_2 production under neutral condition. In addition, the aerobic ammonium-oxidizing bacteria *Nitrosomonas* spp. were found to be highly enriched in the ammonium-containing anoxic condition (Lek Noophan et al., 2009), whereas they were not detected through Illumina sequencing and *amoA*-based qPCR (data not shown) in the treatment of Fe(III) + NH_4^+ in this study. All of these disclosed that the Anammox bacteria Brocadiaceae, *Kuenenia*, and *Jettenia* had potential for Feammox-associated anaerobic ammonium oxidation (**Figure 5A**).

Cooperation between Anammox bacteria and iron(III)-reducers such as *Geobacter* could also complete the Feammox process (**Figure 5B**). The conductive pili of *Geobacter* provide the chance to extend electron transfer ability beyond the outer surface of their cells (Reguera et al., 2005). These pili offer the possibility for *Geobacter* to accept electrons from anaerobic ammonium oxidation by Anammox bacteria through periplasmic or outer membrane electron transfer protein (Reguera et al., 2005). The increase in the gene copy numbers of *nirS*, *nosZ*, *hzsB*, and relative abundances in nitrate reducers/denitrifiers (including *Geobacter*, *Pseudomonas*, *Bacillus*, *Clostridium*, and *Desulfotomaculum*) (Zhou et al., 2019) further indicated the contribution of denitrification, nitrate reduction, Anammox and nitrate reduction dependent iron(II) oxidation to N turnover in the Fe(III) + NH_4^+ treatment during the incubation (**Figures 5A,B**).

Potential Feammox rate was estimated with a value of 0.49 μg N kg^{-1} d^{-1} based on the $^{30}N_2$ production rates, which was comparable to that reported in paddy soil (0.17–0.59 μg N kg^{-1} d^{-1}), intertidal wetland (0.24–0.36 μg N kg^{-1} d^{-1}), and tropical forest soil (about 0.32 mg N kg^{-1} d^{-1}) (Clement et al., 2005; Yang et al., 2012; Ding et al., 2014; Li et al., 2019). However, the contribution of Feammox to N loss was much lower than that of Anammox enrichment from the sludge (4.1×10^6 μg N kg^{-1} d^{-1}) (Chen et al., 2014), suggesting a substantially low N removal efficiency *via* Feammox. Furthermore, the minor contribution ratio of Feammox to N loss in this study was inconsistent with the previous reports in the Anammox sludge, which showed that Fe(III) addition increased the N removal up to 0.8×10^6 μg N kg^{-1} d^{-1} (Chen et al., 2014; Wang et al., 2016). The significantly lower relative abundance of Anammox bacteria in the treatment of Fe(III) + NH_4^+ (**Figures 2A**, **3**, **4C**) than the those reported in the previous wastewater treatment system (Chen et al., 2014; Wang et al., 2016) may be an important reason for low amount of N_2 *via* Feammox. Firstly, limited capability of substrate utilization by Anammox bacteria led to slow growth rate and long doubling time (Jetten et al., 2005). As a result, these Anammox bacteria were overwhelmed by iron(III) reducers that could efficiently obtain energy from dissimilatory iron(III) reduction. Secondly, the relative abundances of the Brocadiaceae, *Kuenenia*, and *Jettenia* decreased in the treatment of Fe(III) + NH_4^+ (**Figure 4C**), which was likely due to the accumulation of NO_2^-/NO_3^- after 12-day incubation (**Supplementary Table 3**). Iron(II) coexistence with NO_2^- (**Supplementary Figure 2**), which might lead to the NO_x^- dependent Fe(II) oxidation, can severely inhibit the activity of Anammox bacteria (Zhao et al., 2014). Thirdly, dilution of Anammox bacteria *via* three generations of subculture may be another important reason for the low activity of Feammox-associated N_2 production decreased during the incubation. Besides, Fe_3O_4 can form from rapid iron(III) reduction with the production of Fe(II) absorbed on the ferric oxides surface and then improve N removal during Feammox process (Kappler et al., 2014; Li H. et al., 2018; Li X. et al., 2018). Hence, it can be inferred that Fe(II) was accumulated with relatively low extent after subculturing in the treatment of Fe(III) + NH_4^+; therefore, the amount of Fe_3O_4 produced in the treatment was lower compared to the sludge reactor in continuous operation.

CONCLUSION

This study demonstrated the occurrence of Feammox in Anammox inoculant-based enrichment. The relative abundances of *Geobacter* and Anammox bacteria such as Brocadiaceae, *Kuenenia*, and *Jettenia* were significantly correlated with $^{15}N_2$ production rates, indicating their potential role in Feammox-involved N removal. We proposed that sole Anammox bacteria or cooperation between Anammox bacteria and *Geobacter* or unclassified Geobacteraceae could complete the Feammox process during the incubation. Our results suggested the potential role of Anammox bacteria in the nitrogen removal *via* the Feammox process.

DATA AVAILABILITY STATEMENT

The datasets presented in this study can be found in online repositories. The names of the repository/repositories and accession number(s) can be found in the article/ **Supplementary Material**.

AUTHOR CONTRIBUTIONS

X-RY, HL, and G-WZ did the experiments, conceived and designed the project, and analyzed the data. J-QS gave assistance

in lab work and laboratory analyses. X-RY wrote the manuscript. X-RY, HL, J-QS, and G-WZ revised the manuscript. All authors read and approved the final manuscript.

FUNDING

This work was supported by the National Natural Science Foundation of China (41771285 and 42021005).

ACKNOWLEDGMENTS

We thank Han Zhang (Institute of Urban Environment, Chinese Academy of Sciences) for kindly supporting the determination of δ^{15}N-nitrate and δ^{15}N-nitrite.

SUPPLEMENTARY MATERIAL

The Supplementary Material for this article can be found online at: https://www.frontiersin.org/articles/10.3389/fmicb.2021.717249/full#supplementary-material

Supplementary Figure 1 | The dynamics of $^{29}N_2$ and $^{30}N_2$ production in the treatment of Fe(III) + NH_4^+ during 22-day incubation.

Supplementary Figure 2 | The time course of abundances of *nirS* and *nosZ*, and concentrations of NO_3^- and NO_2^- in the treatment of Fe(III) + NH_4^+ during 22-day incubation.

Supplementary Table 1 | Characteristic of the initial inoculant slurry.

Supplementary Table 2 | Primers and qPCR processes used in this study.

Supplementary Table 3 | The concentrations of $^{15}NO_x^-$ in the Fe(III) + NH_4^+ treatment after 22-day incubation.

REFERENCES

Cervantes, F. J., Meza-Escalante, E. R., Texier, A. C., and Gómez, J. (2009). Kinetic limitations during the simultaneous removal of p-cresol and sulfide in a denitrifying process. *J. Ind. Microbiol. Biotechnol.* 36, 1417–1424. doi: 10.1007/s10295-009-0628-6

Chen, H., Yu, J. J., Jia, X. Y., and Jin, R. C. (2014). Enhancement of anammox performance by Cu(II), Ni(II) and Fe(III) supplementation. *Chemosphere* 117, 610–616. doi: 10.1016/j.chemosphere.2014.09.047

Clement, J., Shrestha, J., Ehrenfeld, J., and Jaffe, P. (2005). Ammonium oxidation coupled to dissimilatory reduction of iron under anaerobic conditions in wetland soils. *Soil Biol. Biochem.* 37, 2323–2328. doi: 10.1016/j.soilbio.2005.03.027

Ding, B., Chen, Z., Li, Z., Qin, Y., and Chen, S. (2019). Nitrogen loss through anaerobic ammonium oxidation coupled to Iron reduction from ecosystem habitats in the Taihu estuary region. *Sci. Total Environ.* 662, 600–606. doi: 10.1016/j.scitotenv.2019.01.231

Ding, B., Li, Z., and Qin, Y. (2017). Nitrogen loss from anaerobic ammonium oxidation coupled to Iron(III) reduction in a riparian zone. *Environ. Pollut.* 231(Pt 1), 379–386. doi: 10.1016/j.envpol.2017.08.027

Ding, L. J., An, X. L., Li, S., Zhang, G. L., and Zhu, Y. G. (2014). Nitrogen loss through anaerobic ammonium oxidation coupled to iron reduction from paddy soils in a chronosequence. *Environ. Sci. Technol.* 48, 10641–10647. doi: 10.1021/es503113s

Graaf, A. A., Bruijn, P., Robertson, L. A., Jetten, M. S. M., and Kuenen, J. G. (1996). Autotrophic growth of anaerobic ammonium-oxidizing microorganisms in a fluidized bed reactor. *Microbiology* 142, 2187–2196. doi: 10.1099/13500872-142-8-2187

Huang, S., and Jaffé, P. R. (2014). Characterization of incubation experiments and development of an enrichment culture capable of ammonium oxidation under iron reducing conditions. *Biogeosciences* 11, 12295–12321. doi: 10.5194/bgd-11-12295-2014

Jetten, M. S. M., Cirpus, I., Kartal, B., Niftrik, L., Pas-Schoonen, K. T., Sliekers, O., et al. (2005). 1994–2004: 10 years of research on the anaerobic oxidation of ammonium. *Biochem. Soc. Trans.* 33, 119–123. doi: 10.1042/BST0330119

Kanamori, K., Weiss, R. L., and Roberts, J. D. (1989). Ammonia assimilation pathways in nitrogen-fixing *Clostridium kluyverii* and *Clostridium butyricum*. *J. Bacteriol.* 171, 2148–2154.

Kappler, A., Schink, B., and Newman, D. K. (2005). Fe(III) mineral formation and cell encrustation by nitrate dependent Fe(II) oxidizers the nitrate dependent Fe(II) oxidizer strain BoFeN1. *Geobiology* 3, 235–245. doi: 10.1111/j.1472-4669.2006.00056.x

Kappler, A., Wuestner, M. L., Ruecker, A., Harter, J., Halama, M., and Behrens, S. (2014). Biochar as an electron shuttle between bacteria and Fe(III) minerals. *Environ. Sci. Technol. Lett.* 1, 339–344. doi: 10.1021/ez5002209

Kim, C. H., and Hollocher, T. C. (1982). 13N isotope studies on the pathway of ammonia assimilation in Bacillus megaterium and *Escherichia coli*. *J. Bacteriol.* 151, 358–366. doi: 10.1128/JB.151.1.358-366.1982

Klueglein, N., Picardal, F., Zedda, M., Zwiener, C., and Kappler, A. (2015). Oxidation of Fe(II)-EDTA by nitrite and by two nitrate-reducing Fe(II)-oxidizing Acidovorax strains. *Geobiology* 13, 198–207. doi: 10.1111/gbi.12125

Laughlin, R. J., and Stevens, R. J. (2002). Evidence for fungal dominance of denitrification and codenitrification in a grassland soil. *Soil Sci. Soc. Am. J.* 66, 1540–1548. doi: 10.2136/sssaj2002.1540

Lek Noophan, P., Sripiboon, S., Damrongsri, M., and Munakata-Marr, J. (2009). Anaerobic ammonium oxidation by *Nitrosomonas* spp. and anammox bacteria in a sequencing batch reactor. *J. Environ. Manage.* 90, 967–972. doi: 10.1016/j.jenvman.2008.03.003

Li, H., Chi, Z., and Yan, B. (2018). Insight into the impact of Fe3O4 nanoparticles on anammox process of subsurface-flow constructed wetlands under long-term exposure. *Environ. Sci. Pollut. Res. Int.* 25, 29584–29592. doi: 10.1007/s11356-018-2975-1

Li, H., Su, J. Q., Yang, X. R., Zhou, G. W., Lassen, S. B., and Zhu, Y. G. (2019). RNA stable isotope probing of potential Feammox population in paddy soil. *Environ. Sci. Technol.* 53, 4841–4849. doi: 10.1021/acs.est.8b05016

Li, X., Hou, L., Liu, M., Zheng, Y., Yin, G., Lin, X., et al. (2015). Evidence of nitrogen loss from anaerobic ammonium oxidation coupled with ferric iron reduction in an intertidal wetland. *Environ. Sci. Technol.* 49, 11560–11568. doi: 10.1021/acs.est.5b03419

Li, X., Huang, Y., Liu, H. W., Wu, C., Bi, W., Yuan, Y., et al. (2018). Simultaneous Fe(III) reduction and ammonia oxidation process in Anammox sludge. *J. Environ. Sci.* 64, 42–50. doi: 10.1016/j.jes.2017.01.002

Liu, S., Yang, F., Gong, Z., Meng, F., Chen, H., Xue, Y., et al. (2008). Application of anaerobic ammonium-oxidizing consortium to achieve completely autotrophic ammonium and sulfate removal. *Bioresour. Technol.* 99, 6817–6825. doi: 10.1016/j.biortech.2008.01.054

Lovley, D. R. (1991). Dissimilatory Fe(III) and Mn(IV) reduction. *Mircrobiol. Rev.* 55, 259–287. doi: 10.1016/S0065-2911(04)49005-5

Lovley, D. R., and Phillips, E. J. (1988). Novel mode of microbial energy metabolism: organic carbon oxidation coupled to dissimilatory reduction of iron or manganese. *Appl. Environ. Microbiol.* 54, 1472–1480.

Reguera, G., McCarthy, K. D., Mehta, T., Nicoll, J. S., Tuominen, M. T., and Lovley, D. R. (2005). Extracellular electron transfer via microbial nanowires. *Nature* 435, 1098–1101. doi: 10.1038/nature03661

Ren, G. D., Zhang, H. Y., Lin, X. G., Zhu, J. G., and Jia, Z. J. (2014). Response of phyllosphere bacterial communities to elevated CO2 during rice growing season. *Appl. Microbiol. Biotechnol.* 98, 9459–9471. doi: 10.1007/s00253-014-5915-0

Rikmann, E., Zekker, I., Tomingas, M., Vabamae, P., Kroon, K., Saluste, A., et al. (2014). Comparison of sulfate-reducing and conventional Anammox upflow anaerobic sludge blanket reactors. *J. Biosci. Bioeng.* 118, 426–433. doi: 10.1016/j.jbiosc.2014.03.012

Rios-Del Toro, E. E., and Cervantes, F. J. (2016). Coupling between anammox and autotrophic denitrification for simultaneous removal of ammonium and sulfide by enriched marine sediments. *Biodegradation* 27, 107–118. doi: 10.1007/s10532-016-9759-4

Rios-Del Toro, E. E., Valenzuela, E. I., Ramírez, J. E., López-Lozano, N. E., and Cervantes, F. J. (2018). Anaerobic ammonium oxidation linked to microbial reduction of natural organic matter in marine sediments. *Environ. Sci. Technol. Lett.* 5, 571–577. doi: 10.1021/acs.estlett.8b00330

Sawayama, S. (2006). Possibility of anoxic ferric ammonium oxidation. *J. Biosci. Bioeng.* 101, 70–72. doi: 10.1263/jbb.101.70

Schröder, I., Johnson, E., and de Vries, S. (2003). Microbial ferric iron reductases. *FEMS Microbiol. Rev.* 27, 427–447. doi: 10.1016/s0168-6445(03)00043-3

Siemann, S., Caron, F., Riopel, R., and Borraro, V. (2012). Laboratory study on the impact of pH and salinity on the fluorescence signal of natural organic matter (NOM) relevant to groundwaters from a Canadian shield sampling site. *Water Qual. Res. J. Can.* 47, 131–139. doi: 10.2166/wqrjc.2012.028

Strous, M., Kuenen, J. G., Furerst, J. A., Wagner, M., and Jetten, M. S. M. (2002). The Anammox case e a new experimental manifesto for microbiological ecophysiology. *Antonie Van Leeuwenhoek* 81, 693–702. doi: 10.1023/A:1020590413079

Su, J. Q., Wei, B., Ou-Yang, W. Y., Huang, F. Y., Zhao, Y., Xu, H. J., et al. (2015). Antibiotic resistome and its association with bacterial communities during sewage sludge composting. *Environ. Sci. Technol.* 49, 7356–7363. doi: 10.1021/acs.est.5b01012

Tunney, M. M., Einarsson, G. G., Wei, L., Drain, M., Klem, E. R., Cardwell, C., et al. (2013). Lung microbiota and bacterial abundance in patients with bronchiectasis when clinically stable and during exacerbation. *Am. J. Respir. Cell Mol. Biol.* 187, 1118–1126. doi: 10.1164/rccm.201210-1937OC

Tupas, L., and Koike, I. (1990). Amino acid and ammonium utilization by heterotrophic marine bacteria grown in enriched seawater. *Limnol. Oceanogr.* 35, 1145–1155. doi: 10.4319/lo.1990.35.5.1145

Wang, Q., Garrity, G. M., Tiedje, J. M., and Cole, J. R. (2007). Naive Bayesian classifier for rapid assignment of rRNA sequences into the new bacterial taxonomy. *Appl. Environ. Microbiol.* 73, 5261–5267. doi: 10.1128/AEM.00062-07

Wang, X., Shu, D., and Yue, H. (2016). Taxonomical and functional microbial community dynamics in an Anammox-ASBR system under different Fe (III) supplementation. *Appl. Microbiol. Biotechnol.* 100, 10147–10163. doi: 10.1007/s00253-016-7865-1

Westereng, B., Cannella, D., Wittrup Agger, J., Jorgensen, H., Larsen Andersen, M., Eijsink, V. G., et al. (2015). Enzymatic cellulose oxidation is linked to lignin by long-range electron transfer. *Sci. Rep.* 5:18561. doi: 10.1038/srep18561

Yang, W. H., Weber, K. A., and Silver, W. L. (2012). Nitrogen loss from soil through anaerobic ammonium oxidation coupled to iron reduction. *Nat. Geosci.* 5, 538–541. doi: 10.1038/ngeo1530

Yin, S., Li, J., Dong, H., and Qiang, Z. (2019). Enhanced nitrogen removal through marine anammox bacteria (MAB) treating nitrogen-rich saline wastewater with Fe(III) addition: nitrogen shock loading and community structure. *Bioresour. Technol.* 287:121405. doi: 10.1016/j.biortech.2019.121405

Zhang, Z. J., Li, Y., Chen, S., Wang, S., and Bao, X. (2012). Simultaneous nitrogen and carbon removal from swine digester liquor by the Canon process and denitrification. *Bioresour. Technol.* 114, 84–89. doi: 10.1016/j.biortech.2012.03.006

Zhao, R., Zhang, H., Li, Y., Jiang, T., and Yang, F. (2014). Research of iron reduction and the iron reductase localization of anammox bacteria. *Curr. Microbiol.* 69, 880–887. doi: 10.1007/s00284-014-0668-7

Zhou, G. W., Yang, X. R., Li, H., Marshall, C. W., Zheng, B. X., Yan, Y., et al. (2016). Electron shuttles enhance anaerobic ammonium oxidation coupled to iron(III) reduction. *Environ. Sci. Technol.* 50, 9298–9307. doi: 10.1021/acs.est.6b02077

Zhou, G. W., Yang, X. R., Sun, A. Q., Li, H., Lassen, S. B., Zheng, B. X., et al. (2019). Mobile incubator for iron(III) reduction in the gut of the soil-feeding earthworm *Pheretima guillelmi* and interaction with denitrification. *Environ. Sci. Technol.* 53, 4215–4223. doi: 10.1021/acs.est.8b06187

Conflict of Interest: The authors declare that the research was conducted in the absence of any commercial or financial relationships that could be construed as a potential conflict of interest.

Publisher's Note: All claims expressed in this article are solely those of the authors and do not necessarily represent those of their affiliated organizations, or those of the publisher, the editors and the reviewers. Any product that may be evaluated in this article, or claim that may be made by its manufacturer, is not guaranteed or endorsed by the publisher.

frontiers in Microbiology

ORIGINAL RESEARCH
published: 29 October 2021
doi: 10.3389/fmicb.2021.631885

Soluble, Colloidal, and Particulate Iron Across the Hydrothermal Vent Mixing Zones in Broken Spur and Rainbow, Mid-Atlantic Ridge

Mustafa Yücel[1], Serhat Sevgen[1] and Nadine Le Bris[2]*

[1]Institute of Marine Sciences, Middle East Technical University, Mersin, Turkey, [2]LECOB, SU-CNRS, Sorbonne Université, Banyuls-sur-Mer, France

OPEN ACCESS

Edited by:
Sabine Kasten, Alfred Wegener Institute Helmholtz Centre for Polar and Marine Research (AWI), Germany

Reviewed by:
Peter Leslie Croot, National University of Ireland Galway, Ireland
Alexey Kamyshny, Ben-Gurion University of the Negev, Israel

***Correspondence:**
Mustafa Yücel
myucel@ims.metu.edu.tr

Specialty section:
This article was submitted to Microbiological Chemistry and Geomicrobiology, a section of the journal Frontiers in Microbiology

Received: *21 November 2020*
Accepted: *30 September 2021*
Published: *29 October 2021*

Citation:
Yücel M, Sevgen S and Le Bris N (2021) Soluble, Colloidal, and Particulate Iron Across the Hydrothermal Vent Mixing Zones in Broken Spur and Rainbow, Mid-Atlantic Ridge. Front. Microbiol. 12:631885. doi: 10.3389/fmicb.2021.631885

The slow-spreading Mid-Atlantic Ridge (MAR) forms geological heterogeneity throughout the ridge system by deep crustal faults and their resultant tectonic valleys, which results in the existence of different types of hydrothermal vent fields. Therefore, investigating MAR hydrothermal systems opens a gate to understanding the concentration ranges of ecosystem-limiting metals emanating from compositionally distinct fluids for both near-field chemosynthetic ecosystems and far-field transport into the ocean interiors. Here, we present novel data regarding onboard measured, size-fractionated soluble, colloidal, and particulate iron concentrations from the 2018 R/V L'Atalante – ROV Victor research expedition, during which samples were taken from the mixing zone of black smokers using a ROV-assisted plume sampling. Iron size fractionation (<20, 20–200, and >200 nm) data were obtained from onboard sequential filtering, followed by measurement *via* ferrozine assay and spectrophotometric detection at 562 nm. Our results showed the persistent presence of a nanoparticulate/colloidal phase (retained within 20–200 nm filtrates) even in high-temperature samples. A significant fraction of this phase was retrievable only under treatment with HNO_3 – a strong acid known to attack and dissolve pyrite nanocrystals. Upon mixing with colder bottom waters and removal of iron in the higher parts of the buoyant plume, the larger size fractions became dominant as the total iron levels decreased, but it was still possible to detect significant (micromolar) levels of nanoparticulate Fe even in samples collected 5 m above the orifice in the rising plume. The coolest sample (<10°C) still contained more than 1 μM of only nitric acid-leachable nanoparticle/colloidal, at least 200 times higher than a typical Fe concentration in the non-buoyant plume. Our results support previous reports of dissolved Fe in MAR vent plumes, and we propose that this recalcitrant Fe pool – surviving immediate precipitation – contributes to maintaining high hydrothermal iron fluxes to the deep ocean.

Keywords: hydrothermal vents, iron, redox, nanoparticles, marine ecosystems, deep sea

INTRODUCTION

Iron redox cycling is intimately coupled with global carbon, phosphorus, and nitrogen cycles. Several transition metals form cofactors of enzymes but also take part in intra- and extracellular electron transfer and thus are vital for biology (Twining and Baines, 2013). Especially Fe, Zn, Cu, and Ni were essential in global primary production during certain periods of Earth's history to the extent that they might have limited global productivity, providing a direct feedback to planetary evolution (Rickaby, 2015; Moore et al., 2017). Moreover, the precipitation of iron as oxides or sulfides (pyrite-FeS_2) is another major feedback loop in the timing of the atmospheric accumulation of biogenic O_2. This Fe-initiated feedback also resulted in its massive removal from the oceans since the oxidized form of Fe (Fe^{3+}) is insoluble at neutral to alkaline pH if not stabilized in solution by complexation with organics or inorganic ligands, such as sulfides and silicates. Iron is now so scarce in the ocean waters that it limits primary productivity in the so-called "high-nutrient low-chlorophyll" regions, estimated to cover at least one-third of the sunlit ocean (Boyd and Ellwood, 2010). That is why iron fertilization might have driven atmospheric pCO_2 fluctuations over the glacial-interglacial periods (Jickells et al., 2005), but whether the fertilization originated from external sources (dust input) or internal fluxes (upwelling, vents or seafloor sediments) is an ongoing debate (Winckler et al., 2016).

Since their discovery in 1977 with submersible Alvin, hydrothermal vents have been shown to play a major role in oceanic element cycles. In addition to global impact, hydrothermal vent fluxes also support highly productive chemosynthetic seafloor ecosystems (Le Bris et al., 2019). A major internal flux of iron has also been recognized now, but the poor representation of this source in global models yields uncertainty in the iron cycle feedback to the global carbon cycle (Tagliabue et al., 2010, 2016). When ocean currents support vertical export, the vent-derived iron can influence surface ecosystems. For instance, a recent report by Ardyna et al. (2019) showed how hydrothermal (^{3}He enriched) water masses originating from the southern East Pacific Rise can be upwelled along the isopycnals to fertilize phytoplankton blooms in the iron-limited Southern Ocean. That study did not include iron measurements, but recent oceanic transects produced by GEOTRACES (Schlitzer, 2017) showed in all ocean basins how iron can be detected 1000 s km away from deep-sea sources (Resing et al., 2015; Fitzsimmons et al., 2017). Such recent findings posed a contrast with the paradigm that Fe rapidly oxidizes and precipitates, leading to its complete scavenging from plumes close to the emission point. Stabilization by organic complexes in far-field (Sander and Koschinsky, 2011; Kleint et al., 2017) has been established as a plausible mechanism; however, a large gap still remains with regard to the issue of metal stabilization near the source. Organic chelators tend to decompose at the temperatures of vent fluids and kinetic considerations point to previously overlooked inorganic geochemical mechanisms involving the formation of nanoparticles in mixing zones (Yücel et al., 2011; Findlay et al., 2015, 2019). Subsequent organic colloid/particle formation away from the mixing zones could further enhance iron export (Toner et al., 2009, 2016). Based on these studies, it is now widely considered that large-scale oceanic transport of iron might be primarily determined by an unknown interplay between inorganic nanoparticles and organic complexes (Gledhill and Buck, 2012; Fitzsimmons et al., 2015, 2017; Buck et al., 2018; Lough et al., 2019a). The known kinetics of "dissolved" ferrous iron oxidation with oxygen (where iron is assumed to exist as Fe^{2+} hydroxy or carbonate species) does not predict such a high stability of iron. Moreover, a complex set of poorly constrained processes occurring at the interface of hydrothermal fluids and deep-sea water, at scales of nanometers to several 10 s of meters, seem to determine the export of vent iron to the deep-sea.

Very few works have focused on this spatial scale. While landmark geochemical studies focused on the end-members (Von Damm et al., 1998; Seyfried et al., 2011) and established major processes of water-rock reactions leading to vent fluid chemical composition, chemical oceanography studies focused on 10–1000 s of km long water column transects, thus uncovering key aspects of trace element cycling (Wu et al., 2011; Nishioka et al., 2013; Fitzsimmons et al., 2017). Studies on the scales of vent mixing zone interfaces have emerged only recently: one of the first ROV-based rising plume investigations was conducted by Findlay et al. (2015) at MAR (Rainbow, TAG and SnakePit), establishing that a variety of oxides and sulfides is emitted from MAR vents despite the slow-spreading rates and high iron to sulfide (Fe:S > 1) ratios in the end-member fluids. Waeles et al. (2017), working in MAR, employed *in situ* filtration (0.45 µm) and found that lower Fe:S ratios (<1) may result in iron oxidation processes being more important. This supports the view proposed by Yücel et al. (2011) that pyrite nanoparticles form in high-temperature sulfide-rich hydrothermal solutions, and the formation is negligible at higher dilution ratios as the formation of pyrite is kinetically hindered. Findlay et al. (2019) conducted the first mixing zone profiling with the submersible Alvin in the low Fe:S fluids of the East Pacific Rise (EPR) 9°N and confirmed that if any new pyrite nanoparticles form, the process should be constrained to the immediate vicinity of the orifice. These studies demonstrated kinetic constraints in the mixing zones of hydrothermal vents (as opposed to equilibrium speciation approaches). However, the mechanistic controls behind the formation of the larger colloidal pool in which mineral nanoparticles are situated have remained largely elusive.

In this study, we present onboard measured, size-fractionated dissolved iron results from the 2018 R/V L'Atalante – ROV Victor expedition, during which samples were taken from the vertical mixing zone of black smoker (buoyant) plumes with Titanium majors and a syringe (PEP) multi-sampler operated by the ROV VICTOR 6000. Specifically, we aim to:

- Define the controls on iron size fractionation in different vent structures from Broken Spur and Rainbow in the Mid-Atlantic Ridge, including soluble (sFe), colloidal (cFe), and particulate iron (pFe),
- Explore the dynamics of the colloidal pool with additional measurements of nitric acid-leachable nanoparticle colloids (which we abbreviate as cFe-N),

- Compare two different geological areas, with high Fe:S and low Fe:S ratios in end-member fluids at the Rainbow and Broken Spur vent fields, respectively, for their potential to export iron nanoparticles.

STUDY SITES

The Mid-Atlantic Ridge (MAR) is a slow-spreading ridge at a rate of <3 cm/year. The geological heterogeneity throughout the MAR system is under the control of tectonic forces (i.e., extreme attenuation of the crust and formation of detachment faults) in relation to magmatic spreading (Schmidt et al., 2007). This special geology of the MAR results in the formation of different types of hydrothermal vents along the entire ridge system (Kelley and Shank, 2010). To this end, Broken Spur and Rainbow hydrothermal vent fields were examined as two important types of vent systems in the MAR.

The Broken Spur vent field (29° 10' N, 43° 10' W) lies at a depth of ~3,100 m on the crest of a neovolcanic zone in the Mid-Atlantic Ridge (**Figure 1**; Murton et al., 1995), and samples from this field were taken from Spire, Dragon XIII, and Chandelier vent structures. Broken Spur hosts high-temperature black smokers driven by heat extracted from cooling magma. Water-rock reactions with basaltic rocks control the formation and evolution of hydrothermal fluids in the vent field, which has high temperatures (up to 332°C) and low pH vent fluids with a comparable amount of trace metals and a relatively high concentration of sulfides with respect to other vent sites at the MAR (James et al., 1995; Charlou et al., 2010; this study).

The Rainbow vent field is located at 36° 14' N, 33° 54' W at a depth of ~2,300 m on a nonvolcanic ridge in the northern MAR (**Figure 1**; Douville et al., 2002; Charlou et al., 2010). Three individual vent structures (named Fumeur Tres Dense, Fumeur Nouveau, and Magali) were sampled in this vent field. Serpentinized peridotites have the primary role in the evolution of vent fluid geochemistry in the Rainbow field. High-temperature vents (up to 372°C) contain low pH fluids with very high concentrations of Fe and Cl and a relatively low concentration of sulfide with respect to other vents in the MAR (Douville et al., 2002; Charlou et al., 2010; Seyfried et al., 2011; Gartman et al., 2014; Findlay et al., 2015; this work). High concentrations of Cl indicate phase separation in the subsurface and exerts a primary control on metal solubility (Seyfried et al., 2011). Moreover, Rainbow vent fluids show stability in both temporal and spatial scales. Studies carried out in 1997 (Douville et al., 2002), 2008 (Seyfried et al., 2011), and our own study in 2018 show that the fluid composition of Rainbow has not changed substantially over an ~20-year timespan. Samples obtained from individual vents in the Rainbow field exhibit uniform composition, which might indicate that Rainbow fluids might be fed by a single deep source (Charlou et al., 2002; Seyfried et al., 2011).

MATERIALS AND METHODS

Sample Collection and Onboard Measurements of Sulfide and Iron

All hydrothermal fluid samples were collected during the July–August 2018 TRANSECT research cruise to the Mid-Atlantic Ridge with R/V L'Atalante and remotely operated vehicle (ROV) Victor 6000 (Le Bris and The Science Party, 2018). High-temperature hydrothermal fluid samples were collected from individual chimneys in the Rainbow and Broken Spur

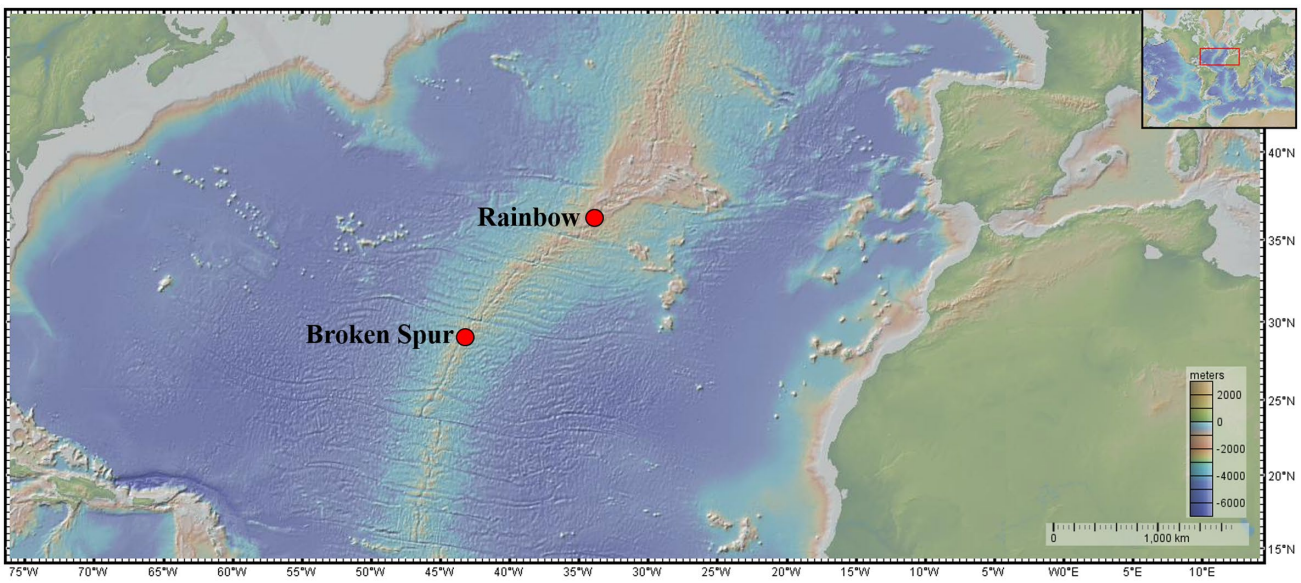

FIGURE 1 | Map showing the location of the vent fields visited along the Mid-Atlantic Ridge. Map courtesy of http://www.geomapapp.org.

hydrothermal fields. Fluids were collected using titanium syringes (also called "major samplers"), a PEP sampler equipped with syringe or PE bags and Niskin bottles where appropriate. We successfully collected plume samples from six different chimneys in Rainbow and Broken Spur (3 each). Each plume sampling included a maximum of six discrete sampling points within the buoyant plume, from the high-T end-member to the coolest part (8–12 m) of the black smoke. The temperatures of the fluids were monitored with high-temperature probes manipulated by the ROV Victor 6000 just before each sampling. Upon retrieval of the fluid samples at ROV Victor 6000 recovery on deck or using the elevator, onboard sample processing was completed within 1 h. Fluid aliquots were extracted for shipboard colorimetric determination of dissolved Fe and dissolved sulfide, while shore-based analysis was carried out for trace metals and major ions.

On board R/V L'Atalante, we measured dissolved free sulfide immediately following sample retrieval *via* the colorimetric methylene blue method with spectrophotometric detection at 670 nm (Cline, 1969) with an Ocean Optics spectrophotometer (detection limit 0.5 μM). For onboard iron measurements, 10 ml of filtered (20 and 200 nm pore size) and non-filtered subsamples were treated with 1 ml 4 N HCl and/or 4 N HNO_3 upon retrieval of the samples (Yücel et al., 2011). HNO_3 was used to dissolve the (nano)particulate pyrite-Fe present in the samples. This acid treatment lasted 6–10 h. All dissolved Fe^{3+} was converted to Fe^{2+} using hydroxylamine hydrochloride as a reducing agent, and the samples were analyzed by the Ferrozine assay for dissolved Fe^{2+} at 562 nm wavelength using an Ocean Optics spectrophotometer (Stookey, 1970) with a 1-cm pathlength cell. As a result, the size fractions were named following established conventions: <20 nm soluble Fe (sFe), 20–200 nm colloidal Fe (cFe), sFe + cFe = dissolved iron (dFe) and >200 nm as particulate Fe (pFe). We add to this an operationally defined HNO_3 extractable fraction minus the HCl extractable iron, abbreviated as cFe-N, as it is composed of colloidal nanoparticulate pyrite and/or non-HCl leachable, but HNO_3 refers to leachable iron oxides. Iron silicate nanoparticles were not leached this way since stronger acids like HF are needed. The detection limit with the ferrozine assay was 0.5 μM, and each of the reported measurements represents an average of two duplicates per sample. The analyses had a precision better than 3%.

On-Shore Analyses of Major Ions and Metals Other Than Iron

Subsamples for shore-based analysis were transferred to polypropylene tubes to measure non-volatile dissolved species in the vent fluids. Filtered (0.2 μm pore size Nylon filters) aliquots were acidified with 1 ml 4 N HCl immediately after subsampling and were stored at −20°C. The concentration of Mg was determined in ion chromatography (IC) with a Dionex CS12-SC separation column, with methane sulfonic acid eluent and CSRS-I suppressor. Filtration through 0.45 μm pore size Nylon filters and 100-fold dilution were applied for each sample before the measurement. On the other hand, the concentrations of Mn and Si were measured by a NexIon 350X Inductively Coupled Plasma Mass Spectrometry (ICP-MS). 1 ml 6 N HNO_3 was added, and 200-fold dilution was applied to all subsamples before measurement. Perkin Elmer multi-element calibration standard solution for metals in 5% HNO_3 with a concentration of 10 μg/ml was used to prepare the calibration standards. An internal Yttrium standard was used to correct the intensity deviations during measurement with ICP-MS. Precision for IC and ICP-MS was less than 3%. All concentrations obtained from IC and ICP-MS analysis were calculated using calibration curves for each element after considering dilution factors and molar mass calculations.

RESULTS

General Observations From the Sites

This study was conducted in a total of 6 black smokers in Broken Spur and Rainbow (**Table 1**). At Broken Spur, we sampled a mature (Spire) and two relatively newly forming (named Chandelier and Dragon XIII) chimney structures. Spire is a tall (>10 m) and complex edifice, the existence of which was also described by James et al. (1995). The largest hydrothermal flow at the very top of the structure was sampled for this study. Chandelier and Dragon XIII were smaller chimneys with less than 2 m in height. As shown in **Table 1**, Broken Spur chimneys had maximum temperatures of 310–332°C. The samples taken from the highest T (orifice) contained high concentrations of co-occurring dissolved Fe (max 187–744 μM) and $\sum H_2S$ (2.7–5.6 mM).

TABLE 1 | General sampling information on vent fluids from Broken Spur (BS) and Rainbow (Rbw).

	Lat. (N)	Lon. (W)	Depth (m)	Victor dive	T-max (°C)	dFe at orifice (μM)	$\sum H_2S$ (mM)	Samplings (m above orifice)
BS Spire	29°10' 5.2"	43°10'28.45"	3,060	690	310	188.2	5.6	0, 0.1, 1, 2, 5
BS Chandelier	29°10'3.27"	43°10'26.22"	3,046	692	n.m.	743.6	3.1	0, 0.1, 1, 3
BS Dragon XIII	29°10'2.96"	43°10'27.59"	3,046	692	332	728.7	2.7	0, 0.1, 1.5
Rbw Magali	36°13'75.25"	33°54'22.83"	2,238	694	372	22791.3	bdl	0, 0.1, 1, 2, 3, 5
Rbw M2 (Fum. Nouveau)	36°13'45.18"	33°54'12.78"	2,321	686	320	4978.6	bdl	0, 0.2, 1.5, 4, 7
Rbw M1a (Fum. Tres Dense)	36°13'45.12"	33°54'3.24"	2,238	684	300	5430.7	bdl	0, 0.3, 2, 3, 5, 12

"nm" not measured bdl: below detection limit – T-max are the highest temperatures observed during the particular sampling at the start of the plume profiling. End-member temperatures may differ.

Rainbow hydrothermal chimneys included a "Magali" structure as well as two unnamed structures, tentatively called M1a (Fumeur Tres Dense) and M2 (Fumeur Nouveau). Their maximum temperatures ranged between 300 and 372°C with dissolved iron concentrations reaching to over 22 mM. Dissolved free sulfide was below detection level in all high-temperature samples. Detailed end-member geochemistry analyses and ecosystem processes resulting from the 2018 R/V L'Atalante TRANSECT expedition will be given in upcoming papers.

Size Fractionation in Plumes and Distribution of HNO_3 Extractable Nanoparticles

Spire plume, near the orifice, contained about 405 µM of total (TFe = dFe + pFe), which decreased to a TFe of 2.8 µM at 5 m above the orifice (**Figure 2A**). Dissolved iron (dFe) decreased from 187.2 to 1.2 µM toward the highest sampling point. Colloidal fraction was less than 1% at the orifice but gradually increased to 16% of TFe at 5 m. The cFe-N was between 1.8 and 5.4 µM, and at 5 m, still detectable (0.12 µM) levels of cFe-N were present (**Figure 2A**). Overall, cFe-N was as high as 18% of the TFe in the Spire plume. Compared to Spire, the rising plume of Chandelier was shorter in height, and in the 3-m distance, no detectable sFe was present but more than half of the TFe was present as cFe (**Figure 2B**). Similar to Spire, the cFe fraction of Chandelier increased with plume height. Dissolved dFe and cFe-N both showed a logarithmic decrease from 743.6 to 2.4 and 8.6 to 0.7 µM, respectively. Nanoparticle Fe (cFe-N) comprised about 1% of TFe but rose to 24% of the cFe pool. In the Dragon XIII chimney, the last sampling of Broken Spur, we found that a maximum cFe (21%) fraction was present at the orifice sample, with the pFe fraction peaking in the mid-plume sample (**Figure 2C**). At 1.5 m height, dFe decreased to 53.5 µM (from 728.7) and the Fe-nano fraction ranged from 25.6 to 0.6 µM. The 25.6 µM Fe-nano level is the highest measured in Broken Spur. This is remarkable in the sense that the concentration belongs to the sample obtained

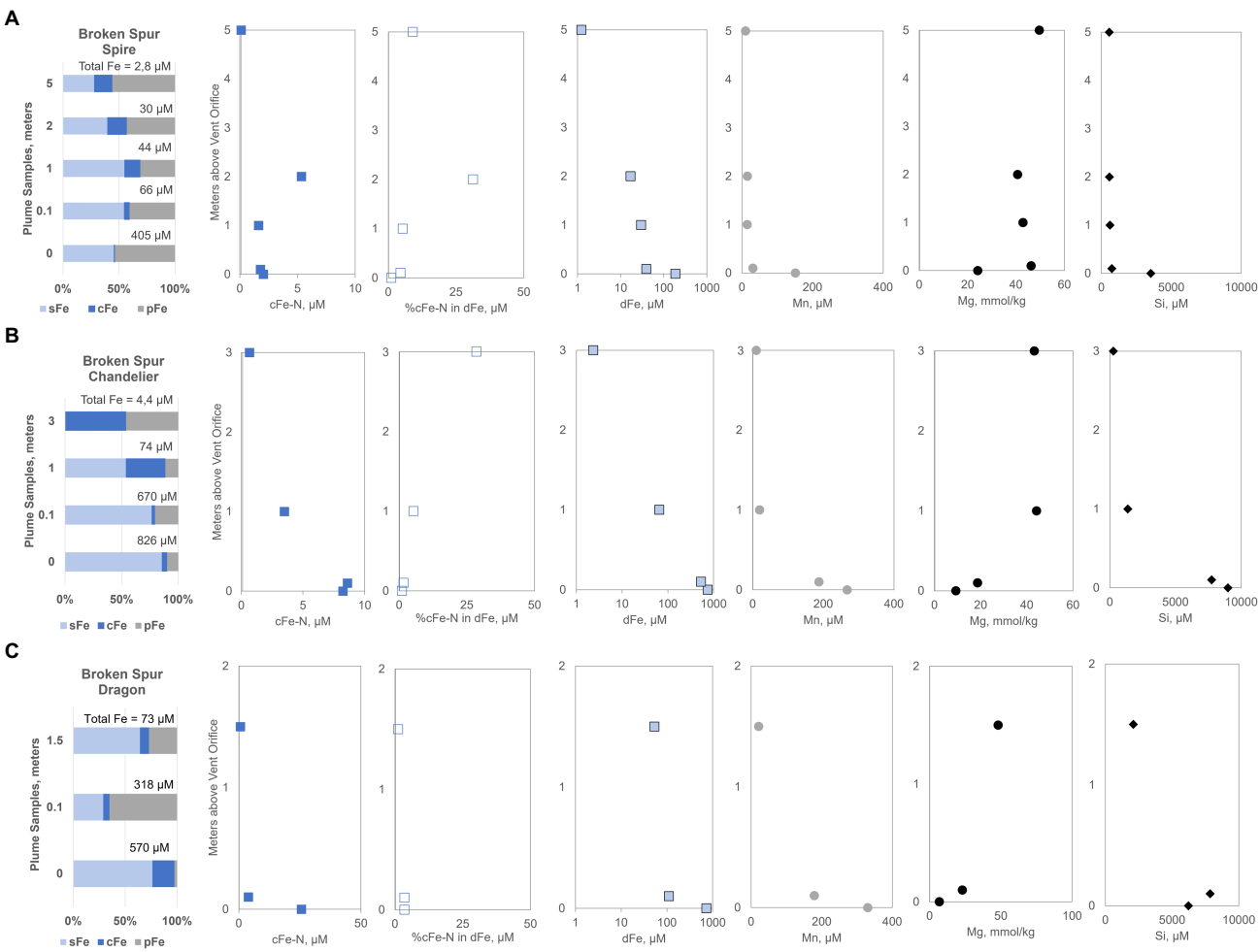

FIGURE 2 | Iron size fractionation data for Broken Spur vent fluids **(A)** Spire, **(B)** Chandelier, and **(C)** Dragon XIII are presented along with profiles containing distance from the orifice vs. measured different chemical species (e.g., cFe-N, dFe, Mn, Mg, and Si). sFe, soluble iron; cFe, colloidal iron; pFe, particulate iron; cFe-N, nanoparticle iron; dFe, dissolved iron.

from the high-T end. This Fe-nano is about 4% of the dFe emitted from the Dragon XIII high-T fluid.

Compared to Broken Spur, the Rainbow sites had much higher iron levels at the orifice (**Supplementary Table S1**). In the Magali plume, about 23,697 μM TFe was emitted, and this decreased to TFe of 131 μM at 5 m (**Figure 3A**). The sFe fraction was overall high, exceeding 90% in the upper 2 m and then decreasing to 52% at 5 m. A significant fraction of cFe (max. 11% of the TFe) was present from the bottom to the top of the sampled area, with cFe-N in the cFe ranging from 1326.4 μM at the orifice to 1.2 μM at 5 m (**Figure 3A**). The cFe-N comprised up to 10% of the dFe pool even 3 m above the orifice. The particulate Fe fraction increased with plume height. In the other two chimneys sampled in Rainbow, we could not perform a full-size fractionation including using the 20-nm filter but obtained results on <200 and >200 nm filtrates. As was the case with other profiles, the additional Fe released after nitric acid treatment still showed a difference, which we equate to the cFe-N fraction assuming these are colloidal nitric acid-leachable nanoparticles. The M2 plume (Fumeur Nouveau) had 11,294 μM TFe at 0.2 m but decreased to 134 μM at 7 m (**Figure 3B**). Actually, the 0.2-m sample had more iron than our "orifice" sample that was supposed to be richer in iron; however, as can be seen in the Mn, Mg and Si tracer results, the 0.2 m sample was much closer to the end-member fluid. Both orifice and 0.2 m samples had almost 100% dFe and the particulate fraction became more important at 4 and 7 m (**Figure 3B**). Significant levels (max 281 μM) of cFe-N were detected but decreased to 1.6 μM at 7 m. The cFe-N pool comprised nearly 9% of all dFe at 1.5 m in this plume. Similarly, the M1a (Fumeur Tres Dense) plume contained mostly dFe near the orifice with maximum levels of 8,233 μM. However, the whole Fe pool in M1a was as pFe at 5 and 12 m, with no detectable dFe and cFe-N at less than 5 m height (**Figure 3C**). At 5 m, the M1a plume still had a TFe level of 104 μM. This is the lowest TFe value when compared to similar heights within the rising plumes of the M2 and Magali hydrothermal vents.

Plume Vertical Profiles of Mg, Mn, and Si

For a better contextual understanding of the mixing processes in the plume and for assessing the mixing status of the samples,

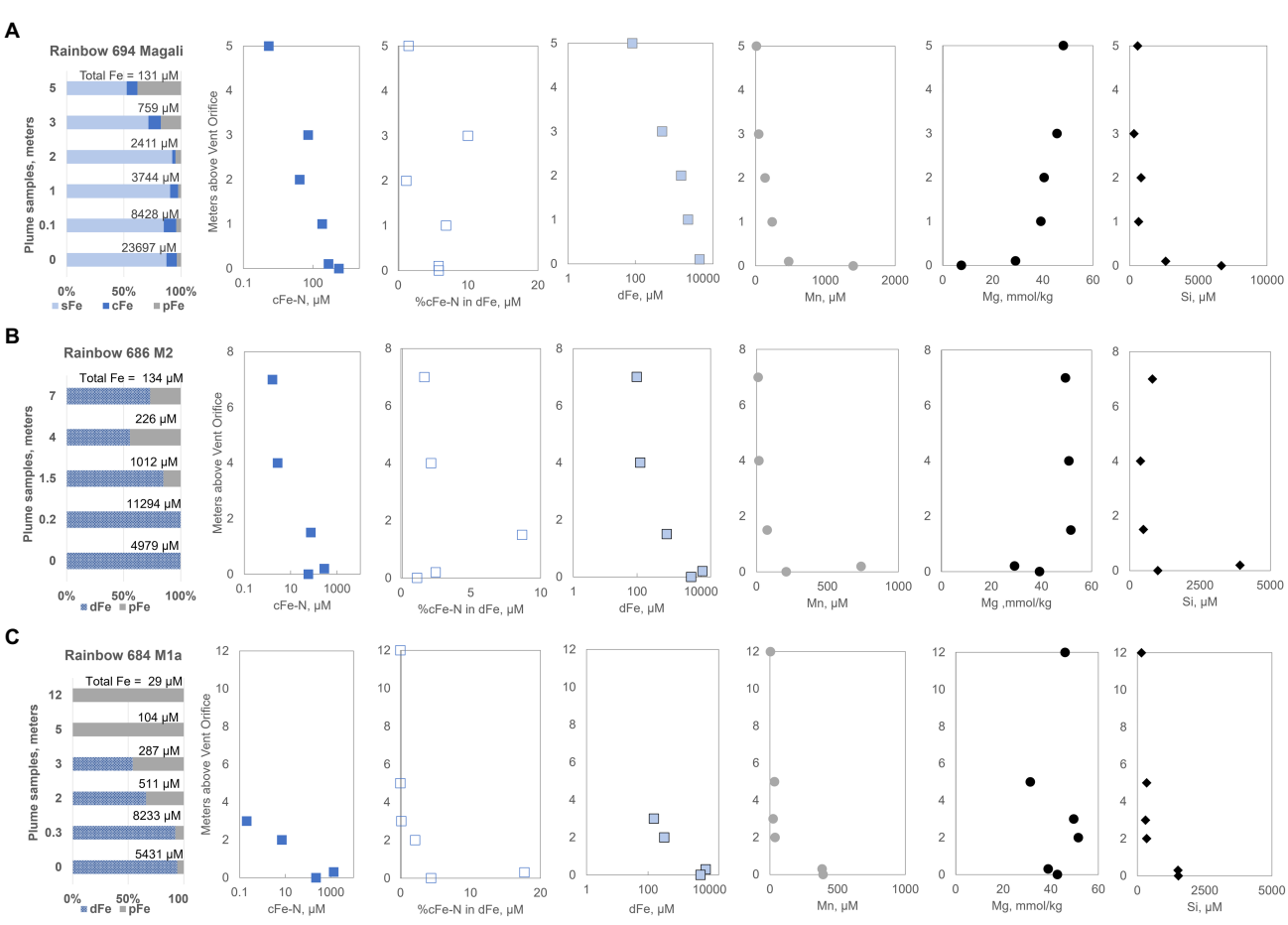

FIGURE 3 | Iron size fractionation data for Rainbow vent fluids **(A)** Magali, **(B)** Fumeur Nouveau (M2), and **(C)** Fumeur Tres Dense (M1a) are presented along with profiles containing distance from the orifice vs. measured different chemical species (e.g., cFe-N, dFe, Mn, Mg, and Si). sFe, soluble iron; cFe, colloidal iron; pFe, particulate iron; cFe-N, nanoparticle iron; dFe, dissolved iron.

additional dissolved tracer data were obtained. We considered Mg as a conservative tracer of seawater with typical depletion in vent fluids and Mn and Si as fluid tracers as they are also sourced from hydrothermal high-T emissions. In Broken Spur, a maximum of 330 μM of dissolved Mn was detected at the orifice of the Dragon XIII chimney (**Figure 2C**). Other chimneys still emitted Mn levels around 200 μM. We observed that in the uppermost 2 m about 10 μM level of Mn is retained in the plume with little variation. At a height of 5 m above the Spire orifice, dissolved Mn was about 9 times higher than dFe (**Figure 2A**). Mg concentrations displayed expected depletion toward the orifice with a minimum of 6.9 mmol/kg measured at Dragon XIII. The Mg profiles of the Dragon XIII and Chandelier plumes display a logarithmic shape implying a regular mixing curve, while the first two samples near the orifice of Spire gave strong indications of a high fraction of seawater mixing just above the orifice (**Figure 2**). Silica concentrations were high: a maximum of 8,991 μM of dissolved Si was found in Chandelier, with decreasing concentrations over the plume height. Several hundred μM of Si was still retained in the upper part of the plume and entered the deep ocean from Broken Spur vents.

Rainbow vents had higher concentrations of Mn (max. 1,398 μM) compared to Broken Spur; however, the Mn levels in the upper part of the plumes had a range of 3–12 μM, similar to that of Broken Spur (**Figure 3**). The maximum Si at the high-T end was 6,670 μM with a range of 153–807 μM. Si was still present beyond the 5-m height. Mirroring the Si profiles, the Magali plume showed a steady decrease with height with a relatively depleted high-T end. M1a and M2 plumes displayed higher levels of seawater mixing, which may also have caused the high fractions of particulates found in these samples.

DISCUSSION

A Dynamic Colloidal Pool Controls Size Fractionation and Nanoparticle Dynamics in Plumes

As summarized in **Figure 4**, the particulate fraction in Broken Spur is significant in all sections of the rising plumes, but in Rainbow, it shows a marked logarithmic increase toward the upper part of the plume. This is possibly related to the lower Fe:S ratios in the Broken spur end-member fluids, which favors the formation of particulates in the high-temperature samples. This would support the findings of Yücel et al. (2011) and Findlay et al. (2015, 2019). In Rainbow, particulate iron formation seems to be largely driven by oxidation in the upper part of the plumes. Although the colloidal fraction is invariant in Rainbow, a slight increasing tendency occurs in Broken Spur. With an average of 15%, the Broken Spur colloidal fraction exceeds that of Rainbow (8%). While quantitatively Rainbow's input is more significant, Broken Spur's lower Fe:S ratios might have favored colloidal iron formation. The colloidal fraction of iron in the Broken Spur proximal vent plumes, presumably made up of mostly sulfides, could be produced in the subsurface or very near the orifice as shown by Yücel et al. (2011) and Findlay et al. (2019) for similar low Fe:S EPR vent fluid and plumes. The colloidal fraction grows toward the upper part of the rising plume as the vent fluid continues to mix with deep-sea water. In Rainbow, oxidative processes probably contribute to particulate formation, but this is not reflected in the colloidal fraction. Two hypotheses can be proposed: 1- a stable colloidal phase is formed early on and transported conservatively upwards, where Fe oxides are quickly transformed into large particles and settle 2- the initial colloidal phases (which form in the high-T fluid) are lost but new phases that form in the plume enter the colloidal phase, implying a dynamic colloidal pool.

For further insights into the composition of the colloidal pool, we also investigated the relationship between the fraction of nitric acid-leachable colloids (cFe-N – which we attribute to Fe mineral nanoparticles except for refractory silicates) in the whole cFe pool mixing with seawater. As shown in **Figures 4C,F**, the range of cFe-N in both sites can be as much as 100% of the whole cFe, and the two vent fields do not show a significant difference in that regard. This maximum is reached around the 40 mM Mg level, which corresponds to the first 1–1.5 m above the orifice, showing that the cFe-N pool is produced below and immediately above the vent orifice. The upper parts of the mixing plume are more labile; hence, HCl extractable colloids become more important. In Broken Spur, this could be due to FeS nanoparticle/cluster formation, which would be retrievable through a mild acid treatment. In Rainbow, the relative stability of the cFe fraction was mentioned earlier, but here, we find that its composition may shift to more labile, plume-forming components. This point then may support the second hypothesis above, implying a dynamic pool of colloids in Rainbow perhaps supplanted by the mixing-induced formation of new phases. Even so, it must be noted that each site at the top of the sampled area emits significant (max 0.7 μM in Broken Spur and 1.6 μM in Rainbow) levels of cFe-N, emphasizing the early production and conservative mixing of possible nanoparticles of pyrite, non-labile iron oxides (goethite, hematite) or more elusive phases of HNO_3 extractable silicates and even organic Fe phases.

Interplay of Silicates, Sulfur, Oxygen, and Iron in Controlling (Nano)Particle Composition

The Rainbow and Broken Spur vent fields provide insight into not only on understanding how much cFe-N is being produced in different vent settings but also how different geochemistry may affect the compositional evolution of (nano)particles both from the subseafloor and throughout the rising plume. It has already been shown that Broken Spur has fluids rich in $\sum H_2S$ and a comparable amount of Fe, which creates low Fe:S ratios. On the other hand, Rainbow produces fluids with much higher Fe:S ratios (Douville et al., 2002; Charlou et al., 2010). It is also important to notice that the relatively high concentrations of other transition metals, such as Cu and Zn (e.g., Cu and Zn: ~260 μM from Seyfried et al., 2011), observed in Rainbow

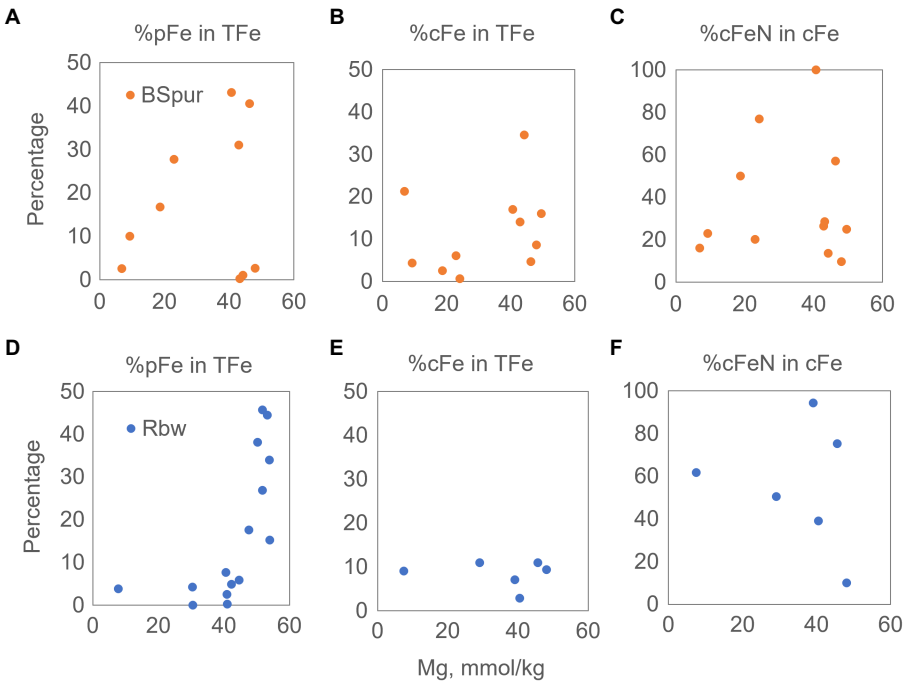

FIGURE 4 | Measured concentration of aqueous Mg versus calculated fractions of %pFe, %cFe in TFe, and %cFe-N in cFe for Broken Spur **(A–C)** and Rainbow **(D–F)** vent fluids. cFe, colloidal iron; pFe, particulate iron; cFe-N, nanoparticle iron; TFe, total iron.

fluids have significant implications on sulfide dynamics in the Rainbow hydrothermal mixing zone since they can precipitate with sulfide species at decreasing temperatures and remove a comparable amount of sulfide from the Rainbow fluids (Findlay et al., 2015).

The distinct geochemical systematics characterizing both vent fields have substantial implications on the quantitative production of cFe-N. For example, one of the main reasons behind the much higher concentration of cFe-N just next to the orifice and throughout the rising plume in the Rainbow vents might be that the Rainbow fluids have a much higher end-member Fe concentration (24–26.5 mM) compared to Broken Spur (570–900 μM). Around 0–0.1 m from the orifice, cFe-N concentrations were between 1,326–467 μM in Magali, 224–1,346 μM in Fumeur Tres Dense, and 57–281 μM in Fumeur Nouveau (**Figures 3A,C**). On the other hand, quantitatively a much smaller cFe-N pool was detected at the immediate exit of the Broken Spur fluids, reaching only 2–1.8 μM in Spire, 8.24–8.61 μM in Chandelier and 25.6–3.9 μM in Dragon XIII (**Figures 2A,C**). Despite the large initial Fe difference at the high-T end of the plume, the cFe-N does not differ significantly in the upper parts of the buoyant plume in the Rainbow fluids when compared to Broken Spur. For example, we have measured 1.23, 1.64, and 0.2 μM of cFe-N in the coolest hydrothermal fluid samples from the Magali, Fumeur Nouveau and Fumeur Tres Dense orifices, respectively. On the other hand, cFe-N was 0.1 μM at 5 m from Spire orifice, 0.67 μM at 3 m from the Chandelier orifice, and an even sharper decrease in Dragon XIII, where cFe-N was measured as 0.62 at 1.5 m from the orifice. It seems, therefore, that although the Rainbow fluids create slightly more cFe-N at the immediate exit from the orifice, a higher fraction of the cFe-N pool is being lost in the rising Rainbow plumes, while the cFe-N in the Broken Spur fluids seems more conservative.

In order to understand the plume dilution and evolution mechanisms creating this shift in the rising plume, correlations for Fe, Si, and Mn were examined for each of the vent fluids. Additionally, since Mg exhibits a conservative behavior during the mixing of end-member hydrothermal fluids with seawater, we preferred to use Mg as a mixing tracer (**Figure 5**). Seawater is rich in Mg, while hydrothermal fluid end-members have near-zero Mg concentrations due to the reactions of fluids with basalt, gabbro, and peridotite at high temperatures and low water/rock ratios (Bischoff and Dickson, 1975; Mottl and Holland, 1978; Seyfried and Bischoff, 1981; Janecky and Seyfried, 1986; Seyfried et al., 2007). Therefore, a mixing line is created between the average end-member fluid compositions of corresponding vent fluids and background seawater (e.g., McDermott et al., 2020). Comparison of element distributions with the mixing line indicates removal and/or enrichment of corresponding element.

Dissolved iron in the Rainbow and Broken Spur fluids exhibits strong positive correlation with Si and Mn (**Figures 6A,D**), except for the Dragon XIII fluids. These strong correlations show that Si is an important cue to iron and manganese geochemistry in both Rainbow and Broken Spur fluids, and its geochemical behavior in the plume might resemble that of Fe and Mn. The strong positive correlation between

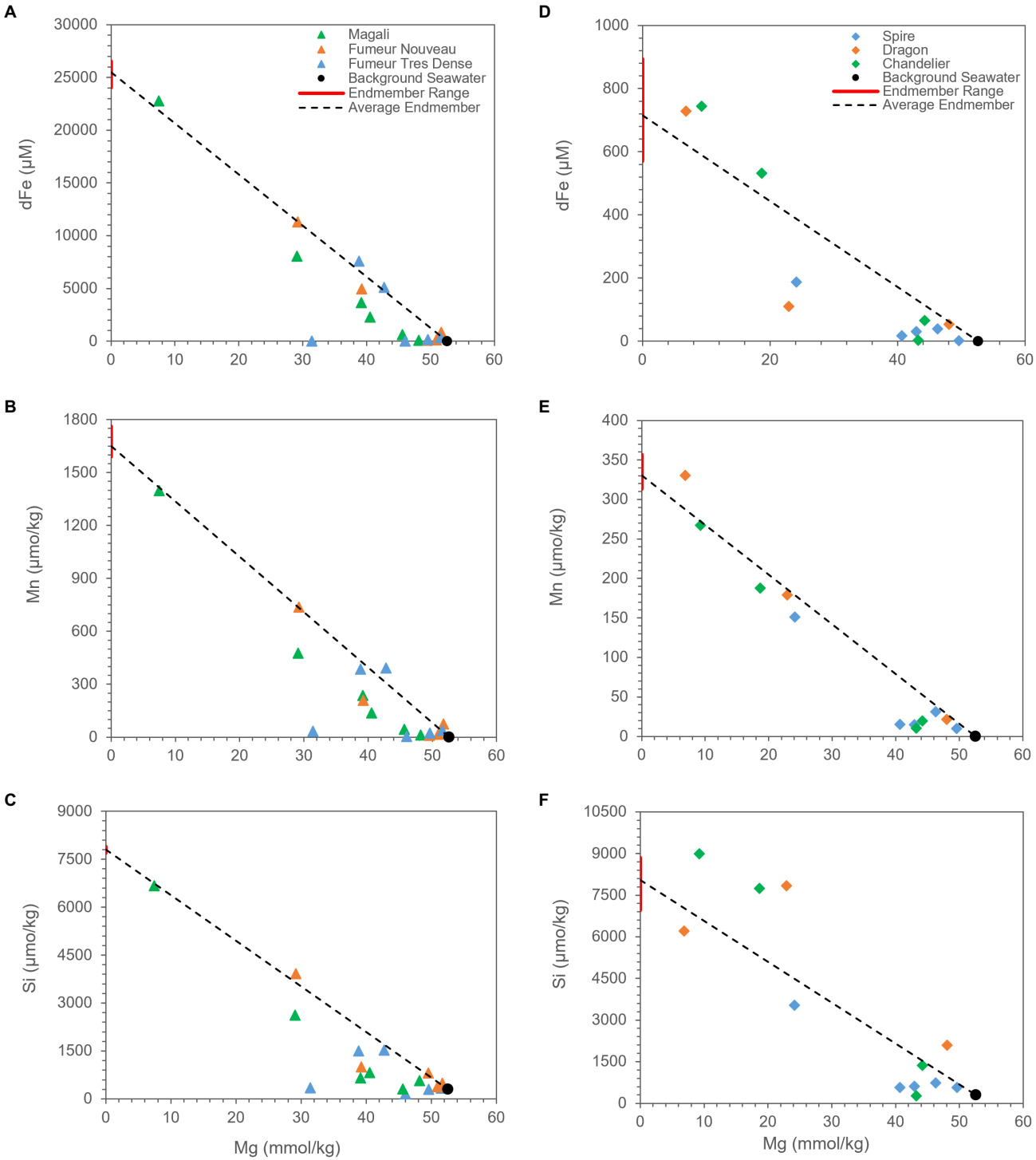

FIGURE 5 | Measured concentrations of aqueous Mg vs. dFe, Mn, and Si for fluid samples from Rainbow **(A–C)** and Broken Spur **(D–F)** vents. For each species, the range in extrapolated zero Mg high-temperature end-member composition is shown with the red bar along the y axis, and the average is shown with a black line projected from seawater composition. Species that exhibit conservative behavior during mixing plot on the line, while species that behave non-conservatively plot above or below the line.

Si and Fe and the similar removal trends they exhibit for some sites might support the hypothesis that Fe and Si precipitate together (or aggregate as nanoparticles) in the rising plume. As has been shown, silicates impact Fe (II) oxidation rates (Jones et al., 2009; Kinsela et al., 2016) and Fe (III) silicate complexation could be critical under high silicate concentrations

(Patten and Byrne, 2017). Therefore, Fe (II) silica co-precipitates may play a role in stabilizing colloids (Mayer and Jarrell, 1996; Francisco et al., 2020). Findlay et al. (2015) indicated that a substantial amount of Fe (in the mM level) would stay in the buoyant plume and might precipitate in and/or be adsorbed by silicate forms. Different studies have shown that Si-containing particles, such as amorphous silica and kaolinite, are present in hydrothermal vent plumes (Feely et al., 1990;

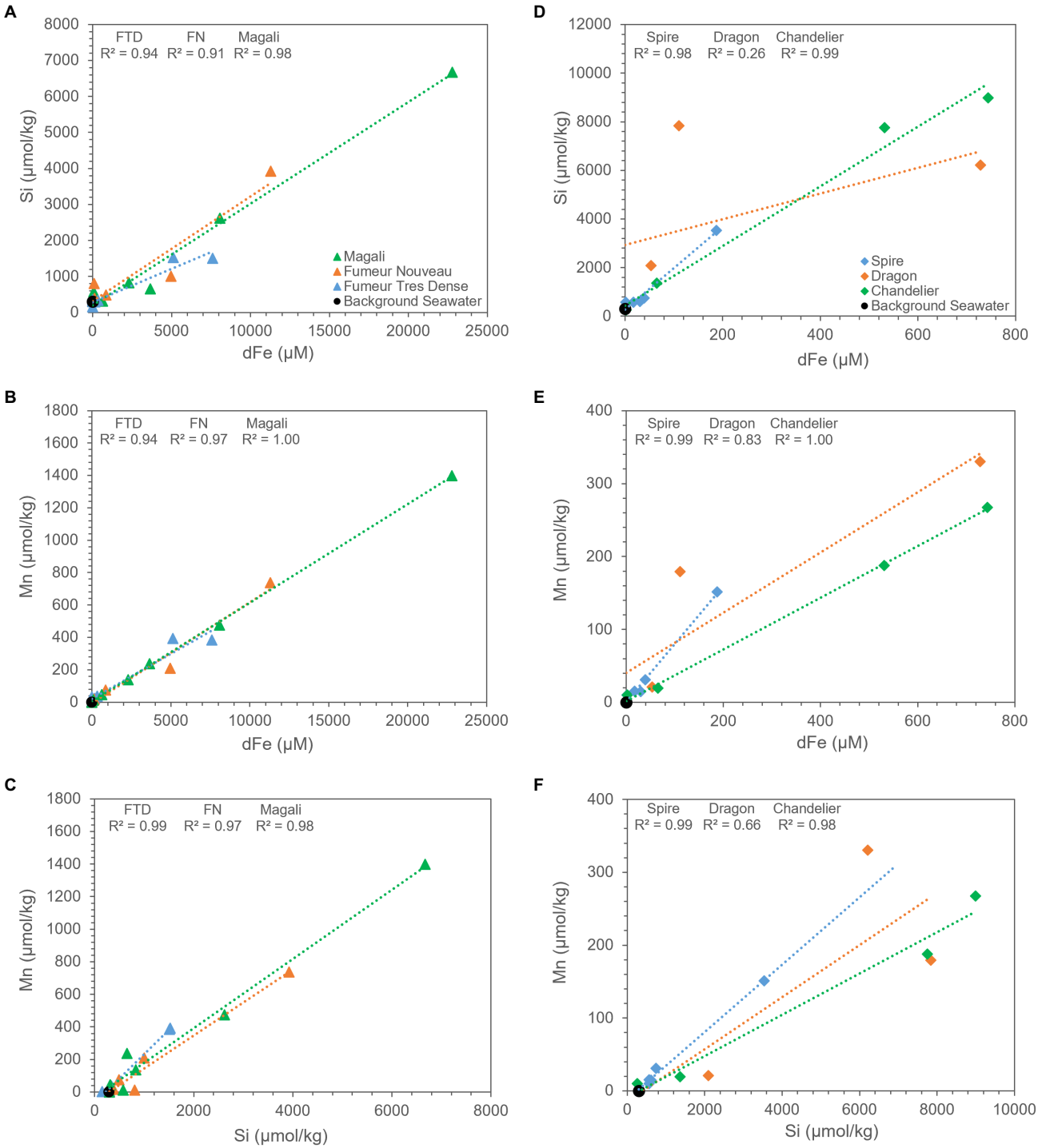

FIGURE 6 | Relationship between measured concentrations of dissolved iron, Si, and Mn in Rainbow **(A–C)** and Broken Spur **(D–F)** vents. Rainbow fluids exhibit very high correlation with Si and Mn in all its vents likewise Broken Spur vent fluids except for Dragon XIII, where scarcity in data might create deviation from correlation for both Si and Mn. Statistical parameters are given on the plots.

Gartman et al., 2014). However, silicate phases might not be restricted to only these forms, and Fe containing silicate (nano)particles have been shown to be an important fraction in plume geochemistry (Gartman et al., 2014; Estes et al., 2018).

Indeed, the existence of iron silicate nanoparticles is evident in Earth history, and recent studies have suggested that they (e.g., stilpnomelane and greenalite) might have been the primary sediments mediating mobilization and transportation of iron in the Precambrian oceans (Rasmussen et al., 2015; Johnson et al., 2018). Furthermore, the oxidation rate of iron in hydrothermal plumes in deep Atlantic waters is very high compared to other basins (e.g., oxidation half-lives of iron are ~17 and ~27 min for Rainbow and TAG plumes at the MAR, respectively) (Field and Sherrell, 2000; Gartman and Findlay, 2020). Different studies have indicated that the oxidation products of dissolved iron (Fe-Ox) are crucial players in plume geochemistry since they form a considerable fraction of the Fe pool and act as strong scavengers for different elements (Mottl and McConachy, 1990; Rudnicki and Elderfield, 1993; Feely et al., 1996; Field and Sherrell, 2000; Breier et al., 2012; Fitzsimmons et al., 2017; Waeles et al., 2017; Hoffman et al., 2018). Therefore, in addition to Fe-Si forms, Fe-Ox might be responsible for sustaining a considerable amount of dissolved iron in the rising plume as well.

Mn is assumed to exhibit conservative behavior during plume development since its oxidation rate is very slow, and it does not tend to precipitate in sulfide phases (Feely et al., 1994; Breier et al., 2012; Resing et al., 2015). However, our data demonstrate that Rainbow and Broken Spur fluids show depletions with respect to Mg (**Figures 5B,E**). In Rainbow fluids, Findlay et al. (2015) observed a similar Mn removal trend within the first 1-m from the vent orifice. It has already been shown that Mn removal rates can differ from basin to basin. Moreover, different processes, such as the microbial oxidation of Mn and the scavenging of Mn with particles like Fe-Ox, might be responsible for Mn removal in the plume (Campbell et al., 1988; Cowen et al., 1990; Dick and Tebo, 2010; Dick et al., 2013). Additionally, Findlay et al. (2015) indicated that Rainbow has much more particulate Mn when compared to other low Fe:S vent fluids, such as TAG. Since Mn oxidation is not expected within the first couple of meters from the orifice, a major portion of particulate Mn might come from the incorporation of Mn into silicate phases and/or the scavenging of Mn by other particles. A strong positive correlation between Mn and Si can be seen in **Figure 6C**, and their similar removal trends are shown in **Figure 5**, which might support the idea that Mn and Si are closely related to each other in the rising plume. As a result, the relatively higher Mn removal trend starting at heights shallower than the orifice in Rainbow fluids might indicate that oxides and silicates have pivotal roles in the compositional evolution of Rainbow plumes when compared to Broken Spur, where Mn removal exhibits relatively higher conservative behavior (**Figures 5B,E**).

Various studies have indicated that sulfide species are responsible for partitioning Fe into mainly sulfide forms in vent fluids (Mottl and McConachy, 1990; Field and Sherrell, 2000). The main controlling mechanism in the formation of Fe bearing sulfide (nano)particles is attributed the Fe:S ratio of the hydrothermal fluids (Field and Sherrell, 2000). For example, German et al. (2002) calculated that precipitation of iron with sulfides accounts for 80–90% of dissolved iron removal in low Fe:S 13°N EPR fluids, while the formation of Fe-Ox particles is responsible for 10–20% of dissolved iron removal. However, Edmonds and German (2004) indicated that the high Fe:S ratio of Rainbow fluids causes only 4% of total Fe precipitating as sulfide minerals. A more recent study conducted by Waeles et al. (2017) showed that a relatively smaller fraction of hydrothermal Fe (<10%) is precipitated as sulfide minerals, and Fe oxidation is a major process in the removal of hydrothermal iron in vent systems. Nevertheless, different studies agree that Fe-sulfide and Fe-Ox phases (as well as mixed oxide/sulfide phases) are essential parts of the plume geochemistry in varying proportions, depending on the setting.

As an additional point, **Figures 2, 3** indicate that Fe fractions (both dFe and cFe-N) exhibit an apparent exponential loss as the hydrothermal plumes rise. Therefore, we examined the e-folding loss rates of dFe and cFe-N in the Rainbow and Broken Spur plumes in order to better estimate the removal trend of these species (**Supplementary Figures S1**, **S2**). This analysis shows that simple dilution is not the only controlling mechanism in the removal of Fe phases, as also indicated in **Figure 5**. On the other hand, the removals are all related to the first order dependence of dFe and cFe-N concentrations. Furthermore, the slopes of the trend lines in **Supplementary Figures S1**, **S2** might give clues about removal rates in the rising plumes. For example, Broken Spur has a higher dissolved iron removal rate (~%33) when compared to the Rainbow rising plume. Accordingly, earlier domination of particulate iron in the Broken Spur plume is valid, as indicated in **Figure 4**. Additionally, the removal rate of cFe-N phases in the Broken Spur plume is much less when compared to dFe. It indicates that stable FeS (nano)particles exhibit more chemical stability. However, the presence of more labile (nano) particles (e.g., oxides) in the Rainbow rising plume decreases the overall stability of cFe-N and increases the rate of removal as the plume evolves.

Our results suggest that Fe-Si and Fe-Ox (nano)particle forms might become a critical fraction of the colloidal pool during fluid ascension and dilution for both vent fields. At Broken Spur, however, a significant fraction of sulfide nanoparticles might exert the primary control on compositional evolution cFe-N in the rising plume. We also suggest that Rainbow fluids have a much more dynamic environment in the case of cFe-N formation as a result of silicates and oxides forming in the plume, while the immediate formation and predominance of sulfide forms in Broken Spur fluids generate more stable forms of cFe-N. Therefore, a dynamic colloidal pool exists at Rainbow and might be responsible for the observation of a shift of a very high concentration of cFe-N at the vent orifice but the removal of a large fraction up in the buoyant plume. Additionally, metal silicate phases are not thought to be extractable with HCl and HNO_3 treatments (Huerta-Diaz and Morse, 1992); therefore, quantitative understanding of the cFe-N silicate pool in the rising plume

is required for future studies. As an additional factor, organic matter should not be entirely disregarded in the high-T mixing zones. Entrainment near and around diffuse and high-T vent orifices, and the stabilization of nanoparticles with OM before the OM is thermally degraded also needs to be taken into account in the near-field export of iron. Hence, in addition to the now better understood role of inorganic sulfide nanoparticles, the complex interplay of silicate phases as well as the organic derivatives from local chemosynthetic-sourced organic matter should be accounted for (Bailly-Bechet et al., 2008; Bennett et al., 2011).

Input of Fe to the Deep Atlantic and Its Role in Biogeochemical Cycles

The lowest temperature samples in our mixing zone profiling (<10°C) still contained at least 0.5 μM of only nitric acid-leachable nanoparticle/colloidal iron, which is approximately 200 times higher than a typical Fe concentration in the non-buoyant plume. The larger colloidal pool (cFe) reached a maximum of 12 μM in the upper part of the mixing zone, constituting a significant flux of cFe to the deep Atlantic. Kunde et al. (2019) reported full water column depth profiles in the Northern Atlantic and found that up to 76% of TFe was cFe in the deep-sea part of the profile and cFe rose to 92% in the samples from a hydrothermal plume, where concentrations increased to as much as 30 nM. They proposed an hourglass shape for Fe vertical distribution in the Northern Atlantic, where cFe becomes the dominant Fe phase in the euphotic zone and deep zone. This is consistent with earlier work by Fitzsimmons et al. (2015), which claims an 89–96 cFe percentage in the plume of the nearby TAG vent field. While it is still unclear whether the cFe detected is fully hydrothermal in origin or represents cFe recycled from sFe and pFe from the vents, it is at least possible to achieve these levels from a simple dilution of a high-T produced colloidal pool, including HNO_3 extractable pyrite-type nanominerals. While Findlay et al. (2015) showed the emanation of Fe, Zn, and Cu sulfides from the MAR, solid state particulate speciation work from the upper part of the plume found no evidence of Fe-sulfide particles in the neutrally buoyant plume of TAG (Ohnemus and Lam, 2015). Lough et al. (2019b) also failed to detect any iron sulfides in the water column in the slow-spreading Von Damm vent field in the Caribbean Sea. Such high Fe:S vent fluids might result in low levels of dissolved sulfide. Accordingly, the slow-spreading systems examined so far perhaps emit limited levels of pyrite nanoparticles, but our results show that they may still be forming in high-T end-members. Silicate-including nanoparticles may also have a dominant role, especially in Rainbow-like systems (Estes et al., 2018; Luther et al., 2020). It can be further proposed that such particles may offer substrates for plume microbes using sulfur or iron as electron acceptors, thus leading to the redissolution and precipitation of iron under different oxide and organic phases.

The extrapolation of our results to broader lengths of the MAR system as well as to the global ridge system is less straightforward, but it can be stated that the spreading rate can exert a first order control on stable iron fluxes. In particular, Rainbow could be representative of serpentinized systems that may be widespread on slow/ultraslow-spreading ridges with a potential for high Fe:S end-members. Previously, based on low ^{3}He emissions and their specific topography, slow-spreading systems were thought to export less Fe to deep ocean basins. Now, at least for slow-spreading MAR, it is becoming established that a persistent colloidal pool is generated due to hydrothermal emissions, and iron nanoparticles may play a role in generating a high flux in the early phase of plume formation. While our digestion scheme did not include silicate fractions, our results on Si, Mg, and Fe collectively show that silicate nanoparticles can play a larger role in this type of slow-spreading system. More work integrating a comparative, multi-site sampling will possibly reveal different ridge or back-arc types generating a specific carrier phase, eventually providing different and improved parametrization possibilities for models. Both deep-sea ecosystem models and carbon cycling (German et al., 2015; Le Bris et al., 2019), as well as global climate models (Tagliabue et al., 2016), can benefit from this. Diffuse hydrothermal sources are also essential contributors of iron to the deep waters (Le Bris et al., 2019; Lough et al., 2019b), and a similar small-scale profiling study and size fractionation analyses are needed to explore the distinct, possibly biologically transformed unique (nano) particle dynamics in and around vents.

Finally, it must be emphasized that understanding such size fractionation and nanoparticle dynamics around vents is vital and not just from the traditional chemical oceanographic perspective that focuses on euphotic zone productivity. Iron speciation and size fractionation, through the high catalytic role of nanoparticles, should play a role in transforming deep-sea organic carbon pools and influence the biological interaction of metals and carbon. Global and regional models can therefore benefit from a better parametrization of iron fluxes, not only from vents, but also other systems such as seeps and reducing sediments. This will be necessary to eliminate uncertainties with regard to carbon cycling and enable better estimations of future climate states as well as improve our understanding of past climate shifts (glacial times, carbon sinks, etc.). The Earth system hosts many seafloor redox gradients, high-T, and diffuse vents to cold seeps and reducing sediments, in most of which filter-passing nanoparticles may be abundant across marine redox gradients where metal turnover is orders of magnitude higher than other ocean zones (**Figure 7**). These nanoparticle fluxes, in turn, could explain the persistence of benthic and hydrothermal iron fluxes in the ocean interior, as consistently reported in various oceanic transects arising from the GEOTRACES project (Resing et al., 2015; Fitzsimmons et al., 2017). Furthermore, nanoparticle and colloid formation and accumulation may amplify under redox oscillations frequently encountered in marine chemoclines (as a result of physical forcing) or in the mixing zone of reduced hot vents with the oxidized, cold seawater. This will gain importance as dramatic changes are anticipated in metal cycles: global warming, marine deoxygenation, and acidification may increase metal mobility in the Earth system, possibly amplifying internal metal fluxes between oceanic compartments (Basile-Doelsch et al., 2015; Eiriksdottir et al., 2015).

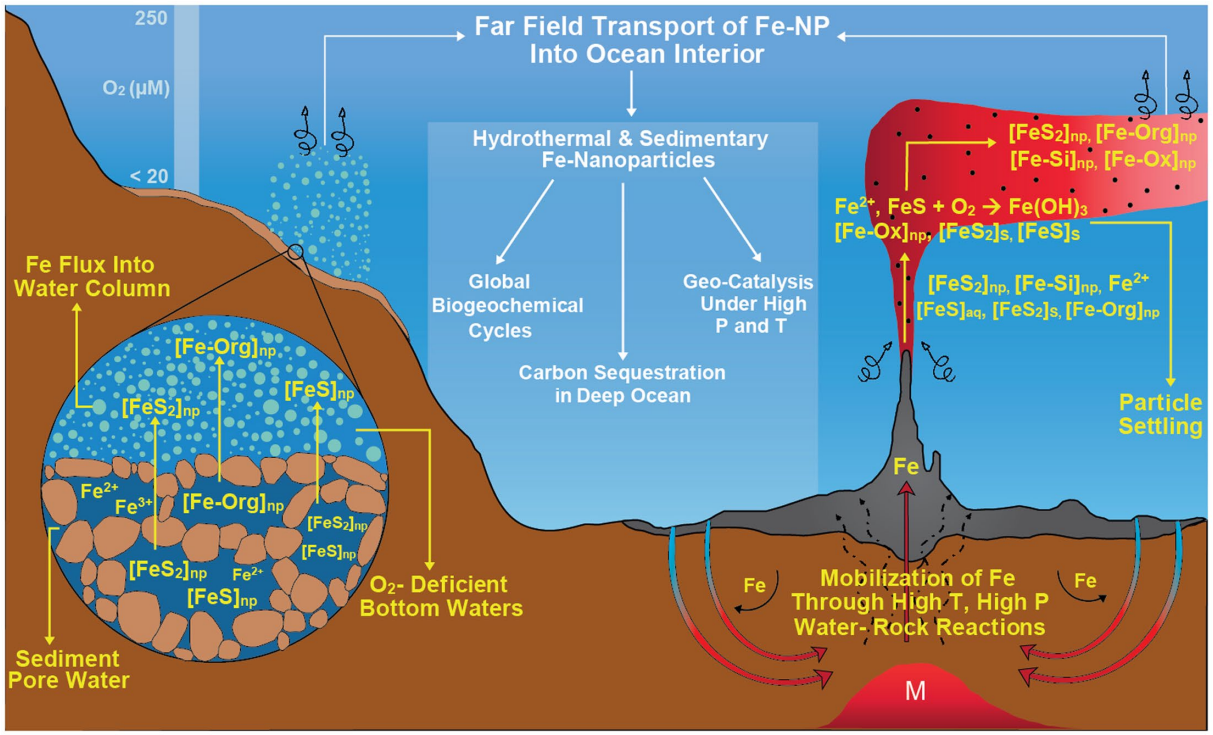

FIGURE 7 | Nanoparticles as an important geochemical actor across naturally occurring marine redox gradients such as high-temperature hydrothermal vents and reducing sediments where metal turnover is orders of magnitude higher compared to other ocean zones. These nanoparticle fluxes might have a primary role in global biogeochemical cycles, carbon sequestration in deep ocean and geo-catalysis under high pressure and temperature conditions.

CONCLUSION

We have observed that a colloidal fraction, cFe, is a persistent feature of hydrothermal vent mixing zone samples from the high-temperature source fluids at the Broken Spur (basalt-hosted) and Rainbow (serpentinite-hosted) vent fields of the Mid-Atlantic Ridge. The cFe fraction is either stable or generally grows with distance from the vent orifice, and our detailed analysis shows that it is a biogeochemically dynamic and significant pool. This colloidal pool changes in composition as the colloidal particles appear to be more HCl extractable in the samples more distant from the orifice. The HNO_3 extractable fraction is significant in the mid-plumes in the sulfide-rich Broken Spur vents. Our results complement previous reports of dissolved Fe in MAR vents. With its rich geological variety of hydrothermal vents, nanoparticle export is a persistent feature of the Northern Mid-Atlantic Ridge. Moreover, we show for the first time that Broken Spur vents, with a different Fe:S end-member ratio, are also a principal source of nanoparticles to the near-field. We propose that this recalcitrant Fe pool – surviving the immediate precipitation – is the fraction that maintains high hydrothermal iron fluxes to the deep ocean. If vent iron inputs are shown to be sustained over different time periods, this previously overlooked mechanism has the capacity to sustain fluxes of ecosystem-limiting metals originating from the ocean's interior.

DATA AVAILABILITY STATEMENT

The original contributions presented in the study are included in the article/**Supplementary Material**; further inquiries can be directed to the corresponding author.

AUTHOR CONTRIBUTIONS

MY and NLB designed the study and steered the sampling during the TRANSECT campaign. MY and SS performed the subsampling, onboard measurements, and sample fixation for on-shore analyses. MY, SS, and NLB analyzed the data and drafted the manuscript. All authors contributed to the article and approved the submitted version.

FUNDING

The cruise was funded by the French Oceanographic Fleet and CNRS-INEE to LECOB (NLB). Transect Cruise DOI: https://doi.org/10.17600/18000513

ACKNOWLEDGMENTS

The authors are grateful to the Master and crew of the 2018 N/O L'Atalante TRANSECT campaign for a very successful cruise

(Transect Cruise DOI: https://doi.org/10.17600/18000513). Specifically, we thank the ROV Victor 6000 group for the excellent seafloor sampling operations. MY acknowledges the Turkish Academy of Sciences, Young Investigator Grant (TÜBA-GEBIP) as well as the Science Academy – BAGEP award, which supported traveling and part of the on-shore analyses. MY acknowledges further support from TUBITAK BIDEB 2247 project (contract no 119C107) DEEPREDOX and DEKOSIM project of METU-IMS for enabling the completion of the analyses and supporting the drafting of this manuscript. We would also like to thank Nimet Alimli for her valuable contributions to the discussion.

SUPPLEMENTARY MATERIAL

The Supplementary Material for this article can be found online at: https://www.frontiersin.org/articles/10.3389/fmicb.2021.631885/full#supplementary-material

REFERENCES

Ardyna, M., Lacour, L., Sergi, S., d'Ovidio, F., Sallée, J. B., and Rembauville, et al., (2019). Hydrothermal vents trigger massive phytoplankton blooms in the Southern Ocean. *Nat. Commun.* 10:2451. doi: 10.1038/s41467-019-09973-6

Bailly-Bechet, M., Kerszberg, M., Gaill, F., and Pradillon, F. (2008). A modeling approach of the influence of local hydrodynamic conditions on larval dispersal at hydrothermal vents. *J. Theor. Biol* 255, 320–331. doi: 10.1016/j.jtbi.2008.08.016

Basile-Doelsch, I., Balesdent, J., and Rose, J. (2015). Are interactions between organic compounds and nanoscale weathering minerals the key drivers of carbon storage in soils. *Environ. Sci. Technol.* 49, 3997–3998. doi: 10.1021/acs.est.5b00650

Bennett, S. A., Statham, P. J., Green, D. R. H., Le Bris, N., McDermott, J. M., Fahnestock, M. F., et al. (2011). Dissolved and particulate organic carbon in hydrothermal plumes from the East Pacific Rise, 9 50'N. *Deep-Sea Res. Part I* 58, 922–931. doi: 10.1016/j.dsr.2011.06.010

Bischoff, J. L., and Dickson, F. (1975). Seawater-basalt interaction at 200°C and 500 bars: implications for origin of sea-floor heavy-metal deposits and regulation of seawater chemistry. *Earth Planet. Sci. Lett.* 25, 385–397. doi: 10.1016/0012-821X(75)90257-5

Boyd, P. W., and Ellwood, M. J. (2010). The biogeochemical cycle of iron in the ocean. *Nat. Geosci.* 3, 675–682. doi: 10.1038/ngeo964

Breier, J. A., Toner, B. M., Fakra, S. C., Marcus, M. A., White, S. N., Thurnherr, A. M., et al. (2012). Sulfur, sulfides, oxides and organic matter aggregated in submarine hydrothermal plumes at 9°50'N East Pacific Rise. *Geochim. Cosmochim. Acta* 88, 216–236. doi: 10.1016/j.gca.2012.04.003

Buck, K. N., Sedwick, P. N., Sohst, B., and Carlson, C. A. (2018). Organic complexation of iron in the eastern tropical South Pacific: Results from US GEOTRACES Eastern Pacific Zonal Transect (GEOTRACES cruise GP16). *Mar. Chem.* 201, 229–241. doi: 10.1016/j.marchem.2017.11.007

Campbell, A. C., Palmer, M. R., and Klinkhammer, G. P. (1988). Chemistry of hot springs on the Mid-Atlantic Ridge. *Nature* 335, 514–519. doi: 10.1038/335514a0

Charlou, J. L., Donval, J. P., Fouquet, Y., Jean-Baptiste, P., and Holm, N. (2002). Geochemistry of high H2 and CH4 vent fluids issuing from ultramafic rocks at the rainbow hydrothermal field (36°14'N, MAR). *Chem. Geol.* 191, 345–359. doi: 10.1016/S0009-2541(02)00134-1

Charlou, J. L., Donval, J. P., Konn, C., Ondréas, H., and Fouquet, Y. (2010). "High production and fluxes of H_2 and CH_4 and evidence of abiotic hydrocarbon synthesis by serpentinization in ultramafic-hosted hydrothermal systems on the Mid-Atlantic Ridge," in *Diversity of Hydrothermal Systems on Slow Spreading Ocean Ridges. Vol. 188.* eds. P. A. Rona, C. W. Devey, J. Dyment and B. J. Murton, American Geophysical Union Monograph Series (Washington, DC: AGU), 265–295.

Cline, J. D. (1969). Spectrophotometric determination of hydrogen sulfide in natural waters. *Limnol. Oceanogr.* 14, 454–458.

Cowen, J. P., Massoth, G. J., and Feely, R. A. (1990). Scavenging rates of dissolved manganese in a hydrothermal vent plume. *Deep-Sea Res.* 37, 1619–1637. doi: 10.1016/0198-0149(90)90065-4

Dick, G., Anantharaman, K., Baker, B. J., Li, M., Reed, D. C., and Sheik, C. S. (2013). The microbiology of deep-sea hydrothermal vent plumes: ecological and biogeographic linkages to seafloor and water column habitats. *Front. Microbiol.* 4:124. doi: 10.3389/fmicb.2013.00124

Dick, G. J., and Tebo, B. M. (2010). Microbial diversity and biogeochemistry of the Guaymas deep-sea hydrothermal plume. *Environ. Microbiol.* 12, 1334–1347. doi: 10.1111/j.1462-2920.2010.02177.x

Douville, E., Charlou, J. L., Oelkers, E. H., Bienvenu, P., Jove Colon, C. F., Donval, J. P., et al. (2002). The rainbow vent fluids (36°14'N, MAR): the influence of ultramafic rocks and phase separation on trace metal content in Mid-Atlantic Ridge hydrothermal fluids. *Chem. Geol.* 184, 37–48. doi: 10.1016/S0009-2541(01)00351-5

Edmonds, H. N., and German, C. R. (2004). Particle geochemistry in the rainbow hydrothermal plume, Mid-Atlantic Ridge. *Geochim. Cosmochim. Acta* 68, 759–772. doi: 10.1016/S0016-7037(03)00498-8

Eiriksdottir, E. S., Gislason, S. R., and Oelkers, E. H. (2015). Direct evidence of the feedback between climate and nutrient, major, and trace element transport to the oceans. *Geochim. Cosmochim. Acta* 166, 249–266. doi: 10.1016/j.gca.2015.06.005

Estes, E. R., Berti, D., Hochella, M. F. Jr., Findlay, A., Gartman, A., Shaw, T. J., et al. (2018). Production and Transport of Fe- and Mg-bearing Silicate Nanoparticles in Hydrothermal Fluids at the East Pacific Rise (9°50'N). American Geophysical Union. 10–14 December 2018. Washington, D.C., USA. Abstract retrieved from SAO/NASA Astrophysics Data System.

Feely, R. A., Baker, E. T., Marumo, K., Urabe, T., Ishibashi, J., Gendron, J., et al. (1996). Hydrothermal plume particles and dissolved phosphate over the superfast-spreading southern East Pacific Rise. *Geochim. Cosmochim. Acta* 60, 2297–2323. doi: 10.1016/0016-7037(96)00099-3

Feely, R. A., Geiselman, T. L., Baker, E. T., and Massoth, G. W. (1990). Distribution and composition of hydrothermal plume particles from the ASHES vent Field at axial volcano, Juan de Fuca Ridge. *J. Geophys. Res.* 95, 12855–12873. doi: 10.1029/JB095iB08p12855

Feely, R. A., Massoth, G. J., Trefry, J. H., Baker, E. T., Paulson, A. J., and Lebon, G. T. (1994). Composition and sedimentation of hydrothermal plume particles from North Cleft segment, Juan de Fuca Ridge. *J. Geophys. Res.* 99, 4985–5006.

Field, M. P., and Sherrell, R. M. (2000). Dissolved and particulate Fe in a hydrothermal plume at 9°45′N, East Pacific Rise: slow Fe (II) oxidation kinetics in Pacific plumes. *Geochim. Cosmochim. Acta* 64, 619–628. doi: 10.1016/S0016-7037(99)00333-6

Findlay, A. J., Estes, E. R., Gartman, A., Yucel, M., Kamyshny, A., and Luther, G. W. III (2019). Iron and sulfide nanoparticle formation and transport in nascent hydrothermal vent plumes. *Nat. Commun.* 10:1597. doi: 10.1038/s41467-019-09580-5

Findlay, A. J., Gartman, A., Shaw, T. J., and Luther, G. W. (2015). Trace metal concentration and partitioning in the first 1.5 m of hydrothermal vent plumes along the Mid-Atlantic Ridge: TAG, Snakepit, and rainbow. *Chem. Geol.* 412, 117–131. doi: 10.1016/j.chemgeo.2015.07.021

Fitzsimmons, J. N., Carrasco, G. G., Wu, J., Roshan, S., Hatta, M., Measures, C. I., et al. (2015). Partitioning of dissolved iron and iron isotopes into soluble and colloidal phases along the GA03 GEOTRACES North Atlantic transect. *Deep-Sea Res. Part II* 116, 130–151. doi: 10.1016/j.dsr2.2014.11.014

Fitzsimmons, J. N., John, S. G., Marsay, C. M., Hoffman, C. L., Nicholas, S. L., Toner, B. M., et al. (2017). Iron persistence in a distal hydrothermal plume supported by dissolved-particulate exchange. *Nat. Geosci.* 10, 195–201. doi: 10.1038/ngeo2900

Francisco, P. C. M., Mitsui, S., Ishidera, T., Tachi, Y., Doi, R., and Shiwaku, H. (2020). Interaction of FeII and Si under anoxic and reducing conditions: structural characteristics of ferrous silicate co-precipitates. *Geochim. Cosmochim. Acta* 270, 1–20. doi: 10.1016/j.gca.2019.11.009

Gartman, A., and Findlay, A. J. (2020). Impacts of hydrothermal plume processes on oceanic metal cycles and transport. *Nat. Geosci.* 13, 396–402. doi: 10.1038/s41561-020-0579-0

Gartman, A., Findlay, A. J., and Luther, G. W. III (2014). Nanoparticulate pyrite and other nanoparticles are a widespread component of hydrothermal vent black smoker emissions. *Chem. Geol.* 366, 32–41. doi: 10.1016/j.chemgeo.2013.12.013

German, C. R., Colley, S., Palmer, M. R., Khripounoff, A., and Klinkhammer, G. P. (2002). Hydrothermal plume-particle fluxes at 13°N on the East Pacific rise. *Deep-Sea Res. Part I* 49, 1921–1940. doi: 10.1016/S0967-0637(02)00086-9

German, C. R., Legendre, L. L., Sander, S. G., Niquil, N., Luther, G. W., Bharati, L., et al. (2015). Hydrothermal Fe cycling and deep ocean organic carbon scavenging: model-based evidence for significant POC supply to seafloor sediments, Earth Planet. *Sci. Lett.* 419, 143–153. doi: 10.1016/j.epsl.2015.03.012

Gledhill, M., and Buck, K. N. (2012). The organic complexation of iron in the marine environment: a review. *Front. Microbiol.* 3:69. doi: 10.3389/fmicb.2012.00069

Hoffman, C. L., Nicholas, S. L., Ohnemus, D. C., Fitzsimmons, J. N., Sherrell, R. M., German, C. R., et al. (2018). Near-field iron and carbon chemistry of nonbuoyant hydrothermal plume particles, southern east pacific rise 15°S. *Mar. Chem.* 201, 183–197. doi: 10.1016/j.marchem.2018.01.011

Huerta-Diaz, M. A., and Morse, J. W. (1992). Pyritization of trace metals in anoxic marine sediments. *Geochim. Cosmochim. Acta* 56, 2681–2702. doi: 10.1016/0016-7037(92)90353-K

James, R. H., Elderfield, H., and Palmer, M. R. (1995). The chemistry of hydrothermal fluids from the broken spur site, 29°N Mid Atlantic Ridge. *Geochim. Cosmochim. Acta* 59, 651–659. doi: 10.1016/0016-7037(95)00003-I

Janecky, D. R., and Seyfried, W. E. (1986). Hydrothermal serpentinization of peridotite within the oceanic crust: experimental investigations of mineralogy and major element chemistry. *Geochim. Cosmochim. Acta* 50, 1357–1378. doi: 10.1016/0016-7037(86)90311-X

Jickells, T. D., An, Z. S., Andersen, K. K., Baker, A. R., Bergametti, G., Brooks, N., et al. (2005). Global iron connections between desert dust, ocean biogeochemistry and climate. *Science* 308, 67–71. doi: 10.1126/science.1105959

Johnson, J. E., Muhling, J. R., Cosmidis, J., Rasmussen, B., and Templeton, A. S. (2018). Low-Fe(III) Greenalite was a primary mineral from neoarchean oceans. *Geophys. Res. Lett.* 45, 3182–3192. doi: 10.1002/2017GL076311

Jones, A. M., Collins, R. N., Rose, J., and Waite, T. D. (2009). The effect of silica and natural organic matter on the Fe(II)-catalysed transformation and reactivity of Fe(III) minerals. *Geochim. Cosmochim. Acta* 73, 4409–4422. doi: 10.1016/j.gca.2009.04.025

Kelley, D. S., and Shank, T. M. (2010). "Hydrothermal systems: a decade of discovery in slow spreading environments, diversity of hydrothermal systems on slow spreading ocean ridges," in *Diversity of Hydrothermal Systems on Slow Spreading Ocean Ridges. Vol. 188.* eds. P. A. Rona, C. W. Devey, J. Dyment and B. J. Murton, American Geophysical Union Monograph Series (Washington, DC: AGU), 369–407.

Kinsela, A. S., Jones, A. M., Bligh, M. W., Pham, A. N., Collins, R. N., Harrison, J. J., et al. (2016). Influence of dissolved silicate on rates of Fe(II) oxidation. *Environ. Sci. Technol.* 50, 11663–11671. doi: 10.1021/acs.est.6b03015

Kleint, C., Pichler, T., and Kochisnky, A. (2017). Geochemical characteristics, speciation and size-fractionation of iron (Fe) in two marine shallow-water hydrothermal systems, Dominica, Lesser Antilles. *Chem. Geol.* 454, 44–53. doi: 10.1016/j.chemgeo.2017.02.021

Kunde, K., Wyatt, N. J., González-Santana, D., Tagliabue, A., Mahaffey, C., and Lohan, M. C. (2019). Iron distribution in the subtropical North Atlantic: the pivotal role of colloidal iron. *Glob. Biogeochem. Cycles* 33, 1532–1547. doi: 10.1029/2019GB006326

Le Bris, N., and The Science Party (2018). Campagne TRANSECT TRANsfert d'Energie dans les Ecosystèmes Chimiosynthétiques en contexte ulTramafique. doi: 10.17600/18000513

Le Bris, N., Yücel, M., Das, A., Sievert, S. M., LokaBharathi, P., and Girguis, P. R. (2019). Hydrothermal energy transfer and organic carbon production at the deep seafloor. *Front. Mar. Sci.* 5:531. doi: 10.3389/fmars.2018.00531

Lough, A. J. M., Connelly, D. P., Homoky, W. B., Hawkes, J. A., Chavagnac, V., Castillo, A., et al. (2019b). Diffuse hydrothermal venting: a hidden source of iron to the oceans. *Front. Mar. Sci.* 6:329. doi: 10.3389/fmars.2019.00329

Lough, A. J. M., Homoky, W. B., Connelly, D. P., Comer-Warner, S. A., Nakamura, K., Abyaneh, M. K., et al. (2019a). Soluble iron conservation and colloidal iron dynamics in a hydrothermal plume. *Chem. Geol.* 511, 225–237. doi: 10.1016/j.chemgeo.2019.01.001

Luther, G. W., Shaw, T.J., Estes, E. R, Berti, D., Hochella, M.F., Yucel, M., et al. (2020). Formation of reactive oxygen species and (iron)silicate (nano) particles in the mixing zone above hydrothermal vent orifices; June 21-26, 2020;. Goldschmidt Conference.

Mayer, T. D., and Jarrell, W. M. (1996). Formation and stability of iron(II) oxidation products under natural concentrations of dissolved silica. *Water Res.* 30, 1208–1214. doi: 10.1016/0043-1354(95)00265-0

McDermott, J. M., Sylva, S. P., Ono, S., German, C. R., and Seewald, J. S. (2020). Abiotic redox reactions in hydrothermal mixing zones: decreased energy availability for the subsurface biosphere. *Proc. Natl. Acad. Sci.* 117, 20453–20461. doi: 10.1073/pnas.2003108117

Moore, E. K., Jelen, B. I., Giovannelli, D., Raanan, H., and Falkowski, P. G. (2017). Metal availability and the expanding network of microbial metabolisms in the Archaean eon. *Nat. Geosci.* 10, 629–636. doi: 10.1038/ngeo3006

Mottl, M. J., and Holland, H. D. (1978). Chemical exchange during hydrothermal alteration of basalt by seawater – I. Experimental results for major and minor components of seawater. *Geochim. Cosmochim. Acta* 42, 1103–1115. doi: 10.1016/0016-7037(78)90107-2

Mottl, M. J., and McConachy, T. F. (1990). Chemical processes in buoyant hydrothermal plumes on the East Pacific Rise near 21°N. *Geochim. Cosmochim. Acta* 54, 1911–1927. doi: 10.1016/0016-7037(90)90261-I

Murton, B. J., Van Dover, C., and Southward, E. (1995). Geological setting and ecology of the broken spur hydrothermal vent field: 29°10′N on the Mid-Atlantic Ridge. *Geol. Soc. Lond., Spec. Publ.* 87, 33–41. doi: 10.1144/GSL.SP.1995.087.01.04

Nishioka, J., Nakatsuka, T., Watanabe, Y. W., Yasuda, I., Kuma, K., Ogawa, H., et al. (2013). Intensive mixing along an island chain controls oceanic biogeochemical cycle. *Glob. Biogeochem. Cycles* 27, 920–929. doi: 10.1002/gbc.20088

Ohnemus, D. C., and Lam, P. J. (2015). Cycling of lithogenic marine particles in the US GEOTRACES North Atlantic transect. *Deep-Sea Res.* 116, 283–302. doi: 10.1016/j.dsr2.2014.11.019

Patten, J. T., and Byrne, R. H. (2017). Assessment of Fe(III) and Eu(III) complexation by silicate in aqueous solutions. *Geochim. Cosmochim. Acta* 202, 361–373. doi: 10.1016/j.gca.2016.12.004

Rasmussen, B., Krapež, B., Muhling, J. R., and Suvorova, A. (2015). Precipitation of iron silicate nanoparticles in early Precambrian oceans marks Earth's first iron age. *Geology* 43, 303–306. doi: 10.1130/G36309.1

Resing, J. A., Sedwick, P. N., German, C. R., Jenkins, W. J., Moffett, J. W., Sohst, B. M., et al. (2015). Basin-scale transport of hydrothermal dissolved metals across the South Pacific Ocean. *Nature* 523, 200–203. doi: 10.1038/nature14577

Rickaby, R. E. M. (2015). Goldilocks and the three inorganic equilibria: how Earth's chemistry and life coevolve to be nearly in tune. *Phil. Trans. R. Soc. A* 373:20140188. doi: 10.1098/rsta.2014.0188

Rudnicki, M. D., and Elderfield, H. (1993). A chemical model of the buoyant and neutrally buoyant plume above the TAG vent field, 26 degrees N, Mid-Atlantic Ridge. *Geochim. Cosmochim. Acta* 57, 2939–2957. doi: 10.1016/0016-7037(93)90285-5

Sander, S. G., and Koschinsky, A. (2011). Metal flux from hydrothermal vents increased by organic complexation. *Nat. Geosci.* 4, 45–150.

Schlitzer, R. (2017).eGEOTRACES - Electronic Atlas of GEOTRACES Sections and Animated 3D Scenes. Available at: http://www.egeotraces.org

Schmidt, K., Koschinsky, A., Garbe-Schönberg, D., de Carvalho, L. M., and Seifert, R. (2007). Geochemistry of hydrothermal fluids from the ultramafic-hosted Logatchev hydrothermal field, 15°N on the Mid-Atlantic Ridge: temporal and spatial investigation. *Chem. Geol.* 242, 1–21. doi: 10.1016/j.chemgeo.2007.01.023

Seyfried, W. E. Jr., and Bischoff, J. (1981). Experimental seawater-basalt interaction at 300°C, 500 bars, chemical exchange, secondary mineral formation and implications for the transport of heavy metals. *Geochim. Cosmochim. Acta* 45, 135–147. doi: 10.1016/0016-7037(81)90157-5

Seyfried, W. E. Jr., Foustoukos, D. I., and Fu, Q. (2007). Redox evolution and mass transfer during serpentinization: An experimental and theoretical study at 200°C, 500 bars with implications for ultramafic-hosted hydrothermal

systems at Mid-Ocean Ridges. *Geochim. Cosmochim. Acta* 71, 3872–3886. doi: 10.1016/j.gca.2007.05.015

Seyfried, W. E. Jr., Pester, N. J., Ding, K., and Rough, M. (2011). Vent fluid chemistry of the rainbow hydrothermal system (36°N, MAR): phase equilibria and in situ pH controls on subseafloor alteration processes. *Geochim. Cosmochim. Acta* 75, 1574–1593. doi: 10.1016/j.gca.2011.01.001

Stookey, L. L. (1970). Ferrozine-a new spectrophotometric reagent for iron. *Anal. Chem.* 42, 779–781. doi: 10.1021/ac60289a016

Tagliabue, A., Aumont, O., DeAth, R., Dunne, J. P., Dutkiewicz, S., Galbraith, E., et al. (2016). How well do global ocean biogeochemistry models simulate dissolved iron distributions? *Glob. Biogeochem. Cycles* 30, 149–174. doi: 10.1002/2015GB005289

Tagliabue, A., Bopp, L., Dutay, J.-C., Bowie, A. R., Chever, F., Jean-Baptiste, F., et al. (2010). Hydrothermal contribution to the oceanic dissolved iron inventory. *Nat. Geosci.* 3, 252–256. doi: 10.1038/ngeo818

Toner, B. M., Fakra, S. C., Manganini, S. J., Santelli, C. M., Marcus, M. A., Moffett, J., et al. (2009). Preservation of iron(II) by carbon-rich matrices in a hydrothermal plume. *Nat. Geosci.* 2, 197–201. doi: 10.1038/ngeo433

Toner, B. M., German, C. R., Dick, G. J., and Breier, J. A. (2016). Deciphering the complex chemistry of deep-ocean particles using complementary synchrotron X-ray microscope and microprobe instruments. *Acc. Chem. Res.* 49, 128–137. doi: 10.1021/acs.accounts.5b00282

Twining, B. S., and Baines, S. B. (2013). The trace metal composition of marine phytoplankton. *Annu. Rev. Mar. Sci.* 5, 191–215. doi: 10.1146/annurev-marine-121211-172322

Von Damm, K. L., Bray, A. M., Buttermore, L. G., and Oosting, S. E. (1998). The geochemical controls on vent fluids from the lucky strike vent field, Mid-Atlantic Ridge. *Earth Planet. Sci. Lett.* 160, 521–536. doi: 10.1016/S0012-821X(98)00108-3

Waeles, M., Cotte, L., Pernet-Coudrier, B., Chavagnac, V., Cathalot, C., Leleu, T., et al. (2017). On the early fate of hydrothermal iron at deep-sea vents: a reassessment after in-situ filtration. *Geophys. Res. Lett.* 44, 4233–4240. doi: 10.1002/2017GL073315

Winckler, G., Anderson, R. F., Jaccard, S. L., and Marcantonio, F. (2016). Ocean dynamics, not dust, have controlled equatorial Pacific productivity over the past 500,00 years. *Proc. Natl. Acad. Sci.* 113, 6119–6124. doi: 10.1073/pnas.1600616113

Wu, J., Wells, M. L., and Rember, R. (2011). Dissolved iron anomaly in the deep tropical–subtropical Pacific: evidence for long-range transport of hydrothermal iron. *Geochim. Cosmochim. Acta* 75, 460–468. doi: 10.1016/j.gca.2010.10.024

Yücel, M., Gartman, A., Chan, C. S., and Luther, G. W. III (2011). Hydrothermal vents as a kinetically stable source of iron-sulphide-bearing nanoparticles to the ocean. *Nat. Geosci.* 4, 367–371. doi: 10.1038/ngeo1148

Conflict of Interest: The authors declare that the research was conducted in the absence of any commercial or financial relationships that could be construed as a potential conflict of interest.

frontiers | Frontiers in Microbiology

ORIGINAL RESEARCH
published: 27 April 2022
doi: 10.3389/fmicb.2022.662219

Quantification of Organic Carbon Sequestered by Biogenic Iron Sulfide Minerals in Long-Term Anoxic Laboratory Incubations

*Nader Nabeh†, Cheyenne Brokaw† and Aude Picard**

School of Life Sciences, University of Nevada, Las Vegas, Las Vegas, NV, United States

OPEN ACCESS

Edited by:
Lei Yan,
Heilongjiang Bayi Agricultural University, China

Reviewed by:
Aditi Sengupta,
California Lutheran University, United States
Adriano Reis Lucheta,
Instituto SENAI de Inovação em Tecnologias Minerais, Brazil
Guanghui Yu,
Tianjin University, China

***Correspondence:**
Aude Picard
audeamelie.picard@unlv.edu

†These authors have contributed equally to this work and share first authorship

Specialty section:
This article was submitted to Microbiological Chemistry and Geomicrobiology, a section of the journal Frontiers in Microbiology

Received: *31 January 2021*
Accepted: *29 March 2022*
Published: *27 April 2022*

Citation:
Nabeh N, Brokaw C and Picard A (2022) Quantification of Organic Carbon Sequestered by Biogenic Iron Sulfide Minerals in Long-Term Anoxic Laboratory Incubations. Front. Microbiol. 13:662219. doi: 10.3389/fmicb.2022.662219

Organic carbon sequestration in sedimentary environments controls oxygen and carbon dioxide concentrations in the atmosphere. While minerals play an important role in the preservation of organic carbon, there is a lack of understanding about the formation and stability of organo-mineral interactions in anoxic environments, especially those involving authigenic iron sulfide minerals. In this study, we quantified organic carbon and nitrogen sequestered in biogenic iron sulfide minerals co-precipitated with sulfate-reducing bacteria (SRB) in freshwater and marine conditions in long-term laboratory experiments. The amounts of C and N associated with biogenic iron sulfide minerals increased with increasing cell biomass concentrations available in the media. C and N levels stabilized over the first 2 months of incubation and remained stable for up to 1 year. Crystalline mackinawite (FeS) formed in all experimental conditions and transformed to greigite only in some experimental conditions. We did not find evidence that this mineral transformation affected C and N levels, neither could we identify the factors that controlled greigite formation. Pyrite did not form in our experimental conditions. While C concentrations in minerals correlated with concentrations of reduced sulfate in both the freshwater and marine media, removal of OC by iron sulfide minerals was more efficient in freshwater than marine conditions. Removal of OC by iron sulfide minerals was also more efficient when cells were present (SRB biomass) in comparison with abiotic incubations with organic mixtures (e.g., tryptone, yeast extract, and casamino acids). Our study highlights the potential for biogenic iron sulfide minerals to quantitatively contribute to organic carbon preservation in anoxic environments.

Keywords: iron sulfide minerals, biomineral, microbial sulfate reduction, *Desulfovibrio*, mackinawite, greigite, organic carbon preservation

INTRODUCTION

The long-term preservation of organic carbon has significant impacts on the global carbon cycle. Over geological timescales, organic carbon sequestration removes carbon dioxide from the atmosphere and releases oxygen into the Earth's atmosphere (Berner and Canfield, 1989; Berner, 1990; Keil, 2017; LaRowe et al., 2020). Sedimentary environments represent the largest

reservoir of organic carbon. Anoxic and reduced conditions promote increased organic carbon burial (Jenkyns, 2010; Raven et al., 2019). Indeed, organic carbon deposition is typically enhanced in coastal and shelf environments, below zones of high primary productivity where oxygen-deficient zones can develop (Keil, 2017; Raven et al., 2021b). Anthropogenically driven climate change is promoting an expansion of oxygen-free zones in the ocean, leading to the enhanced delivery of OC to the seafloor and potentially enhanced preservation (Keil, 2017). While anoxic marine sediments represent the largest long-term organic carbon repository (Canfield, 1994; Burdige, 2007), freshwater sedimentary environments are also significant for the preservation of OC due to their sensitivity to changes in the carbon cycle, especially those driven by human activity (Boye et al., 2017). Microbial communities play an important role in the transformations of organic carbon (Singh et al., 2010; Cavicchioli et al., 2019; LaRowe et al., 2020). While microorganisms are typically assumed to degrade most organic carbon in the environment, they can also play a role in its preservation through mechanisms such as polymerization, sulfurization, or biomineralization (Ogawa et al., 2001; Ingalls et al., 2003, 2004; Chan et al., 2009; Jiao et al., 2010; Picard et al., 2019; Raven et al., 2021b).

Interactions between organic carbon and minerals play a role in long-term organic carbon (OC) preservation (Keil and Mayer, 2014; Hemingway et al., 2019; Kleber et al., 2021). The association of organic compounds with minerals is driven by multiple physical and chemical processes, including physical adsorption and/or strong bonding at mineral surfaces, insertion into clay interlayers, formation of mineral-OC aggregates, co-precipitation with authigenic minerals, incorporation into exopolymeric substances (EPS), and production of biogenic minerals by controlled mineralization (LaRowe et al., 2020). Ligand exchange, ion exchange, and hydrogen bonding are potential driving forces for the aggregation of organic matter and minerals that may strengthen organo-mineral interactions and thus provide a mechanism for OC preservation (Keil and Mayer, 2014). Minerals could stabilize and protect organic matter against alteration, such as weathering, decomposition, and microbial degradation, therefore preserving organic carbon derived from living and dead microbial biomass for long periods of time (Keil and Mayer, 2014).

In anoxic environments, the biogeochemical cycles of iron, carbon, and sulfur are intertwined through microbial activity (Rickard, 2012a; Jørgensen et al., 2019). Reduced sulfur produced by microbial sulfate reduction interacts with Fe(II) to form iron sulfide minerals but also interacts with Fe(III) minerals to form Fe(II) and intermediate-redox sulfur species (Rickard, 2012a; Picard et al., 2016). Sulfate-reducing microorganisms (SRM) can be found in a variety of aquatic environments and are responsible for 97% of Earth's sulfide production in low-temperature environments (Rickard, 2012a). Iron-rich substrates seem to prevent the degradation of organic compounds by microbial metabolic activity. For example, organic carbon preservation occurs due to co-precipitation with ligand-Fe and with Fe oxides in a variety of environments, including surface marine and estuarine environments, as well as in hydrothermal plumes (Lalonde et al., 2012; Barber et al., 2017; Hoffman et al., 2018). The role of OC-Fe ligand and OC-Fe minerals in preserving OC in anoxic environments has hardly been studied (Barber et al., 2017). Sulfide produced by SRM promotes the sulfurization of organic carbon in a variety of marine environments (Raven et al., 2016a,b, 2021b). Additionally, through their influence on the formation of iron sulfide minerals, SRM could also play an important role in the long-term preservation of organic carbon in anoxic sedimentary environments. In laboratory experiments, SRM influence the physical and chemical properties of iron sulfide minerals, and also potentially their mineralogy (Picard et al., 2016, 2018; Mansor et al., 2019). Whether iron sulfide minerals associate tightly with cells (through mineral encrustation) or precipitate away from cells, they associate strongly with organic carbon derived from microbial biomass. Notably, iron sulfide minerals have a strong affinity for proteinaceous material (Picard et al., 2019). Microbial organic carbon associated with biogenic iron sulfide minerals precipitated in anoxic laboratory conditions is still detectable by *X*-ray microscopy after incubations of 2 years (Picard et al., 2019, 2021). Moreover, biogenic minerals are more stable than abiotic minerals precipitated with organic molecules, which indicate the importance of microbial biomass and cellular structures in the preservation of organic carbon.

Here, we quantified concentrations of organic carbon and nitrogen that biogenic iron sulfide minerals can sequester in long-term laboratory experiments. Biogenic minerals were precipitated in the presence of a marine SRB, *Desulfovibrio hydrothermalis* AM13, and a freshwater SRB, *Desulfovibrio magneticus* RS-1 and incubated for up to 1 year at their optimal growth temperature (35 and 30°C, respectively). We also quantified organic carbon sequestration in abiotic experiments with organic mixtures. We evaluated the role of mineralogy, salinity, and type of organic carbon (in biomass vs. organic mixtures without cells) in the sequestration capacity and stability of iron sulfide minerals.

MATERIALS AND METHODS

Microorganisms and Media

Desulfovibrio hydrothermalis AM13 (called *Dh* AM13 hereafter) is a deep-sea marine sulfate-reducing bacterium (SRB) and grows optimally at 35°C (Alazard et al., 2003). *Dh* AM13 was purchased from DSMZ (Deutsche Sammlung von Mikroorganismen und Zellkulturen) under the reference DSM 14728. DSMZ 195c medium (2014 recipe) was used to grow *Dh* AM13. All solutions were prepared with ultrapure water. The following salts were dissolved in 870 ml water to prepare Solution A: 3.00 g Na_2SO_4, 0.20 g KH_2PO_4, 0.30 g NH_4Cl, 21.00 g NaCl, 3.10 g $MgCl_2 \times 6\ H_2O$, 0.50 g KCl, 0.15 g $CaCl_2 \times 2\ H_2O$, and 1.0 ml selenite-tungstate solution (as described in DSMZ 385 medium). Resazurin was omitted. Solution A was gassed for at least 30 min with a N_2/CO_2 gas mixture and autoclaved in a 2-L bottle sealed with a thick black rubber stopper and a screw cap. A buffer solution (final volume 100 ml) was prepared with 5.00 g $NaHCO_3$, gassed for at least 30 min with a N_2/CO_2 gas mixture, and autoclaved in a serum vial sealed

with a blue butyl stopper and an aluminum cap. Solution A and the buffer were mixed in a vinyl anaerobic chamber (Coy Laboratory Products) and supplemented with 1 ml of filter-sterilized SL-10 trace element solution (as described in DSMZ 320 medium) and 10 ml of filter-sterilized vitamin solution (as described in DSMZ 141 medium). Autoclaved sodium DL-lactate syrup (60 w/w%, Sigma) was added to the medium: 5 ml (very high lactate, VHL), 3.1 ml (high lactate, HL), 1.5 ml (low lactate, LL), and 1.0 ml (very low lactate, VLL). Corresponding lactate and sulfate concentrations are given in **Table 1**.

Desulfovibrio magneticus RS-1 (called *Dm* RS-1 hereafter) is a freshwater SRB and grows optimally at 30°C (Sakaguchi et al., 2002). *Dm* RS-1 came from the culture collection of Dr. Dennis Bazylinski at UNLV. A freshwater medium (Ingvorsen and Jørgensen, 1984) was used to grow *Dm* RS-1. All solutions were prepared with ultrapure water. A mineral solution (final volume 1 l after pH adjustment) contained: 1.42 g Na_2SO_4, 0.32 g Na_2HPO_4, 0.11 g KH_2PO_4, 0.25 g NH_4Cl, 1.00 g NaCl, 0.6 g $MgCl_2 \times 6\ H_2O$, 0.20 g $CaCl_2 \times 2\ H_2O$, and 1.0 ml modified Wolfe's trace element solution (as described in DSMZ 141 medium). Sodium DL-lactate syrup (60 w/w%, Sigma) was added to the mineral solution: 5 ml (very high lactate, VHL), 3.0 ml (high lactate, HL), 1.5 ml (low lactate, LL), and 1.0 ml (very low lactate, VLL). The pH of the mineral solution was adjusted to 7.1 before gassing the solution for at least 30 min with a N_2/CO_2 gas mixture and autoclaving it in a 2-L bottle sealed with a thick black rubber stopper and a screw cap. A buffer solution (final volume 50 ml) was prepared with 4.00 g $NaHCO_3$, gassed for at least 30 min with a N_2/CO_2 gas mixture, and autoclaved in a serum vial sealed with a blue butyl stopper and an aluminum cap. The mineral solution and buffer were mixed in the anaerobic chamber and supplemented with 1 ml of selenite-tungstate solution (see above) and 1 ml of vitamin solution (see above). Lactate and sulfate concentrations are given in **Table 1**.

Both SRB couple the incomplete oxidation of lactate with sulfate reduction according to the following reaction (Rabus et al., 2013):

$$2CH_3CHOHCOO^- + {SO_4}^{2-} + 2H^+ \rightarrow 2CH_3COO^- + 2CO_2 + H_2S + 2H_2O \quad \text{Eq. (1)}$$

Preparation of SRB Cultures for Biomass Carbon Quantification

Cultures were prepared in a vinyl anaerobic chamber (Coy Laboratory Products). Media, as described above, were dispensed in serum vials (50 ml of medium per 110-ml glass bottle) and inoculated with 250 µl from a stock culture of *Dm* RS-1 and *Dh* AM13 and incubated for ~1 month at 30°C and 35°C, respectively. Cell pellets were recovered from *Dh* AM13 cultures and from *Dm* RS-1 cultures by centrifugation at 8,000 g for 20 min. Cell pellets were then resuspended in anoxic sterile water for carbon quantification in the elemental analyzer (see below).

Co-precipitation of Iron Sulfide Minerals With Sulfate-Reducing Bacteria and With Organic Mixtures

All experiments were prepared in the anaerobic chamber. The media, as described above, were dispensed in serum vials (50 ml of medium per 110-ml glass bottle). Fe(II) was added to each

TABLE 1 | Cell biomass production in cultures of the two sulfate-reducing bacteria used in this study: marine strain *Desulfovibrio hydrothermalis* AM13 and freshwater strain *Desulfovibrio magneticus* RS-1.

	***Desulfovibrio hydrothermalis* AM13**				***Desulfovibrio magneticus* RS-1**			
	Marine medium: ~21.1 mM sulfate				**Freshwater medium: ~10.0 mM sulfate**			
	VLL	**LL**	**HL**	**VHL**	**VLL**	**LL**	**HL**	**VHL**
Lactate concentration (mM, calculated)	7.0	10.4	21.6	34.8	7.0	10.4	20.9	34.8
Reduced sulfate (mM, expected)	3.5	5.2	10.8	17.4	3.5	5.2	10.0	10.0
Reduced sulfate (mM, measured)	2.7 ± 0.9	3.9 ± 1.2	9.8 ± 0.4	17.5 ± 1.4	4.8 ± 1.3	7.4 ± 2.1	9.8 ± 0.7	10.2 ± 0.4
Cell biomass carbon (mg/L, measured)	33.4 ± 4.0	40.7 ± 1.5	74.8 ± 3.5	106.1 ± 9.3	20.7 ± 5.2	23.1 ± 7.6	26.6 ± 0.9	31.5 ± 2.7
Cell biomass carbon (mmol/L)	2.8 ± 0.3	3.4 ± 0.1	6.2 ± 0.3	8.8 ± 0.8	1.7 ± 0.4	1.9 ± 0.6	2.2 ± 0.1	2.6 ± 0.1
Initial molar C/Fe ratio	0.7 ± 0.2	0.9 ± 0.2	1.6 ± 0.4	2.2 ± 0.5	0.4 ± 0.1	0.5 ± 0.2	0.6 ± 0.1	0.7 ± 0.2

VLL, LL, HL, and VHL refer to the lactate concentrations used in experiments (see "Materials and Methods"). The expected reduced sulfate concentrations were calculated using the typical stoichiometry associated with microbial sulfate reduction of 2 mol of lactate oxidized per 1 mol of sulfate reduced. Actual sulfate concentrations were determined using the barium sulfate assay as described in the Methods section. Concentrations of reduced sulfate (mM) presented here are average values from multiple experiments at a given condition. Biomass carbon concentrations in cell pellets recovered from cultures grown without Fe(II) were determined using an elemental analyzer, as described in the Methods section. Average values and standard deviations were calculated from cell pellets collected from 2 to 5 independent incubations. Biomass carbon concentrations in mg/L were converted to mol/L to calculate total molar biomass C/Fe ratios in incubations. An average concentration of 4.0 ± 0.9 mM Fe(II) was calculated from measurements done in all experiments (whether added at the beginning or at the end of experiments).

vial at a concentration of 4 mM (from a sterile anoxic 1 M $FeCl_2$ solution). For each microorganism and lactate concentration, 10–20 bottles containing the Fe medium were inoculated with 250 µl from a fresh stock culture of *Dm* RS-1 and *Dh* AM13 and incubated at 30°C and 35°C, respectively (Experiments named Fe experiments). When SRB are grown in Fe medium, iron sulfide minerals tend to precipitate near cells and have large mineral particles (Picard et al., 2018). When Fe(II) is added after the bacteria have completed sulfate reduction, iron sulfide minerals precipitate away from cells, and have a small particle size (Picard et al., 2018). Therefore, for some experimental conditions (Experiments named AddFe experiments), we co-precipitated iron sulfide minerals by adding Fe(II) at a concentration of 4 mM (from a sterile anoxic 1 M $FeCl_2$ solution) to fully grown cultures of *Dm* RS-1 and *Dh* AM13 after sulfate concentrations had become stable. Cultures without Fe were prepared as described in the former paragraph. After Fe(II) addition, cultures were placed back at 30°C and 35°C, respectively. At each time point, two serum vials were taken out of the incubator for analysis.

Three sets of abiotic experiments were also prepared (**Table 2**). Iron sulfide minerals were co-precipitated with mixtures of organic molecules (tryptone, yeast extract, and casamino acids) in the marine medium used for *Dh* AM13. Solutions of Bacto tryptone (pancreatic digest of casein), Difco yeast extract, and Bacto casamino acids (acid-hydrolyzed casein) were prepared at 50 g/l each with ultrapure water, degassed with N_2, and autoclaved in sealed serum vials. Marine medium was dispensed in serum vials (50 ml of medium per 110-ml glass bottle). Fe(II) was added to each vial at a concentration of 4 mM (from a sterile anoxic 1 M $FeCl_2$ solution). Then, 1 ml of either organic mixture was added to serum vials. The next day, 1 ml was added from a sterile anoxic sodium sulfide solution (~457 mM) to precipitate all Fe(II) as iron sulfide minerals and provide excess sulfide to the medium. A final concentration of 9.1 mM was estimated and corresponded approximately to the concentration of sulfide produced in experiments with high lactate (HL) concentrations (Picard et al., 2018). Mineral suspensions were incubated at 35°C. At each time point, two serum vials were used for analysis.

TABLE 2 | Summary of experimental conditions for abiotic experiments with organic molecules.

	Abiotic with tryptone Marine medium	Abiotic with yeast extract Marine medium	Abiotic with casamino acids Marine medium
Added sulfide (mM)	9.1	9.1	9.1
Concentration of carbon from organic molecules (mg/L, measured)	428 ± 10	385 ± 4	326 ± 7
Concentration of carbon from organic molecules (mmol/L)	36.0 ± 0.8	32.1 ± 0.3	27.0 ± 0.6
Initial molar C/Fe ratio	9.0 ± 0.2	8.0 ± 0.1	6.8 ± 0.2

Iron sulfide minerals were co-precipitated in the marine medium with either tryptone, yeast extract, or casamino acids. A concentration of 4 mM Fe(II) was used in all experiments; therefore, sulfide was in excess in all conditions and all Fe(II) precipitated as iron sulfide minerals.

Spectrophotometry

Quantification of Soluble Sulfate

Sulfate was quantified in bacterial cultures using the barium sulfate assay as described elsewhere (Kolmert et al., 2000). 100 µl of culture/medium collected from serum vials in the anaerobic chamber were mixed with 900 µl of zinc acetate. Samples were centrifuged at 13,000 g to remove any zinc sulfide precipitates. Supernatants were recovered and mixed with barium chloride (~60 mg) using a vortex mixer. 1 ml of conditioning reagent was added to each sample. The conditioning reagent was prepared with 150 g NaCl, 100 ml pure glycerol, 60 ml of concentrated HCl, and 200 ml of 95% ethanol. Ultrapure water was added to produce 1 l of reagent. Turbidity produced by barium sulfate precipitates was monitored at 420 nm on a Beckman Coulter™ DU-530 spectrophotometer. Sulfate concentrations were determined using a calibration curve prepared with sodium sulfate solutions.

Quantification of Total Ferrous Iron

Total Fe(II) was quantified in experiments using the ferrozine assay (Stookey, 1970). 100 µl of culture collected from serum vials in the anaerobic chamber were mixed with 900 µl of HCl 1 M, which completely dissolved biogenic and abiotic iron sulfide minerals produced in all experiments. 25 µl of the fixed sample was mixed with 975 µl of ferrozine solution, prepared at a final concentration of 0.1% ferrozine in HEPES buffer at pH 7.0. Absorbance was measured at 563 nm after 5 min. Fe(II) concentrations were determined using a calibration curve prepared with ammonium ferrous sulfate solutions.

Solid Phase Preparation for CN Quantification and for *X*-Ray Diffraction

Solid phases were recovered from biomineralization experiments and from abiotic experiments on a regular basis over the course of long-term incubations. For each time point, solid phases were prepared from two different serum vials. Cultures containing minerals and abiotic mineral suspensions (each 50 ml) were transferred to Nalgene tubes sealed with O-ring screw caps in the anaerobic chamber and centrifuged at 8,000 g for 30 min at room temperature. Solid phases were washed with sterile anoxic water in the anaerobic chamber and left to dry afterwards.

Elemental Analysis (Carbon and Nitrogen)

Total carbon (TC), total nitrogen (TN), and CN ratios were determined in solid phases recovered from biomineralization and abiotic mineralization experiments, in cell pellets recovered from cultures grown without Fe, and in stock solutions of organic molecules (used for abiotic experiments) using an Elementar varioMAX analyzer in the CN mode. Dried solid

phases were gently ground in an agate mortar and pestle in the anaerobic chamber and transported to the instrument in air-tight jars. Samples were weighted in stainless steel crucibles just before analysis and loaded into the instrument. Limited air contact with dried minerals did not impact their TC and TN contents. Cell pellets were resuspended in anoxic ultrapure water and transferred to stainless steel crucibles just before analysis. The instrument was calibrated with >99.0% pure L-glutamic acid (Merck). The stability of the instrument was monitored by measuring small amounts of standard materials with a range of C and N contents: low organic content soil standard OAS (Elemental microanalysis, C: 1.86%, N: 0.122%), reagent grade > 98% L-aspartic acid (Sigma, C: 36.10%, N: 10.52%), and Buffalo River sediment standard (NIST 8704, C: 3.351%, N: 0.19%).

X-Ray Diffraction

Powder *X*-ray diffraction was used to determine the mineralogy of solid phases, prepared as described above. Dried minerals were homogenized in 200-proof ethanol using an agate mortar and pestle and subsequently mounted on a zero-diffraction silicon plate (MTI corporation) in the anaerobic chamber. Samples were transported to the instrument in air-tight jars. Powder *X*-ray diffraction (XRD) data were acquired with a Proto AXRD at the Geoscience department of the University of Nevada Las Vegas. *X*-ray diffractograms were acquired using Cu K-α radiation (30 kV-20 mA), between 10° and 60° 2θ angles with increment steps of 0.05° and a dwell time of 1 s.

Experimental Design, Data Processing, and Statistical Tests

Concentrations of cell biomass carbon (**Table 1**) are average values from 2 to 5 cultures grown without Fe(II) for ~1 month. Errors represent ± one standard deviation. For each condition tested, biomineralization experiments consisted of up to 20 replicate serum vials prepared with the same batch of medium, the same solution of $FeCl_2$ and inoculated with the same stock culture (or prepared with the same sulfide solution for abiotic experiments). At each time point, two serum vials were sacrificed to collect liquid samples and minerals; and measured TC, TN and CN represent average values from these two independent samples. Errors represent ± one standard deviation. For each given experimental condition, the concentration of reduced sulfate presented in **Table 1** is an average value of all time points taken after 2 weeks of incubation. The average concentration of 4.0 ± 0.9 mM Fe(II) was calculated from all time points taken in this study. Stabilized data of TC, TN, and CN ratio presented in **Table 3** were calculated by averaging values measured over a period of time during which the values appeared stable. To determine the time at which the data became stable for a given experimental condition, i.e., the time at which values do not change significantly anymore, a one-way ANOVA analysis with a Tukey HSD test was performed to compare data collected at each time point against one other. We used the same range of time to calculate stabilized data for TN contents and for CN rations. To evaluate differences between TC% in iron sulfide minerals co-precipitated with bacteria in cultures grown with Fe(II), e.g. Fe experiments in **Table 3**, and in iron sulfide minerals co-precipitated with bacteria in cultures where Fe(II) was added after growth happened (AddFe experiments), when available, a Student unpaired *t*-test was performed between stabilized values (See **Table 3** to see under which conditions AddFe experiments have been performed). Total carbon concentrations removed from medium (**Table 3**) were calculated by assuming that all 4 mM of Fe(II) precipitated as FeS (mackinawite), therefore producing an average concentration of mackinawite of 352 mg/l. Although in some conditions, Fe(II) was slightly in excess and in some other conditions, greigite was also produced, total carbon concentrations removed from the medium would fall in the same range.

RESULTS AND DISCUSSION

Organo-mineral interactions play an important role in the long-term preservation of organic carbon in a variety of environments, e.g., permafrost, soils, and sediments (Solomon et al., 2012; Keil and Mayer, 2014; Kleber et al., 2015, 2021; Opfergelt, 2020; Wagai et al., 2020). While the majority of minerals in sediments and soils is represented by clays and Fe/Mn oxides (Kleber et al., 2021), there is a lack of understanding of the role of authigenic minerals forming in anoxic environments in the sequestration of organic carbon (OC). In this study, we quantified the OC sequestration capacity of iron sulfide minerals in long-term laboratory experiments. As sulfide production in low-temperature environments is driven by microbial sulfate reduction, we co-precipitated biogenic iron sulfide minerals in marine and freshwater media with varying amounts of biomass from sulfate-reducing bacteria (SRB) and monitored their carbon and nitrogen contents in long-term (>1 year) incubations. We discuss the role of salinity, cells, and mineralogy in building strong and stable organo-mineral associations.

Biomass Carbon Production Varies Between Strains of Sulfate-Reducing Bacteria

Cultures of sulfate-reducing bacteria (SRB) were grown with a fixed sulfate concentration (21.1 mM in the marine medium and 10.0 mM in the freshwater medium) and four different lactate concentrations (7.0 mM VLL, 10.4 mM LL, 20.9–21.6 mM HL, and 34.8 mM VHL) to vary amounts of sulfate reduced and therefore to vary biomass concentrations produced. In cultures of the marine strain *Desulfovibrio hydrothermalis* AM13, lactate was limiting in all conditions, and sulfate was leftover in all conditions (**Table 1**). In cultures of the freshwater strain *Desulfovibrio magneticus* RS-1, lactate was limiting in VLL and LL conditions, while sulfate was limiting and lactate was leftover in HL and VHL conditions (**Table 1**). A concentration of 4 mM Fe(II) was used in all biomineralization experiments; therefore, Fe(II) was the limiting factor to produce iron sulfide minerals. Sulfide was in excess in HL and VHL incubations with *Dh* AM13 and in all incubations with *Dm* RS-1. Although

TABLE 3 | Summary of parameters characterized in iron sulfide minerals: total carbon (TC) content (% w/w), total nitrogen (TN) content (% w/w), C/N ratio, TC content (mg/g mineral), TC sequestered from medium (mg/L and %), and mineralogy.

	Stabilized TC (w/w %)	Stabilized TN (w/w %)	Stabilized C/N ratio	Stabilized TC (mg/g = g/kg)	TC removed from medium (mg/L)	TC removed from medium (%)	Mineralogy
Biotic experiments – *Desulfovibrio hydrothermalis* AM13 (marine medium)							
Dh **Fe** VLL (all)	3.7 ± 0.3	1.5 ± 0.4	2.7 ± 0.7	37 ± 3	14 ± 1	42	Mackinawite†
Dh **AddFe** VLL (2 mo)	4.1 ± 0.3	1.2 ± 0.1	3.5 ± 0.1	41 ± 3	15 ± 1	45	ND
Dh **Fe** LL (all)	5.0 ± 0.6	1.2 ± 0.2	4.2 ± 0.7	50 ± 6	18 ± 2	44	Mackinawite†
Dh **AddFe** LL (all)	5.6 ± 1.8	1.8 ± 0.6	3.1 ± 0.7	56 ± 18	21 ± 7	51	ND
Dh **Fe** HL (>2 mo)	8.3 ± 0.4	2.3 ± 0.6	3.8 ± 0.8	83 ± 4	32 ± 2	43	Mackinawite*† Greigite*†
Dh **AddFe** HL	ND	ND	ND	ND	ND	ND	Mackinawite*
Dh **Fe** VHL (>2 mo)	13.5 ± 0.7	3.3 ± 0.7	4.2 ± 0.7	135 ± 7	55 ± 3	52	Mackinawite† Greigite†
Dh **AddFe** VHL (>2 mo)	11.0 ± 0.6	2.7 ± 0.2	4.1 ± 0.1	110 ± 6	44 ± 2	42	ND
Biotic experiments – *Desulfovibrio magneticus* RS-1 (freshwater medium)							
Dm **Fe** VLL (>1 mo)	3.7 ± 0.3	0.9 ± 0.1	4.1 ± 0.3	37 ± 3	14 ± 1	67	Mackinawite† Greigite†
Dm **AddFe** VLL	ND	ND	ND	ND	ND	ND	ND
Dm **Fe** LL (all)	6.1 ± 1.0	1.8 ± 0.6	3.7 ± 0.7	61 ± 10	23 ± 4	100	Mackinawite† Greigite†
Dm **AddFe** LL	ND	ND	ND	ND	ND	ND	ND
Dm **Fe** HL (all)	9.5 ± 0.7	2.5 ± 0.4	3.8 ± 0.6	95 ± 7	37 ± 3	137	Mackinawite†
Dm **AddFe** HL (>2 mo)	7.5 ± 2.3	1.5 ± 0.7	5.2 ± 1.1	75 ± 23	29 ± 9	107	ND
Dm **Fe** VHL (all)	10.2 ± 1.2	2.3 ± 0.9	3.6 ± 0.9	102 ± 12	40 ± 4	125	Mackinawite†
Dm **AddFe** VHL	ND	ND	ND	ND	ND	ND	ND
Abiotic experiments – organic mixtures (marine medium)							
Abio Tryptone (6 mo)	5.1 ± 0.6	2.3 ± 0.7	2.5 ± 0.8	51 ± 6	19 ± 3	4	Mackinawite#
Abio Yeast extract (6 mo)	5.2 ± 0.8	2.3 ± 1.0	2.5 ± 0.6	52 ± 8	19 ± 2	5	Mackinawite#
Abio Amino acids (6 mo)	1.2 ± 0.1	1.1 ± 0.0	1.0 ± 0.1	12 ± 1	4 ± 1	1	Mackinawite#

Iron sulfide minerals were precipitated in the presence of sulfate-reducing bacteria Desulfovibrio hydrothermalis AM13 (Dh) and Desulfovibrio magneticus RS-1 (Dm; Biotic experiments); in the presence of organic mixtures, e.g., tryptone, yeast extract, and amino acids (Abiotic experiments). "Fe" experiments refer to experiments in which Fe(II) was added to the medium before inoculation of SRB, while "AddFe" experiments refer to experiments in which Fe(II) was added to fully grown SRB cultures. "Stabilized" data correspond to average values of data after values have reached a stable level (data points included in the calculation are indicated between brackets near the experiment name). Fe(II) was added at a concentration of 4 mM in all experiments, therefore producing an average concentration of iron sulfide minerals of 352 mg/l in all experiments. Mineralogy results from Picard et al., 2018, from Picard et al., 2021#, and from this study†.*

the experimental conditions were intended to produce sulfide in excess in all experiments with *Dh* AM13, sulfide was slightly limiting in VLL and LL conditions (**Table 1**). Cell biomass carbon concentrations, determined in cell pellets, increased with increasing sulfate reduced (**Figure 1**; **Table 1**). For *Dm* RS-1 in HL and VHL conditions, biomass concentrations were similar. An increase in the lactate concentration (in VHL vs. HL) did not impact biomass concentrations as the same amount of sulfate was reduced in these two conditions. The biomass yield differed between the two bacteria, with 4.9 g biomass carbon per mol sulfate for *Dh* AM13 and 1.7 g biomass carbon per mol sulfate for *Dm* RS-1. This converts to 9.8 g dry biomass per mol sulfate and 3.4 g dry biomass per mol sulfate, respectively, as the content of carbon of microbial biomass is ≈50% (Bar-On et al., 2018). Biomass carbon yields (typically reported as dry biomass yields in the literature) of other *Desulfovibrio* strains vary between 3.6 g and 13.5 g dry biomass per mol sulfate (with lactate as source of carbon and energy; **Table 4**; Traore et al., 1981, 1982; Ingvorsen and Jørgensen, 1984; Okabe and Characklis, 1992; Cooney et al., 1996). Differences in biomass carbon yields observed between different strains of *Desulfovibrio* do not appear to be related to the origin of the strain, as they range from 3.4 to 13.5 g dry biomass per mol sulfate for freshwater strains and from 3.6 to 9.8 g dry biomass per mol sulfate for marine strains. Instead, if all lactate is used for microbial sulfate reduction, differences in biomass yields between

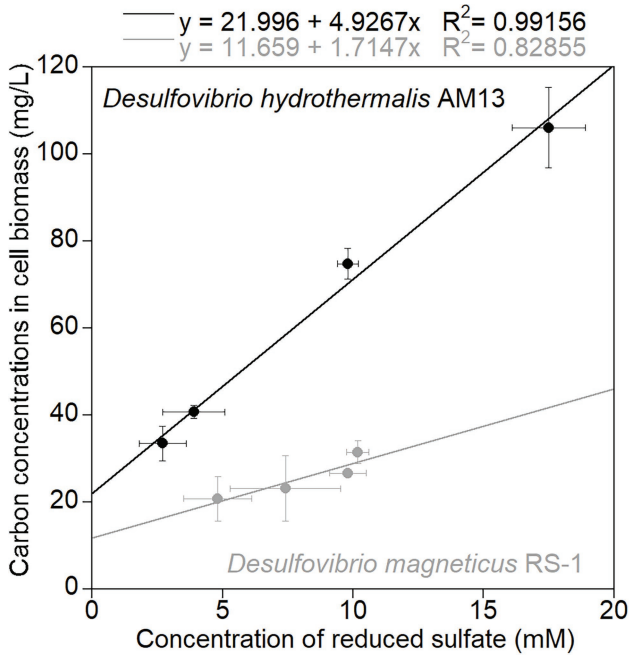

FIGURE 1 | Average carbon concentrations in cell biomass (mg/L) measured in cell pellets recovered from cultures grown without Fe(II), as a function of average concentrations of reduced sulfate (mM). Black circles are data for marine strain *Desulfovibrio hydrothermalis* AM13, and gray circles are data for freshwater *Desulfovibrio magneticus* RS-1. Error bars represent ±one standard deviation. The slope of the linear regressions gives the amount of biomass carbon (g) produced per mol sulfate reduced as: 4.9 g biomass carbon/mol sulfate for *Dh* AM13 and 1.7 g biomass carbon/mol sulfate for *Dm* RS-1.

strains can occur as a result of variations between ATP generation, and/or variations in ATP utilization by anaerobic synthesis (Traore et al., 1982).

The Amount of Carbon and Nitrogen Sequestered by Biogenic Iron Sulfide Minerals Increases With Increasing Biomass Concentrations in the Media

Biogenic minerals precipitated in cultures of freshwater and marine SRB grown with Fe(II) incorporated carbon and nitrogen from the media that contained microbial biomass (**Figure 2**). When Fe(II) is added to the HL medium before inoculation of *Dh* AM13, iron sulfide minerals precipitate at the surface of cells and form crusts closely associated with cells, but also have a larger particle size than abiotic minerals (Picard et al., 2018). Total carbon (TC) contents of iron sulfide minerals increased with increasing initial lactate concentrations (i.e., with increasing concentrations of reduced sulfate *and* increasing concentrations of produced biomass; *Dh*, **Figure 2A**; *Dm* **Figure 2B**, Fe experiments in **Table 3**). In very low lactate (VLL) conditions, TC levels were stable early on and reached their stabilized levels of 3.7 ± 0.3 w/w% for *Dh* AM13 and for *Dm* RS-1 after 2 weeks and 1 month of incubation, respectively. The same was observed for low lactate (LL) conditions, in

TABLE 4 | Estimated biomass carbon and dry biomass yields of *Desulfovibrio hydrothermalis* AM13 and *Desulfovibrio magneticus* RS-1 grown with sulfate and lactate.

	Biomass carbon (g/mol sulfate)	Dry biomass (g/mol sulfate)	References
D. hydrothermalis AM13 (m)	4.9	9.8	This study
D. africanus (m)		3.6	Traore et al., 1982
D. sapovorans (m)		8.7	Ingvorsen and Jørgensen, 1984
D. salexigens (m)		8.0	Ingvorsen and Jørgensen, 1984
D. magneticus RS-1 (fr)	1.7	3.4	This study
D. desulfuricans Essex 6 (fr)		10.8	Cooney et al., 1996
D. desulfuricans Norway 4 (fr)		8.2	Traore et al., 1982
D. gigas (fr)		7.4	Traore et al., 1982
D. vulgaris (fr)		13.5	Traore et al., 1981
D. vulgaris Marburg (fr)		7.1	Ingvorsen and Jørgensen, 1984
D. desulfuricans (fr)		5.4	Okabe and Characklis, 1992

Values are compared with those reported for other Desulfovibrio species. (fr) and (m) indicate freshwater and marine strains, respectively.

which TC levels reached their stable levels of 5.0 ± 0.6 w/w% for *Dh* AM13 and of 6.1 ± 1.0 w/w% for *Dm* RS-1 after 2 weeks and 1 week of incubation, respectively. In cultures of *Dh* AM13 grown in HL medium, the TC content of minerals decreased sharply from ~12.6 ± 2.4 w/w % after 1 week of incubation to reach a stable level of 8.3 ± 0.4 w/w% after 2 months of incubation. TC levels in biogenic minerals precipitated with *Dh* AM13 in VHL medium fluctuated within the first 2 months of incubation before reaching a stable level of 13.5 ± 0.7 w/w%. Minerals older than 6 months produced in VHL medium with *Dh* AM13 were lost due to a malfunction of the elemental analyzer. Based on the observation that TC levels were already stable after 6 months in all other conditions (with both SRB), we assumed that this was also the case for minerals precipitated with *Dh* AM13 in VHL medium (**Figure 2A**). In minerals precipitated in HL and VHL conditions with *Dm* RS-1, TC levels were similar and reached stabilized values of 9.5 ± 0.7 w/w% after 1 week of incubation and 10.2 ± 1.2 w/w% after 2 weeks of incubation, respectively. In both conditions, similar amounts of sulfate were reduced and similar amounts of biomass were produced (**Figures 1, 2B**; **Table 1**). Total nitrogen (TN) contents in iron sulfide minerals showed more variability over time, but overall followed similar trends to TC contents (**Figures 2C,D**). Stabilized C/N ratios of minerals converged to a narrow range of 2.7–4.2 for minerals produced with marine *Dh* AM13 (**Figure 2E**), and of 3.6–4.1 for minerals produced with freshwater *Dm* RS-1 (**Figure 2F**).

Additionally, we measured TC and TN levels, and CN ratios of biogenic minerals precipitated by adding Fe(II) to fully grown cultures of *Dh* AM13 and *Dm* RS-1 in selected conditions (AddFe experiments in **Table 3**). When adding Fe(II) to cultures of *Dh* AM13 after full growth in HL medium, minerals tend

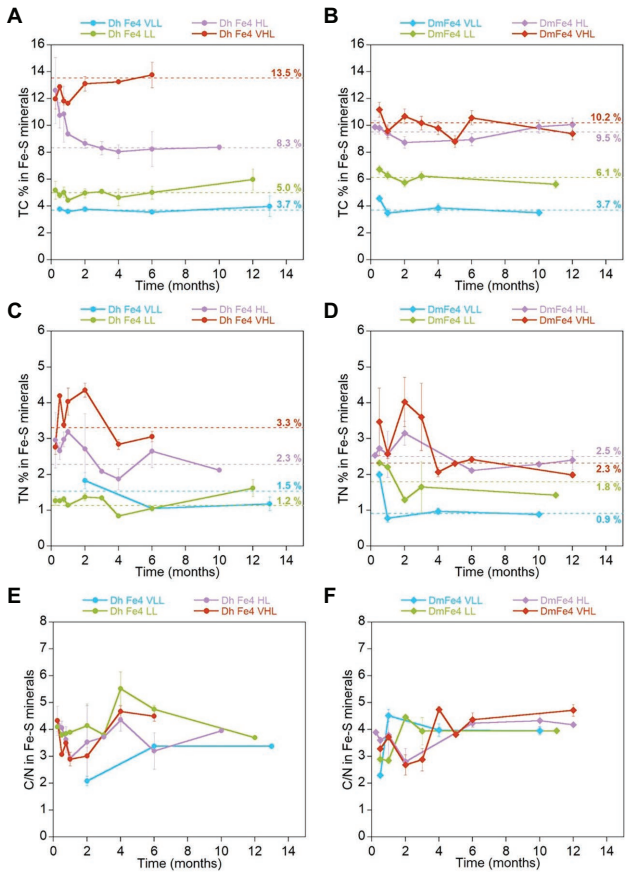

FIGURE 2 | Evolution of the average total carbon (TC) content (w/w %), average total nitrogen (TN) content (w/w %), and average C/N ratio in iron sulfide minerals precipitated in the presence of *Desulfovibrio hydrothermalis* AM13 **(A,C,E)** and in the presence of *Desulfovibrio magneticus* RS-1 **(B,D,F)** as a function of time. Error bars represent ±one standard deviation. Incubations were performed with four different initial lactate concentrations (VLL, LL, HL, and VHL) which controlled the amount of sulfate reduced and biomass produced (**Table 1**; **Figure 1**). Results presented here are from minerals produced in cultures that were grown in the presence of Fe(II). Average values of stabilized levels of TC and TN (see **Table 3** for data points encompassed in stabilized values) are indicated over dashed lines **(A-D)**. TC and TN contents in iron sulfide minerals increase with increasing lactate concentrations in the medium (corresponding to increasing concentrations of reduced sulfate, i.e., increasing concentrations of cell biomass). CN ratios stabilize to a narrow range of values for both bacteria: 2.7–4.2 for marine *Dh* AM13and 3.6–4.1 for freshwater *Dm* RS-1 **(E, F)**.

to precipitate away from cells and have a small particle size similar to this produced without bacteria (Picard et al., 2018). For minerals produced in VLL and LL conditions with *Dh* AM13, average values of TC were not significantly different in Fe and AddFe experiments ($p > 0.05$). In minerals produced in HL conditions with *Dm* RS-1 and in VHL conditions with *Dh* AM13, average values of TC were significantly different in Fe and AddFe experiments ($p < 0.05$; **Table 3**). When cells are grown with Fe(II), the precipitation process occurs over several days. There is the possibility for Fe(II) to interact with the surface of microbial cells, as there is a strong affinity between cations, such as Fe(II), and negatively charged bacterial cell surfaces (Ferris et al., 1987; Beveridge, 1989). As cells grow and produce sulfide, mackinawite precipitates at the surface of cells, while new cells can interact with leftover Fe(II). In contrast, when Fe(II) is added all at once after growth and sulfide production, precipitation of mackinawite is very fast. In conditions producing the highest biomass contents (HL and VHL conditions), the slower process of precipitation might allow for sequestering more biomass.

We previously used scanning transmission *X*-ray microscopy (STXM) coupled with near-edge *X*-ray absorption fine structure spectroscopy (NEXAFS) to determine the type of carbon compounds that can associate with biogenic iron sulfide minerals produced in the presence of *Dh* AM13 in HL medium, whether Fe(II) was provided before inoculation or after growth of the SRB (Picard et al., 2019, 2021). The NEXAFS spectra at the C K-edge of biogenic iron sulfide minerals were deconvolved with standard spectra of proteins, polysaccharides, and lipids and were similar to the C K-edge spectra of non-encrusted bacterial cells reported in other studies (Cosmidis et al., 2015; Picard et al., 2019). The NEXAFS spectra at the N K-edge of biogenic iron sulfide minerals were indicative of fresh proteinaceous material (Picard et al., 2019). Inorganic carbon (e.g., from the carbonate buffer of the medium) and inorganic nitrogen (added as NH_4Cl to the medium) did not contribute significantly to the spectroscopic signatures of iron sulfide minerals (Picard et al., 2019, 2021). Therefore, TC and TN levels in the present study reflect total organic carbon (TOC) and total organic nitrogen (TON) levels in biogenic iron sulfide minerals. Additionally, the spectroscopic signature of organic carbon associated with biogenic iron sulfide minerals did not change over the course of long-term experiments, suggesting no overall partitioning of organic molecules (Picard et al., 2019, 2021). In the present study, we are confirming the quantitative preservation of microbial biomass in iron sulfide mineral aggregates over long periods of time.

While the interactions between iron sulfide minerals (e.g., mackinawite) and heavy metals and pollutants have been extensively studied in the context of bioremediation applications (Chen et al., 2019), to our best knowledge, only two studies have explored TC levels in iron sulfide minerals in laboratory incubations (Balind, 2019; Wang et al., 2019). In experiments co-precipitating mackinawite with dissolved organic carbon extracted with water from soil, corn, and phytoplankton, levels of TOC in mackinawite of up to ~80 mg/g, ~105 mg/g, and ~145 mg/g were measured, respectively. In sorption experiments with the above compounds, levels of TOC in mackinawite were slightly lower and reached levels up to ~45 mg/g, ~65 mg/g, and ~90 mg/g, respectively (Balind, 2019). Overall, this is comparable to our experiments co-precipitating iron sulfide minerals with biomass (up to ~135 mg/g with *Dh* AM13 and up to ~102 mg/g with *Dm* RS-1). In sorption experiments of commercially available iron sulfide FeS and pyrite FeS_2 with dissolved organic matter extracted with water from a peat, TOC levels reached levels up to 1.4 mg/g in FeS and up to 0.065 mg/g in pyrite (Wang et al., 2019). The differences in TOC levels

in the commercially available FeS and freshly precipitated nanocrystalline mackinawite might come from the different nature and crystallinity of minerals. The commercially available FeS might not be mackinawite, therefore preventing comparison with our results and those of Balind (2019). Iron sulfide minerals are less abundant than other types of minerals known to preserve organic carbon [e.g., Fe(III) oxides or clay minerals]; however, they are likely to closely interact with cell biomass when precipitated in anoxic environments. Indeed, in most anoxic environments at the surface of the Earth, microbial sulfate reduction is the source of 97% of sulfide (Rickard, 2012a; Picard et al., 2016); therefore, precipitation of iron sulfide minerals is likely to happen in close proximity to SRB cells. The following is an attempt at estimating the global amount of organic carbon that could potentially be sequestered by biogenic iron sulfide minerals in marine sediments. Estimates of global rates of microbial sulfate reduction in marine sediments vary (Jørgensen, 2021). For the purpose of a rough estimate, we use the lowest overall estimate of 11.3 Tmol of sulfate reduced yearly in marine sediments (Bowles et al., 2014). Not all sulfide produced ends up as iron sulfide minerals; sulfide can interact with organic matter, can be reoxidized to sulfate or intermediate sulfur species, and can precipitate as metastable iron sulfide minerals that will eventually transform to pyrite (FeS_2; Jørgensen, 2021). Of the 11.3 Tmol sulfide produced per year, about 90% are reoxidized (Jørgensen, 2021), therefore leaving ~1 Tmol of sulfide per year that precipitate as iron sulfide minerals. As the first product of interaction between sulfide and ferrous iron is FeS (either as clusters, colloids, or metastable mackinawite; Rickard and Luther, 2007), this gives us an estimated production of 88 Tg of FeS per year. Based on TC measurements done in minerals precipitated in the marine medium with *Dh* AM13 (37–135 mg/g), this translates to 3–12 Tg of organic carbon that can be potentially sequestered by biogenic metastable iron sulfide minerals yearly. Considering our biomass yield of 4.9 g per mol of sulfate for *Dh* AM13, global microbial sulfate reduction would produce ~55 Tg of biomass per year. Obviously, our measurements do not reflect the reality of microbial sulfate reduction in natural environments, as cultures are grown with lactate; however, this illustrates the possibility that enough biomass would be produced to be sequestered by iron sulfide minerals in the range of 3–12 Tg. Interestingly, the global pyrite (FeS_2) formation rate was estimated at ~5 Tg per year in marine sediments (Rickard and Luther, 2007). If metastable iron sulfide minerals are precursors to pyrite formation, the process involves dissolution before reprecipitation as pyrite (Rickard, 2012b), and this would potentially involve some loss of OC. While mineral-associated TC levels obtained in laboratory experiments are not necessarily representative of natural environments, there is recent direct evidence that iron sulfide minerals could be associated with significant amounts of OC in the environment and that it is useful to understand the basic mechanisms of interactions between OC and iron sulfide minerals (Barber et al., 2017; Balind, 2019).

Biogenic Iron Sulfide Minerals Sequester Organic C and N More Efficiently in Freshwater Medium

Stabilized TC levels in iron sulfide minerals produced in freshwater and marine media were correlated with concentrations of reduced sulfate (**Figure 3A**). However, for similar concentrations of reduced sulfate, different cell biomass concentrations were produced by each bacterium (**Figure 1**; **Table 1**). Therefore, we compared the OC removal capacity of iron sulfide minerals in freshwater and marine conditions. In all experiments, a fixed Fe(II) concentration of 4 mM was used. Assuming that all Fe(II) precipitated as iron sulfide minerals, then the same amount of iron sulfide minerals (~352 mg/l) was produced in all experiments. Using values of TC% in iron sulfide minerals, we estimated organic carbon concentrations removed from the medium (**Figure 3B**; **Table 3**). Biogenic iron sulfide minerals produced in marine conditions with *Dh* AM13 captured 42, 45, 44, and 51% of the cell biomass carbon available in VLL, LL, HL, and VHL conditions, respectively. Biogenic iron sulfide minerals precipitated in freshwater conditions with *Dm* RS-1 sequestered 67, 100, 137, and 107% of the available carbon in VLL, LL, HL, and VHL conditions, respectively. *Dm* RS-1 experiments in HL and VHL conditions showed a removal higher than 100%. We hypothesize that this might be due to uncertainties in measuring cell biomass carbon contents in pellets. While SRB can produce extracellular polymeric substances (EPS), their quantification was not possible and we assumed that they would not contribute significantly to organic carbon concentrations. In our incubations, we did not reach saturation levels; therefore, iron sulfide minerals could possibly bind more biomass than the levels we tested in this study. Due to uncertainties measuring biomass concentrations and therefore calculating organic concentrations at equilibrium in the freshwater experiments, we did not attempt to fit our data to adsorption isotherm models. Overall, our data indicate that sequestration of organic matter by iron sulfide minerals is more efficient in freshwater than in marine conditions. In a recent study investigating interactions between natural OM into ferrihydrite, a Fe(III) oxyhydroxide, it was shown that OM adsorbed more on ferrihydrite in low- and mid-ionic strength water (e.g., proxy for freshwater) than in high-ionic strength water (e.g., proxy for seawater). At high-ionic strength, Na^+ ions seem to occupy the surface of minerals and prevent adsorption of organic matter (Tomaszewski et al., 2021).

Cells Play an Important Role in Increasing the TC Contents of Organo-Mineral Aggregates

Abiotic iron sulfide minerals were precipitated in the marine medium with organic mixtures. The amino acid mixture (Casamino acids) and tryptone are mostly made of proteinaceous material, while yeast extract is close to the overall composition of bacteria, with the difference that yeast cells have lysed. TC levels reached 1.2 ± 0.1 w/w%, 5.1 ± 0.6 w/w%, and 5.2 ± 0.8 w/w% after 6 months of incubation with casamino acids, tryptone, and yeast extract, respectively. Despite initial concentrations of organic C in the

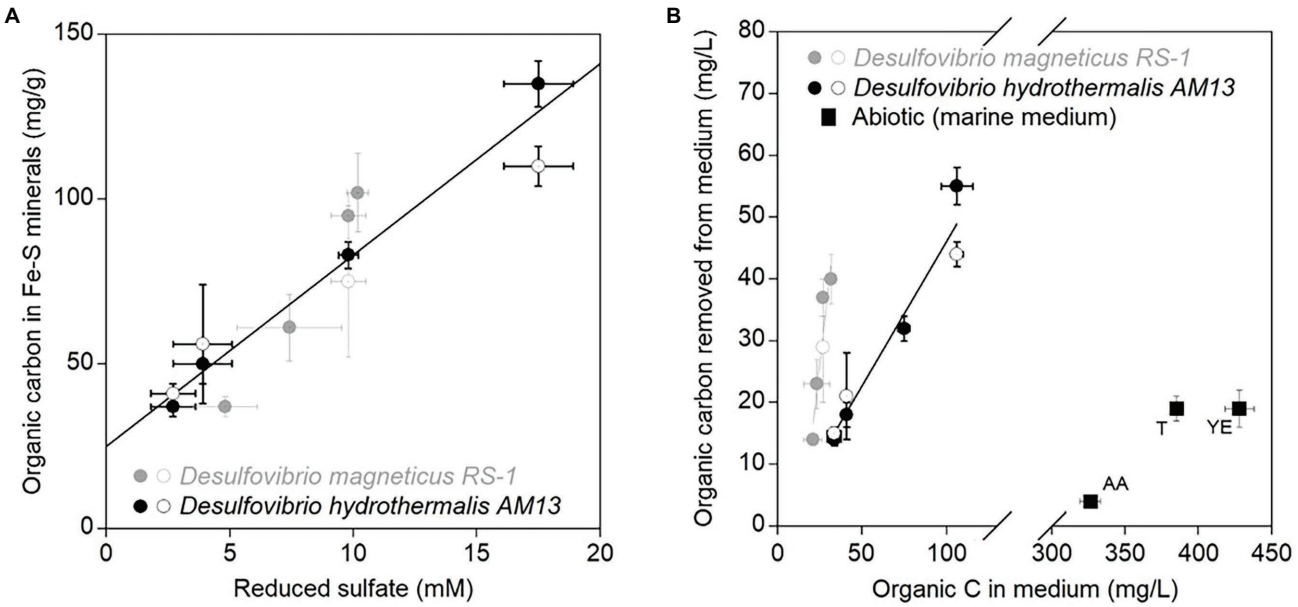

FIGURE 3 | (A) Average stabilized organic carbon contents (mg/g) in biogenic iron sulfide minerals as a function of average concentrations of reduced sulfate (mM). Black circles are data for marine strain *Desulfovibrio hydrothermalis* AM13, and gray circles are data for freshwater *Desulfovibrio magneticus* RS-1. Closed circles are from minerals precipitated in cultures grown with Fe(II) and open circles are from minerals precipitated in cultures to which Fe(II) was added after growth of SRB. Error bars represent ±one standard deviation. The linear regression is calculated for all data points ($R^2 = 0.89$). **(B)** Average organic carbon concentrations (mg/L) removed from the medium in biotic and abiotic experiments by iron sulfide minerals as a function of average organic concentrations of carbon (mg/L) available in the medium. Black circles are data for marine *Dh* AM13, and gray circles are data for freshwater *Dm* RS-1. Closed circles are from minerals precipitated in cultures grown with Fe(II) and open circles are from minerals precipitated in cultures to which Fe(II) was added after growth of SRB. The black linear regression is calculated for all data points from experiments with marine *Dh* AM13 ($R^2 = 0.95$) and the gray linear regression is calculated for all data points from experiments with marine *Dm* RS-1 ($R^2 = 0.89$). Black squares are data from abiotic experiments to which organic mixtures have been used for co-precipitation of minerals: T, tryptone, YE, Yeast extract, and AA, Casamino acids. Error bars represent ±one standard deviation. Iron sulfide minerals have a higher affinity toward organic molecules in freshwater medium than in marine medium. Iron sulfide minerals also have a higher affinity toward cell biomass than organic mixtures in abiotic conditions.

medium three to ten times higher in abiotic experiments than in biotic experiments, and initial molar C/Fe ratios much higher in abiotic experiments, the removal of organic molecules in the medium by iron sulfide minerals was low in abiotic experiments: 6% in incubations with tryptone, 4% in incubations with yeast extract, and 1% in incubations with casamino acids (**Tables 2** and **3**; **Figure 3B**). Our previous spectroscopic study indicated that iron sulfide minerals have affinity for large proteinaceous material (from tryptone and yeast extract) and low affinity for sugars (mannose and glucose; Picard et al., 2021). The results of the present study indicate that presence of cells, and/or cellular structure and architecture play a role in increasing the amount of organic carbon sequestered through organo-mineral associations. This might be explained by the fact that when iron sulfide minerals bind to organic molecules at the surface of cells, the whole cells are preserved in mineral aggregates rather than just the molecules binding to minerals. This is supported by STXM analyses of iron sulfide minerals produced in laboratory experiments. While organic carbon is homogeneously distributed on/in abiotic minerals precipitated with tryptone and yeast extract, in biogenic minerals precipitated with *Dh* AM13 grown with Fe(II) or in cultures to which Fe(II) was added after full growth of SRB, organic carbon has a heterogeneous distribution (Picard et al., 2019, 2021). Indeed, hot spots of organic carbon (i.e., cells) are preserved in iron sulfide mineral aggregates, whether cells are encrusted in minerals or not, and these hot spots are still present after 2 years of incubation (Picard et al., 2019, 2021). The reported patchy occurrence of organic matter in continental margin sediments could therefore be explained by the abundant presence of microbial cells in sedimentary environments (Ransom et al., 1997, 1999). Interestingly, when mackinawite was precipitated with natural organic matter (NOM) extracted with water from phytoplankton, soil, or corn, the TC% in minerals reached levels as high or higher than those in minerals precipitated with SRB in our study (Balind, 2019). The NOM solutions used by Balind were filtered with 0.7 µm filters, which might leave residues of cells or smaller cells go through in the solutions, explaining how higher retention of OC might be possible. The study by Balind also highlights that iron sulfide minerals have a high affinity toward natural OM (Balind, 2019).

Mineralogical Changes Do Not Play an Apparent Role in the Stability of TC and TN Contents in Iron Sulfide Minerals

Dh AM13 can influence iron sulfide mineral transformations. Notably, when *Dh* AM13 is grown in HL medium in the presence of Fe(II), mackinawite starts transforming to greigite

via solid-state transformation after 5 months of incubation, while no transformation is observed in abiotic experiments and in biotic experiments to which Fe(II) is added after full growth of the bacteria (Picard et al., 2018). Mackinawite to greigite transformation was also detected in cultures of *Desulfovibrio vulgaris* grown with Fe(II) grown with Fe(II) after several months of incubation (Mansor et al., 2019). As TC contents in minerals precipitated with marine *Dh* AM13 in HL conditions stabilized after 2 months of incubation, just before mineral transformations started to be measurable by *X*-ray diffractions (XRD), we hypothesized that mineral transformations could potentially influence TC contents in minerals and their long-term stability. We therefore characterized the mineralogy of iron sulfide minerals in all conditions at relevant times during long-term incubations (**Figure 4**). Transformation of mackinawite to greigite was observed, but not in all conditions. In *Dh* cultures, greigite was produced in VHL and HL conditions, while it was not detected when experiments started with LL and VLL concentrations. While we previously started to observe intense peaks representative of greigite in the XRD spectra collected from 5-month-old minerals (**Figure 1** in Picard et al., 2018), we only saw traces of greigite after 6 months of incubation in the present study (**Figure 4**). The same medium was used in both studies, the main difference was that only 1 ml of trace element solution was used in the preparation of media for this study, while 10 ml was used in the former study. This potentially indicates that the microbial influence on mineral formation and transformation could be influenced, directly or indirectly, by the availability of trace elements. However, this observation will require further exploration. In *Dm* cultures, we also observed different outcomes in mineralogical products depending on the starting concentration of lactate. Greigite was detected in LL and VLL conditions, while it was not detected in HL and VHL conditions. We did not detect pyrite in any of the conditions. The absence of pyrite might be explained by the fact that the presence of organic carbon in iron sulfide precipitation experiments seems to inhibit pyrite formation and promote greigite formation (Morse and Wang, 1997; Rickard et al., 2001). However, we were not able to identify parameters that control greigite formation and/or prevent mackinawite transformation in our study. Additional work would be needed for that purpose. In conclusion, mineralogical changes cannot be attributed to changes in TC levels.

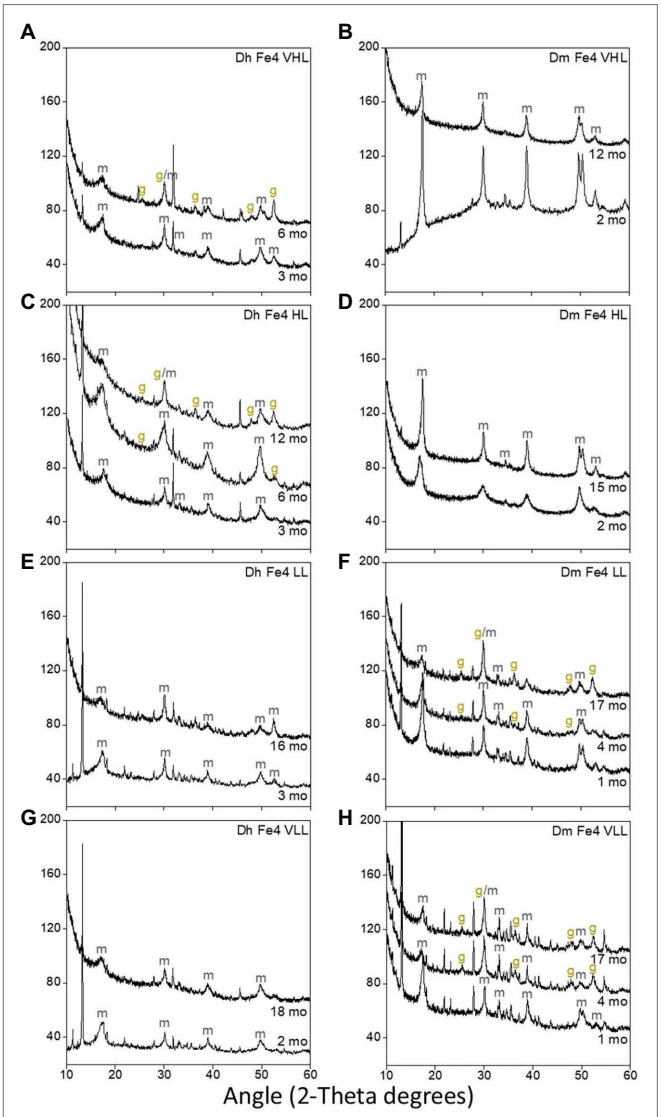

FIGURE 4 | *X*-ray diffraction (XRD) spectra of biogenic minerals precipitated in cultures of Dh AM13 **(A,C,E,G)** and in cultures of Dm RS-1 **(B,D,F,H)**. Only the peaks relevant to iron sulfide minerals have been labeled (*m*, mackinawite; g, greigite). Other peaks visible on theses spectra are form vivianite [Fe(II) phosphate mineral].

CONCLUSION

Climate change will reduce oxygen contents in the ocean and will expand oxygen minimum zones, which will modify organic carbon delivery to sediments (Keil, 2017). Authigenic iron sulfide minerals have the potential to play a role in preserving significant amounts of organic carbon in anoxic environments, concurrently with organic matter sulfurization (Raven et al., 2021a). A better understanding of the mechanisms that form associations between organic carbon and iron sulfide minerals is needed. Specifically, it would be critical to determine the type of interactions between Fe and S in iron sulfide minerals and atoms in functional groups of organic carbon (C, H, O, and N), if bonding is covalent or noncovalent, and if organic carbon can be incorporated in the crystal structure of iron sulfide minerals. A better characterization of the organo-mineral interface is required, although technically challenging at high resolution (Kleber et al., 2021). Adsorption and co-precipitation experiments with individual organic molecules originating from biomass, and with a large variety of natural organic matter mixtures will help understand the dynamics of interactions better. While our experiments show stable interactions between iron sulfide minerals and organic carbon in long-term anoxic incubations, it will be necessary to determine the reactivity

of these interactions with other microorganisms under anoxic conditions, and their stability under oxic conditions. Iron sulfide minerals store preferentially proteinaceous material, which is the preferred food for some other types of microorganisms in subsurface sediments (Lloyd et al., 2013). It is also unknown if SRM can access this organic carbon for their own metabolism. Iron sulfide minerals could also be an energy source for either sulfide- or iron-oxidizing bacteria. Additionally, the effect of mineral transformations on TC contents needs to be investigated as eventually metastable iron sulfide minerals might transform to pyrite, independently of the pyrite formation pathway, or might be oxidized at the oxic-anoxic interface in sediments. Finally, biogenic FeS minerals could also have an impact on the sequestration of trace metals (Co, Cu, and Ni) and important nutrients (N and P), which would in turn influence microbial life in anoxic environments as well as recorded proxies typically used for the reconstruction of past anoxic environments (Large et al., 2017; Gregory et al., 2019). While marine environments represent the largest environment where microbial sulfate reduction happens and iron sulfide mineral precipitation occurs, it is also important to consider freshwater environments. To conclude, there are still numerous questions to investigate related to interactions between iron sulfide minerals and organic carbon; questions that are relevant for the fields of biogeochemistry of past and modern environments, astrobiology, and microbial physiology.

DATA AVAILABILITY STATEMENT

The raw data supporting the conclusions of this article will be made available by the authors, without undue reservation.

AUTHOR CONTRIBUTIONS

AP conceived and supervised the project, performed the experiments, analyzed the data, and wrote the manuscript. NN and CB performed the experiments, carried out the analyses, and contributed to the writing of the manuscript. All authors contributed to the article and approved the submitted version.

FUNDING

This work was funded by a Research Infrastructure grant from the Nevada NASA Space Grant Consortium awarded to AP (grant number NNX15AI02H). NN was supported by a CSUN scholarship from the UNLV Office of Undergraduate Research during the Summer of 2019 and by an NSF EPSCoR Nevada Undergraduate Research Opportunity Program (UROP) scholarship for the academic year 2020-2021. CB was supported by an NSF EPSCoR Nevada undergraduate research opportunity program (UROP) scholarship for the academic year 2021-2022. The publication fees for this article were partially supported by the UNLV University Libraries Open Article Fund.

ACKNOWLEDGMENTS

We thank Brenda Buck (UNLV, Geoscience) for providing access to her elemental analyzer and Dennis Bazylinski (UNLV, School of Life Sciences) for providing access to his laboratory and support. We would like to acknowledge the support from the College of Sciences.

REFERENCES

Alazard, D., Dukan, S., Urios, A., Verhe, F., Bouabida, N., Morel, F., et al. (2003). *Desulfovibrio hydrothermalis* sp. nov., a novel sulfate-reducing bacterium isolated from hydrothermal vents. *Int. J. Syst. Evol. Micr.* 53, 173–178. doi: 10.1099/ijs.0.02323-0

Balind, K. (2019). *Exploring the Affinity and Selectivity of Sedimentary Mackinawite (FeS) Towards Natural Organic Matter*. Montreal, Quebec, Canada: Concordia University.

Barber, A., Brandes, J., Leri, A., Lalonde, K., Balind, K., Wirick, S., et al. (2017). Preservation of organic matter in marine sediments by inner-sphere interactions with reactive iron. *Sci. Rep.* 7:366. doi: 10.1038/s41598-017-00494-0

Bar-On, Y. M., Phillips, R., and Milo, R. (2018). The biomass distribution on earth. *Proc. Nat. Acad. Sci.* 115, 6506–6511. doi: 10.1073/pnas.1711842115

Berner, R. A. (1990). Atmospheric carbon dioxide levels over Phanerozoic time. *Science* 249, 1382–1386. doi: 10.1126/science.249.4975.1382

Berner, R. A., and Canfield, D. E. (1989). A new model for atmospheric oxygen over Phanerozoic time. *Am. J. Sci.* 289, 333–361. doi: 10.2475/ajs.289.4.333

Beveridge, T. J. (1989). Role of cellular design in metal accumulation and mineralization. *Annu. Rev. Microbiol.* 43, 147–171. doi: 10.1146/annurev.mi.43.100189.001051

Bowles, M. W., Mogollón, J. M., Kasten, S., Zabel, M., and Hinrichs, K.-U. (2014). Global rates of marine sulfate reduction and implications for sub–sea-floor metabolic activities. *Science* 344, 889–891. doi: 10.1126/science.1249213

Boye, K., Noël, V., Tfaily, M. M., Bone, S. E., Williams, K. H., Bargar, J. R., et al. (2017). Thermodynamically controlled preservation of organic carbon in floodplains. *Nat. Geosci.* 10, 415–419. doi: 10.1038/ngeo2940

Burdige, D. J. (2007). Preservation of organic matter in marine sediments: controls, mechanisms, and an imbalance in sediment organic carbon budgets? *Chem. Rev.* 107, 467–485. doi: 10.1021/cr050347q

Canfield, D. E. (1994). Factors influencing organic carbon preservation in marine sediments. *Chem. Geol.* 114, 315–329. doi: 10.1016/0009-2541(94)90061-2

Cavicchioli, R., Ripple, W. J., Timmis, K. N., Azam, F., Bakken, L. R., Baylis, M., et al. (2019). Scientists' warning to humanity: microorganisms and climate change. *Nat. Rev. Microbiol.* 17, 569–586. doi: 10.1038/s41579-019-0222-5

Chan, C. S., Fakra, S. C., Edwards, D. C., Emerson, D., and Banfield, J. F. (2009). Iron oxyhydroxide mineralization on microbial extracellular polysaccharides. *Geochim. Cosmochim. Acta* 73, 3807–3818. doi: 10.1016/j.gca.2009.02.036

Chen, Y., Liang, W., Li, Y., Wu, Y., Chen, Y., Xiao, W., et al. (2019). Modification, application and reaction mechanisms of nano-sized iron sulfide particles for pollutant removal from soil and water: a review. *Chem. Eng. J.* 362, 144–159. doi: 10.1016/j.cej.2018.12.175

Cooney, M. J., Roschi, E., Marison, I. W., Comminellis, C., and Von Stockar, U. (1996). Physiologic studies with the sulfate-reducing bacterium Desulfovibrio desulfuricans: evaluation for use in a biofuel cell. *Enzym. Microb. Technol.* 18, 358–365. doi: 10.1016/0141-0229(95)00132-8

Cosmidis, J., Benzerara, K., Nassif, N., Tyliszczak, T., and Bourdelle, F. (2015). Characterization of Ca-phosphate biological materials by scanning transmission *X*-ray microscopy (STXM) at the Ca $L_{2,3}$-, P $L_{2,3}$- and C K-edges. *Acta Biomater.* 12, 260–269. doi: 10.1016/j.actbio.2014.10.003

Ferris, F. G., Fyfe, W. S., and Beveridge, T. J. (1987). Bacteria as nucleation sites for authigenic minerals in a metal-contaminated lake sediment. *Chem. Geol.* 63, 225–232. doi: 10.1016/0009-2541(87)90165-3

Gregory, D., Mukherjee, I., Olson, S. L., Large, R. R., Danyushevsky, L. V., Stepanov, A. S., et al. (2019). The formation mechanisms of sedimentary

pyrite nodules determined by trace element and sulfur isotope microanalysis. *Geochim. Cosmochim. Acta* 259, 53–68. doi: 10.1016/j.gca.2019.05.035

Hemingway, J. D., Rothman, D. H., Grant, K. E., Rosengard, S. Z., Eglinton, T. I., Derry, L. A., et al. (2019). Mineral protection regulates long-term global preservation of natural organic carbon. *Nature* 570, 228–231. doi: 10.1038/s41586-019-1280-6

Hoffman, C. L., Nicholas, S. L., Ohnemus, D. C., Fitzsimmons, J. N., Sherrell, R. M., German, C. R., et al. (2018). Near-field iron and carbon chemistry of non-buoyant hydrothermal plume particle, southern East Pacific rise 15°S. *Mar. Chem.* 201, 183–197. doi: 10.1016/j.marchem.2018.01.011

Ingalls, A. E., Aller, R. C., Lee, C., and Wakeham, S. G. (2004). Organic matter diagenesis in shallow water carbonate sediments. *Geochim. Cosmochim. Acta* 68, 4363–4379. doi: 10.1016/j.gca.2004.01.002

Ingalls, A. E., Lee, C., and Druffel, E. R. (2003). Preservation of organic matter in mound-forming coral skeletons. *Geochim. Cosmochim. Acta* 67, 2827–2841. doi: 10.1016/S0016-7037(03)00079-6

Ingvorsen, K., and Jørgensen, B. B. (1984). Kinetics of sulfate uptake by freshwater and marine species of Desulfovibrio. *Arch. Microbiol.* 139, 61–66. doi: 10.1007/BF00692713

Jenkyns, H. C. (2010). "Geochemistry of oceanic anoxic events," in *Geochemistry, Geophysics, Geosystems*. ed. N. Bhatnagar (Canada: Arcler Education Incorporated).

Jiao, N., Herndl, G. J., Hansell, D. A., Benner, R., Kattner, G., Wilhelm, S. W., et al. (2010). Microbial production of recalcitrant dissolved organic matter: long-term carbon storage in the global ocean. *Nat. Rev. Microbiol.* 8, 593–599. doi: 10.1038/nrmicro2386

Jørgensen, B. B. (2021). Sulfur biogeochemical cycle of marine sediments. *Geo. Perspect.* 10, 145–307. doi: 10.7185/geochempersp.10.2

Jørgensen, B. B., Findlay, A. J., and Pellerin, A. (2019). The Biogeochemical Sulfur Cycle of Marine Sediments. *Front. Microbiol.* 10:849. doi: 10.3389/fmicb.2019.00849

Keil, R. (2017). Anthropogenic forcing of carbonate and organic carbon preservation in marine sediments. *Annu. Rev. Mar. Sci.* 9, 151–172. doi: 10.1146/annurev-marine-010816-060724

Keil, R., and Mayer, L. (2014). "Mineral matrices and organic matter," in *Treatise on Geochemistry: Organic Geochemistry*. eds. P. G. Falkowski and K. H. Freeman (Netherlands: Elsevier Science), 337–359.

Kleber, M., Bourg, I. C., Coward, E. K., Hansel, C. M., Myneni, S. C., and Nunan, N. (2021). Dynamic interactions at the mineral–organic matter interface. *Nat. Rev. Earth Env.* 2, 402–421. doi: 10.1038/s43017-021-00162-y

Kleber, M., Eusterhues, K., Keiluweit, M., Mikutta, C., Mikutta, R., and Nico, P. S. (2015). Mineral–organic associations: formation, properties, and relevance in soil environments. *Adv. Agron.* 130, 1–140. doi: 10.1016/bs.agron.2014.10.005

Kolmert, Å., Wikström, P., and Hallberg, K. B. (2000). A fast and simple turbidimetric method for the determination of sulfate in sulfate-reducing bacterial cultures. *J. Microbiol. Methods* 41, 179–184. doi: 10.1016/S0167-7012(00)00154-8

Lalonde, K., Mucci, A., Ouellet, A., and Gelinas, Y. (2012). Preservation of organic matter in sediments promoted by iron. *Nature* 483, 198–200. doi: 10.1038/nature10855

Large, R. R., Mukherjee, I., Gregory, D. D., Steadman, J. A., Maslennikov, V. V., and Meffre, S. (2017). Ocean and atmosphere geochemical proxies derived from trace elements in marine pyrite: implications for ore genesis in sedimentary basins. *Econ. Geol.* 112, 423–450. doi: 10.2113/econgeo.112.2.423

LaRowe, D., Arndt, S., Bradley, J., Estes, E., Hoarfrost, A., Lang, S., et al. (2020). The fate of organic carbon in marine sediments-new insights from recent data and analysis. *Earth-Sci. Rev.* 204:103146. doi: 10.1016/j.earscirev.2020.103146

Lloyd, K. G., Schreiber, L., Petersen, D. G., Kjeldsen, K. U., Lever, M. A., Steen, A. D., et al. (2013). Predominant archaea in marine sediments degrade detrital proteins. *Nature* 496, 215–218. doi: 10.1038/nature12033

Mansor, M., Berti, D., Hochella, M. F. Jr., Murayama, M., and Xu, J. (2019). Phase, morphology, elemental composition, and formation mechanisms of biogenic and abiogenic Fe-cu-sulfide nanoparticles: a comparative study on their occurrences under anoxic conditions. *Am. Mineral.* 104, 703–717. doi: 10.2138/am-2019-6848

Morse, J. W., and Wang, Q. (1997). Pyrite formation under conditions approximating those in anoxic sediments: II. Influence of precursor iron minerals and organic matter. *Mar. Chem.* 57, 187–193. doi: 10.1016/S0304-4203(97)00050-9

Ogawa, H., Amagai, Y., Koike, I., Kaiser, K., and Benner, R. (2001). Production of refractory dissolved organic matter by bacteria. *Science* 292, 917–920. doi: 10.1126/science.1057627

Okabe, S., and Characklis, W. G. (1992). Effects of temperature and phosphorous concentration on microbial sulfate reduction by Desulfovibrio desulfuricans. *Biotechnol. Bioeng.* 39, 1031–1042. doi: 10.1002/bit.260391007

Opfergelt, S. (2020). The next generation of climate model should account for the evolution of mineral-organic interactions with permafrost thaw. *Environ. Res. Lett.* 15:091003. doi: 10.1088/1748-9326/ab9a6d

Picard, A., Gartman, A., Clarke, D. R., and Girguis, P. R. (2018). Sulfate-reducing bacteria influence the nucleation and growth of mackinawite and greigite. *Geochim. Cosmochim. Acta* 220, 367–384. doi: 10.1016/j.gca.2017.10.006

Picard, A., Gartman, A., Cosmidis, J., Obst, M., Vidoudez, C., Clarke, D. R., et al. (2019). Authigenic metastable iron sulfide minerals preserve microbial organic carbon preservation in anoxic environments. *Chem. Geol.* 530:119343. doi: 10.1016/j.chemgeo.2019.119343

Picard, A., Gartman, A., and Girguis, P. R. (2016). What do we really know about the role of microorganisms in iron sulfide mineral formation? *Front. Earth Sci.* 4:68. doi: 10.3389/feart.2016.00068

Picard, A., Gartman, A., and Girguis, P. R. (2021). Interactions between iron sulfide minerals and organic carbon: implications for biosignature preservation and detection. *Astrobiology* 21, 587–604. doi: 10.1089/ast.2020.2276

Rabus, R., Hansen, T., and Widdel, F. (2013). "Dissimilatory sulfate- and sulfur-reducing prokaryotes," in *The Prokaryotes*. eds. E. Rosenberg, E. DeLong, S. Lory, E. Stackebrandt and F. Thompson (Berlin Heidelberg: Springer), 309–404.

Ransom, B., Bennett, R. H., Baerwald, R., Hulbert, M. H., and Burkett, P.-J. (1999). In situ conditions and interactions between microbes and minerals in fine-grained marine sediments: a TEM microfabric perspective. *Am. Mineral.* 84, 183–192. doi: 10.2138/am-1999-1-220

Ransom, B., Bennett, R., Baerwald, R., and Shea, K. (1997). TEM study of in situ organic matter on continental margins: occurrence and the "monolayer" hypothesis. *Mar. Geol.* 138, 1–9. doi: 10.1016/S0025-3227(97)00012-1

Raven, M. R., Fike, D. A., Bradley, A. S., Gomes, M. L., Owens, J. D., and Webb, S. A. (2019). Paired organic matter and pyrite δ34S records reveal mechanisms of carbon, sulfur, and iron cycle disruption during ocean anoxic event 2. *Earth Planet. Sci. Lett.* 512, 27–38. doi: 10.1016/j.epsl.2019.01.048

Raven, M., Keil, R. G., and Webb, S. M. (2021a). Rapid, concurrent formation of organic sulfur and iron sulfides during experimental sulfurization of sinking marine particles. *Glob. Biogeochem. Cycles* 35:e2021GB007062. doi: 10.1029/2021GB007062

Raven, M. R., Keil, R. G., and Webb, S. M. (2021b). Microbial sulfate reduction and organic sulfur formation in sinking marine particles. *Science* 371, 178–181. doi: 10.1126/science.abc6035

Raven, M. R., Sessions, A. L., Adkins, J. F., and Thunell, R. C. (2016a). Rapid organic matter sulfurization in sinking particles from the Cariaco Basin water column. *Geochim. Cosmochim. Acta* 190, 175–190. doi: 10.1016/j.gca.2016.06.030

Raven, M. R., Sessions, A. L., Fischer, W. W., and Adkins, J. F. (2016b). Sedimentary pyrite $\delta^{34}S$ differs from porewater sulfide in Santa Barbara Basin: proposed role of organic sulfur. *Geochim. Cosmochim. Acta* 186, 120–134. doi: 10.1016/j.gca.2016.04.037

Rickard, D. T. (ed.) (2012a). "Microbial sulfate reduction in sediments," in *Developments in Sedimentology*. Oxford: Elsevier, 319–351.

Rickard, D. T. (ed.) (2012b). "Sedimentary pyrite," in *Developments in Sedimentology*. Oxford: Elsevier, 233–285.

Rickard, D., Butler, I. B., and Oldroyd, A. (2001). A novel iron sulphide mineral switch and its implications for earth and planetary science. *Earth Planet Sc. Lett.* 189, 85–91. doi: 10.1016/S0012-821X(01)00352-1

Rickard, D., and Luther, G. W. (2007). Chemistry of iron sulfides. *Chem. Rev.* 107, 514–562. doi: 10.1021/cr0503658

Sakaguchi, T., Arakaki, A., and Matsunaga, T. (2002). *Desulfovibrio magneticus* sp nov., a novel sulfate-reducing bacterium that produces intracellular single-domain-sized magnetite particles. *Int. J. Syst. Evol. Micr.* 52, 215–221. doi: 10.1099/00207713-52-1-215

Singh, B. K., Bardgett, R. D., Smith, P., and Reay, D. S. (2010). Microorganisms and climate change: terrestrial feedbacks and mitigation options. *Nat. Rev. Microbiol.* 8, 779–790. doi: 10.1038/nrmicro2439

Solomon, D., Lehmann, J., Wang, J., Kinyangi, J., Heymann, K., Lu, Y., et al. (2012). Micro- and nano-environments of C sequestration in soil: a multi-elemental STXM-NEXAFS assessment of black C and organomineral associations. *Sci. Total Environ.* 438, 372–388. doi: 10.1016/j.scitotenv.2012.08.071

Stookey, L. L. (1970). Ferrozine - A new spectrophotometric reagent for iron. *Anal. Chem.* 42, 779–781. doi: 10.1021/ac60289a016

Tomaszewski, E. J., Coward, E. K., and Sparks, D. L. (2021). Ionic strength and species drive iron–carbon adsorption dynamics: implications for carbon cycling in future coastal environments. *Environ. Sci. Technol. Lett.* 8, 719–724. doi: 10.1021/acs.estlett.1c00432

Traore, A. S., Hatchikian, C. E., Belaich, J.-P., and Le Gall, J. (1981). Microcalorimetric studies of the growth of sulfate-reducing bacteria: energetics of Desulfovibrio vulgaris growth. *J. Bacteriol.* 145, 191–199. doi: 10.1128/jb.145.1.191-199.1981

Traore, A. S., Hatchikian, C. E., Le Gall, J., and Belaich, J.-P. (1982). Microcalorimetric studies of the growth of sulfate-reducing bacteria: comparison of the growth parameters of some Desulfovibrio species. *J. Bacteriol.* 149, 606–611. doi: 10.1128/jb.149.2.606-611.1982

Wagai, R., Kajiura, M., and Asano, M. (2020). Iron and aluminum association with microbially processed organic matter via meso-density aggregate formation across soils: organo-metallic glue hypothesis. *Soil* 6, 597–627. doi: 10.5194/soil-6-597-2020

Wang, Y., Zhang, Z., Han, L., Sun, K., Jin, J., Yang, Y., et al. (2019). Preferential molecular fractionation of dissolved organic matter by iron minerals with different oxidation states. *Chem. Geol.* 520, 69–76. doi: 10.1016/j.chemgeo.2019.05.003

Conflict of Interest: The authors declare that the research was conducted in the absence of any commercial or financial relationships that could be construed as a potential conflict of interest.

Publisher's Note: All claims expressed in this article are solely those of the authors and do not necessarily represent those of their affiliated organizations, or those of the publisher, the editors and the reviewers. Any product that may be evaluated in this article, or claim that may be made by its manufacturer, is not guaranteed or endorsed by the publisher.

Advantages of publishing in Frontiers

OPEN ACCESS
Articles are free to read for greatest visibility and readership

FAST PUBLICATION
Around 90 days from submission to decision

HIGH QUALITY PEER-REVIEW
Rigorous, collaborative, and constructive peer-review

TRANSPARENT PEER-REVIEW
Editors and reviewers acknowledged by name on published articles

Frontiers
Avenue du Tribunal-Fédéral 34
1005 Lausanne | Switzerland

Visit us: www.frontiersin.org
Contact us: frontiersin.org/about/contact

REPRODUCIBILITY OF RESEARCH
Support open data and methods to enhance research reproducibility

DIGITAL PUBLISHING
Articles designed for optimal readership across devices

FOLLOW US
@frontiersin

IMPACT METRICS
Advanced article metrics track visibility across digital media

EXTENSIVE PROMOTION
Marketing and promotion of impactful research

LOOP RESEARCH NETWORK
Our network increases your article's readership